IRE IEEE
Transactions
ON AUTOMATIC CONTROL

Volume AC-4 December, 1959 Number 3

PROCEEDINGS OF THE

NATIONAL AUTOMATIC CONTROL CONFERENCE

NOVEMBER 4-6, 1959

DALLAS, TEXAS

PUBLISHED BY THE
PROFESSIONAL GROUP ON AUTOMATIC CONTROL

IRE PROFESSIONAL GROUP ON AUTOMATIC CONTROL

The Professional Group on Automatic Control is an organization, within the framework of the IRE, of members with principal professional interest in Automatic Control. All members of the IRE are eligible for membership in the Group and will receive all Group publications upon payment of prescribed fee.

Annual Fee: $2.00

IRE TRANSACTIONS®
on Automatic Control

George S. Axelby, Editor, Air Arm Division, Westinghouse Electric Corp., Box 746, Baltimore, Md.

Published by the Institute of Radio Engineers, Inc., for the Professional Group on Automatic Control, 1 East 79th Street, New York 21, New York. Responsibility for the contents rests upon the authors, and not upon the IRE, the Group or its members. Individual copies available for sale to IRE-PGAC members at$1.45, to IRE members at $2.20 and to nonmembers at $4.35.

PREFACE

The papers presented in this special issue of the PGAC Transactions were presented at the 1959 National Automatic Control Conference (NACC) held at Dallas on November 4-6, 1959. Although this Conference was planned and sponsored by the IRE Professional Group on Automatic Control, it was actually a joint conference with participation by the American Institute of Electrical Engineers, the Instrument Society of America, the IRE Professional Group on Industrial Electronics, and with the cooperation of the Instruments and Regulators Division of the American Society of Mechanical Engineers and the Electrical Engineering Department of Southern Methodist University.

Because of the sponsorship of a portion of the Conference papers by groups other than the IRE-PGAC, and the initial decision not to publish a Conference Proceedings as such, all of the Conference papers cannot be presented in any one publication. Certain of the papers presented are reserved for publication in the Proceedings of the 1960 Moscow Conference of the International Federation on Automatic Control Conference, in the AIEE Transactions, and the ASME Transactions. In order to indicate the total technical content of the National Automatic Control Conference, this Transactions issue contains those papers sponsored by the PGAC, plus abstracts of all other papers which are being published elsewhere.

The 1959 National Control Conference was the first conference sponsored by the PGAC since its formation in 1952. In prior years, the PGAC has limited its activities to sponsorship of sessions at the IRE National Convention and the IRE Western Engineering Show and Convention (WESCON). When initial plans were made for the 1959 NACC, the Administrative Committee of the PGAC decided to seek the participation of other interested societies so as to make it a joint meeting. The Administrative Committee of the PGAC wholeheartedly supports the idea of one major joint inter-society control meeting each year, because it feels that the benefits from cross-fertilization between the control groups in the various societies, plus the possibilities for substantial improvement in technical content of conference programs, far outweigh the increased difficulties in arrangements which are a natural result of joint participation.

The goal of a true joint annual conference on automatic control will be realized starting in 1960 with the inauguration of a five-year cycle of Joint Automatic Control Conferences, with participation by the IRE PGAC, the AIEE Feedback Control and Recording Systems Committees, the ASME IRD Division, the ISA, and the AIChE. In order to reduce fiscal problems of joint sponsorship, the meetings will be sponsored by a single society each year, with the others on a participating basis. The initial JACC, to be held at MIT on September 7-9, 1960, will be under the sponsorship of the ASME. Succeeding sponsorship will be as follows: 1961 - ISA, 1962 - AIEE, 1963 - AIChE, 1964 - IRE-PGAC.

In agreeing to this five-year cycle of joint meetings, each of the participating societies has agreed to sponsor no other control meetings on a national basis, except for control sessions held as part of regular meetings of the respective societies. Thus, the PGAC for the next five years will sponsor meetings on a national basis only at the IRE National Convention in March of each year, the WESCON Convention in August of each year, and the Joint Automatic Control Conferences. If conference proceedings are not established for the joint conferences, IRE-sponsored papers will be published in special PGAC Transactions issues, such as this one.

Many favorable comments have been received on the 1959 NACC. Speaking in behalf of the PGAC, I would like to thank the participating societies and groups for their interest and assistance, and the hardworking committees who made it all possible. The PGAC looks forward to a continuation of the spirit and success of this meeting in the Joint Automatic Control Conferences.

John E. Ward, Chairman
Professional Group on Automatic Control
November 20, 1959

NATIONAL AUTOMATIC CONTROL CONFERENCE

OFFICERS

Chairman Louis B. Wadel, Electronics Division, Chance Vought Aircraft, Inc., Dallas

Technical Program Chairman George S. Axelby, Air Arm Division, Westinghouse Electric Corporation, Baltimore

Special Program Chairman John M. Salzer, Ramo-Wooldridge Division, Thompson Ramo Wooldridge, Inc., Los Angeles

Local Arrangements Chairman R. N. Hutson, Electronics Division, Chance Vought Aircraft, Inc., Dallas

Treasurer F. W. Tatum, Electrical Engineering Dept., Southern Methodist University, Dallas

Publicity Chairman M. L. Barnett, Astronautics Division, Chance Vought Aircraft, Inc., Dallas

Registration Chairmen H. C. Baker and J. A. Savage, Electrical Engineering Dept., Southern Methodist University, Dallas

TECHNICAL PROGRAM COMMITTEE

N. H. Choksy, Electrical Engineering Dept., Johns Hopkins University

W. M. Gaines, General Electric Co., Tempe, Ariz.

John E. Gibson, School of Electrical Engineering, Purdue University

H. Freeman, Sperry Gyroscope Co., Great Neck, N.Y.

R. E. Kalman, RIAS, Inc., Baltimore, Md.

D. P. Lindorff, Electrical Engineering Dept., University of Connecticut

J. H. Mulligan, Jr., Electrical Engineering Dept., New York University

Arthur S. Robinson, Eclipse-Pioneer Div., Bendix Aviation Corp., Teterboro, N.J.

O. Hugo Schuck, Minneapolis-Honeywell Regulator Company, Minneapolis, Minn.

--and with the assistance of J. G. Truxal, Polytechnic Institute of Brooklyn

SESSION CHAIRMEN

Session I - J. E. Ward (PGAC Chairman), Massachusetts Institute of Technology

Session II - F. W. Tatum, Electrical Engineering Dept., Southern Methodist University

Session III - A. R. Teasdale, Temco Aircraft Corp., Dallas, Texas

Session IV - C. F. Taylor, Daystrom, Inc., La Jolla, California

Session V - M. Marx (for F. Gaynor), General Electric Company, Schenectady, N.Y.

Session VI - J. H. Mulligan, Jr., Electrical Engineering Dept., New York University

Session VII - H. Freeman, Sperry Gyroscope Company, Great Neck, Long Island, N.Y.

Special Session - John M. Salzer, Ramo-Wooldridge Division, Thompson Ramo-Wooldridge, Inc., Los Angeles

IRE TRANSACTIONS ON AUTOMATIC CONTROL, VOLUME AC-4, NUMBER 3, DECEMBER, 1959

PROCEEDINGS OF THE NATIONAL AUTOMATIC CONTROL CONFERENCE

November 4-6, 1959 - Dallas, Texas

TABLE OF CONTENTS

FUNDAMENTAL THEORY OF AUTOMATIC LINEAR FEEDBACK CONTROL SYSTEMS

Isaac M. Horowitz

Research Laboratories, Hughes Aircraft Co., Culver City, California

SUMMARY

The reasons for using feedback are reviewed. The beneficial aspects of feedback are quantitatively expressed in sensitivity functions and noise transmission functions. The physical constraints on the controlled process (or plant) determine the maximum number of independent functions realizable. Any configuration with the same number of degrees of freedom may be used. With this approach the study of conditional feedback, model feedback, combined positive and negative feedback, etc. is of secondary interest. The benefits of feedback are paid for in gain-bandwidth of active elements over and above what is needed to physically do the job. The minimum price that must be paid is independent of configuration.

The system with two degrees of freedom is studied in detail. Two methods are presented for the precise design of a system that will be as insensitive as may be desired to large parameter variations. One method uses root-locus techniques and is suitable for systems with a small number of dominant poles and zeros. The second method is based on frequency response and can be used for systems of any complexity. Numerical examples are given.

Reasons for Using Feedback

What are the reasons for applying feedback to a control system and thereby greatly increasing its complexity, cost, and the design effort ? The answers are given by most textbooks on the subject:

"in the presence of disturbing signals, (feedback) tends to reduce the difference between the actual state and an arbitrarily varied desired state."[1] Also, "...very close tolerances in manufacture and constancy of controller characteristics with time are required to obtain high performance of an open-loop system" (whereas) "with the use of lower precision components or ones subject to wider variation under use, it is still possible to maintain high-precision feedback control performance."[2]

Some authors suggest that another principal reason for using feedback is that it makes a system respond faster or at least that this is one of the advantages of a feedback system.[3,4] It has been pointed out by Truxal, that if there is a desire to speed up a system, it can be done with a suitable prefilter in cascade with the plant, much more cheaply and with considerably less design effort than by means of feedback. The term plant, symbol P, is used in this paper to designate the fundamental portion of the control system that is fixed, such as the power amplifier, servomotor and load, the chemical process, etc. The important point here is that in control systems, feedback is not used as a synthesis tool, (although feedback is used as such in other situations, e.g., active RC synthesis) to attain a desired system transfer function, T, because openloop synthesis is easier and cheaper. In regard to the subject, it is suggested that the term optimum feedback systems should not be used for studies of optimum system response. The response of a plant with a fixed capacity and characteristics is an important problem but it is not at all a feedback problem. Whatever response function the plant may be capable of and which is considered optimum for a particular situation, can always be realized by an open-loop configuration.

Canonic Structures

Accordingly, the two fundamental reasons for using feedback, despite its greater complexity and cost, are,

1. the improvement in the rejection of corrupting signals; the improvement in the system linearity may be included under this
2. the decrease in the sensitivity of the system to variations in the plant.

It is therefore only natural that a feedback system should be evaluated by determining how well it accomplishes these objectives. For this purpose it is imperative that canonic configurations be set up and studied in a fundamental manner. In this connection, automatic control theory can benefit from modern network synthesis theory. For example, once the Foster and Cauer canonic configurations for realizing an LC immitance became available, there was no need to study the practically infinite configurations which are combinations of the four canonic structures. However, in feedback control theory, in the absence of canonic structures associated with studies of their fundamental properties, every new configuration merits special study. This is so despite the fact that writers[5-8] have drawn attention to the common basic properties of the various configurations. The reason for the confusion is probably due to the fact that the central and significant importance of the sensitivity function, defined below, has for the most part been neglected[9] in the literature.

The sensitivity function S_P^T, denoting the sensitivity of the system transfer function to the variations in the plant P, is usually defined[10] as

$$S_P^T = \frac{dT/T}{dP/P} \qquad (1)$$

and is thus the relative change in the system transfer function T, divided by the relative change in the plant P, for infinitesimally small changes. It is the logical quantitative measure of those two properties of feedback because of which feedback is used.

Consider a control system with the following constraints: a single system input and output; no signals can be directed to the output except through the plant; the plant has a single input and output, the plant is fixed, and there is no access to it by the designer except at its input and output. Such a system has only three essential variables: r — the independent input, c — the output, and p — the input to the plant. More variables can be invented, but they can always be eliminated, except for the above three, with no adverse effect on the items of interest: the system response, the sensitivity to plant variations, and the response of the system to noise entering anywhere along the plant. The system is therefore described by no more than six independent transmissions: r to c, c to r, r to p, p to r, p to c, and c to p. The first of these is not allowed, and therefore Fig. 1 is a general block diagram representation of the system under discussion. $P = P_1P_2$ is shown split up, to indicate that noise entering at various points in the plant is included in the study of the system, Interest in the system is concentrated on the transfer function.

$$T = \frac{C}{R}, \qquad (2)$$

S_P^T defined in (1), and the noise transmissions. From Fig. 1,

$$T = \left(\frac{G_1}{1 + G_1G_4}\right)\left[\frac{P}{1 + \frac{P(G_2 + G_1G_3)}{1 + G_1G_4}}\right] = \frac{GP}{1 + L} \qquad (3)$$

Equation (3) defines G and L. Also,

$$S_P^T = S = \frac{1}{1 + L}, \qquad (4)$$

$$T_{n_1} = \frac{P}{1 + L} = PS, \qquad (5)$$

$$T_{n_2} = \frac{P_2}{1 + L} = P_2S, \qquad (6)$$

$$T_{n_3} = \frac{1}{1 + L} = S. \qquad (7)$$

Note that because of the system constraints, T_{n_1}, T_{n_2}, and T_{n_3} are completely determined by S. The latter must therefore be chosen to satisfy the noise specifications as well as those due to plant parameter varations. It is seen that the individual specification of G_1, G_2, etc. is not necessary. If the system has the constraints previously listed and if the interest is only in system response, sensitivity to plant, and response to noise entering in the plant (which includes load), then two and only two independent transmissions (L and G) are all that are needed or even useful. There is no need to clutter the system with any additional blocks. For such a system with its constraints, any structure with two degrees of freedom may be used.

More complicated systems do not result in more than two degrees of freedom, unless some of the constraints are lifted, e.g., in Fig. 1, if the designer has physical access to point x, there is more freedom and three quantities, T, $S_{P_1}^T$ and $S_{P_2}^T$ can be independently controlled. In general if $P = P_1P_2 \ldots P_n$, with n + 1 accessible terminals, of which all but the first have only output signals available, then n + 1 functions, (T, $S_{P_1}^T$, $S_{P_2}^T$, etc.) may be independently realized by means of a feedback structure with n + 1 degrees of freedom. A first step in any system design is the determination of the constraints and the number of degrees of freedom. These in turn determine the number of functions which may be independently controlled. The minimum number of compensating transmissions is then precisely determined. In general, the price paid for the benefits of feedback is in the large gain-bandwidth required of the compensating transmissions. But as soon as the designer has decided how much of the benefits he wants, the compensating transfer functions and their gain-bandwidth products are precisely determined. Therefore, as far as the sensitivities to plant and transmissions of noise entering into the plant are concerned, it doesn't matter at all what kind of system structure is used, so long as it contains the minimum number of independent transfer functions. In short, it is argued that this is a fundamental approach in that it points out the secondary role of the structure and the canonical role of the plant and its constraints. For example, the plant type previously described (Fig. 1, etc.) had only two degrees of freedom, which permits independent realization of T and S_P^T. Two independent functions are required. They are, from (3) through (7),

$$G = \frac{T}{PS}, \qquad (8)$$

$$L = S^{-1} - 1. \qquad (9)$$

Any of a very large variety of structures may be used, such as that shown in Fig. 2. Some of these

configurations have appeared in articles that claim their superiority to the more conventional configurations. In Fig. 2a,

$$G_1 = \frac{T}{PS}, \tag{10}$$

$$H = \frac{1}{G_1 P}\left(\frac{1}{S} - 1\right), \tag{11}$$

In Fig. 2b,

$$G_1 = \frac{T}{PS}, \tag{12}$$

$$H = \frac{1}{P}\left(\frac{1}{S} - 1\right) - G_1. \tag{13}$$

Fig. 2c is the conditional feedback system of Ham and Lang[6] with

$$A = \frac{T}{P}, \tag{14}$$

$$G_2 H = \frac{1}{P}\left(\frac{1}{S} - 1\right). \tag{15}$$

If the system shown in Fig. 2c does have any advantage, it is in the additional freedom provided by using three fuctions so that in (15) only the product is specified. But this freedom is achieved at the price of considerably greater complexity and can be obtained with simpler structures. Fig. 2d is a member of the minor positive feedback loop family, for which extravagant claims have been made and continue to be made. In Fig. 2d,

$$H_2 = \frac{1}{T}(1 - S), \tag{16}$$

$$\frac{T}{SP} = \frac{G_1}{1 - G_1 H_1}. \tag{17}$$

Some comments will now be made on the use of minor positive feedback loops to achieve what are usally claimed as spectacular and superior results. Whatever these results may be it must be possible to express them quantitatively in the specification of S. So the question really is whether it is easier to synthesize the resulting compensating transmissions by means of positive feedback amplifiers than with ordinary amplifiers. This important point is emphasized. The sensitivity function S represents the quantitative desired benefits of feedback. Since $S = (1 + L)^{-1}$, the loop transmission function L is rigidly fixed by S and is available as a rational function in the complex variable s. The additional specification of the system transfer function T definitely fixes the other degree of freedom, G in (8). The problem is therefore completely one of network synthesis, i.e., one of realizing functions with specified poles, zeros and gain constants. It is difficult to generalize on optimum methods of transfer function realization. The science of network synthesis has in fact not been developed to the point where many definite statements can be made on optimum methods. Furthermore it depends a great deal on ones' definition of optimum. However, it may sometimes be possible to achieve a particular relation of gain versus frequency more conveniently by means of positive feedback. Thus, a vacuum tube has a fixed gain-bandwidth product g_m/C, but to achieve a gain factor greater than the amplification factor μ, it may be more convenient to use positive feedback than transformers. This is also the case if sensitivity zeros at $\pm j\omega_0$ (i.e., at a real frequency) are desired. Why one should want such zeros is explained later in the discussion and by (27) and (28). The zeros of S are the poles of L from (4), and transfer poles at real frequencies can be realized only by means of positive feedback. This important point should be emphasized. If there is any real need of minor positive feedback loops in a system, this need becomes apparent from the specification of S. Consequently it is established that there is little point in searching for new and exotic feedback configurations. Instead, one should adopt a synthesis approach, establish the constraints, the degrees of freedom in the system, the desiderata, and how much of the latter is obtainable on the light of the constraints. From such considerations the T, T_n's (noise transmissions) and S functions are specified. If positive feedback or fancy configurations are needed at all, the designer will be forced to use them. Usually, from a practical standpoint, the simplest and least exotic configurations are the best just because of their simplicity.

There is one qualification that should be made. Attention has been concentrated on the sensitivity of the system to the plant and on noise entering anywhere in the plant. But there are secondary considerations, such as the sensitivity of T to the compensating networks and the effect of noise entering into the system through them. Usually the compensation blocks are at a much lower power level and can be well designed at reasonable cost. However, in these matters and in the matter of nonlinearities, one particular structure may be better than another.

The Poor Sensitivity of Designs Based on T Alone

It can easily be shown that in the usual, straightforward, textbook design of a feedback-control system, whether by frequency-response, root-locus, or s-plane methods, there results a T function which is extremely sensitive to plant variations in a very critical part of the frequency band. An example to illustrate this point follows.

Design Example:

The nominal plant transfer function is

$P = \frac{1}{s(s+1)(s+2)}$, the desired value of K_v is 10 and the margin is to be not less than 30°. Fig. 3 presents a typical design using lag compensation. The results are:

$$S = \frac{1}{1+G}$$

$$= \frac{s(s+0.0044)(s+1)(s+2)}{(s+0.08)(s+2.38)(s^2+0.54s+0.49)} \quad (18)$$

$$G = \frac{1.25(s+0.0704)}{s(s+0.0044)(s+1)(s+2)}, \quad (19)$$

$$T = \frac{1.25(s+0.0704)}{(s+0.08)(s+2.38)(s^2+0.54s+0.49)}. \quad (20)$$

S is sketched in Fig. 4. The effect of substantial plant variations is desired. For this purpose the incremental sensitivity function defined by (1) is not satisfactory and a function that gives the effect of gross variations is wanted. Let T_o, L_o, and S_o be the transfer, loop, and sensitivity functions, respectively, when the plant has its nominal value of P_o; let T, L, and S be the corresponding functions at the new plant value, P. Also, let

$$\Delta P = P - P_o, \quad (21)$$

$$\Delta T = T - T_o. \quad (22)$$

By straightforward substitution into (3) and some manipulation it is found that

$$\frac{\Delta T/T}{\Delta P/P} = S_o = \frac{1}{1+L_o}, \quad (23)$$

$$\frac{T_o}{T} = 1 - S_o \frac{\Delta P}{P}, \quad (24)$$

$$\frac{T_o}{T} = \frac{\frac{P_o}{P} + L_o}{1+L_o} \quad (25)$$

Equations (23) through (25) are extremely useful because they enable simple exact calculation of the effect of gross plant variations from the original sensitivity function, or the original loop transmission. In the above example, if the gain constant of P decreases by 20 percent $\Delta P/P = 0.25$. At $\omega = 0.7$ rps, $S(\Delta P/P) = 1.9\angle 44^\circ (0.25) = 0.475 \angle 44^\circ$ and from (24), $T_o/T = 1.38 \angle 14^\circ$, a significant change. If the gain constant of P increases by 1/3, $\Delta P/P = -0.25$ and at $\omega = 0.7$ rps, $T_o/T = 0.73\angle -27^\circ$. At $\omega = 1.0$ rps, $S_o(\Delta P/P) = -0.40\angle 8^\circ$ and $T_o/T = 0.6\angle 5.4^\circ$. The frequencies chosen are at the edge of the useful transmission band. In general, the system overshoot is very sensitive to the behavior of T at the band edge, and precisely in this frequency range, ($\omega \sim 0.7$ rps), the sensitivity of T to P (see Fig. 4) is almost two in magnitude. Despite the use of feedback with all its vaunted advantages, the system response in an important frequency range is more sensitive to plant variations than it would be if there were no feedback at all. A 20-percent change in gain magnitude leads to almost 40-percent overshoot in place of the design value of 25-percent overshoot. While the above represents a typical textbook example of frequency response design methods, the same poor sensitivity results in designs carried out by root-locus or Guillemin synthesis techniques, whether by lag or lead compensation.

The reason for the poor performance of designs such as the above is that only one degree of freedom has been used to secure (by means of gain, phase margins, and bandwidth), basically a satisfactory T function. No attention has been paid to the S function. The fact that in an important frequency range there is positive feedback rather than negative feedback is not too surprising. As Bode [11] demonstrated long ago, the integral of the log of S over frequency is zero, (if L goes to zero at infinity at more than 6 db per octave). and therefore in a practical feedback system there is as much positive feedback as there is negative feedback. The designer, by suitably specifying S, is in control of the situation and obtains the negative feedback where he wants it.

Constraints on Sensitivity Function

Are there any constraints on S, or may it be specified completely at the whim of the designer? From (9), the loop transmission function L, which is a physical transfer function, is $L = S^{-1} - 1$. Now L explicitly contains the plant transfer function P, i.e., let $L = PX$. If P goes to zero at infinity at the rate of 6n db per octave, i.e., if P has n more poles than zeros, then L must have at least n more poles than zeros because X is a physical transfer function. Actually X, being a physical transfer function, must also go to zero at infinity at the rate, say, of 6m db per octave. Therefore, L must have m + n more poles than zeros. But $L = 1/S - 1 = d_s - n_s/n_s$, where

$$S = \frac{n_s}{d_s}. \quad (26)$$

If L is to have m + n more poles than zeros, it is necessary that the first m + n coefficients of the numerator and denominator of S should respectively equal each other. Thus, if m + n = 5, the designer must specify S such that the first five

coefficients of its numerator are respectively equal to the first five coefficients of its denominator. Furthermore, to be of any use, S must of course have the desired behaviour over the finite, important T frequency range. For m + n = 5, S may perhaps have to be of tenth degree in order to do both the above. Specifying the correct S is what is known in network synthesis as an approximation problem, and it is in general a difficult problem. It is in the specification of S and T that the challenge exists of satisfying the specifications with a minimum of gain-bandwidth cost. Fortunately, in practical designs it is possible to use the loop transmission function L in place of S. Two methods for finding an appropriate L function are given in this paper. The first method uses root locus notions and is practical when the system is characterized by a small number of dominant poles and zeros. The second method uses the frequency response approach and can be applied to systems of any complexity. In each case an appropriate L is found from a statement of the maximum plant variations and the desired tolerances on T, in the light of these variations.

Before proceeding with the two methods, more may be said about the S function. The required properties of S (whether they are obtained later by working with L rather than with S is immaterial) form an important part of the design of a feedback control system. S should be specified by simultaneous consideration of the nature of the input, the system, the disturbances, and the desired output. For example, if the input is characterized by step functions and if the steady-state output is to be independent of plant variations, the sensitivity functions must have a zero at the pole of the input, i.e., at the origin. In general,[12] if the characteristic input function has simple poles at $s = s_1, s_2 \ldots$ and double poles at $s = s_a, s_b \ldots$ and if the forced components of the output are to be independent of plant variations, it is necessary that S have simple zeros at $s_1, s_2 \ldots$ and double zeros at $s_a, s_b \ldots$. This is seen as follows. From (2), C = TR.

$$\text{Let} \quad R = \sum \frac{A_n}{s-s_n} + \sum \frac{A_i}{(s-s_i)^2} + \ldots . \qquad (27)$$

$$\text{Then} \quad c(t) = \sum T(s_n) A_n e^{s_n t} + \sum A_i T(s_i) t\, e^{s_i t}$$

$$+ \quad A_i T'(s_i) e^{s_i t} + \ldots + \left\{\text{natural components}\right\} . \qquad (28)$$

If the steady-state or forced components are to be independent of P, it is necessary that

$$\frac{dT(s_n)}{dP} = \frac{dT(s_i)}{dP} = 0, \text{ i.e., that } S_P^T \text{ have zeros}$$

at s_i and s_n. Also $\frac{dT'(s_i)}{dP} = 0$, i.e., it is necessary that S_P^T have double zeros at s_i. These requirements lead naturally to the definition of the error coefficients. An attempt[13] has also been made to define S by considering the statistical properties of the input functions.

S-PLANE DESIGN TECHNIQUE

A procedure for controlling the movement of the dominant T poles in the face of large plant variations is now presented by means of a numerical example.

The plant transfer function is,

$$P = \frac{k}{s(s^2 + 2\xi_p \omega_p s + \omega_p^2)} , \qquad (29)$$

with k varying from 1 to 4 and ξ_p, ω_p are such that the complex pole pair of P may be anywhere in the rectangles ABCD, $\overline{ABCD}$ in Fig. 5. T is desired with a dominant pole pair inside a circle of radius 1.2 centered at $-10 \pm j10$ (R, $\bar{R}$ in Fig. 5). Note that in this example the variations of the plant in the important frequency range are fantastically large. It is realized that T must have more (far-off) poles, and it is specified that they must always be to the left of the line MNN'M' in Fig. 5, (given by x = -40). One may argue over the specific location and shape of MNN'M', but the important point here is that such a choice must be made if one is to work with dominant poles and zeros. The example demonstrates how to proceed after the choice has been made.

The following is the design philosophy. Loop transmission zeros near the desired dominant T poles (Fig. 6), in conjunction with large loop gain, ensure closed loop poles near the zeros, irrespective of the plant-pole locations. The device supplying the zeros must have at least two finite poles. These must be located sufficiently far away to ensure that the specifications with respect to the far-off poles are not violated. Suppose they are located as shown in Fig. 6 at Y, $\bar{Y}$. The danger is that the large loop gains needed to keep the dominant poles relatively stationary will cause the roots along the loci F, $\bar{F}$ to cross the MNN'M' line. To prevent this, the poles at Y, $\bar{Y}$ must be sufficiently far off to the left. Here is seen the price required for keeping T so insensitive over the significant frequency range to such large plant variations. First, a large loop gain is needed and secondly, the large loop gain causes the need for compensating networks with large

bandwidths. The analogue of the equality of positive and negative feedback areas is that the large loop gain, which ensures small movement of one set of poles, causes very large movements in another set, the far-off poles.

A design procedure is now developed for finding the minimum gain-bandwidth required to satisfy the specifications for the simplest type of compensation, i.e., one consisting of a pair of zeros and poles. Consider first the effect of variations, in the gain of L alone, on a pole of T located at R. The pole at R is a root of 1 + L= 0. The nominal gain is

$$K_o = \frac{\pi(p_i R)}{\pi(z_j R)} = \frac{\pi(\text{pole vectors of L to R})}{\pi(\text{zero vectors of L to R})} . \qquad (30)$$

When K varies in value, the root of 1 + L = 0, originally at R, moves to a new point R', such that

$$K = \frac{\pi(p_i R)}{\pi(z_j R')} . \qquad (31)$$

In the present case the root at R is not allowed to drift very much and therefore each $p_i R' \doteq p_i R$ and each $z_i R' \doteq z_i R$, except for the zero z_1 near R. Therefore,

$$K \doteq \frac{\pi(p_i R)}{(z_1 R')\pi_{j\neq 1} z_j R} . \qquad (32)$$

From (30) and (32),

$$\frac{z_1 R}{z_1 R'} \doteq \frac{K}{K_o} . \qquad (33)$$

With this type of approximation it is possible to find relatively quickly the movement of R due to the variations in P .

The nominal value of the plant poles is taken as -6 ± j10 and the nominal value of k_o of (29) is taken as unity. The effect of the motion of the poles of P along ADCBA is found by finding the drift at the corners DCB. If the plant poles have moved to ± j10, from previous approximation method it follows that

$$\frac{zR'}{zR} \doteq \frac{K_o}{K} \frac{(p'R)(\bar{p}'R)}{(pR)(\bar{p}R)} , \qquad (34)$$

with pR = -4, $\bar{p}R$ = -4 + j20, p'R = -10, and $\bar{p}'R$ = -10 + j20. Accordingly,

$$\frac{zR'}{zR} \doteq \frac{K_o}{K} \, 2.6\angle 16^\circ . \qquad (35)$$

R and z may be located at any two points; their relative location determines only the scale of the diagram and its orientation. Once located, however, the point R' is fixed. In Fig. 7, M corresponds to R' of (31) at $K = K_o$ and M' is R' for $K = 4K_o$. The straight line RM is taken as the approximate locus of R' as the plant-pole pair moves along AD, $\bar{A}\bar{D}$. An intermediate point or two may be checked if desired; the straight line approximation is good enough.

The value of R' for the plant poles at C, $\bar{C}$ is likewise found:

$$\frac{zR'}{zR} \doteq \frac{K_o}{K} \frac{(-10 + j8)(-10 + j12)}{(-4)(-4 + j20)} = \frac{K_o}{K}(2.45)\angle -10^\circ . \qquad (36)$$

In Fig. 7, J is the correct R' for (32), for $K = K_o$ and J' for $K = 4K_o$. Similarly for the plant poles at B, $\bar{B}$, a dominant system pole is at N for $K = K_o$ and N' for $K = 4K_o$. The magnitude of zR is now available. The dominant T poles lie inside the region XM'MJNN'X in Fig. 7. (X corresponds to $K = 4K_o$, p' = p.) But from the specifications, this region must be inside a circle of radius 1.2, which determines the scale to be assigned to Fig. 7. The result is that $|zR| \leq 1$.

To locate the zeros of L precisely, it is noted that at the nominal R, $\bar{R}$ (-10 + j10), the net angle of the phasors from the poles and zeros of L must be 180°. The far-off poles of L are not known as yet, so one may wait until they are known or may anticipate that their contribution is negligible and calculate (Fig. 8),

$$180^\circ = \angle pR + \angle \bar{p}R - \angle zR - \angle \bar{z}R + \angle OR . \qquad (37)$$

Since $\angle \bar{z}R \approx 90^\circ$, (37) leads to $\angle zR \approx 146^\circ$, which locates the zeros at $-9.17 \pm j9.45$. Actually the exact location is not critical and the numbers may be rounded off.

Location of the Far-off L Poles

The boundary of the permissible region is the line x = -40 in Fig. 9. At K = 4K, a zero of 1 + L lies on this boundary, say at the point W = -40 x j200 in Fig. 9. At W, the totality of the poles and zeros near the origin appears as a single pole, located, for practical purposes, at the origin. At W, the phasor from the pole at the origin has the angle 101.3°. The other two far-off poles of L must therefore contribute the balance of 180 - 101.3 = 78.7°. The locus of pole positions contributing 78.7° at W is a segment of a circle passing through W. Three other points on the circle are quickly located: the coincident pair on the real axis which contributes 78.7°/2 each; the other two points are on the horizontal lines through W, $\bar{W}$. The first one has zero angle. The second one must therefore have an angle of

78.7^{o} at W, and the point is thus easily located. The circle can now be drawn.

Suppose now that the two far-off poles are located at M, $\bar{M}$ (Fig. 9) on the circle. The value of $K = 4K_o$ which results in a root of $1 + L = 0$ at $W = -40 + j200$ is calculated, (equal to $|(MW)(\bar{M}W)(OW)|$), giving $K_o = (3.3)10^6$. This value of K_o must also give rise to a root of $1 + L = 0$ at $R = -10 + j10$ and the required value of

$$K_o = \left|\frac{(pR)(\bar{p}R)(OR)}{(zR)(\bar{z}R)}\right| \times \left|(MR)(\bar{M}R)\right| > (3.3)10^6$$

(see Figs. 8 and 9). Therefore M, $\bar{M}$ are not correct locations for the far-off poles. Other point-pairs on the circle are tried until a pair is found which gives K_o for the root at R and $4K_o$ for the root at W.

The resulting value of K is not necessarily the lowest and the far-off L poles are therefore not the best in the sense of the smallest bandwidth. A new point on the boundary is attempted, the appropriate circle is drawn, and the process is repeated until the smallest K_o (which corresponds also to the smallest bandwidth) is found. In this particular example, it is approximately $K_o = (3.8)\,10^6$, with

$$L_o = \frac{(3.8)10^6\,(s^2 + 18s + 171)}{s(s^2 + 12s + 136)(s + 240)(s + 290)} . \qquad (38)$$

At $K = 4K_o$, the far-off poles are at $-40 \pm j180$. The root loci of the far-off poles are sketched in Fig 10. At $K = K_o$, the far-off poles are at $-80 \pm j44$. They are practically unaffected by the variation of the plant poles. If the structure shown in Fig. 2a is used,

$$G_1H = \frac{(3.8)10^6\,(s^2 + 18s + 171)}{(s + 240)(s + 290)} . \qquad (39)$$

G_1 is taken as an amplifier whose bandwidth is considerably larger than 300 rps. If the structure if Fig. 4b is used, G_1 has the same value as before and $H = \frac{L}{P} - G_1$. In order that the position constant, K_p, be infinite, $T(O) = 1$, which requires that $H(O) = 0$. Therefore,

$$G_1 = 9350 \text{ and } H = \frac{(3.8)\,10^6\, s(s + 16.7)}{(s + 240)(s + 290)} . \qquad (40)$$

Needless to say, none of the above values need be precisely realized.

The advantage that is usually cited for working in the s plane is that correlation with the transient response of the system is better than with the frequency response. This is true only so long as there are a small number of dominant poles and zeros and then one may design in the above manner to control the movement of the system poles. Actually, greater economy in gain-bandwidth is achieved by using more complicated compensation networks. In any case, when the plant is so complex that it is impossible to characterize the system by a small number of dominant poles and zeros, one must resort to the frequency response method. A frequency response method for designing a system for a desired T and for specific tolerances on T in the face of large plant variations is now presented.

FREQUENCY RESPONSE METHOD

To keep track of T in the face of gross plant variations, one may work with (25). It is best to work with L rather than S, because of the difficult approximation problem involved in the latter when the plant goes to zero at infinity at more than 12 db per octave.

If (25) is used, i.e., $\frac{T_o}{T} = \frac{\frac{P_o}{P} + L_o}{1 + L_o}$, the procedure is to make a polar sketch of $\frac{P_o}{P}$. For example, if $P_o = \frac{k}{s(s + a)}$ and if k, a, respectively, may vary from 1 to 40 and 1 to 4, then an extreme value of $\frac{P_o}{P}$ is $\frac{1}{40}\frac{(s + 4)}{(s + 1)}$ whose locus is a semicircle (Fig. 11). Suppose $-L_o$ has the polar locus shown in Fig. 11. If A and B are points on $-L_o$ and $\frac{P_o}{P}$ for the same frequency ω_x, then from (25), $\frac{T_o}{T} = \frac{AN}{AB}$ at $s = j\omega_x$. For synthesis purposes, the extreme loci of P_o/P are ascertained and the requirements of L_o become clear. In special cases it is possible to adjust the locus of L_o so that over the significant frequency range, $|T_o/T| \doteq 1$ with numerically small L_o. However, the phase of T_o/T is then large. The net effect on the transient response is what really counts. More study of the net effect of small change in $|T|$ and large change in $\angle T$ on its time behavior is required. While in most cases the above can be executed for a specific change in the plant, when the entire range of possible plant variations is considered, it is no longer feasible.

The procedure is best presented by means of a numerical example. The design problem concerns the same plant previously considered (Fig. 5), but the design specifications (not all the same as before) must now be given in terms of frequency response. Suppose the specifications are that in spite of the plant variations, $|T(j\omega)|$ is not to vary by more than ten percent from d.c. up to 15 rps, 30 percent from 15 to 30 rps, 100 percent from 30 to 50, etc. One may argue about the merit of the specifications, but the

purpose here is to present a procedure for satisfying fairly rigorous tolerances.

One might begin with a Bode sketch of the nominal loop transmission, $|L_o(j\omega)|$. The plant poles are poles of L_o and therefore L_o is very large for small frequencies and decreases with frequency. The shape of L_o in the intermediate frequency range is the real design problem. In order to economize on L_o gain-bandwidth, it should be decreased as fast as possible, but then there is the stability problem. Ordinarily, the ideal fastest rate at which L_o can be reduced for a specific gain and phase margin is given by the ideal Bode cutoff characteristic.[14] The latter is a good general guide, but the problem is somewhat different here. Here there is a certain area of variation of P and there are tolerances on $|T(j\omega)|$ in the intermediate frequency range. The shape of L_o must be drawn with these matters in mind. For this purpose the exact expression T_o/T (Eq. 25) is used, i.e.,

$$\frac{T_o}{T} = \frac{\frac{P_o}{P} + L_o}{1 + L_o} \qquad (25)$$

Polar sketches of $P_o/P\,(j\omega)$ for typical frequencies in the lower frequency range are made in Fig. 12. Normally, the information on the plant variations is available in terms of frequency behavior, but in this particular problem it must be obtained from the s-plane data. As the poles of P take on the infinite values of the region bounded by ABCDA in Fig. 5, $P_o/P\,(j\omega)$ is mapped on to a closed region which is defined by mapping the boundary. To map the latter, values for the four points of the rectangle ABCD are found and are joined by straight lines. When it is felt necessary, additional points are calculated. It is a good idea to sketch the boundary of P_o/P for a few points near the band edge of T, (such as 5, 10, 15 rps in Fig. 12) in order to be able to satisfy the specifications with $|L_o|$ as small as possible. In Fig. 12, the P_o/P polar loci are sketched only for $K = K_o$ in order not to clutter the diagram. It is obvious what area is covered, as K assumes values up to $4K_o$. In the intermediate frequency range, Fig. 13, (approximately 50 to 500 rps), near the point where L_o crosses the zero-db line, there is the danger of instability, and the proximity of the $-L_o$ polar locus to the P_o/P locus must be carefully checked. For the latter frequency range, one point need be calculated because at $K = K_o$, $|P_o/P| \doteq 1$. This is apparent from Fig. 13, which contains the polar loci for several values of frequency in the intermediate range. For example, at $s = j100$, $P_o/P\,(j100)$ may be anywhere in the region MNPQ in Fig. 13.

With these two separate polar loci sketches, it is possible to select $|L_o|$ as small as possible to satisfy the specifications. At 15 rps, $|L_o| = 7$ is satisfactory if its phase is between 120^o and 160^o. Taking $|L_o|$ as 17 db at 15 rps, it should be brought down as fast as possible (to conserve gain-bandwidth) and yet satisfy the specifications. A certain amount of trial and error is inevitable at this point because $-L_o$ must be tested on the polar plot while compatible gain and phase for $-L_o$ are obtained from a Bode plot. One might begin with the simplest type of L, 17 db at 15 rps, decreasing at 6 db per octave and finally at 18 db per octave at a sufficiently high corner frequency. For such a simple L_o, if coincident real axis poles at -a are used, the corner frequency, a, must be approximately at 300 rps to satisfy the specifications. The maximum change in $|T|$ is 27 db at about 260 rps. If a is chosen at 200 rps, the system is unstable at a value of P within its region of variation. With a =300,

$$L_{o_1} = \frac{(9.5)10^6}{s(s + 300)^2} \quad ; \qquad (41)$$

this is sketched in Fig. 13. Some economy in gain-bandwidth is obtained by staggering the corner frequencies, e.g.,

$$L_{o_2} = \frac{(8.4)10^6}{s(s + 200)(s + 400)} \quad . \qquad (42)$$

Considerable improvement is effected by using a more complicated loop transmission,

$$L_{o_3} = \frac{(3.5)10^6(s + 100)^2}{s(s + 15)(s + 250)^3} \quad , \qquad (43)$$

which is sketched in Fig. 13. Bode sketches of L_{o_1}, L_{o_2}, and L_{o_3} are shown in Fig. 14.

Root loci of $1 + kL_{o_3} = 0$ are sketched in Fig. 15.

At $k = k_o$,

$$1 + k_o L_{o_3} = \frac{(s^2 + 36s + 2400)(s^2 + 356s + 38{,}000)(s + 373)}{s(s + 15)(s + 250)^3} = \frac{1}{S_P} \quad . \qquad (44)$$

T_o is chosen as

$$T_o = \frac{(10.9)10^3(s + 100)^2(s + 250)^2}{(s^2 + 20s + 200)(s^2 + 36s + 2400)(s^2 + 356s + 38{,}000)(s + 373)} \quad . \qquad (45)$$

If the structure in Fig. 2a is used,

$$G_1 = \frac{T_o}{P_o S_o} = \frac{(10,900)(s^2 + 12s + 136)(s + 100)^2}{(s^2 + 20s + 200)(s + 15)(s + 250)} \quad (46)$$

$$H = \frac{L_o}{G_1 P_o} = \frac{320(s^2 + 20s + 200)}{(s + 250)^2} \quad (47)$$

Note that the complex plant poles do not appear in L_o. They must appear as zeros of G_1 (unless T_o has them as poles), and it looks as if this is a case of cancellation compensation with the attendant worry about the dipoles that result. There is an important difference here. The loop transmission and therefore the sensitivity have been chosen to satisfy the specifications for the system frequency response. The combination of system poles and zeros that exists as the plant parameters drift and age need not concern us because its net effect on the frequency axis is under control. The important thing is to be careful with the original statement of the plant variations and to be sure that an L_o has been chosen to handle them. What about inexact realization of the compensation networks? Clearly, if L_o is not off by an unreasonable amount, the effect is unimportant. It means only that a somewhat different L_o and a somewhat different T_o have been realized. There is nothing critical about L_o and T_o that requires any special attention in the realization of the compensating networks.

The frequency response method has definite advantages over the root locus method. It can be used with plants whose frequency response is available graphically only and which may be very complex. It permits experimentation with complicated loop transmissions in order to economize on the gain-bandwidth product of the compensating networks. Formally, it may be used for any plant, no matter how large and fantastic its parameter variations, so long as these variations are slow in comparison with the system response time. Ignorance of the system can be included. The greater the ignorance, the larger is the equivalent area of parameter variation. Of course, in extreme cases, inordinately large gain-bandwidth is required from the compensating networks. At this point, one may turn to an adaptive or computer-controlled system. The latter may be thought of as a system which periodically measures the plant and readjusts L and G. It is certain that ordinary feedback to handle the problem requires a tremendous gain-bandwidth product, however, against this requirement should be set the cost of the computer and the complex associated equipment for measuring the plant transfer function. Before any claim as to the advantages of the adaptive system may be made, it is necessary to formulate the problem quantitatively by clarifying the plant variations or the designer's ignorance of what these variations may be. It should then be possible to compare the merits of an adaptive design and the design procedure presented here. With regard to the latter, in very difficult design problems requiring enormous gain-bandwidth products, it is always possible to simplify the problem by means of minor feedback loops. The idea is to reduce the area of plant parameter variation by applying at the very outset feedback loops around various portions of the plant. The procedure outlined in this paper may then be applied to the modified plant whose area of variation is now more limited.

CONCLUSIONS

It has been suggested that a synthesis approach be adopted in the linear design of automatic feedback control systems. The basic ingredients in such an approach are the plant constraints which determine the maximum number (n) of independent system functions which can be realized. These system functions, such as plant sensitivity (S_P^T) noise transmissions, etc, incorporate the beneficial aspects of feedback and are the quantitative measure of the reasons for which feedback is used. Any configuration with n degrees of freedom may be used in the actual synthesis. Such an approach removes the customary emphasis on stability and configuration and places it where it belongs—on consideration of the inherent system capabilities and their quantitative formulation. Should an unusual configuration be needed, the designer will be forced to use it. Therefore, the pursuit of exotic configurations, such as conditional feedback, model feedback etc., is unnecessary. The case for n = 2 has been treated in detail.

ACKNOWLEDGMENTS

The author wishes to express his appreciation to L. Weinberg for encouraging the research. The author's original interest in the problem is due to J. G. Truxal and to his emphasis on the fundamental problems in feedback control systems. Acknowledgment is also made to J. Sipress for many valuable and stimulating discussions.

REFERENCES

1. Automatic Feedback Control (book), W. R. Ahrendt, J. F. Taplin. McGraw-Hill Book Co., Inc., New York, N. Y., 1951, p. 1.

2. Servomechanisms and Regulating Systems Design (book), H. Chestnut, R. W. Mayer. J. Wiley and Sons, Inc., N. Y., 1951, p. 8.

3. Reference 2, p. 6.

4. Feedback Control Systems (book), O. J. M. Smith. McGraw-Hill Book Co., Inc., N. Y., 1958, p. 4.

5. Discussion, G. C. Newton, Jr. AIEE Transactions, Applications and Industry, Vol. 74,

1955, pp. 158-9 (Discussion of "Conditional Feedback Systems" by G. Lang and J. Ham, ibid., pp. 152-8

6. Design of Feedback Systems, E. J. Angelo, Jr. Research Report R-449-55, PIB-379, Microwave Research Institute, Polytechnic Institute of Brooklyn, January, 1956.

7. Modern Network Theory and Its Application to Feedback Control, J.G. Truxal. Research Report R-440-55, PIB-372, Microwave Research Institute, Polytechnic Institute of Brooklyn, September 1955.

8. Design of Feedback Systems for Simultaneous Control of Transmission and Sensitivity, I.M. Horowitz, J.M. Sipress. Memorandum No. 9, R-657-58, PIB-585, Microwave Research Institute, Polytechnic Institute of Brooklyn, April 22, 1958.

9. Control-System Behavior Expressed as a Deviation Ratio, J.M.L. Janssen. Article in Frequency Response (book) edited by R. Oldenburger, The MacMillan Co., N.Y., 1956, pp. 131-40.

10. Automatic Feedback Control System Synthesis (book), J.G. Truxal. McGraw-Hill Book Co., N.Y., 1955, p. 120.

11. Network Analysis and Feedback Amplifier Design (book), H.W. Bode. D. Van Nostrand Co., N.Y., 1945, p. 285.

12. Sensitivity Considerations in Active Network Synthesis, J.G. Truxal, I.M. Horowitz. Proc. of Second Midwest Symposium on Circuit Theory, December 1956, Kellogg Center, Michigan State University, East Lansing Michigan, pp. 6-1 to 11.

13. Specification of the Linear Feedback System Sensitivity Function on the Basis of a Minimum Square Error Criterion, William R. Mazer. Research Report R-652-58, PIB-580, Microwave Research Institute, Polytechnic Institute of Brooklyn, April 17, 1958.

14. Reference 11, Chapter 18.

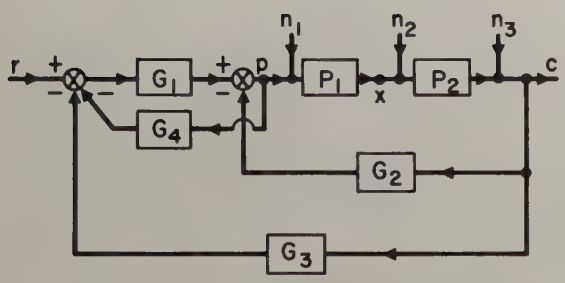

Fig. 1. General configuration for 2-degree system.

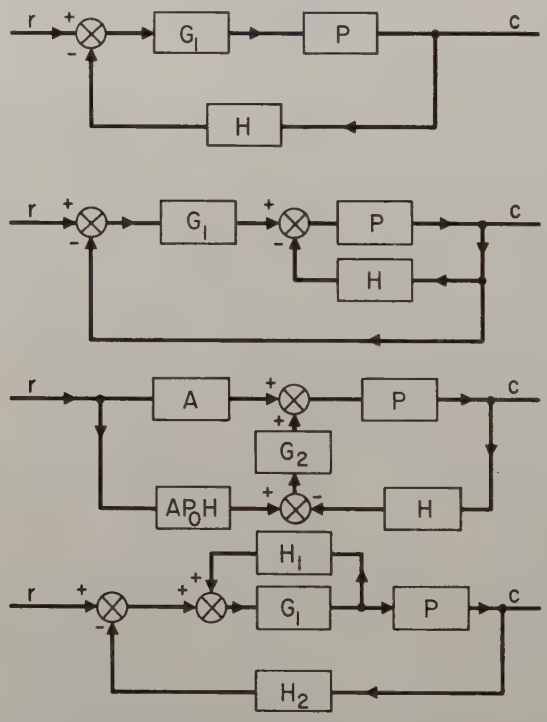

Fig. 2. Some sturctures with 2 degrees of freedom.

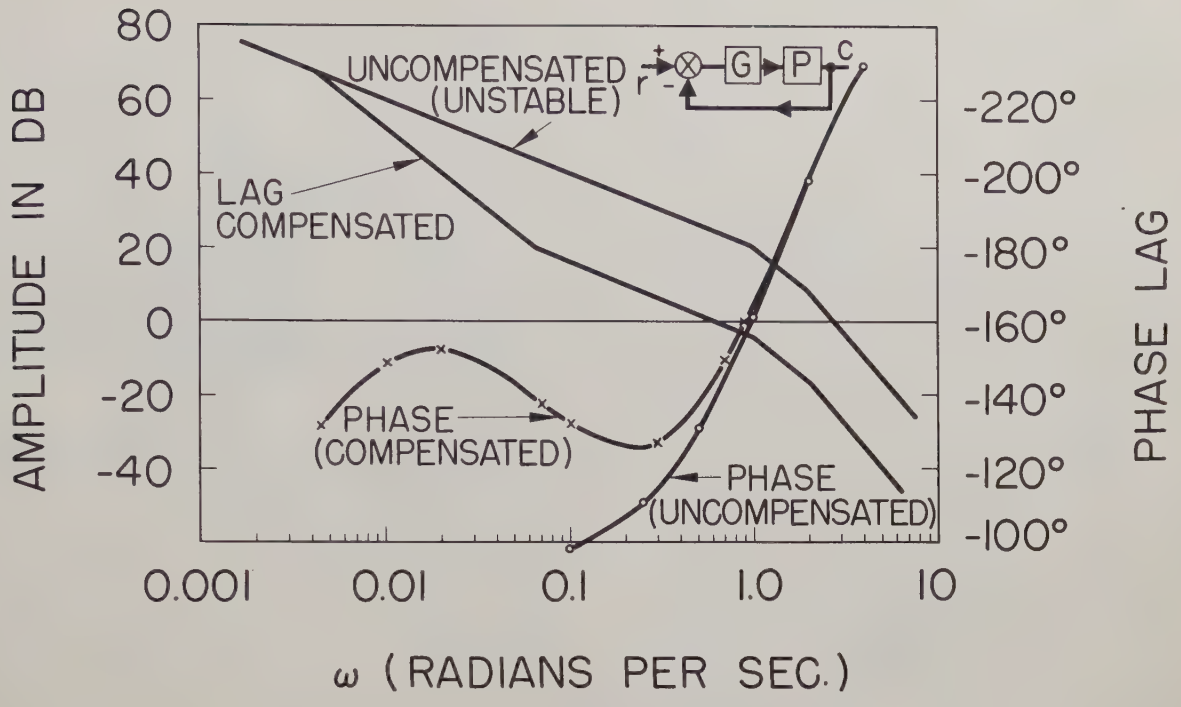

Fig. 3. Typical design-lag compensation.

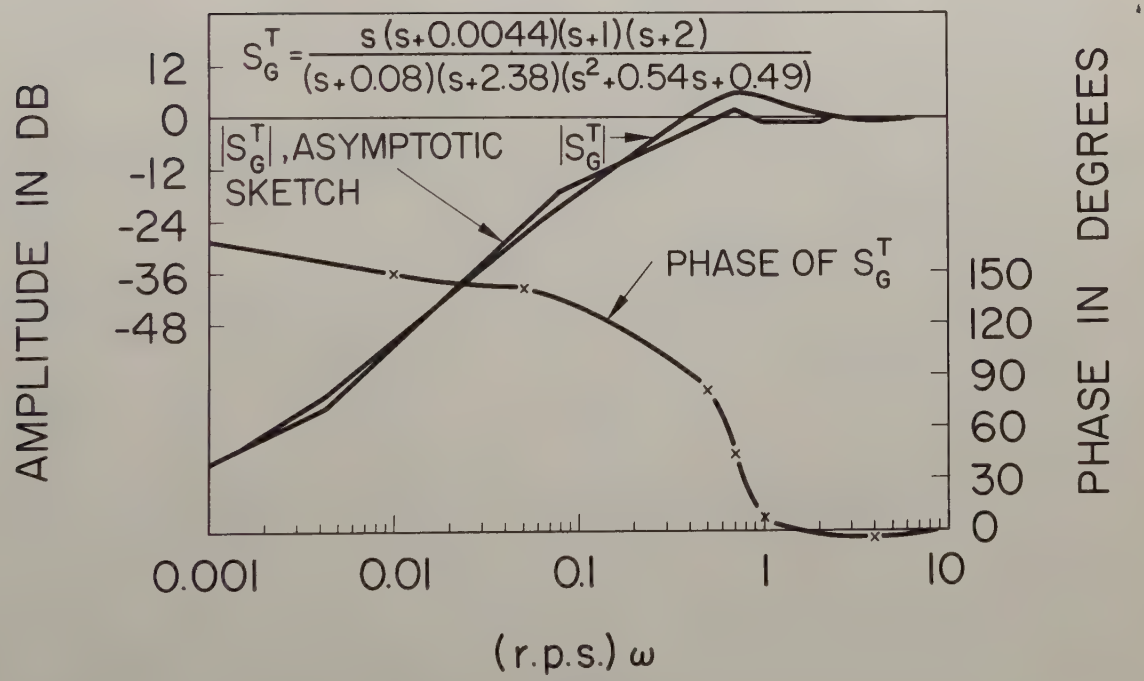

Fig. 4. Sensitivity function for system of Fig. 3.

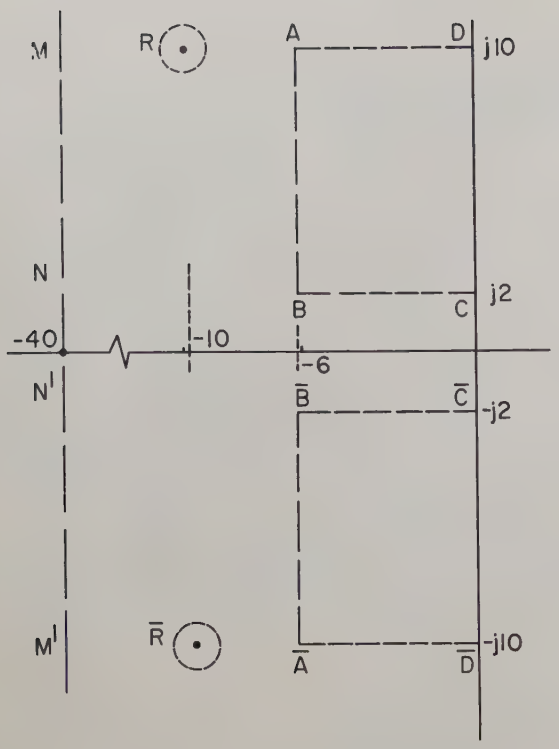

Fig. 5. Area of variation of plant poles.

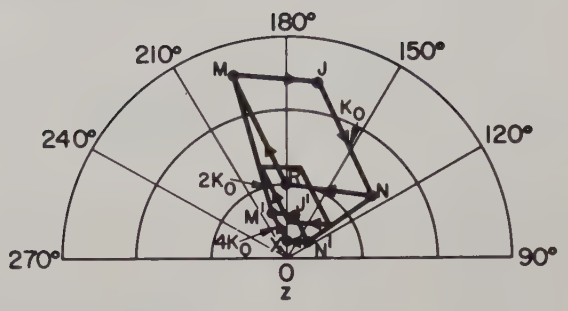

Fig. 7. Area of variation of T poles due to plant pole variations.

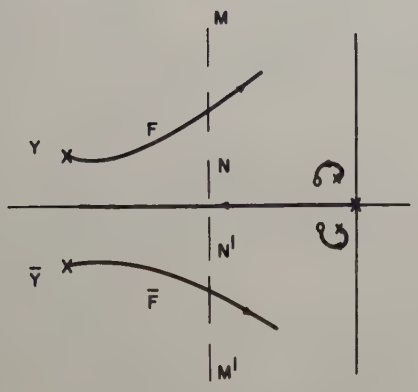

Fig. 6. Design philosophy.

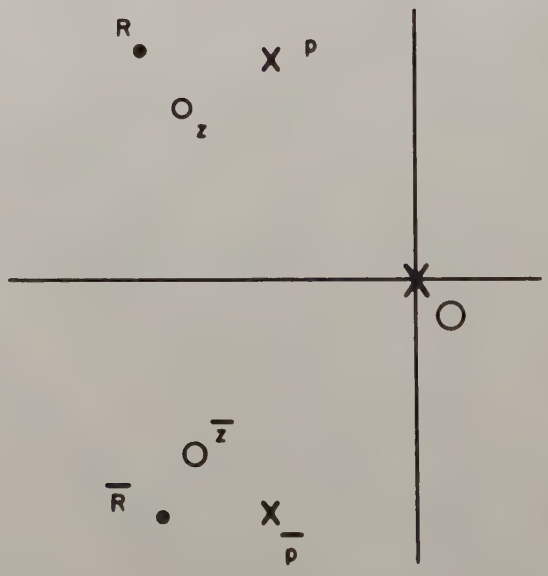

Fig. 8. Construction for locating z.

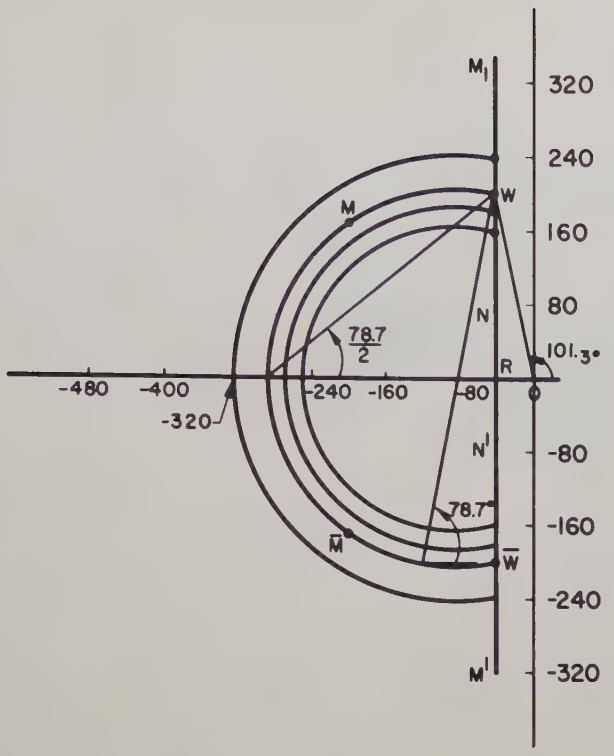

Fig. 9. Construction for locating far-off poles.

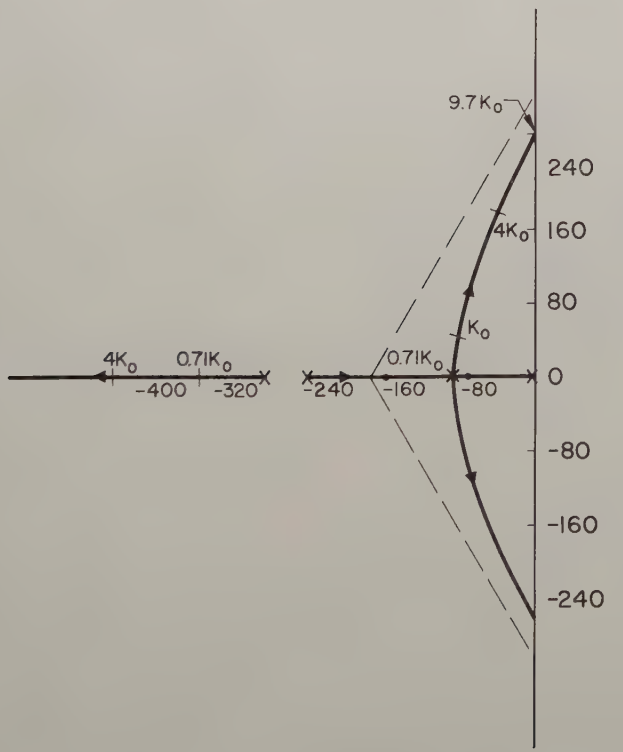

Fig. 10. Root loci of far-off poles.

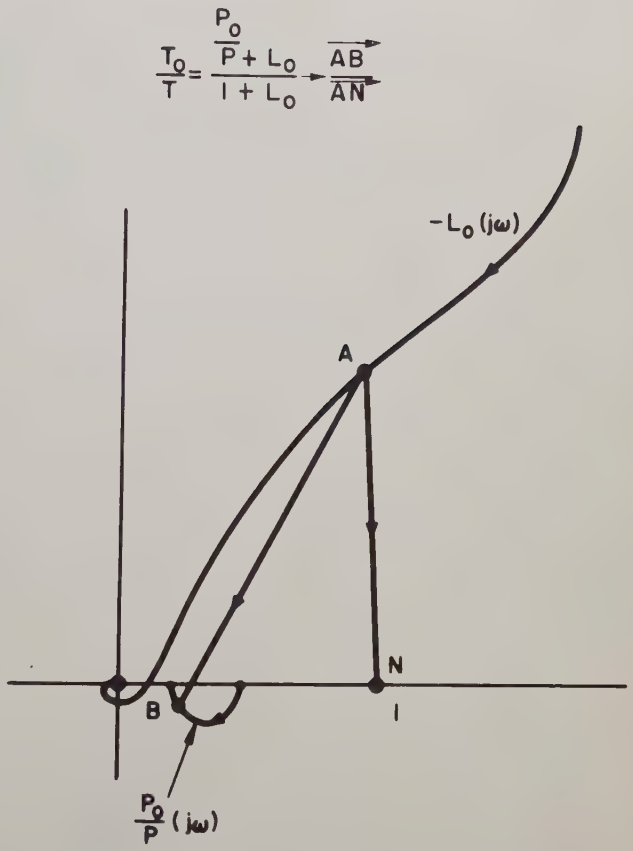

Fig. 11. Construction for evaluating $\frac{T_o}{T}(j\omega)$

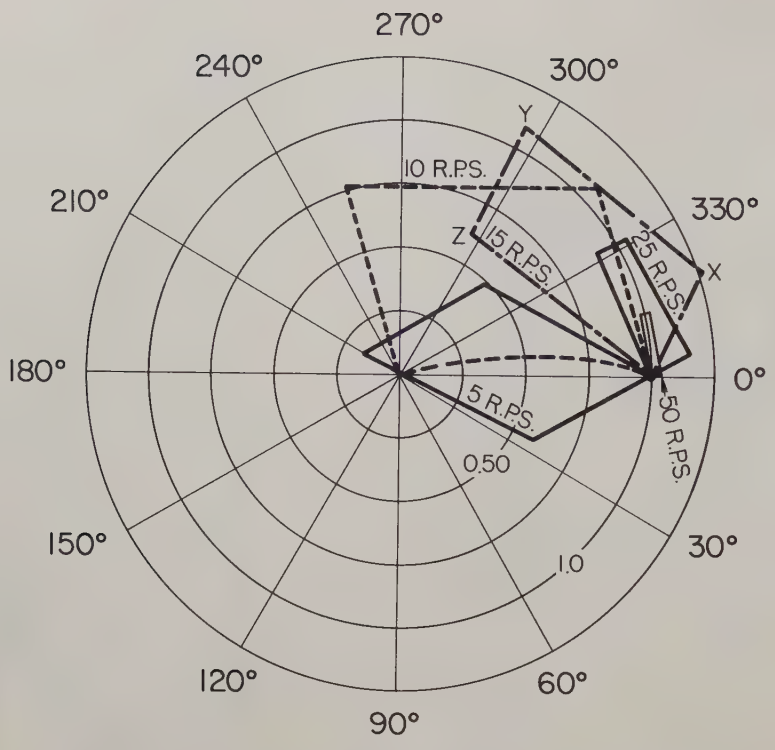

Fig. 12. Polar sketches of $\frac{P_o}{P}(j\omega)$ for typical frequencies.

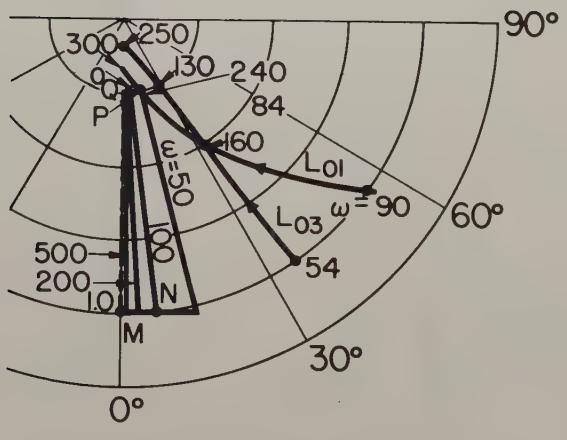

Fig. 13. Construction for finding L_o in intermediate frequency range.

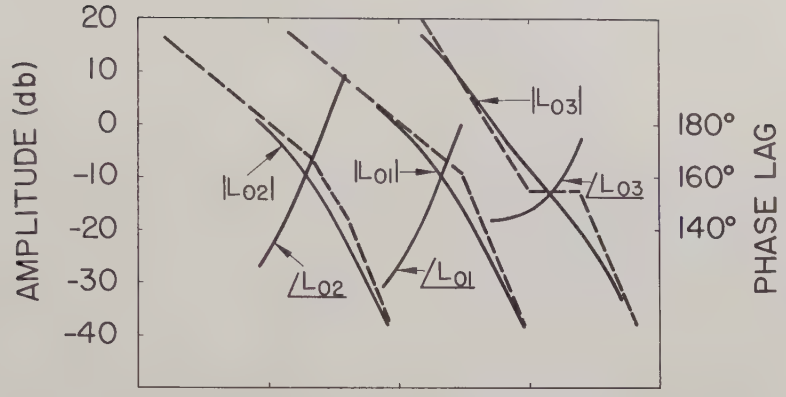

Fig. 14. Three possible L_o functions.

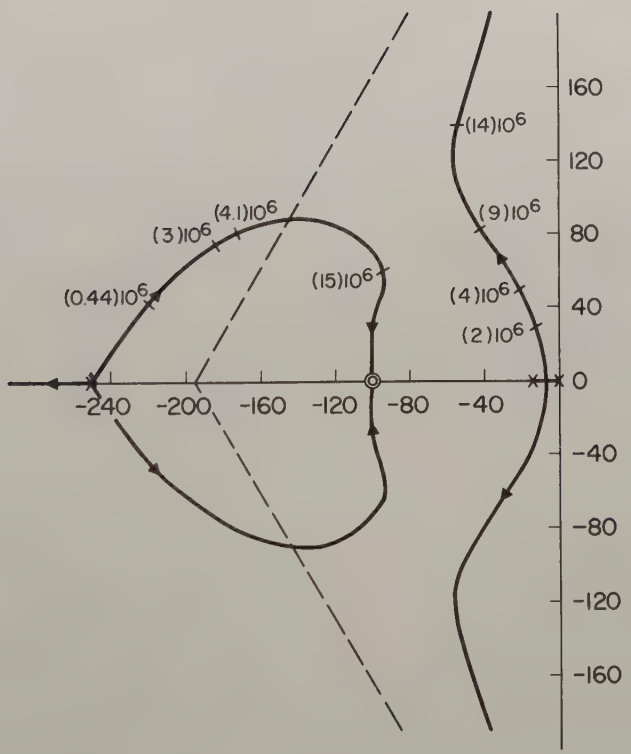

Fig. 15. Root loci of far-off poles.

GENERAL APPROACH TO CONTROL THEORY BASED ON THE METHODS OF LYAPUNOV

R. E. Kalman
RIAS, Inc.
Baltimore, Md.
and
J. E. Bertram
I.B.M. Research Center
Yorktown Heights, N. Y.

Abstract

This discussion is an introduction to the second method of Lyapunov in determining the stability of linear and nonlinear control systems. Although almost universally referred to in Russia and although it is becoming an increasingly important concept, this method has not been used in English-speaking countries because of the lack of suitable translations. This introduction to the method will not be published because it is essentially a condensation and introduction of the authors' paper given in Session IV.

THE IMPACT OF INFORMATION CONVERSION ON CONTROL

Harold Chestnut and Walter Mikelson
General Electric Company
Schenectady, New York

The rapid expansion of components and techniques for information conversion during recent years has provided control systems engineers with new tools for developing new kinds of systems. Nine basic functional tools have been identified which describe the complete information conversion process - sensing, converting, storing, communicating, computing, programming, regulating, actuating, and presenting. Information conversion is forming an important part of broader automatic control systems and an example is cited from the electric utility field.

Introduction

During the past several years the equipment and functions performed by control systems have expanded to include such additional services as programming, data processing, and computing.[1,2,4] More emphasis is being placed on the handling of information, data, and commands by such systems in addition to the important function of controlling power and energy. Whereas previously control systems were used primarily as regulators to maintain constant some desired quantity, now flexible programs of instructions are used to direct control systems to turn out intricate but precisely controlled parts. In addition to regulating and controlling power processes, control systems are being used to provide printed, tape, and/or punched card records of the quality of performance of various controlled or uncontrolled parameters of the process.

The expansion of the work of control systems has broadened the concepts of what constitutes such a system and has pointed toward the need for additions to our vocabulary to describe what is currently taking place. Further the introduction of new equipment making possible new systems has brought about the need for examining the relationships which exist among a number of our newer and older technologies, as for example, automatic computing, instrumentation, and control.[3]

A study has been made by the authors and some of their associates of the fundamental means by which sources of information are sensed and converted into data, operated on, and finally brought into a form where they may be used effectively. The nine basic functional tools identified which describe the complete information conversion process are sensing, converting, storing, communicating, computing, programming, regulating, actuating, and presenting. Definitions of these basic functional tools and examples of their use in control and information handling systems are presented in this paper.

In addition this paper will describe the subject of information conversion systems so that technically oriented people can further discuss the ideas to be found in some systems currently being built as well as those projected into the future. The influence of the new devices and equipments providing information conversion functions on the stability, accuracy and reliability of the systems in which they occur will be mentioned. It is hoped that through a better understanding of the information conversion process, there will be a broader acceptance and more widespread use of advanced ideas in automatic control systems.

Major Categories of Manufactured Products

In contrast with the familiar customer oriented description of manufactured products in such terms as utility, industrial, consumer, or military, it is possible to divide manufactured products broadly into three primary functional categories that describe the job these products perform. These categories - energy conversion, information conversion, and materials conversion - reflect the common technological ties to be found in each of these areas.

1. Energy conversion relates to the generation, transmission, and distribution of energy and its conversion from one form to another.

2. Information conversion pertains to the generation of signals and information which can be used to control energy conversion or materials processes as well as for the presentation of data or entertainment.

3. Materials conversion covers the manufacture of substances having such chemical, electrical, mechanical and other properties as to make possible improved products and equipment for use in further manufacturing processes.

In the fashion of a homely simile, the materials function may be likened to the body of man, the energy conversion function to his muscle power, and the information conversion function to that of his senses and intelligence.

Each of these three primary functions may be present in varying amounts in any particular product or equipment. In some complicated systems, there may be a number of different parts,

some of which are principally in one category, and the remainder of which are definitely in other categories. As shown in figure 1, the whole manufacturing business can be considered to be made up of these three parts.

As shown in figure 2, information conversion equipment can be used to provide controlled inputs to the energy conversion or materials conversion portions of a system so that the actual output is held closer to the value desired for it. Although in many cases the influence of information and energy conversion functions on each other is of great importance from a performance point of view, there is also much to be gained by studying the characteristics of each separately. In the material that follows, particular attention is paid to the information conversion function.

Information Conversion Definitions

Although the concept of information conversion is not one that is characterized by hard and fast definitions, there is merit in setting up general descriptions which help to establish a flavor for the intent of the various terms involved. Despite the fact that some of these definitions may not be adhered to rigorously in all of the material that follows, the basic ideas associated with these terms are as indicated below.

Information - That which conveys meaning such as data, ideas or concepts, narratives, commands or emotions. Although the broad meaning of information also covers the subjective values listed, the emphasis contained in this paper will be on the objective (data) aspects.

Conversion - The process of obtaining data from a system being observed or controlled and translating or modifying it in various ways into information that is useful for control or display. In addition to being applicable to the overall process of information conversion, the term "conversion" is also used to express a particular part of this overall process as described in Table I.

Data - Results of observations or logical operations performed on other data. As such, data can consist of outputs of measuring or sensing devices or of a number of other devices where the data are purely symbolic or numeric. Data can be either analog or digital in form.

Analog Data - Have continuously varying values. Examples of analog data are mechanical positions, electrical voltages, temperature indicators or curve traces.

Digital Data - Have discrete values that may change in a discontinuous fashion. Examples of digital data are numbers, letters, words, punched holes, magnetic poles stored on tape, drum, or cores.

In addition to the broad definitions given above, table I has been prepared which lists the nine functional elements of the information conversion process. A simple definition or explanation of each of these functions is given. In the examples given later for purposes of illustrating typical equipment for performing these functions, the terminal equipment associated with each function is considered to be part of this function.

It is interesting to note that these definitions are not in all cases unique and that some of the devices performing one function may in fact incorporate elements that are of another function. For example, the function of programming will, in general, require that data be stored within the programmer. Likewise, the function of regulating may require that sensing and actuating functions also be performed. The selection of these functional elements has been made with the thought that, to a large extent, it should be possible to describe with a number of these terms, equipment assemblies which perform more than one function.

The criterion that should be applied in using these functional definitions is "what is the principal function that the equipment performs for the user". In this way, the user can more easily identify different devices for the same function and compare them for their relative effectiveness in performing his job. Although occasionally there may be some ambiguity in using these functional definitions, the terms tend to line up with many existing equipments. In addition the use of these relatively few functionally descriptive terms obviates the need for using numerous other words and trade names which fail to convey a clear understanding of their function to the user. Perhaps by using even fewer functions, the same objectives could be met. By using nine, however, it is possible to provide finer shades of meaning than could be realized with a smaller number.

Information Conversion Block Diagram

A general form of the information conversion process may be represented schematically as a block diagram as is shown in figure 3. As shown at the bottom of the figure, primary information enters the system principally through the vehicle of sensors, after which intermediate information or data in the form of digital or analog representation is obtained. At the top of the diagram actuators or presentors are shown to take the information and convert it into useful form. These functions - the sensing, the actuating, and the presenting areas are where the information conversion equipment touches intimately the remainder of the system. It is

important, therefore, that these areas be flexible and adaptable to the needs of the process in the case of sensors, and the need of the user in the case of actuators or presentors. Because of the large number of quantities to be sensed and their varied characteristics, the number of instruments for performing the sensing tends to be large and ever-increasing.

The intermediate functions of information conversion are ones which to a large extent are not ones that act directly upon the user's equipment. The interconnections may be made between any of a number of functions and are made with primary regard to the requirement of the system and its internal design needs rather than with the direct customer specifications as a reference. These functions are the result of a selection of material or equipment which may be fashioned in such a way as to be most convenient for the designers of this equipment and the designers of the system.

Although the nature of the conversion process is materially affected by the character of its inputs and outputs, a certain degree of broad standardization may be possible in this area. Because in many cases the costs in dollars and time of the engineering design to interconnect most efficiently these various intermediate function equipments may exceed the savings in material costs involved in using standard units, the possibility of using standard building blocks for those intermediate functions of the overall system appears to have sufficient merit to warrant further investigation. The block diagram approach does serve to place emphasis on the systems interconnection problem inherent in the information conversion process rather than stressing the custom nature of the design which might otherwise receive major attention.

Information Conversion Functional Tools

The material that follows describes what is meant by the different functional categories of information conversion and gives illustrations of specific equipments which are included in the different areas. The illustrations are merely indicative of the sort of equipment involved and are not meant to exclude other possible equipment. As a general rule, the equipment is identified with the function it performs for the user and not on the technique employed to achieve the result. In many cases, the same technology and engineering principles may be employed in a number of different functional tools. However, it is the use of the equipment that establishes the principal basis for the category in which it is placed.

The terminal equipment, such as an input converter or/and output display unit that is attached to an equipment, is generally considered to be part of the major equipment to which it is appended. The same converter or display unit by itself would be considered as a converter or presentor respectively.

An effort has been made not to include the elemental components such as tubes, transistors, resistors, and capacitors, as functional tools. Rather the emphasis has been placed on considering as the functional tools the more comprehensive assemblies, as for example, servo amplifiers, starting relay panels, and supervisory telemetry, relating to the users functional needs.

1. Sensors - Employ physical effects and principles to generate data.
   Quantities measured:
   - Mechanical--position, length, velocity, acceleration, weight, temperature, pressure, flow, force.
   - Electrical--voltage, current, power, flux, density, torque.
   - Chemical--density, composition, acidity.
   - Optical--intensity, color, wave length.
   - Symbols--numbers, letters, words.

   Examples:
   - Gyroscope, tachometer, x-ray gage.

   Note: Excluded from sensors are simple presentors as, for example, voltmeters and ammeters that are used primarily for display purposes for most sensing devices.

2. Converters - Change form of data to facilitate their transmission, storage, or manipulation without altering their absolute value.
   Types of Conversions:
   - Mechanical--punched cards to punched tape or electrical signals
   - Electrical--electrical voltages to magnetism on tapes, electrical voltage to pulse time modulation.
   - Optical--mechanical photographic code wheels, optical-electrical voltage conversions.

   Examples:
   - Digital-to-analog converters, analog-to-digital converters, shaft encoders and decoders, and code translators.

   Note: Excluded from converters are the terminal equipment performing this function as a part of other equipment as for transmitting and receiving or presenting.

3. Storage Devices - Means for memorizing for short or long periods of time, data instructions, or programs.
   Examples:
   - Mechanical--cards, punched paper tape, program wheels.
   - Electrical--magnetic tape, magnetic drum, core memory, electrostatic storage, relay matrix.
   - Optical--film storage, color filter storage.

   Note: Storage devices may include means for reading information into and out of memory where these are essentially part of same overall equipment.

4. Communicating - Send and receive data from one place to another.
   Examples:
      Electrical--Radio and TV transmitters and receivers, telemetering equipment, microwave links, automatic dispatching, supervisory control, carrier current.
      Optical--Projectors, cameras, light receivers.

5. Computers - Perform basic and more involved mathematical processes of comparing, sorting, adding, subtracting, multiplying, dividing, integrating, etc.
   Examples:
      Navigation computers, fire control computers, static switching equipments, general and/or special purpose computers.
   Note: Analog and/or digital means may be employed. Internal storage as well as intimately associated input and output equipment is generally considered all part of the computer.

6. Programmers - Schedule and direct an operation automatically in accord with an overall plan. Programmers initiate, adjust, sequence, and/or stop a process usually as a function of some prearranged time schedule, or process schedule.
   Examples:
      Machine tool contouring programmer, radio station programmers, cam timer programs, multiplexers, scanners, and distributors.
   Note: Programmers differ from regulators and actuators which are the subsequent elements that perform the energy or power control.

7. Regulators - Operate on a process to maintain its controlled variable in accord with a reference quantity.
   Regulated Quantities--the mechanical, electrical, chemical, optical and other quantities that can be measured (as mentioned under sensing) can be regulated.
   Examples:
      Power supplies, speed variators, amplifiers, position regulators, voltage regulators, and torque controllers.
   Note: In case of manually set regulators, the initiation, adjustment, and stopping equipment associated are considered part of the regulator.

8. Presentors - Display data in a form useful for human intelligence.
   Quantities Presented:
      Visual - Pictures, signs, words, numbers, symbols, meters, dials, colors
      Aural - Music, alarms
      Touch - Pressures
   Examples: Voltmeters, indicators, display consoles, radio and TV sets, data printers, chart recorders.

9. Actuators - Initiate, interrupt, or vary the transmission of power for purposes of controlling energy conversion or materials processes.
   Quantities Actuated:
      Mechanical--position, speed, torque, pressure, tension, force.
      Electrical--voltage, current, charge, flux.
      Hydraulic--flow, pressure.
   Examples:
      Circuit breakers, motor starter panels, generator field controls, power drives, valves, hydraulic power actuators.

Information Conversion as Part of Broader Automatic Control Systems

The examples of information conversion functional tools mentioned in the previous section contained many terms that would be somewhat foreign to the control system engineer of 10 years ago. However, today more and more comprehensive control systems are being designed and built embracing many of these information conversion devices.

Figure 4 illustrates in an elementary form how the conventional feedback control system, shown by solid lines, can be incorporated into a larger automatic control system which may include as supplemental features a programmer, a computer, and a data logger shown in dotted lines. In the physical embodiment of such a system, the various functions of programming, computing, and data processing may all take place in one or more equipments. As indicated in figure 4, the more comprehensive system from information reference to information controlled variable may form an open-loop automatic control system. Although for some systems the outer loop may be closed, the analysis of such a system is generally much the same.

It is comprehensive systems such as these where product quality, plant efficiency, or maximum yield are the true variables being controlled that the newer control system theories and application may be increasingly valuable. These new and challenging problems are ones to which control systems engineers can contribute effectively as they have in the past in the simpler feedback control loops. The characteristics of speed, flexibility, and precision possible with many of the newer components provide today's control system engineer with the possibility of developing and using new control concepts and techniques that have not been employed to any extent with previous conventional methods. Extremum and other self-optimizing ideas are particularly attractive for such applications. Adaptive and self-organizing methods likewise are most promising.

Because the equipment for performing the programming, computing, and/or data processing

may embody many of the same functional devices, these three equipments may actually be incorporated into one which is frequently called by the generic term "computer." Figure 5 shows the familiar block diagram of such a system which is often referred to as a "computer-controlled" system. To the extent that continuous analog data are used throughout, this system is analogous to the feedback control systems of the past in the means for analyzing it and predicting its performance. To the extent that digital data are used with time sharing of the computer's function, quantized and sampled data techniques are required to perform the system's analysis. The increasing trend in information conversion equipments of late has been to stress the importance of the digital methods as the programming and data processing functions have been combined with the computer.[4]

The simple diagram of figure 5, by failing to show the many instruments that perform the input-output functions of sensing, presenting, actuating and communicating, tends to create a distorted picture of the combined control system. As shown in figure 6, where these functions are indicated, the size, cost, performance, and number of these devices may exceed those of the regulating and computing equipment required for the job. Since such practical factors as those listed above have a direct bearing on whether an instrumentation or a computer oriented individual or firm may be called upon to do this work, it is important that the alternate approaches and relative effectiveness of the different equipments be considered and understood. It is apparent that the modern control engineer has to have command of many more subjects and data than the traditional ones of stability and accuracy of linear systems.[3]

One other factor of vital importance in large scale automatic control systems is the subject of reliability. Systems of the sort being considered here are costly, and their use is justified only on systems and processes that are comparably expensive or even more costly. To justify such systems economically, it is essential that they operate and that they "fail-safe." Therefore, it is essential that the reliability of these automatic control systems be very high and that the trouble-shooting and maintenance time be held to a minimum. The demands for reliability will in the future have an increasingly important effect on control systems design and manufacture in all aspects.

Example of Information Conversion Processes Applied to the Electric Utility Field

An application of the information conversion functions to an integrated system is illustrated by the Electric Utility system shown in figure 7. Starting with the fuel into a given boiler-turbine-generator combination, the regulators and actuators of the individual energy conversion devices are indicated as well as the tie-in of the data from these energy conversion elements to a central storage, programming, computer, and presenting system labelled Power Generation Control. Presentors may also be used in conjunction with the individual energy conversion equipments. Controls to the transformers and switchgear equipment and the associated presentation equipment including alarms are also affected by the central power generation control system. In addition, automatic start-up and shut-down routines can be programmed into the power generation control.

Additional power generation capacity in the same station will be handled through a more comprehensive power generation control means that programs the elements of each of the individual power generation units to optimize station performance through the use of computing and storage. The individual power generating stations making up the overall Electric Utility System will in turn be programmed and actuated from a central control system which directs the dispatching of power in response to the demands of the power loads of the remainder of the system. Stored information on such factors as fuel costs, transmission loss characteristics, and availability of various power units will all be taken into account in arriving at the optimum performance for the overall system of many stations. Data presentation in the form of printed records are available for use by engineering, financial, operating, and management people.

The extension of the present feedback control activities into the Electric Utility Field is evident in the above illustration, which indicates an expansion of the control concept to include the broad field of information conversion as well as energy conversion. The above example is merely one application of many that might be chosen to illustrate the combination of energy conversion and control with the newer concepts of information conversion. Other examples in the industrial processing fields, the manufacture of chemicals, the making and shaping of metals, the refining and processing of petroleum, and the preparation of plastics and paper readily come to mind.

Conclusion

The rapid expansion of components and techniques for information conversion during recent years has provided control systems engineers with new tools for developing new kinds of systems. In addition to controlling energy processes, designers are placing increasing emphasis on controlling information and information conversion systems separately or in conjunction with energy or material process systems.

It is hoped that the suggested definitions of information conversion functional terms and the examples of the functional tools will be of help to control systems engineers in describing their systems to ultimate users and in including the dynamic effects of all the system parts. Through the use of these terms a better understanding and a more ready acceptance of the salient features of new control systems may be obtained. The use of more uniform terminology

should help point the way to greater standardizing of equipment functions, as well as input-output characteristics, to achieve improved simplicity, interchangeability and reliability of the overall systems. These systems in many cases are ones which will do better than systems employing traditional control techniques or will do things previously not considered possible.

The purpose of this paper will be served if action is taken by individuals and by the interested technical organizations to expedite the interconnection of information conversion devices and equipments into more comprehensive information conversion and control systems. In this way, the broader use and acceptance of automatic control systems will be facilitated.

Bibliography

1. "Control Engineers Handbook," John G. Truxal, McGraw Hill Book Company, 1958.

2. "Objectives and Trends in Feedback Control Systems," H. Chestnut, Electrical Engineering, Jan. 1958, p. 58-63.

3. "Basic Instrumentation," W. A. Wildhack, Transactions on Industrial Electronics PGIE-5, April 1958, p. 4-9.

4. "Computers and Automation," E. L. Harder, Electrical Engineering, May 1959, p. 508-518.

TABLE I

Table of Definitions of Information Conversion Functional Terms with Respect to Equipment Applications

FUNCTION	DEFINITION OR EXPLANATION
Sensing	Generates primary data which describes phenomenon or things
Converting	Changes data from one form to another to facilitate its transmission, storage or manipulation
Storing	Memorizes for short or long periods of time data, instructions, or programs
Communicating	Transmits and receives data from one place to another
Computing	Performs basic and more involved mathematical processes of comparing, adding, subtracting, multiplying, dividing, integrating, etc.
Programming	Schedules and directs an operation in accord with an overall plan
Regulating	Operates on final control elements of a process to maintain its controlled variable in accord with a reference quantity
Actuating	Initiates, interrupts, or varies the transmission of power for purposes of controlling "energy conversion" or "materials" conversion processes
Presenting	Displays data in a form useful for human intelligence

PRIMARY FUNCTIONAL DIVISION OF MANUFACTURED PRODUCTS

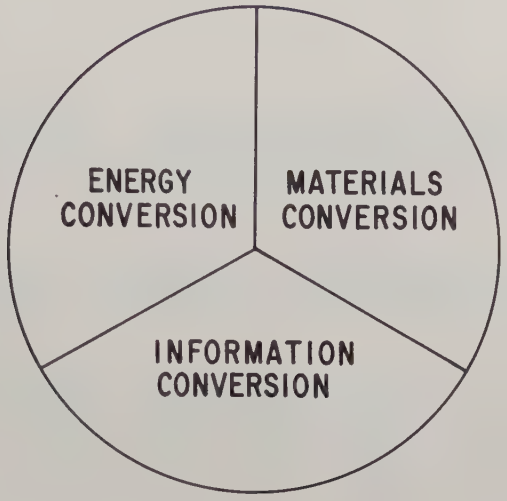

Fig. 1.

CONTROL SYSTEM SHOWING INTERRELATIONSHIP OF INFORMATION, ENERGY AND MATERIALS CONVERSION

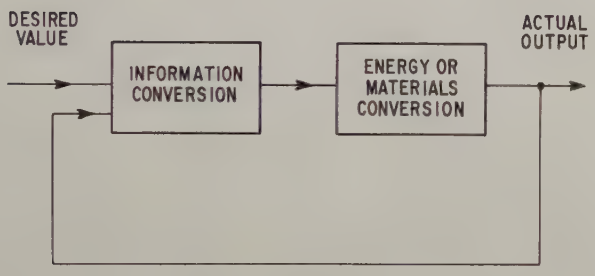

Fig. 2.

COMBINED FEEDBACK CONTROL AND INFORMATION CONVERSION SYSTEM

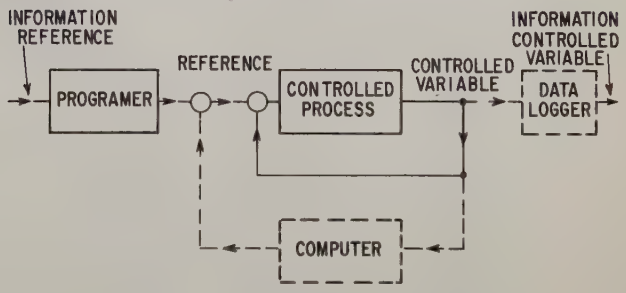

Fig. 4.

BLOCK DIAGRAM OF GENERALIZED INFORMATION CONVERSION SYSTEM

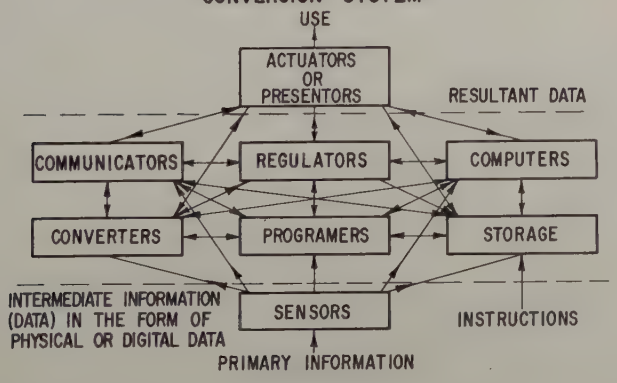

Fig. 3.

COMPUTER-CONTROLLED SYSTEM

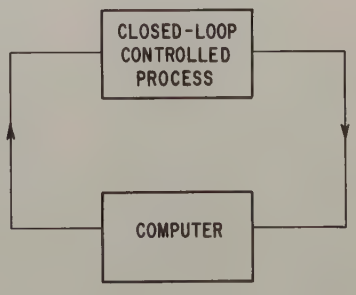

Fig. 5.

COMPUTER-CONTROLLED SYSTEM SHOWING ALSO THE FUNCTIONS OF SENSING, COMMUNICATING, AND PROGRAMING

THE CONCEPT OF CONVENTIONAL CLOSED-LOOP FEEDBACK CONTROL WITH AN OUTSIDE COMPUTING, PROGRAMING LOOP IS ILLUSTRATED

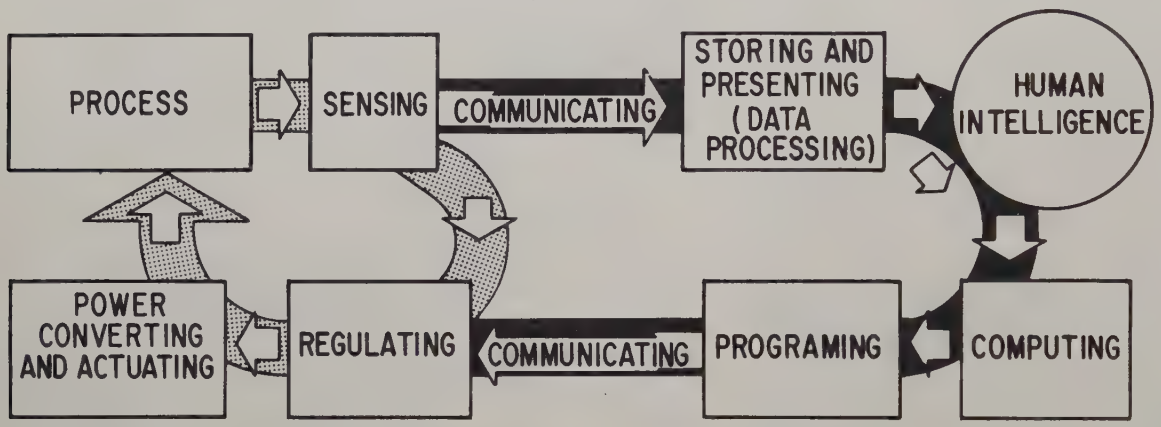

Fig. 6.

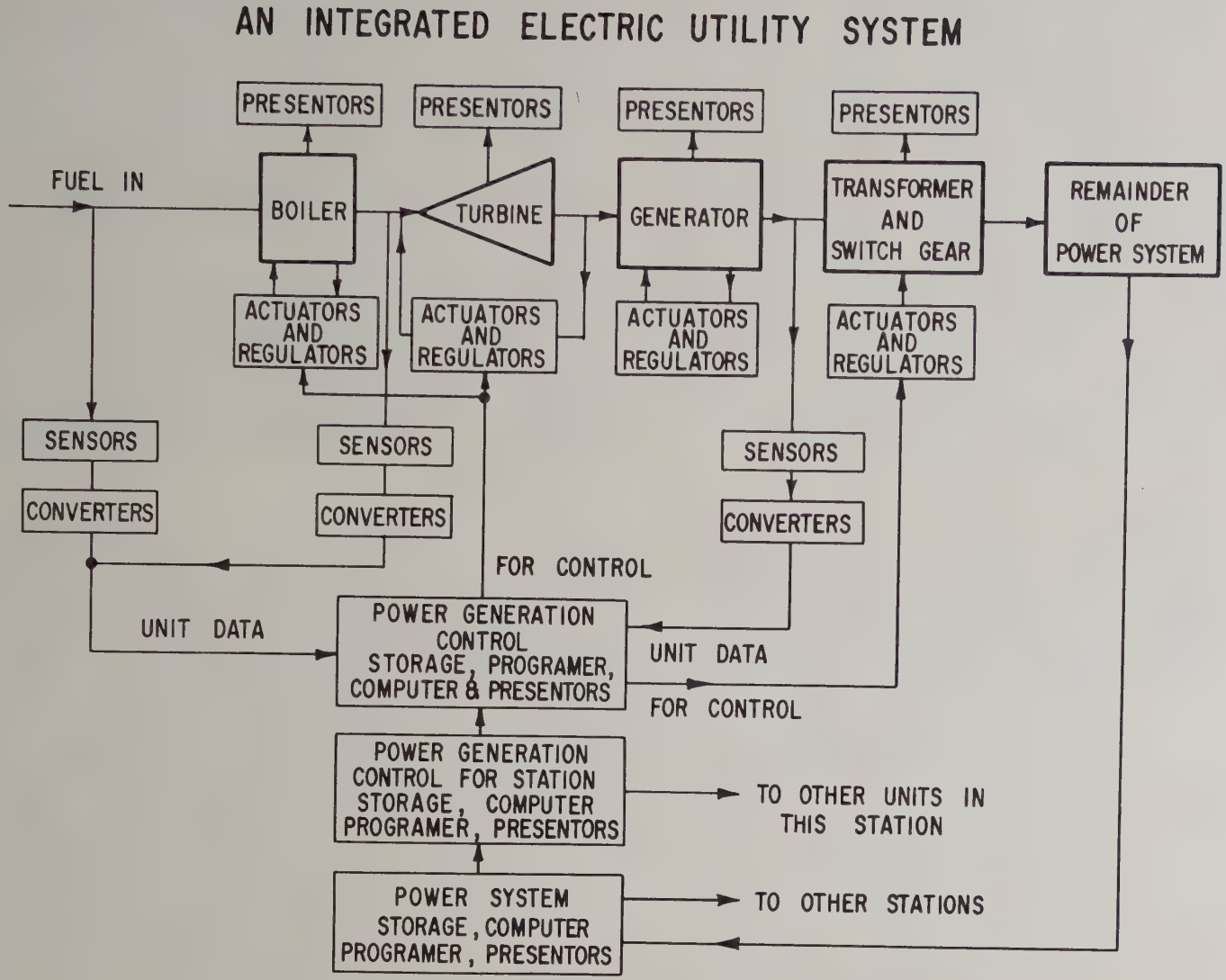
AN INTEGRATED ELECTRIC UTILITY SYSTEM
PRESENTORS
PRESENTORS
PRESENTORS
PRESENTORS
FUEL IN
BOILER
TURBINE
GENERATOR
TRANSFORMER AND SWITCH GEAR
REMAINDER OF POWER SYSTEM
ACTUATORS AND REGULATORS
ACTUATORS AND REGULATORS
ACTUATORS AND REGULATORS
ACTUATORS AND REGULATORS
SENSORS
SENSORS
SENSORS
CONVERTERS
CONVERTERS
CONVERTERS
FOR CONTROL
UNIT DATA
POWER GENERATION CONTROL STORAGE, PROGRAMER, COMPUTER & PRESENTORS
UNIT DATA
FOR CONTROL
POWER GENERATION CONTROL FOR STATION STORAGE, COMPUTER PROGRAMER, PRESENTORS
TO OTHER UNITS IN THIS STATION
POWER SYSTEM STORAGE, COMPUTER PROGRAMER, PRESENTORS
TO OTHER STATIONS

Fig. 7.

CONTROLLED PROPULSION

by

Konrad K. Dannenberg
Army Ballistic Missile Agency
Redstone Arsenal, Alabama

(A Special Session, "Control Problems of the Space Age" was held on Wednesday, November 4, at the Control Conference under the direction of John M. Salzer of Ramo-Wooldridge. The topics included "Controlled Propulsion" by K. K. Dannenberg of the Army Ballistic Agency, "Attitude Control of Space Vehicles" by Dr. C. R. Gates of the Jet Propulsion Laboratory, "Tracking and Path Control" by Dr. R. C. Booton, Jr., of Space Technology Laboratories, Inc., and "Control of the Human Environment" by Dr. Paul Webb, Consultant. Although the authors had not originally planned to publish their papers, Dr. Konrad K. Dannenberg, Director of the Jupiter Project at the Army Ballistic Missile Agency, was able to submit a copy of his paper. Dr. Dannenberg stresses the importance of control and control reliability in the development of missile propulsion systems. His message, timely and important, should be of interest to all control engineers.)

A multiplicity of applications, reaching all the way from new copter propulsion to deep space probes, results in a bewildering variety of propulsion system designs. A brief review cannot exhaustively cover such a huge area of endeavors; therefore, I shall restrict this presentation to rocket propulsion by large liquid propellant boosters.

This limitation to booster engines does not require me to discuss re-ignition and the many other special features we find today on most small-size special purpose engines. In conformance with current trends, I will also restrict my discussion to conventional fuels, such as liquid oxygen, and kerosene. I shall exclude solids, exotic propellants and nuclear propulsion. This approach may sound very unsophisticated to an audience such as you; but on the one hand, the "conventional" chemical engines will still be used in big boosters for a long time to come; and on the other hand, the control engineer has still to contribute a number of major advances in order to get our big missiles safely, reliably, and with clock-work dependability in the air.

For these reasons, I believe it is certainly worth the control engineer's effort to look deeper into this "old fashioned" field of conventionally propelled liquid engines. Today, I want to weigh current design trends in our spacecraft propulsion systems against the past history starting with the V-2 ballistic missile, and going past the "Old Reliable" REDSTONE rocket! I intend very specifically to include the REDSTONE, because it will be the first rocket engine to propel man into space during early "MERCURY" flights.

In order to meet the unprecedented requirements of this venture, the ABMA propulsion engineers have still a rigid and thorough reliability program under way, in spite of the proverbial REDSTONE reliability rating. ABMA's philosophies and presently planned measures are reflected all through this presentation, as it is believed that this trend will soon apply to many more of our present and future projects to be employed for manned space flight.

All engines operate in accordance with the same basic control scheme; they require

1. Start-up, to include ignition.
2. Steady-state operation, oftentimes with special control features added.
3. Cut-off.

Let us discuss these three distinct phases of control requirements separately:

Phase 1

During early development work, it had been considered mandatory to start large liquid engines very slowly and a variety of sequences had been worked up for the V-2 power plant. It was deemed necessary to operate the engine for a brief period of time at a "pre-stage level" before the main thrust of the engine could be turned on. Only three methods of pre-stage operation were carried into the test phase. Two of them, which called for pre-stage operation by having combustion in only one of the eighteen combustion elements of the V-2 thrust chamber, were discarded pretty soon because tremendous problems developed in the non-burning elements of the thrust chamber. The final version of the start-up sequence provided pre-stage operation by throttling the fuel valve opening to a very small gap for fuel passage to all eighteen combustion elements. The liquid oxygen flow was controlled by means of a separate LOX-pre-stage valve which was inserted into the poppet of the LOX main valve. Both designs resulted in a number of problem areas: It was difficult to maintain the close tolerances which were required for the opening of the main fuel valve in order to have accurate flow rates during pre-stage. The completely inclosed LOX pre-stage valve malfunctioned often and could only be repaired after disassembly of the LOX duct. For this reason, a butterfly-type design was employed for the REDSTONE engine, opening in two steps. Later development tests established that an engine the size of the REDSTONE can be ignited without any distinct pre-stage operation if the start-up

is conducted under closely controlled conditions. This redesign reduced the number of control components considerably as shown in Table I.

The propulsion engineers were told to simplify the logistics of propellant supply for large missiles by deletion of the peroxide system; the ATLAS, THOR, and JUPITER engines replaced the peroxide steam plant, therefore, by a LOX-kerosene gas generator. During main stage, the operation is very simple. However, the start-up is a tricky problem. The propellant feed cannot take place in the normal way because the pump is not yet operating to yield the necessary feed pressure. This situation requires the introduction of start tanks which can either be located on ground, thereby creating separation problems; or they can be carried along in the missile for the full duration of the flight, thus adding to missile dead weight and consuming the expensive hardware during each and every firing.

The JUPITER S-3D engine selected the ground start system while other engines carry the tanks along for the flight. Both methods require many additional components for the gas generator controls. It was, therefore, obvious that an advanced design, such as the H-1 engine, for the SATURN vehicle should simplify the start-up procedure. Existing proposals are to use a solid propellant charge to supply the initial turbopump power. This will simplify the start-up system drastically.

The start-up phase has always posed the main problem of liquid engine design. For that reason, considerable changes have taken place in this area. Only a few of the many different control schemes and control components have been discussed here.

Phase 2

In contrast, the steady-state operation of the engine has not experienced too many changes. Designs were under test to provide simultaneous thrust control and mixture ratio control for the V-2. However, the rigid requirements for accuracy and reliability of such a system prevented it from becoming a production item. Therefore, all engine adjustments for main thrust level were made solely during ground testing. Elaborate procedures had been worked out where testing of individual components would yield enough data to graphically compute adjustment orifices for installation in the propellant lines. This method never yielded really accurate data and mixture ratio and thrust level were, in most instances, adjusted during cold calibration water tests. With this method, the accuracy could be almost tripled, but it still was way below accuracy data which could be obtained in a "hot" static firing. Mixture ratio and thrust level adjustment posed a big problem for the wartime mass production of V-2's, with the prevailing alcohol shortage, but it never has become an issue for the relatively small production of REDSTONE, IRBM, or ICBM engines. It has never been seriously considered in this country to replace the final engine acceptance run by cold tests or by component checks only. I believe that this trend will continue at least for early flights during the large booster development. This situation could drastically change, though, once accurate, lightweight and completely reliable control systems become available to do this job satisfactorily during flight by means of automatically computed adjustments. The hardware cost is of only minor importance, as the savings would be tremendous which can be obtained by deletion of the engine and missile acceptance run. I am afraid, however, that the cost of the required development program will put any such system in the far, far distant future.

For similar reasons, propellant utilization systems had never been installed in production missiles although components have been test flown. The small gain in range for just a very few maximum range firings was never considered to be important enough to warrant the installation, into all the missiles, of an expensive, heavy, and possibly unreliable propellant utilization system. The value of thrust control has been disputed often, but it is generally agreed that for first stage boosters it does not enhance greatly the overall performance of the system. For that reason, it is not intended at this time to use a thrust control system for the SATURN booster in order to gain reliability by the simplification of the overall engine system.

To permit flight without propellant utilization controls, special attention should be given to propellant loading. A system has been designed which yields a fill weight accuracy of ±0.10 per cent. The system changes in fuel density that occur during standby and makes the necessary corrections in the LOX to fuel weight ratio. LOX weight is determined by measuring the LOX head pressure and using the LOX density derived from the LOX temperature, similar to the system of the JUPITER missile.

Phase 3

The cut-off portion of the control system has never posed a severe problem. In order to allow the guidance system more time to compute the accurate cut-off velocity and to follow up with the shut-down signal, the V-2 design introduced an eight-ton step (about a third of the main thrust value). The complicated steam supply system to the turbine combined with this eight-ton step created considerable problems due to functional unreliability.

In order to avoid this complication in the REDSTONE missile, it was decided to terminate the engine operation directly from main thrust level. Deviations in total impulse obtained during this period will be compensated by a terminal guidance system which is part of the REDSTONE accuracy scheme. For the JUPITER missile, a solid propellant vernier engine has been introduced which compensates for deviations during the thrust decay. This arrangement avoids complications of the main engine. Cut-off

accuracy is not required for booster engines, and therefore, the H-1 (SATURN) engine will use the same simple cut-off as the JUPITER engine.

The SATURN Booster

At this time, I want to give you a few SATURN facts of interest to the control engineer.

As a historical introduction, I would like to mention that ABMA was among early groups to consider payload capabilities of 10,000 pounds for escape missions and several times this payload weight for orbiting satellites. Initial studies showed that thrust ratings of around 1.5 million pounds would be required for these space missions.

The present SATURN configuration, as originated by ARPA, was selected, based upon available engine hardware, ABMA's favorable experience with these engines in the JUPITER missile and the availability of many required tools and fixtures for booster construction and assembly and resulted in ARPA's decision to sponsor SATURN work. The TITAN and CENTAUR upper stages will be employed in conventional tandem arrangement.

The design intent of the SATURN program is to provide a space vehicle with a high payload capability at the earliest possible date at low cost. Existing and proven hardware will be employed whenever possible to meet this objective, but advancements will be incorporated if they do not adversely affect reliability, cost and/or schedule. This led to the selection of the H-1 engine over its S-3D predecessor.

The structural booster design was studied with particular thoroughness. The nine-tank arrangement--eight smaller tanks mounted around a larger central tank--was selected to take advantage of existing conditions.

The selection of a clustered engine arrangement for the SATURN booster requires a few explanations because the cluster concept appears to be a major contribution to the solution of the reliability problem, especially in consideration of manned space flight. The SATURN booster was designed with a "one-engine-out" capability. The advantage of such redundancy is demonstrated in Table II. The second column in this table shows that clustering will normally result in a lower reliability of the cluster design without an "engine-out" capability. The third column demonstrates that a "one-engine-out" capability improves the reliability of the cluster unless the reliability of the individual engine drops below 95 percent. Further improvements are possible for a "two-engine-out" capability, as shown in the fourth column of Table II. Because this arrangement would involve additional complications and losses in payload capability, it was decided not to employ this system for the SATURN booster. It must be realized that this table is purely a mathematical exercise and does not indicate the effect of clustering on the individual engine reliability rating. It may be that the new environment deteriorates the reliability.

It may well be, though, that the reliability of the individual engine in the cluster improves because not all components and/or systems need to be multiplied and certain redundancies are possible. A study of these effects is under way at ABMA. Results are not yet available.

Another major reliability improvement can be obtained by the application of principally new designs. For example, a new pressure switch has been selected for the SATURN cluster which has shown in component tests that its reliability is superior to any previously tested designs. This pressure switch consists of a Bourdon tube pressure sensing element, an inductance pick-off and a solid-state trigger and switch circuit. The helically twisted Bourdon tube is the only moving part in the pressure switch, and its use results in high sensitivity to pressure changes, but insensitivity to acceleration, shock, and vibration. Although the addition of the electronic circuit increased the number of parts considerably, the overall reliability meets the very high requirements of the SATURN system. The entire engine operation is based on the proper performance of this pressure switch. It monitors proper functioning of the engine prior to take-off and signals engine failure to shut off any improperly operating engine for the "one-engine-out" operation. Because eight of these switches are needed, this new construction element requires the utmost performance in reliability. Conventional pressure switches could not meet the established operational specifications.

The selection of a clustered engine arrangement for the SATURN booster was principally made on the following reasons:

1. The immediate availability was the main consideration for the selection of the cluster design. It is estimated that three to five years of development time can be gained. Moreover, the cluster is likely to stay ahead of the single engine as to its "state of the art" for many more years.

2. The development cost will be much lower than that for developing single chambers of the same output, as development problems may be encountered demanding additional funds to overcome unforeseen obstacles for single-engine development.

3. The manufacturing cost is likely to be lower, at least initially, because assembly-line production techniques can be employed to produce the larger number of smaller engines. The maintenance cost, especially for planned recovery operations, will be lower because smaller subsystems are less costly to replace.

4. The "one-engine-out" capability increases the reliability performance of the booster vehicle.

5. The cluster engine is shorter, and additional design effort would be required for the single engine to compete in this respect with the cluster version.

All these advantageous features should not erroneously imply that large-size single chambers are of no value. On the contrary, sufficient development time and funding can overcome the disadvantages of clusters:

A. Ground checkout of the clustered engines prior to launching and for all static firing operations will require more personnel and preparation time.

B. The cluster weight will always be higher than a competitive and properly designed single-engine version. For missions requiring maximum performance, single engines would thus be preferred.

C. Clustering for more powerful boosters would be difficult.

For these reasons, an early development of reliable single-chamber engines of more than one million pounds thrust output is considered vital for the very large space probes planned for the 1970's.

The control engineer needs to contribute to cluster and large single-engine developments in the following four areas:

1. Creation of new design ideas for breakthrough in dependability of components and systems.

2. Measurable increase of reliability performance by thorough test-to-failure and environmental testing prior to production, but maintained during production as a "quality assurance" type program.

3. Sizable improvements in manufacturing techniques and quality control procedures to augment the reliability program just mentioned.

4. Miniaturization of components without loss of reliability performance in order to permit redundancies to a greater extent than has been possible up to now.

Summarizing, I would like to stress also that space flight demands are oftentimes different from any of our ballistic missile needs. Although the precision and accuracy requirements are comparable in nature, the reliability will have to be stepped up by an order of magnitude if manned space flight is to be included. The demands for range and operating time are oftentimes in entirely different categories than they were during the missile era.

The Russian lead in this field makes it mandatory that we go to work quickly. The tremendous cost of the new ventures necessitates that we do the job right and with utmost efficiency. A good share of the task is yours!

	1953 REDSTONE Engine	1959 REDSTONE Engine
Regulators	4	1
Relief Valves	2	1
Solenoid Valves	12	4
Pressure Switches	6	2
Check Valves	3	0
Test Connections (Valve)	4	1
Pneumatic Filter	0	1
	31	10

Table I

Estimated Reliability of each Engine Cluster	Probability That All 8 Engines Function Properly	Probability That 7 or 8 Engines Function Properly	Probability That 6, 7 or 8 Engines Function Properly
100%	100%	100%	100%
99%	92.28%	99.74%	99.99%
98%	85.08%	98.97%	99.96%
97%	78.37%	97.76%	99.86%
96%	72.14%	96.18%	99.69%
95%	66.3%	94.3%	97.4%
90%	43.0%	81.3%	96.2%
85%	27.2%	65.7%	89.7%

Table II - Theoretical Cluster Reliability Comparison

ATTITUDE CONTROL OF SPACE VEHICLES

Dr. C. R. Gates
Chief of Guidance Systems Analysis
Jet Propulsion Laboratory
Pasadena, Calif.

Abstract

The problem of sensing and controlling the angular orientation of a space vehicle is discussed. Optical, radio, and inertial methods of angle-sensing are described, and application of control torques by reaction jets, flywheels, radiation pressure, and gravitational gradient are compared. Requirements for angular accuracy likely to be imposed by maneuvering, performing measurements for navigation, making scientific measurements, radio communication, and solar cell orientation are described. Attitude control requirements and techniques for earth satellites and deep-space probes are compared.

This discussion will not be published.

TRACKING AND PATH CONTROL

Dr. R. C. Booton, Jr.
Manager, Guidance and Navigation Department
Space Technology Laboratories, Inc.
Los Angeles, Calif.

Abstract

Problems and possible methods of controlling the path of a vehicle in free space are discussed. Difficulties in determining and relaying the vehicle's position are given particular attention.

There are no plans for publishing this discussion.

CONTROL OF THE HUMAN ENVIRONMENT

Dr. Paul Webb, Consultant
Yellow Springs, Ohio

Abstract

The human environment in space is controlled within fairly narrow limits, the range between the limits representing man's ability to adjust without serious strain. Broadly defined, environment includes the makeup of the gaseous artificial atmosphere, gas temperature, movement and humidity, the thermal radiation level, the mechanical force field, and the level of ionizing radiation. From the control standpoint, there is not much to be done about g-forces and radiation. The gaseous atmosphere and the thermal environment offer more opportunity to the control engineer. Biologically speaking, the controllable environment serves two major body functions, respiration and thermoregulation. In the isolated artificial atmosphere of a space cabin the environmental variables which affect these functions are closely interwoven. For example, water vapor pressure and gas movement are involved in both respiratory balance and heat balance. Various approaches to control of the human environment in space will be described. Simple automatic controls in present systems will be discussed. More complex control needs will be suggested for the future systems designed to carry man ever farther into space.

No plans have been made to publish this discussion.

SIGNAL STABILIZATION OF SELF-OSCILLATING SYSTEMS

R. Oldenburger
Purdue University
and
T. Nakada
Tokyo Istitute of Technology

Abstract

The hunt (self-oscillations) of a physical system may often be removed by the introduction of an appropriate stabilizing signal which changes the open loop gain of a closed loop system in a nonlinear manner. The theory of stabilization developed in this paper explains experimental results reported by R. Oldenburger in 1957. With the aid of Fourier series the designer can determine the periodic signal to be inserted at one point in a loop to yield a desired stabilizing input to a nonlinear element in the loop. This is illustrated by sinusoidal and triangular inputs to a nonlinear element. An example where a limiter is the only nonlinearity, is employed to illustrate the theory. The input-output characteristics of nonlinear elements are in practice always modified by the presence of extra signals such as "noise." Further, nonlinearities are always present in physical systems. The effect of extra signals on nonlinearities and system performance is thus of concern in the general study of physical systems, regardless of whether or not the problem of stability is involved. The results of this paper for the problem of stability extend readily to the problem of system performance for arbitrary disturbances.

This paper is to be published in the Proceedings of the First IFAC Moscow Congress by Butterworth Scientific Publications, in 1960.

A ROOT-LOCUS METHOD FOR THE ANALYSIS OF NONLINEAR SERVOMECHANISMS

Malcolm J. Abzug
Douglas Aircraft Company, Inc.,
El Segundo, Calif.

Summary

A root-locus method for the analysis of nonlinear servomechanisms is developed, using the complex convolution theorem of the Laplace transformation. The nonlinear servomechanisms that can be treated by this method are systems that contain nonlinear elements whose input-output relationships can be expressed in the form of power series. With some approximation this includes systems containing ideal relays and linear gains with dead zone.

Transfer functions are developed for odd-power and odd-root nonlinear elements. These transfer functions are valid only for sinusoidal inputs and are functions of the frequency as well as the Laplace Transform variable s. The method is illustrated by a root-locus analysis on a system that includes an ideal relay. Comparison with existing methods using the Kochenburger describing function and with transient solutions shows that the new method is reasonably accurate. The usual root-locus synthesis techniques may be applied to improve nonlinear system performance.

Introduction

Analytical techniques suitable for the analysis and synthesis of nonlinear servomechanisms are not only scarce, but are also incapable of treating all cases of interest. This situation represents an obstacle to the orderly development of the servomechanism field. Nonlinear servomechanisms offer important development possibilities. However, optimum designs will not be produced by cut-and-try methods but will require powerful synthesis techniques.

The present paper is a brief outline of a new analysis method for a class of nonlinear servomechanisms. The nonlinear servomechanisms considered are characterized by elements whose input-output relationships may be expressed by power series.

The approach used in this paper originated in a presentation[1] by Ernst Weber at the Brooklyn Polytechnic Institute's 1956 Symposium on Nonlinear Circuit Analysis. Weber presented a method for the transient analysis of nonlinear systems of the same type analyzed here by a root-locus method.

Variable-Gain Elements

There are variable-gain servomechanism elements whose input-output relationships can be expressed in terms of the following power series:

$$x_o = a_1 x_i + a_3 x_i^3 + a_5 x_i^5 + \cdots$$

$$\cdots + a_{1/3}\, x_i^{1/3} + a_{1/5}\, x_i^{1/5} + \cdots \quad (1)$$

Typical variable-gain elements described by Eq. (1) are shown in Figure 1. Approximations to an ideal relay and to a linear gain with dead zone are shown. H. D. Grief[2] has derived Kochenburger describing functions for simple variable-gain elements of this type. These describing functions give the element's output-to-input amplitude ratio in terms of the amplitude of the sinusoidal input. The describing function for variable-gain elements has no phase shift.

Transfer Function For Odd-Power Variable-Gain Elements

The Kochenburger describing function provides an approximation only to the frequency response of nonlinear elements. An actual transfer function of the Laplace Transform variable s may also be obtained for odd-power variable-gain elements, by complex convolution[3]. Thus, if

$$x_o = (x_i^n)_{n\ \text{odd}} \quad (2)$$

and the input is sinusoidal, i.e., $x_i = X_i \sin \omega t$,

$$\left[G^*(s,\omega)\right]_{\substack{\text{odd}\\ \text{power}}} = \frac{X_o(s,\omega)}{X_i(s,\omega)} = \frac{\mathcal{L}\left\{X_i^n \sin^n \omega t\right\}}{X_i\, \omega/(s^2+\omega^2)}$$

$$= \frac{X_i^{n-1}\, n!\, \omega^{n-1}}{(s^2+9\omega^2)(s^2+25\omega^2)\cdots(s^2+n^2\omega^2)} \quad (3)$$

This transfer function has the following properties that distinguish it from the usual linear transfer function of s:

1. The function G^* is valid only for sinusoidal inputs. The usual linear transfer function of s is independent of the input wave form.

2. The function G^* assumes various values depending upon the input frequency. The usual linear transfer function of s is independent of input frequency.

Transfer Function For Odd-Root Variable-Gain Elements

The transfer functions of variable-gain elements in which the cube root, fifth root, or other odd root of the input is taken cannot be obtained directly by complex convolution. Thus, if

$$x_o = (x_i^{1/n})_{n \text{ odd}}, \tag{4}$$

the Laplace transform of $\sin^{1/n} \omega t$ cannot be obtained by complex convolution of the transforms of known functions of time. However, the required transfer function may be obtained from the preceding results by adding in series a $1/n$-power variable-gain element to the output of an n-power variable-gain element. The final output must be identical to the initial input. The required transfer function must therefore be the inverse of Eq. (3) or

$$\left[G^*(s,\omega)\right]_{\substack{\text{odd} \\ \text{root}}} = \frac{(s^2+9\omega^2)(s^2+25\omega^2)\ldots(s^2+n^2\omega^2)}{X_i^{n-1}\, n!\, \omega^{n-1}} \tag{5}$$

Transfer Functions For Arbitrary Variable-Gain Elements

The input-output relationship of an odd-root variable-gain element is approximately that of an ideal relay. This approximation becomes increasingly better for smaller and smaller values of the fraction. Other nonlinear-control-system elements may be approximated by combinations of odd-power and odd-root variable-gain elements with other forms.

As an example, the combination of a linear gain with a cube-root variable gain produces a fair approximation to a linear gain with dead zone, as can be seen in Figure 1. The G^* transfer function for this combination, calculated from Eq. (5), is

$$\left[G^*\right]_{\substack{\text{linear gain} \\ \text{plus dead zone}}} = 1 - \frac{s^2+9\omega^2}{6X_i^2\ \omega^2}$$

$$= \frac{s^2+\omega^2\ (9-6X_i^2)}{-6X_i^2\ \omega^2} \tag{6}$$

The development of transfer functions for arbitrary variable-gain elements requires only that suitable analytical power series with finite numbers of terms be available to describe the input-output relationships of the elements involved.

Comparison of Transfer and Describing Functions For Variable-Gain Elements

The frequency-response amplitude ratios appropriate to the previously-derived transfer functions for variable-gain elements are obtained in the usual manner by the substitution of $j\omega$ for s. This step permits a direct comparison to be made between the exact frequency-response amplitude ratios and those provided by the Kochenburger describing function. In Table I and in Figure 2, this comparison is made for four simple variable-gain elements. Results of the comparison may be summarized as follows:

1. The describing function and the G^* transfer function are in exact agreement for the third- and fifth-power variable-gain elements.

2. The describing function underestimates the frequency-response amplitude ratio $|G^*(j\omega)|$ for values of input amplitude less than about 1.0 and overestimates it for values of input amplitude greater than about 1.0, for cube-root and fifth-root variable-gain elements.

Root Locus For System With Variable-Gain Elements

The development of transfer functions in which nonlinear-control-system elements are represented by pole-zero distributions suggests that the root-locus method of control-system analysis may be applied. Thus, from Equation (5), a cube-root variable-gain element is seen to contribute an infinite series of zeros on the imaginary axis, located at $s = \pm 3\, j\omega$. At constant values of frequency only one pair of zeros is involved, and a normal root locus may be constructed using these zeros and the poles and zeros for the remainder of the system.

The use of root-locus analysis on a system that includes an ideal relay in the forward path is illustrated in Figure 3. The relay is represented by the G^* transfer function for a cube-root variable-gain element. The open-loop transfer function for the entire system is

$$KG^* = \frac{K(s+3j\omega)(s-3j\omega)}{6E^2\,\omega^2 s(s+1)(s+4)} \tag{7}$$

Equation (7) contains the following:

1. Gain inversely proportional to the square of the system oscillation frequency.

2. Three conventional first-order poles.

3. An infinite set of second-order zeros, located on the imaginary axis at distances from the origin equal to plus and minus three times the system oscillation frequency.

For large values of frequency, such as 10, the imaginary-axis zeros are far from the origin and the root locus is similar to the locus for a linear system, except for the gain values. For small values of frequency the root locus remains close to the asymptote required by the three-pole, two-zero configuration. Instability is indicated in either case for sufficiently large values of the gain-error parameter K/E^2.

Comparison Of Root-Locus, Describing-Function, and Transient-Response Results

Typical transient responses to step inputs for the system including an ideal relay in the forward path are shown as the solid curves in Figure 4. To facilitate comparison with the root-locus method of this paper, the ideal relay is represented by a cube-root variable-gain element in these results. Stable limit cycles at a frequency of 2.0 radians per second with a gain-error-parameter value $K/E^{2/3} = 17.5$ may be predicted for this system by a Nyquist diagram using the Kochenburger describing function. Stable limit cycles are likewise predicted by the root loci of Figure 3 over a range of frequencies and values of K/E^2. A comparison of the root-locus, describing-function, and transient-response results for this system (Figure 5) shows that reasonably accurate results are obtained with the new method.

Effect of Compensation on Nonlinear-System Performance

Compensation to improve the performance of the previously discussed system including an ideal relay evidently involves the addition of poles and zeros to shift the loci of Figure 3 to the left. In particular, it is desired to move those loci at frequencies of 1.0 and above, that cross over into the right half-plane for gain-error-parameter K/E^2 values of about 15. This compensation was chosen as

$$(1.85\ s+1)/(0.185\ s+1) \qquad (8)$$

The compensated root loci are shown in Figure 6. Comparison with the original loci of Figure 3 shows that improved performance is obtained. As an example, for a frequency of 1.0, all closed-loop roots are in the left half-plane for the compensated system, as compared with all closed-loop roots in the right half-plane for the original system for values of K/E^2 above 24.0.

The effects of the compensation, which had been selected on a root-locus basis, on system transient behavior are illustrated as the dotted curves in Figure 4. Stable limit-cycle behavior is obtained again, but the oscillation amplitude is greatly reduced and the oscillation frequency is higher.

The analysis method introduced in this paper, which uses the G^* transfer function in a root locus, presents the characteristics of a nonlinear system as a set of conventional root loci. This approach permits the body of existing experience on the compensation of root loci to be applied.

Conclusions

The following conclusions may be drawn regarding the root-locus method for the analysis of nonlinear servomechanisms presented in this paper:

1. Variable-gain elements, which appear in some nonlinear servomechanisms, have exact transfer functions of the Laplace Transformation variable s, for sinusoidal inputs.

2. Transfer functions of the above type, called G^* transfer functions, exist for elements whose input-output relationship may be expressed in a power series. With some approximation, this includes ideal relays and linear gains with dead zone.

3. The frequency response provided by the Kochenburger describing function is exact for odd-power variable-gain elements but is only approximately correct for odd-root variable-gain elements.

4. Root-locus analysis employing the G^* transfer function provides a reasonably good prediction of system transient response. Synthesis of compensating networks is facilitated, since the characteristics of the composite nonlinear system are presented as a set of conventional root loci.

References

1. Weber, Ernst: Complex Convolution Applied to Nonlinear Problems. Proceedings of the Symposium on Nonlinear Circuit Analysis, Volume VI, pp 409-427. Polytechnic Institute of Brooklyn, New York, April 1956.

2. Grief, H. D.: Describing Function Method of Servomechanism Analysis Applied to Most Commonly Encountered Nonlinearities, Trans. AIEE, Part II, Applications and Industry, Vol. 72, pp. 243-248, 1953.

3. Gardner, M. F., and Barnes, J. L.: Transients in Linear Systems, John Wiley and Sons, Inc., New York, 1942.

TABLE I

DESCRIBING FUNCTIONS, FREQUENCY-RESPONSE AMPLITUDE RATIOS AND TRANSFER FUNCTIONS FOR SIMPLE VARIABLE-GAIN ELEMENTS

ELEMENT	$x_o(t)$	DESCRIBING FUNCTION	FREQUENCY-RESPONSE AMPLITUDE RATIO $\lvert G^*(j\omega) \rvert$	TRANSFER FUNCTION $G^*(s,\omega)$
CUBIC	x_i^3	$\frac{3}{4} X_i^2$	$\frac{3}{4} X_i^2$	$\frac{6 X_i^2 \omega^2}{s^2 + 9\omega^2}$
FIFTH-POWER	x_i^5	$\frac{5}{8} X_i^4$	$\frac{5}{8} X_i^4$	$\frac{120 X_i^4 \omega^4}{(s^2+9\omega^2)(s^2+25\omega^2)}$
CUBE-ROOT	$x_i^{1/3}$	$\frac{1.16}{X_i^{2/3}}$	$\frac{4/3}{X_i^2}$	$\frac{s^2 + 9\omega^2}{6 X_i^2 \omega^2}$
FIFTH-ROOT	$x_i^{1/5}$	$\frac{1.20}{X_i^{4/5}}$	$\frac{8/5}{X_i^4}$	$\frac{(s^2+9\omega^2)(s^2+25\omega^2)}{120 X_i^4 \omega^4}$

ANALYTIC VARIABLE-GAIN ELEMENTS

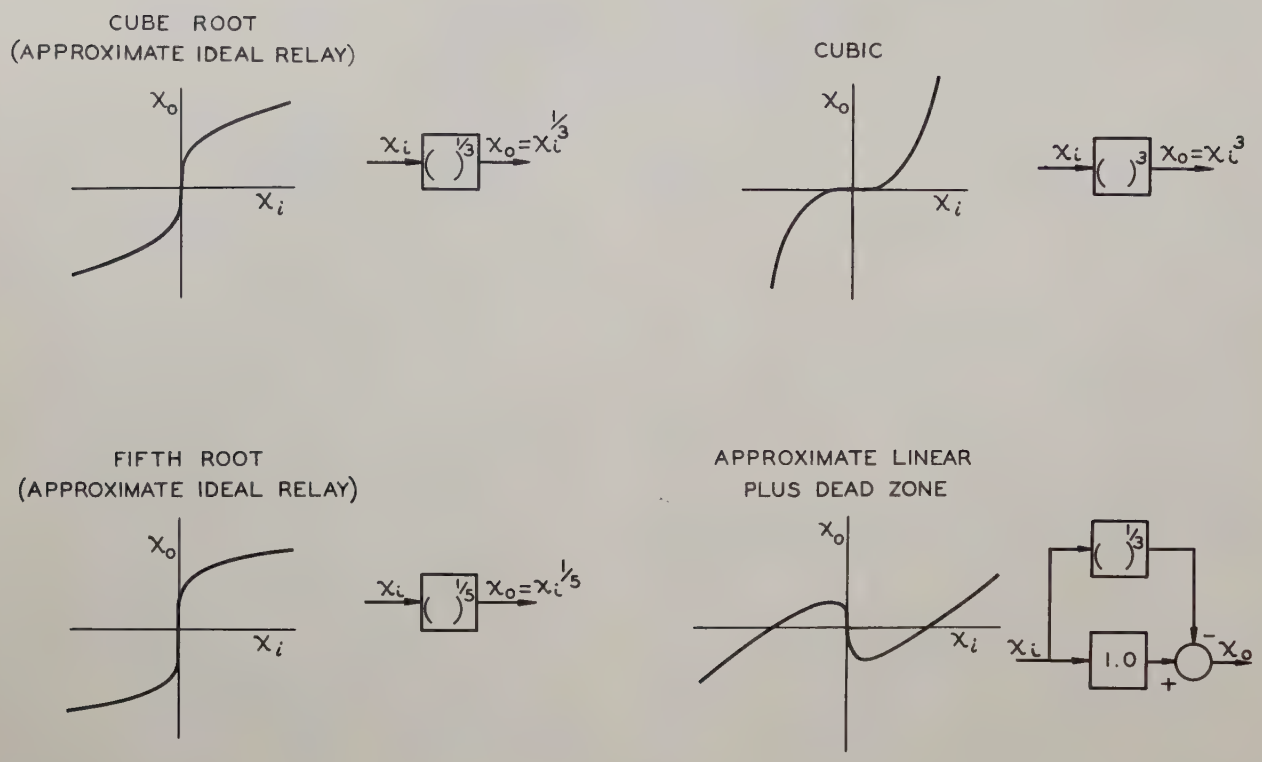

Fig. 1.

EXACT AND APPROXIMATED FREQUENCY RESPONSES

VARIABLE-GAIN ELEMENTS

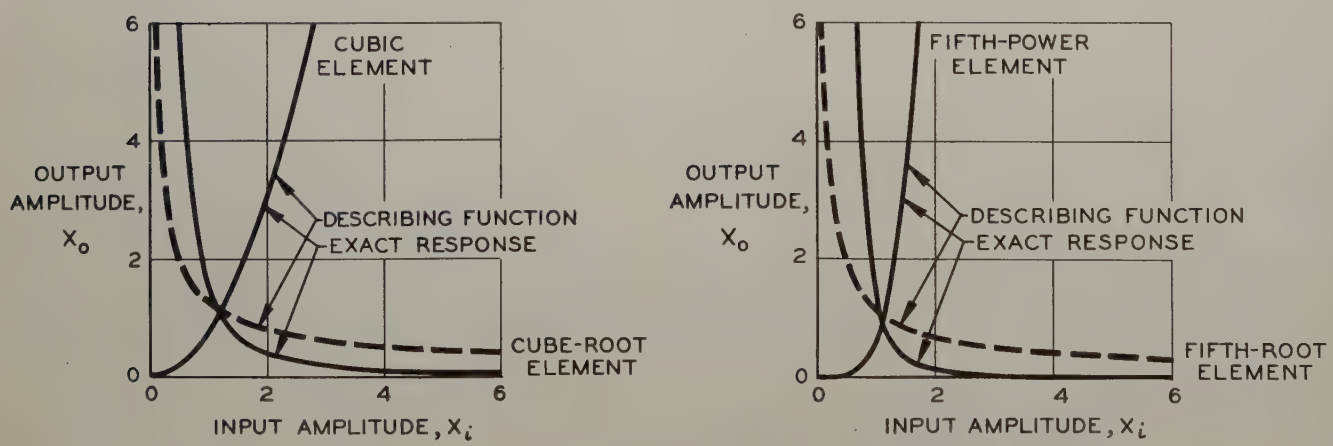

Fig. 2.

CONSTANT-FREQUENCY ROOT LOCI

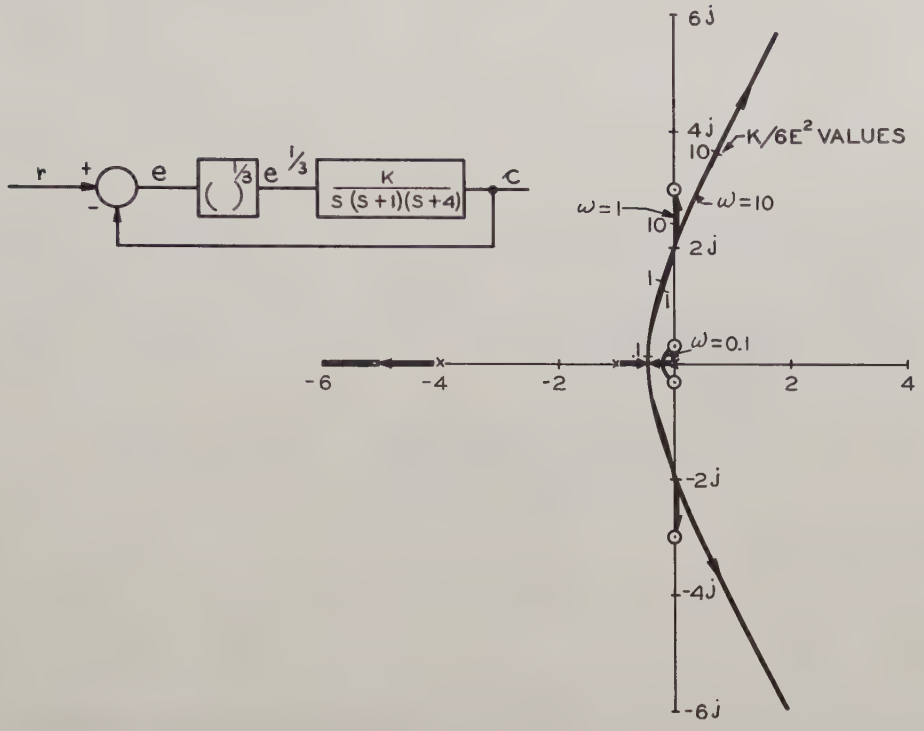

Fig. 3.

EFFECT OF GAIN ON ERROR RESPONSE

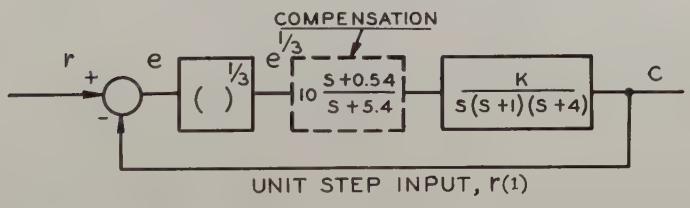

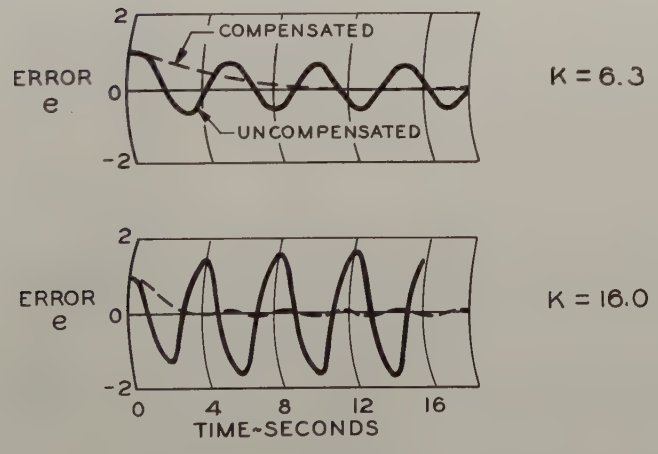

Fig. 4.

MEASURED AND PREDICTED LIMIT CYCLES

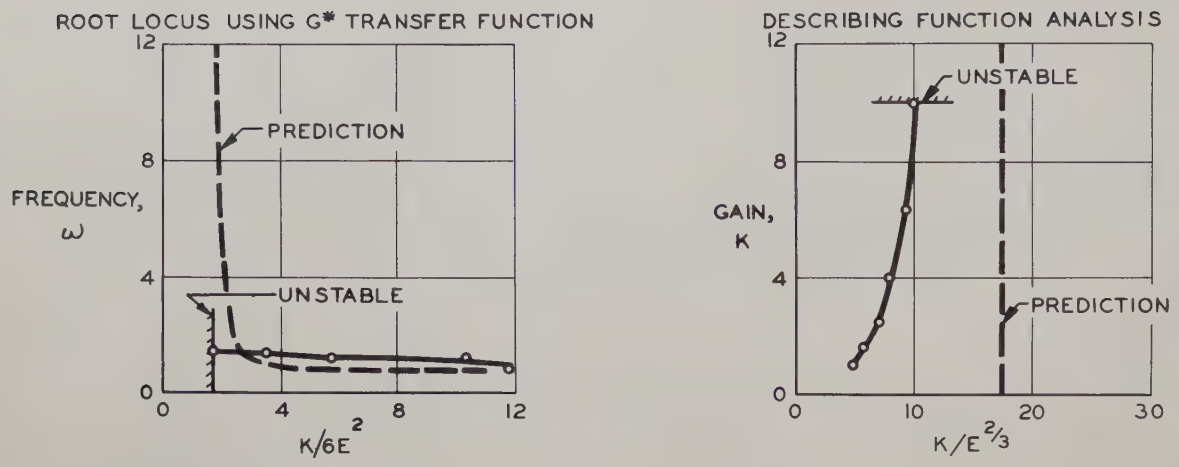

Fig. 5.

CONSTANT-FREQUENCY ROOT LOCI FOR COMPENSATED SYSTEM

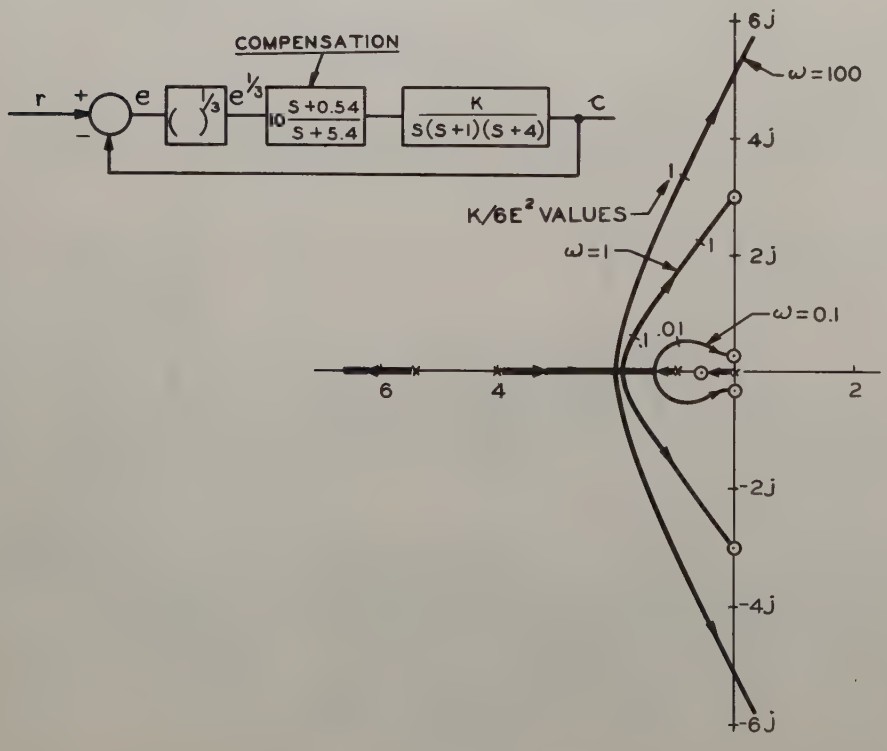

Fig. 6.

SOME NONLINEAR CONTROL TECHNIQUES NOVEL TO CONTROL ENGINEERS EMPLOYED BY A BIOLOGICAL CONTROL SYSTEM

M. Clynes
Rockland State Hospital
Orangeburg, N. Y.

Abstract

The nervous control of heart rate in man was studied through dynamic analysis of experimental results and computer simulation. The heart rate changes caused by respiration were found to be accurately analyzable and predictable, as related by a fifth-order nonlinear differential equation which proved to have specific physiological meaning. The nonlinear characteristics of the equations are interesting in that they also show how neural controls can produce certain dynamic characteristics not normally encountered in control engineering practice.

This paper is to be published in the Proceedings of the First IFAC Moscow Congress by Butterworth Scientific Publications in 1960.

ON THE ANALYSIS OF BI-STABLE CONTROL SYSTEMS

B.E. Amsler and R.E. Gorozdos
Johns Hopkins University, Applied Physics Laboratory
Silver Spring, Maryland

Summary

The basic theory of bi-stable oscillating loop control is first summarized using standard describing function concepts. The effective transfer characteristic of the bi-stable switch is defined in terms of the ratio of both amplitude and frequency of the control error signal to amplitude and frequency of the loop oscillation signal. The effect of variation in loop oscillation amplitude with low frequency control error amplitude is considered. The relationship between switch gain at control frequencies and switch gain at oscillation frequency is noted. The inherent insensitivity of the bi-stable oscillating system to variations in linear loop parameters is discussed. The effect of variation in loop gain of the bi-stable system is compared with the effect of equal variations in a similar linear system.

The possibility of bi-stable loop oscillation at more than one frequency is considered. The conditions are defined which insure oscillation at the intended oscillation frequency. Analog simulation tests used to verify these loop oscillation criteria are outlined.

Basic Theory of Bi-Stable Operation

A bi-stable system is simply the familiar "bang-bang" control system in which the overall loop oscillates about the desired value of the output. Control is achieved by a switching action which applies full control first in one direction and then in the other. The performance of such a system may be defined by specifying a pseudo-linear equivalent gain for the bi-stable element. The magnitude of this low frequency equivalent gain is dependent upon the amplitude of the high frequency loop oscillation signal as it appears at the input to the bi-stable element. In the case of a control system where the loop gain is greatly attenuated at frequencies above the oscillation frequency, the higher order harmonics contained in the oscillation signal are negligible and the oscillation signal may be taken as sinusoidal at the input to the bi-stable switch. The addition of a low frequency control signal then acts to vary the time proportioning of the switching action. This in turn results in a corresponding variation in the output. The basic characteristics of such a system have already been treated in considerable detail so that only a brief summary will be included herein.[1-2]

A simple bi-stable control system is shown in Fig. 1. For purposes of discussion the system error signal E(t) will be separated into two components A(t) and B(t) such that A(t) is the error component due to loop oscillation and B(t) is the additional component due to introduction of a system input signal R(t). The bi-stable switch is indicated by element N. The magnitude of the switch output is L; the sign of the output is the sign of E(t). For the case shown loop oscillation frequency is

$$\omega_o = \frac{1}{\tau},$$

the frequency at which overall loop phase is 2 radians.

Consider first the case where R(t) = 0, B(t) = 0. The amplitude of the fundamental component of switch output is $\frac{4L}{\pi}$. Thus the amplitude of the oscillating input to the switch is given by:

$$|A| = \frac{4}{\pi} L \left| \frac{K}{s(\tau s + 1)^2} \right|_{s = j\omega_o} \qquad (1)$$

For constant amplitude oscillation the effective loop gain at oscillation frequency must be unity. Thus (assuming stable oscillation does occur) the effective gain of the switching element must vary with the linear system parameters in order to maintain exactly unity loop gain at $\omega = \omega_o$. This effective gain at oscillation frequency is in general given by

$$K_o = \frac{1}{|G(j\omega_o)|} \qquad (2)$$

where $G(j\omega_o)$ is the gain of the linear loop elements at $\omega = \omega_o$.

Now consider the case where R(t) ≠ 0. The significant signal waveforms are shown in Fig. 2. For the moment consider only the case where all significant components of R(t) occur at d.c. The resultant d.c. signal component at the input to the switch is B(t); the total input to the switch is thus A(t) + B(t). It is seen that the combination A(t) + B(t) acts to provide dwell time modulation of the square wave C(t) and thus a change in the d.c. system output C(t). From Fig. 2 it is evident that the rate of change of C(t) is a function of the relative amplitude of A(t) and B(t). A decrease in A(t) will result in an increase in the value of C(t) and vice versa. Working directly from Fig. 2 it can be shown that

$$\bar{\dot{C}} = L\frac{2}{\pi}\sin^{-1}\left(\frac{B}{A}\right) \qquad (3)$$

where $\bar{\dot{C}}$ is the amplitude of the d.c. (signal) component of $\dot{C}(t)$. The non-dimensionalized plot of $\bar{\dot{C}}$ versus B/A as defined by Eq. 3 is given as the "d.c." case in Fig. 3.

The d.c. equivalent switch gain as defined by Eq. (3) is seen to vary with both the d.c. error signal amplitude and amplitude of the fundamental component of loop oscillation signal. If the oscillation amplitude A is constant then the gain is specified directly as a function of input error signal amplitude B. However, in any oscillating loop system the amplitude A of the fundamental component of the oscillating switch input signal also varies as a function of the control error signal amplitude B. Thus the effect of variation of amplitude A with B must also be considered.

Referring again to Fig. 2, the amplitude of the fundamental component of switch output oscillation frequency is given by:

$$\dot{C}_1 = \frac{4L}{\pi}\sin\frac{\pi}{T}\left(\frac{T}{2} - 2\Delta T\right)$$

and since $\Delta T = \frac{T}{2\pi}\sin^{-1}\frac{B}{A}$

$$\dot{C}_1 = \frac{4L}{\pi}\left[\sin\frac{\pi}{2} - \sin^{-1}\frac{B}{A}\right] = \frac{4L}{\pi}\cos\left[\sin^{-1}\frac{B}{A}\right]$$

Now taking $\dot{C}_{10} = \left[\dot{C}_1\right]_{B=0} = \frac{4L}{\pi}$ it is seen that

$$\frac{\dot{C}_1}{\dot{C}_{10}} = \cos\left[\sin^{-1}\frac{B}{A}\right]$$

However A is proportional to $\dot{C}_1$ and defining $A_o = A$ when $B = 0$

$$\frac{A}{A_o} = \cos\left[\sin^{-1}\frac{B}{A}\right]$$

from which may be obtained

$$\sin^{-1}\frac{B}{A} = \frac{1}{2}\sin^{-1}\frac{2B}{A_o}$$

Thus, substituting in Eq. (3) the following relationship is obtained:

$$\bar{\dot{C}} = \frac{L}{\pi}\sin^{-1}\frac{2B}{A_o} \qquad (4)$$

and

$$K_N^1 = \frac{\bar{\dot{C}}}{B} = \frac{L}{\pi B}\sin^{-1}\frac{2B}{A_o} \qquad (5)$$

where K_N^1 is the effective value of d.c. switch gain for an oscillating loop system and A_o is the amplitude of oscillation input to the switch when the low frequency control error signal amplitude $B = 0$.

Thus far in the analysis it has been assumed that significant variations in amplitude, B, of the control error component of switch input occur only over many cycles of loop oscillation frequency. However, the analysis has also been extended to cover the case when

$$A(t) = A\sin\omega_o t$$

$$B(t) = B\sin(\omega_s t + \theta)$$

with

$$\omega_o = \frac{p}{q}\omega_s$$

where p and q are such that $p > q$, insuring that $\omega_o > \omega_s$. The analytical work involved is quite lengthy; a summary of this work has been included in the Appendix. However, the results may be simply stated as follows:

For small amplitudes of control error component of switch input the effective gain of the switch at the control error frequency is given by

$$K_N = \frac{2L}{\pi A_o} \qquad (6)$$

for all values of p and q such that $p > q$. Note that this is precisely the result obtained by taking B/A_o small in Eq. 5. For larger values of B/A, the equivalent gain is a function of p and q. A normalized plot of the effective control output versus B/A for various values of p and q is given in Fig. 3. The curves shown for $p = 3$, $q = 1$ and $p = 2$, $q = 1$ represent the upper and lower limits for all p and q. Furthermore, only slight phase shift is introduced into the control signal component by the switching operation even for small values of the ratio p/q. For example with $B/A = .5$ a phase shift of at most 7 degrees is introduced by the switching operating for $p/q = 3$. For all other p/q smaller control signal phase shift is obtained. (See Table I, Appendix). The simple gain value defined by Eq. 6 is of course satisfactory for use in any perturbation study. The curves given in Fig. 3 also indicate that the value of K_N given in Eq. 6 may be used in almost any analysis study in which values of switch input $B > A_o/2$ need not be considered.

On the other hand, it should be noted that values of effective gain K_N are not even defined by Eq. 5 for $B > A_o/2$. This results from the fact that stable loop oscillation can not exist for $B > A_o/2$. In particular if B is raised to and held at value slightly above $A_o/2$ the loop oscillation will die out. Thus the value of low frequency output C will change from L/2, the value obtained for $B = A_o/2$, to L, the value obtained with no loop oscillation. Furthermore, loop oscillation can not be reinitiated until the low frequency error B is reduced to near zero. In a practical case the particular combination of error amplitude for $B > A_o/2$ together with error frequency will determine whether or not the loop oscillation amplitude will be further modulated

by this phenomenon. In the limit a special low frequency loop oscillation characterized by a variation in amplitude of the loop oscillation can result.

Now consider the relationship between the gain of the bi-stable element loop oscillation frequency, K_o, and the gain, K_N, obtained for small B.

Combining Eqs. 2 and 6, we obtain

$$\frac{K_o}{K_N} \times \left| \frac{1}{G(j\omega_o)} \right| \times \frac{\pi A_o}{2L}$$

But from Eq. 1

$$A_o = \frac{4}{\pi} L \left| G(j\omega_o) \right|$$

for $B \to 0$. Thus,

$$\frac{K_o}{K_N} = \frac{1}{\left| G(j\omega_o) \right|} \times \frac{\pi}{2L} \times \frac{4}{\pi} L \left| G(j\omega_o) \right|$$

and

$$\frac{K_o}{K_N} = 2 \qquad (7)$$

Thus the gain of the switch element at oscillation frequency is always just twice the effective low frequency gain, for small amplitudes of control error signal.[1-2]

This relationship may be used to analyze the performance characteristics of such a system for the smaller amplitudes of control error. Consider the example defined by Fig. 1. Based on previous analysis, it is known that for stable oscillation and small B

$$K_o \left| G(j\omega_o) \right| = 1$$

$$\angle G(j\omega_o) = -180^\circ$$

where K_o is the equivalent linear gain of the switch element at oscillation frequency. Thus the loop conditions at stable oscillation frequency ω_o are defined by the point -180° and 0 db on a Nichols plot of the open loop transfer. However, by Eq. 7, the effective low frequency gain of the switch element is one-half the oscillation value. The overall equivalent linear open loop Nichols plot may always be constructed by starting at the frequency ω_o with a gain of -6 db and a phase of -180°.[1]

Insensitivity of the System to Variations in Loop Parameters

From Eqs. 5 and 6 it is seen that the effective low frequency forward loop gain varies inversely as the amplitude A of the oscillation signal at the input to the bi-stable element. If the value of the linear gain K, in Fig. 1, were changed, the amplitude of the input to the switch, A, would also change. This would result in an exactly compensating change in K_N the equivalent gain of the switching element. Such a system would be quite insensitive to variations in linear system parameters, since the change in K_N exactly compensates for the change in K. The loop performance would not be affected by variations in the linear loop gain (assuming of course that the system exhibited negligible dead space and saturation effects over the operating range being considered).

The inherent insensitivity of the bi-stable oscillating system to variation in linear loop parameters can be assessed by considering the effect of some possible variations. For example, addition of an extraneous linear lag in the region $\omega = 2\omega_o$ would have little effect on the gain curve for $\omega < \omega_o$. However, significant increase in phase lag for $\omega > \omega_o/3$ would be obtained. In the case of a linear servo, such an increase in lag would certainly result in a modified response characteristic and could lead to catastropic instability. However, in this non-linear case a new oscillation frequency ω_o' is established at $\omega_o' < \omega_o$. The linear loop gain at this lower frequency is greater than that obtained at $\omega = \omega_o$; the oscillation signal at the switching element input is thus increased resulting in a decrease in equivalent low frequency loop gain K_N. Thus the effective response characteristics are little changed except for the ultimate reduction in system bandwidth obtained with reduced oscillation frequency. In general it is seen that such a system is also relatively insensitive to significant variations in loop phase as well as changes in loop gain. It thus exhibits some of the characteristics of parameter adaptive control while considerable less attention to individual parameter tolerances is required in the design of a practical system of this type.

The inherent insensitivity to loop gain variations is demonstrated in Fig. 4. A simple third order system was simulated on an analog computer. A system having an identical linear loop transfer was also simulated with a constant gain in place of the bi-stable switch element. The open loop linear gain of both simulations was varied as shown. The resultant response to step input is reproduced in Fig. 4. The complete insensitivity of the bi-stable system to these variations in linear loop gain is clearly evident.

Multiple Oscillation Modes in a Bi-Stable System

In the design of a practical system of this type there exists a special fundamental problem which must be considered. In particular, it is required that the intended oscillation frequency be maintained even in the presence of other extraneous loop oscillation modes. It is sometimes found that the -180° loop phase condition occurs at more than one frequency. For example, in an electro-mechanical control system this

condition would occur at normal loop crossover; it might also occur at the mechanical resonant frequency of the output member. Conversely, in a conditionally stable system containing an inherently un-stable element to be controlled, loop oscillation may develop near the low frequency pole associated with the unstable element.

Thus it is necessary to determine:

(a) which of the possible loop singularities (-180° phase condition) represent stable (constant amplitude and frequency) modes and which are the unstable modes at which a particular frequency and amplitude of oscillation cannot be maintained.

(b) the criteria for insuring that a particular desired mode is maintained so that the operating point does not shift to some undesired mode.

The general principles will be illustrated by means of a specific example.

The block diagram for a simple system having more than one possible oscillation mode is shown in Fig. 5. Note that this system is the same as that of Fig. 1 except that there are two feedback paths. It will be assumed that $T_2 \ll T_1$, $K_2 \ll K_1$ and $\zeta_2 \ll 1.0$. The resultant linear loop Bode plot is shown in Fig. 6 for a case where $K_2 = K_1/16$, $T_2 = T_1/8$, $\zeta = .01$. The three possible oscillation conditions (phase = -180°) are circled. The linear loop gain level K_1 was arbitrarily chosen as shown. This, together with the limit level, determines the oscillation amplitude.

For the type of system herein considered it can be shown that the oscillation mode is stable if, at the condition of loop phase = -180°, the phase lag is increasing with increasing frequency. Conversely, decreasing lag with increasing frequency defines an unstable system mode.[3] Thus stable oscillation is, in general, possible at the points $\omega = 1.16/T_1$, and at $\omega = 8.0/T_1$. On the other hand, the point at $\omega = 3.4/T_1$ is an unstable point. This point therefore represents a boundary condition between the two possible stable states. Assuming that certain additional requirements discussed below are satisfied, then the frequency will always return to the lower value for an initial condition of energy less than that defined by the unstable point. For an initial energy higher than the value defined by the unstable point, the oscillation will stabilize at the higher frequency condition. Note that the conditions are alternately stable, unstable, etc. This is in accordance with a general principle of mechanics which requires that for any system, two like (stable or unstable) singularities are always separated by a singularity of the opposite kind.[4]

In a practical control application we would, in general, want only a particular mode to be excited. For example, bi-stable oscillation at a structural resonance mode of a control output member could be catastropic. However, it is entirely possible that some large system transient or noise signal would momentarily drive the system to energy levels beyond that defined by the unstable singularity. This could result in a shift in mode even though this mode was not normally excited. Thus we must define the criterion which insure that oscillation will not occur at some undesired operating mode.

To define this criterion, let us initially assume that a system of the form being considered is oscillating at the higher frequency mode. The overall "low frequency" pseudo-linear Nichols plot can then be drawn by starting with the point -6 db; -180° at oscillation frequency. The typical plot for this particular case is sketched in Fig. 7 as the solid curve. For this particular plot the parameters of Fig. 6 are assumed with the exception of ζ_2 which is raised to 0.05. On a pseudo-linear basis the system is now unstable at the lower frequency point $\omega = 1.16/T_1$ rad/sec. Oscillation will build up at this frequency and take over control of the system. A new pseudo-linear plot results (shown dotted in Fig. 7). Thus in general it is seen that if the linear loop gain at the lower oscillation frequency exceeds that at the higher frequency by more than a factor of two, stable oscillation at the higher frequency is not possible.

The corresponding conditions for insuring that loop oscillation will occur at only the higher of the two frequencies must also be established. Again the criterion is best defined by first assuming oscillation at the lower frequency and then determining the loop conditions which will isure a shift to the higher frequency oscillation mode. We will consider a case wherein the higher oscillation frequency is near to but not exactly an odd harmonic of the lower frequency. Let ω_1 be the lower (assumed) oscillation frequency and ω_2 be the possible higher frequency mode of oscillation where N is an odd integar. The harmonic of ω_1 near $\omega = \omega_2$ is $N\omega_1$. Note that N can only be odd in the absence of a steady state loop error component.

Normal describing function theory assumes that only the fundamental component of switch output is important in determination of the loop operating point. However, if this were true a shift to the higher frequency operating point could not occur, and the higher frequency components of switch output must also be taken into account. Under conditions of a steady state loop oscillation the total switch output signal is given by

$$\dot{C}(t) = \sum_{N = 1,3,5--} \frac{4L}{N\pi} \sin N\omega_1 t$$

Thus the switch input is given by

$$A(t) = \sum_{N = 1,3,5--} \frac{4L}{N\pi} \left|G(jN\omega)\right| \sin (N\omega_1 t + \phi_N)$$

where $G(jN\omega_1)$ is the linear loop transfer for each of the various harmonic components of the square wave switch output. In a majority of practical cases only the fundamental plus the signal component which is near the higher oscillation mode frequency are of significant amplitude. In order to facilitate the analysis this assumption will be made. Thus the switch input is given by

$$A(t) = \frac{4L}{\pi}\left[\,|G(j\omega_1)|\,\sin(\omega_1 t + \phi_1) + \frac{|G(jN\omega_1)|}{N}\,\sin(N\omega_1 t + \phi_N)\right] \qquad (8)$$

where ϕ_1 and ϕ_N are the loop phase shift at $\omega = \omega_1$ and $\omega = N\omega_1$. The switch output and two possible input signal conditions for a case where N = 7 are shown in Fig. 8. Note that with the switch input as shown in Fig. 8 oscillation will be maintained at the lower frequency mode. That is, no further increase in the amplitude of the seventh harmonic signal at switch input can occur in the absence of an extraneous input signal since switching frequency is ω_1. On the other hand if the input amplitude at $\omega = N\omega_1$ were sufficiently increased an additional switch reversal could be made to occur. Note that a further increase in amplitude of the seventh harmonic of switch input would then be obtained as a result of the additional switch reversals. Thus a further increase of high frequency switch input component would result and the oscillation would build up at the upper frequency $N\omega_1$.

It is seen that in general a shift of oscillation to the higher mode can occur in the absence of external forcing signal only if

$$A(t) < 0 \text{ for } 0 < t < \frac{\pi}{\omega}$$

The actual conditions for oscillation mode shift for the general case of non-periodically related modes may be defined as follows. A possible linear loop transfer function was shown in Fig. 6. Let us designate the lower possible oscillation frequency as ω_1 and the higher as ω_2. For purposes of this discussion assume that a particular odd harmonic of ω_1, the lower oscillation frequency, occurs at $\omega = N\omega_1$, which is near to but below the frequency of the higher mode. The conditions for switch reversal are given by setting A(t) in Eq. (8) equal to zero. It was assumed that $\phi_N < 180^\circ$. Thus Eq.(8) can only be satisfied if $\phi_1 > 180^\circ$.

Thus the oscillation frequency ω_1 is "pulled" toward a higher frequency, that is toward ω_2/N. Conversely, if $N\omega_1 > \omega_2$ the frequency would be lowered by any increase in amplitude of switch output at $\omega = N\omega_1$.

The conditions at steady state oscillation with $\omega = \omega_1$ are defined by setting A(t) in Eq.8 equal to zero for $\omega_1 t = 0$. Thus

$$\frac{|G(jN\omega_1)|}{N\,|G(j\omega_1)|} = -\frac{\sin\phi_1}{\sin\phi_N} \qquad (9)$$

In any particular case the resultant value of steady state oscillation frequency together with appropriate gain and phase values can be determined directly using Eq. 9 together with the overall gain and phase characteristics of the system. In this general case where ϕ_1 and ϕ_N are not equal to 180° the condition for unforced shift of oscillation to the higher mode will occur very near to $N\omega_1 t + \phi_N = 3\pi/2$. Substituting this value into Eq. 8 the following gain and phase conditions are defined in order that mode shift can occur.

$$|G(jN\omega_1)| > |G(j\omega_1)|\,N\,\sin\left(\frac{3\pi}{2N} - \frac{\phi_N}{N} + \phi_1\right) \qquad (10)$$

Eqs. 9 and 10 may be employed together with the loop phase and gain characteristics to determine whether or not an undriven mode shift from lower to higher frequency will occur.

One important point should be noted. In many, if not most, of the practical cases an undriven shift from the lower to higher mode may be achieved by a simple increase in gain at the upper critical frequency. For example, in the case defined by Fig. 5 with parameters as defined by Fig. 6 a reduction in the value of the quadratic damping coefficient ζ_2 will always cause mode shift. On the other hand, a different selection in the value of the ratio τ_1/τ_2 will result in a case where undriven shift will not occur for any value of ζ_2. Whether or not the shift will occur may of course be determined from Eqs. 9 and 10.

In order to check the validity of the conclusions outlined above a system similar to that shown in Fig. 5 was simulated on the analog computer. Various values of τ_1/τ_2, K1 and K2 were set into the simulation. The value of which resulted in shift of oscillation mode was noted. Excellent correlation was obtained between measured and predicted values over a rather wide range of parameter variations.

Conclusions

The salient results of the work described above may be summarized as follows:

1. The effective transfer characteristic of the bi-stable switch is a function of the ratio of control error to loop oscillation signal amplitude. The effective transfer is also a function of the ratio of control error to loop oscillation signal frequency. However for switch input signal amplitudes less than about one quarter of the quiescent loop oscillation signal amplitude, the transfer characteristic may be taken as inversely proportional to the loop oscillation signal amplitude. Furthermore, in this case only negligible phase shift of the control error signal is produced by the switching action.

2. The oscillating loop type of system is inherently insensitive to variations of linear loop gain. This insensitivity is a direct consequence of the relationship between loop oscillation signal amplitude and effective switch transfer characteristics as noted above.

In the case of a control system having more than one possible oscillation mode it has been shown that

3. Stable oscillation will only occur at the lower of two possible loop oscillation frequencies when

$$|G(j\omega_1)| > 2 \quad |G(j\omega_2)|$$

where ω_1 is the lower and ω_2 the higher loop oscillation frequency.

4. Stable loop oscillation may occur at either of the two frequencies when

$$|G(j\omega_1)| < 2 \quad |G(j\omega_2)| \ .$$

Whether or not stable oscillation will occur at only the upper of the two frequencies may be determined by applying Eqs. 9 and 10.

5. In those cases where both oscillation modes are stable, selection of the particular oscillation mode is determined by the system input signal or initial conditions.

Appendix

The d.c. equivalent switch gain has been determined for the case where $\omega_o \gg \omega_s$ and is given in Eq. 4. The equivalent switch gain will now be determined for $\omega_s = q/p\ \omega_o$ where $p > q$.

In the system shown in Fig. 1 let $E = A + B$ where A is the error component due to loop oscillation and B is the additional component due to the signal R. Assume $A(t)\ A \sin(\omega_o t + \theta)$ and $B(t)\ B \sin q/p\ \omega_o t$. It can be shown that the equivalent switch gain is a continuous monotonic function of $k = B/A$ and a discontinuous but bounded function of ω_s. It will be assumed that A(t) is not a function of B(t). The error introduced by this approximation will be discussed subsequently.

If p/q is a rational number, $\dot{C}(t)$ will be periodic. If q/p is not a rational number, C(t) will not be periodic. These two cases will be considered separately.

A. Non-Periodic Case

The method used here was used by Bennett[5] and later by Bennett and Kalb[6] in analyzing modulation products. The output of the switch can be expanded as follows:

$$\dot{C}(t) = \dot{C}(x,y) = \sum_{m=0} \sum_{n=0} A_{mn} \cos(mx + ny) + B_{mn} \sin(mx + ny)$$

where $x = pt$ and $y = qt$.

The coefficients are given by

$$A_{mn} = \frac{1}{2\pi^2} \int_{-\pi}^{\pi} \int_{-\pi}^{\pi} \dot{C}(x,y) \cos(mx + ny)\, dx\, dy$$

$$B_{mn} = \frac{1}{2\pi^2} \int_{-\pi}^{\pi} \int_{-\pi}^{\pi} C(x,y) \cos(mx + ny)\, dx\, dy$$

Since $\dot{C}(t)$ is not periodic, there is no loss in generality in assuming θ to be zero.

$$\dot{C}(x,y) = +L \text{ if } \sin x + k \sin y > 0$$

$$= -L \text{ if } \sin x + k \sin y < 0$$

Since $\dot{C}(x,y)$ is an odd function, A_{mn} will be zero. The equivalent switch gain can be determined from B_{01}. By changing variables and inserting the value of $\dot{C}(x,y)$

$$B_{01} = \frac{4L}{\pi^2} \int_0^{\pi} \int_0^{\alpha} \cos y\, dx\, dy$$

where $\alpha = \cos^{-1}(-k \cos y)$

$$B_{01} = \frac{4Lk}{\pi^2} \int_0^{\pi} \frac{1 - \cos^2 y}{\sqrt{1 - k^2 \cos^2 y}}\, dy$$

This can be expressed in terms of complete elliptic integrals of the first and second kind.

$$B_{01} = \frac{8L}{k\pi^2} \left[E - (1 - k^2)K\right]$$

where K and E are the complete elliptic integrals of the first and second kind.

The equivalent switch gain is defined as the ratio of B_{01} to B.

$$K'_N = \frac{B_{01}}{B} = \frac{8L}{\pi^2 k^2 A} \left[E - (1 - k^2)K\right]$$

By expanding E and K into a power series in k

$$K'_N = \frac{2L}{\pi A} \left(1 + \frac{1}{8} k^2 + \frac{3}{64} k^4 + \frac{25}{1024} k^6 + \ldots.\right) \tag{11}$$

B. Periodic Case

In this case, the function C(t) can be expanded as follows:

$$\dot{C}(t) = \sum_{n=0} A_n \cos nt + \sum_{n=1} B_n \sin nt$$

First assume $\theta = 0$. Then $A_n = 0$. The harmonic of interest is B_q.

$$B_q = \frac{2}{\pi} \int_0^{\pi} \dot{C}(t) \sin qt \qquad (12)$$

The pulse width modulated signal $C(t)$ can be resolved into two components.

$$\dot{C}(t) = \dot{C}_S(t) + \dot{C}_I(t)$$

$\dot{C}_S(t)$ is the square wave which is obtained when $k = 0$. B_q will not be a function of $C_S(t)$. $C_I(t)$ contains the necessary information to compute B_q. It will consist of a series of pulses of width α_r and amplitude $\pm 2L$. There will be exactly p values of α in the interval from 0 to k. Call these values α_r, $r = 1,2,3 \ldots p$. These values of α_r can be obtained from

$$\sin p\left(\frac{r\pi}{p} + \alpha_r\right) + k \sin q\left(\frac{r\pi}{p} + \alpha_r\right) = 0$$

Integrating Eq. (12)

$$B_q = \frac{4L}{q\pi} \sum_{r=1}^{p} (-1)^r \left[\cos(a + q\,\alpha_r) - \cos a\right]$$

where $a = \dfrac{qr\pi}{p}$

The equivalent switch gain is defined as the ratio of B_q to B.

$$K'_N = \frac{B_q}{Q} = \frac{4L}{q\pi kA} \sum_{r=1}^{p} (-1)^r \left[\cos(a + q\alpha_r) - \cos a\right] \qquad (13)$$

Eq. 13 can be expanded into a power series in k by first expending it into a power series in α_r. α_r is then expanded into a power series in k. The constant term in the series expansion of α_r is zero; therefore, only each coefficient of the series expansion of K'_N will be the sum of a finite number of terms.

$$K'_N = \frac{4L}{\pi A} \sum_{n=1} C_n k^n \qquad (14)$$

The coefficients C_n can be evaluated for various values of p and q. Substituting these values in Eq. 14

$$K'_N = \frac{2L}{\pi A}\left(1 + \frac{1}{8}k^2 + \frac{3}{64}k^4 + \ldots\right) \text{ if } \frac{p}{q} \neq 2,3,5$$

$$K'_N = \frac{2L}{\pi A} \text{ if } \frac{p}{q} = 2$$

$$K'_N = \frac{2L}{\pi A}\left(1 + \frac{1}{4}k + \frac{1}{8}k^2 + \frac{5}{64}k^3 + \frac{7}{64}k^4 + \ldots\right) \text{ if } \frac{p}{q} = 3$$

$$K'_N = \frac{2L}{\pi A}\left(1 + \frac{1}{8}k^2 - \frac{1}{64}k^3 + \frac{3}{64}k^4 + \ldots\right) \text{ if } \frac{p}{q} = 5$$

If $p \gg 8$, the power series approaches that given by Eq. 11.

C. Periodic Case $\theta \neq 0$

If $\theta \neq 0$, the same analysis can be applied. $C(t)$ will no longer be an odd function; therefore both A_q and B_q must be evaluated. The equivalent switch gain can be given by

$$K'_N = K'_{NB} + j\,K'_{NA}$$

If $\theta = 0$ $K'_{NA} = 0$ and no phase shift is obtained. K'_{NB} and K'_{NA} can be expressed as a power series for arbitrary θ.

$$K'_{NB} = \frac{2L}{\pi p} \sum_{n=0} C_n k^N \qquad (15)$$

where $C_o = 1$ for all p and q

$C_1 = 0$ for all $\frac{p}{q} \neq 3$

$C_1 = \frac{1}{4}\cos 3\theta$ for $\frac{p}{q} = 3$

$C_2 = \frac{1}{8}$ for $\frac{p}{q} \neq 2$

$C_2 = \frac{1}{24}\sin^2 2\theta$ for $\frac{p}{q} = 2$

$C_3 = 0$ for $\frac{p}{q} \neq 3, 5$

$C_3 = \frac{1}{128}\cos 5\theta$ for $\frac{p}{q} = 5$

$$K'_{NA} = \frac{2L}{\pi A} \sum_{n=0} d_n k^n \qquad (16)$$

where $d_o = 0$ for all p and q

$d_1 = 0$ for $\frac{p}{q} \neq 3$

$d_1 = \frac{1}{4}\sin 3\theta$ for $\frac{p}{q} = 3$

$d_2 = 0$ for $\frac{p}{q} \neq 2$

$d_2 = -\frac{1}{8}\sin 4\theta$ for $\frac{p}{q} = 2$

$d_3 = 0$ for $\frac{p}{q} \neq 3,5$

$d_3 = \frac{1}{64}\sin 5\theta$ for $\frac{p}{q} = 5$

From Eqs. 15 and 16 it can be seen that there is some phase shift introduced by the switch for frequencies near ω_o. The maximum phase shift introduced is a function of p,q and k. Table I lists the absolute value of the maximum phase shift for various p and q

TABLE I

p/q	Maximum Phase Shift
3	$\tan^{-1} k/4$
2	$\tan^{-1} k/8$
5	$\tan^{-1} k/64$

D. Change in A due to B

It has been assumed that the amplitude of the loop oscillation frequency is not a function of the signal component B. The error introduced by this assumption will be considered here.

Let $\dot{C}_1$ be the amplitude of the fundamental component of the output of the switch. Using the techniques of the previous analysis, the following is obtained.

$$\dot{C}_1 = \frac{8L}{\pi^2} E \text{ for } \frac{p}{q} \text{ irrational and } p \gg q$$

where E is the complete elliptic integral of the second kind. Expanding E

$$\dot{C}_1 = \frac{4L}{\pi}\left[1 - \frac{1}{4}k^2 - \frac{3}{64}k^4 - \frac{5}{256}k^6 - \ldots\right]$$

The value of $\dot{C}_1$ can also be determined for specific values of p and q.

$$\dot{C}_1 = \frac{4L}{\pi}\left[1 - \frac{1}{4}k^2\right] \quad \text{for } \frac{p}{q} = 2$$

$$\dot{C}_1 = \frac{4L}{\pi}\left[1 - \frac{1}{4}k^2 - \frac{1}{12}k^3 - \frac{3}{64}k^4 - \ldots\right]$$

$$\text{for } \frac{p}{q} = 3$$

If k = .5, the decrease in $\dot{C}_1$ is about seven percent. For values of k less than .25, the decrease in amplitude reduces to approximately one percent.

ACKNOWLEDGEMENTS

A portion of the material described in this paper represents some of the results obtained as part of a doctoral thesis research program conducted by Mr. Gorozdos at the University of Maryland. The aid of Dr. T. C. Gordon Wagner of the Electrical Engineering Department is gratefully acknowledged.

REFERENCES

1. Carrier Controlled Servo - J.C. Lozier, "Electrical Engineering" December 1950, pp. 1052-1056.

2. Servomechanisms - L.A. MacColl (Book) D. VanNostrand Company, New York, N.Y. 1945

3. Sinusoidal Analysis of Feedback-Control Systems Containing Non-Linear Elements - E.C. Johnson "AIEE Transactions" Vol. 71, Part II, 1952, pp. 169-181

4. Non-Linear Mechanics - N. Minorsky (Book) Edwards Brothers, Ann Arbor, Michigan, 1947

5. New Results in the Calculation of Modulation Products - W.R. Bennett, "Bell System Technical Journal", Vol. XII, 1933, pp. 228-243

6. Ferromagnetic Distortion of a Two Frequency Wave, R.M. Kalb and W.R. Bennett "Bell System Technical Journal", Vol. XIV, 1935, pp. 322-359

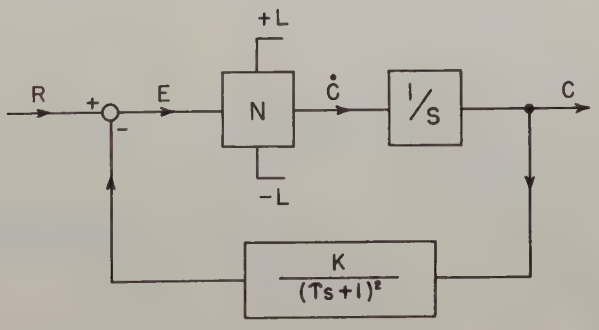

Figure 1. Simple Bi-stable Control System

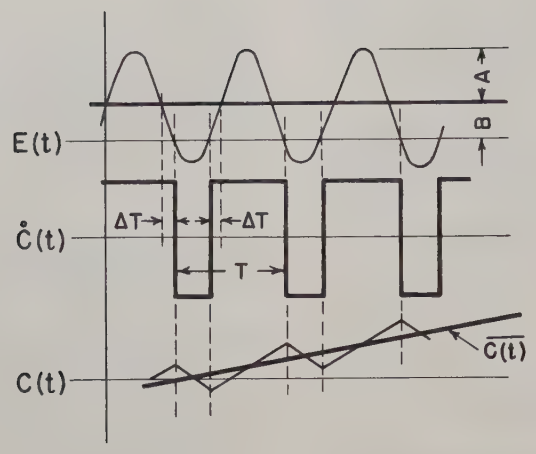

Figure 2. Typical Signals for Oscillating Bi-stable Control System

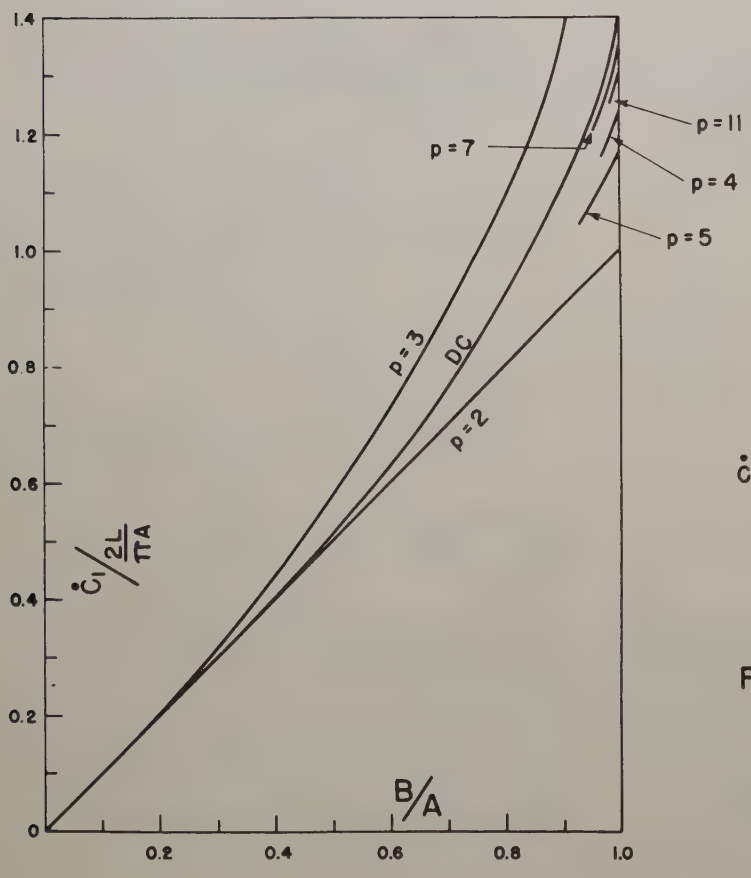

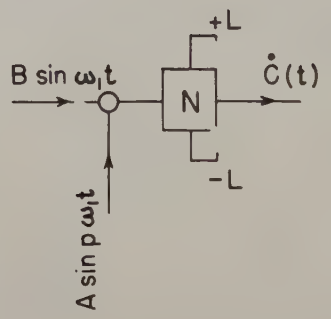

$\dot{C}_1$ is amplitude of output signal component of $\omega = \omega_1$

Figure 3. Normalized Output of Bi-stable Switch Versus Ratio of Signal to Oscillation Amplitude

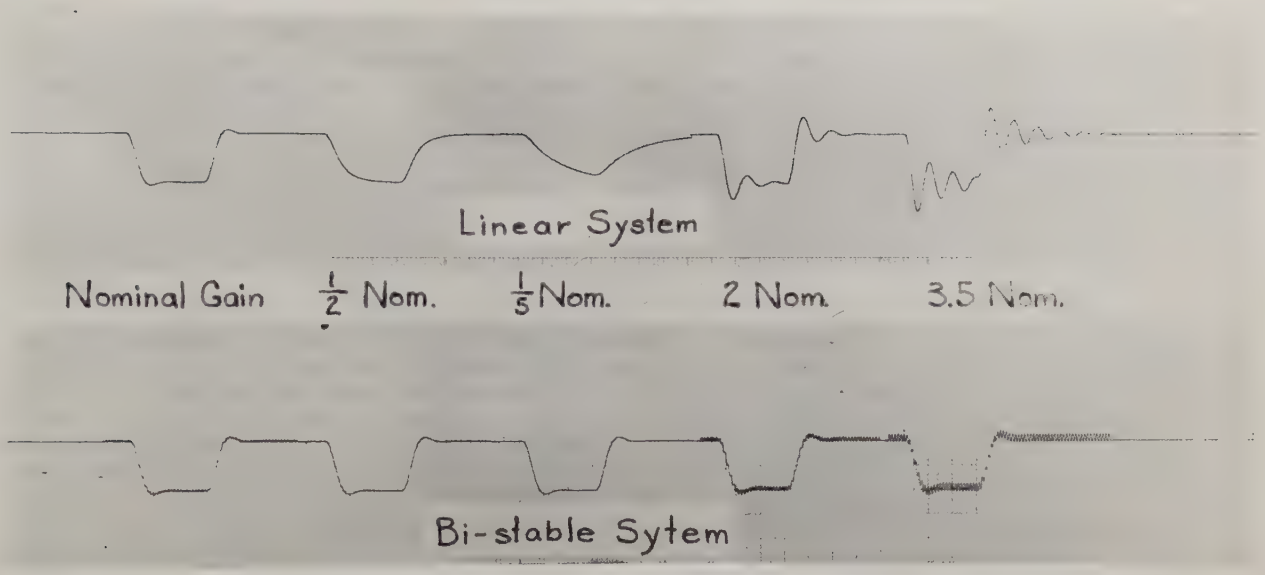

Figure 4. Performance of Bi-stable and Linear Systems with Various Values of Loop Gain.

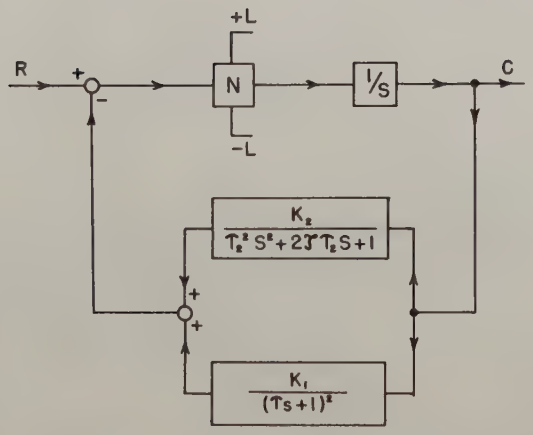

Figure 5. Bi-stable System Having Two Possible Oscillation Modes.

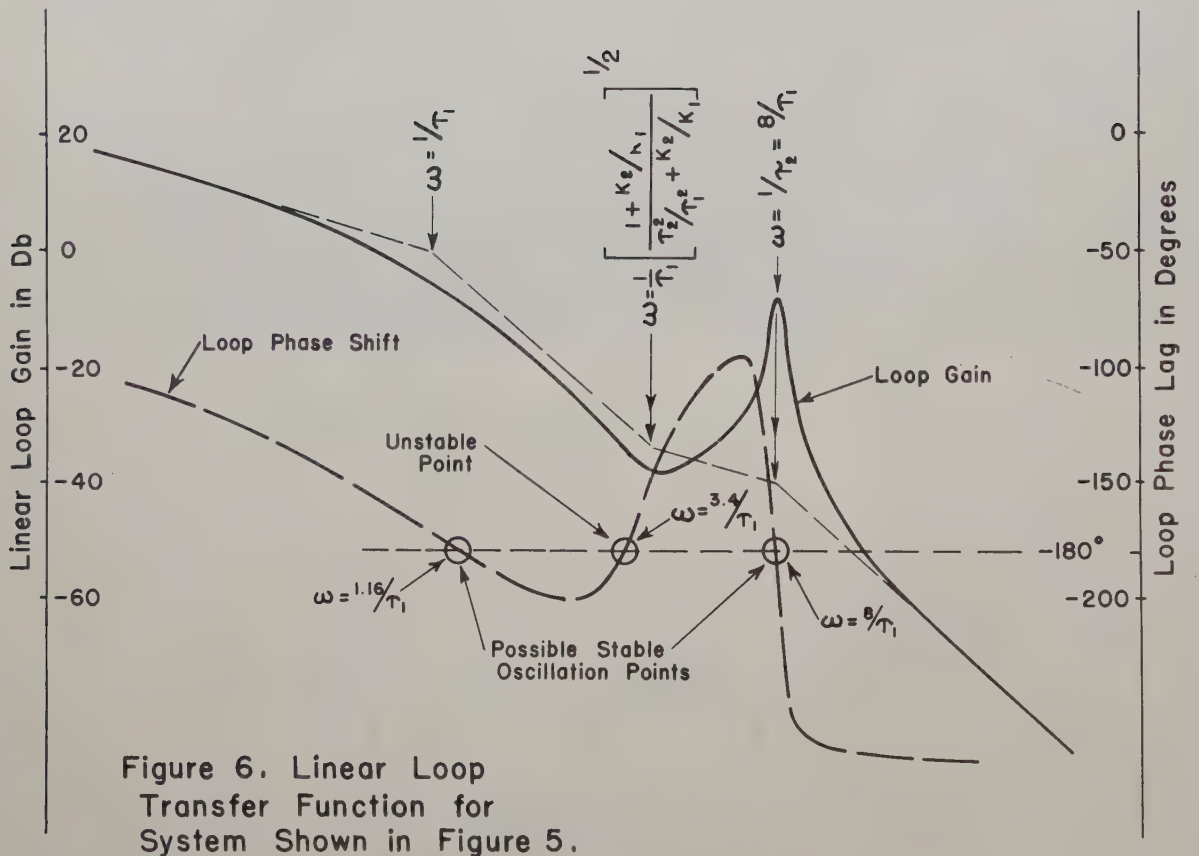

Figure 6. Linear Loop Transfer Function for System Shown in Figure 5.

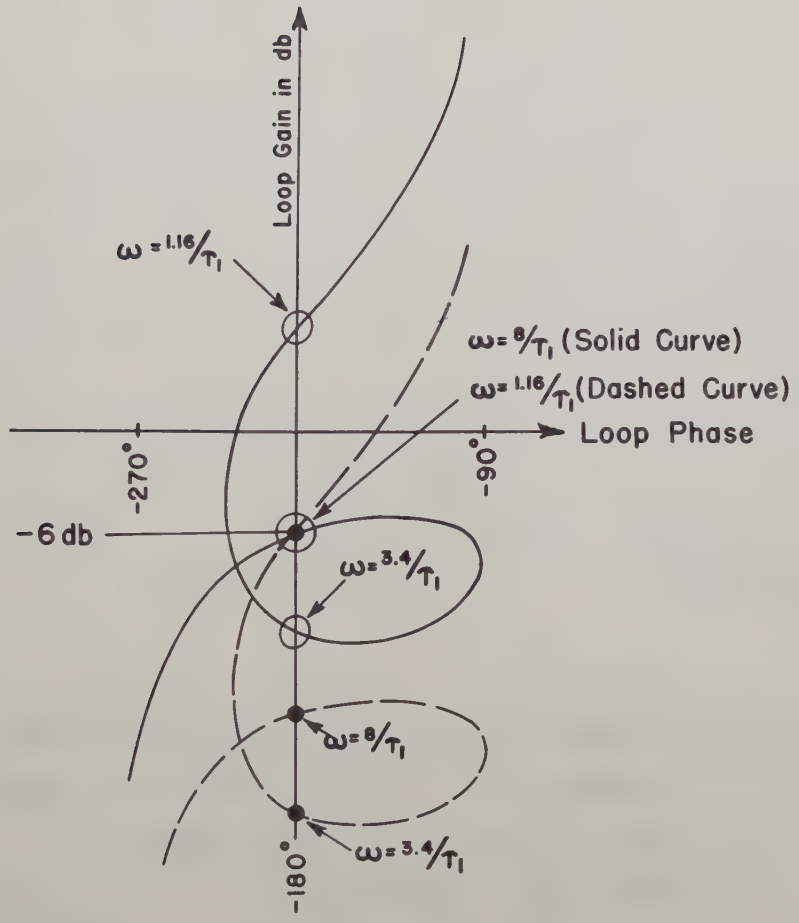

Figure 7. Nichols Plot Illustrating Conditions Required for Shift of Oscillation from Higher to Lower Frequency.

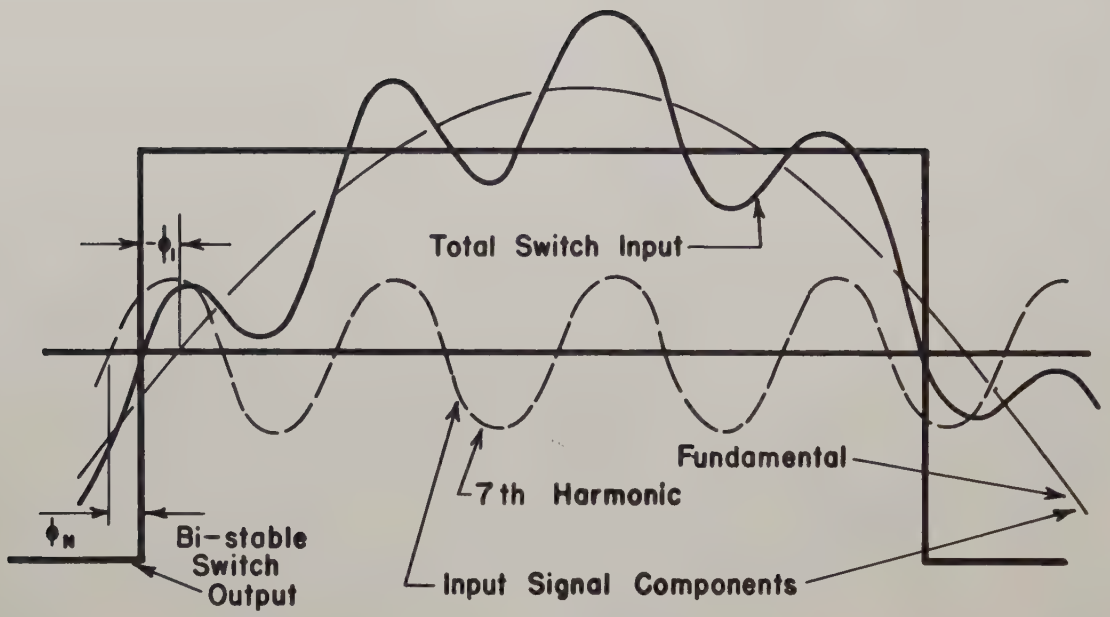

Figure 8. Switching Signals for Bi-stable System with Large Value of Loop Gain at Seventh Harmonic of Switching Frequency.

EFFECT OF POWER SOURCE REGULATION ON THE RESPONSE OF A CONTROL SYSTEM AMPLIFIER

Ralph J. Kochenburger
University of Connecticut

Abstract

Many feedback control systems employ amplifiers that incidently convert energy from one physical form to another. Amplification is accomplished by variation of a parameter that changes such conversion properties. Among a number of examples are variable-displacement hydraulic pumps and "Ward-Leonard" systems of motor control. Conventional linear response analyses usually are based upon the assumption of an "ideal" input energy source. Actual practice displays many instances when such an assumption is not valid. The load imposed on the controlled output may have a significant effect on the input power source. The method presented here takes such non-ideal characteristics into account.

This paper is to be published in the Proceedings of the First IFAC Moscow Congress by Butterworth Scientific Publications in 1960.

PENDULOUS VELOCITY METER CONTROL SYNTHESIS

S. G. Shutt & S. A. White
Autonetics
North American Aviation, Inc.
Downey, Calif.

Summary

An acceleration sensing instrument is essential to an automatic inertial navigation system. A velocity meter (VM) is a singly-integrating, acceleration-sensing instrument which has become important in providing precise, continuous velocity information for navigation of a wide variety of vehicles, from submarines to ballistic missiles.

The increased autonavigator accuracy achievements and objectives have placed greater emphasis on instrument and associated instrument electronics error sources and their design to minimize these errors. This paper is primarily concerned with error sources which are affected by the design of the VM servo control amplifier. The environmental conditions, the pendulous nature of the VM, and the accuracy specifications are analyzed to provide requirements for synthesis of a VM servo control amplifier to achieve the desired system operation.

Introduction

Automatic inertial navigation is a form of dead reckoning which has been gaining importance in the past ten years. Several desirable characteristics of this type of system account for its increased use. Among the most significant advantages are high accuracy, fast time response and being completely self-contained independent of external interference. This type of system is used in a wide range of applications; from submarine to ballistic missile guidance.

A typical inertial navigation system has a gyro-stabilized platform with an orthogonal coordinate system fixed to the platform of known orientation. A gimballing structure supports the platform to the vehicle providing complete maneuverability of the vehicle. On the platform are mounted acceleration sensing instruments with sensitive axes colinear with the platform coordinate axes. In some systems the acceleration sensing instruments are of the singly-integrating type or velocity meters. The pendulous velocity meter (VM) is of particular interest and is to be discussed in this paper.

The concept of applying Newton's second law of motion to navigation is not new, however, the application of many specialties and new techniques have been required to achieve a functional system of useful accuracy operating in a realistic environment. Navigational instrument design has reached a very high level in the art and science of force balance. Many error sources of a pendulous velocity meter must be considered in producing a successful velocity meter system. Some of these errors can not be changed by the control amplifier. Those which can be influenced by the control amplifier design are analyzed in this paper to establish the requirements of the VM control amplifier. From the error considerations, the control amplifier design is synthesized.

Description of Pendulous Velocity Meter Operation

Operation is based on the principle of sensing deflections of the pendulous element from null under the action of acceleration, and applying a torque back to the pendulum to restore null via some form of rotary coupling characterized by generating a torque which is a linear function of rotational velocity. The coupling, which is a differentiating device, may be visualized as a liquid-shear coupling or as a magnet-and-conductor arrangement as in an automobile speedometer. The relationship is expressed in Eq. (1).

$$P\ddot{\rho} = D\dot{\sigma} \tag{1}$$

where

P = pendulosity or pendulum unbalance

$\ddot{\rho}$ = input acceleration

D = torque applied to pendulum proportional to motor angular velocity

$\dot{\sigma}$ = angular velocity of motor shaft

If the torque balance stated in Eq. (1) is maintained, the velocity at any time, assuming zero initial conditions, is given in Eq. (2) by integration of both sides of Eq. (1).

$$P\int_0^{\dot{\rho}} d\dot{\rho} = D\int_0^{\sigma} d\sigma$$
$$\dot{\rho} = \frac{D}{P}\sigma \tag{2}$$

The motor shaft angle, σ, is then a continuous measure of input velocity, $\dot{\rho}$.

Function of Control Amplifier

It is the function of the control amplifier to maintain the torque balance expressed in Eq. (1). An input acceleration acting on the pendulum unbalance will cause the pendulum to rotate on an ultra low friction bearing. An angular pickoff will detect the pendulum angle and provide an electrical input signal to the control amplifier proportional to the pendulum angle. The control amplifier will amplify, compensate, and provide

power back to the VM motor to rotate the torque motor at the proper speed to hold the pendulum (via the coupler) at near null position and maintain the desired torque balance. The primary question, so far as this paper is concerned, is; how small a null is required for a given accuracy operating in a known environment?

Nomenclature

D_d = damping coefficient between pendulum and torque motor shaft about the y axis

D_p = damping coefficient between pendulum and VM case about the y axis

E = torque motor applied voltage

E_s = torque motor starting voltage

f = frequency

F(o) = zero frequency control amplifier gain

F(s) = control amplifier transfer function

G = 1/H

H = stiffness, defined as the ratio of torque applied to the pendulum to the resulting pendulum angle

H_o = zero frequency stiffness

I = moment of inertia of pendulum
I_{xx}, I_{yy}, I_{zz} = principle moments of inertia with respect to xyz coordinate system
I_{xy}, I_{xz}, etc. = products of inertia. The pendulum coordinate system is oriented so that these terms are zero

J = Polar moment of inertia as seen at motor shaft

K = open loop gain

K_h = K/D_p

K_m = motor velocity constant

K_p = spring constant between pendulum and VM case about the y axis

K_t = motor torque constant

K_v = motor back emf constant

K_2 = pendulum pickoff relating pendulum angle to voltage

M = angular momentum of pendulum as defined in Eq. (5)

m_p = mass of pendulum

P = pendulosity of pendulum. $P_z = P = r_{cg}\, m_p$
$P_x = P_y = 0$

P_{max} = peak motor $I_a{}^2 R_a$ losses

P_n, z_n = n^{th} pole, zero of F(s)

q = $\sqrt{\omega_m K}$

R_a = motor armature resistance

R_{xy} = cross-correlation function

r_{cg} = distance between origin of xyz and center of mass of the pendulum

s = Laplace transform operator

S(f) = Spectral density

t = time

T = total torque applied to pendulum

T_m = motor time constant

β = mechanical viscous friction as seen at motor shaft (contains D_d)

θ = absolute pendulum angle, angle of xyz coordinate system with respect to XYZ

θ_p = $\theta_y - \phi_y$ = pendulum angle with respect to VM case about the y axis

θ_{ps} = pendulum angle to start torque motor rotation

ρ = distance separating the origins of xyz and XYZ

σ = absolute angle of torque motor shaft

ϕ = absolute VM case angle, angle of $x_1 y_1 z_1$ coordinate system with respect to XYZ

ψ = stiffness phase angle

ω_m = $1/T_m$

i,j,k, unit vectors along the coordinate axes of xyz

Subscripts x, y, z identify the parameter to a specific axis; such as, $\ddot{\rho}_{x1}$ is the acceleration of VM case along the x_1 axis.

Derivation of VM Transfer Function

A three dimensional analysis of the pendulum is performed, from which a block diagram is constructed and several error sources made apparent.

Figure 1 indicates the general VM configuration with coordinate axes shown. Three orthogonal coordinate systems are used; X, Y, Z is an inertial reference, x, y, z is placed in the VM pendulum, and x_1, y_1, z_1 is placed in the VM case and torque motor but not rotating with the motor.

A summation of applied torques acting on the pendulum will yield the desired relationships; this is expressed as a vector equation

$$T = \frac{dM}{dt} + \dot{\theta} \times M + r_{cg}\, m_p \times \frac{d^2\rho}{dt^2} \tag{3}$$

If the origin of the pendulum coordinate system were placed at the pendulum cg then Eq. (3) would reduce to the more common form of Euler's equation. It is convenient, however, to avoid the relative translational motion between the origin of xyz and $x_1y_1z_1$ by placing xyz at the pendulum pivot.

Equation (3) can be expanded into three components of torque about each pendulum axis in the following matrix:

$$T = \begin{pmatrix} I_{xx} & I_{xy} & I_{xz} \\ I_{yx} & I_{yy} & I_{yz} \\ I_{zx} & I_{zy} & I_{zz} \end{pmatrix} \begin{pmatrix} \ddot{\theta}_x \\ \ddot{\theta}_y \\ \ddot{\theta}_z \end{pmatrix} + \begin{pmatrix} i & j & k \\ \dot{\theta}_x & \dot{\theta}_y & \dot{\theta}_z \\ M_x & M_y & M_z \end{pmatrix} + \begin{pmatrix} i & j & k \\ P_x & P_y & P_z \\ \ddot{\rho}_x & \ddot{\rho}_y & \ddot{\rho}_z \end{pmatrix} \tag{4}$$

and

$$M = \begin{pmatrix} I_{xx} & I_{xy} & I_{xz} \\ I_{yx} & I_{yy} & I_{yz} \\ I_{zx} & I_{zy} & I_{zz} \end{pmatrix} \begin{pmatrix} \dot{\theta}_x \\ \dot{\theta}_y \\ \dot{\theta}_z \end{pmatrix} \tag{5}$$

Of primary importance is the torque acting about the y axis; this is given in Eq. (6) with the cross products of pendulum inertia and P_x and P_y equal to zero.

$$T_y = I_{yy}\,\ddot{\theta}_y + \dot{\theta}_z\,\dot{\theta}_x\,(I_{xx} - I_{zz}) - P_z\,\ddot{\rho}_x \tag{6}$$

The input axes of the platform system are with respect to the VM case, so that the input acceleration $\ddot{\rho}_x$ and input rotations $\dot{\theta}_z$ and $\dot{\theta}_x$ must be broken into components referred to x_1 y_1 z_1 or

$$\ddot{\rho}_x = \ddot{\rho}_{xl} \cos(\theta_y - \phi_y) + \ddot{\rho}_{zl} \sin(\theta_y - \phi_y) \tag{7}$$

which reduces, for a small difference angle, to

$$\ddot{\rho}_x = \ddot{\rho}_{xl} + \ddot{\rho}_{zl}(\theta_y - \phi_y) = \ddot{\rho}_{xl} + \ddot{\rho}_{zl}\,\theta_p \tag{8}$$

Also, the angular rates, $\dot{\theta}_z$ and $\dot{\theta}_x$, are transformed to the VM case axes

$$\dot{\theta}_z = \dot{\phi}_z + \dot{\phi}_x\theta_p \tag{9}$$

$$\dot{\theta}_x = \dot{\phi}_x - \dot{\phi}_z\theta_p \tag{10}$$

From Fig. 1 it is observed that the applied torque to the pendulum about the y axis, L_y, is given by Eq. (11).

$$T_y = -D_p(\dot{\theta}_y - \dot{\phi}_y) - K_p(\theta_y - \phi_y) - D_d(\dot{\theta}_y - \dot{\sigma}_y) \tag{11}$$

Combining Eqs. (6), (8), (9), (10) and (11), taking the Laplace transform with zero initial conditions and rearranging

$$\left[I_{yy}s^2 + (D_p + D_d)s + K_p\right]\theta_y(s) + (I_{xx} - I_{zz})\left[\dot{\phi}_x\dot{\phi}_z(1 - \theta_p(s)^2) + \dot{\phi}_x{}^2\theta_p(s) - \dot{\phi}_z{}^2\theta_p(s)\right] = \left[D_p s + K_p\right]\phi_y(s) + D_d\,\dot{\sigma}_y(s) + P\ddot{\rho}_{xl}(s) + P\ddot{\rho}_{zl}(s)\theta_p(s) \tag{12}$$

A second equation can be considered as a two dimensional problem and is the transfer function of a motor with voltage input and shaft-angle output, as expressed in Eq. (13)

$$\frac{\sigma_y(s)}{E} = \frac{K_m}{s\left(\frac{s}{\omega_m} + 1\right)} \tag{13}$$

Equations (12) and (13) are used to construct the block diagram representing the VM servo, see Fig. 2. The block diagram is then a representation of the VM servo loop which is to be stabilized by the control amplifier, F(s).

VM Servo System Requirements

Requirements of the control amplifier, to stabilize the servo system represented in Fig. 2 so that Eq. (1) is approximated within specified accuracy, are considered next. Several properties of the system must be determined to establish design parameters of the control amplifier. The amplifier design characteristics are determined by investigating error sources and establishing parameters and gains so that the errors associated with the controller are acceptable compared with performance specifications. Specifications generally call out

1. threshold acceleration, $\ddot{\rho}_{et}$
2. threshold velocity, $\dot{\rho}_{et}$
3. maximum allowable acceleration error, $\ddot{\rho}_{em}$
4. maximum allowable velocity error, $\dot{\rho}_{em}$
5. maximum input acceleration, $\ddot{\rho}_{xlm}$
6. maximum cross axis acceleration $\ddot{\rho}_{zlm}$
7. spectral density of noise environment

Stiffness

It is convenient to relate all error sources and gains required to meet the accuracy specification in terms of stiffness as a function of frequency. Stiffness is defined, here, as the ratio of applied torque acting on the pendulum to the resulting pendulum angle. All error sources are then related to the same plot, Fig. 4. Amplifier requirements can then be established so that all errors related to amplifier design are within the allowable values.

Consider the VM servo loop as

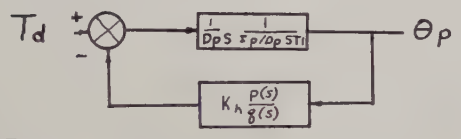

$$H = \frac{T_d}{\theta_p} = D_p s \left(\frac{I_{yy}}{D_p} s + 1\right) + K_h \frac{p(s)}{q(s)}$$

These variables are usually represented on a stiffness chart as shown below

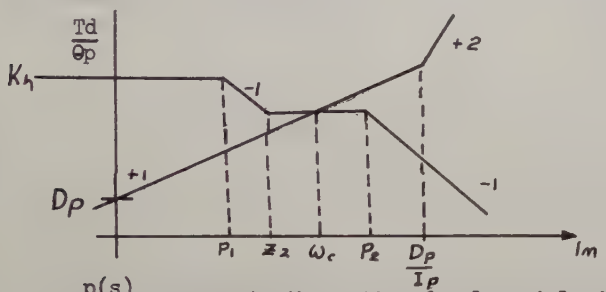

where $\frac{p(s)}{q(s)}$ represents the ratio of polynomials in s determined by the motor break frequency, $\frac{1}{Tm}$, and the equalizer $F(s) = \frac{(\frac{s}{z1} + 1)(\frac{s}{z2} + 1)}{(\frac{s}{p1} + 1)(\frac{s}{p2} + 1)}$ where z_1 is set about $\frac{1}{Tm}$ and ω_c is the open loop crossover frequency.

The system can be designed on the stiffness chart. For general design purposes the compensation break frequencies, maximum and minimum stiffness values should be set and indicated on the stiffness chart.

It is convenient to normalize stiffness. Consider the system without compensation for a moment as shown below.

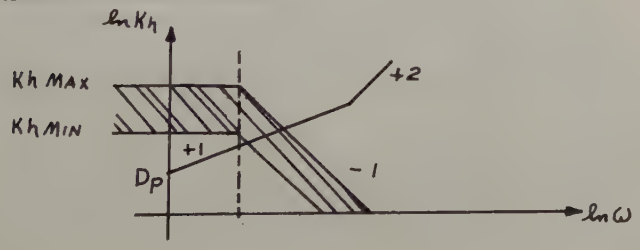

The uncompensated system may lie anywhere in the shaded area. If K_h is normalized about D_p, the ordinate becomes the loop gain K. If the frequency is normalized about the motor break frequency, the plot becomes:

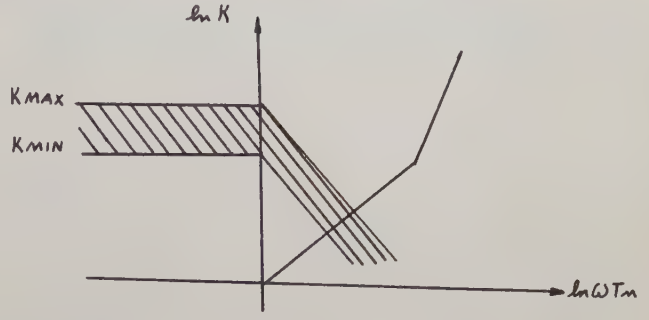

Minimum Stiffness Requirements

There are errors which can be decreased with increasing stiffness. These error sources are analyzed separately, but added together to arrive at a minimum stiffness curve above which the VM servo loop must operate, as indicated in Fig. 4. The first six effects are all low frequency considerations which establish zero frequency stiffness; the seventh is primarily a mid-frequency effect which determines the minimum stiffness.

Cross-axis coupling. The pendulous nature of the VM makes it sensitive to the linear acceleration along the axis orthogonal to the input and pivot axes. This is observed from Eq. (8); the input acceleration, $\ddot{\theta}_{x1}$, is in error by

$$\ddot{\theta}_e = \ddot{\theta}_{z1}\,\theta_p \qquad (14)$$

$\ddot{\theta}_{x1}$ P is the input torque to the pendulum which must be balanced by the feedback torque, but to get a feedback torque there must be an angle θ_p. The stiffness is then

$$\frac{\ddot{\theta}_{x1} P}{\theta_p} = H_o \qquad (15)$$

Combining (14) and (15)

$$H_o = \frac{\ddot{\theta}_{z1m}\,\ddot{\theta}_{x1m}}{\ddot{\theta}_{em}} P \qquad (16)$$

All accelerations of Eq. (16) are known from the system specification. P is also known for a given VM.

Velocity threshold. A starting voltage is required at the torque motor to start rotation as indicated in Fig. (5a). There must be rotation, $\dot{\sigma}_y$, before a torque can be applied back to the pendulum to counter an input acceleration. During the time the motor voltage is below the motor starting voltage, there can be an input acceleration, but there will be no output indication; this gives rise to a velocity threshold which is a function of the low frequency servo gain.

At low frequency the pendulum transfer function reduces to

$$P\,\ddot{\varepsilon}_{xl} = (D_p + D_d)\,\dot{\theta}_p \tag{17}$$

for no rotation of the VM case $\phi_y = 0$ and negligible spring constant K_p. No feedback torque is applied since the motor is not rotating; the servo is open loop. By integration of (17)

$$P\int_0^{\dot{\varepsilon}_{et}} d\dot{\varepsilon} = (D_p + D_d)\int_0^{\theta_{ps}} d\theta_p$$

$$P\,\dot{\varepsilon}_{et} = (D_p + D_d)\,\theta_{ps} \tag{18}$$

where θ_{ps} is the pendulum angle required to produce motor starting voltage and related to motor starting voltage by

$$\theta_{ps}\,K_2 F(o) = E_s \tag{19}$$

The zero frequency stiffness, from Fig. 2, is

$$H_o = K_2\,F(o)\,K_m\,D_d \tag{20}$$

Combining Eqs. (18), (19), and (20),

$$H_o = \frac{E_s\,K_m\,D_d\,(D_p + D_d)}{P\,\dot{\varepsilon}_{et}} \tag{21}$$

Again all quantities of (21) are known from the specification or from the VM.

Amplifier null drift. The required stiffness to take care of an amplifier drift, referred to the output, is the same as given by Eq. (21) with E_s replaced by E_d and $\dot{\varepsilon}_{et}$ replaced by $\dot{\varepsilon}_{em}$

$$H_o = \frac{E_d\,K_m\,D_d\,(D_p + D_d)}{P\,\dot{\varepsilon}_{em}} \tag{22}$$

where E_d is maximum allowable amplifier null drift voltage referred to the amplifier output.

Velocity error. The maximum low frequency torque applied to the pendulum is $P\,\ddot{\varepsilon}_{xlm}$ which generates a pendulum angle θ_{pm}; the stiffness is then

$$H_o = \frac{P\,\ddot{\varepsilon}_{xlm}}{\theta_{pm}} \tag{23}$$

Combining Eq. (23) and (18) with θ_{ps} and $\dot{\varepsilon}_{et}$ replaced by θ_{pm} and $\dot{\varepsilon}_{em}$

$$H_o = \frac{\ddot{\varepsilon}_{xlm}\,(D_p + D_d)}{\dot{\varepsilon}_{em}} \tag{24}$$

Acceleration error. A pendulum spring constant, K_p, will give rise to an acceleration error for a non-null pendulum angle. The spring torque is interpreted as an input acceleration and given by

$$\theta_p\,K_p = P\,\ddot{\varepsilon}_{em} \tag{25}$$

Combining Eq. (25) and (23)

$$H_o = \frac{\ddot{\varepsilon}_m}{\ddot{\varepsilon}_{em}}\,K_p \tag{26}$$

This acceleration error can be considered as part of the VM scale factor, but then K_p and the control amplifier gain must not change a specified amount. It is more desirable to reduce this error as expressed in Eq. (26).

Acceleration threshold. Acceleration threshold does not change the scale factor in a linear fashion and must be made small. The torque balance between allowable acceleration threshold and spring torque is given by

$$\theta_{ps}\,K_p = P\,\ddot{\varepsilon}_{et} \tag{27}$$

Combining Eqs. (19), (20), and (27)

$$H_o = \frac{K_m\,D_d\,E_s\,K_p}{P\,\ddot{\varepsilon}_{et}} \tag{28}$$

Periodic cross-axis acceleration effects. The pendulous type velocity meter is susceptable to errors introduced by translational input components along the cross-axis when they are correlated with the pendulum deflection as a function of time.

If an acceleration exists simultaneously along input and cross-axis, the total resultant torque about the pendulum pivot axis may be seen to be

$$T(t) = P\,\ddot{\varepsilon}_{xl}(t) + P\,\theta_p\,\ddot{\varepsilon}_{zl}(t) \tag{29}$$

The first term of Eq. (29) is the component of acceleration which is meant to be sensed, the second term being an error. The resulting error torque is

$$T_e(t) = P\,\theta_p(t)\,\ddot{\varepsilon}_{zl}(t) \tag{30}$$

The average error torque and the corresponding acceleration error are

$$\overline{T} = P\,\overline{\theta_p(t)\,\ddot{\varepsilon}_{zl}(t)} \tag{31}$$

$$= P\,R_{\theta_p \ddot{\varepsilon}_{zl}}(0) \tag{32}$$

$$\ddot{\varepsilon}_{em} = R_{\theta_p \ddot{\varepsilon}_{zl}}(0) \tag{33}$$

The acceleration error may be related to the spectrol density by

$$\ddot{\varepsilon}_{em} = \frac{1}{2}\int_{-\infty}^{\infty} S_{\theta_p\,\ddot{\varepsilon}_{zl}}(f)\,df \tag{34}$$

which may be shown to be equal to

$$\ddot{\varepsilon}_{em} = \frac{1}{2}\int_{-\infty}^{\infty} S_{\ddot{\varepsilon}_{xl}\,\ddot{\varepsilon}_{zl}}(f)\,G^*(j2\pi f)\,df \tag{35}$$

where $G(s) = \dfrac{\theta_p(s)}{\ddot{\varepsilon}_{xl}(s)}$ (36)

Spectral density is a convenient criterion to employ since data are usually available. However, cross-spectral density data are normally not tabulated. A simplified and probably more realistic approach to the noise problem is to assume that the noise on the input and cross-axis is actually components of a single signal applied in the plane defined by the two axes under consideration, at an angle α from the input axis. This insures a worst possible case consideration.

$$\ddot{\theta}_{em} = \frac{\sin 2\alpha}{4} \int_{-\infty}^{\infty} S_{\ddot{\theta}_n \ddot{\theta}_n}(f) G^*(j 2\pi f)\, df \qquad (37)$$

Now, $G(s) = \frac{P}{H(s)}$ where H(s) is defined as the pendulum stiffness, or

$$H(s) = \frac{T_d(s)}{\theta_p(s)};\ H(j\omega) = |H|\ e^{j\psi} \qquad (38)$$

Let us now further assume that $\alpha = 45°$ maximizing $\ddot{\theta}_{em}$, yielding:

$$\ddot{\theta}_{em} = \frac{P}{4} \int_{-\infty}^{\infty} \frac{S_{\ddot{\theta}\ddot{\theta}}(f)}{H(j 2\pi f)}\, df \qquad (39)$$

$$= \frac{P}{2} \int_{0}^{\infty} \mathrm{Re}\, \frac{S_{\ddot{\theta}\ddot{\theta}}(f)}{H(j 2\pi f)}\, df \qquad (40)$$

$$= \frac{P}{2} \int_{0}^{\infty} \frac{S_{\ddot{\theta}\ddot{\theta}}(f) \cos\psi}{|H|}\, df \qquad (41)$$

Assuming a worst minimum value for $|H|_{min}$ to be essentially constant and a worst possible value of $\cos\psi$

$$\ddot{\theta}_{em} = \frac{P}{2|H|_{min}} \int_{0}^{\infty} S_{\ddot{\theta}\ddot{\theta}}(f)\, df \qquad (42)$$

Now this can be examined in two ways. We may consider $S_{\ddot{\theta}\ddot{\theta}}$ to be composed of band limited white noise of amplitude η up to some frequency, fn, or as a sum of sinusoidal signals, $a_j \sin 2\pi f_j t$, near the resonant frequency of the stiffness curve. Assuming the sum of the two,

$$\int_{0}^{\infty} S_{\ddot{\theta}\ddot{\theta}}(f) df = \eta^2 fn + \sum \frac{a_i^2}{4} = |P| \qquad (43)$$

$$\ddot{\theta}_{em} = \frac{P}{2} \frac{|P|}{|H|_{min}} \qquad (44)$$

The minimum allowable stiffness, determined by this criteria, is given by Eq. (44).

It is sometimes found that the vibration and allowable acceleration error specifications require the stiffness, as determined by Eq. (44), to be higher than is desirable. In this case cross-axis acceleration effect is analyzed after the system parameter gains have been established by using Eq. (41) which includes the phase angle, ψ.

Minimum gain to avoid servo saturation. Multiply the total anticipated input amplitude spectrum $S(\omega)$ consisting of noise plus signal by $\frac{P}{D_p \theta_{pmax}}$ where θ_{pmax} is the pendulum displacement which causes servo saturation. This is the translated input amplitude spectrum curve which is plotted on the normalized stiffness chart. To avoid amplifier saturation, the normalized stiffness curve must lie above the translated input - amplitude spectrum curve as shown in Fig. 4.

Compensation

A later section will show that we wish to restrict the compensation to the form

$$F(s) = \frac{(\frac{s}{z_1} + 1)(\frac{s}{z_2} + 1)}{(\frac{s}{p_1} + 1)(\frac{s}{p_2} + 1)} \text{ where } p_2 > z_2 > z_1 > p_1 \qquad (45)$$

and higher frequency noise - attenuating lags are introduced. Now, on the normalized stiffness plot p_1, p_2, z_1 and z_2 as a function of loop gain may be determined. The phase margin may be expressed as:

$$PM = 2 \tan^{-1}\left(\frac{p_1}{\omega_m}\right)^{\frac{1}{2}} + 38° \left(\frac{\omega_m}{K}\right)^{\frac{1}{2}} \left(\frac{p_1}{\omega_m}\right)^{3/4} - 90° \qquad (46)$$

p_1 is determined graphically. Let $\frac{z_2}{p_2} = \frac{p_1}{\omega_m}$. The compensation loci as the gain is varied is plotted on Fig. 3 and indicated again on Fig. 4.

Maximum Gain Determination

Excessive gain causes hot spots in the instrument due to copper losses in the motor which should be held to a minimum. Motor acceleration is related to the copper losses by:

$$\ddot{\sigma} = \frac{K_t}{\beta} \sqrt{\frac{P_{max}}{R_a}}\, \frac{s}{\frac{J}{\beta} s + 1} \qquad (47)$$

For frequencies sufficiently far below ω_c,

$$\frac{T_s}{\theta_p} = \frac{\ddot{\sigma} D_d}{s\, \theta_p} = \frac{\ddot{\sigma} D_d H}{s\, T_d} < \frac{\ddot{\sigma}_{max}}{T_{d\,max}} \frac{D_d H}{s} \qquad (48)$$

For the moment, consider $H = K_h \frac{(\frac{s}{z_2} + 1)}{(\frac{s}{p1} + 1)}$

Then $\frac{Ts}{\theta_p} < \frac{\ddot{\sigma}_{max}}{T_{dmax}} \frac{D_d}{s} K_h \frac{(\frac{s}{z_2} + 1)}{(\frac{s}{p1} + 1)}$ (49)

$$\frac{Ts}{\theta_p} < \frac{K_t}{\beta} \frac{D_d K_h}{T_{dmax}} \sqrt{\frac{P_{max}}{R_a}}\, \frac{(\frac{s}{z_2} + 1)}{(\frac{s}{p1} + 1)(\frac{J}{\beta} s + 1)} \qquad (50)$$

$$= K_h K' \frac{(\frac{s}{z_2} + 1)}{(\frac{s}{p1} + 1)(\frac{J}{\beta} s + 1)} \qquad (51)$$

where $K' = \frac{Kt}{\beta} \frac{Dd}{Tdmax} \sqrt{\frac{Pmax}{R_a}}$

Sketching on a standard stiffness chart for frequencies up to ω_c.

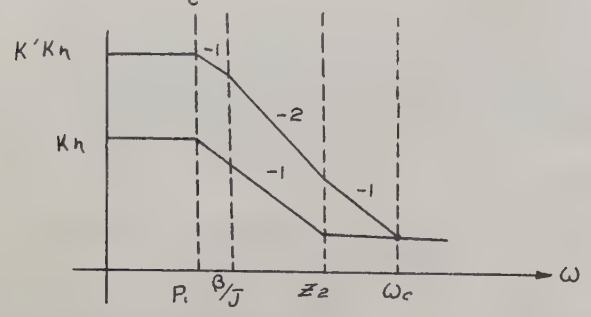

From the above we may write:

$$\omega_c < \frac{K'\beta}{J} \text{ but } \omega_c = K\frac{p_1}{z_2} = \frac{K_h}{D_p}\frac{p_1}{z_2} \tag{52}$$

$$K_H < D_p \frac{z_2}{p_1}\frac{K'\beta}{J} = \frac{D_p}{J}\frac{z_2}{p_1}\frac{Kt\ Dd}{Tdmax}\sqrt{\frac{Pmax}{Ra}} \tag{53}$$

For sufficiently large values of loop gain, one may show that for optimum phase-margin setting

$$\frac{z_2}{p_1} \simeq \sqrt{\frac{K}{.42\omega_m}} \tag{54}$$

Then

$$K < 2.38\omega_m\frac{Pmax}{R_a}\left(\frac{Kt\ Dd}{J\ P\ \ddot{\theta}_{xlm}}\right)^2 \text{ at } \omega = p_1 \tag{55}$$

which may be applied to the normalized chart.

If K is between its maximum and minimum allowable values as established in previous sections, then it follows that:

$$\sqrt{\frac{K_{min}\omega_m R_a}{P_{max}}}\ P\ \frac{\ddot{\theta}_{xlm}\ J}{K_t} < D_d \tag{56}$$

Non-linearities

The VM poses some interesting problems in equalization in that the open-loop cross over frequency must be better than two orders of magnitude less than the open-loop gain using an RC network with small valued components. The most obvious approach would be to use a filter whose profile is shown as Fig. 5d giving rise to a system whose Nyquist diagram is indicated in Fig. 5c.

The small deadband in the motor as shown in Fig. 5a causes a limit cycle at point B and system and environmental noise tend to cause a limit cycle to exist at point A, as the conventional describing-function technique will bear out. One is entirely limited to a network of the form $F_1(s)$ as shown in Fig. 5d with higher frequency lags for noise attenuation.

Effects of Case Rotations

As the reader has seen earlier, rotation of the VM case also applies a torque to the pendulum and affects the output. However, we will show that the effects are negligible. The variables ϕ_x, ϕ_y and ϕ_z represent changes in the inertially stable platform angular attitude. Assume the following:

$$\phi_x = \phi_{x\ max} \sin(\omega_1 t + \alpha) \tag{57}$$

$$\phi_y = \phi_{y\ max} \sin(\omega_2 t + \beta) \tag{58}$$

$$\phi_z = \phi_{z\ max} \sin(\omega_3 t + \delta) \tag{59}$$

Examining first the torques developed by ϕ_x and ϕ_z

$$T_{d_{\phi xz}} = \left[I_{xx} - I_{zz}\right]\left[\dot{\phi}_x\dot{\phi}_z + \dot{\phi}_x^2\theta_p - \dot{\phi}_y^2\theta_p\right] \tag{60}$$

$$= mr^2\Big[\phi_{xmax}\phi_{zmax}\omega_1\omega_3\cos(\omega_1 t+\alpha)\cos(\omega_3 t+\delta) + \theta_p\phi_{xmax}^2\omega_1^2\cos^2(\omega_1 t+\alpha) - \theta_p\phi_{zmax}^2\omega_3^2\cos^2(\omega_3 t+\delta)\Big]$$

The maximum average or bias torque is sensed when $m = n$, $\alpha = \delta$

$$\overline{T_{d_{\phi xz\ max}}} = \frac{mr^2}{2}\Big[\phi_{xmax}\phi_{z\ max}\omega_3^2 + \theta_p(\phi_{x\ max}^2\omega_3^2 - \phi_{zmax}\omega_3^2)\Big]$$

$$\frac{mr^2\omega_3^2}{2}\phi_{xmax}\phi_{zmax} \tag{61}$$

In practice, this bias torque is far too small to be even sensed by the system. The effect of ϕ_y on θ_p may be shown as follows: Assume that the pendulum angle resulting from ϕ_y is less than θ_{ps}. Then:

$$\frac{\theta_p}{\phi_y} = -\frac{I_{yy}s^2 + D_d s}{I_{yy}s^2 + (D_p + D_d)s + K_p} \tag{62}$$

The equivalent disturbing torque is

$$T_{d\phi_y} = -\dot{\phi}_y(I_{yy}s + D_d) \tag{63}$$

$$\overline{T_{d\phi_y}} = 0 \tag{64}$$

Nonsinusoidal values of ϕ_x, ϕ_y, and ϕ_z, i.e. transients, are of such amplitude and duration that their effects are negligible.

Conclusion

A study was conducted to determine the source and magnitude of the errors which are inherent in a pendulous type velocity meter. Of the errors examined, the effects of those which could be minimized by the controller were discussed in this paper. Controller requirements were established which would minimize these errors. Non-linear properties of the VM servo loop imposed requirements on the design of the VM control amplifier; these were also considered. The results of the error analysis and the controller requirements

were presented graphically on a stiffness chart which clearly indicated the permissible region in which the controller must operate.

Acknowledgement

Many talents and specialized skills have been required to develop a system as broad and complex as a velocity meter and VM control amplifier. Messrs. J. M. Slater, D. E. Wilcox, J. N. Schmidt, W. R. Evans, R. B. Higley, T. Mitsutomi, E. E. Pentecost, J. M. Rogers and a great many others have contributed their specialized talents and leadership to make the pendulous velocity meter successful. The authors wish to thank those who have contributed to this effort and for the opportunity to write this paper.

Bibliography

1. Curtis, T. E. and Slater, J. M., "Inertial Navigation in Submarine Operations of 1958", Navigation, Los Angeles, Spring, 1959.

2. Mitsutomi, T., "Characteristics and Stabilization of an Inertial Platform", IRE Transactions on Aeronautical and Navigational Electronics, June 1958, Vol ANE-5, No. 2, pp 95-105.

3. Slater, J. M., "Measurement and Integration of Acceleration in Inertial Navigation", The American Society of Mechanical Engineers, Paper No. 56-A-160.

4. Slater, J. M. and Duncan, D. B., "Inertial Navigation", Aeronautical Eng Review, January 1956, Vol 15, pp 49-53.

5. Slater, J. M. "Gyroscopes for Inertial Navigators", The American Society of Mechanical Engineers, Paper No. 57-SA-39.

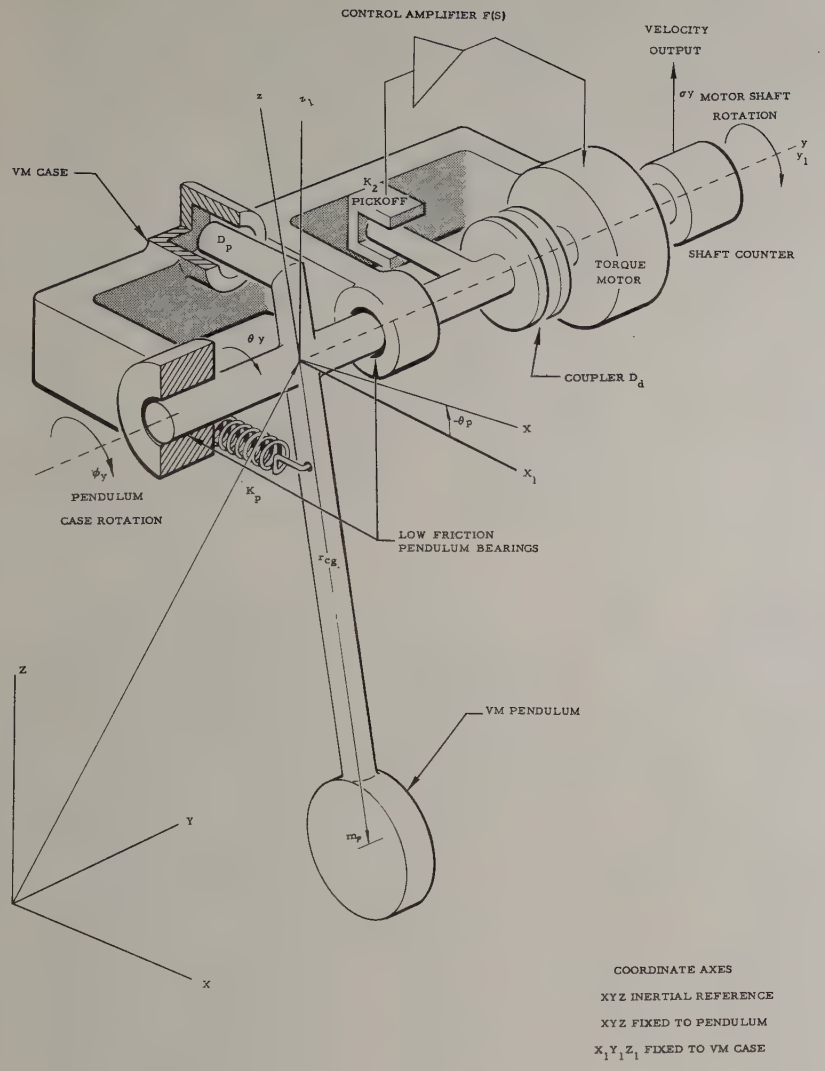
CONTROL AMPLIFIER F(S)
VELOCITY OUTPUT
MOTOR SHAFT ROTATION
VM CASE
PICKOFF
TORQUE MOTOR
SHAFT COUNTER
COUPLER D_d
PENDULUM CASE ROTATION
LOW FRICTION PENDULUM BEARINGS
VM PENDULUM
COORDINATE AXES
XYZ INERTIAL REFERENCE
XYZ FIXED TO PENDULUM
$X_1Y_1Z_1$ FIXED TO VM CASE

Fig. 1.

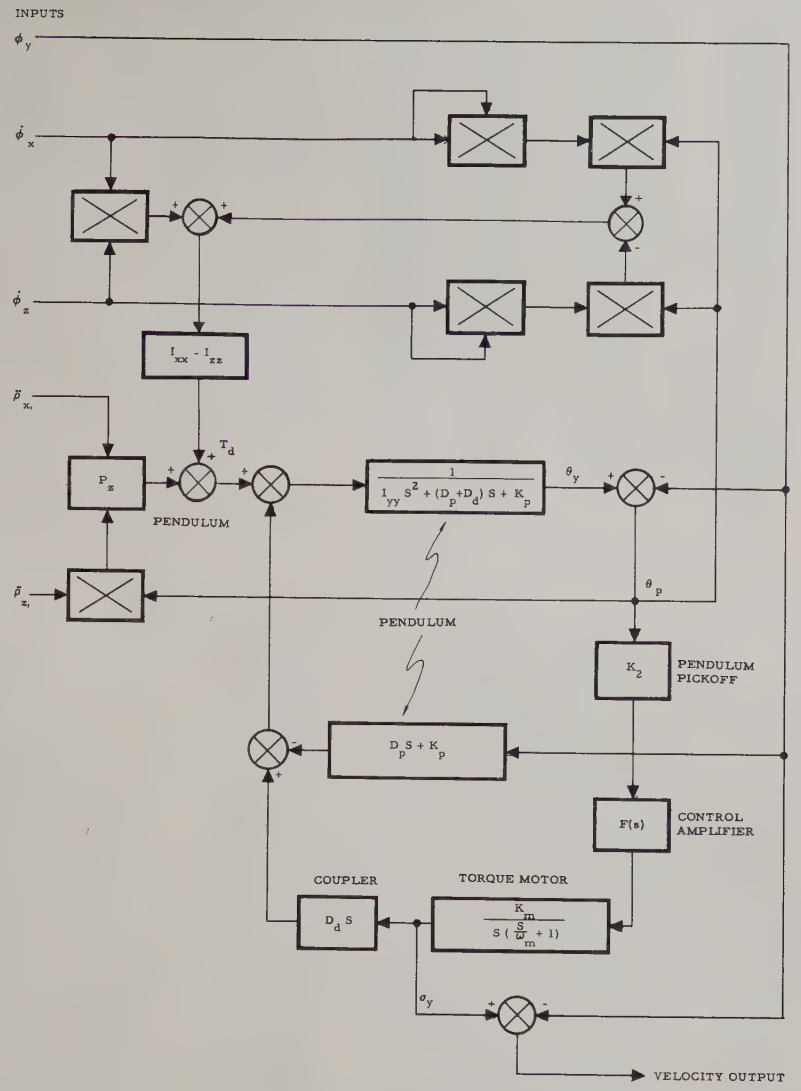
INPUTS
$I_{xx} - I_{zz}$
T_d
P_z
PENDULUM
$\frac{1}{I_{yy}S^2 + (D_p+D_d)S + K_p}$
PENDULUM
K_2
PENDULUM PICKOFF
$D_pS + K_p$
F(s)
CONTROL AMPLIFIER
COUPLER
D_dS
TORQUE MOTOR
$\frac{K_m}{S(\frac{S}{W_m}+1)}$
VELOCITY OUTPUT

Fig. 2.

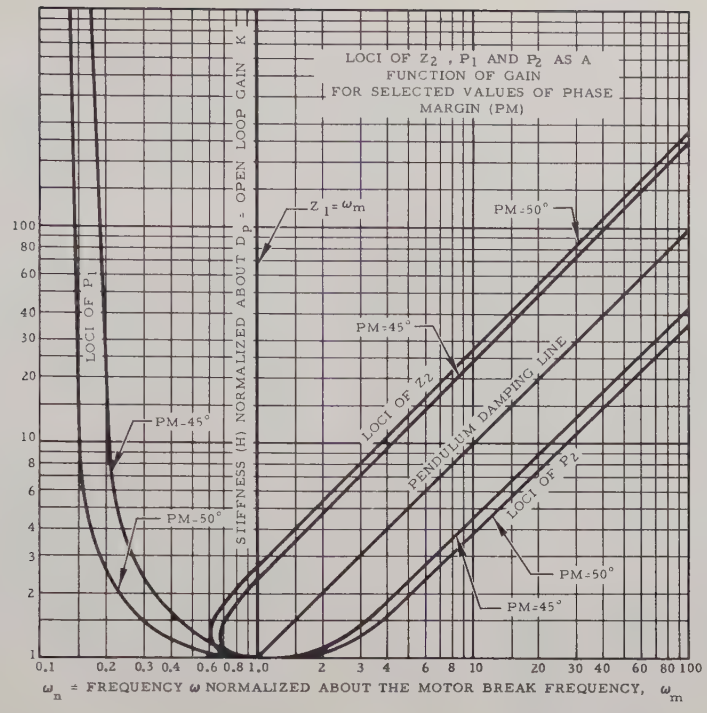
LOCI OF Z_2, P_1 AND P_2 AS A FUNCTION OF GAIN FOR SELECTED VALUES OF PHASE MARGIN (PM)
STIFFNESS (H) NORMALIZED ABOUT D_p = OPEN LOOP GAIN K
LOCI OF P_1
$Z_1 = \omega_m$
PM=50°
PM=45°
PM=45°
LOCI OF Z_2
PENDULUM DAMPING LINE
LOCI OF P_2
PM=50°
PM=45°
PM=50°
PM=45°
100
80
60
40
30
20
10
8
6
4
3
2
1
0.1
0.2
0.3
0.4
0.6
0.8
1.0
2
3
4
6
8
10
20
30
40
60
80
100
ω_n = FREQUENCY ω NORMALIZED ABOUT THE MOTOR BREAK FREQUENCY, ω_m

Fig. 3.

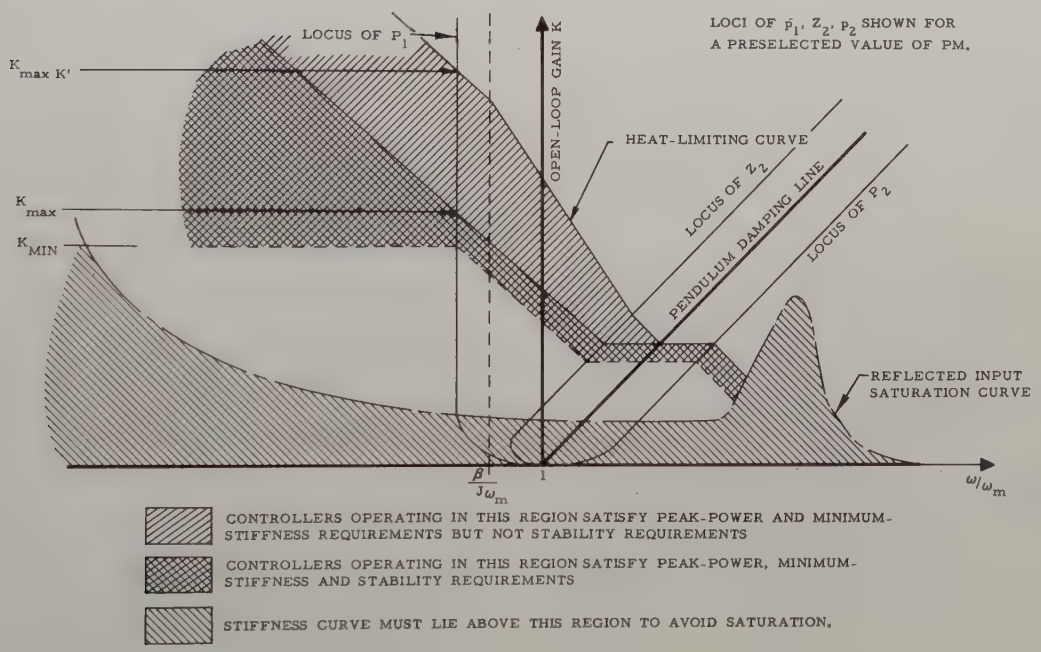
LOCUS OF P_1
LOCI OF P_1, Z_2, P_2 SHOWN FOR A PRESELECTED VALUE OF PM.
K_{max} K'
OPEN-LOOP GAIN K
HEAT-LIMITING CURVE
K_{max}
K_{MIN}
LOCUS OF Z_2
PENDULUM DAMPING LINE
LOCUS OF P_2
REFLECTED INPUT SATURATION CURVE
$\frac{\beta}{J\omega_m}$
1
ω/ω_m
CONTROLLERS OPERATING IN THIS REGION SATISFY PEAK-POWER AND MINIMUM-STIFFNESS REQUIREMENTS BUT NOT STABILITY REQUIREMENTS
CONTROLLERS OPERATING IN THIS REGION SATISFY PEAK-POWER, MINIMUM-STIFFNESS AND STABILITY REQUIREMENTS
STIFFNESS CURVE MUST LIE ABOVE THIS REGION TO AVOID SATURATION.

Fig. 4.

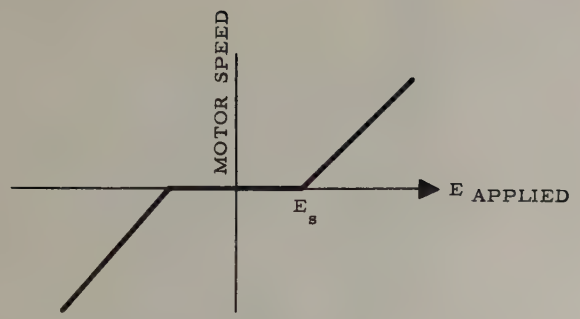

MOTOR VOLTAGE - SPEED CHARACTERISTICS

Fig. 5A.

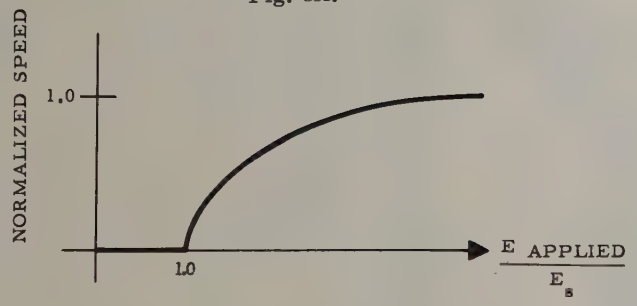

INPUT VOLTAGE NORMALIZED

MOTOR DESCRIBING FUNCTION INDICATED

Fig. 5B.

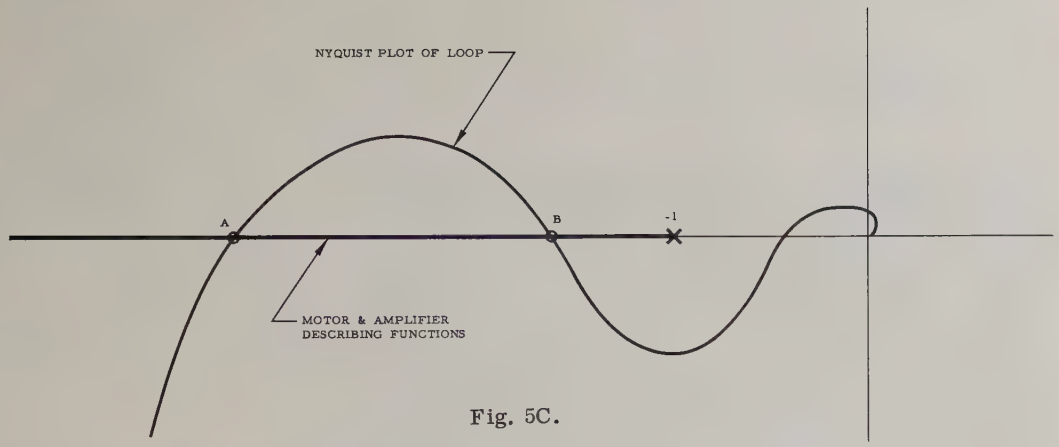

Fig. 5C.

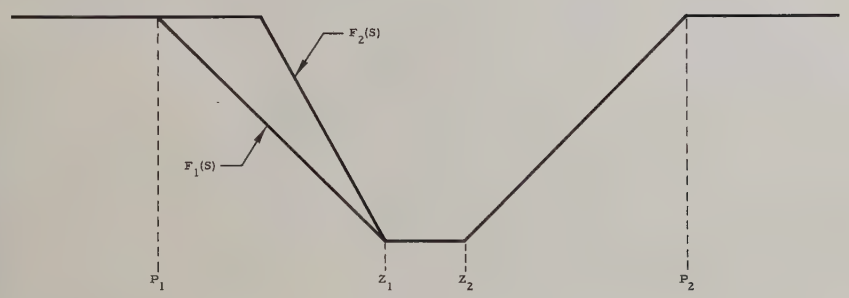

Fig. 5D.

THE ANALYSIS OF DEMODULATING COMPENSATING NETWORKS

Gordon J. Murphy and John F. Egan
Technological Institute
Northwestern University
Evanston, Illinois

Technological Institute
Northwestern University
Evanston, Illinois

Summary

The subject of this paper is the analysis of periodically switched electric networks. A method for determining a sampled-data system which is equivalent to a given member of a class of periodically switched electric networks is first presented. A technique for determining the response of the system to a given input function is then discussed in detail.

Next it is shown that it is possible to identify a time-invariant electric network with the same response to a step-function input as the envelope of the response of the switched network exhibits when the input to the switched network is a suddenly applied constant-amplitude sinusoid at the switching frequency. This "equivalent" d-c network can be utilized to advantage in the design of carrier systems in which periodically switched electric networks are employed as compensators.

Examples are then presented to illustrate the application of the theory, and the results obtained by this method are compared with those obtained by a different method, proposed earlier.

Finally, it is pointed out that the response calculated by the use of the method presented in this paper is theoretically exact and that the technique can be extended to encompass a wide class of periodically switched linear systems.

Introduction

For various reasons, the use of synchronous switches or choppers in feedback control systems is becoming ever more common. The networks incorporating the choppers cannot be analyzed simply by the well known techniques for the analysis of linear networks with constant parameters because the effect of the switching is to alter network parameters periodically. It is natural, therefore, to attempt to apply in the analysis of such networks some technique which has satisfactorily been employed in the analysis of systems with time-varying parameters. The use of one such technique, based on the z-transformation,[3] is presented in this paper.

Representation of a Periodically Switched Passive Network as a Sampled-Data System

The widespread use of synchronous vibrators (or "choppers") in electric networks has given rise to a need for a convenient method for analyzing periodically switched electric networks of the type illustrated in Fig. 1. If the form and the values of the components of the output network in such a system are known, then the output, e_4, of the complete system is determined by the values of e_2 at the instants the switch armature leaves the left-hand contact. Since these discrete values of e_2 occur periodically, it follows that the switching operation may be regarded as conventional sampling, and that the network illustrated in Fig. 1 is equivalent to a conventional sampled-data system.

The method used to obtain a sampled-data system which is equivalent to a given network of the general type illustrated in Fig. 1 is presented below. For illustrative purposes special forms of the general network are chosen. One particular network, shown in Fig. 2, is of practical interest and has been studied by Bolie[1] for $R_2 = \infty$ and $e_1(t)$ an amplitude-modulated sinusoid with carrier frequency equal to the switching frequency.

The switch in the circuit illustrated in Fig. 2 is actuated at a constant rate of $1/T$ times per second. Ideally, the effect of the switch is to complete the circuit between terminals 1 and 2 for

$$kT \leq t < (k+\delta)T, \quad k = 0,1,2,\ldots, \tag{1}$$

where

$$0 < \delta < \tfrac{1}{2} \tag{2}$$

is the dwell time of the contacts, and to complete the circuit between terminals 2 and 3 for

$$(\tfrac{2k+1}{2})T \leq t < [(\tfrac{2k+1}{2}) + \delta]T, \quad k=0,1,2,\ldots. \tag{3}$$

In so doing, it has the effect of closing the left-hand loop (thus impressing $e_1(t)$ upon the series RC Circuit) for $kT \leq t < (k+\delta)T$ and opening the left-hand loop for $(k+\delta)T \leq t < (k+1)T$. Furthermore, it has the additional effect of sampling the output of the low-pass network comprised of R_1 and C at the instants

$$t = (k+\delta)T, \quad k = 0,1,2,\ldots \tag{4}$$

and storing a proportional electric charge on the capacitor at those instants. Finally, in closing the right-hand loop, it permits this stored charge to flow through the resistance R_2, with the result that the output $e_3(t)$ is a train of pulses, each of width δT seconds, with leading edges of adjacent pulses separated by T seconds.

For $kT \leq t < (k+\delta)T$, then $e_2(t)$ is identical to the voltage which would appear across the terminals of the capacitor C if the switch were inoperative and in its left-hand position for $t > 0$ provided that

a) $e_1(t)$ be replaced by

$$e_m(t) \triangleq e_1(t)p(t), \tag{5}$$

where

$$p(t) = \sum_{k=0}^{\infty} \left\{u_{-1}(t-kT) - u_{-1}[t-(k+\delta)T]\right\} \tag{6}$$

where $u_{-1}(t)$ is the unit step function with discontinuity at $t = 0$ and

b) the contribution to $e_2(t)$ on

$nT \leq t < (n+\delta)T$ due to $e_m(\tau)$ for $\tau < nT$ be eliminated

and

c) the charge on the capacitor at $t = kT$ be made

$$q(kT) = Ce_3[(\frac{2k-1}{2} + \delta)T-]. \tag{7}$$

Since the system is linear, the complete response can be obtained by superposition. The contribution to $e_2(t)$ due to $e_m(t)$ is

$$e_\alpha(t) = \mathcal{L}^{-1}G(s)E_m(s), \tag{8}$$

where

$$G(s) \triangleq \frac{1}{\tau_1 s + 1}, \tag{9}$$

with

$$\tau_1 \triangleq R_1C, \tag{10}$$

is the transfer function of the network on the left.

The contributions to $e_2(t)$ on $nT \leq t < (n+\delta)T$ due to $e_m(\tau)$ for $\tau < nT$ and $q(kT)$ for $k < n$ can be eliminated by introducing as a second input in addition to $e_m(t)$ to a unit with transfer function $G(s)$ volts per volt a voltage

$$e_\beta(t) \triangleq -R_1C\sum_{k=0}^{\infty} e_2[(k+\delta)T-]u_o[t-(k+\delta)T+]. \tag{11}$$

Finally, the charge on the capacitor at $t = kT$ can then be made to satisfy (7) by introducing into the unit with transfer function $G(s)$ volts per volt a third input,

$$e_\gamma(t) \triangleq R_1q(0-) + R_1C\sum_{k=1}^{\infty} e_3[(\frac{2k-1}{2}+\delta)T-]u_o(t-kT), \tag{12}$$

where $q(0-)$ is the initial charge on the capacitor (at $t = 0-$).

In the special case considered by Bolie,

$$R_2 = \infty. \tag{13}$$

For this condition, the value of $e_2[(k+\delta)T]$ is simply memorized for the following $(1-\delta)T$ seconds. (That is, the pulses comprising $e_3(t)$ have flat tops.) Such an output is readily obtained in a block diagram by introducing at the output of the block representing a unit with transfer function $G(s)$ an ideal sampler that operates at $t = (k+\delta)T$, $k = 0,1,2,\ldots$ and following this sampler with a delay unit with dead time of $(1-2\delta)T/2$ seconds and then a clamper with transfer function

$$G_C(s) = \frac{1 - e^{-T\delta s}}{s}. \tag{14}$$

Thus, it is seen that, for $R_2 = \infty$ and $q(0-) = 0$, the network illustrated in Fig. 2 can be represented by the block diagram shown in Fig. 3(a). Finally, it can easily be shown that, insofar as the relations between $e_3(t)$, $e_m(t)$, and $e_1(t)$ are concerned, the block diagram shown in Fig. 3(b) is equivalent to that shown in Fig. 3(a). Furthermore, the operation of sampling at $t = (k+\delta)T$, $k = 0,1,2,\ldots$, is equivalent to advancing the signal to be sampled by δT seconds, sampling at $t = kT$, and retarding the resulting train of impulses by δT seconds.

For the system studied by Bolie,

$$e_1(t) = e_i(t)\cos(\Omega t + \varphi), \tag{15}$$

where the carrier frequency is

$$\Omega = \frac{2\pi}{T} \text{ rad/sec}. \tag{16}$$

It follows that in that system

$$e_m(t) = e_i(t)\cos(\Omega t + \varphi)p(t). \tag{17}$$

In general, if

$$f_3(t) = f_i(t)\cos(\Omega t + \theta)p(t), \tag{18}$$

the process of deriving $f_3(t)$ from $f_1(t)$ can be represented either as shown in Fig. 4(a) or as shown in Fig. 4(b), because of the commutative property of the operation of multiplication. The representation in Fig. 4(b) is very convenient because of its physical interpretation as the modulation of a chopped sinusoid by the input function $f_1(t)$. Accordingly, it is convenient to use the block diagram shown in Fig. 5 to represent the network illustrated in Fig. 2 with $q(0-) = 0$, $R_2 = \infty$, and $e_1(t)$ given by (15). Then, by the use of a simple and well known technique, the block diagram can be reduced to the form shown in Fig. 6.

The significance of Fig. 6 is as follows:

(a) there is a closed-loop sampled-data system, in which samples are taken at $t = kT$, with closed-loop transfer function

$$\frac{C}{R}(z) = \frac{1}{1 - H(z)}, \tag{19}$$

where $H(z)$ is the z-transform corresponding to $\frac{1 - e^{-(1-\delta)Ts}}{s} G(s)$.

(b) the Laplace transform of the input to the closed-loop sampled-data system is

$$R(s) = e^{\delta Ts}G(s)\mathcal{L}[e_i(t)\cos(\Omega t + \varphi)p(t)] \tag{20}$$

$$= e^{\delta Ts}G(s)\mathcal{L}[e_i(t)f_4(t)], \tag{21}$$

where

$$f_4(t) \triangleq \cos(\Omega t + \varphi)p(t). \tag{22}$$

(c) Each of the impulse functions (at $t = kT$) comprising $c(t)$ is delayed by $T/2$ seconds and then clamped for δT seconds, with the result that $e_3(t)$ consists of a set of rectangular pulses of width δT seconds, with leading edges at $t = (\frac{2k+1}{2})T$.

Determination of the Response of the Periodically Switched Passive Network to a Given Input

It is evident in Fig. 6 that

$$R(z) = \mathcal{Z}[e^{\delta Ts}G(s)E_m(s)]. \tag{23}$$

In general,

$$E_m(s) = \mathcal{L}[e_i(t)f_4(t)] \tag{24}$$

$$= \frac{1}{2\pi j}\int_{c_1-j\infty}^{c_1+j\infty} E_i(p)F_4(s-p)\,dp, \quad (25)$$

where $c_1 < [\text{Re } s]$ is greater than the abscissa of absolute convergence of $E_i(p)$; and, in particular, if

$$e_i(t) = E_o u_{-1}(t), \quad (26)$$

then

$$E_m(s) = E_o\frac{(s\cos\varphi - \Omega\sin\varphi)(1-e^{-\delta Ts}\cos\Omega\delta T)}{(s^2+\Omega^2)(1-e^{-Ts})} + E_o\frac{\sin\Omega\delta T(\Omega\cos\varphi + s\sin\varphi)e^{-\delta Ts}}{(s^2+\Omega^2)(1-e^{-Ts})}. \quad (27)$$

If the input to the system illustrated in Fig. 6 is a step of voltage of magnitude E_o, then, it follows that

$$R^*(s) = \frac{E_o}{1-e^{-Ts}}\frac{1}{2\pi j}\int_{c-j\infty}^{c+j\infty}\frac{e^{\delta Tp}}{(p^2+\Omega^2)(\tau_1 p+1)[1-e^{-T(s-p)}]}$$

$$\{p\cos\phi - \Omega\sin\phi)[1-e^{-\delta Tp}\cos\Omega\delta T] + e^{-\delta Tp}\sin\Omega\delta T(\Omega\cos\phi + p\sin\phi)\}\,dp \quad (28)$$

$$= \frac{KE_o e^{2sT}}{(e^{sT}-1)(e^{sT}-e^{-T/\tau_1})} \quad (29)$$

where

$$K \triangleq \frac{\Omega\tau_1\sin(\Omega\delta T+\varphi) + \cos(\Omega\delta T+\varphi) - e^{-\delta T/\tau_1}(\Omega\tau_1\sin\varphi + \cos\varphi)}{\Omega^2\tau_1^2+1}. \quad (30)$$

Accordingly, under the conditions stated above,

$$R(z) = \frac{KE_o z^2}{(z-1)(z-e^{-T/\tau_1})}. \quad (31)$$

The pulse transfer function H(z) in (19) can be determined also by contour integration or by the use of tables. However, it is often convenient to use the following alternative method.* Expanding H(s) in partial fractions yields

$$H(s) = \frac{1-e^{-(1-\delta)Ts}}{s(\tau_1 s+1)} = \frac{1}{s} - \frac{1}{s+1/\tau_1} - \frac{e^{-(1-\delta)Ts}}{s} + \frac{e^{-(1-\delta)Ts}}{s+1/\tau_1}. \quad (32)$$

Then

$$H(z) = \frac{z}{z-1} - \frac{z}{z-e^{-T/\tau_1}} - \frac{1}{z-1} + \frac{e^{-\delta T/\tau_1}}{z-e^{-T/\tau_1}} \quad (33)$$

$$= \frac{e^{-\delta T/\tau_1} - e^{-T/\tau_1}}{z-e^{-T/\tau_1}}, \quad (34)$$

and

$$\frac{C(z)}{R(z)} = \frac{1}{1-H(z)} \quad (35)$$

$$= \frac{z-e^{-T/\tau_1}}{z-e^{-\delta T/\tau_1}}. \quad (36)$$

Substituting the right-hand side of (31) into (36) and solving for C(z) then yields

$$C(z) = \frac{KE_o z^2}{(z-1)(z-e^{-\delta T/\tau_1})}. \quad (37)$$

The inverse z-transform of this C(z) is

$$c(t) = \frac{KE_o}{1-e^{-\delta T/\tau_1}}\sum_{k=0}^{\infty}(1-e^{-\delta T/\tau_1}e^{-k\delta T/\tau_1})u_o(t-kT). \quad (38)$$

Finally, the effect of the delay and the clamping action is to convert this train of impulses to the pulse train

$$e_3(t) = \frac{KE_o}{1-e^{-\delta T/\tau_1}}\sum_{k=0}^{\infty}[1-e^{-(k+1)\delta T/\tau_1}]\left\{u_{-1}[t-(\tfrac{2k+1}{2})T] - u_{-1}[t-(\tfrac{2k+1}{2}+\delta)T]\right\}. \quad (39)$$

Thus, it is seen that if the input to the network illustrated in Fig. 6 is given by (26), then the output of the network has the form illustrated in Fig. 7. For an input step of given polarity, the sign of the output is determined by the carrier frequency Ω, the time constant τ_1, the dwell time δT, and the phase angle φ.

The value φ_m of φ for which the sensitivity of the network is maximum can be found by differentiating the right-hand side of (30) with respect to φ and equating the result to zero for $\varphi = \varphi_m$. Thus it is found that

$$\varphi_m = \arctan\frac{\Omega\tau_1\cos\Omega\delta T - \sin\Omega\delta T - \Omega\tau_1 e^{-\delta T/\tau_1}}{\Omega\tau_1\sin\Omega\delta T + \cos\Omega\delta T - e^{-\delta T/\tau_1}}. \quad (40)$$

One of the two principal solutions for φ_m yields a train of positive pulses for $e_3(t)$; the other yields negative pulses. Except for this difference in polarity, the output is independent of the choice of the solution to (40).

The d-c network which responds to a unit step as the envelope of the response of the switched network under consideration responds to the step of carrier impressed upon the input terminals of this network is a cascade connection of an amplifier or an attenuator and the familiar lag network with a transfer function of

$$G(s) = \left[\frac{K}{(1-e^{-\delta T/\tau_1})}\right]\frac{\frac{\tau_1(1-e^{-\delta T/\tau_1})}{\delta}s+1}{\frac{\tau_1}{\delta}s+1}. \quad (41)$$

This equivalent d-c network is illustrated in Fig. 8.

Example 1

The values of the parameters of the system illustrated in Fig. 2 are

1) $T = 1/400$ second
2) $\delta = 0.4$
3) $\varphi = \varphi_m$
4) $R_1 = 10^6$ ohms
5) $C_1 = 10^{-6}$ farad.

Determine the response of this system to the input

$$e_1(t) = \cos(\Omega t + \varphi), \quad (42)$$

given that the system is initially quiescent

(i.e., $q(0-) = 0$).

Substitution of the given values of T, δ, R_1, and C_1 into the right-hand member of (40) yields

$$\varphi_m = 108^\circ \text{ or } 288^\circ.$$

Choosing $\varphi_m = 288^\circ$ to obtain positive pulses and substituting this value along with the given values of the other parameters of the system into (30) yield

$$K = 7.57 \times 10^{-4}. \tag{44}$$

Finally, (39) becomes

$$e_3(t) = 0.757 \sum_{k=0}^{\infty} [1-(0.999)^{k+1}] \left\{u_{-1}[t-(\tfrac{2k+1}{2})T] - u_{-1}[t-(\tfrac{2k+1}{2}+\delta)T]\right\}, \tag{45}$$

where

$$T = 0.0025 \tag{46}$$

and

$$\delta T = 0.001. \tag{47}$$

It should be noted that this result can be obtained much more readily by replacing the switched network with its equivalent d-c network, shown in Fig. 8, and determining the response of the d-c network to a unit step applied at t = 0. The actual output of the switched network can then be drawn under the graph of the response of the d-c network so as to have the appearance indicated in Fig. 7.

Comparison of Results Obtained

Bolie has solved the same problem,† and he presents the solution in his (21). However, because of a slight error in computation, this solution is not quite correct. Since

$$\frac{\sin 0.4\pi}{0.4\pi} = 0.757 \tag{48}$$

and not 0.753 as stated by Bolie, his solution is correctly given by

$$G(t) = E(0)e^{-t/2.5} + 0.757V[1-e^{-t/2.5}]. \tag{49}$$

For the case under consideration,

$$E(0) = 0 \tag{50}$$

and

$$V = 1. \tag{51}$$

Hence, Bolie's solution to this particular problem is

$$G(t) = 0.757(1-e^{-t/2.5}). \tag{52}$$

Accordingly, the amplitude of the pulse commencing** at $t = kT$, $k = 1,2,3,\ldots$, is

$$P_k = 0.757(1-e^{-kT/2.5}) = 0.757(1-e^{-0.001k}) \tag{53}$$

$$= 0.757(1-0.999^k), \tag{54}$$

which is identical to the result obtained in (45) by the use of z-transforms.

Extension to the Case Where R_2 Is Finite

If the resistance R_2 is finite, rather than infinite as assumed in the analysis presented above, the same general approach can be used. However, it is then necessary to modify the transfer functions of the feedback element and the output element in Fig. 6 so as to account for the discharge of the capacitor during the intervals in which terminals 2 and 3 in the circuit diagram in Fig. 2 are connected. This has been done, and the resulting sampled-data system has been analyzed to determine the response of the corresponding network to a step input of modulation of the carrier. The results are shown in Fig. 9, for a network identical to that in the preceding example, except that R_2 = 100,000 ohms.

Example 2

The network illustrated in Fig. 1 is sometimes employed also as a lead compensator in carrier control systems. For this purpose the input is an ideal modulator, output network #1 is reduced to a pair of conductors, with a transfer function of unity, and output network #2 is eliminated entirely, (that is, the output of the system is e_4). The circuit diagram then has the appearance shown in Fig. 10, wherein it is evident that the problem of analyzing the network under discussion is very closely related to the problem of analysis described in detail in Example 1.

At any instant at which the circuit illustrated in Fig. 10 is closed, as shown,

$$e_4(t) = e_1(t) - e_2(t). \tag{55}$$

Since the $e_2(t)$ in Fig. 10 is the $e_2(t)$ in Fig. 2, and since

$$e_4(t) = 0 \tag{56}$$

at any instant at which the circuit is open, the sampled-data system illustrated in Fig. 11 defines a mathematical model of the network under discussion, if

$$G_1(s) \triangleq \frac{R_1Cs}{R_1Cs+1} \tag{57}$$

and

$$G_2(s) \triangleq \frac{1}{R_1Cs+1}. \tag{58}$$

It is evident in Fig. 11 that the z-transform of $e_4(t)$ can be determined by simple application of the well defined rules for the analysis of sampled-data systems. What is actually desired, however, is not $e_4(kt)$, $k = 0,1,2,3,\ldots$, but rather either $e_4(t)$ itself or at least the envelope of $e_4(t)$. For this reason, the modified z-transform is used instead of the ordinary z-transform. Thus, it is found that

$$e_4[(n-1+m)T] = \mathcal{Z}_m^{-1}\left\{G_1E_m(z,m) + \frac{G_1G_3(z,m)G_4E_m(z)}{1-G_3G_4(z)}\right\}, \tag{59}$$

where

$$G_1E_m(z,m) \triangleq \mathcal{Z}_m[G_1(s)E_m(s)], \tag{60}$$

$$G_3(s) \triangleq e^{-\delta Ts}\left[\frac{1-e^{-(1-\delta)Ts}}{s}\right], \tag{61}$$

$$G_4(s) \triangleq e^{\delta TS} G_2(s), \tag{62}$$

and

$$G_1G_3(z,m) \triangleq \mathcal{Z}_m[G_1(s)G_3(s)]. \tag{63}$$

It can be shown that if

$$e_1(t) = e_i(t)\sin \Omega t \tag{64}$$

and

$$e_i(t) = E_o\, u_{-1}(t) \tag{65}$$

and

$$\delta = \tfrac{1}{2}, \tag{66}$$

then

$$E_4(z,m) = \frac{E_o}{(R_1^2C^2\Omega^2+1)(z-1)(z-e^{-T/R_1C})} \left\{ \begin{array}{l} (R_1C\Omega\cos 2\pi m + R_1^2C^2\Omega^2\sin 2\pi m)(z-e^{-T/R_1C}) \\ - R_1C\Omega\, e^{-mT/R_1C}(z + e^{-T/2R_1C}) \end{array} \right\}$$

$$- \frac{R_1C\Omega E_o\, e^{-mT/R_1C}(1-e^{-T/R_1C})z}{(R_1^2C^2\Omega^2+1)(z-1)(z-e^{-T/R_1C})(z-e^{-T/2R_1C})}, \qquad 0 \le m < \tfrac{1}{2}. \tag{67}$$

It follows from (67) that, under the specified conditions,

$$e_4[(n+m)T] = \frac{E_o}{R_1^2C^2\Omega^2+1} \left\{ \begin{array}{l} R_1C\,\Omega\cos 2\pi m + R_1^2C^2\Omega^2\sin 2\pi m \\ - \dfrac{2R_1C\,\Omega}{1-e^{-T/2R_1C}}\, e^{-mT/R_1C} \\ + R_1C\,\Omega\coth\dfrac{T}{4R_1C}\, e^{-(n+2m)T/2R_1C} \end{array} \right\},$$

$$n = 0,1,2,\ldots,\ 0 < m < \tfrac{1}{2}. \tag{68}$$

Furthermore,

$$e_4[(n+m)T] = 0, \quad n = 0,1,2,\ldots,\ \tfrac{1}{2} < m < 1. \tag{69}$$

It can be shown that if two such networks are connected back-to-back and diode clippers are introduced so as to eliminate the spikes in the output waveform the resulting circuit is equivalent to the d-c network illustrated in Fig. 12, with

$$K = \frac{R_1C\,\Omega}{R_1^2C^2\Omega^2+1}\left[\cos\theta + R_1C\,\Omega\sin\theta - \frac{2}{1-e^{-T/2R_1C}}\, e^{-\frac{\theta T}{2\pi R_1C}} + \coth\frac{T}{4R_1C}\, e^{-\theta T/2\pi R_1C}\right], \tag{70}$$

where

$$\theta \triangleq \frac{\pi}{2} - \arctan\frac{1}{R_1C\,\Omega}, \tag{71}$$

and

$$R_1' = \frac{2K(R_1^2C^2\Omega^2+1)}{R_1C\Omega\left(\cos\theta + R_1C\,\Omega\sin\theta - \dfrac{2}{1-e^{-T/2R_1C}}\, e^{-\theta T/2\pi R_1C}\right)} R_1 \tag{72}$$

and

$$R_2' = \frac{2K(R_1^2C^2\Omega^2+1)}{R_1C\Omega\left(\coth\frac{T}{4R_1C}\, e^{-\theta T/2\pi R_1C}\right)} R_1 \tag{73}$$

and

$$C' = C. \tag{74}$$

A graph of $e_4(t)$, plotted from (68) and (69), is shown in Fig. 13 for R_1 = 3990 ohms, C = 10^{-7} farad, and T = 1/400 second.

Conclusions

Periodically switched electric networks can be analyzed as sampled-data systems. The use of the z-transformation to describe the operation of such systems yields a convenient, compact, and relatively simple solution. When this approach is used, it is not necessary to limit consideration to those systems in which the input $e_1(t)$ and the output $e_3(t)$ are modulated carriers with non-negative envelopes, as in Bolie's method. Moreover, the solution obtained by the method presented in this paper is theoretically exact and the technique can be extended to encompass a wide class of periodically switched linear systems.

Alternatively, the problem can be solved by the use of difference equations. This has been done, and the results thus obtained are of course identical to those presented in this paper.

Since the compensation obtained in a carrier control system by the use of switched networks of the kind discussed in this paper is independent of carrier frequency, such compensating networks are superior to the more conventional a-c compensating networks for most applications.

The analysis of carrier control systems which are compensated by a synchronously switched network of the kind under discussion can be considerably simplified by the substitution of an "equivalent" d-c network for the switched compensator and the substitution of an amplifier with appropriate gain for the modulator in the block diagram of the system. Although the analysis then yields only an approximation to the actual response of the system, considerable insight into the performance of the system can thus be attained. Accordingly this procedure is of value at least in the early stages of design.

REFERENCES

1. Victor W. Bolie, "Analysis of a Special Purpose RC Filter Incorporating a Periodically Conducting Bilinear Element," IRE Proc., vol. 42, no. 9, pp. 1435-1438, September, 1954.
2. William K. Linvill, "Sampled-Data Control Systems Studied Through Comparison of Sampling with Amplitude Modulation," A.I.E.E. Trans., vol. 70, pt. II, pp. 179-188, 1951.
3. J. R. Ragazzini and Lofti Zadeh, "The Analysis of Sampled-Data Systems," A.I.E.E. Trans., vol. 71, pt. II, pp. 225-232, 1952.
4. John G. Truxal, Automatic Feedback Control System Synthesis, McGraw-Hill Book Company, New York, 1955, p. 511.
5. Eliahu I. Jury, Sampled-Data Control Systems, John Wiley and Sons, Inc., New York, 1958.

6. J. R. Ragazzini and F. G. Franklin, Sampled-Data Control Systems, McGraw Hill Book Company, New York, 1958.

7. G. J. Murphy, Control Engineering, D. Van Nostrand Company, Inc., Princeton, N. J., 1959.

8. G. J. Murphy and J. F. Egan, "The Analysis of Compensating Detectors for A-C Control Systems," NEC Proc., vol. XV (1959).

FOOTNOTES

*See, for example, Automatic Feedback Control System Synthesis, John G. Truxal, McGraw-Hill Book Company, Inc., New York, 1955, p. 554.

†See p. 1438 of reference 1.

**It should be noted that Bolie chose his time origin to coincide with t = - T/2 on the abscissa used earlier in this paper.

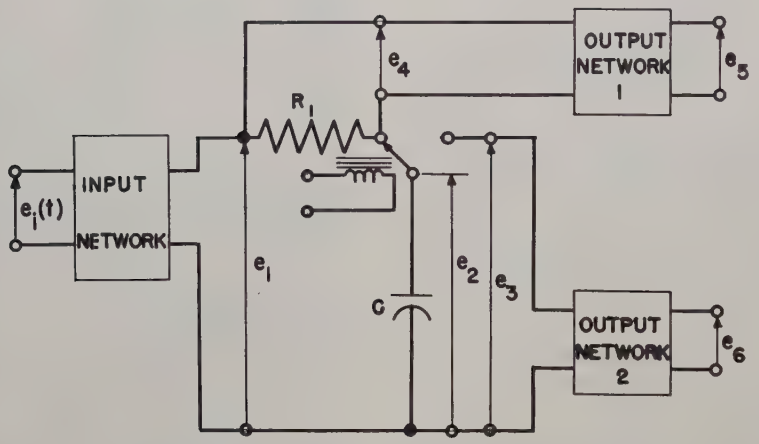

Fig. 1. Diagram of a class of periodically switched electric networks.

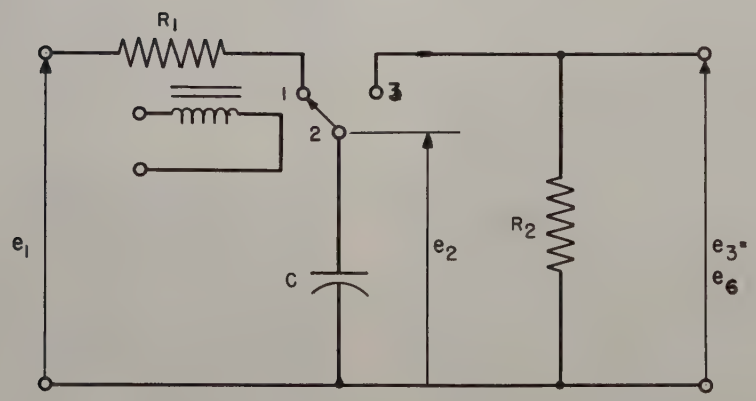

Fig. 2. A particular example of the type of network illustrated in Fig. 1.

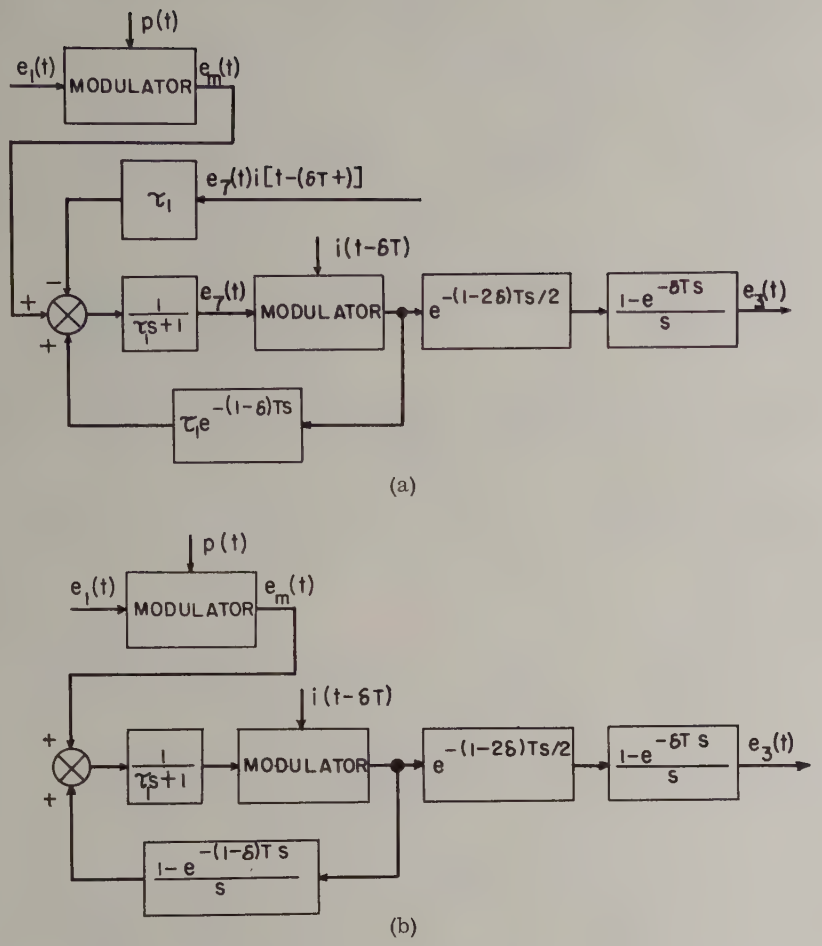

Fig. 3. Block diagram representation of the network illustrated in Fig. 2 with $R_2 = \infty$.

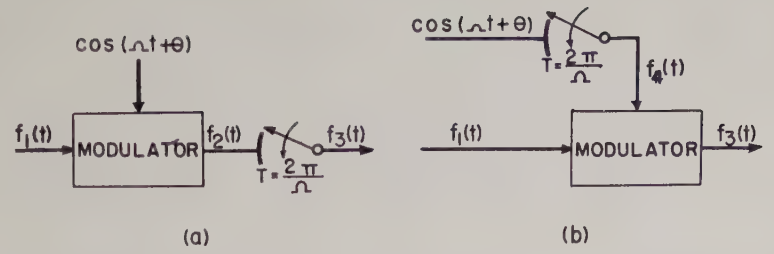

Fig. 4. Equivalent diagrammatic representations of the modulating-and-switching process.

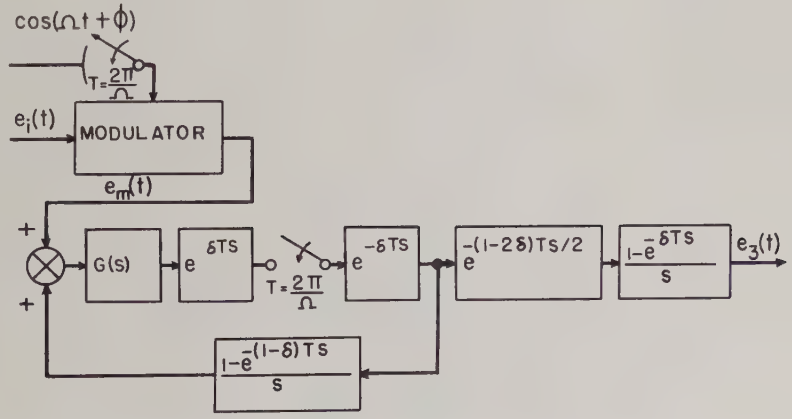

Fig. 5. Block diagram of a sampled-data system equivalent to the system illustrated in Fig. 3.

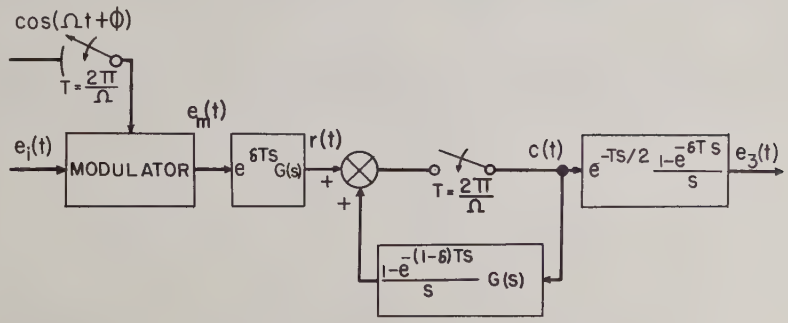

Fig. 6. Block diagram of a sampled-data system equivalent to the system illustrated in Fig. 5.

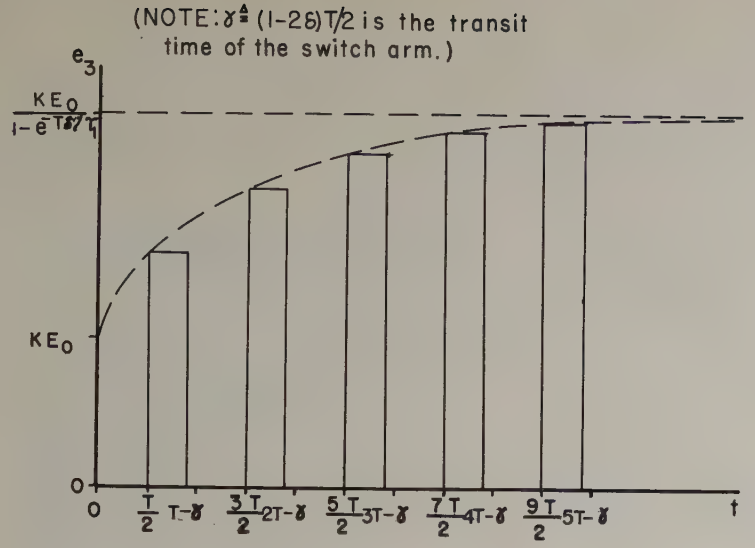

Fig. 7. Response of the system shown in Fig. 6 to a step function.

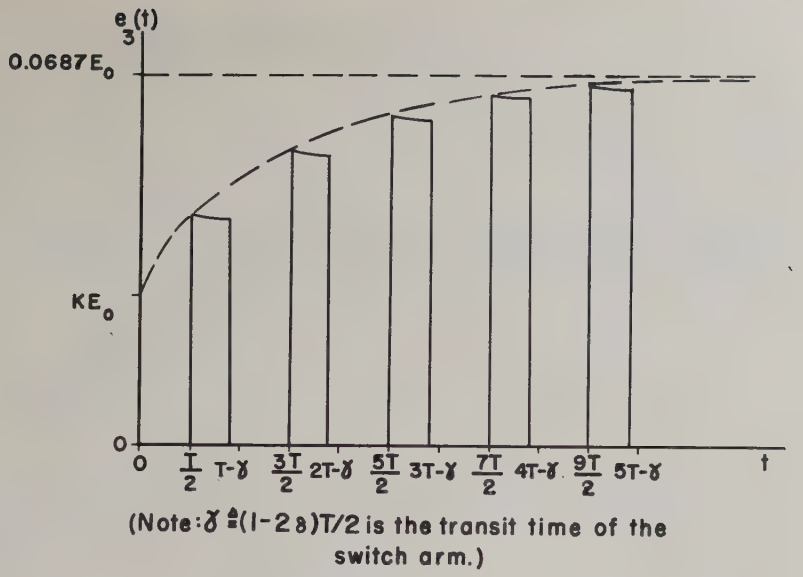

Fig. 9. Response of the network illustrated in Fig. 2, with finite R_2, to a step of modulation of the carrier.

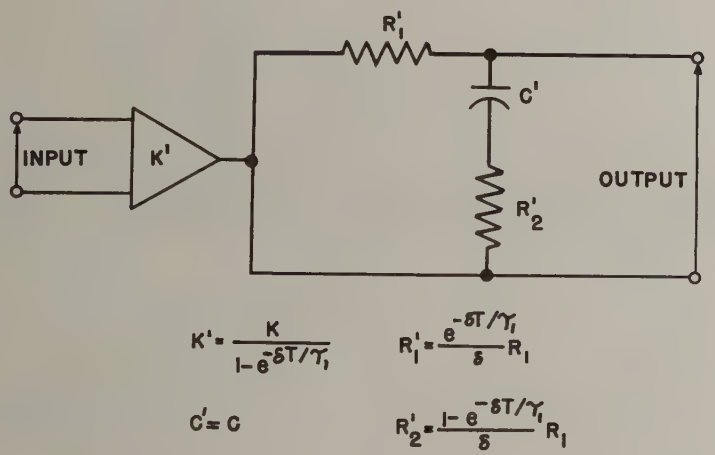

Fig. 8. The d-c network equivalent to the switched network in Example 1.

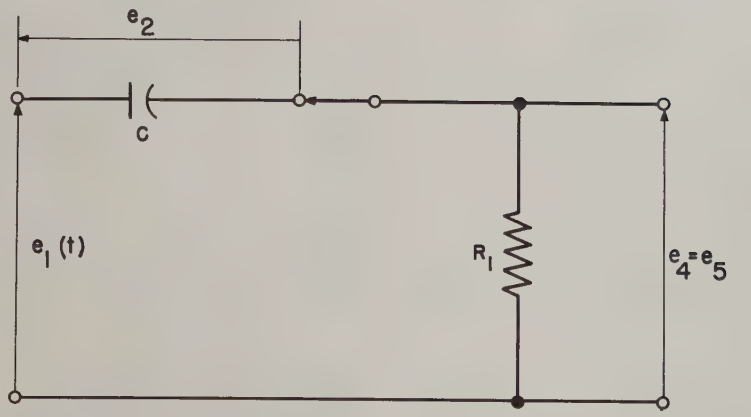

Fig. 10. A demodulating lead network for use in carrier control systems.

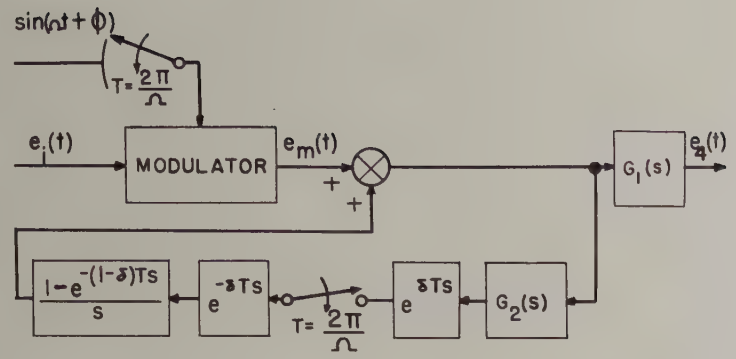

Fig. 11. A sampled-data system that defines a mathematical model of the network illustrated in Fig. 10.

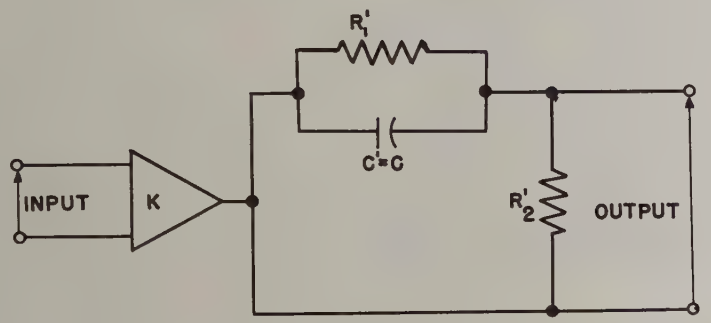

Fig. 12. A d-c network equivalent to the network illustrated in Fig. 10.

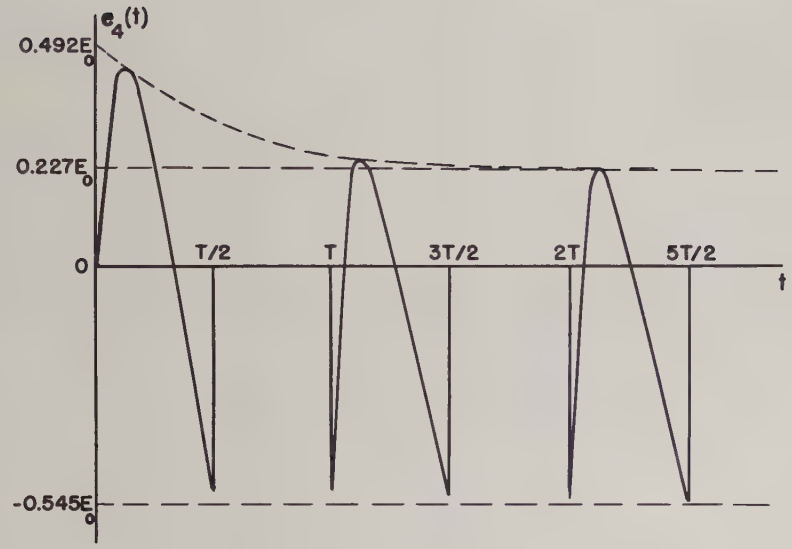

Fig. 13. Response of the network illustrated in Fig. 10 to a step input of magnitude E_o for $R_1 = 3990$ ohms, $C = 10^{-7}$ farad, $T = 1/400$ second, and $\delta = 1/2$.

MATHEMATICAL MODELS FOR COMPUTER CONTROL SYSTEMS

T. M. Stout
Thompson-Ramo-Wooldridge Products Company
Los Angeles, Calif.

Abstract

Mathematical models are often needed for design and justification of computer control systems prior to installation. They may also become an integral part of the control system itself, providing a means for rapid and periodic determination of the best operating conditions. Using fundamental physical and chemical principles, relationships are written to describe typical process operations. Both steady-state and dynamic models are considered. By means of "constants" which will be modified by the control computer, the models can accommodate slow and minor changes arising from variables whose effects are poorly understood. Some applications of the models are mentioned.

This paper is to be published in the Proceedings of the First IFAC Moscow Congress by Butterworth Scientific Publications in 1960.

MULTI-LOOP AUTOMATIC TEMPERATURE CONTROL SYSTEM DESIGN FOR FLUID DYNAMICS FACILITY HAVING SEVERAL LONG TRANSPORT DELAYS

G. J. Fiedler J. J. Landy
Sverdrup & Parcel Engineering Co.
St. Louis, Missouri

Summary. This paper describes the systems analysis and design of an automatic temperature control system in the world's largest fluid dynamics testing complex consuming 470 megawatts of drive power. The plant treated in this paper can be described mathematically as a 110th order system having 130 feedback loops. Facility component characteristics are mostly non-linear, with prominent distributed parameters and ten long, variable fluid transport delay times. Important simplifications introduced to make the analysis and design work tractable include: (a) Application of the mathematical analogy between the theory of electric transmission lines and gas flow to validate the separation of temperature and pressure variations, (b) Selection of control frequency to permit lumped-parameter representation, (c) Design and construction of special computer devices and circuitry to simulate transport delays from 0.2 to 141 seconds in length. These valid simplifications reduce the plant to a 14th order system having about 50 feedback loops. The simplified system is simulated on an analog computer for economical synthesis and design of the controllers.

Introduction

The basic purpose of this work is to design an effective automatic control system for stagnation air temperatures in the stilling chamber and in the plenum re-entry duct in the wind tunnel complex illustrated in Figure 1. It is necessary that cooling water flow rate and temperature be controlled simultaneously in order to obtain the required system responses. Performance criteria realized is $\pm$ 0.5% accuracy in transient and steady-state during all disturbances and the controlled variable overshoot does not exceed the specified value of 1.07 when making set-point changes over most of the operating range. The analysis is complicated by non-linearities in system characteristics, apparent interactions of pressure and temperature, prominent distributed parameters and long transport delays. The work is notable for the simplifications developed to make the analysis of this complex system both technically feasible and economical. These simplifications include: (1) Disclosure of two modes of propagation of temperature variations and their subsequent use in separating temperature and pressure effects, (2) Selection of control frequency to permit lumped parameter representation, (3) Development of new analog computer devices and circuitry for simulation of transport delays ranging up to 141 seconds.

The complex consists of three large interconnected wind tunnels which form a single dynamic unit. This complex forms a major part of the USAF Arnold Engineering Development Center, Tullahoma, Tennessee. The testing for this particular facility is done in the Supersonic Propulsion Wind Tunnel 16' x 16' test section which is also equipped with a boundary layer flow control system. Full scale propulsion engines for rockets and missiles are tested under environmental conditions corresponding to speeds from Mach 1.5 to 4.5 and at altitudes from sea level to over 120,000 feet.

The material relating to compressor dynamics and the propagation of temperature and pressure variations is based in part upon unpublished work of R. J. Kochenburger, V. B. Haas, Jr. and V. E. Scottron of the University of Connecticut; and ASME Transactions Paper No. 56-IRD-21 by T. R. Stalzer and G. J. Fiedler. New circuitry for transport delay simulation is developed and designed by R. J. W. Koopman, Head, and L. R. Brown, R. Ozment and D. F. Wann of the instructional staff, Department of Electrical Engineering, Washington University, St. Louis.

The Systems Analysis

The physical diagram of the system is shown in Figure 1 which illustrates the configuration and connection of system components into the integrated complex. An accurate mathematical description of the various plant components is developed using all valid simplifications.

The mathematical development of system transfer functions which follows employs the theory of small perturbations.[1] The linearizing process used employs the principle of the total differential $F = f(x, y, z)$, thus:

$$dF = \frac{\partial F}{\partial x} dx + \frac{\partial F}{\partial y} dy + \frac{\partial F}{\partial z} dz \qquad (1)$$

The linearized variables are transformed using the Laplace operator before writing the system equations and constructing the system transfer diagram. To conserve space these operations are

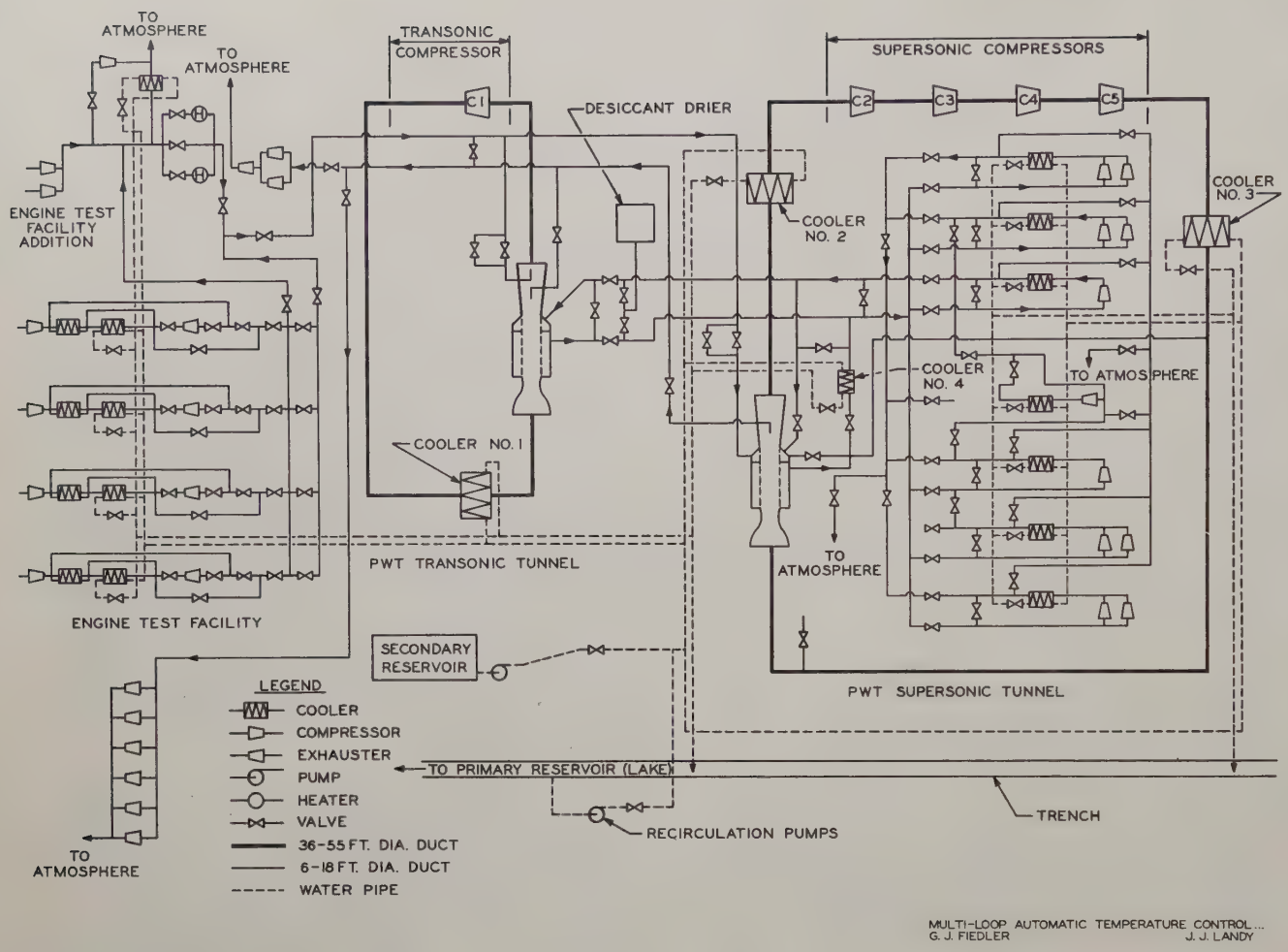

Fig. 1 Plant Schematic Diagram

not always shown in detail in the material that follows.

This paper involves several branches of engineering, each having long established upper and lower case symbols for the variables treated. This precludes strict conformity with the conventional use of lower and upper case letters for variables before and after Laplace transformation. Due to the large number of variables used, symbols are defined with each development for clarity.

Component Characteristics

Compressor Dynamics. The compressor dynamics are defined by the application of the principles of fluid mechanics and turbo-machinery.[2] The energy equation for gas flow is:

$$u_1 + \frac{p_1 v_1}{J} + \frac{V_1^2}{2gJ} + \frac{Z_1}{J} + Q = u_2 + \frac{p_2 v_2}{J} + \frac{V_2^2}{2gJ} + \frac{Z_2}{J} + \frac{W_s}{J} \qquad (2)$$

Where:

$$h = u + \frac{pv}{J} = C_p T \qquad (3)$$

Assuming an adiabatic compressor process, the heat $Q = 0$. Also for this process $Z_1 = Z_2$. Making these deletions and substituting Equation (3) into Equation (2) results in:

$$-\frac{W_s}{J} = C_p T_1 + \frac{V_1^2}{2gJ} - \left(C_p T_2 + \frac{V_2^2}{2gJ}\right) \qquad (4)$$

The negative sign is used for W_s to account for the compressor process where work is done on the fluid.

Since,

$$C_p T_1 + \frac{V_1^2}{2gJ} = C_p T_{ti} \qquad (5)$$

$$C_p T_2 + \frac{V_2^2}{2gJ} = C_p T_{to} \qquad (6)$$

Substituting these expressions into Equation (4)

results in:

$$-\frac{Ws}{J} = C_p(T_{to} - T_{ti}) \tag{7}$$

The adiabatic efficiency or temperature rise ratio is:

$$\mathcal{E}_t = \frac{W \text{ ideal}}{W \text{ actual}} = \frac{C_p(T_{to} - T_{ti})}{C_p(T_{toa} - T_{ti})} = \frac{T_{to} - T_{ti}}{T_{toa} - T_{ti}} \tag{8}$$

The use of the isentropic relationship and equation of state results in the following:

$$p_i v_i^{\gamma} = p_o v_o^{\gamma} \tag{9}$$

or,

$$\left(\frac{p_i}{p_o}\right)^{\frac{1}{\gamma}} = \frac{v_o}{v_i} = \frac{T_{to} p_i}{p_o T_{ti}}$$

or,

$$\frac{T_{to}}{T_{ti}} = \frac{p_o}{p_i}\frac{p_o^{-1/\gamma}}{p_i^{-1/\gamma}} = \left(\frac{p_o}{p_i}\right)^{\frac{\gamma-1}{\gamma}} \tag{10}$$

Combining this with Equation (8) results in:

$$\mathcal{E}_t = \frac{\left[\left(\frac{p_o}{p_i}\right)^{\frac{\gamma-1}{\gamma}} - 1\right] T_{ti}}{T_{toa} - T_{ti}} \tag{11}$$

Substituting the isentropic factor Y:

$$Y = \frac{T_{to} - T_{ti}}{T_{ti}} = \left(\frac{p_o}{p_i}\right)^{\frac{\gamma-1}{\gamma}} - 1 \tag{12}$$

results in:

$$\mathcal{E}_t = \frac{Y\, T_{ti}}{T_{toa} - T_{ti}} \tag{13}$$

The modified Euler equation for an axial-flow compressor[2] is:

$$E = \frac{V_t V_a}{Jg}(\tan\alpha_1 - \tan\alpha_2) \tag{14}$$

This equation is further modified by Ω, the so-called work-done factor[2] as follows:

$$E = \frac{\Omega\, V_t V_a}{J\, g}(\tan\alpha_1 - \tan\alpha_2) \tag{15}$$

Equating (7) and (15) and substitution of Equation (12) and the relation:

$$C_p = \frac{\gamma}{\gamma - 1}\frac{R}{J}$$

gives:

$$\frac{\frac{\gamma}{\gamma-1} RYT_{ti}}{\frac{V_t^2}{g}} = \frac{\Omega V_a}{V_t}(\tan\alpha_1 - \tan\alpha_2) \tag{16}$$

Let,

$$\eta = \frac{\Omega V_a}{V_t}(\tan\alpha_1 - \tan\alpha_2) \tag{17}$$

Therefore, Equation (16) now reads:

$$\eta = \frac{Y\left(\frac{\gamma-1}{\gamma}\right)RT_{ti}}{V_t^2/g} \tag{18}$$

The following three equations together with Equations (11) and (18) govern compressor behavior:

Compression ratio:

$$r_p = \frac{p_o}{p_i} = (Y+1)^{\frac{\gamma}{\gamma-1}} \tag{19}$$

Isentropic factor:

$$Y = \left[\left(\frac{p_o}{p_i}\right)^{\frac{\gamma-1}{\gamma}} - 1\right] = \frac{\eta\, V_t^2/2g}{(\gamma/\gamma - 1)RT_{ti}} \tag{12}$$

Output temperature:

$$T_{toa} = T_{ti}\left(1 + \frac{Y}{\mathcal{E}_t}\right) \tag{20}$$

Where:

E	= energy transfer to fluid	BTU/lb
V	= axial or through-flow velocity	ft/sec
v_1	= specific volume, inlet	ft^3/lb
v_2	= specific volume, outlet	ft^3/lb
V_1	= inlet velocity	ft/sec
V_2	= outlet velocity	ft/sec
p_i	= total inlet pressure	lbs/ft^2
p_o	= total outlet pressure	lbs/ft^2
h	= static enthalpy	BTU/lb
g	= gravitional constant	ft/sec^2
C_p	= specific heat constant pressure	BTU/lb/deg
Z_1	= energy due to elevation, inlet	ft
Z_2	= energy due to elevation, outlet	ft
Q	= heat transfer to fluid	BTU/lb
J	= mechanical heat equivalent	ft-lb/BTU
n	= impeller speed	rpm
d	= diameter impeller	ft
q_1	= volume flow, inlet	ft^3/sec
q_2	= volume flow, outlet	ft^3/sec
R	= gas constant	ft/°R
s	= Laplace operator	1/seconds
t	= time	seconds
τ	= time constant	seconds
T_{ti}	= total temperature inlet, actual	°R
T_{to}	= total temperature outlet, ideal	°R
T_{toa}	= total temperature outlet, actual	°R
T_i	= input temperature, convective	°R
T_o	= output temperature, convective	°R
T_1	= static temperature, inlet	°R
T_2	= static temperature, outlet	°R
u_1	= internal energy, inlet	BTU/lb

u_2	= internal energy, outlet	BTU/lb
V_t	= peripheral velocity	ft/sec
W_s	= total shaft work	ft-lb/lb
Y	= isentropic factor	numeric
γ	= ratio of specific heats	numeric
η	= pressure rise ratio	numeric
$\mathcal{E}_t$	= temperature rise ratio	numeric
α_1	= angle between tangent to mean blade profile line and entrance velocity vector	degrees
α_2	= angle between tangent to mean blade profile line and exit velocity vector	degrees

The pressure-rise and temperature-rise ratios are characteristic of particular operating conditions for specific compressor units. It is convenient to work with the slopes of these curves at the operating point. Since curves of η and $\mathcal{E}_t$ versus volume flow with speed as a parameter are available, two dimensionless quantities are defined which make use of the slope at the operating point. These are:

Pressure-rise factor:

$$K_\eta \triangleq \frac{\partial \eta}{\partial q/n} \frac{q/n}{\eta} \tag{21}$$

Temperature-rise factor:

$$K_t \triangleq \frac{\partial \mathcal{E}_t}{\partial q/n} \frac{q/n}{\mathcal{E}_t} \tag{22}$$

Applying linearizing techniques, Equation (19) may be expressed as follows:

$$dp_o = \frac{p_o}{p_i} dp_i + \frac{\gamma}{\gamma - 1} \frac{p_o}{Y + 1} dY \tag{23}$$

Also, from Equation (12) the increment in Y can be expressed as:

$$dY = \frac{-Y}{T_{ti}} dT_{ti} + \frac{Y}{\eta} d\eta + \frac{2Y}{n} dn \tag{24}$$

From Equation (21) the following is derived:

$$d\eta = -K_\eta \eta \left(\frac{dq}{q} - \frac{dn}{n}\right) \tag{25}$$

The volume flow q is related to the weight flow w by the expression:

$$\rho q = w$$

$$q = \frac{w}{\rho} = \frac{wRT_{ti}}{p_i} \tag{26}$$

where ρ = density in lb/ft^3.

The differential is:

$$dq = \frac{q}{w} dw - \frac{q}{p_i} dp_i + \frac{q}{T_{ti}} dT_{ti} \tag{27}$$

The change in pressure, a function of four variables, is found by combining Equations (23), (24), (25) and (27). This gives:

$$dp_o = \frac{p_o}{p_i}\left(1 + \frac{\gamma}{\gamma - 1} \frac{Y}{Y + 1} K_\eta\right) dp_i - \frac{\gamma}{\gamma - 1} \frac{p_o}{T_i} (1 + K_\eta) \left(\frac{Y}{Y + 1}\right) dT_{ti} - \frac{\gamma}{\gamma - 1} \frac{p_o}{w} \frac{Y}{Y + 1} K_\eta \, dw + p_o \frac{\gamma}{\gamma - 1} \frac{Y}{Y + 1} (2 + K_\eta) \frac{dn}{n} \tag{28}$$

The change in total temperature is formed by taking the total differentials of Equations (20) and (22) resulting in Equations (29) and (30).

$$dT_{toa} = \frac{T_{toa}}{T_{ti}} dT_{ti} + \frac{T_{toa} - T_{ti}}{Y} dY - \frac{T_{toa} - T_{ti}}{\mathcal{E}_t} d\mathcal{E}_t \tag{29}$$

$$d\mathcal{E}_t = -K_t \mathcal{E}_t \left(\frac{dq}{q} - \frac{dn}{n}\right) \tag{30}$$

These equations are then combined with Equations (24) and (27) resulting in:

$$dT_{toa} = \left[1 - \frac{T_{toa} - T_{ti}}{T_{ti}} (K_\eta - K_t)\right] dT_{ti} - \frac{T_{toa} - T_{ti}}{w} (K_\eta - K_t) \, dw + \frac{T_{toa} - T_{ti}}{p_i} (K_\eta - K_t) \, dp_i + (T_{toa} - T_{ti})(2 - K_t + K_\eta) \frac{dn}{n} \tag{31}$$

Equations (28) and (31) are expressed in terms of total temperature increments. It is necessary to separate the wave-transmitted component from the convectively-transmitted component and to express the temperature increment in terms of the latter component. This is done by substitution of the following relationships which are developed later in this paper:

$$dT_{toa} = dT_o + \frac{\gamma - 1}{\gamma} \frac{T_{to}}{p_o} dp_o \tag{32}$$

and,

$$dT_{ti} = dT_i + \frac{\gamma - 1}{\gamma} \frac{T_{ti}}{p_i} dp_i \tag{33}$$

Expressed in terms of convectively-transmitted components Equation (28) becomes:

$$dp_o = \frac{p_o}{p_i}\left(\frac{1 + \frac{K_\eta\, Y}{\gamma - 1}}{Y + 1}\right) dp_i - \frac{\gamma}{\gamma - 1}\,\frac{Y}{Y + 1}\,(1 + K_\eta)\,\frac{p_o}{T_i}\,dT_i$$

$$- \left(\frac{\gamma}{\gamma - 1}\,\frac{Y}{Y + 1}\,K_\eta\,\frac{p_o}{w}\right) dw + p_o\,\frac{\gamma}{\gamma - 1}\,\frac{Y}{Y + 1}\,(2 + K_\eta)\,\frac{dn}{n} \qquad (34)$$

Expressed in terms of convective-transmitted components Equation (31) becomes:

$$dT_o = \left[\frac{(\gamma - 1)\,T_{ti} + (K_\eta - K_t)\,(T_{toa} - T_{ti})}{\gamma\, p_i} - \frac{\gamma - 1}{\gamma}\,\frac{T_{toa}}{p_i}\,\frac{1 + \frac{K_\eta\, Y}{\gamma - 1}}{Y + 1}\right] dp_i$$

$$+ \left[1 - \frac{T_{toa} - T_{ti}}{T_{ti}}\,(K_\eta - K_t) + \frac{T_{toa}}{T_{ti}}\,\frac{Y}{Y + 1}\,(1 + K_\eta)\right] dT_i$$

$$- \left[\frac{T_{toa} - T_{ti}}{w}\,(K_\eta - K_t) - \frac{T_{toa}}{w}\,\frac{Y}{Y + 1}\,(K_\eta)\right] dw$$

$$+ \left[(T_{toa} - T_{ti})\,(2 - K_t + K_\eta) - \frac{T_{toa}\, Y}{Y + 1}\,(2 + K_\eta)\right] \frac{dn}{n} \qquad (35)$$

These relationships are shown on compressor block diagram Figure 2.

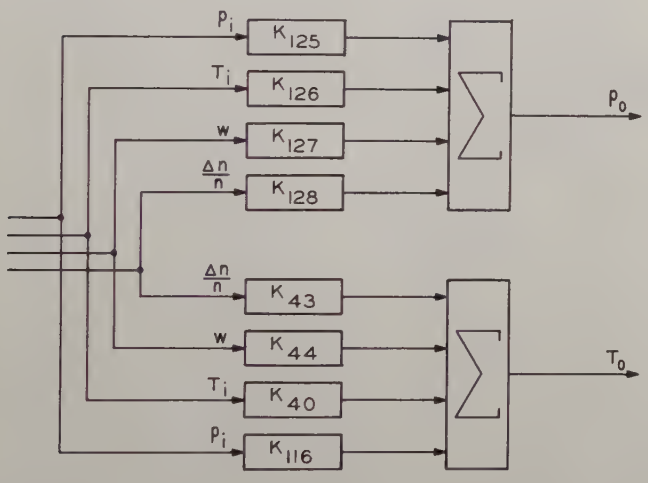

Fig. 2 Block Diagram of Compressor

Cooler Dynamics - Parallel Flow (Cooler 2). The cooler dynamics are analyzed by writing the heat balance equations for the air side, the water side, and the heat transferred[3] as indicated on Figure 3. The following assumptions are made:

1. The average air-water temperature difference in the cooler is the logarithmic mean temperature difference.

2. The heat storage capacity of the quantity of air present in the cooler at any instant is negligible in comparison with the heat storage capacity of cooler metal and water.

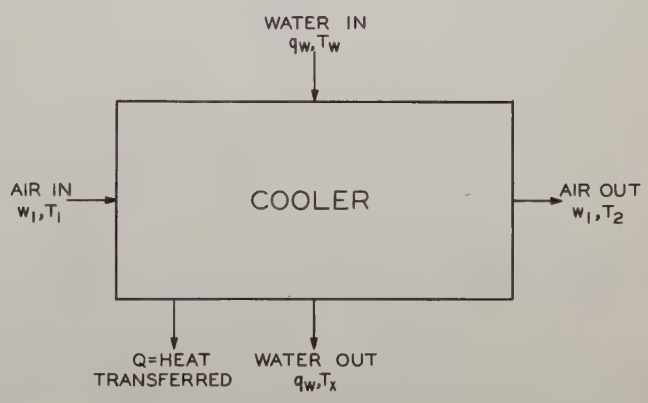

Fig. 3 Cooler Schematic Diagram

3. The value of the over-all heat transfer coefficient is constant for the small variations in flow and temperature encountered.

The air-side equation[3] is:

$$C_p\, w\, T_d - Q_h - C_p\, w\, T_{ai} = 0 \qquad (36)$$

The water-side equation[3] is:

$$C_w\, q_w\, T_w + Q - \frac{D}{2}\,\frac{d}{dt}\,(T_w + T_x) = C_w\, q_w\, T_x \qquad (37)$$

The heat transferred, Q_h, is:

$$Q_h = UA\,\Delta T_m = UA\,\frac{(T_d - T_w) - (T_{ai} - T_x)}{\ln \frac{(T_d - T_w)}{(T_{ai} - T_x)}} \qquad (38)$$

Where:

A	= Cooler airside surface area	ft^2
C_w	= Specific heat of water	BTU/lb/°F
C_p	= Specific heat of air	BTU/lb/°F
D	= Heat to raise cooler 1°F	BTU/°F
q	= Water flow thru cooler	lbs/sec
Q	= Heat flow	BTU/sec
Q_h	= Heat transferred	BTU/sec
s	= Laplace complex operator	1/sec
T_d	= Cooler inlet air temperature	°F
T_{ai}	= Cooler outlet air temperature	°F
T_w	= Cooler inlet water temperature	°F
T_x	= Cooler outlet water temperature	°F
U	= Heat transfer coefficient	BTU/sec/°F/ft^2
w	= Weight flow of air	lbs/sec
ΔT_m	= Log mean temperature difference	°F

Applying the linearizing technique to the air side and combinaing Equations (36) and (38) results in:

$$C_p wT_d(s) + C_pT_dW(s) - C_p wT_{ai}(s) - C_pT_{ai}W(s) = UAK_aT_d(s) + UAK_bT_{ai}(s) + UAK_cT_w(s) + UAK_dT_x(s) \quad (39)$$

Where:

$$K_a = \frac{\partial \Delta T_m}{\partial T_d} = \frac{\ln \frac{(T_d - T_w)}{(T_{ai} - T_x)} - \left[1 - \frac{(T_{ai} - T_x)}{(T_d - T_w)}\right]}{\left[\ln \frac{(T_d - T_w)}{(T_{ai} - T_x)}\right]^2}$$

$$K_b = \frac{\partial \Delta T_m}{\partial T_{ai}} = \frac{-\ln \frac{(T_d - T_w)}{(T_{ai} - T_x)} - \left[1 - \frac{(T_d - T_w)}{(T_{ai} - T_x)}\right]}{\left[\ln \frac{(T_d - T_w)}{(T_{ai} - T_x)}\right]^2}$$

$$K_c = \frac{\partial \Delta T_m}{\partial T_w} = \frac{-\ln \frac{(T_d - T_w)}{(T_{ai} - T_x)} - \left[\frac{(T_{ai} - T_x)}{(T_d - T_w)} - 1\right]}{\left[\ln \frac{(T_d - T_w)}{(T_{ai} - T_x)}\right]^2}$$

$$K_d = \frac{\partial \Delta T_m}{\partial T_x} = \frac{\ln \frac{(T_d - T_w)}{(T_{ai} - T_x)} - \left[\frac{(T_d - T_w)}{(T_{ai} - T_x)} - 1\right]}{\left[\ln \frac{(T_d - T_w)}{(T_{ai} - T_x)}\right]^2}$$

Solving Equation (39) for T_x, the cooler outlet water temperature, and transforming results in:

$$T_x(s) = \frac{C_p(T_d - T_{ai})}{UAK_d} W(s) + \frac{(wC_p - UAK_a)}{UAK_d} T_d(s) - \frac{(UAK_b + wC_p)}{UAK_d} T_{ai}(s) - \frac{K_c}{K_d} T_w(s) \quad (40)$$

Then applying the linearizing technique to the water side, Equations (37) and (38), followed by transforming gives:

$$(T_x - T_w)C_wQ(s) + qC_wT_x(s) - qC_wT_w(s) + \frac{D}{2} sT_x(s) + \frac{D}{2} sT_w(s) = UA\left[K_aT_d(s) + K_bT_{ai}(s) + K_cT_w(s) + K_dT_x(s)\right] \quad (41)$$

Equations (40) and (41) are solved simultaneously for T_{ai} the air outlet temperature as a function of air inlet temperature, air mass flow, quantity of cooling water and temperature of cooling water.

$$T_{ai}(s) = K_{36}T_d(s) + K_{37}W(s) + K_{38}Q_w(s) + K_{39}T_w(s) \quad (42)$$

K_{36}, K_{37}, K_{38} and K_{39} are long complicated expressions but have the simple forms:

$$K_{36b} \frac{(1 + \tau_1 s)}{(1 + \tau_2 s)}; \qquad K_{37b} \frac{(1 + \tau_5 s)}{(1 + \tau_2 s)}$$

$$K_{38b} \frac{1}{(1 + \tau_2 s)}; \qquad K_{39b} \frac{(1 - \tau_7 s)}{(1 + \tau_2 s)}$$

The numerator time constants are womewhat smaller than their counterparts in the denominators. The gain and time constants are both functions of the rates-of-flow and temperatures of the inlet and outlet air and cooling water. An interesting feature of these dynamics is the non-minimum phase characteristic. The numerator time constant in the K_{39} term is negative and investigation shows that the parallel-flow arrangement causes this phase characteristic. However, the assumption of constant reservoir water temperature for the non-recirculation modes of cooler operation effectively opens the loop eliminating this characteristic.

Cooler Dynamics - Counter Flow (Cooler 3). The cooler dynamics are the same as the parallel-flow case except for the heat transfer term Q_h which is defined for counter-flow as follows:

$$Q_h = UA\ \Delta T_m = UA \frac{(T_b - T_x) - (T_c - T_w)}{\ln \frac{(T_b - T_x)}{(T_c - T_w)}} \quad (43)$$

Using this expression, the over-all transfer function similar to Equation (42) is found to be:

$$T_c(s) = K_1T_b(s) + K_2W_b(s) + K_3Q_w(s) + K_4T_w(s) \quad (44)$$

K_1, K_2, K_3 and K_4 are long complicated expressions but have the simple forms:

$$K_{1b}\frac{(1 + T_6s)}{(1 + T_3s)}; \quad K_{2b}\frac{(1 + T_8s)}{(1 + T_3s)};$$

$$K_{3b}\frac{1}{(1 + T_3s)}; \quad K_{4b}\frac{(1 + T_{10}s)}{(1 + T_3s)}$$

The numerator time constants are somewhat smaller than the time constants in the denominators. The gain and time constants are functions of the rates-of-flow and the temperatures of the inlet and outlet air and cooling water. These transfer functions are similar to the parallel-flow cooler except the non-minimum phase characteristic is not encountered.

Cooler Dynamics - Recirculation Mode. For light cooler loads the cooling surface area is reduced in discrete steps. However, after the limit is reached it is necessary to further reduce the cooler efficiency by increasing the cooling water inlet temperature. This is done by pumping a controlled mixture of the heated cooler outlet water and cold reservoir water back through the cooler. Consequently, for this mode of operation dynamic air temperatures are controlled by varying both the cooling water flow rate and temperature simultaneously. For Cooler 2 transfer functions K_{111} to K_{114} determine the heated cooler water outlet temperatures. They are obtained by simultaneous solution of Equations (40) and (41), and are complicated expressions of air and water rates-of-flow and temperatures. Transfer functions K_{93} to K_{96} are derived from similar equations for Cooler 3. These cooler transfer functions also have the same form previously identified with coolers under non-recirculation modes of operation. The complicated cooler dynamics involving several feedback paths in the recirculation mode of operation are obvious by reference to Figure 4.

In addition to the above the non-minimum phase characteristic previously identified with the parallel-flow coolers is encountered. However, the excess phase shift caused by this factor is negligibly small at cross-over frequency compared with the phase shift caused by the long transport delays.

The water temperature change is defined in the following manner. The total heat contained in the water after mixing and at the entrance to the cooler is the sum of the total heat of the cold water and the hot recirculated water. Assumption of negligible heat storage in the mixing valve and line, results in:

$$qT_w = q_cT_{cw} + q_hT_x \quad (45)$$

$$q = q_c + q_h \quad (46)$$

Where:

q	= Mixed water flow	lbs/sec
T_w	= Mixed water temperature	^oF
q_c	= Cold water flow	lbs/sec
T_{cw}	= Cold water temperature	^oF
q_h	= Recirculated water flow	lbs/sec
T_x	= Recirculated water temperature	^oF

Linearizing and transforming Equations (45) and (46) gives:

$$T_wQ(s) + qT_w(s) = T_{cw}Q_c(s) + T_xQ_h(s) + q_hT_x(s) \quad (47)$$

and,

$$Q(s) = Q_c(s) + Q_h(s) \quad (48)$$

Substituting Equation (48) into Equation (47) and solving for $T_w(s)$ the transform of the temperature of cooling water leaving the cooler gives:

$$T_w(s) = K_{87}Q_c(s) + K_{88}Q_h(s) + K_{89}T_x(s) \quad (49)$$

Where:

$$K_{87} = \frac{T_{cw} - T_w}{q}; \quad K_{88} = \frac{T_x - T_{cw}}{q}; \quad K_{89} = \frac{q_h}{q}$$

These symbols are for use with Cooler No. 2. Similar symbols for Cooler No. 3 are designated K_{90}, K_{91}, and K_{92}.

Mixing Dynamics. The temperature of fluid resulting from the combining of two (or more) streams entering a mixing point is developed as follows assuming heat in = heat out; with no heat stored.

w_1T_1 = air flow and temperature entering mix point
w_2T_2 = air flow and temperature entering mix point
w_3T_3 = air flow and temperature leaving mix point

Equating these flows and solving for the leaving air temperature gives:

$$T_3 = \frac{w_1T_1 + w_2T_2}{w_3} \quad (50)$$

This form of equation constructed for the appropriate number of air streams, followed by linearizing and transforming is the basis of the mixing process transfer functions designated K_9 to K_{15} and K_{20} to K_{35} inclusive. The procedure is straight-forward and is omitted.

Test Section Temperature. The test section temperature can be written as follows:[4]

$$T_s = \left[\frac{T_o}{1 + \frac{\gamma - 1}{2}M_t^2}\right]\left[\frac{(7M_t^2 - 1)(M_t^2 + 5)}{36M_t^2}\right] \quad (51)$$

Where:

T_o = stagnation temperature

M_t = test section Mach number

The usual straightforward linearizing and transforming process is applied and is omitted here. This results in:

$$T_s(s) = K_{85}T_o(s) + K_{86}M_t(s) \qquad (52)$$

Test Section Mach Number. The Mach number in the test section can be written as:[4]

$$M_t = \frac{w_o\sqrt{R\,T_s}}{A_t p_t\ \sqrt{\gamma\, g}} \qquad (53)$$

Where:

w_o	= stagnation weight flow	lbs/sec
T_s	= test section temperature	^oF
A_t	= test section area	ft^2
P_t	= test section pressure	lbs/ft^2

The customary and straightforward linearizing and transforming process is applied and results in:

$$M_t(s) = K_{82}T_s(s) + K_{84}W(s) + K_{84a}P_t(s) \qquad (54)$$

Weight-Flow of Air Through Cooler. The frictional flow of air through a pipe can be approximated by:[5]

$$w = \sqrt{\frac{2g(p_i - p_o)p_i}{RBT_i}} \qquad (55)$$

Where:

$$B = \frac{4\ell^3 f}{d} \qquad (56)$$

Weight-Flow of Air Through Valve or Nozzle. Research tests conducted by the University of Michigan indicate that the nozzle equation[4] adequately expresses flow through butterfly valves at and above critical pressure ratios. The weight-flow through a valve or nozzle at sub-critical pressure ratios is given by the equation:

$$w = \frac{2.055\ Ap_i f_1}{\sqrt{T_i}} \qquad (57)$$

Where:

$$f_1 = \sqrt{\left(\frac{p_2}{p_1}\right)^{1.43} - \left(\frac{p_2}{p_1}\right)^{1.71}}$$

for $\frac{p_2}{p_1} \geq 0.528$ (sub-critical flow)

$= 0.257$

for $\frac{p_2}{p_1} \leq 0.528$ (critical flow)

The usual linearizing and transforming procedure results in:

$$W(s) = K_{62}T_i(s) + K_{63}P_i(s) + K_{64}P_o(s) + K_{66}A(s) \qquad (58)$$

Weight-Flow Through Scavenging Scoop. This expression is developed by use of the continuity equation:[4]

$$w = \frac{0.92\ AM_t p_i}{\sqrt{T_i}} \qquad (59)$$

The usual linearizing and transforming procedures result in:

$$W(s) = K_{79}T_i(s) + K_{81}M_t(s) + K_{83}P_i(s) \qquad (60)$$

Fluid Transport Dynamics. Data presented later in the paper shows that practically all of the total temperature variations are transmitted through the ducting system at the local fluid velocity. The heat exchange with tunnel walls is a negligible part of the total. This process can be described for a fixed delay by the following development. The Taylor series expansion shows that:

$$f(t - \tau) = f(t) - \tau f'(t) + \frac{\tau^2}{2!}f''(t) - \frac{\tau^3}{3!}f'''(t) + \ldots \qquad (61)$$

where $f'(t)$, $f''(t)$, $f'''(t)$ are time derivatives.

Substitution of the Laplace operator s for differentiation yields:

$$f(t - \tau) = \left[1 - \tau s + \frac{(\tau s)^2}{2!} - \frac{(\tau s)^3}{3!} + \ldots\right]F(s) \qquad (62)$$

Since this is the series expansion for ϵ^{-st} the result is:

$$f(t - \tau) = F(s)\epsilon^{-st} \qquad (63)$$

This expression is used for the transport delays in the air and water circuits.

Water Flow Dynamics - Frictional Loss. The relationship for hydraulic loss due to pipe friction from fluid mechanics[6] is:

$$h_\ell = \frac{f\ell}{d}\ \frac{V^2}{2g} \qquad (64)$$

$$N_R = \frac{V\,d\,\rho}{\mu\, g} \qquad (65)$$

Where:

A	= area	ft^2
d	= diameter of pipe	ft
f	= friction factor - function of N_R	numeric
g	= acceleration, gravity	ft/sec^2
h_ℓ	= head loss	ft
ℓ	= length of pipe	ft
N_R	= Reynolds number	numeric

V	= velocity	ft/sec
w	= weight flow	lb/sec
ρ	= specific weight of fluid	lb/ft^3
μ	= viscosity	$lb\text{-}sec/ft^2$

The pressure drop Δp in psi can be expressed as:

$$\Delta p = \frac{\rho h_\ell}{144} \tag{66}$$

$$V = \frac{w}{\rho A} \tag{67}$$

Equating (64) and (66) and substituting Equation (67) gives the pressure drop-flow relationship:

$$\Delta p = \frac{f\ell w^2}{\rho d A^2 2g\ 144} = r_1 w^2 \tag{68}$$

For a given section of piping r_1 is a constant. Transfer function K_{131} is the pump characteristic. Transfer functions K_{132} and K_{134} are of the form $(r_1 + sL)$. The L factor is defined in the next paragraph.

Water Flow Dynamics - Acceleration Loss. The relationship describing head loss due to fluid acceleration is expressed by:

$$F = ma \tag{69}$$

Where the force on an element d_x of fluid is:

$$F = (p_1 - p_2)A \tag{70}$$

$$m = \frac{w'}{g} = \frac{\ell A \rho}{g} \tag{71}$$

Where w' = weight in lbs. Other symbols are as previously defined.

Also,

$$\frac{dw}{dt} = aA\rho$$

$$a = \frac{1}{A\rho}\frac{dw}{dt} \tag{72}$$

Combining Equations (71) and (72) gives:

$$ma = \frac{\ell}{g}\frac{dw}{dt} \tag{73}$$

Equating (70) and (73) results in:

$$(p_1 - p_2) = \frac{\ell}{Ag}\frac{dw}{dt} = L\frac{dw}{dt} \tag{74}$$

The parameter $L = \frac{\ell}{Ag}$ is the hydraulic inductance or inertance.

Where:

F	= force	lbs
m	= mass	$lbs\text{-}sec^2/ft$
a	= acceleration	ft/sec^2
w'	= weight of air	lbs
w	= weight flow	lbs/sec
g	= acceleration, gravity	ft/sec^2
A	= area	ft^2
ℓ	= length	ft
L	= hydraulic inertance	sec^2/ft^2
ρ	= density of fluid	lbs/ft^3
p_1	= upstream pressure	lbs/ft^2
p_2	= downstream pressure	lbs/ft^2

For a given pipe section L is a constant. Transfer functions K_{132}, K_{134} and K_{138} define the fluid accelerating time constants.

Water Flow Dynamics - Valve Loss. Head loss through a valve is derived from fluid mechanics[6] as follows:

$$h_v = \left\{\frac{1}{C_v^2}\left[1 - \left(\frac{A_2}{A_1}\right)^2\right] - \alpha_2\left[1 - \frac{\alpha_1}{\alpha_2}\left(\frac{A_2}{A_1}\right)^2\right]\right\}\frac{V_2^2}{2g} \tag{75}$$

Where:

α_1 = inlet velocity coefficient

α_2 = outlet velocity coefficient

Since α_2 is usually much smaller than $\frac{1}{C_v^2}$ and $\frac{\alpha_1}{\alpha_2}$ is usually close to unity, an approximate relationship for h_v is:

$$h_v = \frac{1}{C_v^2}\left[1 - \left(\frac{A_2}{A_1}\right)^2\right]\frac{V_2^2}{2g} \tag{76}$$

Since A_2 is much smaller than A_1 a further simplification results in:

$$h_v = \frac{1}{C_v^2}\frac{V_2^2}{2g} = \frac{w^2}{2C_v^2 g A_2 \rho}$$

This can be expressed as:

$$h_v = \frac{w^2}{K_a A_2} \tag{77}$$

Where:

$$K_a = C_v^2\,\rho\,(2g)$$

This factor is the basis of transfer functions K_{133}, K_{135} and K_{136}.

Valve Flow Characteristics. The relationship between valve area and valve stem position for an equal-percentage valve is also characteristic of the butterfly valve over the useable control range and can be expressed by:[7]

$$x = K \ln \frac{A}{A_o} \tag{78}$$

Where:

x	= valve stem position, % of travel	numeric
K	= constant	numeric
A	= valve open area	ft^2
A_o	= valve area at minimum controllable flow	ft^2

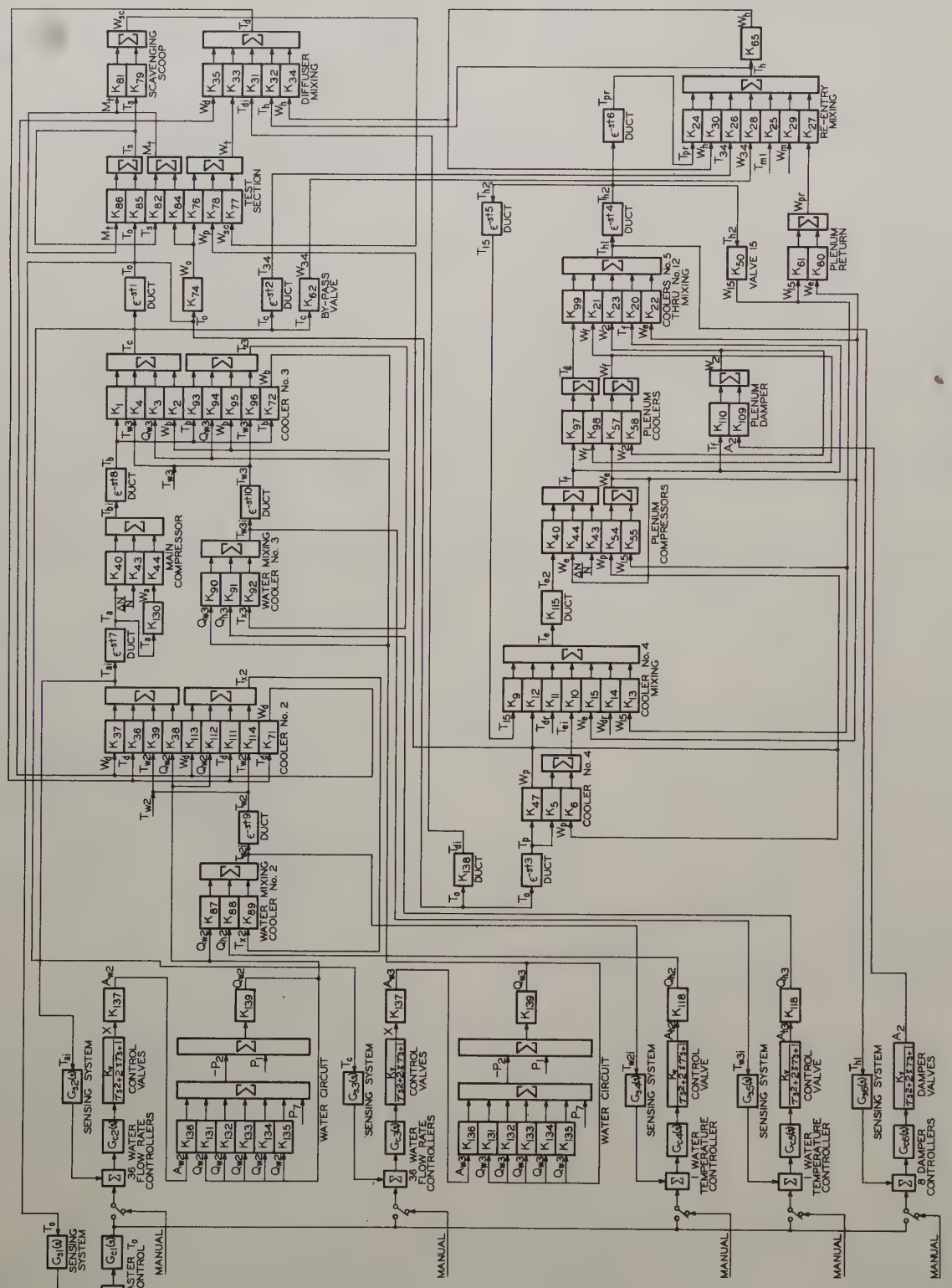

Fig. 4 System Transfer Function Diagram

Therefore:

$$dx = \frac{K}{A}\, dA$$

$$\frac{dA}{dx} = \frac{A}{K} = K_v \qquad (79)$$

This expression is the basis of transfer function K_{137} on Figure 4.

System Characteristics

The system-wide aspects of the complex plant processes are analyzed for the purpose of effecting all possible simplifications to facilitate the analysis and design work. The simplifications are discussed in the following paragraphs.

Separation of Pressure and Temperature Variations. Disturbances due to extreme engine throttle bursts and noise cause excursions from nominal values in both temperature and pressure. Pressure variations travel in ducting sections at sonic velocity. It is assumed that there is negligible leakage and negligible heat exchange to the tunnel walls. To develop the relationship between wave-transmitted temperature variations and pressure variations, the aerodynamics continuity equation and the net force equation are used[8] as indicated on Figure 5.

$$-\frac{\partial M}{\partial t} = w + \frac{dw}{d\lambda}\, d\lambda - w \qquad (80)$$

This equation states that the rate of decrease in mass within the elementary volume is equal to the net rate of mass flow out of the volume. The mass equation is:

$$M = \rho A d\lambda \qquad (81)$$

Differentiation results in:

$$\frac{\partial M}{\partial t} = -A\, \frac{\partial \rho}{\partial t}\, d\lambda \qquad (82)$$

For the assumed isentropic duct process:[4,8]

$$\frac{\partial p}{\partial \rho} = \mu_c^2/g \qquad (83)$$

Using this relation gives:

$$\frac{\partial w}{\partial \lambda} = \frac{-Ag}{\mu_c^2}\, \frac{\partial p}{\partial t} = C\, \frac{\partial p}{\partial t} \qquad (84)$$

The net force equation states that the net force acting on the fluid within the elementary volume is equal to the time rate-of-change of momentum within the volume plus the net out-flow through the surface of the volume[8]. Therefore,

$$pA - \left(p + \frac{\partial p}{\partial \lambda}\, d\lambda\right)A = \frac{\partial}{\partial t}\, \frac{(MV)}{g} + \frac{\partial}{\partial \lambda}\, \frac{(wV)}{g}\, d\lambda \qquad (85)$$

Since,

$$M = A\rho\, d\lambda \qquad (81)$$

and,

$$V = \frac{w}{A\rho} \qquad (86)$$

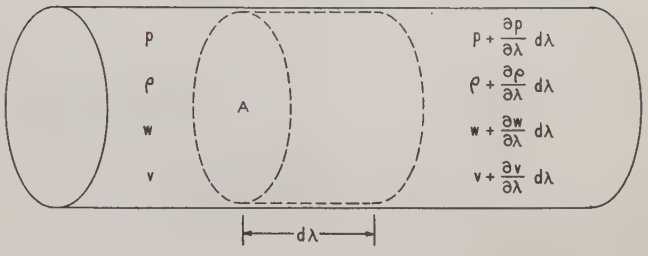

Fig. 5 Ducting Section for Development of Distributed Parameter Equations

Equation (85) becomes:

$$-\frac{\partial p}{\partial \lambda} = \frac{1}{Ag}\, \frac{\partial w}{\partial t} + \frac{w}{Ag}\, \frac{\partial V}{\partial \lambda} + \frac{V}{Ag}\, \frac{\partial w}{\partial \lambda} \qquad (87)$$

Since the velocity is small and does not change significantly with distance, Equation (87) can be re-written as follows:

$$-\frac{\partial p}{\partial \lambda} = -\frac{1}{gA}\, \frac{\partial w}{\partial t} = L\, \frac{\partial w}{\partial t} \qquad (88)$$

For the foregoing derivation:

M	= mass	$lb\text{-}sec^2/ft$
w	= weight flow	lb/sec
ρ	= specific weight	lb/ft^3
A	= duct area	ft^2
V	= average velocity	ft/sec
g	= acceleration, gravity	ft/sec^2
p	= pressure	lbs/ft^2
T	= temperature	^oR
R	= 53.3	ft/deg
γ	= ratio of specific heats	C_p/C_v
t	= time	sec
λ	= distance along duct	ft

Equations (84) and (88) are analogous to the well known equations[8] for current and voltage as functions of time and space along an electric transmission line having zero conductance and zero resistance.

The sonic velocity is:[4,8]

$$\mu_c = \sqrt{\frac{1}{\frac{1}{Ag} \cdot \frac{A}{\gamma RT}}} = \sqrt{\gamma g RT} \qquad (89)$$

And the surge impedance is:

$$Z_{cp} = \frac{\partial p}{\partial w} = \frac{1}{Ag}\, \sqrt{\gamma g RT} = \frac{\mu_c}{Ag} \qquad (90)$$

The following assumptions apply to the preceeding work:

1. The disturbances in pressure and temperature are small so that average values of μ_c may be used.

2. The cross-section area is uniform for a given section.

3. The process is isentropic, there are no energy losses between the ends of the line, and impedances may be lumped at the end of the line.

4. Mach numbers are small compared to unity.

For large Mach numbers the relationship for the isentropic condition is derived from aerodynamic relationships[4] as:

$$\frac{\gamma}{\gamma - 1}\left[1 + (\gamma - 1) M^2\right] \frac{dT_w}{T_t}$$

$$= \left[1 + \gamma M^2\right] \frac{dp}{p} - \gamma M^2 \frac{dw}{w} \qquad (91)$$

Where:

$$M = \frac{V}{\mu_c} = \frac{w}{Ap}\sqrt{\frac{RT_t}{\gamma g}} \qquad (92)$$

Equation (91) reduces to:

$$\frac{\gamma}{\gamma - 1} \frac{dT_w}{T_t} = \frac{dp}{p} \quad \text{for } M << 1 \qquad (93)$$

The linearized and transformed form of this relationship is:

$$T_w(s) = \frac{\gamma - 1}{\gamma} \frac{T_{ti}}{p_i} P(s) \qquad (94)$$

Components such as compressors and coolers do not follow the isentropic relationship. Disturbances applied to them give rise to some total change in temperature designated as ΔT_t. If there is an accompanying pressure change, ΔP, part of this change, i.e., the ΔT_w component of the above relation, will be transmitted along with the pressure wave.

The remainder of the temperature change ($\Delta T_t - \Delta T_w$) will be transmitted convectively and will travel through the system at the air flow velocity. The generalized form of Equations (32) and (33) is:

$$\Delta T(s) = \Delta T_t(s) - \Delta T_w(s)$$

$$= \Delta T_t(s) - \frac{\gamma - 1}{\gamma} \frac{T_{ti}}{p_i} P(s) \qquad (95)$$

Calculations made with the use of Equations (31), (35) and (94) show that the convectively-transmitted temperature variations are predominant and the wave-transmitted components of the temperature variations are negligible for this facility. Furthermore, the pressure and the wave-transmitted temperature variations have propagation rates of 1160 to 1230 feet per second compared to the 70 to 200 feet per second for the predominant convectively-transmitted temperature variations. Therefore, it is concluded that there are no interactions between the dynamic pressure variations and the convectively-transmitted temperature variations. This permits the severing of all pressure and temperature process loops and produces a valid major simplification in the analytical work.

Space Effects - Distributed Parameters. To validate lumped-parameter treatment of the water circuit shown on Figure 1, the control frequency is selected to limit the error in lumped representation to a very small value. This is done by basing calculations on the longest pipe section. This length, 5500 feet in this facility, together with the fluid characteristics and velocity are fixed elements. The control frequency is the only pertinent variable subject to control and it is calculated by making the 5500 foot long pipe length correspond to a selected fraction of a wave length. A value of 10 degrees is used in this case as follows:

$$C = \left(\frac{E}{\rho}\right)^{1/2} \qquad (96)$$

Substituting in Equation (69) for the water circuit results in a sound velocity of 4700 feet per second. Using the relation:

$$f = \frac{C}{\lambda} \qquad (97)$$

results in a value of f = 0.0237 cps. This corresponds to cross-over frequency $\omega_c = 0.1485$ radians per second. This is more than ample because of the long transport delays in the air and water circuits.

Where:

C	= sound velocity	ft/sec
E	= bulk modulus of elasticity	lbs/ft^2
ρ	= fluid density	$lbs\text{-}sec^2/ft^4$
f	= frequency	cps
ω	= frequency	rad/sec
λ	= wave length	ft/cycle

Space Effects - Transport Delays. The mathematical difficulties of solving equations involving the transform of the displaced time function e^{-st} make the electronic computer solution of such equations highly desirable. In this facility the number and length of time delays ranging up to 141 seconds makes the use of operational amplifier means of simulation impracticable even for the largest computing laboratories. A review of the literature indicates that delays of this magnitude have not been previously simulated. This makes necessary the design and construction of suitable devices utilizing other principles. This problem is solved by the use of the device shown in Figure 6(a).

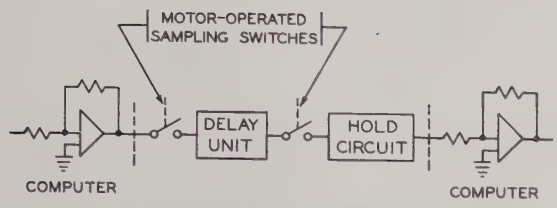

(a) Simulator Schematic

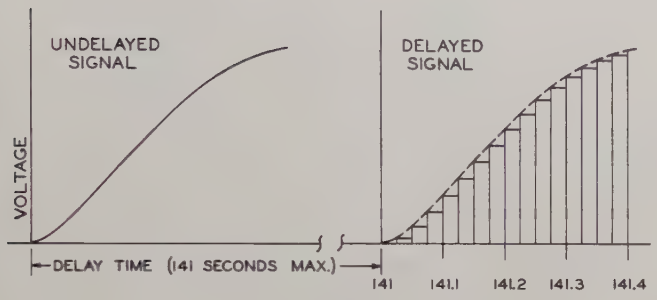

(b) Simulator Response

Fig. 6 Transport Delay Unit

The computer voltages to be delayed are applied to low-loss capacitors mounted on motor-driven, rotating disks through copper commutator bars and brushes on the periphery of the disc. The spacing of the brushes and the speed of the disks are designed to achieve the required time delays and sampling rates. The signal voltages are then fed into suitable hold circuits before re-insertion into the computer. A typical test of the time-delay simulator equipment response is indicated on Figure 6(b) and proved the accuracy to be of approximately the same order as that of the balance of the computer circuitry.

Equations for Simplified Uncontrolled System. After the above simplifications have been made, the system equations are written and the system transfer diagram shown on Figure 4 is constructed. The linearizations and transformations are straight-forward, routine mathematical operations and are omitted to conserve space. The linearized and transformed equations are listed below:

(a) Air Circuit:

$$T_c(s) = \left\{\frac{(K_{1a} + K_{2a}K_{72})\left[\left(\frac{K_{1a}T_{1N} + K_{2a}K_{72}T_{2N}}{K_{1a} + K_{2a}K_{72}}\right)s + 1\right]}{T_{1D}s + 1}\right\}T_b(s) + \frac{K_{3a}}{(T_{3D}s + 1)}Q_{w3}(s) + K_{4a}\frac{(T_{4N}s + 1)}{(T_{4D}s + 1)}T_{w3}(s) \quad (98)$$

$$T_o(s) = T_c(s)e^{-st_1} \quad (99)$$

$$T_p(s) = T_o(s)e^{-st_3} \quad (100)$$

$$T_{34}(s) = T_c(s)e^{-st_2} \quad (101)$$

$$T_{el}(s) = \left\{\frac{(K_{5a} + K_{6a}K_{47})\left[\left(\frac{K_{5a}T_{5N} + K_{6a}K_{47}T_{6N}}{K_{5a} + K_{6a}K_{47}}\right)s + 1\right]}{T_{5D}s + 1}\right\}T_p(s) \quad (102)$$

$$T_e(s) = K_9T_{15}(s) + K_{10}T_{el}(s) + K_{12}K_{47}T_p(s) + K_{13}K_{50}T_{h2}(s) + K_{15}W_e(s) \quad (103)$$

$$T_f(s) = K_{40}K_{115}T_e(s) + K_{43}\frac{\Delta N}{N}(s) + K_{44}W_e(s) \quad (104)$$

$$T_{h1}(s) = (K_{20} + K_{23}K_{110})T_f(s) + (K_{21}K_{57} + K_{22})W_e(s) + K_{21}K_{58}W_2(s) + K_{23}K_{109}A_2(s) + K_{99}T_g(s) \quad (105)$$

$$T_g(s) = \frac{K_{97a}(T_{97N}s + 1)}{(T_{97D}s + 1)}T_f(s) + \frac{K_{98a}(T_{98N}s + 1)}{(T_{98D}s + 1)}W_f(s) \quad (106)$$

$$T_{h2}(s) = T_{h1}(s)e^{-st_4} \quad (107)$$

$$T_{15}(s) = T_{h2}(s)e^{-st_5} \quad (108)$$

$$T_{pr}(s) = T_{h2}e^{-st_6} \quad (109)$$

$$T_h(s) = \frac{K_{24}}{1 - K_{30}K_{65}}T_{pr}(s) + \frac{K_{25}}{1 - K_{30}K_{65}}T_{ml}(s) + \frac{K_{26}}{1 - K_{30}K_{65}}T_{34}(s) + \frac{K_{27}}{1 - K_{30}K_{65}}W_{pr}(s) + \frac{K_{28}K_{62}}{1 - K_{30}K_{65}}T_c(s) + \frac{K_{29}}{1 - K_{30}K_{65}}W_m(s) \quad (110)$$

$$T_d(s) = \frac{(K_{31} + K_{33}K_{76}K_{74})}{(1 - K_{35}K_{71})}T_o(s) + \frac{(K_{33}K_{77})}{(1 - K_{35}K_{71})}W_{sc}(s) + \frac{(K_{33}K_{47}K_{78})}{(1 - K_{35}K_{71})}T_p(s) + \frac{(K_{32} + K_{34}K_{65})}{(1 - K_{35}K_{71})}T_h(s) \quad (111)$$

$$T_{ai}(s) = \left\{ \frac{(K_{36a} + K_{37a}K_{71}) \left[\left(\frac{K_{36a}T_{36N} + K_{37a}K_{71}T_{37N}}{K_{36a} + K_{37a}K_{71}} \right) s + 1 \right]}{(T_{36D}s + 1)} \right\} T_d(s)$$

$$+ \frac{K_{38a}}{(T_{38D}s + 1)} Q_{w2}(s) + \frac{K_{39a}(T_{39N}s + 1)}{(T_{39D}s + 1)} T_{w2}(s) \quad (112)$$

$$T_a(s) = T_{ai}(s)\, e^{-st_7} \quad (113)$$

$$T_{bi}(s) = K_{40}T_a(s) + K_{43} \frac{\Delta N}{N}(s) + K_{44}W(s) \quad (114)$$

$$T_b(s) = T_{bi}(s)e^{-st_8} \quad (115)$$

$$T_t(s) = K_{85}T_o(s) + K_{86}M_t(s) \quad (116)$$

$$W_{pr}(s) = K_{60}W_e(s) + K_{50}K_{61}T_{h2}(s) \quad (117)$$

$$W_{sc}(s) = K_{79}T_s(s) + K_{81}M_t(s) \quad (118)$$

$$M_t(s) = K_{82}T_s(s) + (K_{74}K_{84})T_o(s) \quad (119)$$

$$W_2(s) = K_{109}A_2(s) + K_{110}T_f(s) \quad (120)$$

$$W_f(s) = K_{57}W_e(s) + K_{58}W_2(s) \quad (121)$$

$$W_e(s) = K_{47}K_{54}T_p(s) + K_{50}K_{55}T_{h2}(s) \quad (122)$$

$$T_{w2}(s) = (K_{87} + K_{89}K_{112})Q_{w2}(s) + K_{88}Q_{H2}(s) + (K_{89}K_{111} + K_{89}K_{71}K_{113})T_d(s) + K_{89}K_{114}T_{w2}(s) + K_{89}K_{113}W_d(s) \quad (123)$$

$$T_{w3}(s) = (K_{90} + K_{92}K_{94})Q_{w3}(s) + K_{91}Q_{H3}(s) + (K_{92}K_{93} + K_{92}K_{72}K_{95})T_b(s) + K_{92}K_{96}T_{w3}(s) + K_{92}K_{95}W_b(s) \quad (124)$$

$$T_{w2}(s) = T_{w2i}(s)e^{-st_9} \quad (125)$$

$$T_{w3}(s) = T_{w3i}(s)e^{-st_{10}} \quad (126)$$

(b) Water Circuit:

$$P_1(s) - P_2(s) = K_{139}Q_w(s) = (K_u + sK_v)Q_{w3}(s) \quad (127)$$

$$P_2(s) - P_3(s) = K_{131}Q_w(s) = f(q_{w3})Q_{w3}(s) \text{ (pump characteristic)} \quad (128)$$

$$P_3(s) - P_4(s) = K_{132}Q_w(s) = (K_w + sK_x)Q_{w3}(s) \quad (129)$$

$$P_4(s) - P_5(s) = K_{133}Q_{w3}(s) = \frac{2(P_4 + P_5)}{Q_{w3}}Q_{w3}(s) \quad (130)$$

$$P_5(s) - P_7(s) = K_{134}Q_{w3}(s) = (Kg + sK_h)Q_{w3}(s) \quad (131)$$

$$P_6(s) - P_7(s) = K_{135}Q_{w3}(s) + K_{136}A_{w3}(s) = \frac{2(P_6 - P_7)}{Q_{w3}}Q_{w3}(s) + \frac{2(P_6 - P_7)}{A_{w3}}A_{w3}(s) \quad (132)$$

The above system equation array is obtained from the transfer diagram on Figure 4 after valid simplifications and substitutions are made. Since these operations are straightforward the work is not shown.

The uncontrolled water circuit equations are written in terms of pressure drops. The K_{131} term is the pump characteristic and the K_{133} and K_{135} terms are valve resistance terms in Equation (77). The K_{132}, K_{134} and K_{139} transfer blocks are combined resistance and inductance terms of the form (r + sL) as indicated in Equations (68) and (74). The K_{137} term is the valve area versus position relationship from Equation (79);transfer functionsK_{71} and K_{72} are developed by the use of the continuity equation.[4] The transfer blocks K_{54} to K_{58} and K_{76} to K_{78}, K_{115} and K_{138} have values of 1.0.

The uncontrolled system equations are solved for the control ratios in a purely routine manner, consequently these details are omitted. For use with the transfer diagram Figure 4, these control ratios are:

For Non-Recirculation Mode of Cooler Operation:

$$\frac{T_o(s)}{Q_{w3}(s)} \; ; \quad \frac{T_o}{Q_{w2}}(s)$$

For Recirculation Mode of Cooler Operation:

$$\frac{T_o(s)}{Q_{w3}(s),\, T_{w3}(s)} \; ; \quad \frac{T_{w3i}}{Q_{h3}}(s) \; ;$$

$$\frac{T_o(s)}{Q_{w2}(s)\, T_{w2}(s)} \; ; \quad \frac{T_{w2i}}{Q_{h2}}(s)$$

For Plenum Cooler By-Pass Damper Operation:

$$\frac{T_{h1}}{A_2}(s)$$

These control ratios are very long and complex polynomials in s, and reveal many hundreds of interesting process interactions. However, the discussions of these interactions are outside the scope of this paper.

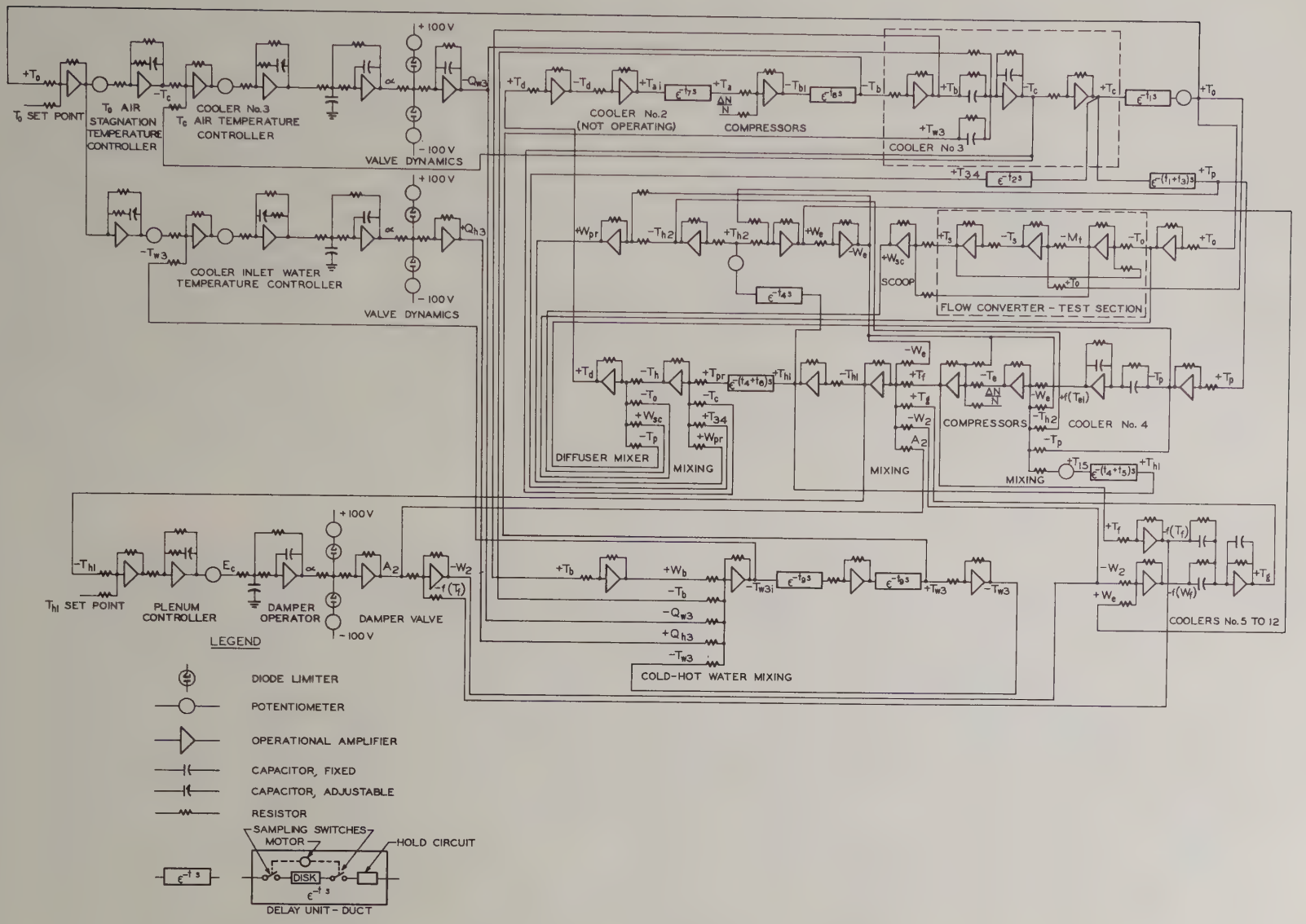

Fig. 7 Computer Circuitry

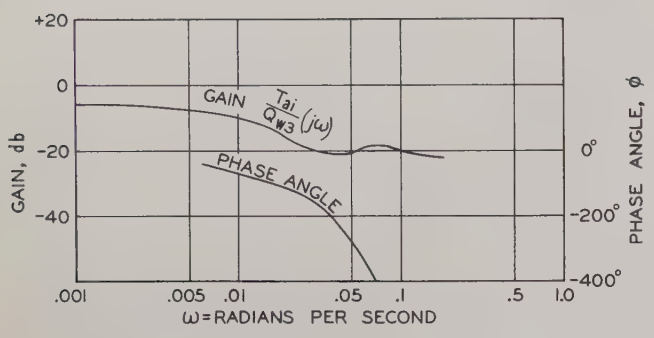

Fig. 8 Frequency Response Plot, Cooler Outlet Air Temperature as Function of Cooling Water Flow Rate, Open Loop - Uncontrolled Plant

Control System Synthesis

The uncontrolled plant equations (98) to (132) are simulated on the analog computer using standard procedures. The accuracy of the simulation is checked by comparison of analytically-developed uncontrolled system responses with the same responses obtained on the analog computer. This also checks the operation of the computer.

The computer circuitry for one mode of cooler operation is shown on Figure 7. This diagram also shows the locations and connections of the sampling devices used for simulation of the transport delays. The excessive phase shift caused by a large transport delay is shown on Figure 8. Servo design principles are applied to design the controllers and other elements of the control loop. The entire control loop is simulated and connected into the uncontrolled plant circuitry. From a "map" of the large number of operating points a relatively few points are carefully selected to cover the plant operating points a relatively few points are carefully selected to cover the plant operating envelope. The computer is used to conveniently adjust controller responses until the transient and steady-state performance criteria for reference input and design disturbances are satisfied for each selected operating point.

The computer responses show that design criteria are satisfied with standard electronic controllers provided controller modifications are made to obtain a 0.1% proportional band. The responses shown on Figure 9 illustrate the superior performance obtained when the cooler inlet water temperatures are automatically and continuously adjusted by the master stagnation air temperature controller in cascaded configurations. Cascaded controller arrangements are also necessary to control the stagnation air temperature because of the physical location of the two coolers over 1000 feet upstream of the stilling chamber.

This installation requires a total of 83 electronic controllers and 191 pneumatically-operated control valves as indicated on Fig. 4.

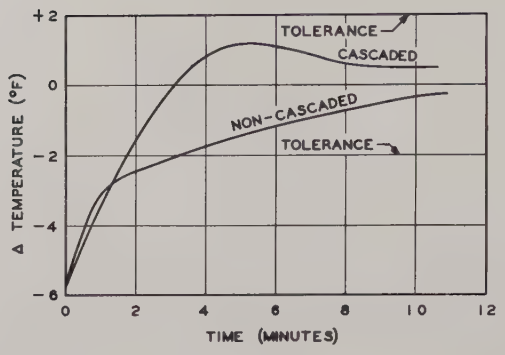

Fig. 9 System Responses with Cascaded and Non-Cascaded Water Temperature Control

Conclusions

1. This paper demonstrates that an integrated systems analysis based on valid simplifications makes the synthesis and design of electronic control systems for the largest dynamic processes technically feasible and economical.

2. The simplified techniques used contrast markedly in terms of difficulty with the usual analytical approach using partial differential and transcendental equations for systems involving time and space variables.

3. The analysis discloses the existence of unknown facility capabilities for: (1) Testing larger engines, (2) Expanded transient testing. Also, important savings are realized in control system hardware cost when compared to a previous design made without a systems analysis.

Bibliography

1. H. Chestnut and R. W. Mayer, "Servomechanisms and Regulating System Design," Volume 2, McGraw-Hill Book Co., Inc., New York, N.Y.; 1957.

2. D. G. Shepherd, "Principles of Turbomachinery", MacMillan Co., New York, N.Y.; 1956.

3. D. Q. Kern, "Process Heat Transfer", McGraw-Hill Book Co., Inc., New York, N.Y.: 1950.

4. H. W. Liepman and A. E. Puckett, "Introduction to Aerodynamics of A Compressible Fluid", John Wiley and Sons, Inc., New York, N.Y.; 1947.

5. J. K. Salisbury, Editor, "Kent's Mechanical Engineers Handbook - Power", 12th Edition, John Wiley and Sons, Inc., New York, N.Y.; 1950.

6. John K. Vennard, "Elementary Fluid Mechanics" John Wiley and Sons, Inc., New York, N.Y.; 1947.

7. D. P. Eckman, "Industrial Process Control", John Wiley and Sons, Inc., New York, N.Y.; 1945.

8. T. R. Stalzer and G. J. Fiedler, "Criteria for Validity of Lumped-Parameter Representation of Ducting Air-Flow Characteristics", ASME Transactions Paper No. 56-IRD-21, May 1957.

SOME LINEAR AND NONLINEAR ASPECTS OF HOT GAS SERVO DESIGN

R. V. Halstenberg
Convair San Diego
San Diego, California

Summary

Gas servos are considered from a feedback analysis standpoint with emphasis on systems such as would be most suitable for missile applications. Linearized equations are presented for the case where the piston is operating off-center. The basic stability and response problems are investigated and some of the characteristics of acceleration, pressure, and transient pressure feedback are considered.

The use of a thin plate orifice for compensation use is considered and a quasi-linear analysis is carried out in order to obtain a better feel for this type of operation. A criterion for the presence and severity of a jump resonance is derived and applied to certain gas servo feedback configurations. Limiting elsewhere in the system is investigated as a means by which the jump resonance caused by saturation of the valve might be avoided.

Introduction

Hot gas servos offer a number of advantages for missile applications, but they also present a number of relatively difficult problems. One of the foremost of these problems is that of controlling the dynamic response of an actuator which is driven by an extremely compressible fluid. Although other phases of gas servo development are equally important and equally interesting, this paper will deal only with dynamic response considerations.

A review of the history of hot gas servos reveals one very important point. Hot gas servos have unquestionably been held back because they do not measure up to some of the rules of thumb for the dynamic response of a hydraulic servo. Since a gas servo is not a hydraulic servo, these rules do not necessarily apply. It appears that new standards and concepts are required in general and especially with regard to dynamic characteristics.

One point of terminology requires some clarification. The actual temperature of the gas has very little to do with the things discussed here. Thus the term "gas servo" is used in the text so as to include cold as well as hot gas systems. The word "hot" has been used in the title because of its present popular usage in connection with this type of work.

Linear Considerations

Basic Equations

The linearized equations for operation at any point in the cylinder are of interest. Shearer[1] gives expressions from which the following equation may be readily obtained.

$$W_a - W_b = \frac{2AP_o}{R_g T} \times \frac{dx}{dt} + \frac{1}{k R_g T}\left(V_{ao}\frac{dP_a}{dt} - V_{bo}\frac{dP_b}{dt}\right) \quad (1)$$

Appendix IV lists and defines all symbols and the notation conventions are as shown in Figure 1. Equation 1 is limited by the small disturbance assumptions discussed by Shearer and by the assumption that the areas of both sides of the piston are equal. If it is further assumed that the valving introduces the same mass of gas on one side of the piston as it removes from the other, then the following may be written for the case of a blocked piston.

$$\frac{dP_a}{dt} V_{ao} = -\frac{dP_b}{dt} V_{bo} \quad (2)$$

A relationship between cylinder pressure rates and differential pressure is also required.

$$\frac{d\Delta P}{dt} = \frac{dP_a}{dt} - \frac{dP_b}{dt} \quad (3)$$

Inspection of Equation 1 shows that is consists of a piston rate term which is independent of pressure fluctuations and a pressure rate term which is independent of piston rate. Thus Equation 1 may be combined with Equations 2 and 3. It is convenient to first solve for differential pressure in terms of piston pressures.

$$\frac{dP_a}{dt} = \frac{V_{bo}}{(V_{ao} + V_{bo})} \times \frac{d\Delta P}{dt} \quad (4)$$

$$\frac{dP_b}{dt} = \frac{-V_{ao}}{(V_{ao} + V_{bo})} \times \frac{d\Delta P}{dt} \quad (5)$$

The final combination eliminates piston pressures as variables and introduces differential pressure instead.

$$W_a - W_b = \frac{2AP_o}{R_g T} \times \frac{dx}{dt} + \frac{2 V_{ao} V_{bo}}{k R_g T(V_{ao}+V_{bo})} \times \frac{d(P_a - P_b)}{dt} \quad (6)$$

In order to achieve a reasonable result, it is necessary to assume that the difference of the weight rates of flow into the two sides of the piston is directly proportional to valve displacement.

$$W_a - W_b = K_y Y \tag{7}$$

A careful study of valving[1,2] will show that this is not entirely true in all cases, but that the assumption is sufficiently close to the actual case to give useful results.

In the general case the gas servo could have a load consisting of a mass, a damper, and a spring which is expressed in Laplace notation as

$$A(P_a - P_b) = Ms^2x + Bsx + K_L x \tag{8}$$

Combining Equations 6, 7, and 8, in Laplace notation gives a relationship between valve position and piston position.

$$K_y Y = \frac{2AP_o}{R_g T} sx + \ldots$$

$$\ldots + \frac{2 V_{ao} V_{bo}}{k R_g T (V_{ao} + V_{bo})} \left(\frac{M}{A} s^3 x + \frac{B}{A} s^2 x + \frac{K_L}{A} sx \right) \tag{9}$$

$$\frac{x}{Y} = \frac{\frac{A k R_g T (V_{ao} + V_{bo}) K_y}{2M V_{ao} V_{bo}}}{s\left(s^2 + \frac{B}{M} s + \frac{K_L}{M} + \frac{k P_o (V_{ao} + V_{bo}) A^2}{M V_{ao} V_{bo}} \right)} \tag{10}$$

An extremely useful concept is that of the gas spring-load mass natural frequency.

$$\omega_P = \sqrt{\frac{k P_o (V_{ao} + V_{bo}) A^2}{M V_{ao} V_{bo}}} \tag{11}$$

Incorporating this concept into Equation 11 gives a more compact form of the valve-to-piston transfer function.

$$\frac{x}{Y} = \frac{K_y R_g T}{2 A P_o} \times \frac{\omega_P^2}{\left(s^2 + \frac{B}{M} s + \frac{K_L}{M} + \omega_P^2 \right)} \tag{12}$$

The damping term, B, as used above comes from a damper on the load. In most applications the load has little or no damping and the use of an artificial damper to give added stability is extremely undesirable. Certain terms which arise from open-centered valves or from leakage across the piston also give damping, but unless the quiesent flow through the open-centered valve is extremely large or unless the sealing across the piston is extremely poor, these contributions are, at best, small. The best assumption for gas servo work is zero damping in the general case.

Inspection of the expression for the gas spring-load mass natural frequency shows that the lowest value occurs when the piston is centered. This minimum frequency is essentially determined by the stall force and the stroke of the piston. Noting that P_o must be less than P_s, Equation 11 can be quite easily modified to give an upper limit for the lowest natural frequency.

$$\omega_{P\ min} < \sqrt{\frac{4\ kAP_s}{M\ \ell_T}} \tag{13}$$

It is, of course, possible to raise this value in a specific case by over-designing the piston so as to give more stall force than is actually required. This may be justified in some cases, but weight, space, and gas consumption all get increased along with the frequency.

Many applications for gas servos have a load which consists of a mass only. In these cases the open loop natural frequency of the servo becomes simply the gas spring-mass frequency. The corresponding expression for a hydraulic servo is as follows.

$$\omega_{hyd} = \sqrt{\frac{4A\beta_H}{M\ \ell_t}} \tag{14}$$

Since the value for the bulk modulus of hydraulic oil is usually a very large number, the hydraulic natural frequency is usually much larger than that of a gas servo designed to do the same job. However, as temperatures are increased the oil becomes softer and if a 1500 degree F. oil were available, the two frequencies would probably be comparable. Another point to be considered is that the actuator is usually not mounted to structure that can be considered as infinitely stiff. Thus the natural frequency to be considered in stabilizing the hydraulic servo could be the mounting spring-load mass frequency, and the stiffness advantage of cooler hydraulics would not be fully realized. It cannot be stated unqualifiedly that hydraulic servos have a large stiffness advantage over gas servos in every case.

Stability Problem

In order to gain some appreciation for the stability problem which gas servos present, consider a valve and actuator with a pure mass load sized such that the open loop natural frequency is 40 radians per second. This seems to be a reasonable value from past studies. A damping ratio of 0.1 will be assumed in order to demonstrate that any reasonable values of damping which could result from valving or leakage are insufficient to make any appreciable difference. Valve actuating dynamics are assumed to be equivalent to a first order lag which corners at 120 radians per second, but this also has very little effect on the basic problem. A Bode plot of the normalized system is shown in Figure 2. If a gain margin of 6 db. is desired, the highest allowable loop gain would be 5 per second if position feedback only were used.

This low value of gain is certainly totally unsatisfactory for any missile control system and the 0.1 damping ratio that allows the gain to be even that high is giving the gas servo the benefit of the doubt insofar as probable values is concerned. Further inspection of Figure 2 shows that the addition of large amounts of velocity feedback will not allow higher position gains because the phase shift drops so rapidly from -90 to -270 degrees. Even if the velocity did allow stable operation at higher position gains, the velocity would slow down the system and nullify any response advantages.

In order to realize high position gains and fast responses from a system such as shown in Figure 2, it is necessary to either prevent the -180 degree point from occurring so near the resonant frequency or it is necessary to bring the phase shift back above -180 degrees at some higher frequency. Sketching a Nyquist plot for this type of system will show this quite clearly. Either of the above techniques requires more than 90 degrees of phase lead from the feedback. Expressed differently, the feedback must contain a higher derivative of position than the first. This higher order feedback can be obtained in a number of ways, the most obvious being acceleration and pressure.

Acceleration

Since some of the characteristics of gas servos will be investigated by means of root locus plots, the open loop transfer functions will be given in root locus form. Valve actuation dynamics will be neglected in order to evaluate the basic trends. If the feedback consists of position, velocity, and acceleration, if the load is mass only, and if damping terms are negligible, the transfer function is as follows.

$$\frac{Y_{out}}{Y_{in}} = \frac{\omega_P^2}{s(s^2+\omega_P^2)} \left(K_a s^2 + K_v s + K_x\right) \tag{15}$$

$$\frac{Y_{out}}{Y_{in}} = \omega_P^2 K_a \times \frac{\left(s^2 + \frac{K_v}{K_a} s + \frac{K_x}{K_a}\right)}{s\left(s^2 + \omega_P^2\right)} \tag{16}$$

Figure 3a shows a root locus plot for K_v set to zero and the frequency of the numerator quadratic less than that of the denominator quadratic. It is seen that the gain can be made rather high, that damping is added, and that the closed loop always has a resonance at a frequency lower than that of the open loop. In Figure 3b the numerator frequency has been made higher than that of the denominator. The closed loop natural frequency has been increased, but the system is hopelessly unstable. The effect of adding velocity is shown in 3c and 3d. It is now possible to have a response which is essentially a well-damped second order with a high resonant frequency. Figure 3d shows the case where the phase shift of the open loop is allowed to drop below -180 degrees after which sufficient lead is added to bring it back. Crossing into the right half plane and returning presents nonlinear problems which will be discussed later. Based purely on linear considerations, the above has shown that with properly chosen acceleration, velocity, and position feedback, the basic gas servo characteristics can be controlled to a point where any desired response is possible: the real limiting factor is valve actuating dynamics.

It is most unfortunate that the accelerometers available today are unsuitable for use on this type of system. They are excessively noisy and would respond to missile acceleration as well as piston motions. Double differentation of position pickups by electronics does not appear to be a satisfactory solution. The practical limitations of instrumenting acceleration for feedback purposes have caused most workers in the gas servo field to turn to some form of pressure feedback. Several forms of pressure feedback can be incorporated directly into the valving in a relatively simple manner. Reethof [2] describes a flapper valve that has extremely simple inherent pressure feedback. Figure 4 shows a more recently developed valve and actuator. The unit has built-in transient pressure feedback but the valve assembly is seen to be quite compact. The unit shown in Figure 4 was built for test and development purposes and actually contains some extra complications in the form of adjustments.

Pressure Feedback

Using the same conditions and assumptions that led to Equation 16, the open loop transfer function for a gas servo with differential pressure, velocity, and position feedback is

$$\frac{Y_{out}}{Y_{in}} = \frac{\omega_P^2}{s(s^2+\omega_P^2)} \left(K_P \frac{\Delta P}{x} + K_v s + K_x\right)$$

For the pure mass load, area times differential pressure is equal to mass times acceleration.

$$\frac{Y_{out}}{Y_{in}} = \frac{\omega_P^2}{s(s^2+\omega_P^2)} \left(K_P \frac{M}{A} s^2 + K_v s + K_x\right) \tag{18}$$

$$\frac{Y_{out}}{Y_{in}} = \omega_P^2 K_p \times \frac{M}{A} \times \frac{\left(s^2 + \frac{K_v A}{K_P M} s + \frac{K_x A}{K_P M}\right)}{s\left(s^2 + \omega_P^2\right)} \tag{19}$$

The similiarity between Equations 16 and 19 has led to a tendency to think of pressure feedback as being exactly the same as acceleration. This is true linearly for the case given here: a load consisting of a mass only and the system driven from the valve input. However, it is not true in general. If the system had some damping or a load spring, the equations would not be nearly so

similar. If an external force were to be applied to the piston, the initial pressure feedback action would be exactly opposite to that of acceleration.

Nonlinear Considerations

Friction

A very practical difference between pressure and acceleration feedback is their behavior in the presence of friction. If there is a small position error, the system must build up differential pressure in order to move the piston and eliminate the error. Pressure feedback will fight this pressure buildup and possibly even allow this small error to persist by returning the valve to neutral. Acceleration will do nothing to discourage the pressure buildup until friction has been broken out and the piston is moving.

Experience with hydraulic servos can lead to underrating friction as a problem in gas servos. It takes time to build up pressure to break out friction, and during this time the piston is not moving. There will, therefore, always be some part of a varying input to which a gas servo will not respond. It is important to hold load friction and piston friction as small as possible, operate with as much position feedback as possible, and avoid anything which aggravates the friction problem.

Transient Pressure Feedback

Since acceleration seems to be impractical, and since pressure feedback does tend to aggravate the friction problem, transient pressure feedback becomes attractive. Here, pressure is fed back through a high pass filter so as to be effective only a those higher frequencies where it is required for stability. One possible mechanization of the high pass filter is shown in Figure 1. Any change in P_b is sensed by the small piston immediately. After some time, sufficient gas leaks through the orifice such that P_f equals P_b and the net effect becomes zero. The arrangement in Figure 1 does not give transient differential pressure feedback, but rather transient pressure from one side of the cylinder. This will be discussed at greater length later.

Using the same assumptions and steps that led to Equation 19, the open loop transfer function for transient pressure, velocity, and position feedback is as follows.

$$\frac{Y_{out}}{Y_{in}} = \frac{\omega_P^2}{s(s^2+\omega_P^2)} \times \left[\frac{\frac{K_P M}{A} s^3 + K_v s^2 + \left(K_x + \frac{K_v}{\tau_T}\right) s + \frac{K_x}{\tau_T}}{s + 1/\tau_T} \right] \quad (20)$$

The cubic cannot be factored in general terms, but factoring specific cases will give a numerator first order that very nearly cancels the denominator first order and a quadratic that is about the same as would be obtained if pressure feedback were used. Solution of a few actual cases will show that the linear responses can be made essentially the same for either pressure or transient pressure. One difference is their behavior in the presence of nonlinearities. Another difference is that transient pressure is stiffer to external disturbances at the lower frequencies. Both of these differences result from the fact that transient pressure has little or no effect at the low frequencies.

Transient pressure compensation can also be achieved by the addition of stabilizing volumes as developed by Shearer[1]. However, these volumes are not considered suitable for use where weight or space are factors. The added volumes must exceed the cylinder in weight and size if an open loop damping ratio above 0.2 is required.

Thin Plate Orifice

The orifice used in the mechanization of the high pass filter can be somewhat of a problem. If a long thin tube (or a capillary resistance) is used, the high pass filter can be satisfactorily described by a linearized equation. Fabrication is somewhat more difficult but analysis is simplified. If a thin plate orifice is used, the reverse is true. The behavior of a thin plate orifice is determined by the nonlinear curve shown in Figure 6. Flow per pressure drop can be linearized about any point. However, when the operating point is zero flow, the flow per pressure drop becomes infinite. This leads to a transient pressure feedback time constant of zero which simply means no feedback. In this situation the servo would have a limit cycle such that the oscillating pressure across the orifice would result in a time constant other than zero. The operating point would be shifted upward onto a portion of the curve with a finite slope. However, the thin plate orifice is not unsatisfactory for this application since the ever-present friction will prevent the limit cycle. Figure 5 shows computer results for a gas servo containing thin plate orifice transient pressure feedback. Figure 5a is a step response without friction and Figure 5b shows the effect of adding relatively little friction. Appendix I contains an analysis which should give a better feel for the behavior of a system with this type of characteristic. An additional point to be considered is that the thin plate orifice characteristic should give superior results so far as positioning in the presence of friction is concerned. The pressure feedback is washed out much sooner for the small pressure fluctuations, so there is a minimum resistance to the pressure build up to break out friction and make small corrections.

It is not necessary to use true differential pressure into the high pass network. Pressure from one side of the cylinder can be used but appears to be subject to certain limitations. When the operating point of the piston is moved from one end of the cylinder to the other, it will be found that the response changes markedly. At one end the maximum allowable position gain may be limited, although recent computer studies have shown that the

addition of a relatively small stabilizing volume on one end (about one fifth of the cylinder volume) will allow the gain to be raised considerably. With transient differential pressure or transient pressure from both sides of the piston, the response can be made essentially uniform throughout the stroke. Although more work on this subject is required, it appears that the choice between one and two sides should depend on the requirements of each specific application.

Jump Resonance

It can be seen from Figure 3 that the highest performance gas servo feedback configurations allow the open loop phase shift to either approach or go below -180 degrees at frequencies where the amplitude ratio is quite large. Going below -180 degrees and returning can be shown to present the possibility of a large amplitude saturation limit cycle. It would seem reasonable that the case where the phase shift approaches but does not cross -180 should not be entirely free from saturation problems. Application of the criterion developed in Appendix II demonstrates that such is the case. Barely avoiding a saturation limit cycle leaves the system subject to tremendous jump resonances.

One solution, of course, would be to avoid the higher performance feedback combinations. Another possibility is to build sufficient capability into the system such that the actuator bottoms out before the valve saturates at those frequencies which present jump problems. Neither of these methods are really satisfactory unless they are compatible with system requirements. However, the latter suggests a third solution. That is, purposely add a second nonlinearity to avoid the undesirable effects of an inherent nonlinearity.

Torque Motor Limiting

If the gas servo has built-in transient pressure feedback, it would seem that saturating the other valve inputs might be a solution. The transient pressure feedback represents most of the phase lead in the loop whereas the position and velocity components of the feedback have been found to do very little for stability. In many cases the other valve inputs consist of input, position feedback, and velocity feedback, all summed into an amplifier as electrical signals. They can be limited to some specific value by limiting in the amplifier or by judicious selection of the torque motor which the amplifier drives. A method for determining the value for this intentional saturation is presented in Appendix III. The limit will usually be such that the input can drive the valve into full saturation in the absence of pressure transients. A final point is that this nonlinear "compensation" cannot be used with pressure feedback because the input could not command full differential pressure from the servo. In this case, the limit would be such that the input could saturate the valve in the absence of either steady state or transient pressures.

Conclusions

With properly chosen feedback, the linearized dynamic response of a gas servo is limited by the valve actuating dynamics. Second derivative feedback is required in most systems for stability and the first derivative (velocity) is necessary if it is desired to achieve a response above the open loop natural frequency. If better instrumentation were available, acceleration would be the best source of the second derivative for proportional systems. Pressure feedback is relatively easy to realize, but leaves something to be desired in the way of steady state positioning accuracy. Transient pressure feedback seems to be the best solution since it can also be achieved rather easily and has zero effect in the steady state.

Transient pressure feedback can be mechanized with either a linear flow resistance or a thin plate orifice, the thin plate orifice being much more difficult to analyze. Configurations that give closed loop frequencies above the open loop frequency in the linear region of operation will usually have large jump resonances during operation which drives the valve into saturation. Limiting the authority of the torque motor can be used to avoid the jumps in systems with transient pressure feedback.

Appendix I

Analysis of Nonlinear Transient Pressure Feedback

Assuming that the thin plate orifice is the only nonlinear element in the system, a good indication of the response of the system can be obtained by establishing the behavior for all values of the nonlinearity. The nonlinearity in this case is the time constant of the high pass filter that gives transient pressure feedback.

Given a system with the parameters which are listed as follows.

K_x = 117 inches per second per inch error.

K_v = 4.37 inches per second per inch per sec.

K_p = .155 inches per second per psi.

M = 1.0 pound second squared per inch.

A = 1.77 square inches.

ω_p = 40 radians per second.

τ_M = 1/120 second.

These values are substituted into Equation 20 and the equation of the denominator is written. The high pass time constant is carried along as the only variable.

$$\frac{16800}{s(s^2+1600)(s+120)} \quad \frac{s^3}{s+1/\tau_T} + 50\ (s+26.8) + 1=0 \quad (21)$$

Equation 21 is manipulated so as to isolate the variable in question.

$$-\frac{1}{\tau_T} = s\left[\frac{s^4+128s^3+19360s^2+1032000s+22.6x10^6}{s^4+128s^3+2560s^2+1032000s+22.6x10^6}\right] \quad (22)$$

Factoring the numerator and denominator by root locus or other means gives a form which can be investigated by root locus.

$$\tau_T = \frac{-(s^2+44s+6830)(s+150)(s+22)}{s(s^2+64s+1600)(s^2+64s+14100)} \quad (23)$$

The root locus plot of Equation 23 is shown in Figure 7.

Only the oscillatory roots have been shown in Figure 7 since they are of the most interest. The servo is unstable for time constants less than 0.014. As the time constant is increased, the damping is improved and the frequency is reduced. Only at the low values of time constant is the response objectionable.

Evaluation of Time Constant

In order to obtain an equivalent time constant for a thin plate orifice and a volume, it is necessary to assume that the flow into the volume is proportional to the pressure drop across the orifice. This assumption can be made for some specific operating point on the curve shown in Figure 4.

$$\frac{W\sqrt{T}}{A_e P} = C_s \frac{(P-P_F)}{P} \quad (24)$$

By using Equation 1 with zero piston rate and the variables for one side set to zero for the behavior of the fixed volume, an expression for the time constant can be obtained.

$$\tau_T = \frac{V_F}{A_e C_s k R_g \sqrt{T}} \quad (25)$$

For the above example, the fluid medium is assumed to be air at 1500 degrees F. A reasonable ratio of chamber volume to effective area has been found to be 8000 inches based on large amplitude computer investigations. Solving Equation 25 for the value of C_s to just give a stable time constant shows that any value of C_s below 14 will give stable operation. The curve in Figure 6 drops off so sharply near zero that it is difficult to determine the exact pressure ratio for a slope of 14, but it is at a pressure ratio of less than 0.01. No attempt will be made to prove that this pressure ratio is less than the friction expressed in a similar manner, but experience will show that it is. The low amplitude, higher frequency instability will be damped out by friction in this case.

Appendix II

Jump Resonance Criterion

The nonlinearity of interest here is saturation so the derivation will be carried out for saturation and such other nonlinearities as happen to fall within the limitations that it will be convenient to assign. Inspection of the method will show that it can be extended so as to include other classes of nonlinear functions. Describing functions are used so all of the usual describing function assumptions apply. It is also assumed that the describing function is real (no phase shift) and that it is a function of input amplitude only. The criterion for the maximum jump requires that the greatest valve of the describing function be unity and that this value of unity corresponds to a region of linear operation.

The standard equation for the summing junction of a simple servo is:

$$\overline{R} = \overline{C} + \overline{E}. \quad (26)$$

The bar above the variable denotes a phasor quantity having both magnitude and direction. The magnitude of the phasors will be represented by omitting the bar. If the phase angle between $\overline{E}$ and $\overline{C}$ is θ, then the magnitudes of all three variables is given by the law of cosines. Dividing by C squared gives an expression for the closed loop amplitude ratio.

$$\left[\frac{R}{C}\right]^2 = 1 + \left[\frac{E}{C}\right]^2 + \frac{2E\cos\theta}{C} \quad (27)$$

By definition and basic assumptions, the output is equal to the product of the error, the describing function, and the linear transfer function.

$$C = ENG \quad (28)$$

Combining Equations 27 and 28 gives:

$$\left[\frac{R}{C}\right]^2 = 1 + \frac{1}{N^2G^2} + \frac{2\cos\theta}{NG} \quad (29)$$

Various considerations will show that if the closed loop amplitude ratio is to have some peak value as N (and therefore E) varies, then the square of the reciprical of that ratio must go through a minimum value. To determine any minimum values of Equation 29, simply differentiate and equate the result to zero.

$$\frac{d\left[\frac{R}{C}\right]^2}{dN} = -\frac{2}{G^2N^3} - \frac{2\cos\theta}{GN^2} = 0 \quad (30)$$

$$\cos\theta = -\frac{1}{NG} \quad (31)$$

Equation 31 defines the condition for the occurrence of a jump resonance in terms of the open loop transfer function. One obvious set of conditions immediately excludes most servos from the possibility of having a jump: the linear transfer function must be greater than unity when the cosine of the phase shift is negative.

Substituting Equation 31 into 29 gives an expression for the maximum nonlinear value of the closed loop amplitude ratio.

$$\frac{1}{\left[\frac{R}{C}\right]^2_{max}} = 1 - \cos^2\theta = \sin^2\theta \qquad (32)$$

The characteristic of the jump resonance which is actually of greatest interest is the height of the jump above the expected linear value. Allowing N to go to unity in Equation 29 gives the expected linear value of amplitude ratio. The ratio of the greatest jump to the linear value is now readily found.

$$\frac{\left[\frac{R}{C}\right]^2_{max}}{\left[\frac{R}{C}\right]^2_{lin}} = \frac{1 + \frac{1}{G^2} + \frac{2\cos\theta}{G}}{\sin^2\theta} \qquad (33)$$

$$= \frac{\sin^2\theta + \cos^2\theta + \frac{2\cos\theta}{G} + \frac{1}{G^2}}{\sin^2\theta} \qquad (34)$$

This ratio is given the symbol γ for convenience and the above factored to give:

$$\gamma^2 = \frac{(G\sin\theta)^2 + (1 + G\cos\theta)^2}{(G\sin\theta)^2} \qquad (35)$$

The above equation is a family of straight lines on the complex plane. All of the lines pass through the minus one point with a slope which is given as follows.

$$m = \frac{1}{\sqrt{\gamma^2 - 1}} \qquad (36)$$

These lines are valid only to the left of minus one. With a complex plane plot of the open loop transfer function, it is a simple matter to find which frequencies present potential problems and just how severe the problem is. Figure 8 shows the open loop of the system studied in Appendix I with a fixed time constant of 0.05 second. A jump of 6 db. above the linear response in the region of 46 radians per second is possible.

The stability of the forced oscillation still remains to be investigated. From Equation 26,

$$2RdR = 2CdC + 2EdE + 2C\cos\theta\, dE + 2E\cos\theta\, dC. \qquad (37)$$

$$R\frac{dR}{dE} = (E + ENG\cos\theta) + \frac{dC}{dE}(ENG + E\cos\theta) \qquad (38)$$

Reference 3 shows that if the right side of the above equation is greater than zero, the forced nonlinear oscillation is stable. For stability,

$$(1 + NG\cos\theta) + G\left(N + \frac{E\,dN}{dE}\right)(NG + \cos\theta) > 0. \qquad (39)$$

This expression may be simplified by inserting the condition of interest as given in Equation 31.

$$\left(1 + \frac{E}{N}\frac{dN}{dE}\right)\left(NG - \frac{1}{NG}\right) > 0 \qquad (40)$$

Since NG at this condition is greater than unity, the final stability relationship is

$$\frac{E}{N} \times \frac{dN}{dE} > -1 \qquad (41)$$

It will suffice at this point to state that the above relation has been investigated for the saturation describing function and that the oscillation corresponding to Equation 31 is stable.

Appendix III

Limiting to Avoid Jump Resonance

A gas servo with built in transient pressure feedback can be represented by the block diagram shown in Figure 9. The input, position feedback, and velocity feedback are electrical signals and are summed into an amplifier and torque motor combination. The transient pressure feedback is summed with the torque motor output at the valve as shown in Figure 1. Using the symbols as shown in Figure 9, the equation of the valve summing junction in phasor form is

$$\overline{L} = \overline{Q} + \overline{V} \qquad (42)$$

Solving the triangle gives

$$L^2 = V^2 + Q^2 + 2VQ\cos\angle FT \qquad (43)$$

Solving for the ratio of L to V in the region of linear operation gives the following.

$$\frac{L^2}{V^2} = 1 + \frac{Q^2}{V^2} + \frac{2Q\cos\angle FT}{V} \qquad (44)$$

$$\frac{L^2}{V^2} = 1 + (FT)^2 + 2\,FT\cos\angle FT \qquad (45)$$

Equation 45 can be solved to give a limit for the electrical valve input, L, which will not allow saturated operation of the valve at those frequencies which show up as having saturation problems. The process is to determine the minimum ratio of L to V in the frequency range of interest and then solve for the maximum allowable value of L by using the V which corresponds to the valve being just at the saturation valve. The situation is complicated somewhat by the fact that the effective value of M

can be 1.27 times the limit, by the fact that slight saturation of the valve may not cause a jump resonance, and also by the fact that the above assumes that the valve saturates when the valve command reaches some certain value independent of frequency. However, the procedure given above will give a reasonable value from which to start a closer examination, if a closer examination is desired.

Since FT is the section of the loop containing the stabilizing lead, the angle of FT should be less than 90 degrees. Thus, Equation 45 should always give a limit for L which is greater than the limit on V, and the electrical signal should be able to drive the valve into full saturation in the absence of pressure transients.

A possible objection to this type of limiting is that the response willbe slowed down somewhat for the larger input commands. Unless some other method can be found, the choice is well-defined: have a fast system with a jump resonance, use feedback which results in a slower system without a jump resonance, or incorporate torque motor limiting so as to have the fast response for most inputs and a slower response to the large inputs. Most systems should not be severely restricted by this limiting since normal operation does not usually require that the valve spend prolonged periods of time in the saturated state.

Appendix IV

Nomenclature

The units given form a consistent set. Other units are certainly possible.

- A - piston area, square inches.
- A_e - effective orifice area of high pass filter, square inches.
- B - damping coefficient, pounds per inch per second.
- C - the output of any servo.
- C_s - linearizing coefficient for the thin plate orifice flow characteristic, degrees to the one-half power per second.
- E - the error signal of any servo.
- F - the transient pressure feedback transfer function.
- G - the open loop transfer function of any servo.
- k - the ratio of specific heats of the gas.
- K_a - acceleration feedback gain, inches per second per inch per second squared.
- K_L - load spring constant, pounds per inch.
- K_p - pressure feedback gain, inches per second per psi.
- K_v - velocity feedback gain, inches per second per inch per second.
- K_x - position feedback gain, inches per second per inch of position error.
- K_y - valve gain, pounds per second per inch.
- L - the torque motor component of valve input.
- l_t - the total stroke of the piston, inches.
- M - load mass, pound seconds squared per inch.
- m - the slope of the constant γ lines.
- N - saturation describing function.
- P - the driving pressure of a thin plate orifice, psi.
- P_a - pressure in the extend side of the cylinder, psi.
- P_b - pressure in the retract side of the cylinder, psi.
- P_f - pressure in the averaging chamber of the high pass filter, psi.
- P_o - average cylinder pressure, psi.
- P_s - supply pressure, psi.
- Q - the transient pressure component of feedback.
- R - the input to any servo.
- R_g - gas constant, inches per degree Rankine.
- s - the Laplace operator.
- T - gas temperature, degrees Rankine, and also the transfer function from valve to piston.
- t - time, seconds.
- V - valve, position.
- V_{ao} - average volume of the extend side of the cylinder, cubic inches.
- V_{bo} - average volume of the retract side of the cylinder, cubic inches.
- V_f - volume of the averaging chamber of the high pass filter, cubic inches.
- W - gas weight flow through a thin plate orifice, pounds per second.
- W_a - gas weight flow into the extend side of the cylinder, pounds per second.
- W_b - gas weight flow into the retract side of the cylinder, pounds per second.
- x - piston position, inches.
- Y - valve displacement from neutral, inches.
- Δ_P - differential pressure across the piston, psi.
- γ - the maximum possible jump resonance peak above the amplitude ratio of the linear system.
- θ - the phase angle of the open loop transfer function of any servo.
- τ_M - valve actuation time constant, seconds.
- τ_T - transient pressure feedback time constant, sec.
- ω_{hyd} - the natural frequency of the fluid spring and the load mass in a hydraulic servo, radians per second.
- ω_p - the natural frequency of the gas spring and the load mass in a gas servo, radians per second.

Acknowledgement

The material in this paper is based on work done by the author at Convair, San Diego as part of company sponsored programs. Any material that was not developed directly on these programs was certainly suggested by the results of these programs. The author also wishes to express appreciation to the Stratos Division of the Fairchild Engine and Airplane Corporation for their permission to use and publish the photograph that appears as Figure 4.

References

1. J. L. Shearer, "Study of Pneumatic Processes in the Continuous Control of Motion with Compressed Air - I & II", ASME Trans., pp. 233 - 249; Feb. 1956.

2. G. Reethof, "Analysis and Design of a Servomotor Operating on High-Pressure Compressed Gas", ASME Trans., pp. 875 - 883; May 1957.

3. Ze'ev Bonenn, "Stability of Forced Oscillations in Nonlinear Feedback Systems", IRE Trans. on Automatic Control, PGAC-6, pp. 109 - 111; December 1958.

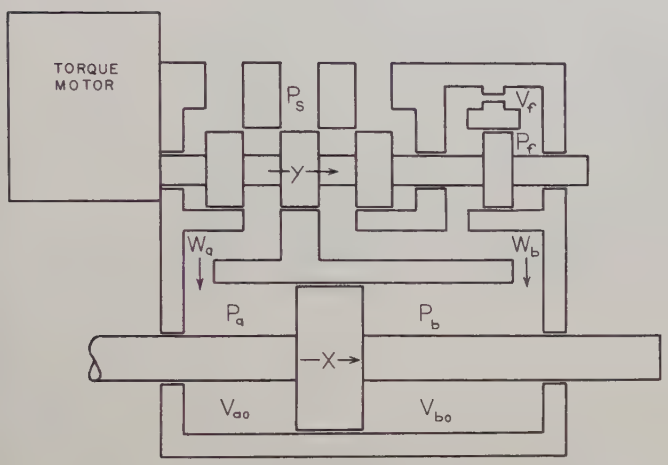

Fig. 1. Gas Servo Schematic.

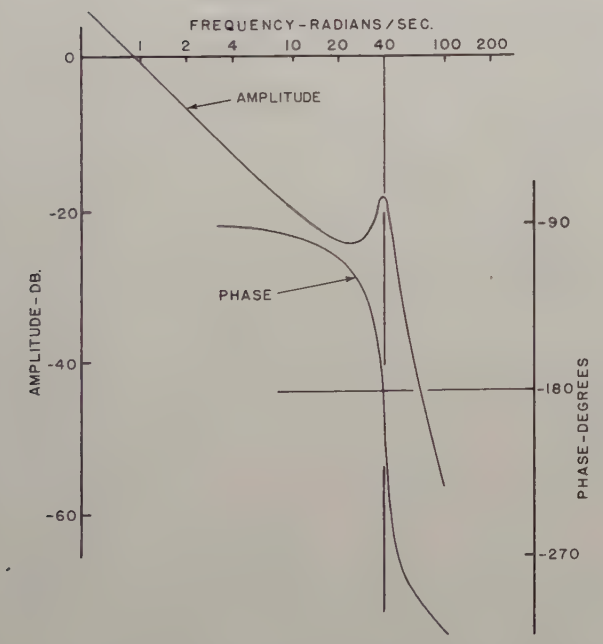

Fig. 2. Bode Plot of Valve-to-Piston Transfer Function.

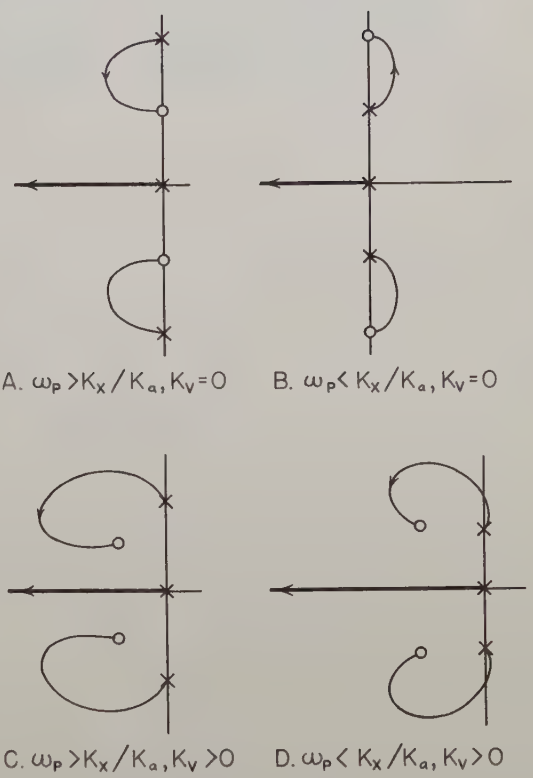

Fig. 3. Effect of Various Feedback Combinations.

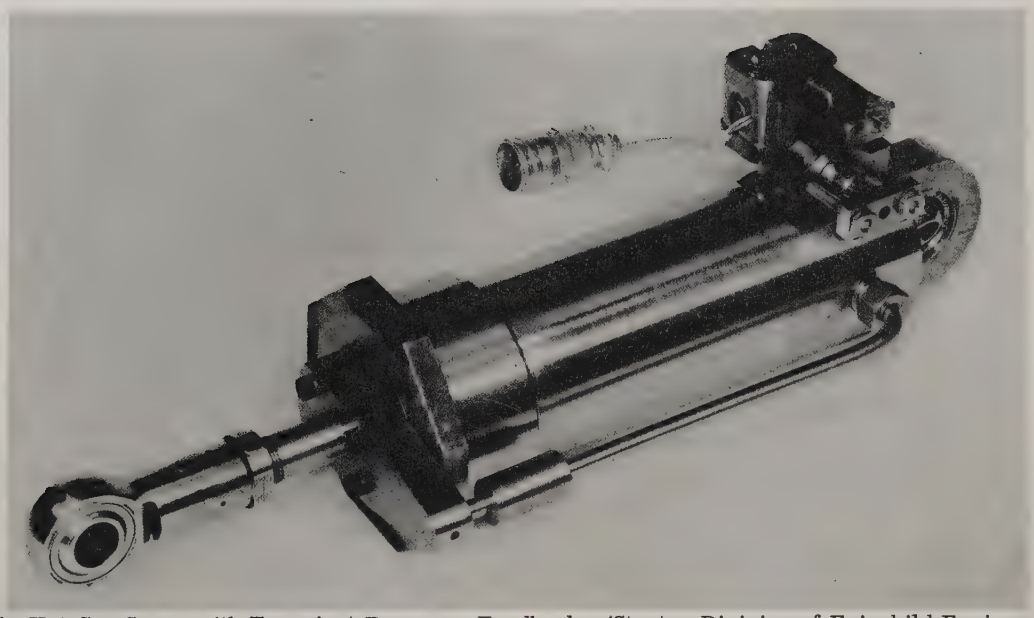

Fig. 4. Hot Gas Servo with Transient Pressure Feedback. (Stratos Division of Fairchild Engine and Airplane Corp.)

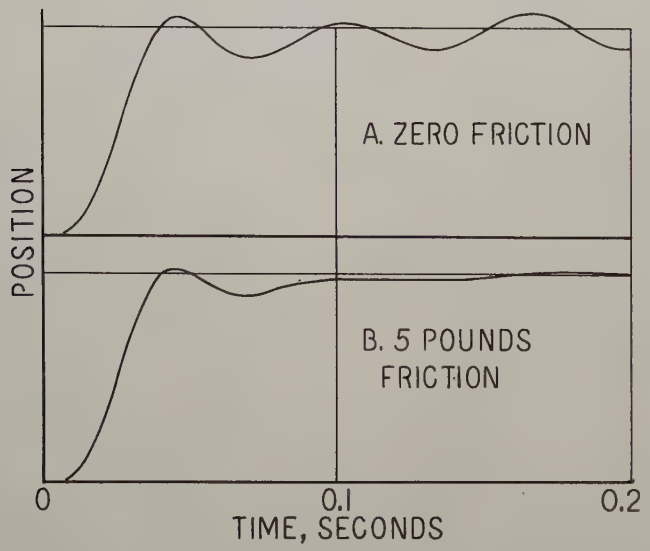

Fig. 5. Computer Results for Thin Plate Orifice Feedback.

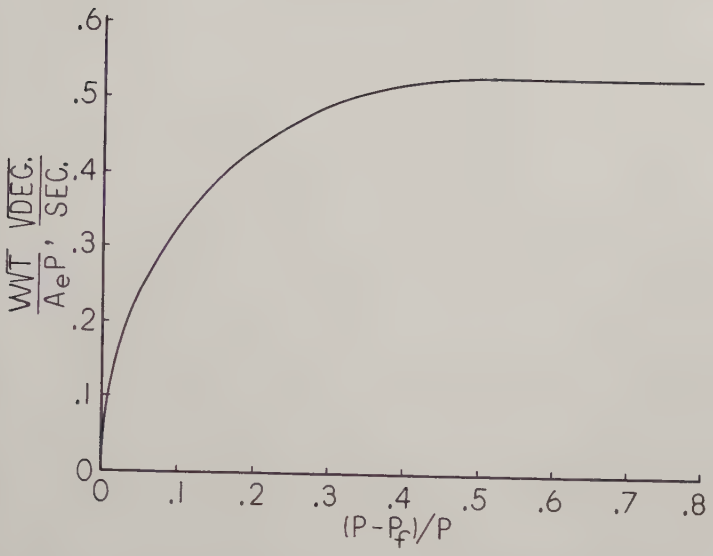

Fig. 6. Thin Plate Orifice Flow Characteristic for Air.

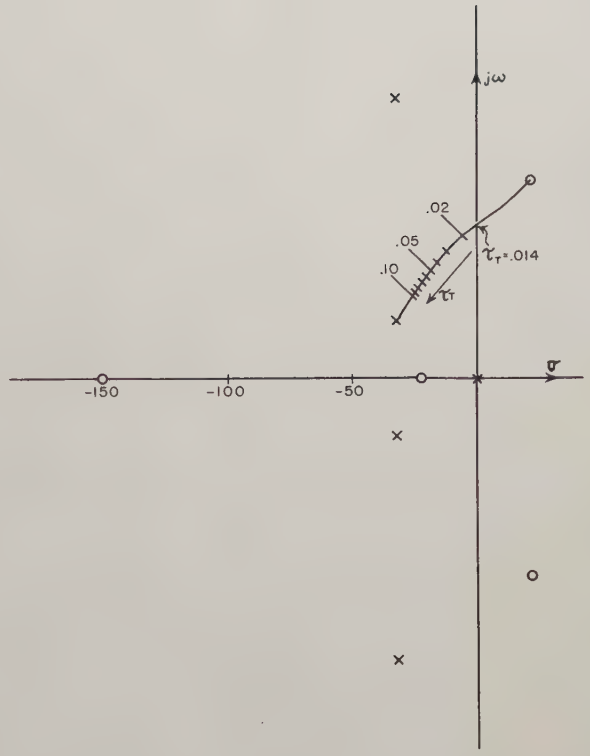

Fig. 7. Effect of Nonlinear Time Constant.

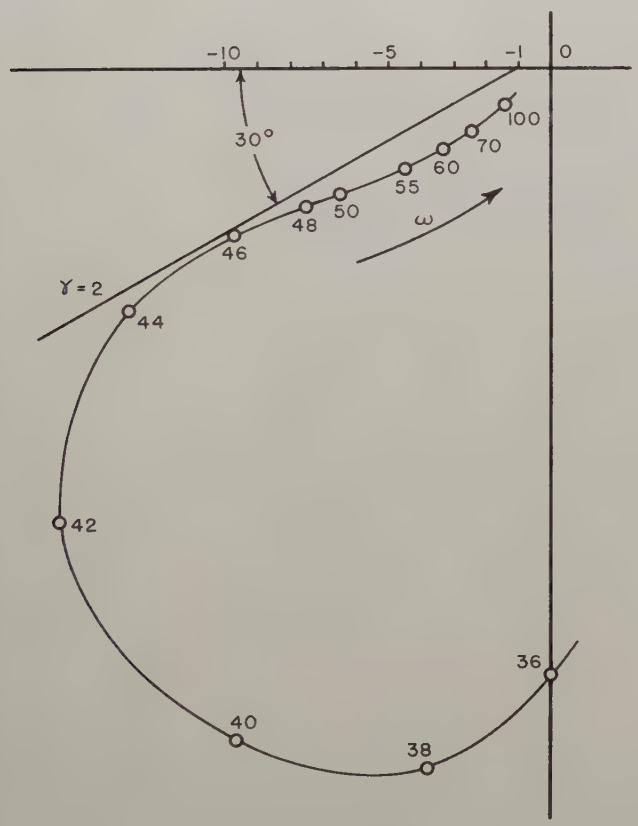

Fig. 8. Application of Jump Resonance Criterion.

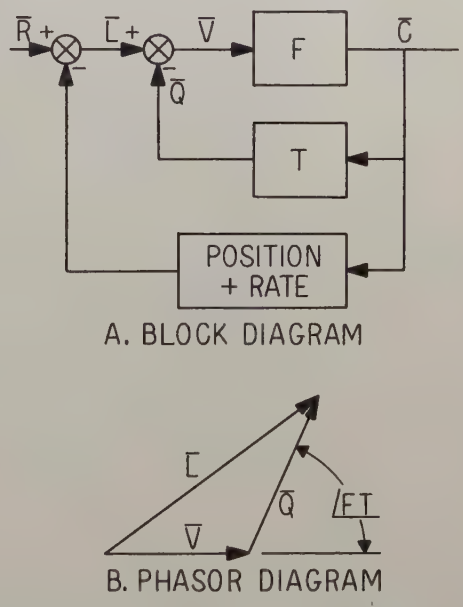

Fig. 9. Relationships for Torque Motor Limiting.

TOPOLOGICAL TECHNIQUES FOR THE SOLUTION OF MULTI-LOOP SAMPLED SYSTEMS

R. Ash, W. H. Kim, and G. M. Kranc
Department of Electrical Engineering
Columbia University
New York, N. Y.

Abstract

This paper presents a flow-graph approach for analyzing multi-loop sampled-data systems. Two techniques for finding the sampled output are examined. These are, first, construction of a "sampled" signal flow graph from the original system; second, a general gain formula which can be directly applied to the original system. The theorems necessary to establish the formula are rigorously proved.

The first technique allows two possible modes of solution. The sampled output can be found directly from the sampled flow graph by the use of Mason's formula, or in case of a more complicated multi-loop system, the problem of enumerating nontouching feedback loops can be simplified by the use of topological matrices. Techniques developed in the paper are also applied to the solution of multirate systems.

This paper has been published by the American Society of Mechanical Engineers as ASME Paper No. 59-NAC-1.

SYNTHESIS OF THIRD ORDER CONTACTOR CONTROL SYSTEMS

Irmgard Flügge-Lotz
Stanford University

Abstract

A dynamic system is given with a transfer function of third order (one real pole, two complex poles, and two zeroes). It is desired to design a contactor control which yields a near-optimum follow-up of a given input. For zero-seeking systems and for step-inputs an "optimum" control problem can be defined easily; however, a general solution of the optimum problem is not yet available. The known particular cases yield switching surfaces in the phase space which depend on the particular pole and zero locations (parameter set). The realization of such surfaces is rather difficult and usually demands digital computer equipment. The author and her associates suggest in this paper switching functions which can be realized easily and which give good response for different parameter sets. Particular attention is given to the occurrence of discontinuities in linear switching functions and their advantages and disadvantages; to different types of chatter, which may or may not improve the system performance; to discontinuities in the switching function which can be avoided by feeding the output of the contactor back into the switching function. Analog computer tests show the performance of systems with linear switching functions. The choice of the coefficients in this linear switching function is discussed. The influence of imperfections of the control system on its performance is investigated. Comparison to linear feedback control systems are included.

This paper is to be published in the Proceedings of the First IFAC Moscow Congress by Butterworth Scientific Publications in 1960.

ON THE GENERAL THEORY OF CONTROL SYSTEMS

R. E. Kalman
RIAS, Inc.
Baltimore, Md.

Abstract

This paper deals with further advances of the author's recent work on optimal design of control systems and Wiener filters. Specifically, we consider the problem of designing a system to control a plant when (1) not all state variables are measurable, (2) the measured state variables are contaminated with noise, and (3) there are random disturbances.

An explicit design procedure (well adapted to digital computation) is presented. In addition, some fundamental new concepts (controllability, observability, etc.) are introduced. A general theory of control systems is outlined which answers many basic questions (what is controllable? why? how?) and gives a highly efficient method of computation.

This paper is to be published in the Proceedings of the First IFAC Moscow Congress by Butterworth Scientific Publications in 1960.

ON OPTIMAL COMPUTER CONTROL

J. E. Bertram and P. E. Sarachik
I.B.M. Research Center
Yorktown Heights, N. Y.

Abstract

This paper is concerned with the optimal computer control of a linear dynamic element of plant. It is required that the outputs of the plant exactly equal a set of desired outputs at the uniformly spaced time instants, t, t_N, t_{2N}, ... The system is optimal in the sense that a quadratic form of the control effort, which is proportional to the control energy, is a minimum. The optimal system is shown to be a linear, periodically time-varying feedback system, in which the generation of the control input is related to the solution of the adjoint equations of the plant. The paper concludes with a discussion of the effects of uncontrolled inputs and certain problems encountered in making the system adapt to slow parameter variations.

This paper is to be published in the Proceedings of the First IFAC Moscow Congress by Butterworth Scientific Publications in 1960.

CONTROL SYSTEM ANALYSIS AND DESIGN VIA THE SECOND METHOD OF LYAPUNOV: (I) CONTINUOUS-TIME SYSTEMS (II) DISCRETE TIME SYSTEMS

R. E. Kalman
RIAS, Inc.
Baltimore, Md.
and
J. E. Bertram
I.B.M. Research Center
Yorktown Heights, N. Y.

Abstract

I - Continuous-Time Systems - The "second method of Lyapunov is the most general approach currently in the theory of stability of dynamic systems. After a rigorous exposition of the fundamental concepts of this theory, applications are made to (a) stability of linear stationary, linear nonstationary, and nonlinear systems; (b) estimation of transient behavior; (c) control-system optimization; (d) design of relay servos. The discussion is essentially self-contained, with emphasis on the thorough development of the principal ideas and mathematical tools. Only systems governed by differential equations are treated here. Systems governed by difference equations are the subject of a companion paper.

II - Discrete-Time Systems-The second method of Lyapunov is applied to the study of discrete-time (sampled-data) systems. With minor variations, the discussion parallels that of the companion paper on continuous-time systems. Theorems are stated in full but motivation, proofs, example, and so on, are given only when they differ materially from their counterparts in the continuous-time case.

Part I has been published by the American Society of Mechanical Engineers as Paper No. 59-NAC-2.

Part II has been published by the American Society of Mechanical Engineers as Paper No. 59-NAC-3.

ADAPTIVE FLIGHT CONTROL

O. H. Schuck
Minneapolis-Honeywell Regulator Company
Minneapolis, Minn.

Abstract

Need for adaptive control systems is explained, and results obtainable with two forms are discussed. Recognized approaches to achieving self-adaptive action are indicated; integrating and nonintegrating techniques are compared. One non-integrating form, the model-bistable system, is taken as an example, and analysis of its operation is developed. Its application to flight control is described, and its limitations in this and other applications are discussed. Effects of system performance requirements, including nature of input signals and disturbances, on the choice of adaptive control type are considered. Relations of mechanistic adaptive control systems to those found in the biological organism are discussed.

This paper is to be published in the Proceedings of the First IFAC Moscow Congress by Butterworth Scientific Publications in 1960.

ELECTRONIC SOLID-STATE AUTOMATIC FLIGHT CONTROL SYSTEMS

The three papers that follow describe a series of developments that have made possible completely electronic solid-state automatic flight control systems, free of moving parts between the input sensors and the output actuators.

Solid-state automatic flight control systems are not new. They have been a working reality for several years now, and have established an enviable record of performance and reliability. The present solid-state flight control systems utilize electromechanical components to perform a number of key system functions. It is expected that systems utilizing the new all-electronic techniques will be superior with respect to size, weight, cost and reliability when compared to their electromechanical counterparts. In addition, the all electronic systems will be particularly compatible with the coming generation of multiplexed airborne digital computing systems.

Figure 1 presents the block diagram of an illustrative signal chain, arranged to emphasize the three areas to be discussed in the papers that follow. The input signal E_1 is an ac voltage that is synchronized, filtered, and gain adjusted before emerging as ac voltage E_2.

The first paper that follows describes electronic function storage and gain control, areas represented by the diagonally shaded boxes in Figure 1. High performance flight control systems, designed to control vehicles that are to operate over widely varying flight conditions, require some form of automatic control of the gains of individual channels in order to compensate for major variations in effective airframe dynamics. The techniques illustrated in Figure 1 include both the classical stored function approach, in which the required gains are stored as functions of variables that are sensed or computed in flight, and one class of adaptive systems in which the difference between a desired and a computed figure of merit is integrated to derive the gain control signal. Figure 1 illustrates the fact that these techniques, and alternate adaptive implementations, are both competitive and compatible. That is, the attainment of a given dynamic performance specification may require an adaptive technique, a stored function technique, or a combination of these approaches. The requirement for a combined approach can stem either from a strict transient specification or from the need to vary the adaptive figure of merit with flight conditions in order to fully realize potential dynamic performance without exceeding airframe capabilities.

The first paper concentrates on new all-electronic implementation techniques for two dimensional function storage that achieve a new flexibility in function approximations and that are readily applicable to combined adaptive stored function control systems. This paper also briefly summarizes the characteristics of electronic switching circuitry for ac signal voltages. Such switching devices are used both in function storage implementations and in the implementation of over-all system switching when actuated by digital logical circuitry.

The second paper deals with the horizontally lined box of Figure 1. In selected modes of automatic flight control system operation it is necessary to remove the effect of any signal present at E_1, while retaining the capability of responding to any variation in E_1 that occurs after a given switching instant. The synchronizer satisfies the first condition by introducing a signal E_b equal and opposite to E_1 when the switch is closed. The second condition is satisfied by memorizing the value of E_b at the instant that the switch is opened. The second paper presents new all-electronic techniques for achieving this precise long-time memory.

The third paper deals with the problems of integration and filtering of ac signals, illustrated in Figure 1 by the vertically lined boxes. In this illustrative example, the integrator is being utilized to build up an adaptive control signal from a voltage proportional to the error between actual and desired figure of merit. In actual flight control systems, integrators are also used directly in the signal chains in areas of high accuracy, low bandwidth control. In addition, integrators are the central element in high pass and low pass filter implementations. The third paper describes new all-electronic, pulse-controlled integrators capable of performing precise integration and, in suitable feedback configurations, of filtering ac signals.

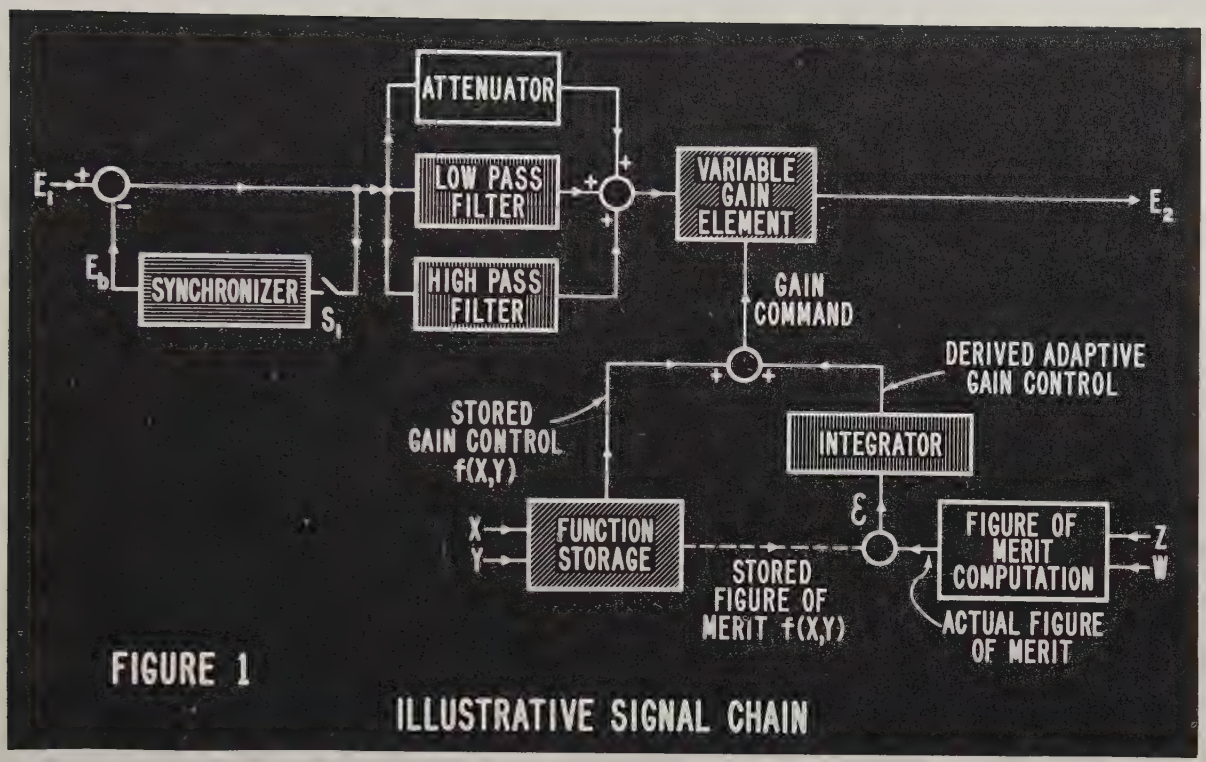

FIGURE 1

ILLUSTRATIVE SIGNAL CHAIN

ELECTRONIC GAIN CONTROL IN AUTOMATIC FLIGHT CONTROL SYSTEMS

William Henn and Eugene L. Boronow

Bendix Aviation Corporation
Eclipse-Pioneer Division
Teterboro, New Jersey

Introduction

This paper deals with the problems involved in implementing electronic, stored function, control of automatic flight control system channel gains. Systems of this type utilize sensed variables to actuate a set of stored functions in such a manner that correct precomputed attenuations are automatically introduced in the channel ac signal lines. Since the greatest attraction of the stored function technique arises when the sensed variables required to actuate a given channel number only one or two, this paper will concentrate on electronic techniques for implementing the one or two variable case, with the understanding that these techniques can be extended to more complex situations when this is required.

Consider the problem of specifying the gain of a given channel as a function of two variables. While it is sometimes possible to derive the required gain as a well defined analytic function, in most cases the basic data is derived from a series of simulation runs in which one parameter is held constant while the second parameter is varied over its operating range. The repetition of this process for a number of chosen values of the first parameter results in a finite family of curves as illustrated in Figure 1. These curves define lines on the required continuous gain surface. The ideal surface can then be approximated by one that passes precisely through each boundary curve and linearily varies from one boundary curve to the next as a function of the first parameter.

The standard technique for implementing channel gain control as a function of two variables involves three basic steps:

1) The surface is first approximated by a combination of the sums and products of a new set of single variable functions in X and Y, utilizing techniques already well defined in the literature. For example, a typical approximation might be

$$F(X, Y) = F_a(X) + F_b(Y) + F_c(X) F_d(Y).$$

In general the number of sum and product terms depends on the required accuracy and on the complexity of the surface that is being approximated.

2) The single variable functions are stored in the winding configuration of nonlinear potentiometers, using one potentiometer per function.

3) The single variable functions are then combined in the prescribed manner.

In a multiple channel system this technique results in the system configurations illustrated in Figure 2a. The variables X and Y are converted to shaft rotations at a centralized location. All system gain adjust potentiometers are mounted in this central assembly, with all F(X) potentiometers driven by the X shaft and all F(Y) potentiometers driven by the Y shaft. The signal leads from all channels are routed to this location, through the applicable potentiometers, and back to the channels from which they came.

The electronic techniques presented in this paper can be used either as direct replacements for these electromechanical implementations or in new configurations that do not require sum and product approximations. Direct replacement is applicable to the generation of single variable functions and to simple multi variable functions that are readily approximated by a small number of sum and product terms. The elimination of sum and product approximations is of greatest value in the generation of more complex multi variable functions.

The use of electronic techniques for direct replacement alone offers several major advantages including:

1) The requirement for routing all ac signals that are to be gain adjusted to a single central location is eliminated. Instead, the system configuration is as illustrated in Figure 2b. The elements that implement the electronic function generation and gain control are combined with the normal ac channel amplifier circuits, with centralized control exercised through the distribution of dc voltages proportional to X and to Y. When more than one channel is to be actuated by the same function, it is possible to generate the required function centrally distributing the resultant dc control signals to the remotely located signal attenuators.

2) The requirement for electromechanical devices, including servo mechanisms and sliding contact potentiometers, is eliminated, thereby increasing system reliability and reducing system size and weight.

3) Individual functions that heretofore could be substantially changed only by redesigning the corresponding potentiometers can be changed easily, in the field if necessary, by simply replacing a small number of fixed resistors.

In addition to the very desirable features that have been summarized above, the new electronic techniques make possible the complete elimination of the substantial inaccuracies introduced by sum and product approximations of complex multi variable functions. These complex functions can now be generated directly from the original family of function curves specified by the simulation runs.

Techniques applicable to the electronic implementation of channel gain control as a function of a single variable are described in the first section of this paper. The application of these techniques to channel gain control as a function of two variables is described in the second section.

The Appendix of this paper presents electronic techniques for switching ac signals under dc voltage control. This requirement is common to electronic function generation, electronic memory, electronic integration and general automatic flight control signal switching.

Functions of a Single Variable

A simple method for generating a function of a single variable is to approximate the required function by a series of steps. An approximation of this type can be implemented very simply by switching a fixed attenuating resistor into the signal channel over the proper range of the sensed variable. Electronic techniques for implementing signal switching are discussed in the Appendix.

This step method of channel gain control is quite limited, however, in that it will yield only a rough approximation to the required function unless a large number of steps are used. A more accurate approximation can be obtained utilizing a series of constant-slope line segments instead of the steps. In this process, each straight-line segment has associated with it both a slope and an initial value at the point of junction with the preceding segment. The location of junction points depends upon the shape of the curve being synthesized. As each junction point is reached, a new straight-line segment having a new slope may be switched in using diode switching. The entire function generator is thus a diode-resistance matrix. The channel gain control is implemented by generating a dc signal defining the required channel gain. This dc signal controls an ac attenuator inserted in the signal channel to produce the required attenuation, as illustrated in Figure 3. The attenuator to be discussed in this paper is a magnetic modulator in which the attenuation is determined by a dc current in the control winding. This control current is generated in the following manner:

A single change in slope can be achieved with one diode and one resistor, as shown in Figure 4. When the input voltage E is applied to the single-diode circuit of Figure 4a, the current i flowing in the circuit is determined by either of two conditions. For values of $E < e_1$ the current i is zero (assuming a perfect diode). For values of $E > e_1$ the current i is given by $i = \frac{E - e_1}{R}$. This relationship is shown graphically in Figure 4b. The break point is at e_1 and the slope is given by $\frac{1}{R}$.

The circuit of Figure 4a can be simplified by using a single Zener diode to replace both the conventional diode and the voltage source e_1. Although both Zener diode and conventional

diode techniques are feasible, the latter will be used to illustrate the various function shaping techniques.

Multiple changes in slope can be achieved by using several diodes and resistors, as shown in Figure 5. The circuit of Figure 5a produces a current-voltage relationship as shown graphically in 5b. Two break points may be noted. For all applied voltages less than e_2, the diode D_2 is cut off and the circuit response is identical to that of the single-diode circuit. When the input voltage exceeds e_2, however, diode D_2 will conduct and an additional break point will be introduced at e_2. The slope is given by $\frac{1}{R_1}$ for the straight-line segment between e_1 and e_2 and by $\left(\frac{1}{R_1} + \frac{1}{R_2}\right)$ for the segment beyond e_2.

The introduction of the control winding resistance (R_L) of the magnetic modulator as part of the dc circuit is shown in Figure 6. The transfer characteristic implemented is one having only increasing slope segments as shown in the accompanying curve. This same configuration can be used to obtain a decreasing slope by adjusting the bias current of the magnetic modulator and reversing the connection of the control winding (R_L). Further, by having a center tapped control winding, and two separate function generators, one containing elements determined by its increasing slope segments, and the other containing elements of its decreasing slope segments, a method of slope reversal is introduced. Such a system is depicted in Figure 7a.

The requirement for floating power supply voltages implied by Figure 6 is eliminated in the configuration illustrated in Figure 7b. Here, the voltage divider $\frac{R_{1b}}{R_{1a} + R_{1b}}$ controls the voltage break point, while the parallel combination of R_{1a} and R_{1b} controls the change in slope. Specifying the required break point and slope change therefore uniquely defines both R_{1a} and R_{1b}. A common grounded power supply is used to provide the single dc reference voltage. Figure 7c presents the output of a system implemented in this manner. For this photograph the modulator was actuated by a fixed ac input voltage and the gain control current was derived from the oscilloscope horizontal sweep voltage.

A number of alternate procedures for producing the required gain control circuits can be readily derived. For example, at the expense of additional circuitry, each segment of the curve can be made independent of the other, using resistors to define the initial value and slope of each segment independently. The most applicable method will depend on the complexity of the function to be generated and on required accuracy.

Functions of Two Variables

For those cases where the function of two variables can be easily approximated by the sums and products of single variable functions, the magnetic modulators can be used to effect the required combination of separately formed single variable functions. This process can be implemented by specifying the interconnection of the magnetic modulators and of their control windings. The sum of two functions can be formed utilizing a control winding consisting of two identical center-tapped coils. Such a function

$$F(X, Y) = F_1(X) + F_2(Y)$$

is illustrated in Figure 8. The product of two functions can be formed by utilizing two modulators in cascade as shown in Figure 9a. A photograph of the detected response of such a system is presented in Figure 9b. Note in particular that the Y input cannot control the shape of the curve, only its amplitude is effected. Functions containing both the sums and products of single variable functions such as

$$F(X, Y) = \left[F_2(X) + F_1(Y)\right] F_3(X)$$

can be implemented as shown in Figure 10.

The generation of a function of two variables by the techniques described above is desirable only when the sum and product approximation is simply derived and yields a sufficiently accurate result. When these conditions are not met is becomes desirable to utilize the original family of data curves and to develop means for interpolating between these curves to obtain the required function. In the electronic implementation to be described, the functions $F_n(X)$ are stored as single variable functions as shown in Figure 1. The Y dc voltage is coded and used to automatically select

the proper upper and lower bound X functions. For example, the voltage Y_p defined as $Y_2 < Y_p < Y_3$ will select $F_2(X)$ as the lower bound and $F_3(X)$ as the upper bound. The interpolation between these two bounding functions is accomplished by a process of fading-in $F_3(X)$ and fading-out $F_2(X)$ under the control of the voltage Y_p.

The selection of the proper boundary functions is implemented by an electronic switching network as shown in Figure 11. This network consists of a series of Schmitt Trigger Circuits, each designed to fire at a specified Y_i, and appropriate gating designed to achieve the required selection. Thus for Y_p as defined above, all Schmitt triggers up to S. T. 3 are in the B state and S. T. 3 and all the remaining Schmitt triggers are in the A state. Therefore only the G_2 line will be excited.

The fading-in process is accomplished by multiplying $F_3(X)$ by an increasing ramp function, P_1 determined by Y_p, utilizing cascaded modulators. The fading out process multiplies $F_2(X)$ by a decreasing ramp, P_2. The sum of these two products gives the desired function

$$F(X, Y) = \left[\frac{Y_3 - Y_p}{Y_3 - Y_2}\right] F_2(X) + \left[\frac{Y_p - Y_2}{Y_3 - Y_2}\right] F_3(X).$$

The implementation of this interpolation procedure is illustrated in Figure 12. The product $P_1 \cdot F_2(X)$ is obtained by cascading modulators 1 and 3 and the product $P_2 \cdot F_3(X)$ results from cascading modulators 2 and 4. The sum of these products is obtained by combining the outputs of modulators 2 and 4 in a series-aiding arrangement. The input ac signal to be attenuated by this network is connected to the inputs of both modulator 1 and modulator 3. Zone selection is accomplished by the electronic switch previously described and by the gating structure shown in Figure 13. The resultant waveforms are as shown in Figure 14. Experimental oscilloscope wave forms illustrating interpolation from the lower bound to the upper bound of a selected zone are presented in Figures 15 and 16. This example illustrates the substantial changes in function, size and shape that can be readily achieved utilizing these new techniques.

ACKNOWLEDGEMENT

The contributions of Dr. A. S. Robinson to the system design and of Mr. M. Teitelbaum, Mr. D. Aviv and Mr. V. Garofalo to the circuit design and construction of the feasibility models of this system are gratefully acknowledged.

APPENDIX A

ELECTRONIC SWITCHING CIRCUITS

The techniques for controlling parametric gain and for generating functions of several independent variables are based on a high-speed solid-state switching capability. Electronic switching circuits are advantageous in that they inherently eliminate such undesirable relay properties as mechanically moving parts, contact bounce and chatter, susceptibility to increasing contact resistance with time, limitations in transmitting extremely low signal levels such as null or small error voltages, and appreciable time lag between actuation and closure. Electronic switching circuits can be designed to retain such desirable relay properties as extremely low transfer impedance in the "ON" position, high transfer impedance in the "OFF" position, essentially undistorted signal wave shape, and signal transfer operation independent of the circuit input and output impedance levels. Additional advantages offered by electronic switching in computing and control systems include high-speed operation, reduced power requirements, greater packaging flexibility, and ability to withstand severe shock and vibration.

The replacement of a relay signal switching system by an electronic equivalent requires recognition of the fact that arrays of relay contacts perform two separate and distinct functions: that of connecting a given set of inputs to a given set of outputs (signal transfer or switching functions), and that of controlling which of these connections are to be made at any given time (logic function). In the all-electronic system to be described these two functions are implemented separately and independently. This physical separation of the signal transfer mechanism for the logic and control mechanism enhances the over-all flexibility of system logical design, and makes possible the sharing of logic circuitry with a reduction in the number of electronic "solenoids" and "contacts" which would otherwise be required. In this respect, Boolean algebra techniques and matrix methods are particularly applicable in offering an organized and logical approach to reducing the amount of switching circuitry required in a given application.

Electronic switching can be implemented for ac as well as dc voltages, both at power levels and at signal levels. The discussion which follows considers the switching of signal level ac carrier voltages. These electronic switches employ conventional dc AND and OR gates to perform the required system logic, and "signal transfer gates" to perform the desired switching function. The "signal transfer gate" is characterized by an ac input, an ac output, and a dc control line that regulates the connection of input to output. When the dc control voltage is at one extreme state, the ac connection is made; while when the dc control voltage is in the opposite extreme state, the ac connection is opened.

Although this basic concept can be implemented using diodes, transistors, magnetic components, or combinations of these elements, diode circuitry is the simplest, as illustrated in Figure 17. The common basis in these circuits is the single switching diode, which when biased in one direction appears as a low-impedance element permitting signal transmission, and when oppositely biased appears as a high-impedance element blocking signal transmission. In its simplest form, when direct coupling can be used, the gate reduces to a single diode.

Improved circuit performance can be achieved by adding selected components. The signal suppression diode shown in the circuitry of Figure 18 makes possible a suppression ratio of 10^7 with respect to undesirable signals in the "OFF" state. This improved performance allows for design trade-off toward relieving the back-resistance specifications otherwise imposed on the gating diode.

The response of a diode gate is almost instantaneous as illustrated in Figure 19, depending upon electron transit time within the diode. However, in the capacitor coupled case, this instantaneous response is superimposed on a dc transient which appears in "OFF" to "ON" switching. The circuit shown in Figure 20 is designed to compensate for this RC transient

and eliminate it completely for those applications in which it is not tolerable.

These all-electronic switching circuits have been built and tested, and their operation verifies theoretically predicted performance. Indications of comparative reliability must be made in an over-all systems context, however, rather than considering a one-for-one replacement. In most typical control systems, the switching circuitry is greatly simplified as a result of the separation of the logic function from the signal transfer function. Thus, the resultant all-electronic solid-state signal switching system is often smaller, lighter, less power-consuming, and more reliable than its relay system counterpart.

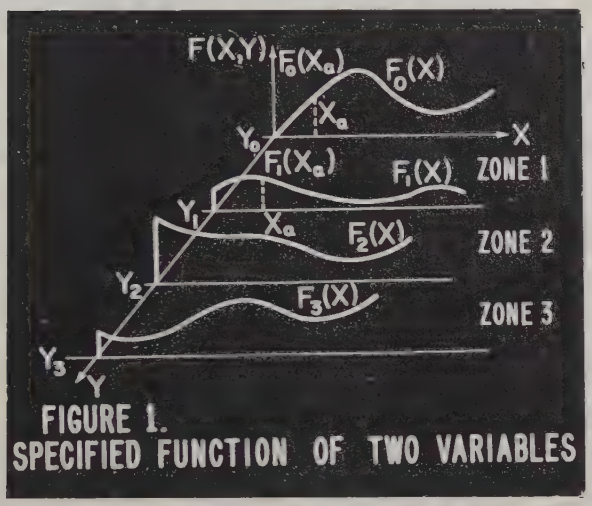

FIGURE 1.
SPECIFIED FUNCTION OF TWO VARIABLES

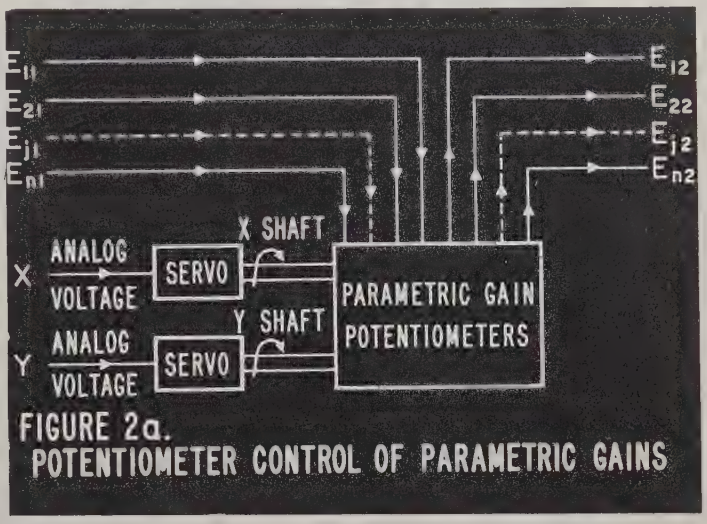

FIGURE 2a.
POTENTIOMETER CONTROL OF PARAMETRIC GAINS

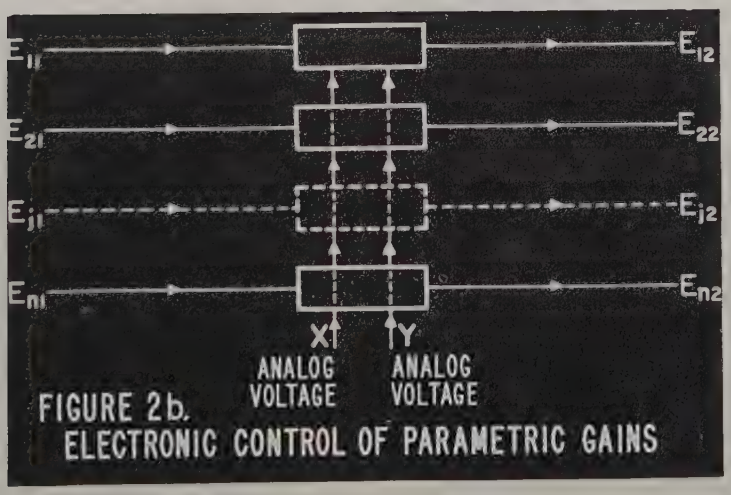

FIGURE 2b.
ELECTRONIC CONTROL OF PARAMETRIC GAINS

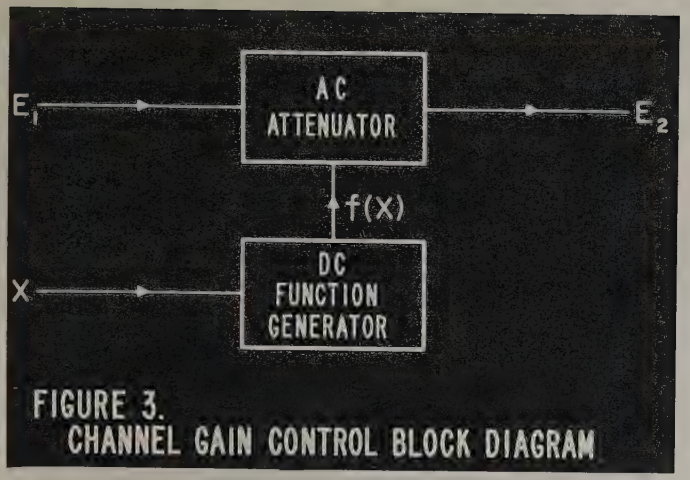

FIGURE 3.
CHANNEL GAIN CONTROL BLOCK DIAGRAM

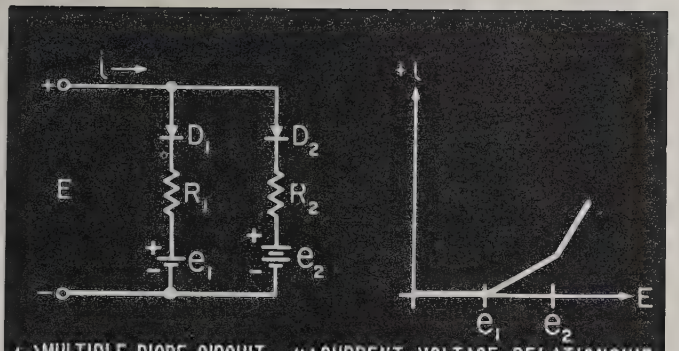

(a) MULTIPLE DIODE CIRCUIT (b) CURRENT-VOLTAGE RELATIONSHIP

FIGURE 5.
MULTIPLE DIODE GENERATION OF POSITIVE SLOPES

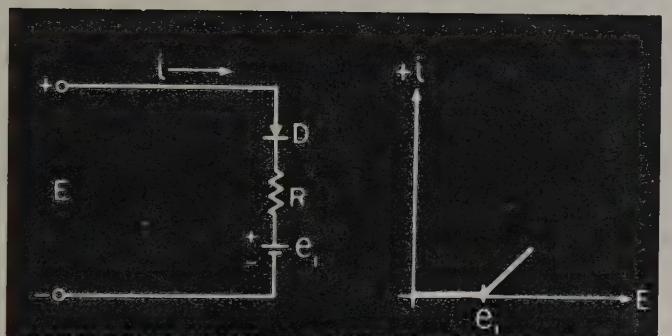

(a) SINGLE DIODE CIRCUIT (b) CURRENT-VOLTAGE RELATIONSHIP

FIGURE 4.
SINGLE DIODE GENERATION OF POSITIVE SLOPES

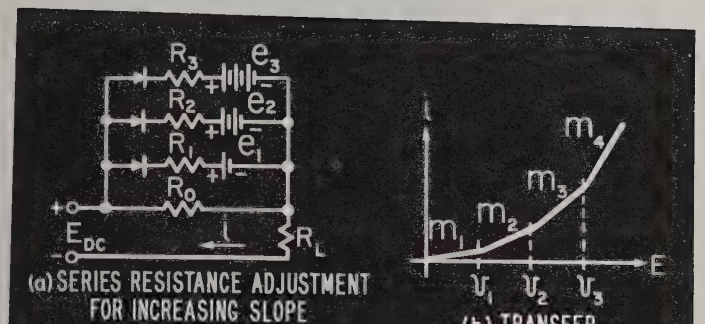

(a) SERIES RESISTANCE ADJUSTMENT FOR INCREASING SLOPE

(b) TRANSFER CHARACTERISTICS

FIGURE 6.
MULTIPLE DIODE GENERATION OF CONCAVE SLOPE CHANGES

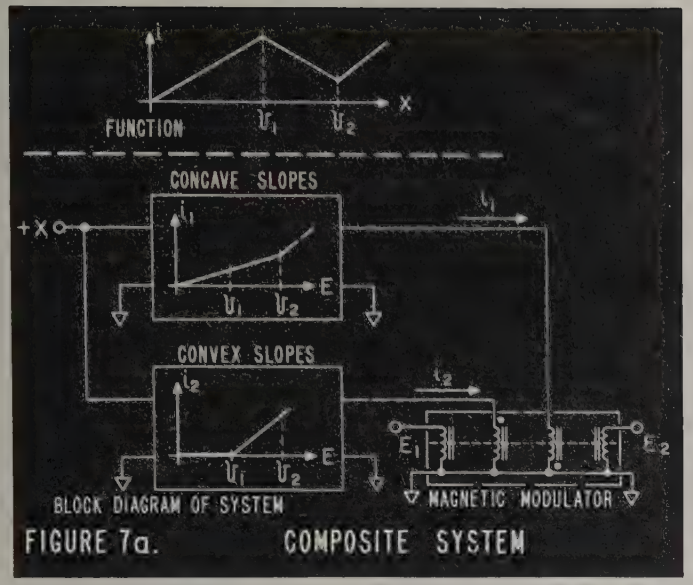

FIGURE 7a. COMPOSITE SYSTEM

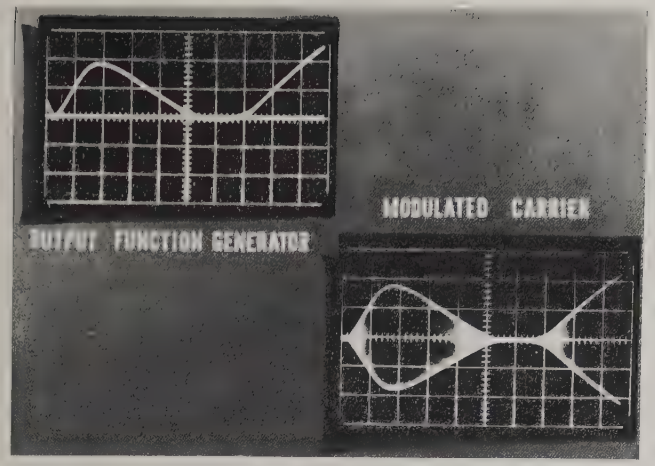

Fig. 7C.

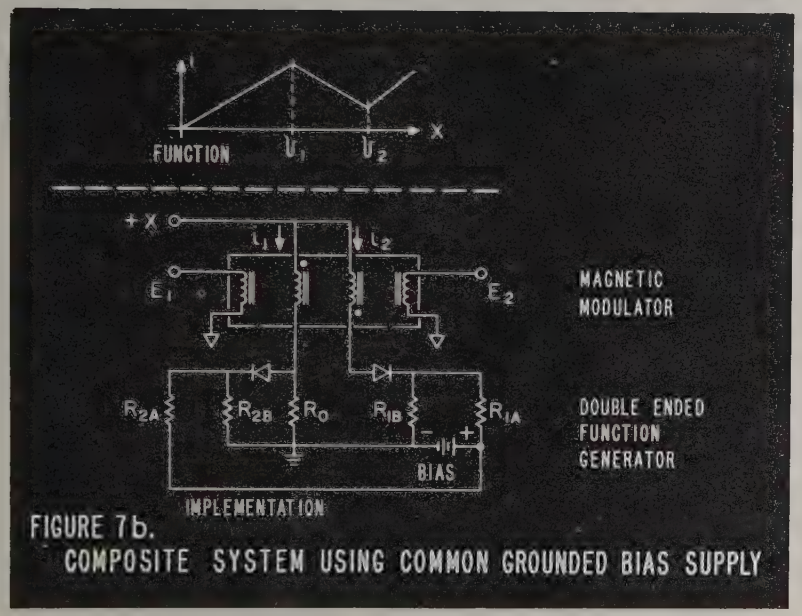

FIGURE 7b.
COMPOSITE SYSTEM USING COMMON GROUNDED BIAS SUPPLY

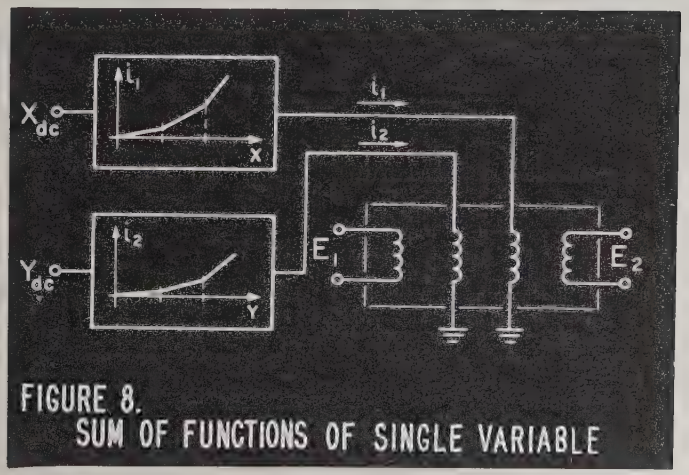
FIGURE 8.
SUM OF FUNCTIONS OF SINGLE VARIABLE

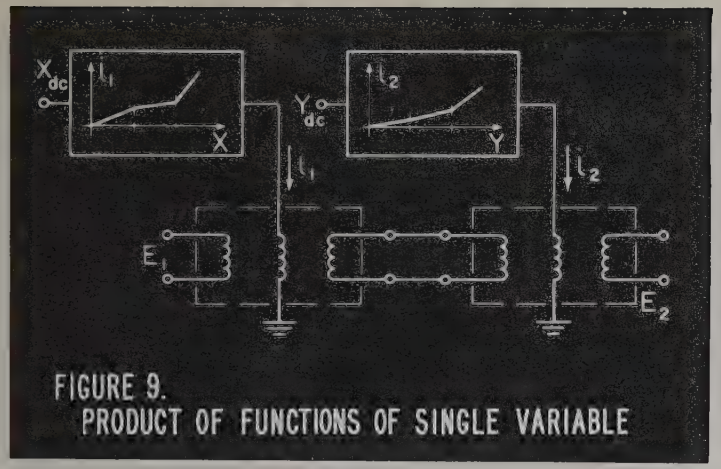

FIGURE 9.
PRODUCT OF FUNCTIONS OF SINGLE VARIABLE

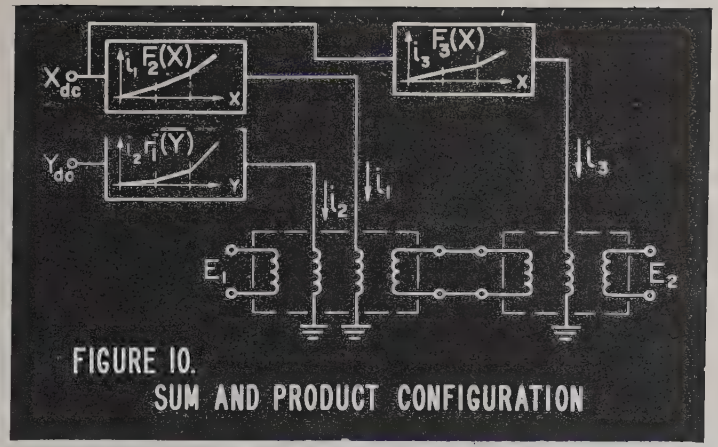

FIGURE 10.
SUM AND PRODUCT CONFIGURATION

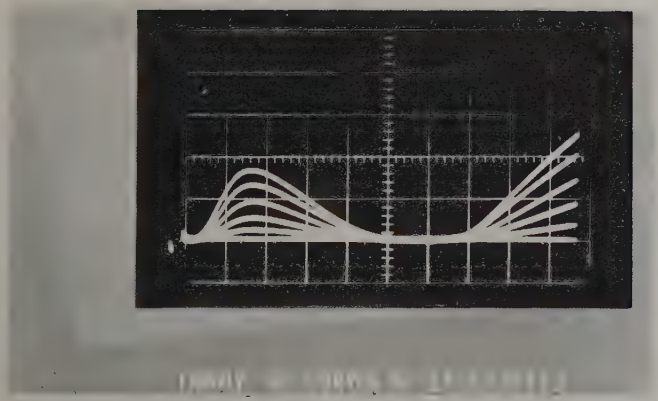

Fig. 9B.

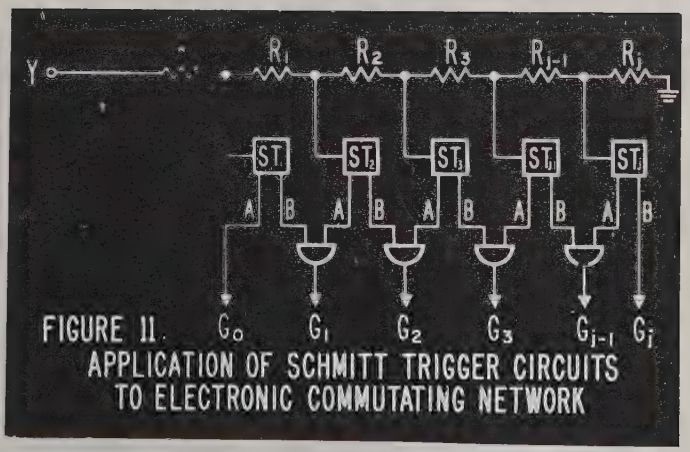

FIGURE 11.
APPLICATION OF SCHMITT TRIGGER CIRCUITS
TO ELECTRONIC COMMUTATING NETWORK

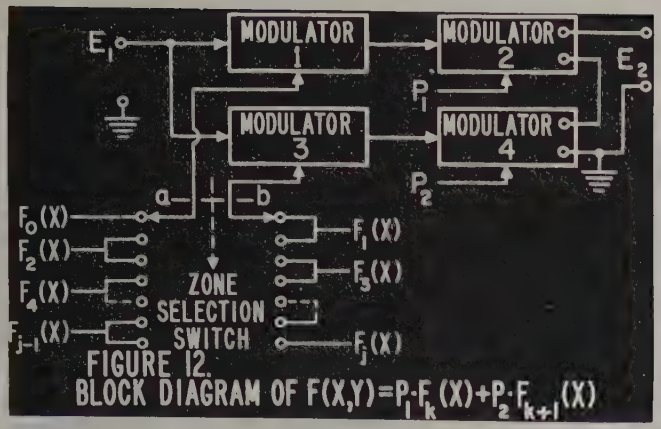

FIGURE 12.
BLOCK DIAGRAM OF $F(X,Y)=P_1 \cdot F_k(X)+P_2 \cdot F_{k+1}(X)$

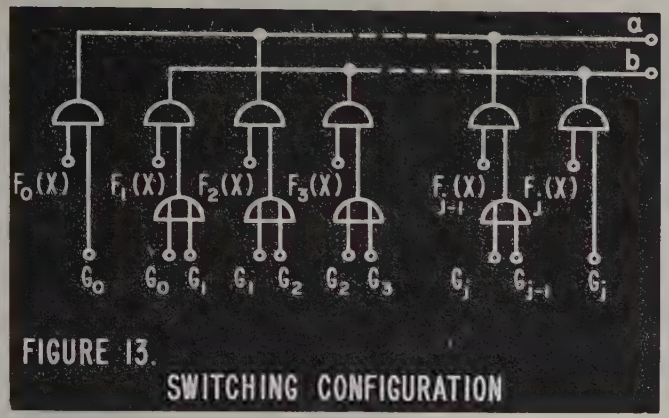

FIGURE 13.
SWITCHING CONFIGURATION

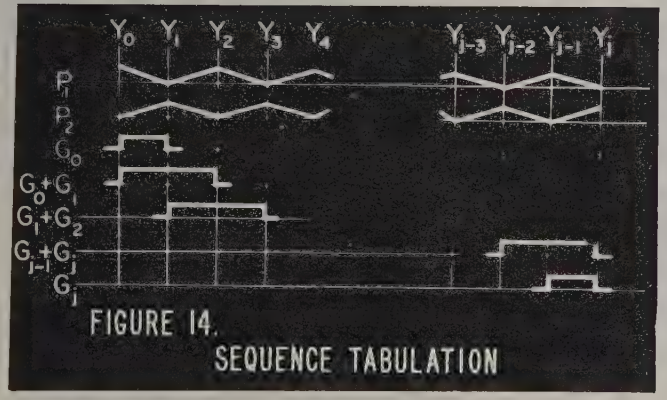

FIGURE 14.
SEQUENCE TABULATION

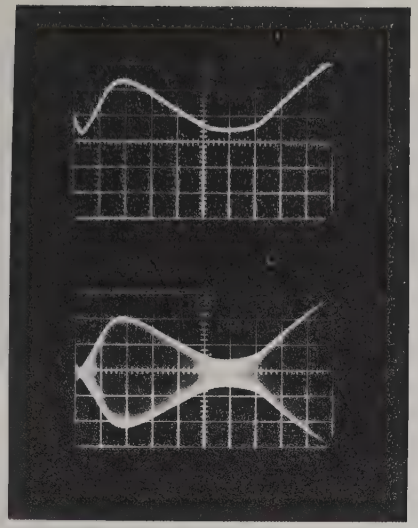

(a)
Initial Function

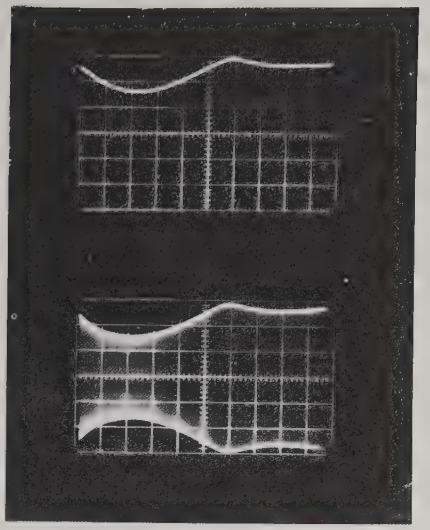

(b)
Final Function

Independent Functions Used as Limits of Continuous Interpolation

Fig. 15.

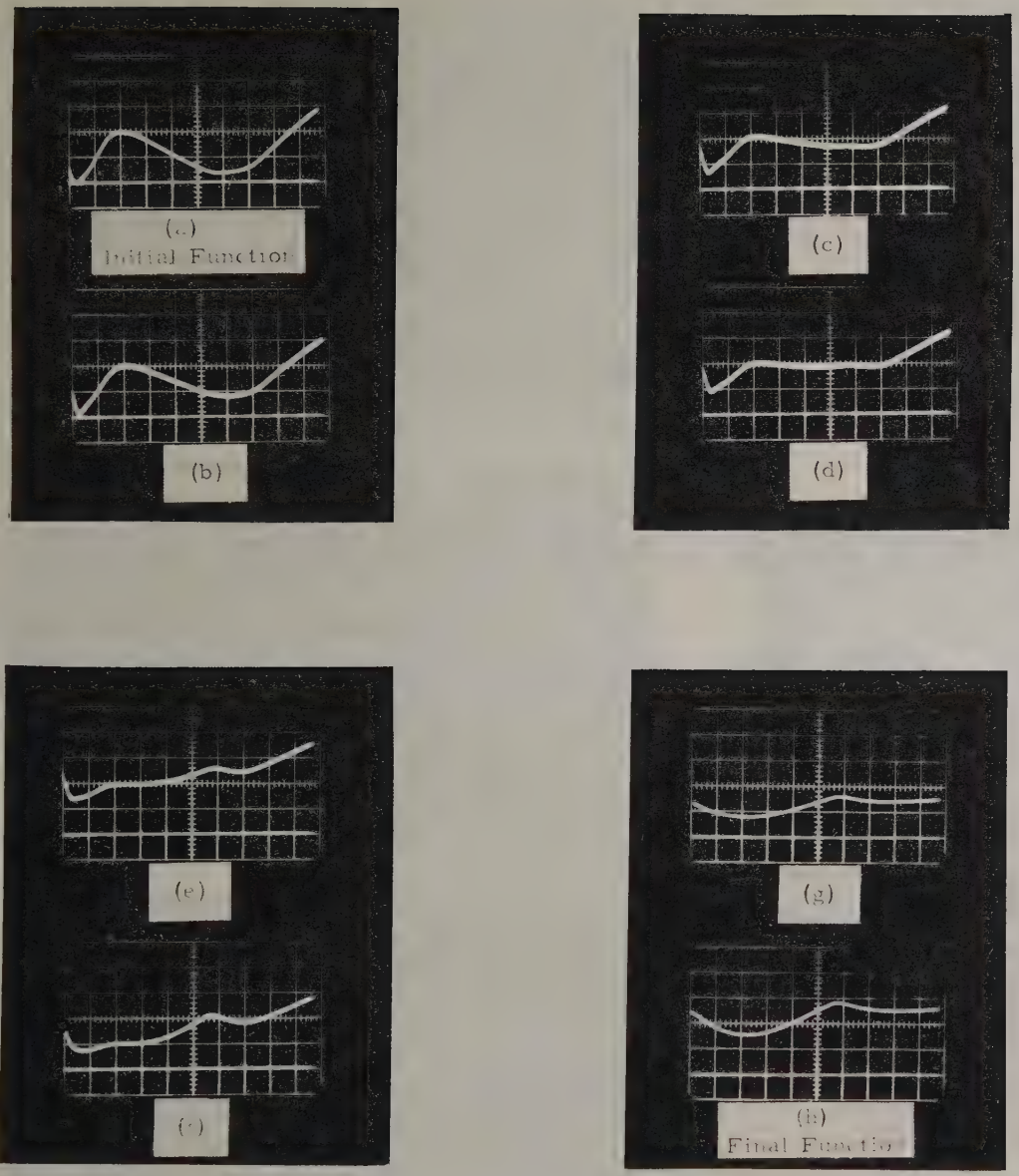

Fig. 16. Continuous Interpolation of One Step in Sequential Order

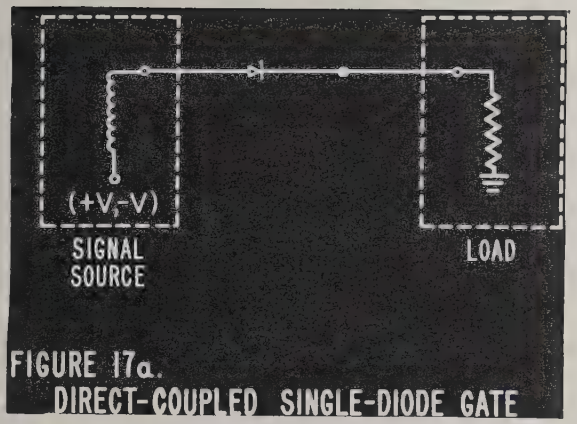

FIGURE 17a.
DIRECT-COUPLED SINGLE-DIODE GATE

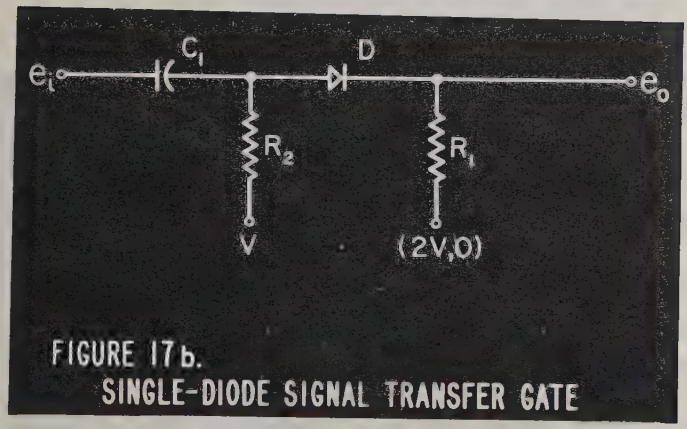

FIGURE 17b.
SINGLE-DIODE SIGNAL TRANSFER GATE

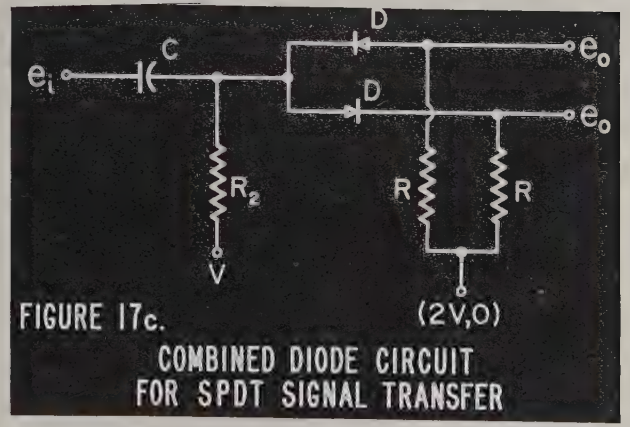

FIGURE 17c.
COMBINED DIODE CIRCUIT
FOR SPDT SIGNAL TRANSFER

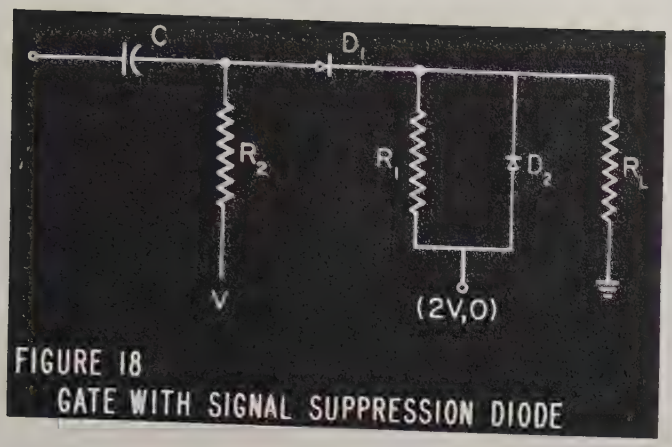

FIGURE 18
GATE WITH SIGNAL SUPPRESSION DIODE

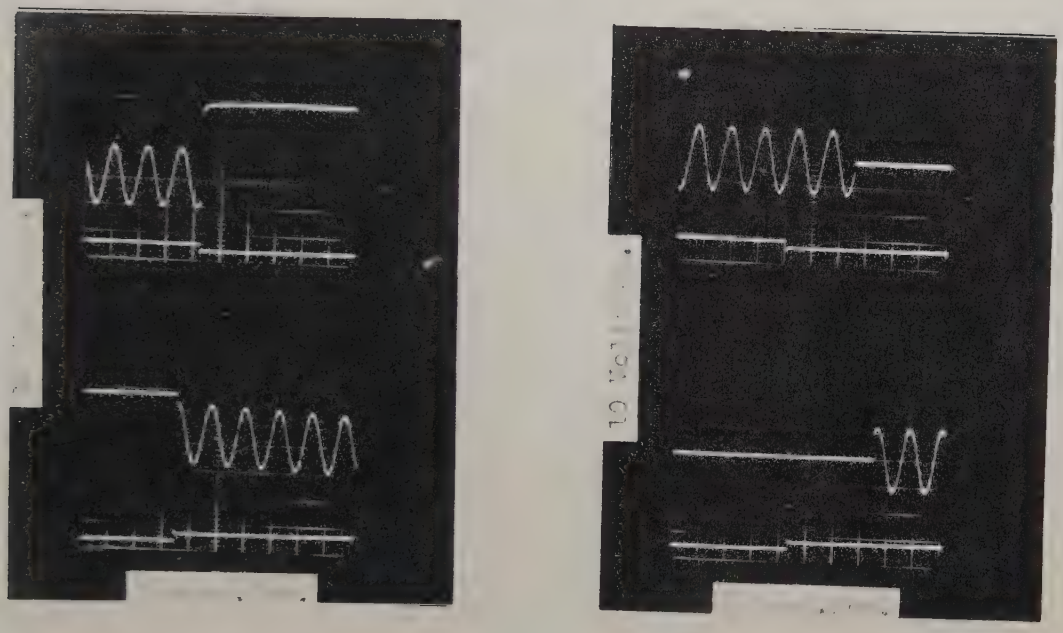

(a)
DIODE GATE

(b)
RELAY

Fig. 19. Oscillographs Comparing Actuating Delay. (a) Diode Gate (b) Relay

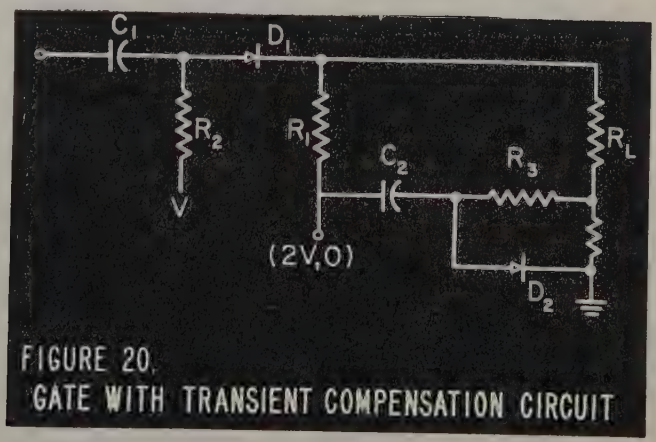

FIGURE 20.
GATE WITH TRANSIENT COMPENSATION CIRCUIT

ELECTRONIC MEMORY IN AUTOMATIC FLIGHT CONTROL SYSTEMS

David H. Blauvelt and Arthur S. Robinson

Bendix Aviation Corporation
Eclipse-Pioneer Division
Teterboro, New Jersey

Introduction

The ability to store an ac voltage that represents an initial problem condition or an intermediate computation result is an important requirement in many automatic flight control systems. Relatively standard carrier memory systems use one of two general methods: either an electromechanical servo system, in which the servo loop is opened to produce the memory feature; or an electronic system which converts to dc, uses a dc memory, and then modulates to restore the carrier. The first system has the disadvantage of slow response and the need for heavy electromechanical components. The second system is limited by the demodulator and modulator inaccuracies and by the relatively short time constants achievable with solid-state dc memories. This paper describes a fast, accurate, infinite time constant electronic solid-state memory for use in ac control systems. This memory system is based on the characteristics of the transfluxor.

Transfluxor Operation

The transfluxor is a ferrite core device combining the square loop properties of the magnetic material with a multiple flux path in such a manner that the device may function as an ac memory with a nondestructive readout.

Figure 1 illustrates an RCA type XF-1501 transfluxor.[1] Two pertinent magnetic paths may be traced on the core, one formed by leg 1 and leg 2 and the other by legs 2 and 3. The transfluxor contains three windings. The control winding W_1 is used to control the magnetic state around the large aperture. The excitation winding W_3 is used to excite the output portion of the core around the small aperture. The output voltage is induced on winding W_2.

The transfer characteristic between the transfluxor input drive current and the transfluxor output voltage is shown in Figure 2. At point ⓐ the transfluxor is saturated in one direction, and has a small residual output due to air coupling. As the input current becomes more negative, E_T remains essentially constant until a threshold current is reached. As the current is increased beyond this value the system output also increases until point ⓜ is reached. Any increase in current beyond this point will result in a decrease in output. In order to remove this possibility, operation is restricted to the region below point ⓒ. If upon reaching point ⓒ, the input current is reduced to zero, the transfluxor output will decrease slightly to point ⓓ. As the current is increased in the opposite direction the transfluxor output voltage will drop slightly again until point ⓔ is reached. As the current is increased beyond this point, the transfluxor output voltage decreases and operation returns to point ⓐ. If at any time the input current is reduced to zero and then increased in the opposite direction, the system will move along a line approximately parallel to ⓒⓓⓔ. Thus the system output will change slightly when the control current is removed.

Electronic Memory System

The electronic memory system has two modes of operation controlled by an electronic switch.[2] When the switch is closed, it operates as a simple feedback control system in which the transfluxor output is compared with the system input and the error between them is used to drive the transfluxor so as to reduce the error and cause the system output to follow the system input. When the switch is open, the transfluxor input is removed, thus causing the transfluxor output to remain constant at the value existing when the switch was opened. The system block diagram is shown in Figure 3.

The change in transfluxor output when a dc control current is removed is not permissible when the transfluxor is used as a memory device, since the system output would change when it is switched from the follow-up mode to the

memory mode. This undesirable effect can be eliminated by using a pulse type input drive in which the control current exists for only a very small fraction of the time. Therefore, the system output is essentially the same for both the follow-up mode and the memory mode. Two types of pulse drives can be used at W_1: a current drive from a high impedance source, or a voltage drive from a low impedance source. The operation of these two types of sources is different in that with a series of constant magnitude current pulses the final flux condition is established by the first pulse and all future pulses have no effect. A series of constant magnitude voltage pulses will create a series of incremental flux changes in the transfluxor with each increment being proportional to the magnitude and the duration of the voltage pulse. This voltage drive technique is discussed in further detail in the paper that follows. [3]

A second consideration in the design of the input drive circuitry is the over-all system stability. It is necessary to establish a delay between the system error and the transfluxor control current to prevent system oscillation. If a current source is used to drive the transfluxor control winding, this delay is obtained by using an RC delay network in the signal chain to delay the control current with respect to the error signal. If a voltage source is used to drive the control winding, the driving current is determined by the initial conditions and the integral of the voltage signal. This integration produces the required delay between error and control current. Both current and voltage source drives have been used in laboratory systems. The current drive causes an appreciable delay in the output each time the error changes sign. The voltage drive will therefore be described in this paper.

Two methods have been used to supply the input voltage drive pulses for the transfluxor. The first method shown in Figure 4 is to demodulate and filter the error signal to produce a dc voltage whose magnitude and sign is determined by the magnitude and phase of the error signal. The dc voltage is then sampled by a 6 diode gate to produce a series of pulses which are fed into a complementary push-pull amplifier having a low output impedance.

The second type of input drive, shown in Figure 5, is essentially the same but eliminates the demodulator and filter by sampling the carrier at the peak of the sine wave. This method however requires additional circuitry to synchronize the sampling pulses to the error sine wave.

The results obtained with these two drives are equivalent in most aspects and are illustrated in Figure 6. The initial error signal saturates the amplifier producing constant voltage pulses at the sampler output. Each pulse produces a fixed incremental change in the transfluxor output. As the error is reduced, the amplifier comes out of saturation reducing the magnitude of the drive pulses into the transfluxor and therefore reducing the incremental changes in the transfluxor output as the system approaches the steady state condition.

The output drive has been chosen as a sinusoidal current source operating at 20 kc. The frequency was made high to increase $\frac{d\phi}{dt}$ and thus increase the output voltage. It was also found necessary to remove the output excitation when the input drive pulse is applied in order to prevent interaction between them. This is accomplished by the electronic switch. The output conversion device consists of a diode detector, a filter and a magnetic modulator arranged such that the transfluxor output is peak detected and then modulated at the proper carrier frequency. This output circuitry is illustrated in Figure 7.

The operation of the memory system in the memory mode is determined by the characteristics of the transfluxor. Since the magnetic state of the transfluxor cannot change unless a signal is applied to the input winding, the system will exhibit an infinite memory with no deterioration.

The most important characteristic of the memory system in the follow-up mode is its ability to follow the input signal. The maximum follow-up rate is determined by the sampling rate, the filter time constant if used, and the maximum output increment caused by each sample. The maximum sampling rate is determined by the carrier frequency if the error sine wave is sampled directly. The size of the maximum increment is determined by the required system accuracy. The filter time constant is determined by the amount of ripple voltage which can be tolerated which is again determined by the required system accuracy. It is therefore possible to trade speed of response for accuracy.

A typical system operating at a 400 cycle carrier frequency, using either a demodulated error signal or a directly sampled error signal type of input drive, is capable of responding to a step input in 40 milliseconds as shown in Figure 8. This response time can readily be decreased by increasing the carrier frequency. This permits a decrease in the required filter time constant and an increase in the sampling rate. Therefore doubling the carrier frequency will cut the response time in half. The lower limit of response time attainable by increasing the carrier frequency is determined by the propagation time of a signal around the loop.

ACKNOWLEDGMENT

The contributions of Mr. William Lasch to the circuit design and bench testing of the feasibility model of this system are gratefully acknowledged.

REFERENCES

1. J. A. Rajchman, A. W. Lo, "The Transfluxor", Proceedings of the I.R.E., March 1956, Vol. 44, No. 3, pp. 321-332.

2. E. Boronow and W. Henn, "Electronic Gain Control in Automatic Flight Control Systems", National Automatic Control Conference, November 1959.

3. A. S. Robinson, "Pulse Controlled Integration in Automatic Flight Control Systems", National Automatic Control Conference, November 1959.

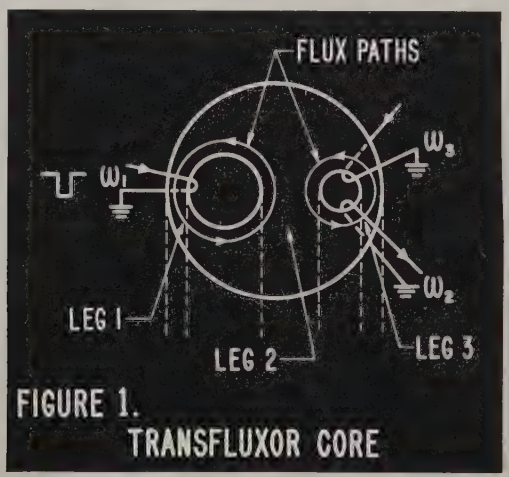

FIGURE 1.
TRANSFLUXOR CORE

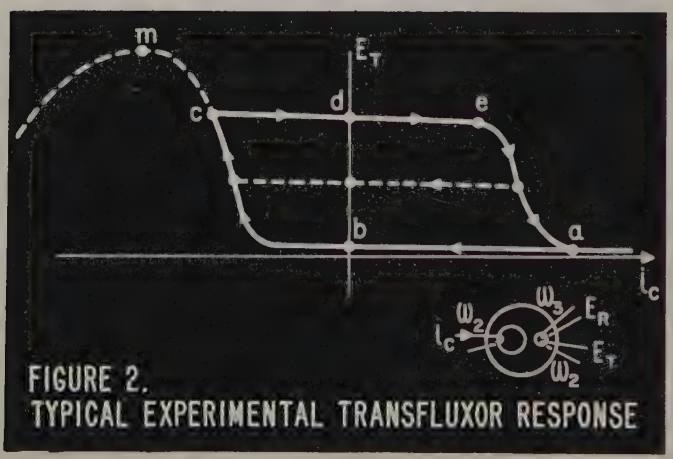

FIGURE 2.
TYPICAL EXPERIMENTAL TRANSFLUXOR RESPONSE

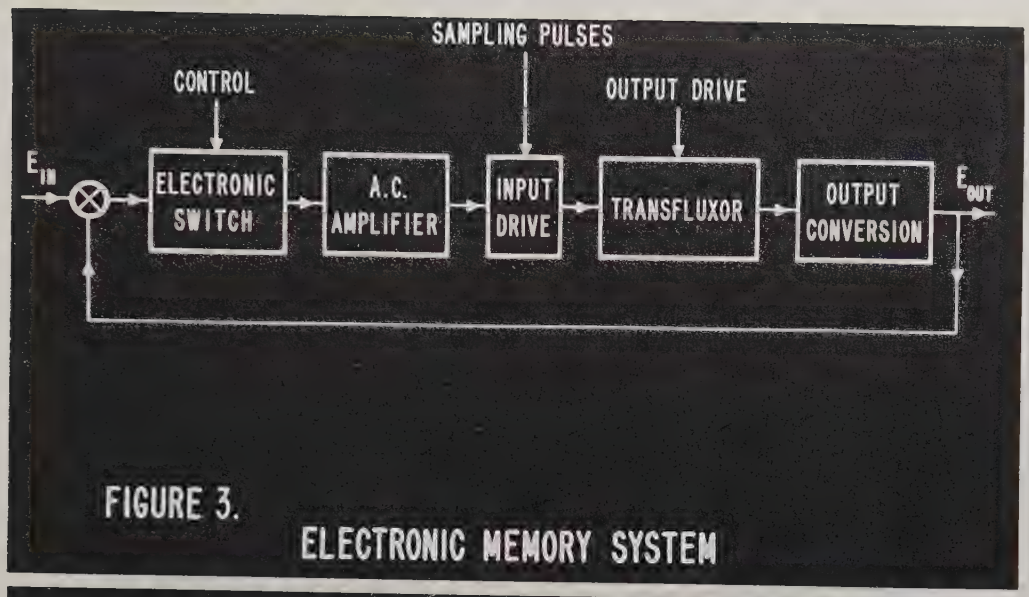

FIGURE 3.
ELECTRONIC MEMORY SYSTEM

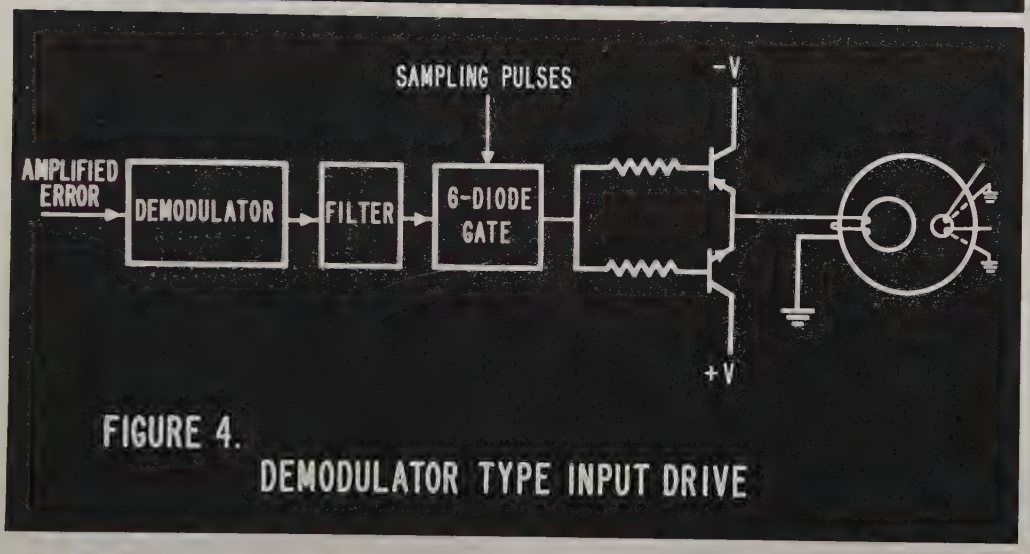

FIGURE 4.
DEMODULATOR TYPE INPUT DRIVE

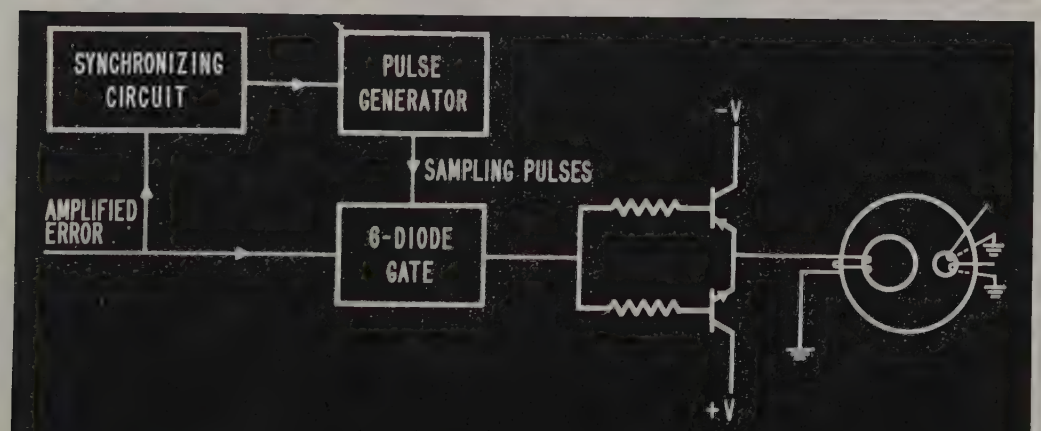

FIGURE 5.
DIRECT SAMPLING INPUT DRIVE

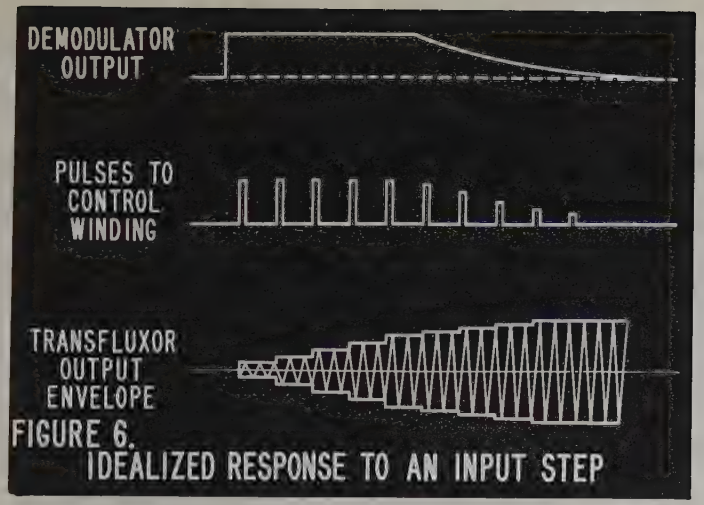

FIGURE 6.
IDEALIZED RESPONSE TO AN INPUT STEP

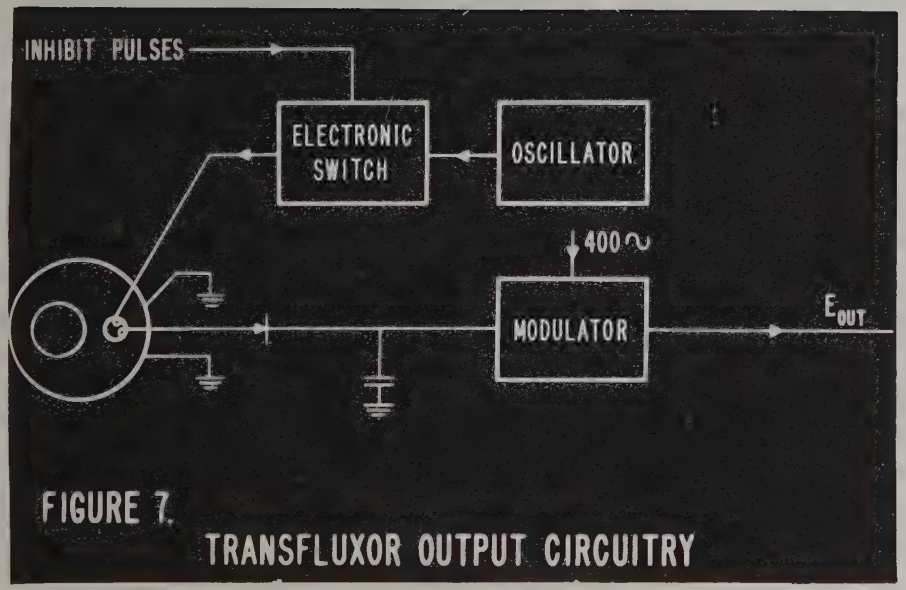

FIGURE 7.
TRANSFLUXOR OUTPUT CIRCUITRY

Modulator Output Wave Forms

System Data: Pulse Rate 400 cps, Pulse Width 1.0 μ sec.

Input Step 0 → 0.5 volt sweep starts at step.

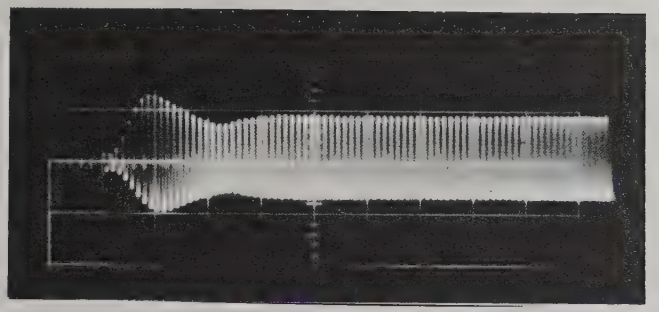

Vert. Sens.
0.5 volt/major div.

Horiz. Sens.
20 millisec/major div.

Input step 0.5 → 0 volt sweep starts at step.

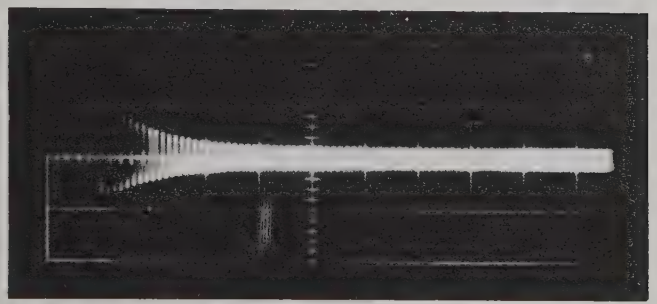

Vert. Sens
0.5 volt/major div.

Horiz. Sens.
20 millisec/major div.

Fig. 8. STEP RESPONSE OF TRANSFLUXOR SYNCHRONIZER

PULSE CONTROLLED INTEGRATION IN AUTOMATIC FLIGHT CONTROL SYSTEMS

Arthur S. Robinson

Bendix Aviation Corporation
Eclipse-Pioneer Division
Teterboro, New Jersey

Introduction

A standard technique that is currently widely used for the integration of ac voltages is illustrated in Figure 1. The combination of amplifier and motor acts to drive the rate generator at a speed such that the feedback voltage E_3 is approximately equal in magnitude to the input voltage E_1. If the rate generator characteristic is truly linear, the shaft Θ is then rotating at a speed that is directly proportional to the input voltage. Shaft position is therefore directly proportional to the integral of the input voltage. An ac output is achieved by measuring shaft position with a potentiometer excited by a fixed ac reference voltage. The accuracy of this technique is a function of the rate generator transfer characteristic, the amplifier gain, and the gear train and output potentiometer accuracies, although the rate generator characteristic is usually the limiting factor.

This paper describes two types of all electronic pulse controlled ac voltage integrators based on the characteristics of the transfluxor. The first technique requires a single transfluxor per integrator and is suitable for medium accuracy applications. The second technique utilizes two transfluxors per integrator and is suitable for applications requiring substantially higher accuracies.

Open Loop Sampled Data Integration

A simple, although in practice accuracy limited, technique for achieving ac integration utilizing a single pulse-controlled transfluxor is presented in Figure 2. Since this approach achieves integration by incrementally changing the transfluxor control flux at discrete intervals of time, it has been designated "open loop sampled data integration". The input ac signal E_1 is periodically sampled at its peak value by sampling pulses that are derived from a pulse generator synchronized to the system ac reference. If the period of the ac voltage is $1/f$, the sampling period is K/f, where K is fixed by the sampling rate control. The sampled pulses (E_a) are applied to the transfluxor control winding through a very low impedance driver. If the impedance of this driver is sufficiently small, and if the resistance of the control winding is sufficiently low, the flow of current in the control winding is limited only by the back EMF generated by the changing control flux. During a given pulse

$$\left|E_a\right| = N \frac{d\Phi}{dt} \quad , \text{ so that}$$

the change in flux in a given period of time is directly proportional to the magnitude of E_a. Each such flux change is transmitted from the control to the output aperture and appears as a change in the output E_b. Since the output is proportional to the total flux transferred to the output aperture, the transfluxor output at any given instant will be proportional to the sum of the values of E_1 at all prior sampling instants, and will therefore be proportional to the integral of E_1. Since the sampling pulses always sample a fixed reference point on the input sine wave, this technique is automatically sensitive to the phase of the input voltage. This system will also operate with an input E_1 in the form of a phase sensitive dc voltage, in which case it is no longer necessary to synchronize the sampling pulses to the system ac reference.

The waveforms presented in Figure 3 illustrate a situation in which an ac input voltage E_1 goes through zero, reversing phase. For purposes of this illustration K = 2, and the sampling pulses result in the indicated voltage pulse train E_a at the control winding input. The first E_a pulse introduces a flux $\Delta\Phi$ in the control winding that is immediately reflected as an increase in the output E_b. The second E_a voltage pulse is half the amplitude of the first, and results in half the increase in output E_b. The third pulse reverses this process, and the fourth pulse returns the output to its initial condition. The pulse currents that must flow in the transfluxor control winding in order to achieve this response are not linearly related to the voltage pulse amplitudes. The current response I_a presented in Figure 3 is explained in further detail

in Figure 4.

The transfluxor is initially at point A. The first pulse moves it through the trajectory ABCD, the second pulse through DCEF, the third through FGHI, and the fourth through IHJK. These highly nonlinear currents are achieved automatically by creating a situation in which current flow is limited only by the rate of flux change.

Of course in practice the assumption of low impedance drive and negligible control winding resistance can only be achieved to a limited degree. The actual existance of such impedances results in a reduction in voltage drive as control current flows, so that operation of this system becomes dependent on particular transfluxor characteristics. Because of this effect practical circuits of this type result in integrators of medium accuracy and resolution, suited to many applications, but of limited usefulness in meeting precision specifications. It is possible to improve the system accuracy by introducing an auxiliary winding on the transfluxor control leg and using a feedback amplifier to drive the transfluxor until the output of this winding indicates the correct rate of flux change. This approach complicates required circuitry, however, and while workable, substantially reduces the advantage of simplicity that would normally be associated with the open loop sampled data approach.

Closed Loop Sampled Data Integration

In order to achieve a high precision integrator substantially independent of transfluxor characteristics and actuating pulse waveforms, a two transfluxor closed loop sampled data integrator has been developed. The principle on which this system is based is presented in Figure 5. In effect, the integrator consists of two transfluxor memories[1] sharing a common ac amplifier and supplemented with additional electronic switching and control circuitry.

The input ac voltage E_1 is first passed through a center tapped transformer so that two ac voltages equal in magnitude to E_1 are available, one in phase and the other 180 degrees out of phase with the system reference carrier. An electronic switch selects one of these two voltages under control of dc voltages on lines © and ©. Specifically, when line © is high $E_c = -E_1$, and when line © is high $E_c = +E_1$. The ac output of the two transfluxor memory units are combined as shown to provide an error signal $\mathcal{E}$ that is equal to $-E_1 + E_a - E_b$ when line © is high and to $+E_1 + E_a - E_b$ when line © is high. The amplified error signal E_d is automatically switched to E_e when line ⓐ is high and to E_f when line ⓑ is high. Further, when line ⓐ is low E_e is zero and when line ⓑ is low E_f is zero.

In operation, the control circuits generate the following voltage sequence under control of the pulse input, with the indicated result:

Basic Cycle

State	a	b	c	E_c	E_e	E_f	Action
1	1	0	1	$-E_1$	E_d	0	Control Memory A
2	0	0	1	$-E_1$	0	0	Guard Zone
3	0	1	0	E_1	0	E_d	Control Memory B
4	0	0	0	E_1	0	0	Guard Zone
				Repeat			
5	1	0	1	$-E_1$	E_d	0	Control Memory A
6	0	0	1	$-E_1$	0	0	Guard Zone
etc.							

TABLE I

In state 1 the system is in a configuration that drives E_a, the output of memory A, to equal the sum of $E_1 + E_b$. In state 2 the control to memory A is opened, so that this value of E_a is stored. The introduction of state 2 guards against spurious transients that might otherwise occur if the system were thrown immediately into state 3. In state 3 the system is in a configuration that drives E_b, the output of memory B, to equal the sum of $E_1 + E_a$. State 4 opens the control to memory B so that this value of E_b is stored. State 5 is the same as state 1, etc.

As a result of this action, at any given instant the transfluxor memory under control holds the sum of the present value of the input plus the output of the second transfluxor memory, which in turn holds the sum of all prior samples of the input. The output of the transfluxor under control is therefore directly proportional to the integral of the input signal. The output of the system can be obtained

1. D. H. Blauvelt and A. S. Robinson, "Electronic Memory in Automatic Flight Control Systems", National Automatic Control Conference, November 1959.

through an electronic switch as the output of the transfluxor memory that is being or just has been controlled. A simpler and often adequate technique is to derive the output from one transfluxor memory, such as E_a alone , in which case the output voltage will change after four state transitions rather than after two transitions.

Since the purpose of even numbered states is to disconnect the transfluxor drive circuits in order to guard against spurious transients, and to prepare for the next sampling command pulse, it is sometimes convenient to derive the pulses that generate the even numbered states artifically in the control circuits, supplying only the pulses that move the system into the odd numbered states on the pulse input line. With such an arrangement, a single pulse on the pulse input line moves the system into an even numbered state for a very short period of time, and then advances it to an odd numbered state, where it rests. Pulses on the input line spaced T seconds apart then result in very short (T_o) transients to an even numbered state after each pulse, with a return to the odd numbered state for the remaining $T - T_o$ seconds of the input pulse period.

A typical control configuration that implements this approach is presented in Figure 6. When the system is first actuated, a reset pulse to both flip flops assures that both lines ⓒ and ⓓ are high and resets the two transfluxor memories so that E_a and E_b start from zero. Since ⓒ and ⓓ are high, line ⓐ is also high and the system is in state 1. A single pulse on the control input will immediately set flip flop #1, moving the system to state 2. T_o seconds later this pulse will appear at the output of the delay line and will reset flip flop #1 which in turn will set flip flop #2, moving the system into state 3 (line ⓑ high) where it will rest until the arrival of another pulse input.

Key closed loop sampled data waveforms are presented in Figure 7 for a constant input ac voltage E_1. The illustrated output voltage E_2 is based on the assumption that the optional output electronic switch is used and that it is actuated by the ⓒ and $\overline{ⓒ}$ signals in such a manner that the output is E_a when ⓒ is high and E_b when $\overline{ⓒ}$ is high. Under these conditions the system approximates the transform $\frac{1}{TS}$ and the output changes every T seconds. It is generally necessary to insert an attenuator (k) in series with the integrator input, in which case the transform becomes $\frac{k}{TS}$. The number of steps per second can then be adjusted by varying T, after which k can be adjusted to obtain the required over-all integration constant.

The configuration as shown is automatically phase sensitive in that when the phase of the input voltage E_1 is reversed, the direction of integration of the output E_2 will automatically change accordingly.

The major advantages of the closed loop sampled data integrator lie in its high potential accuracy and in its capability to act as a true time integrator when supplied with constant frequency pulses (in which case the integration rate is proportional to the pulse frequency) or to act as an integrator with respect to a variable that is not time, but that is available in the form of a single pulse for each incremental change in the variable. It is important to note that when acting as a true time integrator, the integration rate can be readily adjusted from seconds to hours or days by appropriately controlling the pulse input. This capability for precise integration over extended periods of time is one that is particularly difficult to obtain in conventional analog integrators.

The high integrator accuracy is due to the fact that the transfluxors are enclosed in high gain feedback loops, so that the system is substantially independent of transfluxor characteristics. In addition, the system is independent of the waveforms of the actuating pulses. System accuracy and resolution are fixed primarily by the gain of the ac amplifier and by the transmission accuracy of the electronic switches. Dynamic performance is fixed by the time required to control a given memory unit to its new value. An additional practical consideration relates to the degree of distortion in the sine wave outputs of the memory units. The permissible distortion is dependent on required integrator accuracy and on the selected mode of transfluxor drive. In general, the technique that achieves transfluxor control by sampling amplified ac error signal directly requires more freedom from distortion than the technique that utilizes a phase sensitive detector after the ac amplifier and before the transfluxor control sampler.[2]

2. Ibid

The 400 cps circuits described in the preceding paper require a settling time in response to a step command in the order of 40 milliseconds. The maximum number of integration steps per second using these circuits would therefore be in the order of 20 PPS. As noted in the circuit description, an increase in system carrier frequency would directly decrease the memory settling time, so that such a change would directly increase the permissible integration sampling rate.

A fundamental consideration in the specification of closed loop sampled data integrators relates to the permissible size of output voltage transitions. If the maximum permissible incremental output voltage change is ΔE_{2max}, and the minimum sampling period is T_{min}, the maximum rate of change of output voltage is $\Delta E_{2max}/T_{min}$. For a maximum input voltage of E_{1max}, the maximum permissible value of $k = \Delta E_{2max}/E_{1max}$. For example, if $\Delta E_{2max} = 0.5$ volts, T = 50 milliseconds and $E_{1max} = 1$volt, the maximum rate of change of output voltage will be 10 volts per second, corresponding to the 1 volt input and a value of k of 0.5. If the maximum output voltage is 50 volts, it will be reached under these conditions in 100 steps.

The system accuracy depends on the distribution of error at sampling instances, which in turn depends on both the characteristics of the system inputs and on the portion of the transfluxor characteristics that are utilized during the integration process. For example, in the problem outlined above, if the feedback amplifier is designed to control the transfluxor memories to within a maximum residual error of .1 mv at each step, a worst case analysis would indicate a cumulative output error of 10 mv after the 100 steps required to reach the 50 volt output. For smaller input voltages both the required number of steps and the cumulative error would increase. This type of analysis is pessimistic, however, in that a system capable of achieving a maximum residual error of .1 mv under all conditions will have a lower error over a major portion of the transfluxor operating region, since the amount of required drive varies with the transfluxor operating point and the direction of transfluxor control. In addition to this effective decrease in magnitude of error, the error sign will, in fact, vary from step to step so that a rigorous error analysis should be based on statistical criteria. If random conditions prevail, the error of .1 mv per step is likely to result in a cumulative error of only 1 mv after 100 steps.

In practice it is expected that closed loop sampled data integrators with accuracies in the order of 1 part in 1,000 will be readily obtainable, while accuracies of 1 part in 10,000 may be obtainable with proper care and with suitably restricted operating conditions.

The use of these integrators to implement high pass and low pass ac filters is quite straightforward, as illustrated in Figure 8. The major new feature of these filters is that their filtering characteristic is under pulse control. Filter break frequencies can therefore be varied during flight in a simple and precise manner, particularly suited to digital control.

ACKNOWLEDGEMENT

The contributions of Mr. William Lasch to the circuit design and bench testing of the feasibility model of this system are gratefully acknowledged.

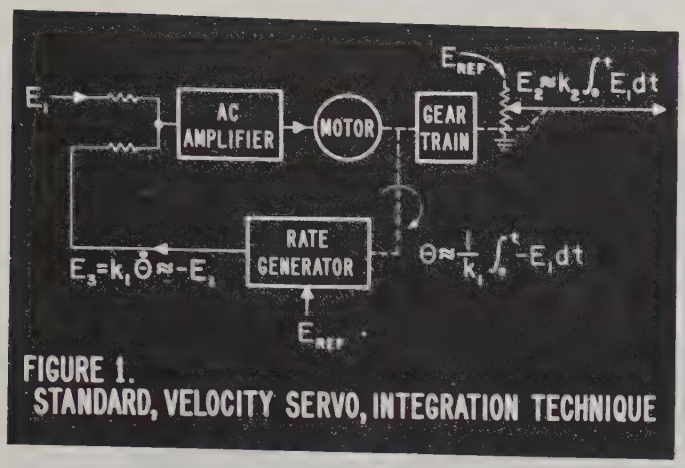

FIGURE 1.
STANDARD, VELOCITY SERVO, INTEGRATION TECHNIQUE

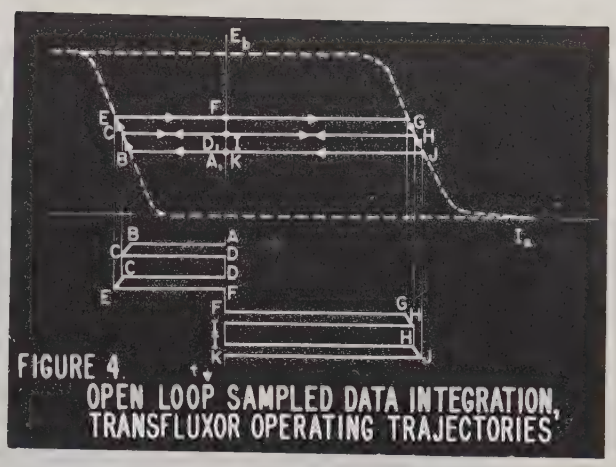

FIGURE 4.
OPEN LOOP SAMPLED DATA INTEGRATION,
TRANSFLUXOR OPERATING TRAJECTORIES

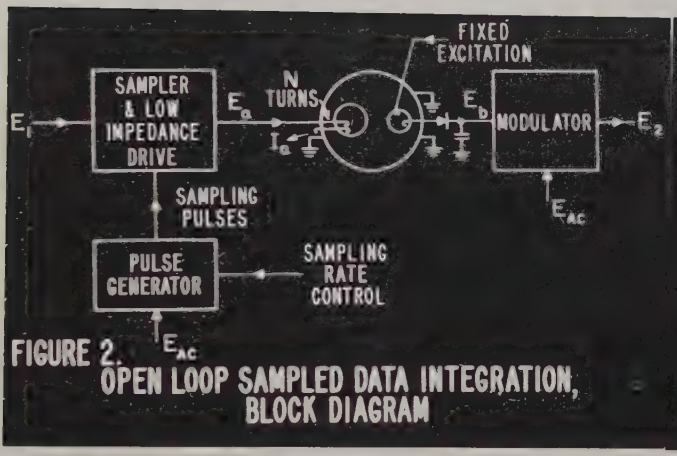

FIGURE 2.
OPEN LOOP SAMPLED DATA INTEGRATION,
BLOCK DIAGRAM

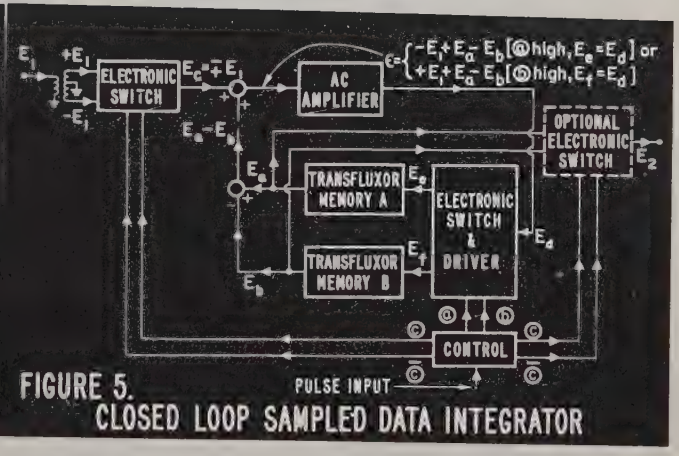

FIGURE 5.
CLOSED LOOP SAMPLED DATA INTEGRATOR

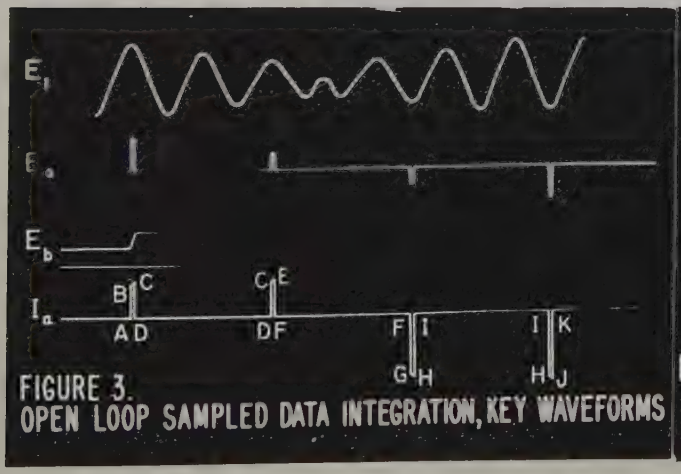

FIGURE 3.
OPEN LOOP SAMPLED DATA INTEGRATION, KEY WAVEFORMS

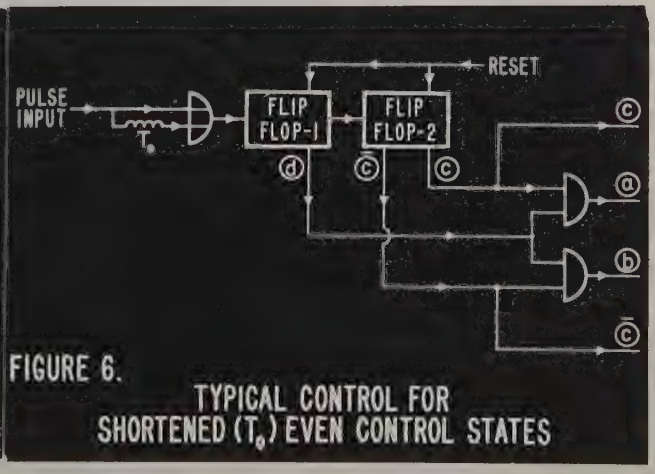

FIGURE 6.
TYPICAL CONTROL FOR
SHORTENED (T_o) EVEN CONTROL STATES

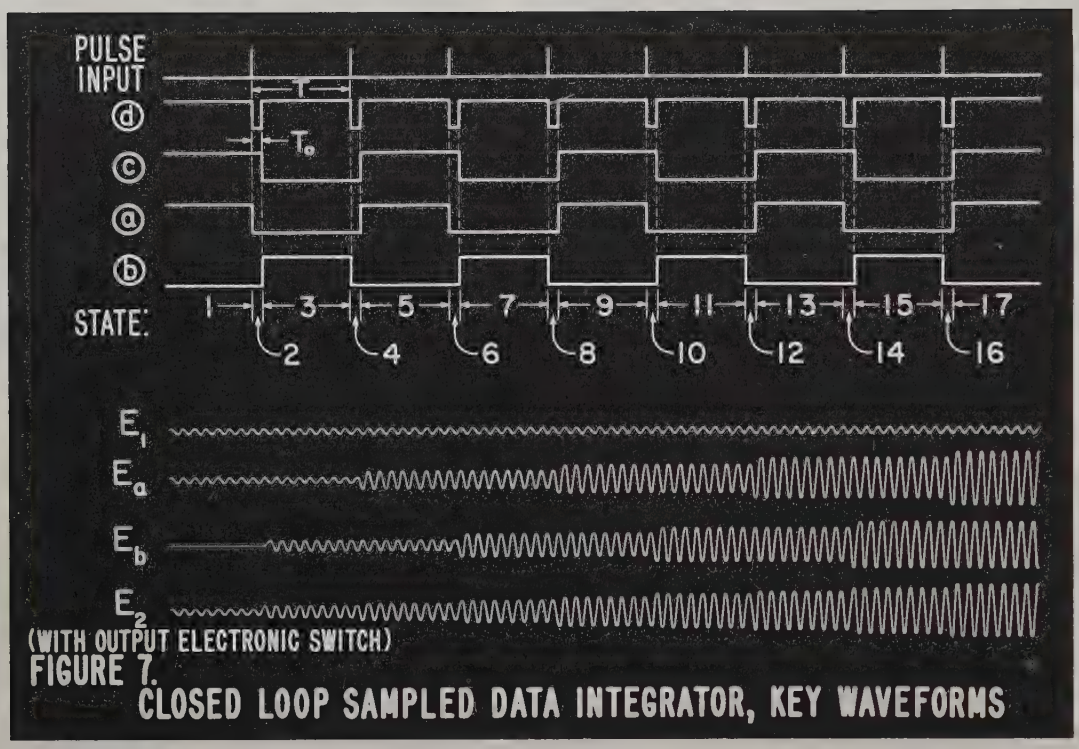

(WITH OUTPUT ELECTRONIC SWITCH)

FIGURE 7.
CLOSED LOOP SAMPLED DATA INTEGRATOR, KEY WAVEFORMS

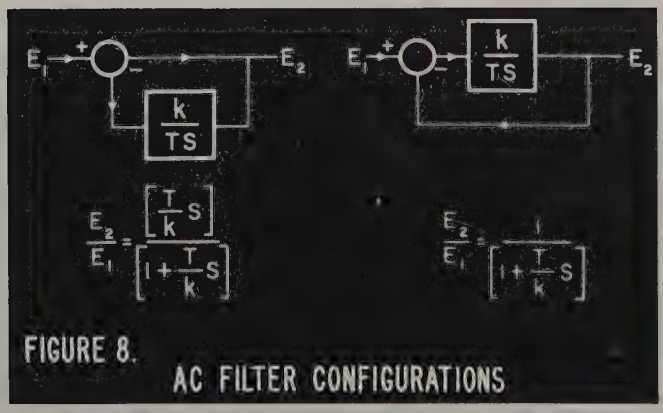

FIGURE 8.
AC FILTER CONFIGURATIONS

REACTION WHEEL ATTITUDE CONTROL FOR SPACE VEHICLES

Ronald W. Froelich and Harry Patapoff

Space Technology Laboratories, Inc.
Los Angeles, California

Summary

An attitude control system consisting of motor-driven inertial wheels in conjunction with an over-riding mass ejection system is proposed for use in space vehicles. Control by mass ejection is used to compensate for initial distrubances during separation from the booster, and for removal of unwanted momentum stored in the wheels. The use of reaction wheels permits fine, damped attitude control.

A laboratory model of a single-axis control system was constructed for experimentation and evaluation. The choice of a suitable platform configuration, selection of a prime mover for the inertial wheel, and the philosophy in the design of the electronics and pneumatics are discussed. Emphasis was placed upon minimization of weight and power consumption. System evaluation includes a discussion of efficiencies, reliability, and torque-speed-power relationships.

Sources of disturbances, methods of sensing, and general equations of motion are presented in the Appendix.

Introduction

The use of inertial wheels is a feasible and relatively simple method for controlling the attitude of a space vehicle. A wide, continuous range of control torques is obtainable, permitting fine, damped attitude control. Furthermore, the generation of these control torques does not require any interaction with ambient fields, which vary with altitude and position. Control torques are derived by inertial means, and are therefore independent of the location of the vehicle.

The low weight requirement, low power consumption, and attainable reliability should make a reaction wheel control system appealing for future space programs. This is especially true in cases where precise attitude control is required for a long period of time, and where electrical energy is to be generated in flight by means of solar cells or nuclear power supplies.

An experimental laboratory model of a single-axis control system was constructed from off-the-shelf components, employing several novel techniques in circuitry. The purpose of constructing such a model was to resolve major problems associated with the design and construction of logic circuitry, power amplifier, and prime mover, in order to obtain a system in which weight and power consumption are minimized. Insofar as practical, single-axis control of a space vehicle was simulated in order to evaluate performance and reliability.

Without employing a major research program, a practical three-dimensional reaction wheel attitude control system for a space vehicle can be constructed with only minor modifications of the system employed in the laboratory model.

System Description

A hybrid system, consisting of a motor-driven inertial wheel and an auxiliary mass ejection system employing constant thrust gas jets, is considered here. Cold pressurized helium is used for thrust generation.

The motor-driven wheel is mounted upon a platform suspended horizontally by means of knife edges. Angular deviations of the platform from the desired attitude are sensed, and the resulting error signals are used to accelerate the wheel in the direction of the deviations. The reaction torque on the platform reduces these deviations to zero. Figure 1 shows a block diagram of the wheel system.

The reaction wheel system is in essence a momentum transfer and storage device, absorbing momentum from the platform. The steady-state behavior of the system in the presence of a constant disturbance torque is a constant acceleration of the wheel, whose reaction torque on the platform is equal and opposite to the disturbance. In the absence of disturbances, constant wheel speed is maintained.

The function of the pneumatic system is to remove undesired momentum from the vehicle or wheel. It is used to reduce any large angular rates imparted to the platform, and to insure that the inertial wheel speed is maintained below a pre-set level. This level is governed by the maximum speed of the motor and by power losses, which are a function of wheel speed. If the wheel speed exceeds this pre-set value, the tachometer activates the pneumatic system and sufficient impulse is generated to reduce the wheel speed. The system then reverts to wheel control.

A block diagram of the pneumatic system appears in Figure 1. The relay has a specified dead-space within which the reaction wheel system operates. The pneumatic system is also an over-riding system for the reaction wheels. If any large spurious disturbance should occur during wheel control, pneumatic control is initiated either when the attitude deviation exceeds the deviation corresponding to the relay dead-space

value, or when the platform angular rate becomes sufficiently large.

The Laboratory Model

In constructing a laboratory model of a single-axis reaction wheel control system, emphasis was placed upon minimizing power and weight requirements, and attaining reliable operation for at least one year. A description of the platform, the prime mover, the electronics, the sensor, and the pneumatics follows (see Figure 2).

The Platform

A desirable platform configuration is one in which the frictional effects of the suspension system are negligible. The methods of suspension considered were (1) the use of precision ball bearings with platform motion about a horizontal or vertical axis, (2) use of high pressure air bearings, (3) suspension vertically by wire, (4) the use of knife edges, and (5) fluid immersion. A configuration using knife edges for the bearing surfaces was chosen, giving a "teeter-totter" motion to the platform. This method of suspension was chosen because of its low frictional torque level, simplicity, and relatively short construction time. The frictional torque level of the knife edges is of the order of 0.015 oz-in., which is sufficiently low compared to the other distrubances encountered in the system. An enclosure for the platform was also added to eliminate the disturbing effects of air currents in the laboratory. Initially, the power supply and electronics were external to the platform, but the frictional effects of the interconnecting leads were not tolerable. As a result, all components including power, gas, sensor, and telemetry were mounted on the platform. To accomodate this apparatus, a platform approximately 3 feet by 1 foot was chosen, pivoted to give maximum moment of inertia.

Power on the platform was provided by Sonotone Type "X" hermetically sealed batteries, chosen to maintain platform balance during the battery's active discharge period. Hermetically sealed batteries eliminate any shift of the center of gravity of the platform due to vapor discharge or motion of liquid.

It was found that platform bending made it difficult to maintain the center of gravity of the platform exactly at the contact point of the knife edge. To remedy this situation, braces were added to make it more rigid and integration was incorporated in the control system to limit platform deviation to small angles.

The Motor

Initial investigations were made of the specifications of all motors feasible for use in rotating the inertial wheel. The results of these investigations follow.

A-C Motors. A squirrel-cage motor does not adapt itself to speed control at zero or at low speeds without undue over-heating.

The speed of an a-c synchronous motor can be controlled by varying the frequency and amplitude of the applied voltage. In theory, this is the ideal motor for speed control. To accomplish speed control, however, it is necessary to vary the frequency and amplitude of the applied current to zero for zero speed while maintaining a constant phase shift to the motor. This can only be accomplished down to approximately 30 per cent of the full-speed values, after which excessive armature heating occurs at lower speeds. As use of this motor thus appears to be impractical, it was not included in the original studies, although it was reserved as a possibility for use at a later date.

An a-c servo motor adapts itself well to speed control, has reasonable linear torque curves over at least 80 per cent of its range, has efficiencies of about 30 per cent at maximum power output from the motor, and is readily available for testing from several manufacturers. One inherent problem with this type of motor is that excitation must be supplied to the main winding of the motor at all times when the motor is in use. To reduce this standby power to a minimum it was decided (a) that a power unbalance should exist in the servo motor to be used on the laboratory platform and (b) that more power should be consumed in the control winding of the motor than is consumed in the main winding of the motor by a ratio of at least 4 to 1. The final ratio is dependent upon the capabilities of the amplifier system.

D-C Motors. A shunt-wound motor is well adapted to speed control, provided the field is fixed at maximum excitation and the armature voltage is varied. This type of motor always has one winding connected across the supply voltage requiring power. This motor was not entirely discounted, although it was not chosen for initial investigation.

A d-c servo motor is similar in operation to the shunt-wound motor discussed above, but exhibits better and more linear torque characteristics. It requires more power under stall conditions for the same case size, since a d-c servo motor is, in effect, only a modified d-c shunt motor with a stronger field. If the motor were made larger, then the power required to produce the necessary flux could be reduced. This type of motor would reduce the required power in the main winding of the motor under standby conditions. As this motor leaves much to be desired from the standpoint of efficiency, it was not used.

A d-c permanent magnet motor has only one winding, good stall torque, and is more efficient than most other types of small d-c motors. As with all d-c motors, brushes could create problems at high altitudes unless the motors were

hermetically sealed. It does not have linear torque curves, but is still the most promising of the regular d-c type motors. Since it is a single-winding motor, no power is required for a second winding, as in the case of the a-c motor under standby conditions. One problem inherent with any d-c motor with brushes is the inability to control running speed over a range greater than 7 or 8 to 1. However, with suitable electronics, such as a velocity servo loop, it is possible to overcome this difficulty.

An electronically commutated d-c motor using special inside-out construction techniques is presently under development and evaluation at Space Technology Laboratories, Inc. The motor is quite efficient, requires no flywheel (the physical rotated mass has sufficient moment of inertia) and has no brushes to cause high-altitude problems. In this motor, the position of the flux field is sensed by two balanced bridges using magneto-resistive or Hall effect in bismuth or other suitable material.

On the basis of the above considerations, a d-c permanent magnet motor, an a-c servo motor, and an electronically commutated d-c motor were chosen as possible prime movers for the wheel.

Since speed information is used in the logic functions of the system, a simple two-pole a-c permanent magnet tachometer is incorporated as an integral part of the motors to sense speed.

The Electronics

Two basic speed control systems have been designed for use with the motors: (a) a 400-cps system to drive the a-c servo motor, and (b) a 10,000-cps time-modulated system to drive the permanent magnet and d-c electronically commutated motors.

A-C Motor Power Amplifier. As system efficiencies for both the a-c and d-c motors are extremely important, it was decided to employ switching techniques to drive the motors. With these techniques, all the circuitry is either completely off and no power is dissipated in any portion of the circuit, or all the circuitry is completely on, i.e., in a condition of saturation, and the maximum possible power is delivered to the load.

In the case of the a-c motor, 400-cps square wave excitation is provided to the main winding of the motor (see Figure 3). To achieve speed control, the signal for the control winding is developed as follows.

The square wave applied to the main winding of the motor (Waveform 1, Figure 4) is integrated and amplified to provide a sawtooth waveform (see Waveform 2, Figure 4). This waveform is clamped to an appropriate level by two Zener diodes. Bias is varied on the base of the transistor to which the clamped sawtooth waveform is applied. Error voltage variation of the bias at the transistors causes amplification of only a portion of the waveform in direct proportion to the bias voltage, producing Waveform 3, Figure 4. The output signal of this stage is amplified through a high-gain amplifier to produce a square wave which varies in duration symmetrically about the 90° centerline (see Waveform 4, Figure 4).

This signal is then applied to a power amplifier driving the control winding. The motor is reversed by changing the polarity of the square-wave voltage applied to the main winding. A null amplifier is used to process the incoming d-c error signal to the system; the output of the null amplifier, when amplified in two Class B complimentary amplifiers, serves to change the bias level in the control amplifier circuitry.

Several novel features have been incorporated into the a-c speed control circuitry. In order to switch the power transistors in the power amplifiers cleanly into saturation, it is necessary to have an available voltage more positive than battery voltage, since the transistors are used in an emitter-follower configuration. This voltage is obtained by means of a step-down transformer, which is connected across the 400-cps voltage supplied to the main winding of the motor. The output of this transformer feeds a full-wave rectifier and develops approximately three-fourths volt out of an r-c filter. This voltage, when added to the positive battery potential, insures that the power transistors are in a state of full saturation.

Chopper stabilization is incorporated into the null amplifier circuitry to reduce long term d-c drift. Excitation to the solid state choppers is provided by transformer coupling to the excitation supplied to the main winding of the a-c servo motor.

As the system has been designed for operation at high temperatures, all transistors used in the circuitry are silicon.

The square-wave generator used as a time base is a hybrid multivibrator. This three-transistor multivibrator is inherently more temperature stable than two-transistor multivibrators, as the frequency of its output is dependent only upon the temperature coefficient of one small capacitor.

The efficiency of this system, in terms of useful power delivered to the load compared to the power consumed by the amplifier, is approximately 85 per cent.

D-C Motor Power Amplifier.

Power System. In the d-c power system, a square-wave type of controlled time-duration voltage is developed to drive both the permanent magnet and the electronically commutated d-c motors. The amplifier was designed to drive the d-c motors on the theory that if a d-c motor were

pulsed at a sufficiently high frequency, the inductance of the motor winding would integrate these pulses and provide filtered d-c to the motor. Speed control would then be achieved by varying pulse width. Figure 5 is a block diagram of the d-c system.

The error signal from the attitude sensor controls the "on time," T_Q, of a one-shot multivibrator (see Figure 6). Another hybrid multivibrator determines the starting time for the one-shot. The output from the first hybrid and width control one-shot are summed in an AND gate. The output of the AND gate is amplified and used to drive the power amplifier connected to the motor winding. This controlled-time speed system is used for both the d-c permanent magnet and d-c electronically commutated motor.

As no 400-cps excitation is available in the d-c amplifier system, the power transistor used in the power amplifier is driven into saturation by means of a pulse current transformer. Since no excitation is available for solid-state choppers, the error signal amplifier is of complimentary symmetry design. A stable hybrid multivibrator is again used for the time base.

The efficiency of this driving amplifier in terms of power delivered to the load compared to power consumed by the amplifier is in excess of 90 per cent.

Commutation System. The electronically commutated motor is basically a two-winding motor. Two identical channels of electronics are used to commutate the windings. A typical channel consists of a level sensitive trigger circuit which receives its intelligence from the flux sensitive bridge that indicates the position of the flux pattern. The output of the level sensitive trigger circuit trips a flip-flop which drives a switching amplifier, connecting the proper end of the motor winding at the proper time to the correct voltage.

Velocity Servo Loop. Since a typical motor tested in the laboratory had an acceleration time of ten seconds from zero to maximum speed and a deceleration time of two minutes, an internal velocity servo loop was added to make system response linear. However, since the times involved in attitude control of space vehicles are on the order of several minutes rather than seconds, addition of this velocity loop may not be necessary.

The velocity servo loop incorporates a dual input photoelectric tachometer whose output, through suitable logic, supplies a voltage whose magnitude is directly proportional to the speed of the motor and whose polarity is dependent upon the direction of rotation of the motor. The output of the tachometer logic is summed with the platform error input signal, amplified by a high gain amplifier, and applied to the error signal amplifier in the power amplifier system. To provide the greatest possible stability, chopper stabilization is used in the high gain amplifier and summing portions of the servo loop.

With the addition of the velocity servo loop, both the acceleration and deceleration times of the motor are approximately ten seconds. The resulting system has better than one per cent speed linearity over its entire range.

The Sensor

To conserve power and to minimize circuitry and weight on the platform, it was decided that the input sensor should consist of: (a) a light beam placed at a convenient distance from the table to establish a reference, and (b) a visible pickup device mounted on the edge of the table to detect attitude error. Gyros are a readily available alternate which could have been used instead of the visible sensor. However, since gyros require heater power as well as three-phase excitation, a heater amplifier and a static inverter would have to be added to the platform, resulting in greatly increased battery drain, platform weight, and system complexity. Furthermore, it would be necessary to process the intelligence coming from the gyros in demodulators, etc., complicating the system even more.

The visible sensor consists of a simple single lens which focuses the light at the rear of the cylinder (see Figure 7), where photo transistors have been mounted. The output of the sensor, either a positive or negative signal, depending on the platform's angular relationship with the incoming light rays, is amplified and used to control the associated power amplifier systems. Both position and integral feedback with lead-lag shaping are employed in the system.

As mentioned previously, a simple two-pole a-c tachometer is mounted on the motor's shaft. The output signal from the tachometer is applied across an active tuned q-multiplier circuit. The output of this circuit is an a-c frequency directly dependent upon the speed of the motor, whose amplitude has been modified by the q-multiplier. This signal is converted to a d-c voltage in a simple passive a-c to d-c circuit. This d-c clamp voltage is then used to actuate a relay, which controls the solenoid valve action in the pneumatic system of the platform. To achieve equal gas discharge times for each end of the platform, an RC time constant determines the on-time of a master relay, which actuates the appropriate slave gas solenoid valve.

The Pneumatics

Gas is stored on the platform in four tanks whose outputs are manifolded together to maintain uniform pressure in each tank. These tanks are mounted symmetrically with respect to the center of gravity of the platform, so that no shift in the center of gravity occurs during gas discharge. The manifold output of the tanks is reduced in a two-stage pressure regulator and then piped to the solenoids mounted at the ends of the table. Figure 8 shows the gas solenoid, nozzle, and sensor mounted on the end of the table.

General

Reliability

The ultimate goal in the design of this system is to achieve a high degree of reliability, and operate unattended for a period of a year or longer. The system will require little or no calibration and no selection of components, as all components are available as off-the-shelf items. Circuits have been specially designed for stability. Switching techniques keep the transistors cool and virtually no power is dissipated in the transistors because of the high circuit efficiencies, which further tend to increase the reliability of the system.

Torque, Speed, Power Relationships

The laboratory model provided a useful stall torque of 1 oz-in., a motor speed of 12,000 rpm (before gas jet firing), and a maximum no-load speed of 20,000 rpm, while consuming approximately 9 watts of energy to maintain a constant wheel speed. The signal circuitry required to process the incoming signal requires an additional 3 to 4 watts. The system has a motor time constant of about 10 seconds for wheel acceleration from 0 to 12,000 rpm. The ratio of moment of inertia of the platform to that of the wheel was approximately 400,000 to 1. This system, with minor modifications, could be further reduced to give a 10 watt per axis system, yielding 1 oz-in. of torque.

The ultimate design goal of a system of this type would be (1) to consume no more than 10 to 15 watts for a 3-axis system, (2) to deliver torques on the order of 1/2-oz-in., with approximately the same speed capability, and (3) to function unattended for a year or longer. The weight of this system would be no more than 10 to 15 lbs. The system described in this report approaches these design goals.

Space Vehicle Control

Three-dimensional attitude control of a space vehicle can be achieved with three channels, as described above, mounted with the wheel spin axes along the vehicle principle axes of inertia. Thrust for the auxiliary mass ejection system can be generated by means of compressed gases, as in the laboratory model. Use of monopropellants or bipropellants, vaporized liquids, ion ejectors, plasma jets, etc., are also feasible for thrust generation. The control system may be simplified somewhat by eliminating the tachometer. Wheel control continues until saturation occurs, at which time any disturbance present will cause the vehicle to drift until the attitude corresponds to the dead-space value of the mass-ejection system. Firing of the jets will then drive the wheels out of saturation, where wheel control resumes.

Design Considerations

In addition to specifying attitude requirements to achieve successful operation of a specific space mission, it is necessary to have some knowledge of the causes of deviations from the desired attitude, of how such deviations can be sensed, and how they can be corrected. The gyroscopic effects of the inertial wheels must also be considered in the design of a control system. Sources of disturbances, methods of sensing, and three-dimensional equations of motion are presented in the Appendix.

Selection of Control Equations

Referring to the equations of motion presented in the Appendix, it can be seen that the control problem is to make the wheel momenta, with respect to the vehicle, suitable functions of the deviations from the reference, so that the resulting vehicle equations of motion have the desired stability and response characteristics. In applications where relatively large deviations in attitude can be tolerated, a control equation in which the wheel momenta are linear functions of the deviation angles and their rates may be satisfactory. Constant wheel speeds, then, result in constant attitude errors. If attitude deviation requirements are stringent, integration can be incorporated into the control system to eliminate these errors.

Although the control equations selected for a single-axis control system may provide satisfactory performance and stability, it is by no means conclusive that three independent single-axis control channels, each a function of the corresponding deviation angle, will provide adequate performance for three-dimensional control. In the case of an orbiting vehicle in which the reference axes rotate at orbital frequency (this, in the absence of disturbances, results in a periodic transfer of momentum between wheels at orbital frequency), and in the presence of periodic disturbance torques at or near orbital frequency, stability problems may arise. More sophisticated control equations may then be necessary.

Appendix

Source of Disturbances

Disturbance torques which act to perturb the vehicle from the desired orientation may arise from the following sources:

1. Rotating parts within the vehicle.
2. Inertial cross-coupling due to differences in principal moments of inertia.
3. Interaction with ambient gravitational, magnetic, and electric fields
4. Incident and emitted radiation.
5. Particle impingements.
6. Aerodynamics.

Because of present lack of knowledge of the environment to which a space vehicle will be subjected, only crude estimates of the magnitudes of disturbances can be made. It is difficult to generalize since these disturbances depend upon the vehicle configuration. The vehicle should, then, be designed to minimize these disturbing effects.

Methods of Sensing

There are a number of sensing methods that can be incorporated into a space vehicle control system. These methods can be divided into four basic classes:

1. Sensing by inertial means.
   Devices which fall into this category are gyroscopes, accelerometers, pendulums, vibrating masses, etc.

2. Sensing by sighting of celestial bodies.
   Such devices are horizon scanners, sun seekers, moon seekers, and star trackers.

3. Sensing by interaction with ambient fields.
   Such methods are quite restricted, in that ambient fields vary with altitude and orbital position. For very low altitudes use can be made of the atmospheric pressure gradient. The earth's magnetic field varies considerably with orbital position, so that some programming must be used with such a system. The observation of the differential gravitational forces on the various parts of the vehicle requires extremely sensitive instrumentation in measuring this gravitational gradient.

4. Sensing by ground observation of signals transmitted from the vehicle.
   The field pattern of a narrow radar beam transmitted from the vehicle can yield attitude information. Correction signals are then transmitted to the vehicle from the ground station.

Although the sensing methods listed above have their limitations and disadvantages, the control designer has a relatively broad selection of feasible methods of attitude sensing.

Equations of Motion

Let the reference coordinate system consist of the xyz axes, with the origin located at the center of mass of the vehicle. It is assumed, for generality, that the position of the vehicle center of mass is known as a function of time. The angular velocity, $\vec{\omega}_{ref}$, of the reference frame, then, is also known as a function of time. It has components ω_x, ω_y, and ω_z, directed along the x, y, and z axes, respectively.

$$\vec{\omega}_{ref} = \omega_x \vec{e}_x + \omega_y \vec{e}_y + \omega_z \vec{e}_z \qquad (1)$$

Let XYZ form an orthogonal set of body-fixed axes directed along the principal axes of inertia of the vehicle, which has principal moments of inertia I_X, I_Y, and I_Z. The angular velocity, $\vec{\omega}_{body}$, of these body-fixed axes, in inertial space, has components ω_X, ω_Y, and ω_Z, directed along the X, Y, and Z axes, respectively.

$$\vec{\omega}_{body} = \omega_X \vec{e}_X + \omega_Y \vec{e}_Y + \omega_Z \vec{e}_Z \qquad (2)$$

Since the sensing elements will, in general, measure deviations from the reference, it may be desirable to express the body rates in terms of these deviations. The angular velocity of the reference frame, the body axes, and the angular velocity, $\vec{\omega}_{rel}$, of the body axes relative to the reference frame, are related by:

$$\vec{\omega}_{body} = \vec{\omega}_{ref} + \vec{\omega}_{rel} \qquad (3)$$

Let us define these deviation angles by the three rotations θ_3, θ_1, and θ_2, in that order, which transform the reference axes, xyz, into the body axes, XYZ. θ_3 is a rotation about the z axis, transforming xyz into x'y'z. θ_1 is a rotation about the x' axis, transforming x'y'z' into x'Yz' θ_2 is a rotation about the Y axis, transforming x'Yz' into XYZ. This sequence was selected so that θ_1 and θ_2 correspond to the gimbal angles of a gimballed "pointer" that is aligned with one of the reference axes. The choice of deviation angles, however, is arbitrary. The unit vectors in the two sets of axes are then related by:

$$\begin{bmatrix} e_X \\ e_Y \\ e_Z \end{bmatrix} = \begin{bmatrix} a_{11} & a_{12} & a_{13} \\ a_{21} & a_{22} & a_{23} \\ a_{31} & a_{32} & a_{33} \end{bmatrix} \begin{bmatrix} e_x \\ e_y \\ e_z \end{bmatrix} \qquad (4)$$

where:

$$a_{11} = \cos\theta_2 \cos\theta_3 - \sin\theta_1 \sin\theta_2 \sin\theta_3$$

$$a_{12} = \cos\theta_2 \sin\theta_3 + \sin\theta_1 \sin\theta_2 \cos\theta_3$$

$$a_{13} = -\cos\theta_1 \sin\theta_2$$

$$a_{21} = -\cos\theta_1 \sin\theta_3$$

$$a_{22} = \cos\theta_1 \cos\theta_3$$

$$a_{23} = \sin\theta_1$$

$$a_{31} = \sin\theta_2 \cos\theta_3 + \sin\theta_1 \cos\theta_2 \sin\theta_3$$

$$a_{32} = \sin\theta_2 \sin\theta_3 - \sin\theta_1 \cos\theta_2 \cos\theta_3$$

$$a_{33} = \cos\theta_1 \cos\theta_2$$

This transformation is shown in diagram in Figure 9.

Euler's equations, which describe the general motion of a body about its center of mass are:

$$I_X\dot{\omega}_X + (I_Z - I_Y)\,\omega_Z\omega_Y = (L_D)_X + (L_W)_X$$

$$I_Y\dot{\omega}_Y + (I_X - I_Z)\,\omega_X\omega_Z = (L_D)_Y + (L_W)_Y \qquad (5)$$

$$I_Z\dot{\omega}_Z + (I_Y - I_X)\,\omega_Y\omega_X = (L_D)_Z + (L_W)_Z$$

where the terms on the right-hand side of equation (5) are the components of the external disturbance torque, $\vec{L}_D$, on the vehicle, and, $\vec{L}_W$, the torque due to the motion of the wheels.

Using equations (3) and (4), the components of the vehicle angular velocity, in inertial space, directed along the body axes then become:

$$\omega_X = a_{11}\omega_x + a_{12}\omega_y + a_{13}(\omega_z + \dot{\theta}_3) + \dot{\theta}_1 \cos\theta_2$$

$$\omega_Y = a_{21}\omega_x + a_{22}\omega_y + a_{23}(\omega_z + \dot{\theta}_3) + \dot{\theta}_2 \qquad (6)$$

$$\omega_Z = a_{31}\omega_x + a_{32}\omega_y + a_{33}(\omega_z + \dot{\theta}_3) + \dot{\theta}_1 \sin\theta_2$$

Let H_X, H_Y, and H_Z represent the components of the total angular momentum, $\vec{H}$, of the X, Y, and Z wheels relative to the vehicle frame. The torque upon the vehicle due to the motion of the wheels becomes:

$$\vec{L}_W = -\frac{d}{dt}(H_X\vec{e}_X + H_Y\vec{e}_Y + H_Z\vec{e}_Z) \qquad (7)$$

or

$$-\vec{L}_W = \dot{H}_X\vec{e}_X + \dot{H}_Y\vec{e}_Y + \dot{H}_Z\vec{e}_Z + \vec{\omega}_{body} \times \vec{H} \qquad (8)$$

The components of $\vec{L}_W$ along the body axes are:

$$-(L_W)_X = \dot{H}_X + H_Z\omega_Y - H_Y\omega_Z$$

$$-(L_W)_Y = \dot{H}_Y + H_X\omega_Z - H_Z\omega_X \qquad (9)$$

$$-(L_W)_Z = \dot{H}_Z + H_Y\omega_X - H_X\omega_Y$$

The general equations of motion of a vehicle with reaction wheels, then, are given by equations (5), (6), and (9). The moments of inertia of the vehicle are now defined to include the moments of inertia of the wheels. These equations are not in a form that can be suitably used for conventional control system synthesis. However, they can be reduced to a more tractable form by linearization, so that the resulting expressions are ordinary differential equations with constant coefficients. Conventional servo techniques can then be applied.

For the single-axis laboratory model the equation of motion, excluding disturbances, is

$$I\ddot{\theta} = -\dot{H} = -J\dot{\omega} \qquad (10)$$

where

I = platform moment of inertia

θ = platform angular deviation

H = wheel momentum

J = wheel moment of inertia

ω = wheel speed

The control equation is

$$\dot{H} = \mu K_m J \frac{(s+k)(\tau_1 s+1)}{(\tau_m s+1)(\tau_2 s+1)}(\theta_c - \theta) \qquad (11)$$

where

μ = amplifier gain

K_m = motor gain

k = integrator gain

τ_m = motor time constant

τ_1 = lead time constant of shaping network

τ_2 = lag time constant of shaping network

θ_c = commanded platform deviation

Amplifier and integrator gains and lead-lag time constants were selected to yield a 50 per cent damped system.

References

1. Roberson, R. E., "Attitude Control of a Satellite Vehicle - An Outline of the Problems", presented at the Eighth International Congress of Astronautics, Barcelona, Spain, October 1957.

2. Roberson, R. E., "Torques on a Satellite Vehicle from Internal Moving Parts", Journal of Applied Mechanics, June 1958.

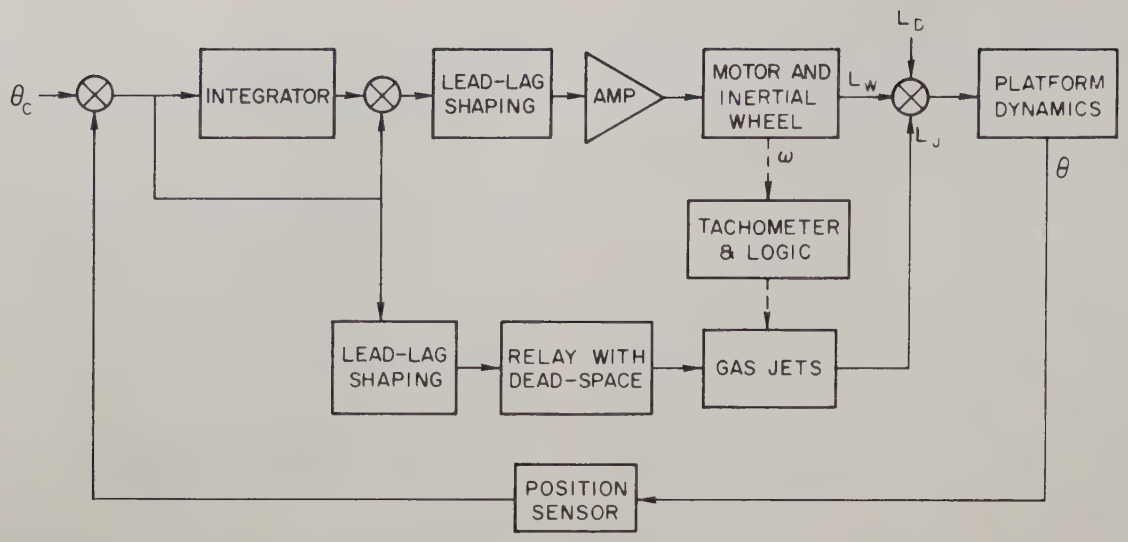

θ = ATTITUDE DEVIATION
θ_C = COMMANDED ATTITUDE DEVIATION
ω = INERTIAL WHEEL SPEED
L_W = WHEEL CONTROL TORQUE
L_J = GAS JET CONTROL TORQUE
L_D = DISTURBANCE TORQUE

Fig. 1. Block Diagram of Laboratory Model of Single-Axis Control System.

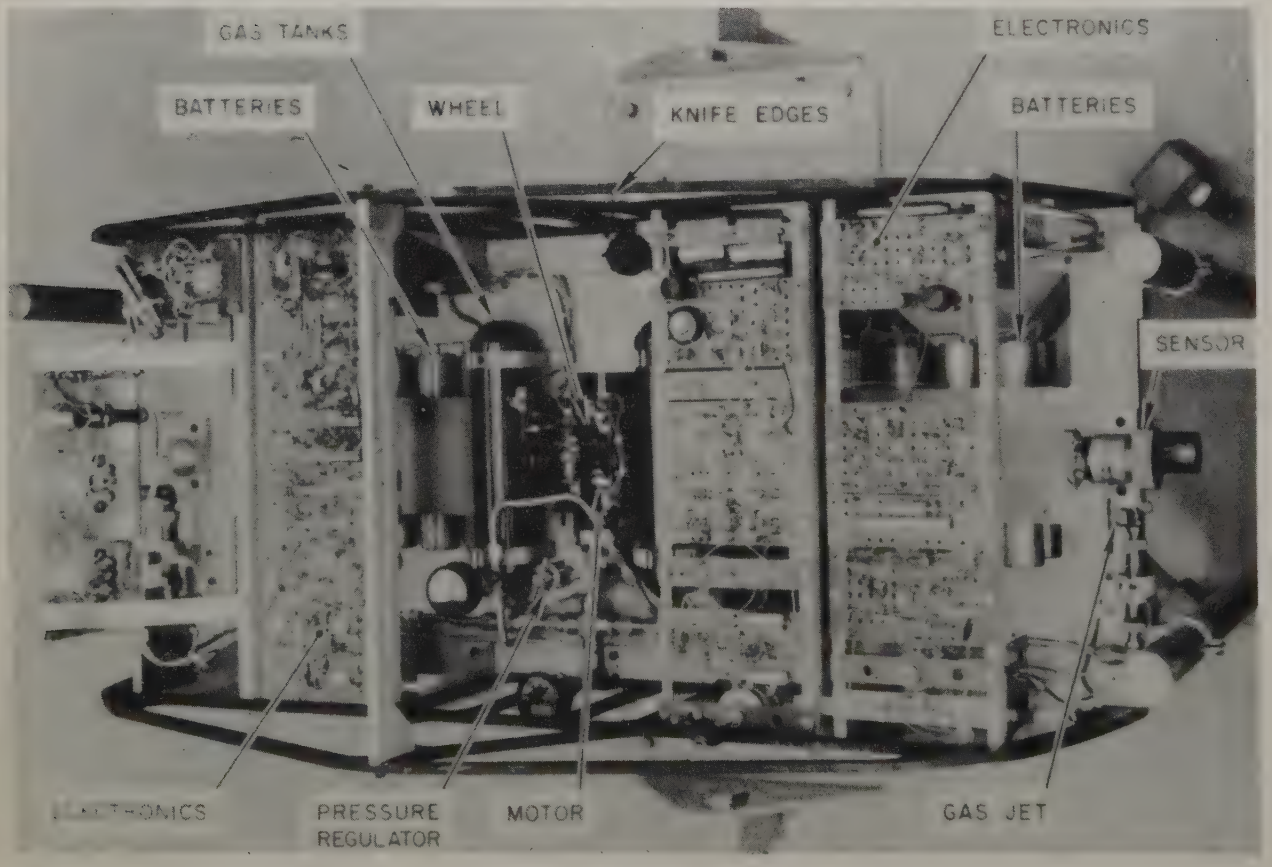

Fig. 2. Laboratory model.

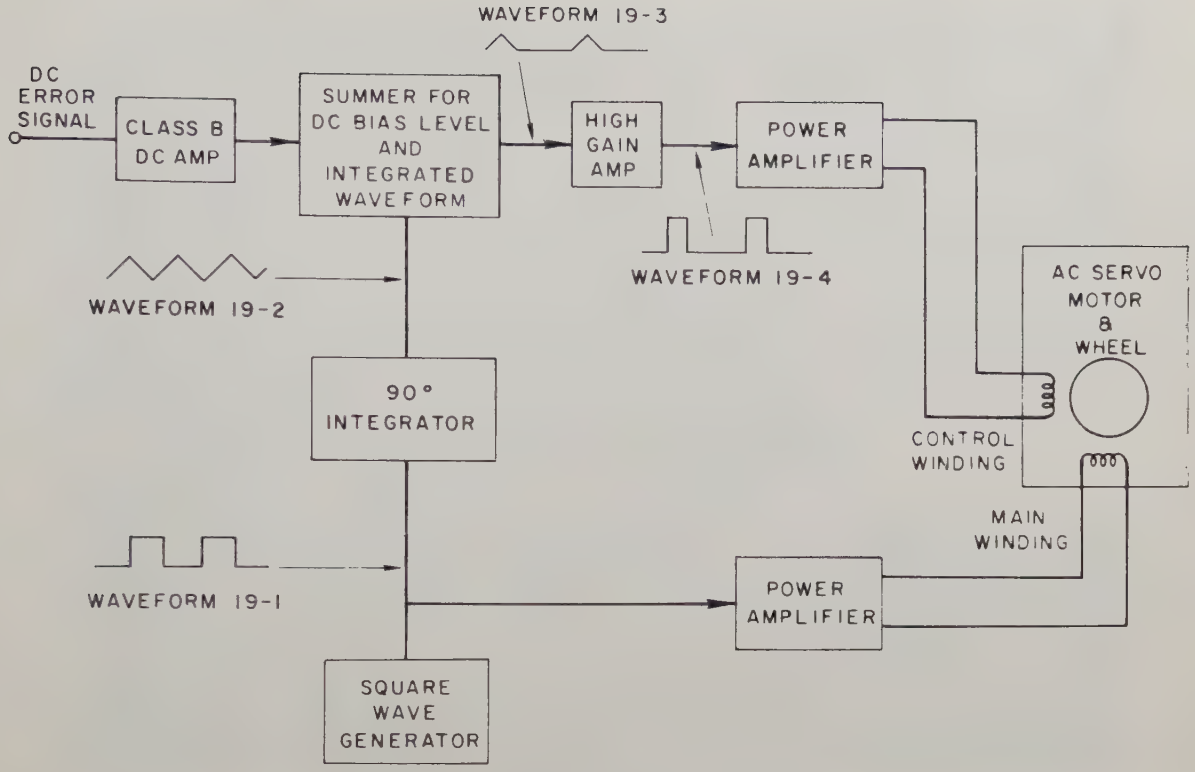

Fig. 3. Block Diagram of A-C System.

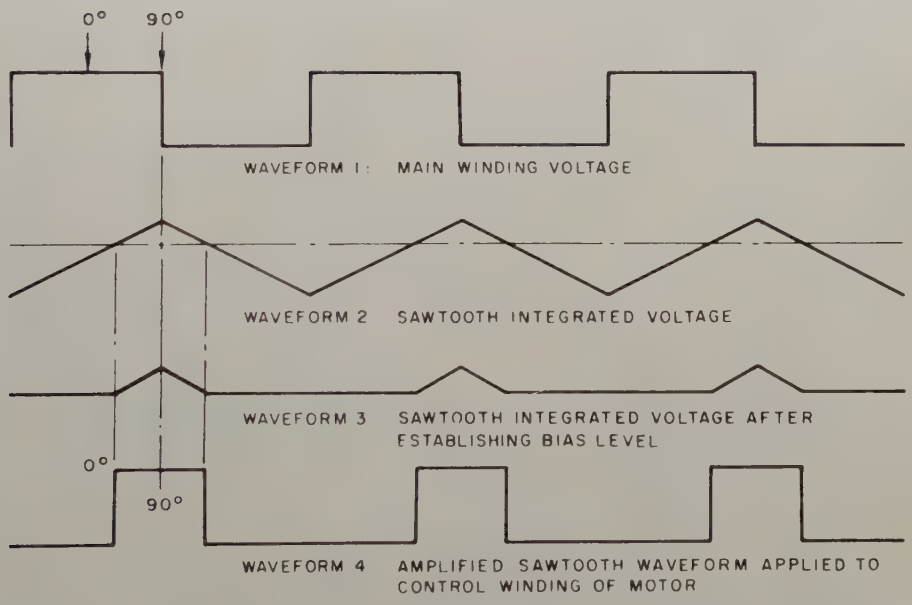

Fig. 4. Waveforms of Control Circuitry of A-C System.

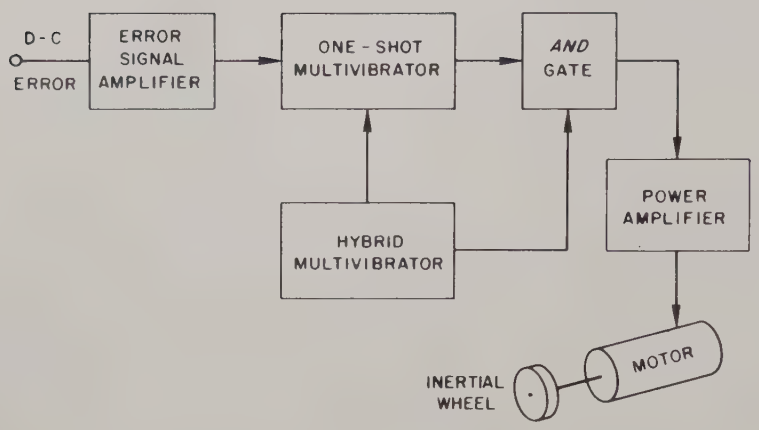

Fig. 5. Block Diagram of the D-C Speed Control System.

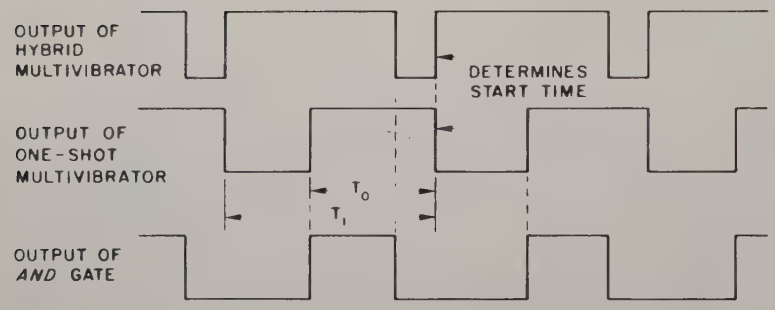

Fig. 6. Essential Waveforms in the D-C System.

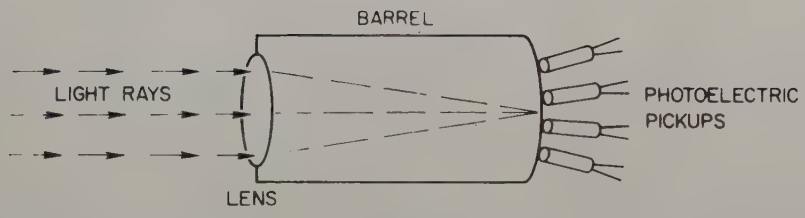

Fig. 7. Mechanics of Sensor.

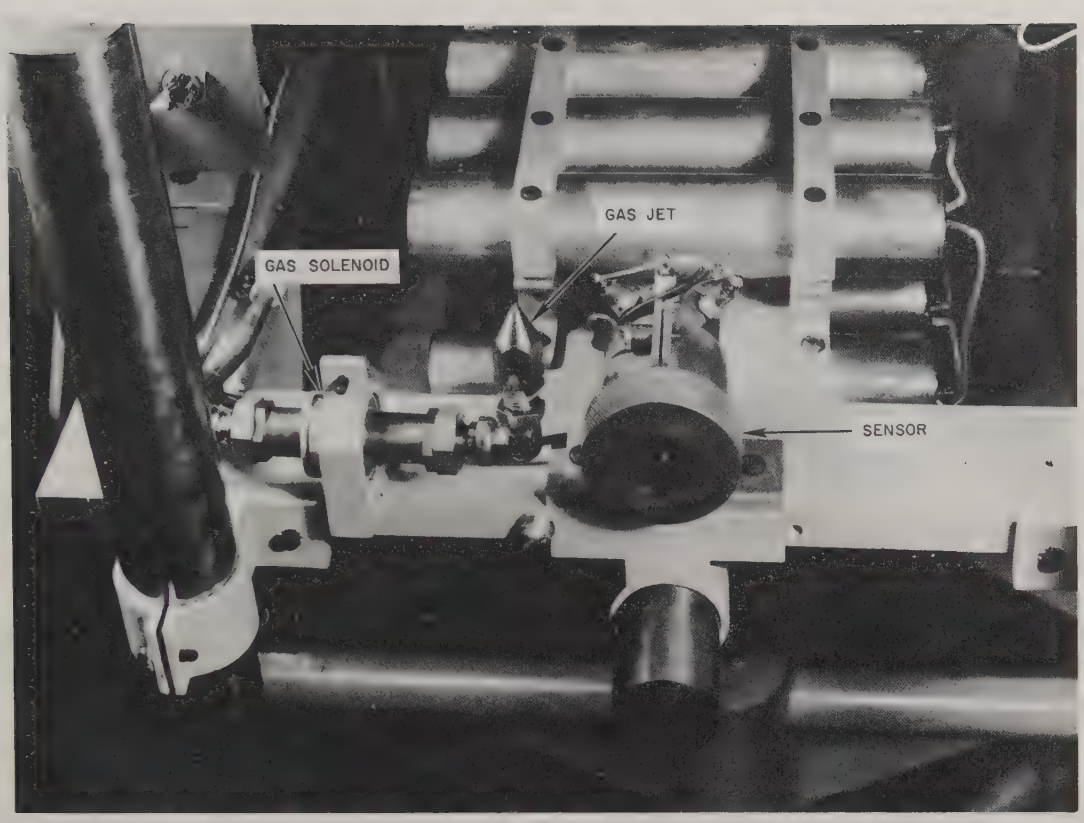

Fig. 8. Gas Solenoid and Sensor Mounted on Table.

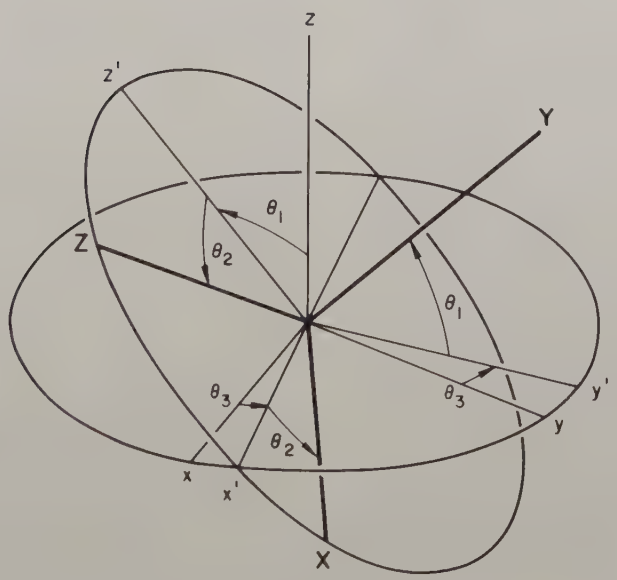

Fig. 9. Deviation Angles.

D-DECOMPOSITION ANALYSIS OF AUTOMATIC CONTROL SYSTEMS

Rolf W. Lanzkron
Martin Corporation
Orlando, Florida

Thomas J. Higgins
University of Wisconsin
Madison, Wisconsin

Summary

Development of the basic theory of D-decomposition by a general polynomial expression, the characteristic function of a linear lumped parameter automatic control system, is followed by account of: the basic theory of parametric stability; unity-feedback variable-gain analysis, with subsequent generalization to numeric and frequency-dependent feedback; transient response determination; and sampled-data system analysis, as effected by D-decomposition theory. Application of theory in practice is illustrated by numerous illustrative examples.

I. Introduction

A. Purpose of Paper

The purpose of this paper is threefold: to direct attention to a powerful means of control systems analysis of which little, if anything, has been written hitherto in English; to develop a critical, integrated and well-detailed account of theory facilitating control theory analysis by this method of D-decomposition; and to exemplify application of this development by illustrative numerical examples.

B. Usefulness of the Content

The essential usefulness of the content of this paper is, perhaps, best illuminated by note of the course of development and current use of a much-used mode of analysis somewhat akin to the method of D-decomposition, in that each comprises a conjunction of graphic and analytic procedure: namely, the method of root-locus. Thus, following original note of the basic concept of the method of root-locus and of its use for determination of the maximum gain demarking the limit of stability of a unity feedback system by Evans (in 1948), a considerable number of investigators have explored the possibilities of this method for servomechanism analysis over the subsequent years to-date. In consequence of this extensive study, a considerable body[1] of root-locus (and associated) theory has been gradually developed that enables facile analysis of various phases of control systems work to which it is well-suited; and the essential content of this body of theory, as evidenced in textbooks and publications, both has passed into the domain of study of basic servomechanism and automatic control theory in engineering schools and has become a basic tool in control system design in practice.

Now much the same possibilities of development, scholastic exemplification, and usefulness in practice attend the method of D-decomposition, so-called by its originator Neimark in virtue of his use of the classical operator $D \equiv d/dt$. Neimark, a Russian mathematician, originated this procedure for use in his work on delimiting the zeros of polynomial expressions. The possible use of this procedure for demarking the domain of stability of a control system, hence as a stability criterion in the same sense that Cauchy's principle of argument provides a procedure for demarking the domain of stability in the guise of Nyquist's well-known criterion, was remarked (circa 1947) by Meerov and Neimark. Subsequently, use of D-decomposition has been extended to some other phases of control systems analysis. But, as inferred from a reading of the available papers[1] shows, the present state of the development of the method of D-decomposition would seem to roughly parallel that of the earlier developments in the root-locus method.

Now it is possible to develop the method of D-decomposition in much the same degree as has been done for the root-locus method; and as the possibilities of use are fully as great and the facileness and flexibility of use for some purposes are even better than for the root-locus method, it is obviously most desirable that this be effected. A substantial advance in this direction is enfolded in the Ph.D. thesis[2] of the first-named author. A concise presentation of certain major aspects of this thesis comprises the context of the present paper.

C. Scope of Paper

Section 2 comprises a development of the basic theory of D-decomposition by a general polynomial expression, interpretable as the characteristic function of a linear lumped-parameter control system. Section 3 advances the basic theory of parametric stability analysis. Section 4 presents an account of certain basic theory in control system analysis for a unity-feedback system by the method of D-decomposition, wherein gain is taken as the variable parameter. Section 5 comprises complementary account of the theory underlying determination of transient response by the method of D-decomposition. Section 6 generalizes application of D-decomposition methods to control systems with numeric and, more broadly, frequency-dependent feedback. Section 7 develops D-decomposition analysis for sampled-data servomechanisms. Section 8 comprises a summary of essential results. A short list of some pertinent references concludes the paper.

2. Basic Theory of D-Decomposition

A. Basic Theory of D-Decomposition by a Characteristic Polynomial

Consider the polynomial equation

$$(1)\quad f(s) \equiv A_o(a,b)s^n + A_1(a,b)s^{n-1} + \ldots + A_n(a,b) = 0$$

where the coefficients $A_i(a,b),(i=1,\ldots,n)$, of the characteristic polynomial $f(s)$ are functions of two parameters (a,b). Let, as is commonly the case in practice, the A_i be linear functions of these parameters: thus, $A_i(a,b)=k_i' + k_i'a + k_i''b$. In such case (1) can be recast as

(2) $f(s) \equiv (k_o+k_o'a+k_o''b)s^n +$

$$(k_1+k_1'a+k_1''b)s^{n-1}+\ldots+(k_n+k_n'a+k_n''b) = 0$$

Setting s = jw in (2) yields

(3) $f(jw) \equiv (k_o+k_o'a+k_o''b)(jw)^n+(k_1+k_1'a+k_1''b)(jw)^{n-1}$

$$+\ldots+(k_n+k_n'a+k_n''b) = 0$$

Collecting the terms multiplying a, those multiplying b, and the remainder of the terms of (3) gives

(4) $f(jw) \equiv aP(jw) + bQ(jw) + R(jw) = 0$

wherein P(jw), Q(jw) and R(jw) are polynomials in jw given by

(5) $P(jw) = \sum_{i=0}^{n} k_i'(jw)^{n-i}$

(6) $Q(jw) = \sum_{i=0}^{n} k_i''(jw)^{n-i}$

(7) $R(jw) = \sum_{i=0}^{n} k_i(jw)^{n-i}$

Expressing P(jw), Q(jw) and R(jw) in terms of their real and imaginary parts by

(8) $P(jw) = P_1(w) + jP_2(w)$

(9) $Q(jw) = Q_1(w) + jQ_2(w)$

(10) $R(jw) = R_1(w) + jR_2(w)$

wherein $P_1(w),\ldots, R_2(w)$ are polynomials in w and substituting accordingly in (4) gives

(11) $f(jw) \equiv [aP_1(w)+bQ_1(w)+R_1(w)] +$

$$j[aP_2(w)+bQ_2(w)+R_2(w)] = 0$$

As a complex quantity equals zero only if its real and imaginary parts are each equal to zero, it follows from (11) that simultaneous satisfaction of the equations

(12) $aP_1(w) + bQ_1(w) = -R_1(w)$

(13) $aP_2(w) + bQ_2(w) = -R_2(w)$

are necessary and sufficient conditions that w be a value which satisfies (11), and thus that the corresponding value s = jw satisfy (1).

From (5), (6) and (7), it follows that $P_2(w)$, $Q_2(w)$ and $R_2(w)$ are polynomials comprised of odd powers of w. Accordingly, (13) can be recast as

(14) $awP_2'(w) + bwQ_2'(w) = -wR_2'(w)$

wherein $P_2'(w)$, $Q_2'(w)$ and $R_2'(w)$ are polynomials comprised of even powers of w. In turn, (14) is equivalent to the pair of equations

(15a) $w = 0$

(15b) $aP_2'(w) + bQ_2'(w) = -R_2'(w)$

Solution of (12) and (13) by Cramer's rule gives

(16) $a=[-Q_2(w)R_1(w)+Q_1(w)R_2(w)]/\Delta(w)=D_1(w)/\Delta(w)$

(17) $b=[-P_1(w)R_2(w)+P_2(w)R_1(w)]/\Delta(w)=D_2(w)/\Delta(w)$

wherein

(18) $\Delta(w) = \begin{vmatrix} P_1(w) & Q_1(w) \\ P_2(w) & Q_2(w) \end{vmatrix}$

and $D_1(w)$ and $D_2(w)$ are defined by

(19) $D_1(w) = Q_1(w)\,R_2(w) - Q_2(w)\,R_1(w)$

(20) $D_2(w) = P_2(w)\,R_1(w) - P_1(w)\,R_2(w)$

Now (16) and (17), and correspondingly (12) and (13), comprise the parametric representation of a curve in the (a,b) plane. Elimination of the parameter w between either of these two sets of equations yields an equation enfolding this curve: say

(21) $F(a,b) = 0$

The geometric significance of (16), (17) and (21) are as follows. If s' = jw' is a specified arbitrary value on the imaginary axis of the s-plane which satisfies (1), then w' is a value which satisfies (12) and (13). In turn, if $w' \neq 0$, it is then a value which satisfies (12) and (15b). The corresponding values (a',b') of (1) for which such is true are given explicitly by (16) and (17) on substituting w' therein. This pair of values locates a point (a',b') in the (a,b) plane corresponding to the point s' = jw' in the s-plane. Then inasmuch as (21) is obtained by elimination of w between (16) and (17), or between (12) and (13), or--since the factor w cancels out in the ratios of (16) and (17)--between (12) and (15b), it follows that the curve defined by (21) enfolds all points of the (a,b) plane which are such that an arbitrary point s = jw of the imaginary axis of the s-plane, <u>other than the origin</u>, is a solution of (1). Thus, the curve defined by (21) contains the "map" of all points of the imaginary axis of the s-plane, other than the origin, afforded by the characteristic polynomial f(s) of (1).

If w' = 0, then (13) is satisfied in virtue of (15a), but simultaneous satisfaction of (12) requires that

(22) $aP_1(0) + bQ_1(0) = -R_1(0)$.

Thus, the values (a',b') such that s' = jw' = 0 is a solution of (1) are enfolded by (22); i.e., the straight line defined by (22) enfolds all points of the (a,b) plane whereof the coordinates (a,b) are corresponding values of (a,b) such that

the point $s = jw = 0$ of the imaginary axis of the s-plane is a solution of (1).

Accordingly, the curves defined by (21) and (22) contain the "map" of the whole of the imaginary axis of the s-plane on the (a,b)-plane as afforded by the characteristic polynomial f(s) of (1). If one or both of a and b are actual functions of w, the mapping is conformal and plot of this map divides, or "decomposes", the (a,b)-plane into regions, some corresponding to the right-half of the s-plane, the remainder to the left-half of the s-plane. The corresponding subdivided plane is termed the "D-decomposition of the (a,b)-plane", as afforded by the characteristic polynomial f(s). The terminology "D-decomposition" stems from Neimark's original use of D, rather than s, as a symbol in the characteristic polynomial of (1): As it is now well-established in the Russian literature, it appears expedient to retain this designation rather than to shift to the corresponding terminology of "s-decomposition".

If both a and b are constants, the D-decomposition is effected, but the correspondence of regions to the right and left halves of the s-plane may not hold.

B. Illustrative Example

In exemplification of the analysis of Section 2-A, consider the D-decomposition afforded by the characteristic polynomial

(23) $f(s) \equiv 10as^3+(11a+10)s^2+(11+a)s+b = 0$

Correspondingly,

(24) $P_1(w) = -11w^2$

(25) $P_2(w) = w(-10w^2+1)$

(26) $Q_1(w) = 1$

(27) $Q_2(w) = 0$

(28) $R_1(w) = -10w^2$

(29) $R_2(w) = 11w$

Herewith (18), (19) and (20) yield

(30) $\Delta(w) = (10w^2-1)w$

(31) $D_1(w) = 11w$

(32) $D_2(w) = (100w^4+111w^2)w$

Substituting appropriately in (16) and (17) gives

(33) $a = 11/(10w^2-1)$

(34) $b = (100w^4+111w^2)/(10w^2-1)$

Eliminating w between these two equations gives

(35) $F(a,b) \equiv 121a^2+1441a-110ab+1210 = 0$

Substituting in (22) gives

(36) $b = 0$

Confirmatively, if $b = 0$ in (23), then a can assume any value and $s = jw \equiv 0$ is yet a solution of (23). Hence the real axis $b = 0$ enfolds the "map" of the origin of s-plane. If $w \neq 0$, then the coordinates (a,b) of a point on the curve defined by (35) may be corresponding values of (a,b) such that the points $s = \pm jw$, w real and positive, $w \neq 0$, satisfy (23). Thus, the map of the whole of the imaginary axis of the s-plane, as afforded by f(s) in (23), is furnished by the curves defined by (35) and (36).

3. Delimitation of Stability by D-Decomposition

A. Basic Theory of Parametric Stability Analysis

Per well-known theory,[3] the nature of the stability of a control system with characteristic equation (1) is linked with the roots of this latter as follows: if all roots of this equation be in the left-half of the s-plane, the system is stable; if any roots lie in the right-half of the s-plane or if any multiple roots be on the imaginary axis, the system is unstable; if roots of multiplicity one be on the imaginary axis and the remainder of the roots lie in the left-half of the s-plane, the system is limitedly stable. Accordingly, determination of the variation of the nature of the stability of a system with parametric characteristic equation (1) comprises, effectively, determination of the variation of the nature of the roots of (1), thus of the zeros of the characteristic polynomial f(s) of (1), with variation of the parameters (a,b).

Now, as noted in Section 2, the D-decomposition of the (a,b)-plane afforded by the characteristic polynomial f(s) entails a division of the (a,b)-plane into regions by a multiply-branched curve which enfolds the conformal trace of the imaginary axis of the s-plane on the (a,b)-plane. By a well-known theorem in conformal mapping, the area of the s-plane to the left of the imaginary axis as this is traversed by a point moving from $w = -\infty$ to $w = +\infty$ corresponds to the area in the (a,b)-plane which is to the left of the curve traced in this plane by the map of the moving point in the s-plane when $\Delta(w)$ in (18) is positive, and to the right of the curve so traced when $\Delta(w)$ is negative. Herewith, therefore, the regions of the D-decomposition of the (a,b)-plane can be identified with the corresponding right and left halves of the s-plane, as illustrated in Fig. 1.

Now in virtue of the linearity of coefficients of (1) in the parameters (a,b), as indicated specifically in (2), a point in the s-plane corresponds to a single point in the (a,b)-plane, as indicated by (16) and (17). Accordingly, a necessary and sufficient condition that a system be stable is (inasmuch as all zeros of f(s) must be in the left-half of the s-plane) that points

of the (a,b)-plane corresponding to the zeros of f(s) lie in the region of the (a,b)-plane which is the map of the left-half of the s-plane. These two corresponding regions may conveniently be termed the stable regions of the respective planes. A ready identification of the possible stable regions stems from shading these regions in the immediate vicinity of the corresponding boundaries afforded by the jw-axis of the s-plane and its map in the (a,b)-plane--as in Fig. 1.

With this correspondence of the s and (a,b)-planes in hand, consider variation of the parameters (a,b) from, say, (a',b') to (a",b"). Therewith, in virtue of the multiple-valued mapping of the (a,b)-plane on the s-plane, the associated set of zeros of f(s) varies from, say, the set of values s' to a set of values s". Suppose that the initial point (a',b') is in the stable region of the (a,b)-plane. Correspondingly, the set of zeros s' is in the stable region of the s-plane, and thus all zeros of the set have negative real parts. Let now (a,b) vary from (a'b') in such fashion that it crosses the stability boundary and thus takes up the position (a",b") in the unstable region. Then the corresponding set of zeros s" enfolds one or more zeros with positive real parts. If it is of interest to know the number with positive real parts, this can be obtained as follows.

Since, in general, (16) and (17) are even-powered in w^2, it follows that both + w' and -w' (where w' is an arbitrarily-specified value of w) correspond to the same point (a,b) on the branch of the stability boundary furnished by (16) and (17). Thus, in crossing this boundary once from the stable to the unstable region, two of the set of zeros of f(s) experience a change from negative real part to positive real part. On the other hand, crossing the branch enfolded by (22) corresponds to passage through the origin of the s-plane. Accordingly, one of the set of zeros of f(s) will experience a change from the negative real part to the positive real part.

B. Illustrative Example

The D-decomposition of the (a,b)-plane afforded by the characteristic equation (23) of the illustrative example of Section 2-B and indication thereon of the stable region are shown in Fig. 2. This figure is effected as follows. The hyperbola and the straight line demarking the (a,b)-plane are defined respectively by (33), (34) and by (36). As by (33) and (34) the parameters a and b have the same sign for a specified value of w, only those portions of the branches of the hyperbola which appear in the first and third quadrants of the (a,b)-plane can possibly comprise the map of the jw-axis of the s-plane, $w \neq 0$; further a portion of the branch in the third quadrant corresponds to imaginary values of w; hence must be excluded--as shown. The corresponding shading indicating the stable region is effected as follows. For the branch of the hyperbola in the first quadrant, $\Delta > 0$ when $w > (1/10)^{1/2}$; whence the stable domain lies to the left of the traverse of the branch in the direction of increasing positive w. Next, as another part of the boundary of the stable domain is afforded by the real axis b = 0, defined by (36), the stable region lies above the positive portion and below the negative portion of the real axis. Finally, as a necessary condition for stability is that all coefficients in (23) be of the same sign, b must be of the same sign as a in the stable region. Herewith, then, the whole of the stable domain is demarked as in Fig. 2.

It is of interest to corroborate this demarkation by use of, say, Routh's criterion. Thus, from the characteristic equation (23), rewritten here for convenience of reference,

$$(37)\quad 10as^3 + (11a + 10)s^2 + (a+11)s + b = 0$$

Routh's criterion yields

(38)	$10a$	$a + 11$
(39)	$11a+10$	b
(40)	$[(11a+10)(a+11)-10ab]/(11a+10)$	0
(41)	b	0

Necessary and sufficient conditions that the system be stable are that all coefficients in (37) be of the same sign and that each element of the first column be of the same sign. Consider, first, positive values. Then from (38), (40) and (41) it must be that $a > 0$, which encompasses the necessity of the coefficient condition $a > -11$ and of $a > -10/11$ that stems from (39); $11a^2+131a+110-10ab > 0$, whereof the left-member is coeval with the polynomial obtained on eliminating w between (33) and (34), as given by (35); and $b > 0$. The region defined by these three conditions is precisely the part of the stable domain evidenced in the first quadrant of Fig. 2. Consider, secondly, that the elements of the first column are all negative. Then, from (39), (40) and (41) and the coefficient condition it must be that $a < -11$, which encompasses the necessity of $a < 0$ that stems from (38) and $a < -10/11$ which stems from (39); $11a^2+131a+110-10ab > 0$; and $b < 0$. The region defined by these three conditions is precisely the remaining part of the stable domain evidenced in the third quadrant of Fig. 2.

C. Conclusion

Thus, in the illustrative example of Section 2-B, analysis by Routh's criterion confirms the correctness of the parametric stability analysis afforded by the D-decomposition. In reference to this corroboration, and in conclusion of this section, it is to be noted that though a parametric stability analysis can always be effected by use of Routh's or Hurwitz's criterion, if the parametric characteristic polynomial is other than a simple quadratic or cubic, the pertinent analysis is lengthy to effect, and verges on the intractable for high-order equations. On the other hand, the nature of the D-decomposition method is such that stability analysis is easily effected for any

order or degree of parametric complexity of the characteristic equation --whence its powerfulness and usefulness for parametric stability analysis.

4. Basic Control Theory Analysis by D-Decomposition

A. D-decomposition with Gain as Variable Parameter

Consider a unity-feedback single-loop control system with block diagram as in Fig. 3. Thereof the standard form of the forward transfer function G(s) is

$$(42)\quad G(s)=KG'(s)=K\prod_{i=1}^{n}[(s/a_i)+1]/\prod_{j=1}^{m}[(s/b_j)+1]$$

and the closed-loop transfer function is

$$(43)\quad C(s)/R(s)=KG'(s)/[1+KG'(s)]$$

whence division of the numerator and denominator of the right-hand member by G'(s) yields

$$(44)\quad C(s)/R(s) = K/\{K+[1/G'(s)]\}$$

The characteristic equation of the system of Fig. 3 is, therefore, afforded by

$$(45)\quad K+[1/G'(s)] = 0$$

and thus, equivalently, by

$$(46)\quad K= -1/G'(s)$$

If s traverses the imaginary axis of the s-plane from w=-∞ to w =+ , the map of the moving point in the K(s) = -1/G'(s)--plane furnishes the D-decomposition of this plane.

Let the real part K_r of K(jw) be designated by u, the imaginary part K_i by v. Then

$$(47)\quad K(jw)=K_r(w)+jK_i(w)\equiv u(w)+jv(w)=-1/G'(jw)$$

Let the polynomials in jw comprising the numerator and denominator of G'(jw), as indicated in (42), be designated by P(jw) and Q(jw). Thus,

$$(48)\quad G'(jw) = P(jw)/Q(jw)$$

Evidencing the real and imaginary parts of P(jw) and Q(jw) by

$$(49)\quad P(jw) = P_1(w) + jP_2(w)$$

$$(50)\quad Q(jw) = Q_1(w) + jQ_2(w)$$

as in Section 2, substituting therefrom in (48) and thencefrom into (47), and rationalizing the right-hand member of the resulting expression gives

$$(51)\quad K_r(w)\equiv u(w)=-[Q_1(w)P_1(w) - Q_2(w)P_2(w)]/[P_1^2(w)+P_2^2(w)]=D_1(w)/\Delta(w)$$

$$(52)\quad K_i(w)\equiv-[Q_2(w)P_1(w)-Q_1(w)P_2(w)]/[P_1^2(w)+P_2^2(w)]=D_2(w)/\Delta(w)$$

wherein, paralleling (18) to (20),

$$(53)\quad \Delta(w) = P_1^2(w) + P_2^2(w)$$

$$(54)\quad D_1(w) = -[Q_1(w)P_1(w)-Q_2(w)P_2(w)]$$

$$(55)\quad D_2(w) = -[Q_2(w)P_1(w)-Q_1(w)P_2(w)]$$

As $\Delta(w)$ in (53) is the sum of two squares, $\Delta(w)$ is positive for all values of w. Accordingly, the stable region of the decomposed K(s)-plane lies always to the left side of the plot of K(jw) as this is traversed in the direction of increasing w. This may be so shaded correspondingly to enable quick recognition of the stable region--as typified in Fig. 4.

B. Determination of Ranges of Stability

In the system of Fig. 3, with overall transfer function C(s)/R(s) as defined in (43), the gain constant K is a real constant, positive values corresponding to degenerative feed-back and negative values to regenerative feedback. Correspondingly, those portions of the real axis of the K(s)-plane which fall within the stable region of the D-decomposition of this plane comprise the ranges of K for which the system is stable. Obviously, the values of K corresponding to the limits of these ranges are the values of the K-coordinates of the points of intersection of the plot of K(jw) with the K_r-axis. These end-point values of K, and the corresponding values of w scaled on the plot of K(jw), are critical values of performance--hence, they may appropriately be termed critical values of K and w and be designated by K_{cr} and w_{cr}, as in Fig. 4.

C. Determination of Frequency Response

The D-decomposition of the K(jw)-plane enables rapid determination of the overall frequency response C(jw)/R(jw) of the system of Fig. 4. Thus, relative to Fig. 5, let K_o designate an arbitrarily-specified gain; $\vec{ab}$ the directed vector from the origin to the point $(K_o,0)$; $\vec{ac}$ the directed vector from the origin to an arbitrarily-selected point on the plot of K(jw), at frequency w_1. Then

$$(56)\quad \vec{ab} = K_o$$

and

$$(57)\quad \vec{bc} = \vec{ab}-\vec{ac} = K_o-K(jw_1) = K_o+[1/G'(jw_1)]$$

It follows from (44) that

$$(58)\quad C(jw)/R(jw)\equiv M(w)e^{j\,\theta(w)}= K_o/\{K_o+[1/G'(jw_1)]\} = \vec{ab}/\vec{bc}$$

Thus,

(59) $M(w) = \overline{ab}/\overline{bc}$

and

(60) $\theta(w) = (\text{angle } \overrightarrow{ab} - \text{angle } \overrightarrow{bc}) = -\text{angle } \overrightarrow{bc}$

since angle ab = 0.

The real and imaginary parts of C(jw)/R(jw) are likewise easily found from the D-decomposition of the K(jw)-plane, as typified in Fig. 5. Thus, taking $C(jw)/R(jw) = p(w) + jq(w)$ yields

(61) $p(w) = M(w) \cos \theta(w)$

and

(62) $q(w) = M(w) \sin \theta(w)$

It follows from Fig. 5, whereon $\overrightarrow{ad}$ is a directed perpendicular to $\overrightarrow{bc}$, that as $\cos(\pi + \theta) = \overline{bd}/\overline{ab}$ and $\sin(\pi + \theta) = \overline{ad}/\overline{ab}$, that

(63) $\cos \theta = -(\overline{bd}/\overline{ab})$

(64) $\sin \theta = -(\overline{ad}/\overline{ab})$

whereof θ carries its own sign according to the usual trigonometric conventions. Substitution from (59), (63) and (64) in (61) and (62) gives the desired expressions

(65) $p(w) = -(\overline{ab}/\overline{bc})(\overline{bd}/\overline{ab}) = -\overline{bd}/\overline{bc}$

(66) $q(w) = -(\overline{ab}/\overline{bc})(\overline{ad}/\overline{ab}) = -\overline{ad}/\overline{bc}$

These expressions for p(w) and q(w) are of use in determination of the transient response of the system of Fig. 3 from the overall frequency response, as afforded by D-decomposition of the K(jw)-plane, as is discussed in detail in the following Section 5.

D. Conclusion

Determination of the gain K_m yielding a specified maximum magnitude M_m of the overall frequency response, commonly taken as 1.3 or 1.4, often comprises a prime phase of design of a control system as in Fig. 3. K_m is easily afforded by D-decomposition, as is detailed in Section 6, in somewhat more general form, together with a numerical example which amply illustrates the ease with which the overall frequency-response characteristics; the critical values K_{cr} of gain K limiting the ranges of stability and the corresponding values w_{cr}; the maximum magnitude M_m of the frequency response which corresponds to specified gain K_o; and the gain K_m yielding a specified maximum magnitude M_m of frequency response can be determined by use of the D-decomposition of the K(jw)-plane, as afforded by plot of K(jw) from (47).

5. Determination of Transient Response By D-Decomposition

A. Expression of Transient Response in Terms of Frequency Response

Determination of the transient response c(t) of a servomechanism from knowledge of its frequency response C(jw) reduces, essentially, to effecting the inversion of the transform C(s) of the response c(t). Thus, by well-known theory, if

1. All singularities of C(s) are to the left of the imaginary axis, the w-axis, of the s-plane;
2. F(s) approaches zero with respect to the phase of s as $s \to \infty$ for $-\pi/2 \leq$ phase $s \leq \pi/2$; and
3. $\int_{-\infty}^{\infty} |F(jw)|\, dw$ converges,

then in the complex inversion theorem for C(s)

(67) $c(t) = (1/2\pi j) \int_{c_o - j\infty}^{c_o + j\infty} C(s)\, e^{st} ds$

the conditions 1, 2, and 3 above are such that c_o can be taken as zero; whence the line of integration $s_o = c_o + jw$ pertinent to (67) is the imaginary axis defined by s = jw, and thus (67) becomes

(68) $c(t) = (1/2\pi) \int_{-\infty}^{\infty} C(jw)\, e^{jwt}\, dw$

In practice, the transient response commonly desired is that produced by unit step-function input, wherefor r(t) = u(t), and R(s) = 1/s. If, then, the overall transfer function of the system is denoted by F(s), the transform of the corresponding response is C(s) = R(s)F(s) = F(s)/s. By the final value theorem $c(\infty) = F(0)$. Accordingly, writing C(s) = F(0)/s + [F(s)-F(0)]/s, substituting in (67), inverting the first term, and replacing the second by its equivalent from (68) yields

(69) $c(t) = F(0)u(t) + (1/2\pi) \int_{-\infty}^{\infty} [F(jw) - F(0)](e^{jwt}/w)\, dw$

In lumped-parameter systems the transfer function results as the ratio of two polynomials in s: thus,

(70) $F(s) = (a_o + a_1 s + \ldots + a_n s^n)/(b_o + b_1 s + \ldots + b_n s^n)$

Substituting s = jw in (70) and rationalizing yields an expression of the form

(71) $F(jw) = P(w) + jQ(w)$

wherein P(w) and Q(w) are, respectively, even and odd functions of w. Further, inasmuch as Q(w) is odd in w, Q(0) = 0; and thus

(72) $F(0) = P(0)$

Substituting from (71) and (72) in (69) gives

(73) $c(t)=P(0)u(t)+(1/2\pi)\int_{-\infty}^{\infty}$

$$\left\{[P(w)+jQ(w)-P(0)]/w\right\}\ (\cos wt+j\sin wt)dw$$

By argument based on P(w) and Q(w) as even and odd functions, it is easily deduced that

(74) $c(t) = (2/\pi)\int_{0}^{\infty}[P(w)/w]\ \sin wt\ dw$

or

(75) $c(t)=P(0)+(2/\pi)\int_{0}^{\infty}[Q(w)/w]\ \cos wt\ dw,$

each valid for $t>0$.

B. Trapezoidal Evaluation of Transient Response Integrals

As evidenced in Section 4 by (65) and (66), the real and imaginary parts P(w) and Q(w) of the overall frequency transfer function F(jw) of (71) can be evaluated by use of the D-decomposition of the K(jw)-plane. This fact, and the fact that c(t) as given by (74) and (75) is expressed in terms of P(w) and Q(w), suggests that the transient response can also be evaluated by use of D-decomposition. Such is actually the case and can be effected as follows.

Suppose, first, that P(w) is such that it can be trapezoidally approximated as in Fig. 6. Then, approximately,

(76) $P(w) = P(0)$ $\qquad 0\leq w\leq w_o$

(77) $P(w) = P(0)-[(w-w_o)/(w_1-w_o)]P(0)$ $\qquad w_o\leq w\leq w_1$

(78) $P(w) = 0$ $\qquad w\geq w_1$

Substituting accordingly in (74) gives

(79) $c(t)=(2/\pi)P(0)\left\{\int_{0}^{w_o}[(\sin wt)/w]dw+\right.$

$$\int_{w_o}^{w_1}[(\sin wt)/w]dw$$

$$\left.-\int_{w_o}^{w_1}[(w-w_o)/(w_1-w_o)][(\sin wt)/w]dw\right.$$

or

(80) $c(t)=(2/\pi)P(0)\left\{Si(w_1t)+[1/t(w_1-w_o)]\right.$

$$(\cos w_1t-\cos w_ot)$$

$$\left.+[w_o/(w_1-w_o)][Si(w_1t)-Si(w_ot)]\right\}$$

wherein the Si function is defined by

(81) $Si(wt) = \int_{0}^{w}[(\sin wt)/w]dw$

On defining $x = w_o/w_1$ and $t' = w_1t$, (80) can be written in the form

(82) $c(t)/P(0)=(2/\pi)\left\{Si\ t'+[1/t'(1-x)]\right.$

$$(\cos t'-\cos xt')$$

$$\left.+[x/(1-x)](Si\ t'-Si\ xt')\right.$$

A table of values of the right-hand member of (82) is given in Reference 4. It furnishes immediately the value of c(t)/P(0) for specified values of x and t'.

Commonly, P(w) cannot be approximated by a single trapezoid as in Fig. 6. However, P(w) can always be approximated by an algebraic superposition of, say, n such trapezoids, as detailed in several books on automatic control theory. In such case the i-th trapezoidal component yields the contribution $c_i(t)/P_i(0)$ to the total response c(t); and summation accordingly by

$c(t)=\sum_{i=1}^{n}P_i(0)[c_i(t)/P_i(0)]$ gives the desired transient response c(t).

An expression for c(t) analogous to that of (82) is readily deduced in similar fashion from (75): but as a table of values similar to that mentioned for use with (82) is not available, this equation is not as convenient to use.

C. Determination of Curves of Constant P(w) and Q(w)

Substitution from (47) in (58) yields

(83) $C(jw)/R(jw)=K_o/[(K_o-u) - jv]$

Rationalizing the right-hand member of (83), and noting (71), yields

(84) $P(w) = (K_o^2-K_ou)/[(K_o-u)^2 + v^2]$

and

(85) $Q(w) = K_ov/[(K_o-u)^2 + v^2]$

Simple algebraic manipulation of (84) and (85) gives

(86) $\left\{u-K_o[1-0.5\ P^{-1}(w)]\right\}^2+v^2=[K_o/2\ P(w)]^2$

and

(87) $(u-K_o)^2+[v-0.5\ K_oQ^{-1}(w)]^2 = [K_o/2Q(w)]^2$

Equation (86) evidences the curves of constant P(w) as a family of circles in the K(jw)-plane, with centers at the points $\{K_o[1-0.5\ P^{-1}(w)],\ 0\}$ on the K_r-axis and of radii $|K_o/2\ P(w)|$. Similarly, (87) evidences the curves of constant Q(w) as a family of circles, with centers at the points $[K_o, K_o/2\ Q(w)]$ and of radii $|K_o/2\ Q(w)|$. In particular, the circle P(w) = 0 is the straight line (a circle of infinite radius)

passing through the point $(K_o,0)$; and the circle $P(w) = 1$ is the circle centered on the point $[K_o/2,0]$ and of radius $|K_o/2|$. Illustratively, these two circles and some of the other members of the two sets of orthogonal circles are exhibited in Fig. 7, for $K_o = 4$.

D. Criterion for Single Trapezoidal Approximation of P(w)

Conjunction of the D-decomposition of the K(jw)-plane, as afforded by plot of $K(jw)=-1/G'(jw)$ from (47), and the double family of circles of constant P(w) and Q(w), enables direct approximate calculation of c(t) from (74) and/or (75). For the intersection of the K(jw)-plot with, say, a P-circle furnishes the value $P(w_i)$ for the frequency w_i corresponding to the point of intersection. If, then, these values are obtained at equal increments (Δw) over the significant (usually finite) range $0 < w < w'$, outside of which $P(w)=0$, the right-hand member of (74) can be calculated by numerical integration yielding

$$(88)\quad c(t)=(2\Delta w/\pi)\sum_{i=1}^{i=(w'/\Delta w)}[P(w_i)/w_i]\sin w_i t$$

A corresponding calculation with values furnished by the intersections of the K(jw)-plot and the Q-circles yields

$$(89)\quad c(t)=P(0)+(2\Delta w/\pi)\sum_{i=1}^{i=(w'/\Delta w)}[Q(w_i)/w_i]\cos w_i t$$

Now it often ensues in practice that the plot of P(w) versus w can be significantly approximated by a single trapezoid. That is, appropriate choice of the single trapezoid and calculation therewith from (82), and thus determination of c(t) directly from values entered in the mentioned table of Reference 4, yields an approximate numerical or graphical delineation of c(t) which is in excellent agreement with the actual delineation. Obviously, it is most desirable to know the conditions under which such rapid delineation of the transient response c(t) is possible.

To ascertain such, consider first that $F(jw)=P(w)+jQ(w)$ is such that the P(w)-plot actually comprises a single trapezoid, as in Fig. 6. Then the D-decomposition furnished by plot of K(jw) relative to the circles of constant P(w) and Q(w) will be as evidenced in Fig. 8. Namely, over the range $0 \leq w \leq w_o$ wherefor $P(w) = 1$, the plot is tangent (coincident) to the circle of constant $P(w) = 1$; departs from it at $w = w_o$ such as to intersect successive circles of decreasing constant values of P(w) as w runs over the range $w_o \leq w \leq w_1$; becomes tangent to the line of constant P(w) $= 0$ at $w = w_1$; and thereafter remains tangent (coincident) to this line.

Correspondingly, if the actual plot of P(w) versus w can be well-approximated by a single trapezoid, such will be manifested by the fact that the actual plot of K(jw) will be substantially coincident with the circle $P(w) = 1$ over a range $0 \leq w \leq w_o$; whence the approximate frequency of departure from approximate tangency furnishes the desired approximation to w_o; will intersect successive circles of decreasing values of constant P(w) as w increases up to a value w_1 at which it intersects the line of constant $P(w) = 0$; and thereafter will tend to intersection with (usually) circles of small negative values of constant P(w) as w approaches infinity. A typical plot of K(jw) is so illustrated in Fig. 9.

If, in particular, as is often the case, the plot of K(jw) tends, after a certain angular span over which it is substantially tangent to both the circle of constant $P(w) = 1$ and the circle of radius K_o centered at the point $(K_o,0)$ for the range $0 \leq w \leq w_o$, thereafter to remain outside of the "K_o-circle"; and the radially measured distance between K_o-circle and the plot of K(jw) continually increases, the plot of P(w) versus w is especially well-approximated by a single pertinently-chosen trapezoid.

In conclusion, it is to be noted that when the P(w)-plot can be trapezoidally approximated, and thus c(t) is directly furnished by use of the values of the mentioned table, the overshoot in c(t) cannot substantially exceed 18% at most: for the largest value of c(t) tabulated in this table is 1.178. Further, the settling-time t_s, defined as the time required for c(t) to both come within plus or minus a certain percentage of the final value, can be substantially delimited by inspection of the table. Thus, illustratively, for the commonly used value of $\pm$ 5%, this table yields $\pi/w_1 \leq t \leq 4\pi/w_1$.

E. An Illustrative Example

To illustrate the foregoing analysis without obscurement by heavy, but routine, algebraic and trigonometric manipulation, consider the system as in Fig. 3 whereof the forward link is of transfer function

$$(90)\quad G'(jw) = 1/jw(1+jw)$$

and thus

$$(91)\quad K(jw) = -jw(1+jw) = w^2-jw$$

and the gain is $K_o = 0.5$. The plot of K(jw) is as in Fig. 10. The plot is substantially tangent to the P(w) = 1 circle from w = 0 up to w = 0.127, crosses the P(w) = 0 line at w = 0.72, does not cut the K_o-circle, and departs appreciably from it after a span of 30°. Thus, $w_o = -0.127$ and $w_1 = 0.72$; whence x = 0.175. Use of the values used in plotting Fig. 10 (interpolating by inspection between x = 0.15 and x = 0.2) and noting that $t = t'/0.72$ yields values of response c(t) as plotted in Fig. 11.

Corroboratively, direct inversion of the

transform of the response

(92) $C(s) = 0.5/s(s^2+s+0.5)$

yields the time response

(93) $c(t) = 1 + 1.414\, e^{-0.5t} \sin(0.5t-135^o)$

and plot from (93) on Fig. 11 gives a curve which well-approximates that first obtained.

If, now, $K_o=2$, the plot of K(jw) is relative to the corresponding K_o-circle as in Fig. 12. As over the range $0 \leq w \leq 1.75$ it lies substantially inside the K_o-circle, it follows both that the transient response c(t) cannot be effected as simply as for $K_o=0.5$ and that the percent overshoot will be substantially greater than 18%. Corroboratively, inversion of the transform of the transient response

(94) $C(s) = 2/s(s^2+s+2)$

yields

(95) $c(t) = 1+1.07\, e^{-0.5t}\sin(1.32t-110.7^o)$

and plot of this response yields an overshoot of approximately 30%, as evidenced in Fig. 11.

F. Conclusion

The foregoing illustrative example amply evidences the technique for determination of approximate transient response by use of D-decomposition, the rapidity with which it can be obtained when the analysis is applicable, and the general use of the P-circles for ascertaining whether or not the percent overshoot of this response is less than the specified value of 18%.

Finally, it is to be noted that when the response cannot be evaluated rapidly in the manner illustrated by the illustrative problem for $K_o = 0.5$, the intersections of the K(jw)-plot with the P(w)-circles or Q(w)-circles afford values of P(w) or Q(w) which enable rapid graphical or numerical computation of the integrals of (74) or (75), and thus of c(t).

6. Generalization to Nonunity Feedback Systems

It is often the case in practice that a control system is other than of unity feedback as in Fig. 3. Accordingly, it is obviously desirable to extend the theory developed for this latter system to encompass the more general case of nonunity-feedback systems. Such systems comprise two broad categories: those whereof the transfer function of the feedback link is a numeric, including 1 as a special case; and those whereof the transfer function of the feedback link is frequency-dependent. It is convenient to consider each in turn, in the stated order.

A. Numeric Transfer Function

By well-known theory, the overall transfer function of the general system with block diagram as in Fig. 13 is

(96) $C(s)/R(s) = KG'(s)/[1+KG'(s)H(s)]$

whence the characteristic equation is

(97) $1 + KG'(s)H(s) = 0$

For the case under consideration, H(s) a numeric-say H, (96) reduces to

(98) $C(s)/R(s) = KG'(s)/[1+KHG'(s)]$

and (97) to

(99) $1 + KHG'(s) = 0$

Denoting KH by K_o, and taking as in (46) that $K(jw) = -1/G'(jw)$, enables recast of (98) as

(100) $C(jw)/R(jw)=(1/H)\left\{K_o/[K_o-K(jw)]\right\}$

In that the bracketed term in (100) is identical with the right-hand member afforded by (58), it follows that relative to Fig. 5,

(101) $K_o/[K_o-K(jw)] = \vec{ab}/\vec{bc}$

and that as (1/H) is of zero phase, the phase of C(jw)/R(jw) is yet the angle θ of Fig. 5. Substituting accordingly in (100) gives

(102) $C(jw)/R(jw)=M(w)e^{j\theta(w)}=(1/H)(\vec{ab}/\vec{bc})e^{j\theta}$

Now as by (102), $M(w) = (1/H)(\overline{ab}/\overline{bc})$, and as $K_o = \overline{ab}$, it follows that the maximum value M_m of M(w) for a specified gain K_o corresponds to the minimum value R of bc, and thus is afforded by $M_m = (1/H)(\overline{ab}/R)$. Corroboratively, if H = 1, then $M_m = (\overline{ab}/R)$, in agreement with (59).

Further, determination of the gain K_o which yields a specified maximum value M_m of M(w) can be effected by the simple artifice of recasting the determination as that for K_o which yields the specified maximum value $M_m' = M_mH = \overline{ab}/\overline{bc}$. Herewith, then, determination of the desired value of K_o proceeds as remarked in Section 4-D.

Again, the critical values of gain and frequency delimiting the ranges of stability are furnished as detailed in Section 4-B.

The curves furnishing the real and imaginary parts of C(jw)/R(jw)=P(w)+jQ(w) are easily obtained. Taking

(103) $K(jw) = K_r + jK_i = u + jv$

and substituting accordingly in (100) gives

(104) $P(w) + jQ(w) = (K_o/H)[K_o-u-jv]$

Rationalizing the right-hand member of (104), comparing real and imaginary parts of the two members, and manipulating the resulting expressions for P(w) and Q(w) yields

$$(105)\quad \left\{u - K_o\,[1-1/2HP(w)]\right\}^2 = [K_o/2HP(w)]^2$$

and

$$(106)\quad (u-K_o)^2 + [v-K_o/2HQ(w)]^2=[K_o/2HQ(w)]^2$$

Corroboratively, if H = 1, these expressions reduce to the corresponding expressions of (86) and (87).

Comparison of (86) and (105) and of (87) and (106) evidences identity of corresponding pairs of equations except for replacement of P(w) by HP(w) and of Q(w) by HQ(w). Accordingly, it follows: that the double family of circles in Fig. 7, for unity feedback, can be used for numeric feedback providing only that the constant values characterizing the circles are interpreted as values of constant HP(w) and HQ(w); and that the intersections of these circles with a scaled plot of K(jw) thereon yields corresponding values of w,HP(w), and HQ(w). These furnish, in turn, plots of P(w) versus w and Q(w) versus w for a specified value of H.

Next, knowledge of these values enables numerical or graphical delineation of the transient response c(t) to unit step-function input through use of (88) or (89), or by trapezoidal approximation through use of (82).

Finally, determination of the pertinent circles of P(w) = 1, P(w) = 0, and the K_o-circle, enabling use of the criterion for limited overshoot developed in Section 5, is easily effected. For: from (105) the circle of constant HP(w) wherefor P(w) = 1 is that centered at $\{K_o[1-(1/2H)],0\}$ and of radius $|(K_o/2H)|$; that for P(w) = 0 is the vertical line through the point $(K_o,0)$, and the K_o-circle is that centered at the point $(K_o,0)$ and tangent to the just-established circle wherefor P(w) = 1. These circles, and other members of the family of constant P(w)-circles, together with a plot of K(jw) are typified in Fig. 13 for H = 2. Obviously, the plot of K(jw) relative to the K_o-circles is such that the criterion limiting overshoot to a maximum of approximately 18% is satisfied.

B. Frequency-dependent Feedback

If the feedback link is frequency-dependent, it follows from (97) that

$$(107)\quad K(jw) = -1/G'(jw)H(jw)$$

Determination of the overall frequency response now proceeds as follows. Equation (96) can be recast in the form

$$(108)\quad H(s)\,C(s)/R(s) = K/[K+1/G'(s)H(s)]$$

Then as the right-hand member of (108) is identical with the right-hand member of (44) except for replacement of G'(s) by G'(s)H(s), it follows that the D-decomposition indicated in Fig. 5, wherefor K(jw) is now as in (107), yields $H(jw)\cdot C(jw)/R(jw) = \vec{ab}/\vec{bc}$. If, on this figure 1/H(jw) is evidenced for convenience, it then follows as typified in Fig. 14 that

$$(109)\quad C(jw)/R(jw)=M(w)e^{j\theta(w)}=$$
$$\vec{ac}_1(\vec{ab}/\vec{bc})=\vec{ac}_1(\vec{ab}/\vec{bc})e^{-j(\theta'-\beta)}$$

Herewith, the real and imaginary parts of C(jw)/R(jw) = P(w) + jQ(w) are readily established, enabling determination of transient response c(t) from (88) and (89). Further, the critical values of gain and frequency delimiting the ranges of stability are furnished by Fig. 14, in the same manner as furnished by Fig. 4 for unity feedback.

Finally, it is to be noted that in virtue of the frequency dependence of H(jw), the curves of constant P(w) and Q(w) are intractable, to the end that a criterion delimiting approximate maximum overshoot cannot be evolved as for numeric feedback.

C. Analytic Delimination of Stability by D-decomposition

Although, as just remarked, the critical values of gain K_{cr} and frequency w_{cr}, as furnished by D-decomposition afforded by (107), can be obtained from the graphical delineation of Fig. 14, it is also of interest to advance an equivalent analytic determination of these values which, often, is more convenient to use if these values alone are of prime interest.

Now, both as remarked earlier in connection with Fig. 4 and as evidenced here in the corresponding Fig. 14, the desired values K_{cr} and w_{cr} are those associated with the intersection of the K(jw)-plot with the K_r-axis: thus the values wherefor $K_i(w) = 0$. Taking now $K(jw) = -1/G'(jw)H(jw) = -q(jw)/p(jw)$ in analogy with (48), it follows from (52) that

$$(110)\quad K_i(w)=[p_1(w)q_2(w)-p_2(w)q_1(w)]/$$
$$[p_1^2(w)+p_2^2(w)] = 0$$

Accordingly, the desired values of w_{cr} are afforded by the zeros of $K_i(w)$, thus by solution of

$$(111)\quad p_1(w)q_2(w) - p_2(w)q_1(w) = 0$$

providing that, as is commonly the case, $[p_1^2(w)+p_2^2(w)] \neq 0$. With these values in hand, (51) yields the desired values of K_{cr} as

$$(112)\quad K_{cr} = [p_1(w)q_1(w)-p_2(w)q_2(w)]/$$
$$[p_1^2(w)+p_2^2(w)]_{w=w_{cr}}$$

D. An Illustrative Example

Consider determination of the critical values K_{cr} and w_{cr} for the system of page 230 of Reference 5 whereof the forward link comprises a cascaded combination of amplifier, amplidyne and motor such that

(113) $K(jw) = -(jw)(1+0.05jw)(1+0.2jw)$

Then, as $K(jw) = -[q_1(w) + jq_2(w)]/[p_1(w)+jp_2(w)]$, simple algebraic manipulation of the right-hand member, yielding

(114) $K(jw) = 0.25w^2 - j(w-0.01w^3)$

gives

(115) $q_1(w) = -0.25w^2$

(116) $q_2(w) = w - 0.01w^3$

(117) $p_1 = 1$

(118) $p_2 = 0$

Substitution accordingly in (111) yields

(119) $w(0.01w^2 - 1) = 0$

whence $w_{cr} = 0$ and 10. Substituting these values in the real part of (114) gives $K_{cr} = 0$ and $K_{cr} = 25$. Correspondingly, the stable range is $0 < K < 25$.

In closure of this section, it may be noted that the especial value of this procedure for delimiting the ranges of stability, as compared with effecting such by use of Routh's or Hurwitz's criterion, is that the values of w_{cr} are furnished; and that complicated and interdependent equations need not be solved to determine the values of K_{cr} -- which is a lengthy task for even a cubic equation; and polynomial equations up to order 8 are not uncommon in modern control work.

E. Conclusion

The theory evolved in this section for the cases of numeric and frequency-dependent feedback both provides generalization of that developed in Sections 4 and 5 for unity feedback systems and enables investigation by use of the method of D-decomposition of means of improving the operating performance of a system by compensation. Limitations of spaces preclude detail here: the interested reader is referred to References 2 and 6 for a lengthy account of theory and illustration by numerical examples.

7. Analysis of Sampled-Data Systems by D-Decompensation

An important class of systems in modern control practice is that of sampled-data systems. In view of the power and usefulness of D-decomposition procedures for the analysis of continuous-type systems, as detailed in previous sections, it is naturally of interest to ascertain whether sampled-data systems can be similarly analyzed. Such is the case -- as is evidenced by the following account of the delimitation of stability.

A. Basic Theory of Delimitation

By well-known theory, the overall transfer function of the unity-feedback sampled-data system with error-sampled forward link G(s) is

(120) $C(s)/R^*(s) = KG'(s)/[1+KG'^*(s)]$

wherein the starred transfer function $G'^*(s)$ of the forward link is

(121) $G'^*(s) = (1/T) \sum_{n=-\infty}^{\infty} G'(s+jnw_s)$

T is the period of sampling, and $w_s = 2\pi/T$ is the (angular) frequency of sampling. From (120) the characteristic equation of the system is

(122) $1 + KG'^*(s) = 0$

and thus by (121) and (122) the D-decomposition of the K(jw)- plane is afforded by

(123) $K(jw) = -T/\sum_{n=-\infty}^{\infty} G'[j(w + nw_s)]$

It is not infrequently the case in practice that the summation of the right-hand member of (123) is sufficiently approximated by the term for n=0. If so, (123) reduces to

(124) $K(jw) = -T/G'(jw)$

Denoting T by

(125) $T = 1/H$

yields

(126) $K(jw) = -1/HG'(jw)$

Now (126) is essentially identical with the decomposition yielded by (99). Accordingly, when the approximation of (124) is valid, D-decomposition analysis of a sampled-data system can be effected as detailed in Section 6 for nonunity numeric feedback systems.

When the approximation of (124) is not valid, it is expedient to effect analysis in terms of z-transforms, rather than s-transforms, as furnished by change of the transform variable through

(127) $z = e^{sT}$; thus, $s = (1/T) \ln z$

Recalling the convention that $G'^*(s) = G'^*[(1/T)\ln z] \equiv G'(z)$, starring each side of (120), and substituting accordingly in the resulting expression yields

(128) $C(z)/R(z) = KG'(z)/[1+KG'(z)]$

whereof for lumped-parameter systems G'(z) is the

ratio of two polynomials P(z) and Q(z) in z; thus,

$$G'(z) = P(z)/Q(z) \tag{129}$$

By (128) the characteristic equation in z is

$$1 + KG'(z) = 0 \tag{130}$$

Now under the transformation of (127) the imaginary axis of the s-plane, defined by s=jw, maps into the curve in the z-plane defined by $z=e^{jwT}$. But as $z = e^{jwT}$ is periodic in 2π, it follows that the strip of the imaginary axis, defined by $w_o \leq w < (2\pi/T) + w_o$, whereof w_o is an arbitrarily-specified value, is mapped on a circle of unit radius centered at the origin of the z-plane; Further, as $z = e^{j\pi(\sigma+jw)} = e^{T\sigma} e^{jwT}$, the strip of the s-plane defined by $w_o \leq w < (2\pi/T) + w_o$, $-\infty \leq \sigma \leq \infty$, is mapped on the whole of the z-plane, the *right*-hand semistrip mapping outside the unit circle. Thus, in the z-plane the boundary of stability is the unit circle, and the stable domain is the interior of this circle.

If, then, in general

$$z = a + jb \tag{131}$$

the boundary of stability is defined by

$$a^2 + b^2 = 1 \tag{132}$$

By (132), $b = (1-a^2)^{1/2}$, and substitution accordingly in (131) yields

$$z = a + j\,(1-a^2)^{1/2} \tag{133}$$

Thus, by (130) and (133), the D-decomposition in the z-plane is afforded by

$$K[a+j(1-a^2)^{1/2}] = K_r(a) + jK_i(a) = (-1/G')[a+j(1-a^2)^{1/2}] \tag{134}$$

Now the values of gain delimiting the ranges of stability are real values; and thus, as in previous sections, these are afforded by the points of intersection of the plot of the right-hand member of (134) with the K_r-axis. Thus, just as outlined for continuous systems in Section 6, the critical values K_{cr} are found by equating the imaginary part, $K_i(a)$, of the right-hand member of (134) to zero; solving the resulting expression for the values of a_{cr}; substituting these values in the real part, $K_r(a)$; and thus obtaining the desired critical values, K_{cr}, of gain. Analytically, this implies denoting the right-hand member of (134) by

$$(-1/G')[a+j(1-a^2)^{1/2}] = p(a) + jq(a). \tag{135}$$

whereof p(a) and q(a) are ratios of two polynomials as in (51) and (52), imposing the condition

$$q(a) = 0 \tag{136}$$

solving (136) to obtain one or more values $a = a_{cr}$; and substituting pertinently to get

$$K_{cr} = p(a_{cr}) \tag{137}$$

The corresponding critical values of frequency w_{cr} are determined by note that (127) gives

$$z = e^{jwT} = \cos wT + j \sin wt \tag{138}$$

and comparison of (131) and (138) gives

$$a = \cos wT \tag{139}$$

Solution of (139) for w and substitution of $a = a_{cr}$ yields

$$w_{cr} = (1/T) \cos^{-1} a_{cr} \tag{140}$$

or, alternatively,

$$w_{cr} = (w_s/2\pi) \cos^{-1}(a_{cr}) \tag{141}$$

B. An Alternative Procedure

From (129) and (130) it follows that K(z) can be expressed, in general, as

$$K(z) = -K' \prod_{j=1}^{m} (z-z_j) \Big/ \prod_{i=1}^{n} (z-z_i) \tag{142}$$

If now, z is a point on the unit circle, then $(z-z_i)$ is a vector drawn from the point z_i to the point z; of modulus $|z-z_i|$ and of the phase, say, ϕ_i; and correspondingly for $(z-z_j)$; as typified in Fig. 15 for real z_i and z_j, which is commonly the case in practice. Accordingly,

$$K(z) = K'\left[-\prod_{j=1}^{m} |z-z_j| \Big/ \prod_{i=1}^{n} |z-z_i|\right] e^{j\left(\sum_{j=1}^{m} \phi_j - \sum_{i=1}^{n} \phi_i\right)} \tag{143}$$

Now K(z) is real when

$$\sum_{j=1}^{m} \phi_j - \sum_{i=1}^{n} \phi_i = k\pi \quad (k=0,\pm 1,\ldots) \tag{144}$$

It is evident from Fig. 15 that A and B will be points where z is such that (144) is satisfied; hence for $z = e^{j0}$ and $z = e^{j\pi}$, K(z) is real and thus yields critical values. At A,

$$w_{cr} = \pi/T \tag{145}$$

and thus

$$K_{cr} = -K' \prod_{j=1}^{m} |-1-z_j| \Big/ \prod_{i=1}^{n} |-1-z_i| \tag{146}$$

At B, w = 0 and

$$K_{cr} = -K' \prod_{j=1}^{m} |1-z_j| \Big/ \prod_{i=1}^{n} |1-z_i| \tag{147}$$

Finally, the possibility exists that at

points on the unit circle other than $z = \pm 1$, the condition of (144) is satisfied. Such can be ascertained by test for a particular system.

C. An Illustrative Example

Consider a system whereof $w_s = 4$ and the transfer function $G'(s)$ of the forward link is

(148) $G'(s) = 1/s(s+1)$

Substituting as indicated in (120) gives

(149) $C(s)/R^*(s) = [K/s(s+1)]/[1+(K2/\pi)\sum_{n=-\infty}^{\infty} 1/(s+jnw_s)(s+1+jnw_s)]$

wherefrom the function affording D-decomposition is

(150) $K(jw) = -(\pi/2)/\sum_{n=-\infty}^{\infty} 1/(jw+jnw_s)(jw+1+jnw_s)$

Approximating (150) by the terms for n=0 and -1 yields

(151) $K(jw) = (\pi/2)[1/(jw)(jw+1)+1/(jw+j4)(jw+j4+1)]$

For w=1, simple but lengthy computation yields

(152) $K(j1) = 2.08 \angle -40^\circ$

For w=2, similar calculation yields

(153) $K(j2) = 3.14 \angle 0^\circ$

Hence, trial as evidenced establishes that $K_{cr} = 3.14$ at $w_{cr} = 2$. Similarly, trial yields $K_{cr} = 0$ at $w_{cr} = 0$. These values afford an approximate check on the following rigorous calculation by use of D-decomposition, as outlined in Sections 7-A and B above.

Substituting appropriately in (128) yields

(154) $C(z)/R(z) = \dfrac{Kz(1-e^{-\pi})/(z-1)(z-e^{-\pi/2})}{1+Kz(1-e^{-\pi})/(z-1)(z-e^{-\pi/2})}$

which is easily reduced to

(155) $C(z)/R(z) = 0.792Kz/[(z-1)(z-0.208)+0.792\ Kz]$

Accordingly, the function affording D-decomposition is

(156) $K(z) = -(z-1)(z-0.208)/0.792z$

and thus

(157) $K[a+j(1-a^2)^{1/2}] = [-1.525(a-1)]-j[(1-a^2)^{1/2}]$

By (136)

(158) $(1-a^2)^{1/2} = 0$

and thus

(159) $a_{cr} = \pm 1$

Substituting $a = 1$ in (137) gives

(160) $K_{cr} = 0$

and substituting $a = -1$ gives

(161) $K_{cr} = 3.05$

Substituting $a_{cr} = 1$ and -1 in turn in (141) gives

(162) $w_{cr} = 0$ and 2

Confirmatively, for solution as indicated by Fig. 16, comparison of (146) and (156) yields

(163) $K_{cr} = -(-1-1)(-1-0.208)/-0.792 = 3.05 \angle 0^\circ$

corresponding, by (145), to $w_{cr} = 2.0$. Similarly, (147) yields

(164) $K_{cr} = -(1-1)(1-0.208)/0.792 = 0$

corresponding to $w_{cr} = 0$.

D. Conclusion

Comparison of corresponding values for $w_{cr}=2$ as given approximately by (153) and accurately by (161), respectively 3.14 and 3.05, evidences a fair approximation. Thus, the error in the first approach is approximately three per cent. Several more terms would be required to obtain a better accuracy with corresponding increase in the labor of obtaining K_{cr}, which even then can be done only by trial as in the two-term approximation. Alternative to this classical approach, delimitation of stability ranges by use of D-decomposition provides a rapid, straightforward procedure for obtaining corresponding values of K_{cr} and w_{cr}, by either of the two procedures detailed in Sections 7-A and B above.

8. Conclusions

The essential values of this paper may be summarized as follows:

1. Attention is directed in Section 1 to the possibilities of developing the concept of D-decomposition into a means of control systems analysis which, in scope, facility of use, and flexibleness of application, could compare favorably with what has been effected with the basic concept of root-locus.
2. Certain aspects of the desired domain of theory is effected in Sections 2 to 7 inclusive.
3. Application in practice of each major phase of the body of theory based on use of D-decomposition, as developed in Sections 2 to 7, is exemplified by one or more illustrative numerical examples.

4. Yet other aspects of theory, illuminated by numerical examples, are detailed in Reference 2 from which this paper stems, and in Reference 6.
5. Comparison of the total available content of this paper and the just-cited references with the content of the numerous papers on root-locus analysis cited in the inclusive bibliography of Reference 1 both evidences the fulfillment of the possibility expressed in item 1 above and the additional possibility of considerably extending the development to-date.
6. Finally, it is to be noted that in virtue of the fulfillment of the tutorial nature of one of the purposes stated in Section 1-A, namely--to advance an integrated account of the method of D-decomposition in English--a portion of the earlier sections on basic aspects of D-decomposition theory comprises content which is well-disseminated in Russian control literature. However, the remaining context, comprising part of the principal contents of Reference 2 (other parts of which are being published in Reference 6) were original to the authors at the time Reference 2 was completed.

References

1. T. J. Higgins, "Classified Bibliography on Automatic Control Systems: Part II. Root Locus and Associated Procedures," A.I.E.E. Conference Paper No. CP58-1270; 1958. See References 67-69 re Russian writings on D-decomposition.

2. R. W. Lanzkron, "D-Decomposition Analysis of Automatic Control Systems," Ph.D. Thesis, Department of Electrical Engineering, University of Wisconsin, Madison, Wisconsin, June 1956.

3. T. Amlie and T.J. Higgins, "A General Theory for Determination of the Stability of Linear Lumped-Parameter Multiple-Loop Servomechanisms (and Other Feedback Systems)," A.I.E.E. Transactions, vol. 74, Part II, 1955, pp. 134-147.

4. V. V. Solodovnikov, "Application of Trapezoidal Frequency Characteristics for Determining the Performance of Automatic Control (in Russian)," Avtomatkia i Telemekhanika, vol. 10, 1949, pp. 362-376.

5. H. Chestnut and R. W. Mayer, "Servomechanism and Regulating Systems," John Wiley and Sons, Inc., New York, N. Y., 1951, p. 85.

6. R. Lanzkron and T.J. Higgins, "Design of Compensation Networks for Automatic Control Systems by D-decomposition with Several Variables," forthcoming paper.

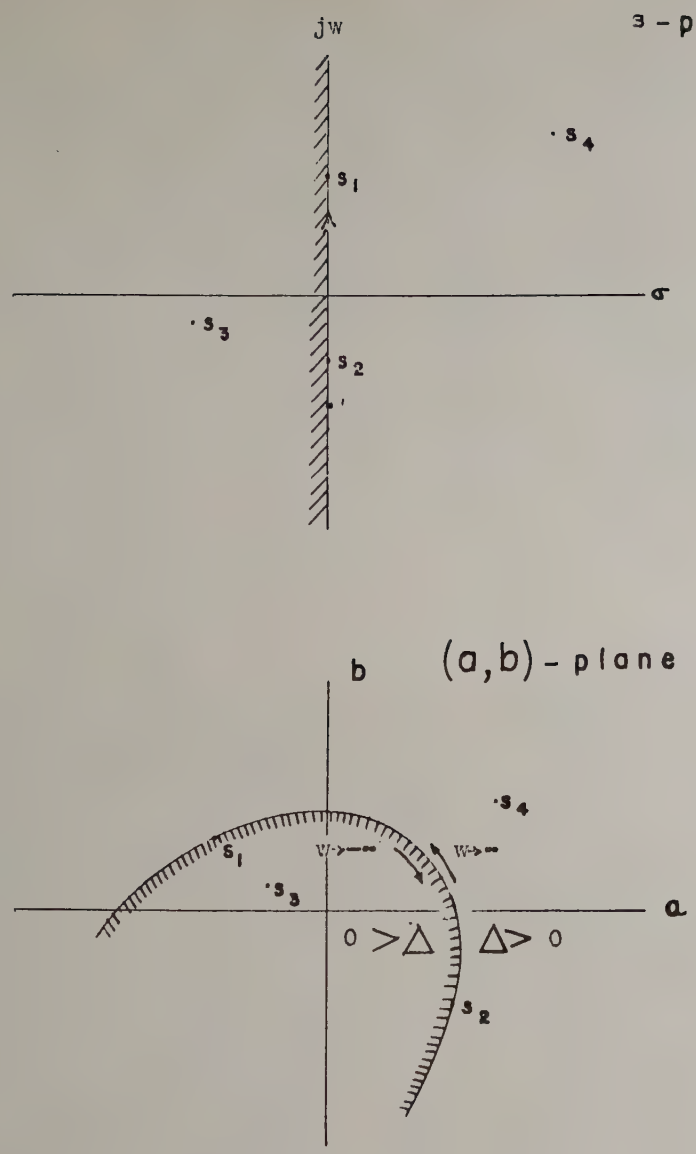

Fig. 1 Mapping of the s-plane on the (a,b)-plane.

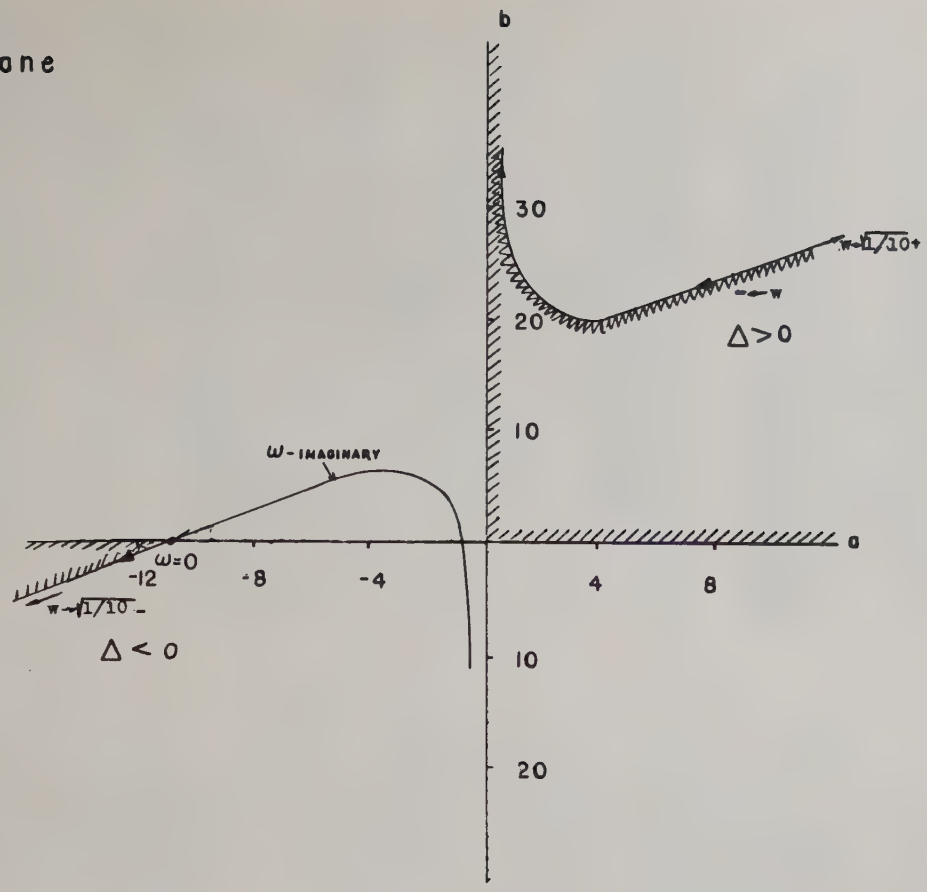

Fig. 2. The D-decomposition for a seryomechanism with characteristic equation, $10as^3 + (11a+10)s^2 + (11+a)s + b = 0$.

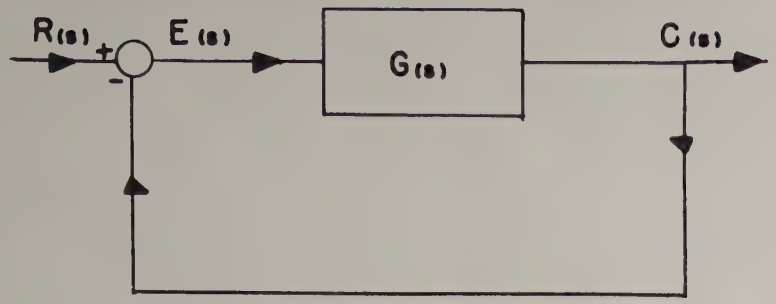

Fig.3. Block diagram of a unity-feedback control system.

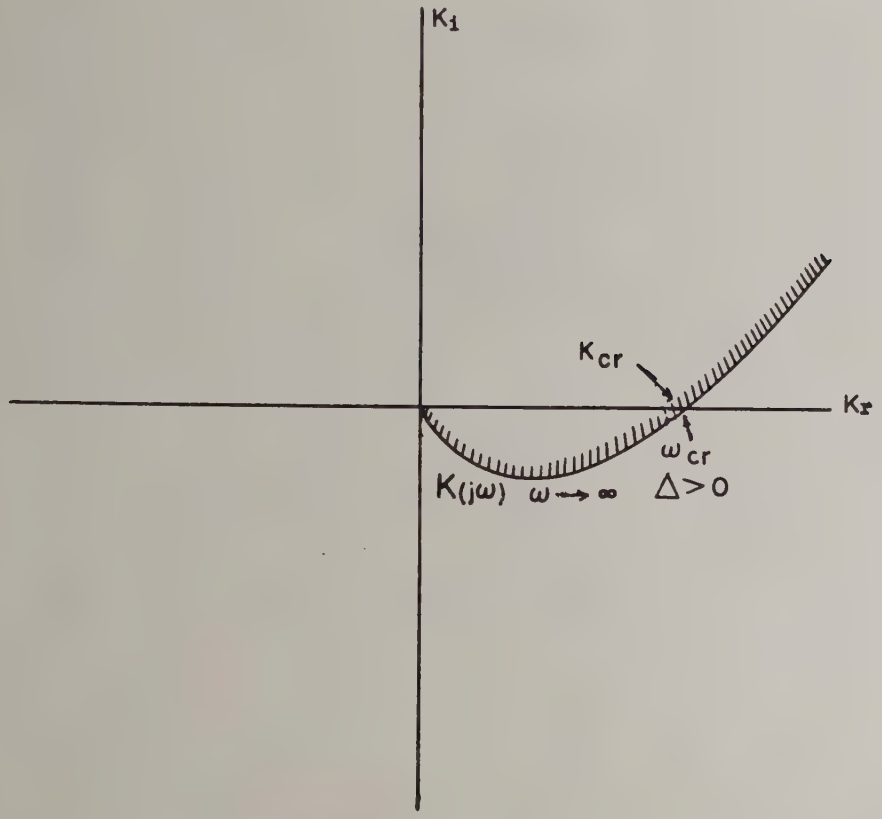

Fig.4. Plot typifying the K(jw)-curve and associated critical values of K and w.

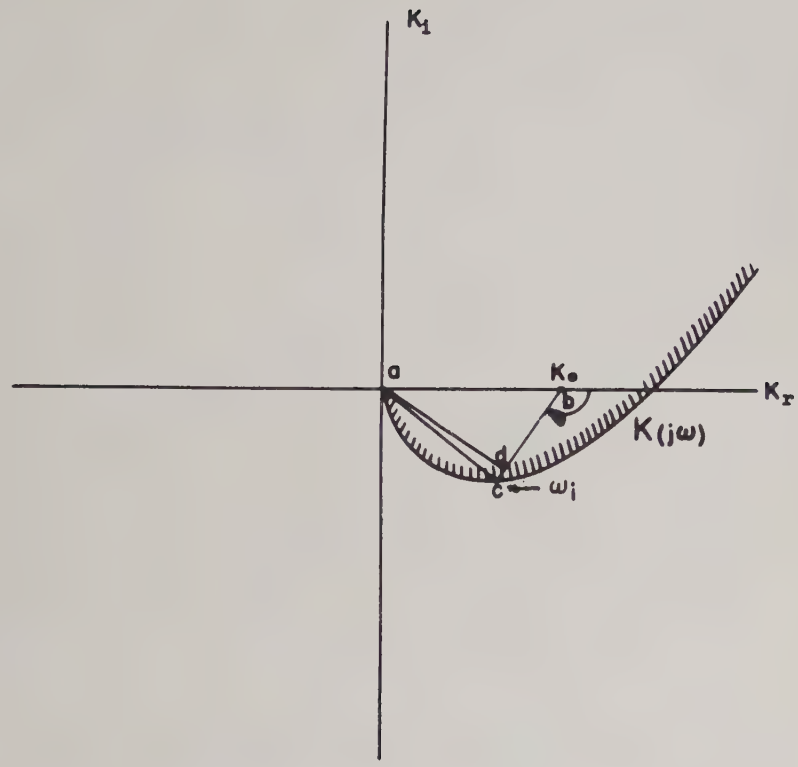

Fig.5. Determination of C(jw)/R(jw), P(w) and Q(w) for a specified K(jw).

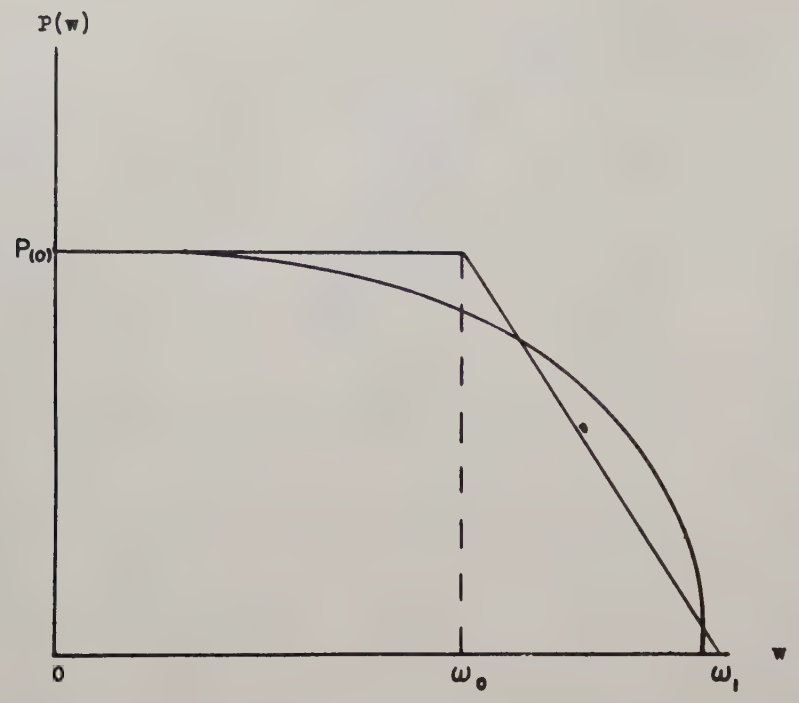

Fig. 6. Approximation of P(w) by line segments.

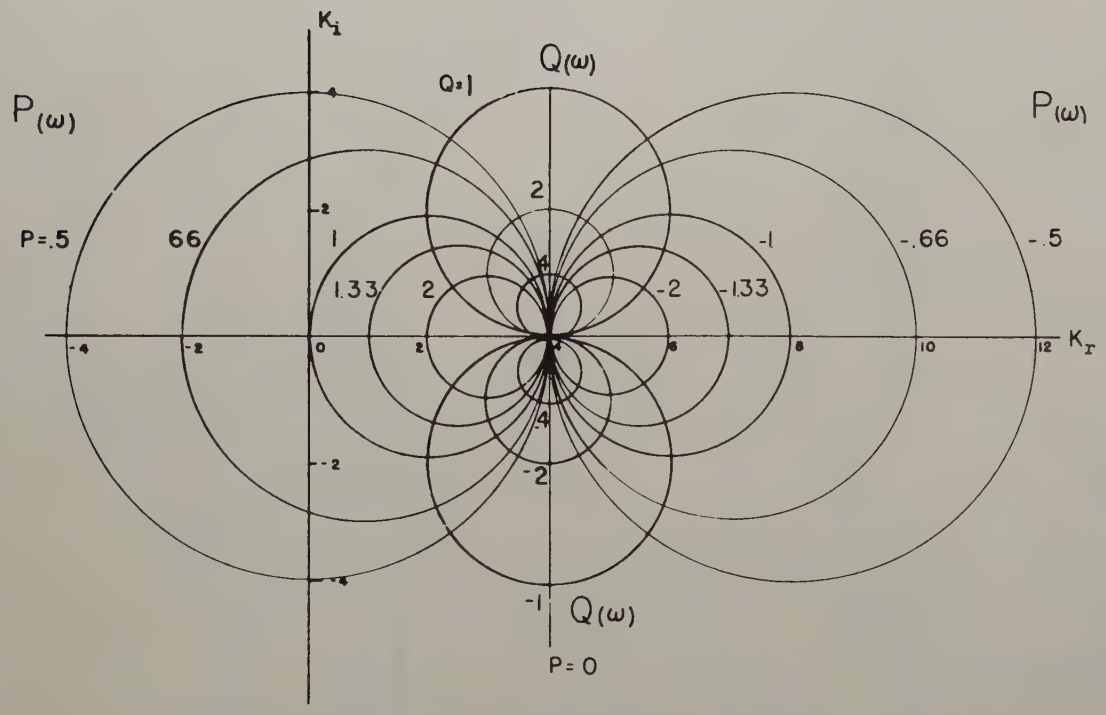

Fig. 7. Orthogonal family of curves of constant P(w) and constant Q(w).

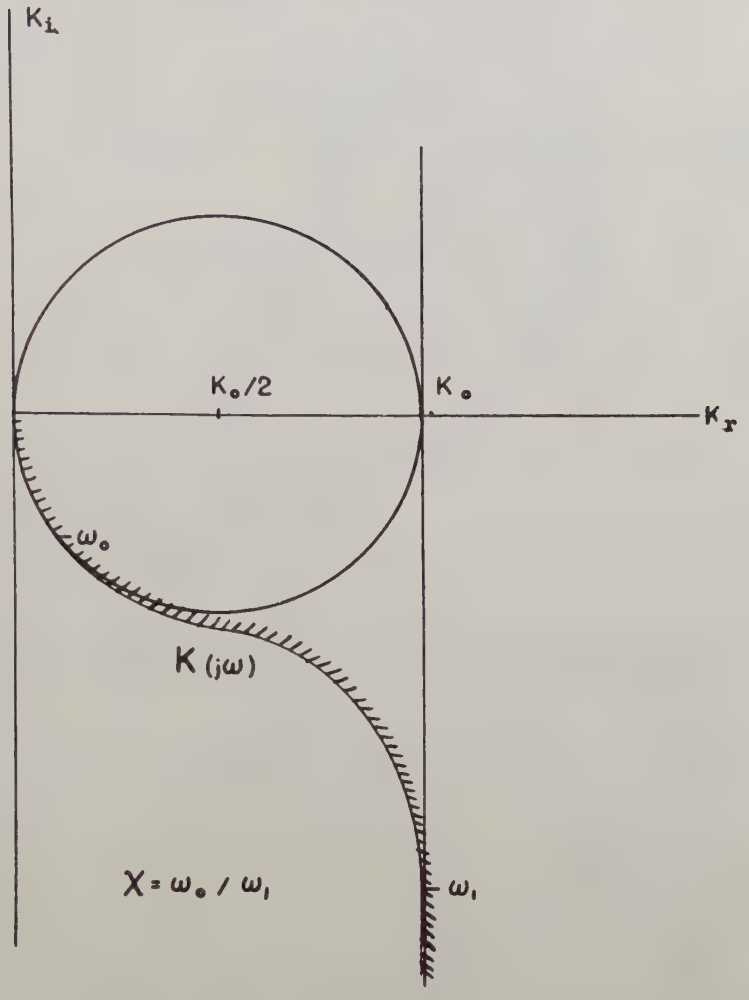

Fig. 8. Plot of K(jw) for a system whereof the P(w) curve is approximation by two line segments as in Fig. 6.

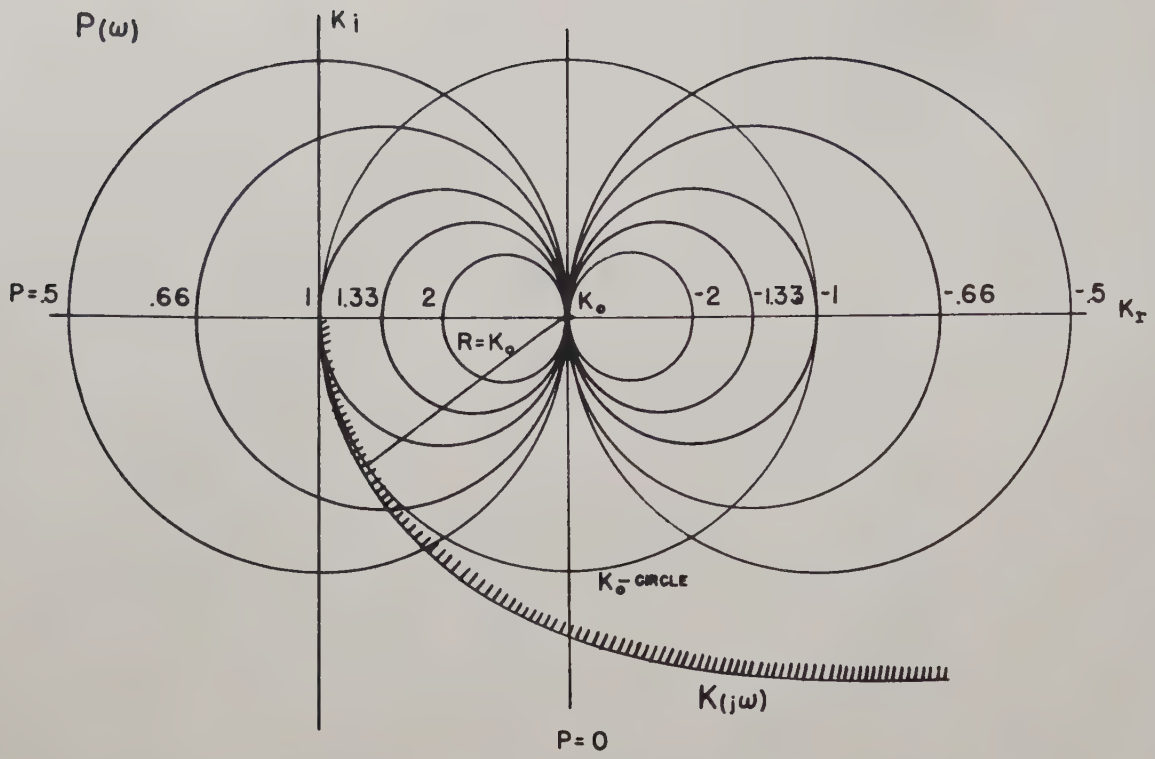

Fig. 9. Plot typifying K(jw)-curve for a system whereof the overshoot is less than 18%.

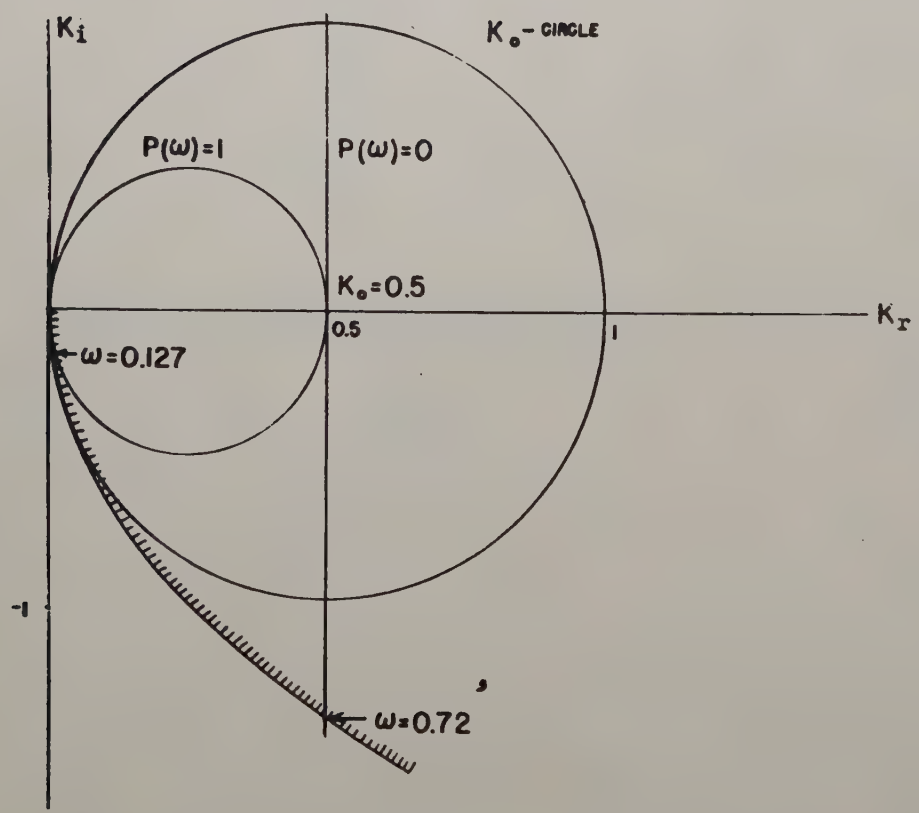

Fig. 10. Plot of K(jw) for $K_0 = 0.5$.

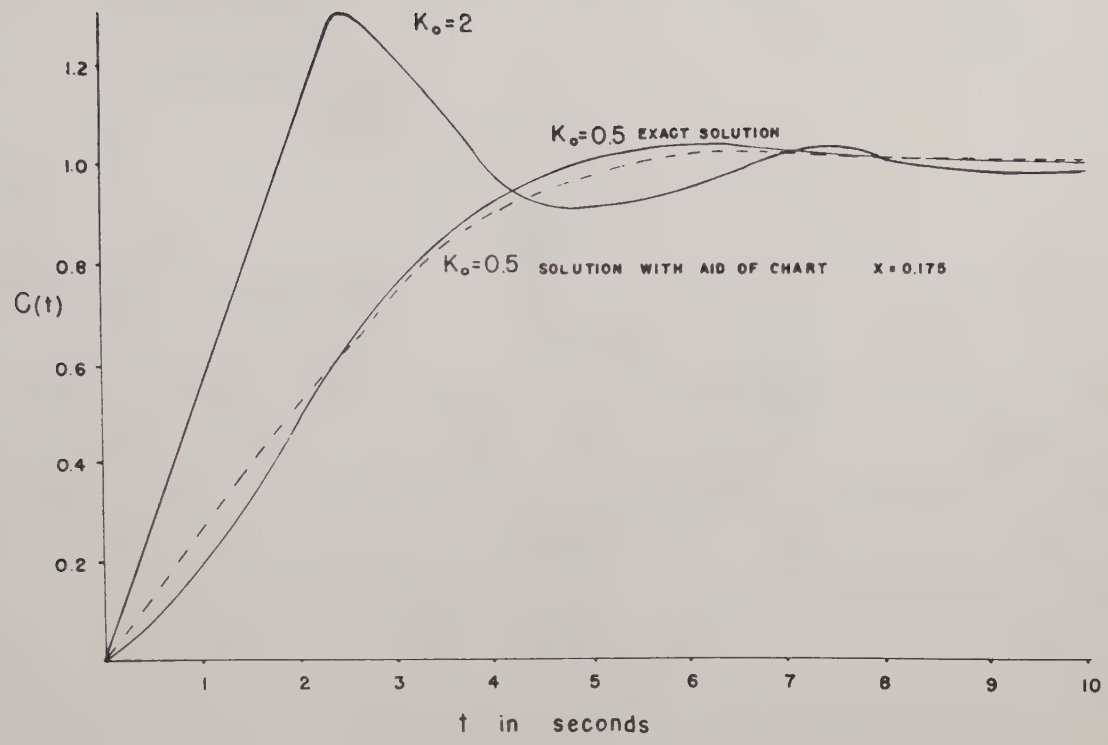

Fig.11. The actual transient response and the corresponding approximate transient response for the system of Fig. 12. K_o = 0.5 and K_o = 2.

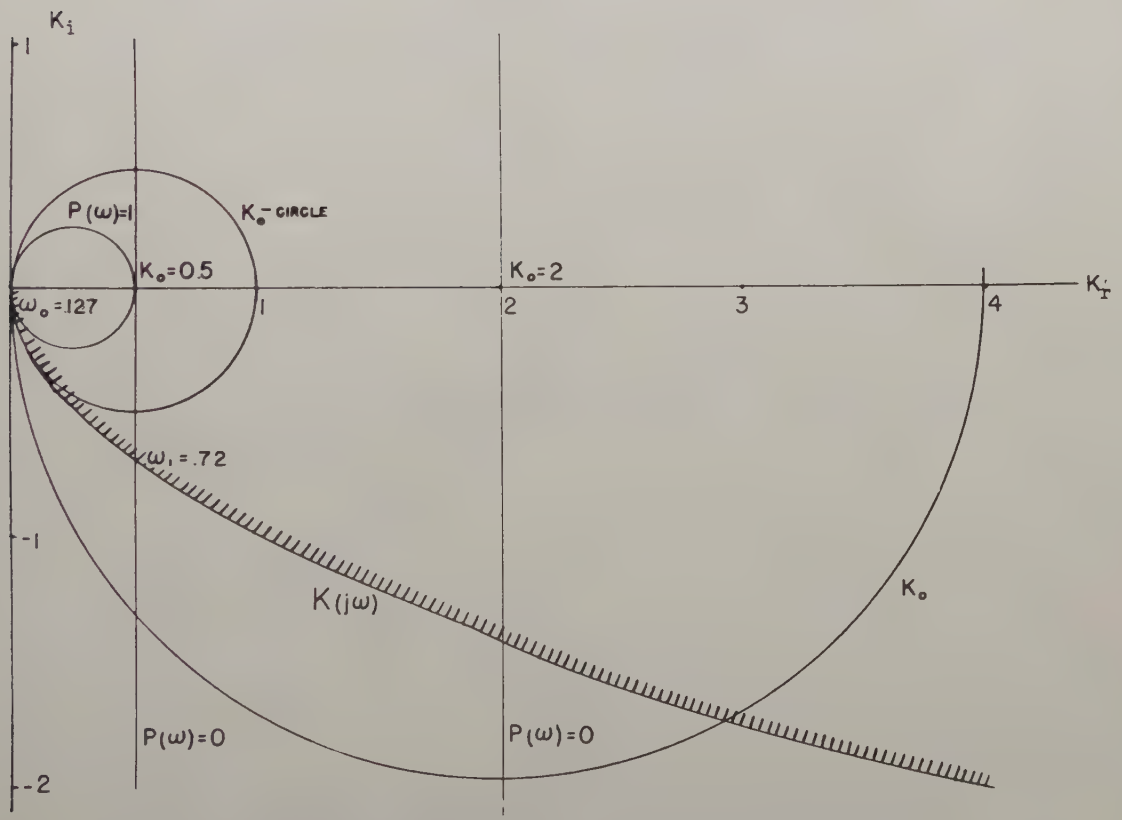

Fig.12. Plot of K(jw) enabling determination of the transient response of the unity-feedback system whereof K(jw) = -jw(1+jw): for K_o = 0.5 and K_o = 2.

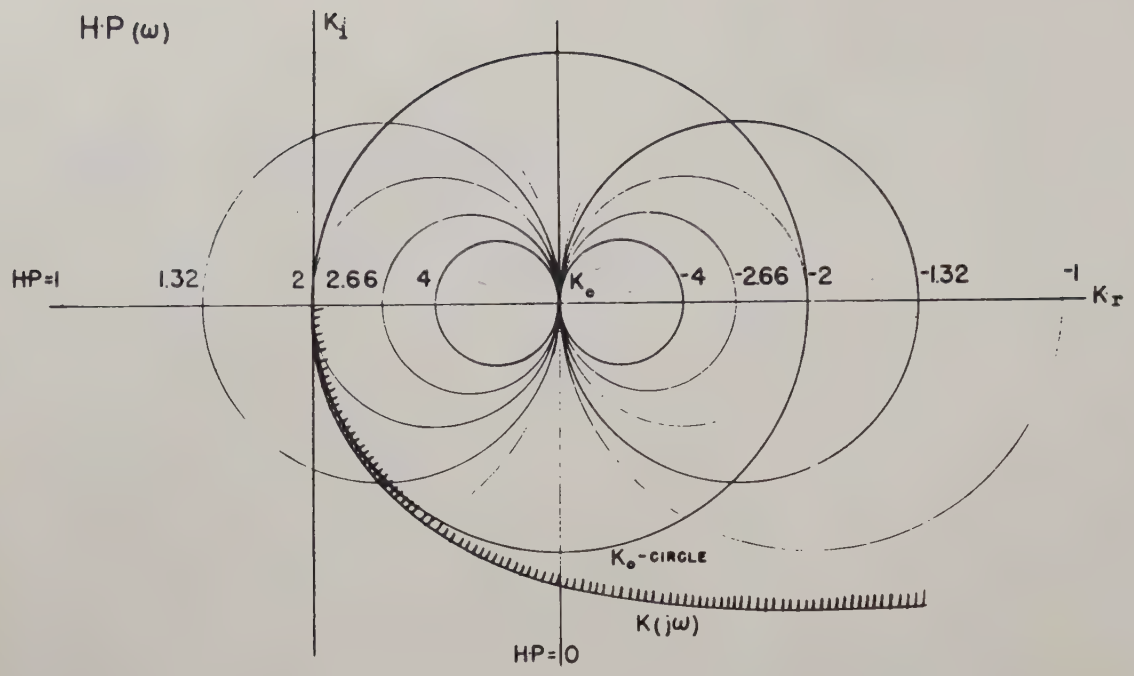

Fig.13. Plot of K(jw)-curve on the family of curves of $H \cdot P(\dot{w})$ = constant pertinent to a nonunity servomechanism with numeric feedback constant H.

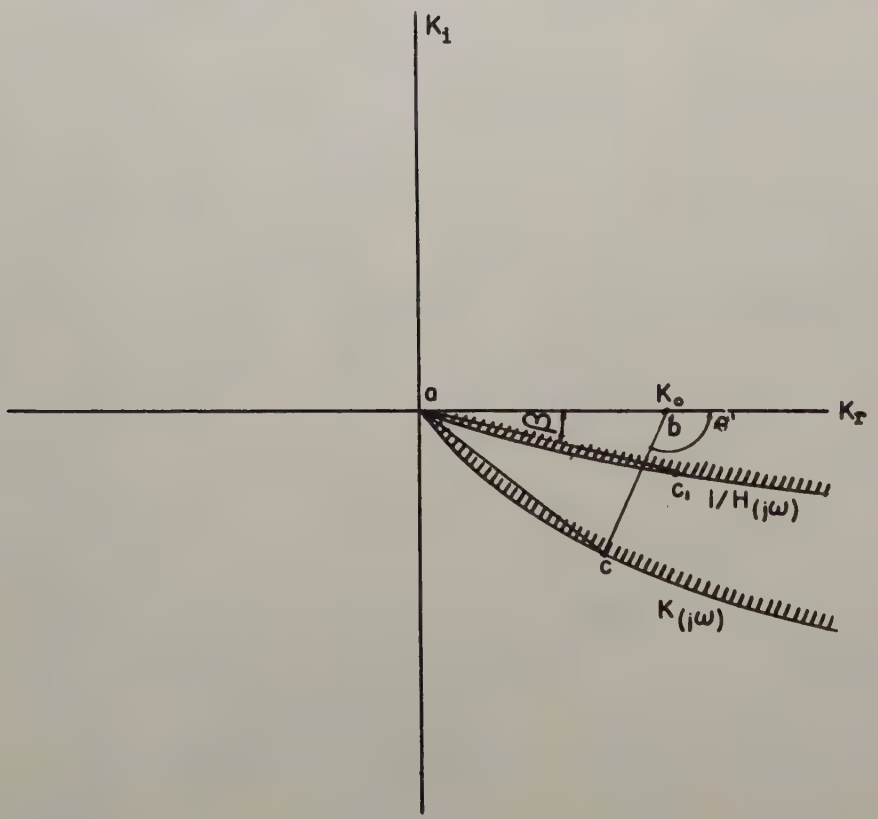

Fig.14. Determination of C(jw)/R(jw) for a nonunity-feedback system from plot of K(jw) and 1/H(jw) curves.

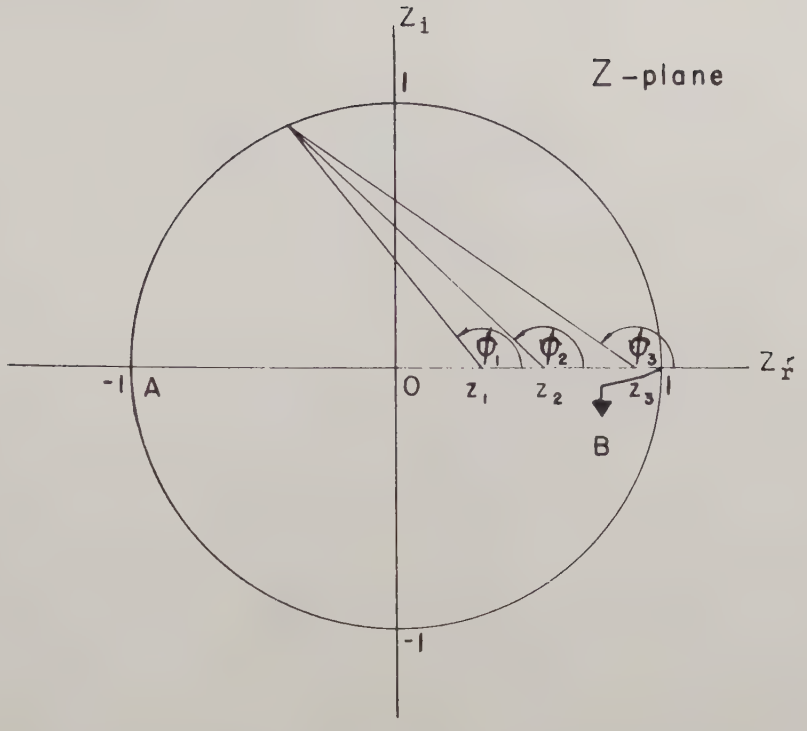

Fig.15. Graphical determination of K_{cr} and W_{cr} from knowledge of the poles and zeros of the characteristic function.

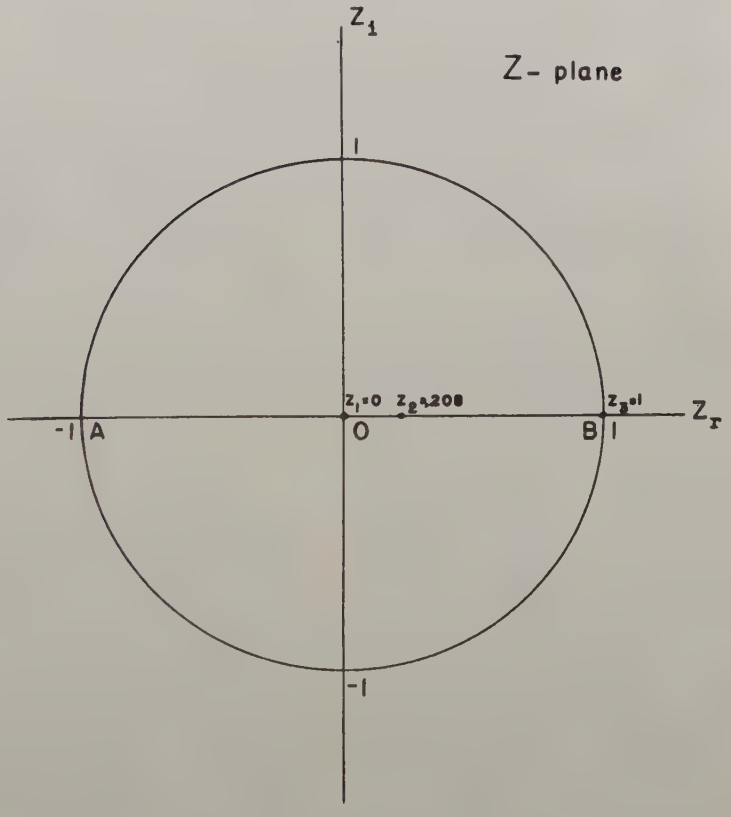

Fig.16. Graphical determination of K_{cr} and W_{cr} for a system with $K(z) = -(z-1)(z-0.208)/0.792\,z$.

OPTIMIZATION OF THE ADAPTIVE FUNCTION BY THE Z-TRANSFORM METHOD

S. S. L. Chang
New York University

Abstract

A study is made on the optimization of the adjustment process in a self-optimizing system under rather general assumptions. The system is designed to keep a performance parameter m either at a prescribed value or at an unknown extremal value. A direct measurement on m is made and the adjustment is based on measured m only. Factors considered are (1) the finite measuring interval, (2) the necessity of looking ahead one interval, (3) the probable error in measurement, and (4) the changing situation. A set of weighting factors on present and past data, and the proper value of test bias for extremal seeking systems, are determined by a least square optimization process. The criterion of optimization is least reduction in m for peak seeking systems and least square error in m for systems with prescribed value of m. Two types of extremal seeking systems are studied. The alternate biasing systems are found to be superior in performance compared to the derivative sensing systems.

This paper has been published by the AIEE as Paper No. CP 59-1296.

APPLICATION OF POLE-ZERO CONCEPTS TO DESIGN OF SAMPLED-DATA SYSTEMS

D. P. Lindorff
University of Connecticut
Storrs, Connecticut

Summary

This paper relates the pole-zero configuration of an error-sampled control system to the transient and steady-state response in a form amenable to straightforward synthesis procedures. The approximate transient response, as defined by percent overshoot and rise time, is specified for a generalized quadratic model in terms of readily discernable parameters. The steady-state error coefficients are developed in terms of the closed-loop poles and zeros. Several examples are used to illustrate the procedure and indicate certain practical conclusions.

Introduction

In the literature various approaches to the synthesis of sampled-data control systems have been proposed. Most of the techniques concerned with response to deterministic inputs have been accomplished in the time domain.[1-3] The feasibility of this approach has been dependent upon the employment of a cancellation procedure which reduces the system impulse response to a sufficiently simplified form to permit the time response to be readily determined. There are several reasons why an alternative synthesis procedure in the complex frequency domain is highly desirable. A foremost reason is the opportunity it affords of recognizing dominant response characteristics of the system from inspection of the pole-zero locations, without resorting to cancellation. In addition, bandwidth concepts are more readily related to the complex-frequency configuration, this being an important consideration when confronted with random noise.

Some interest has been shown in establishing a basis for design in the complex frequency domain;[4] the purpose of this paper will be to pursue this subject further by discussing from a new point of view the transient and steady-state behavior of a sampled-data system in terms of the pole-zero locations in the $z=e^{sT}$ plane. Where possible, simple graphical relationships are introduced so as to allow the salient characteristics of the system to be deduced by inspection. In order to permit time response characteristics to be related to pole-zero locations essentially by inspection, it has been necessary to be content with a specification of the system response at the sampling instants only. This is not considered to be a serious compromise since in any given situation it is readily apparent whether or not the system is well behaved between the sampling instants, and in fact, for the vast majority of practical control systems a knowledge of the response at the sampling instants is fully adequate.

Examples are presented which illustrate the application of the design concepts to several practical situations. The effect of a time delay in the computer is analyzed in terms of its effect upon transient and steady-state performance. In addition the effect of an analog lag network is discussed.

It will be convenient at the outset to state certain well known relationships. Reference is made to the error-sampled model shown in Figure 1. Recognizing $F^*(z)$ as a rational polynomial in $z=e^{sT}$, a root locus can be plotted in the z plane to map the roots of the characteristic equation $(1 + F^*(z))$. The response at the sampling instants is in turn determined by the pulsed transfer function

$$\frac{C^*}{R}(z) = \frac{F^*(z)}{1 + F^*(z)} \tag{1}$$

The real inversion integral yields the response sequence in accordance with (2).

$$c(nT) = \frac{1}{2\pi j} \oint R^*(z) \frac{F^*(z)}{1 + F^*(z)} z^{n-1} dz \tag{2}$$

By consideration of (2), it may be seen that the residue of a pole in close proximity to a zero tends to be diminutive. By this line of reasoning it is possible to identify the dominant poles in a given situation. It follows that zeros too may or may not be dominant. For example, it will be seen that an isolated zero may have a pronounced effect upon the system transient response, as can an isolated pole. The role of dipoles, as might be expected, will be shown to be closely related to steady-state performance.

Generalized Quadratic Model

Just as in the case of continuous control systems, a pair of dominant quadratic roots occur often enough in practice to justify devoting special attention to the so-called quadratic sampled-

data system. Figure 2 represents two special cases wherein the pulsed transfer function exhibits the presence of quadratic roots. In each case the presence of a zero is noted; the location of this zero will be seen to have a critical effect upon the transient response. It can be shown that a single zero is generally associated with the quadratic system and therefore the equation for the generalized quadratic model will be expressed in the form of (3).#

$$\frac{C^*}{R}(z) = \frac{k(z-z_1)}{(z-p_1)(z-\bar{p}_1)} \qquad (3)$$

By considering different functions for G(s) and $D^*(z)$ in Figure 1, the quadratic-model configuration can be made quite general.

Relative Stability

In the interests of defining the relative stability of the quadratic model, an approximate relationship between the step-response overshoot and the geometry of the pole-zero configuration of the quadratic model will be developed. This will be accomplished by defining the percent overshoot of a continuous response function, $c_o(t)$, which passes through the sampled points, c(nT). It should be stressed at this point that the actual continuous response, c(t), is not specified by the quadratic model. Certain restrictions, therefore, must be placed upon the pole locations of (3) to insure that $c_o(t)$ closely characterizes an actual continuous response, c(t) — tantamount to the qualification that the response at the sampling instants provides an adequate sampling of the response characteristics.

It is shown in Appendix I that the percent overshoot of $c_o(t)$ is uniquely specified by the quadratic-model configuration in terms of α and ζ. These parameters are useful in that they relate directly to the pole-zero locations in (3). The angle α may be defined by the geometrical construction in Figure 3. Note that positive or negative values are assigned to α, depending upon whether the perpendicular projection is respectively to the right or to the left of the pole. Thereby the position of the zero is uniquely defined by α for any given pole location. It will be seen in (18) of Appendix I that $\cos\alpha$ appears in the expression for the step response, pointing directly to the effect of the zero location upon overshoot.

The parameter, ζ, defined as the damping ratio in the conventional sense, is mapped from a limited range of the s plane $\left(-\frac{\pi}{T} < \text{Im } s < \frac{\pi}{T}\right)$ onto the z plane as shown in Figure 4, in accordance with the defining equations associated with the figure. Thus ζ is defined uniquely by a given pole location.

The percent overshoot of $c_o(t)$ is plotted in Figure 5 as a function of α and ζ. These parameters in turn uniquely define a quadratic system configuration.

It remains to be seen what restrictions must be imposed upon the system in order that $c_o(t)$ typify the true response. This is assured provided that there are a sufficient number of samples per half cycle of the oscillatory mode. In Appendix I it is shown that in order to be certain of at least two samples per half cycle, the quadratic poles must lie within the first and fourth quadrants of the z plane. Hence the loci of constant ζ as appearing in Figure 4 are restricted to this region. In addition, as the poles approach the vicinity of the origin (dead-beat response) the accuracy of the method deteriorates, and other synthesis procedures are better employed.[1-3] Although the dead-beat design is not handled by this technique, the effect of migration of the poles toward the origin may be established. This will be illustrated in Example I.

Rise Time

Having defined the percent overshoot of $c_o(t)$ in terms of α and ζ, it is also convenient to specify the rise time in terms of these same parameters. For this purpose, rise time will be defined as

t_p = time to reach the first peak in the step response

In Appendix II it is shown that the approximate rise time of the quadratic model is given by

$$t_p = k\,T\,\frac{\pi}{\phi} \qquad (4)$$

where

T = sampling period

ϕ = argument of quadratic pole, p_1

and k as defined in (25) is a parameter which, for convenience, is plotted in Figure 5 as a function of α and ζ. It is noted that the parameter, k, reflects the effect of the zero in (20).

#The necessity for the zero in (3) may be shown by considering the initial value of the first difference of the impulse response sequence which for g(0)=0 is given by

$$\lim_{z\to\infty}\left[(z-1)\,G^*(z)\right] = g(T) - g(0) = g(T)$$

If the initial value of the first difference is to be non-zero, as is usually the case, the order of the numerator must be one less than the order of the denominator.

Application of the above concepts will now be made to specific examples.

Example I

The system described in Figure 6 will be used to illustrate how the approximate percent overshoot and rise time can be determined from a knowledge of the pole-zero configuration. It is seen that the plant typifies a type-2 system with proportional-plus-derivative compensation. The clamp-type hold is used conventionally to filter the error samples. The open-loop pulsed transfer function for this system is given by (5) and provides the basis for plotting the root locus as a function of system gain.

$$\frac{C^*}{E}(z) = KT\left(\frac{T}{2}+1\right)\frac{\left[z+\frac{\frac{T}{2}-1}{\frac{T}{2}+1}\right]}{(z-1)^2} \qquad (5)$$

This locus is plotted in Figure 7 for a sampling period of T=2/3. Inspection of (5) above indicates that for this sampling period a zero is formed at z=0.5. The transient response of the system will be examined for two particular gain settings resulting in two different quadratic configurations denoted by Cases A and B.

Consider the evaluation of the percent overshoot for Case A, representing the lower of the two gain settings. The two parameters, α and ζ must first be evaluated. As illustrated in Figure 7, α is seen to be + 45°. ζ is found from Figure 4 by plotting the value of the complex root which for this case is at $z = \sqrt{2}\, e^{j\frac{\pi}{4}}$. It is seen that $\zeta = 0.4$. Using these values of α and ζ the percent overshoot is taken from Figure 5 to be 55%.

The rise time for Case A is found from (4). With T = 2/3, ϕ = 45°, and k = 0.6 as taken from Figure 5 for the values of α and ζ above, t_p=1.6.

Table I summarizes the data for the two cases considered, comparing the exact values of percent overshoot and rise time with the approximate values obtained from Figure 5. As would be expected, a higher accuracy is obtained for Case A than for Case B, since in the latter case the pole locations marginally satisfy the requirements which insure that the response be adequately characterized by its sampled values — i.e., that the poles lie in the first and fourth quadrants, and avoid the vicinity of the origin. In spite of this restriction, however, the effect of migration of the poles toward the origin can be established; for instance, in this example the results summarized in Table I indicate that migration of the poles toward the origin represents a destabilizing influence. This is a result which is strictly attributable to the sampling action since it is readily shown that the continuous model of this type-2 quadratic system experiences a stabilizing effect with increasing gain.

It should be noted that the location of the zero with respect to the poles (as indicated by the value of α) has a pronounced effect upon the overshoot. For example, consideration of the values of ζ alone would erroneously indicate a more stable configuration in Case B than in Case A (See Table I). This interdependence of parameters is clearly demonstrated by the curves in Figure 5.

Other quadratic configurations can be readily studied in a like manner. It is generally observed from Figure 5 that, for a fixed location of poles, the migration of the zero in the direction of increasing α is in the direction of decreasing response time, while the overshoot passes through a minimum value. In the following section the steady-state response will be discussed in terms of closed-loop pole-zero locations.

Generalized Error Coefficients and Error Constants

The steady-state error response to a slowly varying input has been expressed in terms of generalized error coefficients as pertaining to continuous systems.[5] An equivalent analysis can be made of the sampled error relative to the system in Figure 1. Thus, if it is assumed that an input can be represented by the three-term power series

$$r(t) = a_0 + a_1 t + a_2 t^2 \qquad (6)$$

over the time range of interest, and if the characteristic response modes of the system have subsided, the steady-state error sequence is shown in Appendix III to be of the form

$$e(nT) = \frac{1}{1+K_p}\left[a_0 + a_1 nT + a_2 (nT)^2\right] + \frac{1}{K_v}\left[a_1 + a_2 T(2n+1)\right] + \frac{1}{K_a}\left[2a_2\right] \qquad (7)$$

The coefficients K_p, K_v, and K_a are the familiar error constants which can be defined in a variety of ways. The simplest definition is perhaps obtained from the open-loop transfer function — for example[6]

$$K_v = \frac{1}{T}\lim_{z\to 1}\left[(z-1)\,G^*(z)\right] \qquad (8)$$

Since the underlying objective of this paper is to present synthesis procedures which utilize pole-zero concepts, the error constants in (7) will be expressed in an alternative form. Thus if

the closed-loop pulsed transfer function relating to Figure 1 is denoted by

$$\frac{C}{R}^*(z) = K\frac{\prod^{m}(z-z_i)^{q_i}}{\prod^{1}(z-p_i)^{r_i}} \tag{9}$$

it is shown in Appendix IV that the error constants can be expressed as

$$\frac{1}{1+K_p} = \left[1 - \frac{C}{R}^*(z)\right]_{z=1}$$

$$\frac{1}{K_v} = T\left[\sum^{1}\frac{r_i}{1-p_i} - \sum^{m}\frac{q_i}{1-z_i}\right] \tag{10}$$

$$\frac{1}{K_a} = -\frac{1}{K_v^2} + \frac{T^2}{2}\left[\sum^{m}\frac{q_i}{(1-z_i)^2} - \sum^{1}\frac{r_i}{(1-p_i)^2}\right]$$

The above equations are analogous to those derived by Truxal for continuous systems.[5]

The relationship for the velocity constant in (10) will be used in two examples to follow. In these examples a dominant quadratic system will be analyzed by the techniques described above. As in the discussion of transient response the assumption is made here that the steady-state response is well represented by the response at the sampling instants.

Example II

In this example the effect of a time delay, as would arise from the computation time of a computer, will be considered. The system is described in Figure 8. Both the sampling period and the delay time are taken to be equal to one second. A root locus for the system is plotted in Figure 9 together with a root locus for the same system without time delay. The respective gains are set so as to cause the quadratic roots in both cases to occur at a value of $\zeta = 0.6$.

In order to estimate the relative stability of the system which incorporates the time delay, reference will be made to the quadratic model as previously discussed. The system function given in Figure 8 differs from the quadratic-model configuration by a factor involving a real root near the origin. To a first approximation this real root will be considered to be at z=0; the percent overshoot is then essentially independent of the real root, and can be determined by the method previously described in terms of the quadratic-model configuration. The summary of results in Table II indicates that this approximation is justified, and that the relative stability in this case is simply determined from the quadratic configuration by α and ζ. For shorter sampling periods the accuracy of this approximation improves.

An analysis of the effect of time delay upon steady-state performance is of interest. For this purpose it is again useful to consider the actual system transfer function to be approximated by the system function without delay multiplied by a factor z^{-1}, as shown in (11).

$$\frac{k_2(z-z_1)}{(z-\rho)(z-P_2)(z-\bar{P}_2)} \approx \frac{k_1(z-z_1)}{z(z-P_1)(z-\bar{P}_1)} \tag{11}$$

Here it is assumed that the quadratic poles are essentially the same for the same value of ζ. Again the accuracy of this approximation improves as the sampling period is decreased. Let the velocity constants be defined according to:

K_{v1} = velocity constant for system without time delay

K_{v2} = velocity constant for system with time delay

It then follows from (10) and (11) that

$$\frac{1}{K_{v_2}T} \approx \frac{1}{1-0} + \frac{1}{K_{v_1}T} \tag{12}$$

Solving for K_{v_2}

$$K_{v_2} \approx \frac{K_{v_1}}{1+K_{v_1}T} \tag{13}$$

Equation (13) is of interest in showing the approximate dependence of the velocity constant upon a time delay, assuming the relative stability to be held constant.

Other examples of higher order systems which may be characterized by a dominant quadratic mode occur when there is a dipole associated with the closed loop function. Such cases may arise as a consequence of high-frequency poles in the analog part of the system. Alternatively a lag network in the analog portion of the system may be responsible for forming a dipole in the vicinity of z=1. This latter case will be discussed in the following example.

Example III

With reference to Figure 1 it will be assumed that the error channel consists of a sampler and clamper followed by an analog function

$$G_1(s) = \frac{K\,(10s+1)}{s(s+1)(100s+1)} \qquad (14)$$

With a sampling period of T=1 the resulting open-loop pulsed transfer function can be shown to be given by

$$\frac{C^*}{E}(z) = \frac{K(0.1e^{-1})(z+0.74)(z-0.9)}{(z-1)(z-e^{-1})(z-0.99)} \qquad (15)$$

A value of gain, K, must now be chosen which is compatible with a satisfactory step-response overshoot. For K = 0.41 the root locations shown in Figure 10 are obtained. The transient response is seen to be controlled essentially by the basic quadratic configuration; the dipole is responsible for a long duration transient of small magnitude, typical of the well-known characteristic attributed to lag-network compensation. The dipole, however, effects the steady-state performance. Application of (10) to the pole-zero configuration of Figure 10 gives

$$\frac{1}{K_v T} = \left[\frac{2d}{\ell^2} - \frac{1}{1-z_1}\right] + \left[\frac{1}{1-\rho} - \frac{1}{1-z_2}\right] \qquad (16)$$

$$= 2.84 - 2.5$$

It can be readily appreciated that the effect of the dipole in the vicinity of z=1 is to increase the system K_v by reducing the magnitude of $1/K_vT$ above.

Conclusions

A synthesis technique has been presented which utilizes pole-zero concepts in the determination of transient and steady-state performance of an error-sampled control system. Attention has been focused upon dominant pole-zero configurations, particularly with relation to a generalized quadratic model. A primary purpose has been to present an alternate approach to the well documented cancellation procedures. System non-linearities and noise may often prevent the effective use of compensation by cancellation and in fact dictate the need first to understand the dominant characteristics of the uncompensated system.

Three examples are discussed for the purpose of illustrating the techniques by means of some practical applications.

A disadvantage of using pole-zero concepts in the z domain stems from the difficulty which is encountered in specifying the zeros of a pulsed-transfer function from a knowledge of the associated analog transfer function, except in the simplest cases. An approximate mapping technique is a step toward solving this problem, and is a subject for further study.

Appendix I

A quadratic sampled-data system will be defined by the function

$$\frac{C^*}{R}(z) = \frac{K(z-z_1)}{(z-p_1)(z-\bar{p}_1)} \qquad (17)$$

where K is specified by the requirement

$\left[\frac{C^*}{R}(z)\right]_{z=1} = 1$, i.e., that there by zero steady-state error to a step input. The step response sequence is found from (2) to be

$$c(nT) = 1 - \left|\frac{1}{\cos\alpha}\right| \left| p_1^n \right| \sin(n\phi + \theta_1 + \theta_2) \qquad (18)$$

where

ϕ = argument p_1

θ_1 = argument $(1-\bar{p}_1)$

θ_2 = argument (p_1-z_1)

$\alpha = \theta_1 + \theta_2 - \frac{\pi}{2}$

The angle α defined above is measured conveniently by the geometrical construction in Figure 3.

A continuous function, $c_o(t)$, which passes through the points c(nT) is of the form

$$c_o(t) = 1 - \left(\frac{1+r^2-2\zeta r}{1-\zeta^2}\right)^{\frac{1}{2}} e^{-\zeta\omega_n t} \sin\left(\sqrt{1-\zeta^2}\,\omega_n t + \psi\right) \qquad (19)$$

where

$$\psi = \tan^{-1}\frac{r\sqrt{1-\zeta^2}}{1-\zeta r} + \cos^{-1}\zeta$$

The percent overshoot of (19) will be used to characterize the actual overshoot of the quadratic-system response. It will be useful at this point to write the Laplace transform of (19) as

$$C_o(s) = \frac{1}{s}\left[\omega_n r \frac{\left(s + \frac{\omega_n}{r}\right)}{\left(s^2 + 2\zeta\omega_n s + \omega_n^2\right)}\right] \qquad (20)$$

It can be readily seen that the percent overshoot of the response in (19) is uniquely specified by ζ and r. It is desired, however, that the percent overshoot of (19) be defined by the pole-zero locations in (17). ζ is conveniently and uniquely determined from a knowledge of the location of $z=p_1$ providing that the complex poles in (20) are defined to be within the zero-order strip $\left(-\frac{\pi}{T} < \mathrm{Im}\ s < \frac{\pi}{T}\right)$. Loci of constant ζ are plotted in Figure 4, corresponding to this restricted region in the s plane. A second inde-

pendent relationship for ζ and r is conveniently obtained from a measurement of α. By identifying terms in (18) and (19), it is seen that $\alpha = \psi - \frac{\pi}{2}$. Thus α is seen to be a function of ζ and r as desired.

The curves of percent overshoot in Figure 5, as referring to (19), are plotted as a function of ζ and α since these parameters are readily determined from an inspection of the pole-zero locations of (17).

It remains to be shown that the function, $c_o(t)$, closely approximates the continuous response of the system if certain restrictions are placed upon the locations of p_1. For this purpose reference is made to (18). Noting that the number of samples per half cycle of the oscillatory mode is given by π/ϕ, it is observed that there will be at least two samples per half cycle if $\phi < \pi/2$. Thus, the conjugate poles, p_1 and $\bar{p}_1$, should lie in the first and fourth quadrant as a necessary condition that $c_o(t)$ closely represent the true response. In addition it will be observed that if p_1 lies close to the origin, the decrement factor, p_1^n, may become much more rapid than the oscillation frequency, in which case the sampling rate is too slow compared to the response time to insure that $c_o(t)$ closely bounds the true response. These restrictions can be applied intelligently in any given problem without placing undue constraints on the design objective.

Appendix II

The response time of the quadratic sampled-data system will be defined as the time, $t=t_p$, at which $c_o(t)$ in (19) reaches its first peak. By equating the derivative of $c_o(t)$ equal to zero, it is seen that t_p satisfies the equation

$$\sqrt{1-\zeta^2}\,\omega_n t = \pi - \tan^{-1}\frac{r\sqrt{1-\zeta^2}}{1-r\zeta} \tag{21}$$

Recognizing the identity between terms in (18) and (19) it follows that

$$n\,\phi = \sqrt{1-\zeta^2}\,\omega_n t \tag{22}$$

If nT=t is defined as a continuous variable then

$$\frac{\phi}{T} = \sqrt{1-\zeta^2}\,\omega_n \tag{23}$$

whereupon (21) yields

$$t_p = k\,T\,\frac{\pi}{\phi} \tag{24}$$

where

$$k = 1 - \frac{\tan^{-1}\dfrac{r\sqrt{1-\zeta^2}}{1-r\zeta}}{\pi}$$

T = sampling period

ϕ = argument of p_1

The parameter, k, can be more conveniently expressed by noting that in (18) and (19), $\theta_1 + \theta_2 = \psi$. Using the appropriate substitutions

$$k = \frac{\pi}{2} + \alpha - \cos^{-1}\zeta \tag{25}$$

From (25) contours of constant k have been plotted in Figure 5.

Appendix III

Consider the system described in Figure 1 for which the error response function is defined by

$$\frac{E^*}{R}(z) = W^*(z) \tag{26}$$

The class of inputs to be considered are of the form

$$r(t) = a_o + a_1 t + a_2 t^2 \tag{27}$$

where it is assumed that terms beyond t^2 can be neglected. The z transform of r(t) is therefore given by

$$R^*(z) = \frac{a_o z}{z-1} + \frac{a_1 T z}{(z-1)^2} + a_2 T^2 \frac{z(z+1)}{(z-1)^3} \tag{28}$$

If $W^*(z)$ is expanded in a power series about the point z=1, the sampled error can be expressed as

$$E^*(z) = W(1)R^*(z) + W'(1)(z-1)R^*(z) + \frac{W''(1)}{2!}(z-1)^2 R^*(z) + \ldots \tag{29}$$

If the system is assumed to be in the steady state at t=0, then for t>0 the error, e(nT), can be evaluated from (29) by considering only the residues due to the complex frequencies of $R^*(z)$. The result is found in a straightforward manner to be

$$e(nT) = W(1)\left[a_o + a_1 nT + a_2 (nT)^2\right] + T\,W'(1)\left[a_1 + a_2 T(2n+1)\right] + \frac{T^2 W''(1)}{2}\left[2a_2\right] \tag{30}$$

By relating $W^*(z)$ to $G^*(z)$ through the equation $W^*(z) = \frac{1}{1 + G^*(z)}$ and using the definitions[6]

$$K_p = \lim_{z \to 1} G^*(z)$$

$$K_v = \frac{1}{T} \lim_{z \to 1} \left[(z-1)\, G^*(z)\right] \tag{31}$$

$$K_a = \frac{1}{T^2} \lim_{z \to 1} \left[(z-1)^2\, G^*(z)\right]$$

it follows that (30) can be expressed as

$$e(nT) = \frac{1}{1 + K_p}\left[a_o + a_1 nT + a_2 (nT)^2\right]$$

$$+ \frac{1}{K_v}\left[a_1 + a_2 T(2n+1)\right] \tag{32}$$

$$+ \frac{1}{K_a}\left[2a_2\right]$$

Appendix IV

The purpose of this appendix is to indicate the method of deriving (10). Only the derivation of the expression for K_v will be given in detail, however, since the expressions for K_p and K_a are derived in a similar manner.

Using (29) it follows that

$$\frac{C^*}{R}(z) = 1 - W(1) - W'(1)(z-1) - \frac{W''(1)}{2!}(z-1)^2 - \ldots \tag{33}$$

Identifying terms in (30) and (32) it is seen that

$$\frac{1}{K_v T} = W'(1) = -\left[\frac{d}{dz}\frac{C^*}{R}(z)\right]_{z=1} \tag{34}$$

For the error-sampled model, let it be assumed that the steady-state error sequence to a step disturbance is zero, and hence $\left[\frac{C^*}{R}(z)\right]_{z=1} = 1$.

Therefore (34) can be written in the form

$$\frac{1}{K_v T} = -\left[\frac{\frac{d}{dz}\frac{C^*}{R}(z)}{\frac{C}{R}(z)}\right]_{z=1} = -\left[\frac{d}{dz} \ln \frac{C}{R}(z)\right]_{z=1} \tag{35}$$

If the system pulsed transfer function is denoted by

$$\frac{C^*}{R}(z) = \frac{K \prod^{m} (z-z_i)^{q_i}}{\prod^{l} (z-p_i)^{r_i}} \tag{36}$$

and (36) is substituted into (35) it follows directly that

$$\frac{1}{K_v T} = \sum^{l} \frac{r_i}{(1-p_i)} - \sum^{m} \frac{q_i}{(1-z_i)} \tag{37}$$

Acknowledgement

The research described in this paper was done at the University of Connecticut under the sponsorship of the International Business Machines Corporation in cooperation with the U. S. Air Force.

References

1. "General Synthesis Procedure for Computer Control of Single and Multi-Loop Linear Systems," R. E. Kalman, J. E. Bertram, Trans. of A.I.E.E., Vol. 77, Part II, 1958.

2. "Digital Computers in Feedback Control Systems," J. R. Ragazzini, I.R.E. Convention Record, Part IV, pp. 33-42, 1957.

3. "Discrete Compensation of Sampled-Data and Continuous Control Systems," Trans. of the A.I.E.E., Vol. 76, Part II, pp. 317-325,1957.

4. "Correlation Between Root-Locus and Transient Response of Sampled-Data Control Systems", Trans. of the A.I.E.E., Vol. 75, Part II, pp. 427-435, 1956.

5. "Automatic Feedback Control System Synthesis", J. G. Truxal, McGraw-Hill Book Co., Inc., New York, 1955.

6. "Additions to Z-Transformation Theory for Sampled-Data Systems," G. V. Lago, Trans. of the A.I.E.E., Vol. 74, Part II, pp. 403-408, 1955.

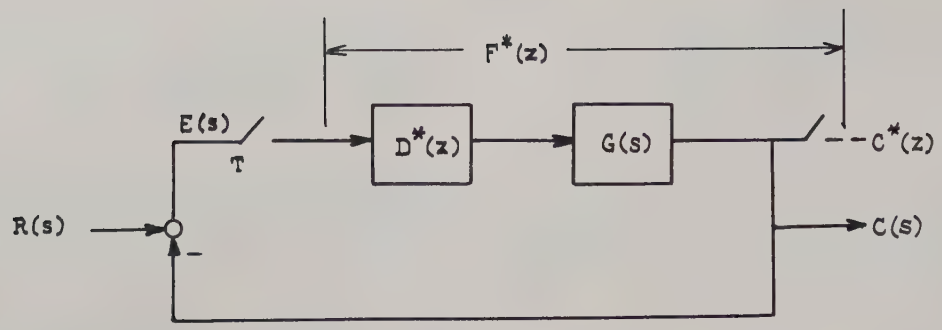

Fig. 1. Error Sampled Model.

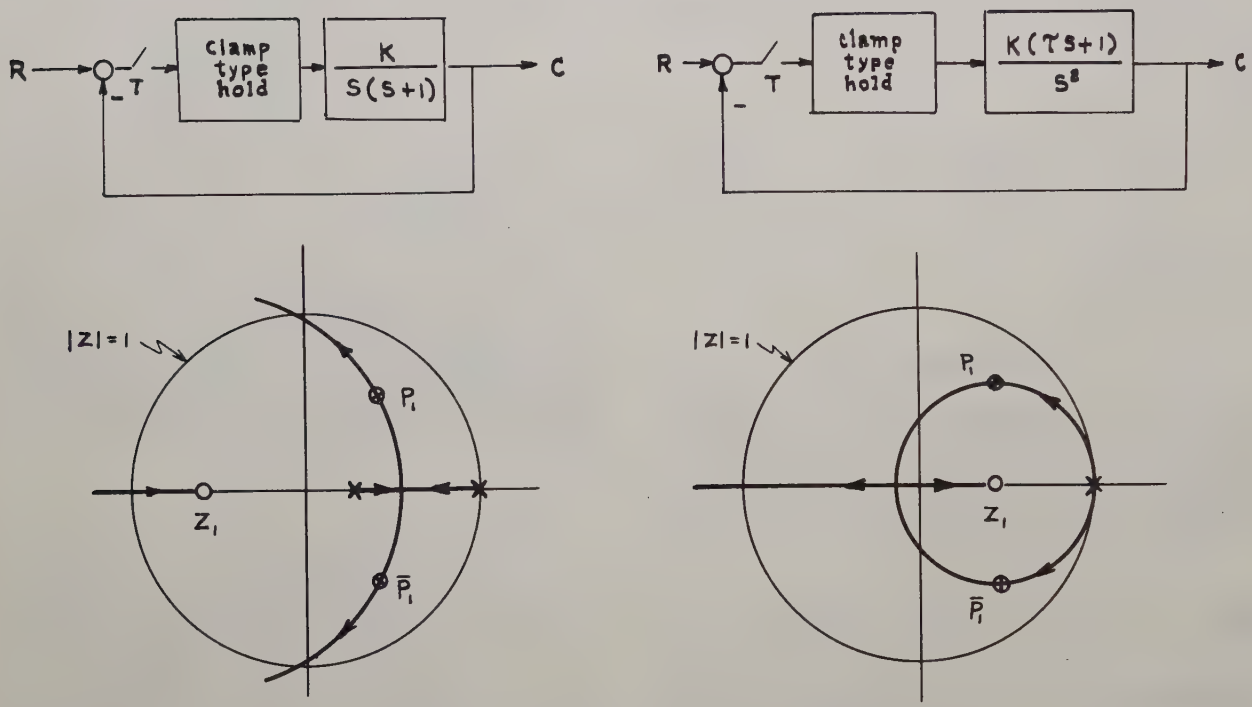

Fig. 2. Illustrations of Quadratic System.

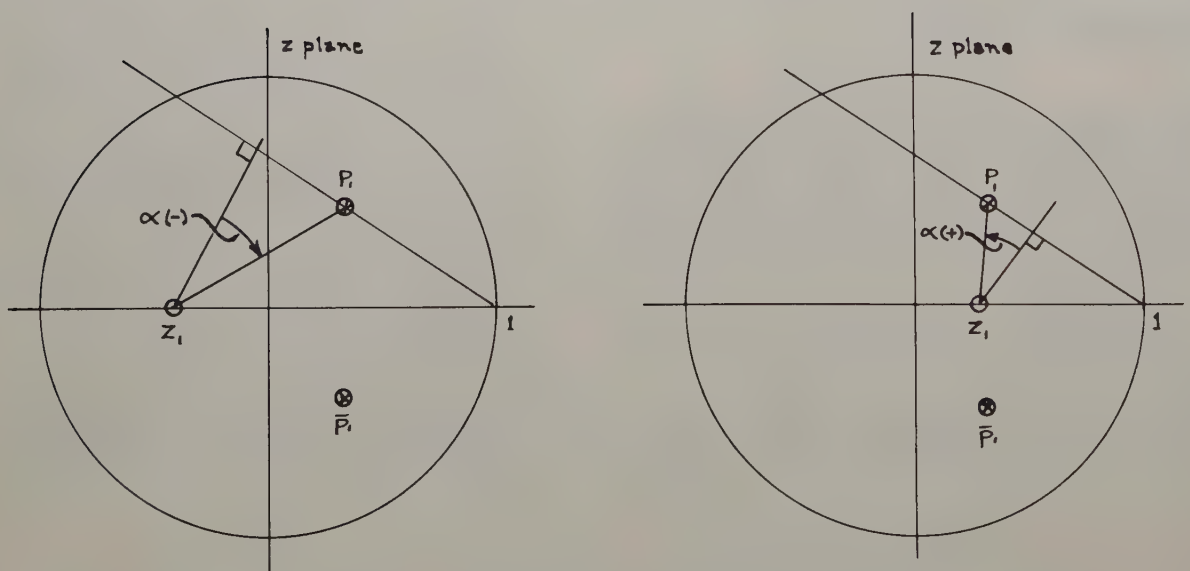

Fig. 3. Geometrical Representations of α .

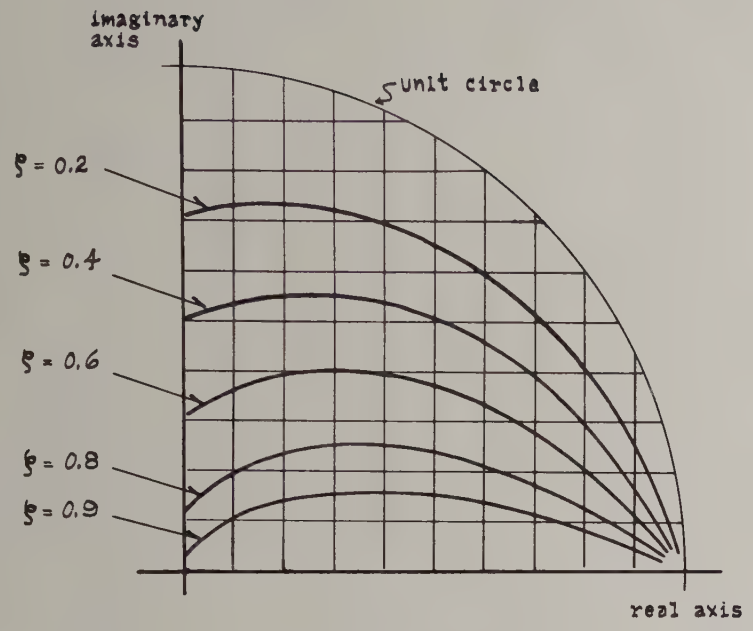

Fig. 4. Loci of Constant ζ.

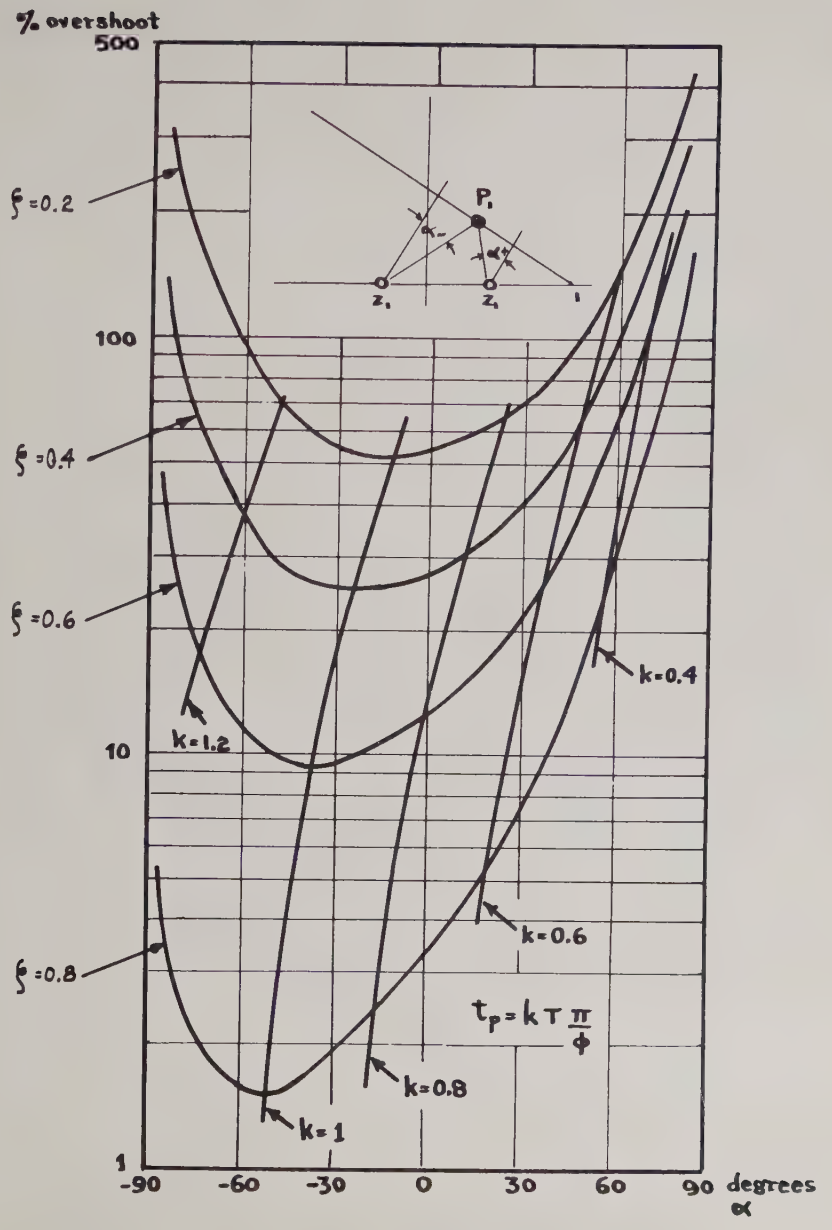

Fig. 5. Transient Response Curves for the Quadratic System.

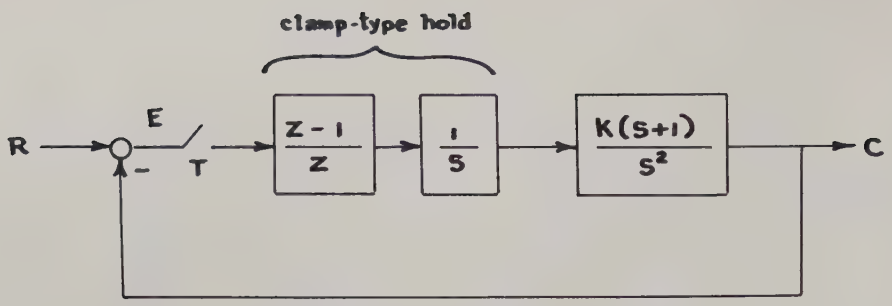

Fig. 6. Quadratic System of Example I.

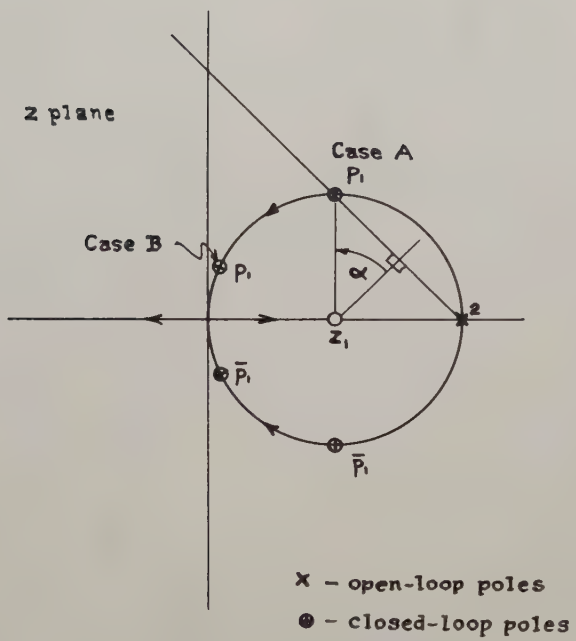

Fig. 7. Root Locus of Example I.

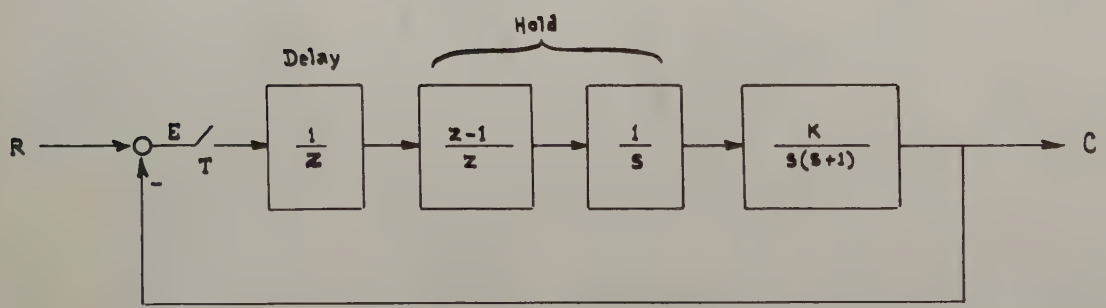

$$\frac{C^*}{R}(z) = \frac{k_2(z-z_1)}{(z-\rho)(z-p_2)(z-\bar{p}_2)}$$

Fig. 8. System Used in Example II.

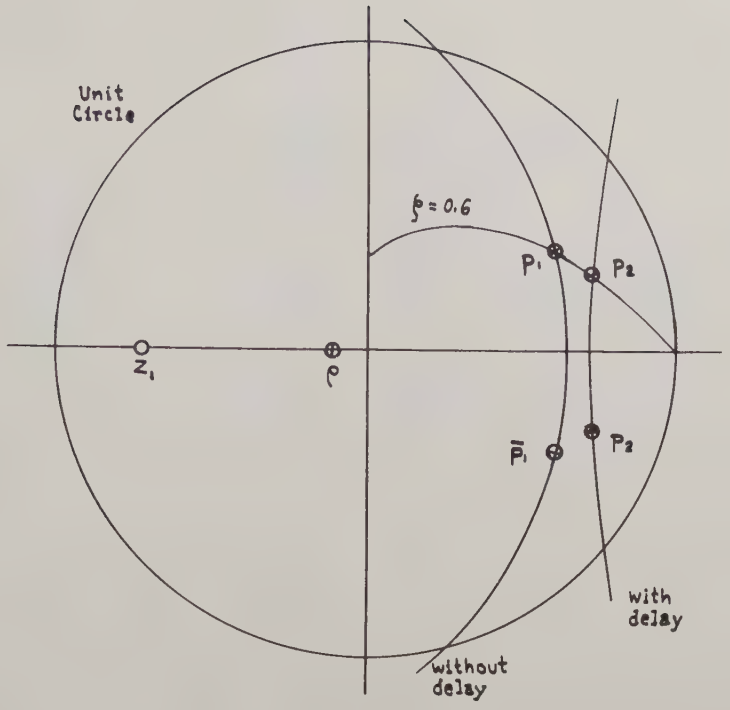

Fig. 9. Root Loci of Example II.

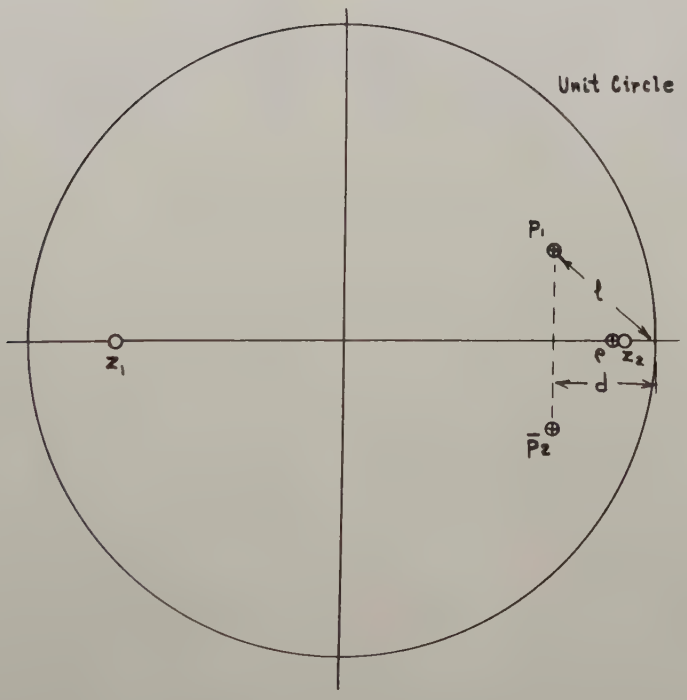

Fig. 10. Pole-Zero Configuration of Example III.

Table I-Results of Example I.

Case	Pole Location P_1	α (Fig.3)	ζ (Fig.4)	Approximate % Overshoot (Fig.5)	Actual % Overshoot	Approx. Rise Time t_p (Fig.5)	Actual Rise Time t_p
A	0.5+j0.5	+45°	0.4	55	56	1.6	1.6
B	0.04+j0.2	+78°	0.76	115	93	0.45	0.67

Table II-Results of Example II.

System	α (degrees)	Percent Overshoot (Fig. 5)	Actual Percent Overshoot	K_v
With Delay	37.5	9.5	9	0.24
Without Delay	36.5	9.5	9	0.4

SYNTHESIS OF FEEDBACK SYSTEMS WITH SPECIFIED OPEN-LOOP AND CLOSED-LOOP POLES AND ZEROS

W. E. Carpenter
Space Technology Laboratories, Inc.
P. O. Box 95001
Los Angeles 45, California

Abstract

This paper describes a graphical method for synthesizing a compensation network where the fixed poles and zeros of the open-loop system are given and the closed-loop poles and zeros are independently specified. The resulting network is general in that it may have both real and complex poles and zeros. The method does not rely on cancellation techniques to determine the compensation network which is often simpler than one which would have resulted from the use of such techniques. In contrast to the Bode and Nyquist methods, wherein phase and gain requirements over a frequency band are used to generate compensation networks, this approach uses requirements at points in the s-plane, such as those imposed by desired transient response, to construct a solution of the problem. The graphical procedure is iterative. In many cases, convergence is rapid, and several techniques are suggested throughout the paper to further increase the speed of solution.

Introduction

The problem of synthesizing compensation networks may be attacked by one of several methods. Guillemin[1] suggests a method which usually requires the cancellation of some of the fixed poles and zeros of the open-loop system except possibly one pole at the origin. The principal of cancellation is also used by Aseltine's inverse root-locus method.[2] Walters[3] has shown that a complex, closed-loop pole may be fixed in the s-plane by angular measurements.

It is possible to use analytical methods involving phase and gain equations constructed from measurements made at given poles and zeros, but this would require the simultaneous solution of a number of nonlinear equations, usually a difficult task. When using the Bode and Nyquist methods, on the other hand, one must attempt to generate networks from phase and gain requirements over a frequency band so that a straightforward approach to the solution is not always readily apparent, particularly when transient response is an important consideration. The method to be described below avoids the first of these difficulties by using an iterative, graphical procedure and mitigates the second by using the phase and gain requirements at points in the s-plane to generate the network.

Method

Fundamental Equations

Let there be q zeros and p poles in the compensation network. Mortensen[4] has shown that, if the gain of the system is not specified,

$$p + q \geq n - 1 \qquad (1)$$

where n is the total number of fixed closed-loop poles. If gain is specified, $p + q \geq n$.

A brief discussion will explain why these equations are valid. The poles of the closed-loop system may be viewed as n parameters which are to be specified independently. To accomplish this, n variables which can be adjusted independently are needed in the open-loop system. One of these is the gain of the open-loop system, unless it is specified; the remainder are the locations of the open-loop poles and zeros. This implies that $(n - 1)$ variable poles and zeros are required in the compensation network to permit specification of the locations of n closed-loop poles. If the gain of the open-loop system is specified, one more pole or zero must be found in the compensation network to offset the lack of freedom to specify this variable.

In the work to follow, assume that gain is not specified. Then the equations below describe the phase and gain at fixed poles or zeros in the s-plane for a negative feedback, open-loop system. The feedback sign convention for the following work is described in the later section on theory.

1. The phase measured at an open-loop pole, using all closed-loop poles and zeros, is zero, i.e.,

$$\text{Phase}\left[Y(s_o)\right] = 0 + n(360^o)$$

where s_o is an open-loop pole and n is an integer or zero. This arises from the inverse-root locus relations.*

* The following identity is used:

$$\frac{\dfrac{KGH}{1 + KGH}}{1 - \dfrac{KGH}{1 + KGH}} = KGH$$

where H is the feedback transfer function, a ratio of polynomials in s. The identity shows that if $H \neq 1$, H may always be included as a part of G(s) in equation (2), in the section on theory. Therefore, zeros of the closed-loop system will be considered as zeros of the open-loop system in this method.

2. The phase measured at a closed-loop pole, using all open-loop poles and zeros, is 180°, i.e.,

$$\text{Phase}\left[G(s_c)\right] = 180^\circ + n(360^\circ)$$

where s_c is a closed-loop pole and n is an integer or zero.

The locus of complex poles or zeros satisfying either of the above constant-phase requirements at a point in the s-plane, other than on the real axis, is an arc of a circle which passes through the point of measurement and has its center on the real axis, as shown in the following diagram (proof of this is given in Appendix I).

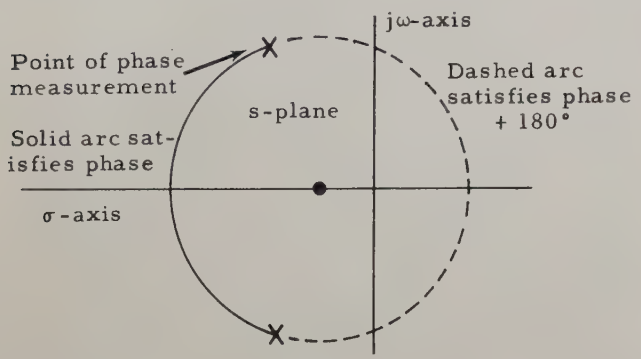

Using the relations stated under 1 and 2 above, it is sometimes possible to construct two arcs which will intersect at a point which satisfies both phase requirements.

At this point, an example will be given to show the use of the phase relations just cited in locating a compensation network in the complex plane. The solution is illustrated on Figure 1. It is assumed that the three closed-loop and three open-loop poles shown in the figure are fixed and that open-loop gain is not specified. Equation (1) indicates that there may be a unique solution if $p + q = 2$, since $n = 3$. Therefore, two relations are needed to determine the compensation network. Since the two sets of poles, one open-loop and one closed-loop, are complex, there are two phase relations which may be used to find two zeros.

If two zeros are used, no new poles will be generated, and all three closed-loop positions will be satisfied by the two phase relations arising at the complex pole positions. The phase lead needed at the complex, closed-loop pole is about 215° and at the complex, open-loop pole, it is about 119°. These relations permit the construction of two arcs which intersect to give the pair of complex zeros shown in Figure 1.

Although it has not been proven that the complex zero solution with $p + q = n - 1$ is unique, it appears most probable that this is true. For this reason, ordinarily one would not search for another solution for this problem once one had been found. However, at this point it may be noted that the arcs constructed from the lag requirements at the complex poles may assist in finding compensation poles and also in locating the closed-loop poles resulting from the addition of compensation poles. Compensation poles must lie on the 145° lag-arc or the real axis, and the additional closed-loop poles must lie on the 241° lag-arc or the real axis. A gain relation can be used at the closed-loop poles to locate compensation poles on the arc or the real axis exactly. However, this is not illustrated on Figure 1 because the use of two poles as compensation will result in an unstable system.

The final possibility, one pole and one zero, may also be discarded, since the points would have to lie on the real axis and no conceivable placement on the axis could satisfy the phase requirements at both of the complex poles simultaneously.

There are cases for which the exact solution of equation (1) is not possible if the system is restricted to negative feedback.* In addition, solutions of equation (1) for some cases may not seem desirable to the designer, even though negative feedback may be used, because of problems of physical realizability. In these cases, the solution must be carried out with $p + q > n - 1$.

The listing of phase and gain relations is continued below.

3. The phase measured at a zero, using open-loop poles and zeros, is $\theta + n(360^\circ)$, where θ is the phase measured at the zero using closed-loop poles and zeros, and n is an integer or zero.

4. The gain must be the same at all closed-loop poles when measured using open-loop poles and zeros, i.e.,

$$K = \frac{1}{\left|G(s_c)\right|}$$

where s_c is a closed-loop pole.

5. The gain must be the same at all open-loop poles when measured using closed-loop poles and zeros, i.e.,

$$K = \frac{1}{\left|Y(s_o)\right|}$$

where s_o is an open-loop pole.

6. If the number of poles is greater than the number of zeros, the gain measured at an open-loop pole is equal to the gain measured at a closed-loop pole.

*It can be shown that $p + q + 1$ solutions always exist for either positive or negative feedback. (See Reference 4.)

Procedure

Listed below are suggested steps for finding a suitable compensation network.

1. Measure the phase and gain at the fixed, complex poles and zeros, both closed- and open-loop, using the poles and zeros as noted in 1, 2, 3, 4 and 5 above. It will help in directing the later work to list the phase and gain required of the compensation network to produce the poles and zeros at which the measurements were made.

2. Determine the number and approximate location of the poles and zeros which exactly satisfy the phase of both the open- and closed-loop systems and roughly equalize the gain among the poles of each system.

A general description of methods that may be used to find this approximate compensation network follows.

The poles and zeros may be added one at a time or in complex pairs. After each addition, Step 1 should be repeated. The total number of poles and zeros added to the compensation network must be at least large enough to satisfy equation (1). At the same time, of course, the final number of open-loop poles or zeros in the system must be at least equal to the total number of closed-loop poles specified.

When more zeros than poles must be added, the system may be made physically realizable by assuming that the poles which must accompany the excess zeros lie very far out on the negative real axis, where their contribution to the phase measurements may be neglected.*

It is easiest to work from phase relations as much as possible. In fact, for some problems, the selection of the compensation network can be accomplished from the phase relations alone.

It is usually desirable to select first the poles and zeros which must be placed between various open- and closed-loop poles and zeros on the real axis, beginning at the extreme right. The poles and zeros so selected should simultaneously help to satisfy the phase and gain requirements in the complex part of the s-plane.

When working in the complex portion of the s-plane, very often the arcs which satisfy the phase requirements at two points will intersect, thus yielding a single conjugate pair of complex poles or zeros. However, if these arcs do not intersect, it may mean that there are two real poles or zeros which will satisfy the phase requirements.* The interval bounded by these poles or zeros will contain the intersections of the arcs with the real axis. The choice between a pair of poles or zeros depends upon whether the phase required is lag or lead, respectively. A special case arises if both phase requirements lie between 0° and 180°. In this instance, the requirements may be satisfied by a pole and a zero on the real axis. Some techniques for constructing these real poles and zeros have been worked out, but as yet they are slower than iterative procedures.

If there are more open-loop poles than specified closed-loop poles, additional closed-loop poles will result whose locations are not known. If these extra closed-loop poles are to be exactly specified in location, at least one compensation pole or zero must be added to the open-loop system for each newly specified pole. Also for each specified pole one additional equation in the next step of this procedure must be found. If there are only one or two extra open-loop poles, and if complex, fixed, open-loop poles exist, it is usually simpler than using additional relations, to choose only an approximate location in some part of the s-plane where the closed-loop poles will not interfere with the closed-loop specifications on response. Since the compensation network being constructed in this step will satisfy phase exactly, the final location of these poles will be controlled to some extent by the phase it contributes to the complex, open-loop pole positions.

An alternative to the above is to use in the next step only equations derived from closed-loop poles. This will avoid the necessity of locating the extra closed-loop poles, since all of the measurements will concern only open-loop poles and zeros. However, if this is done, all control over the extra closed-loop poles will be lost.

3. Given n fixed closed-loop poles, construct $(n-1)$ independent equations from measurements at fixed open- or closed-loop poles or zeros. Choose as many phase equations as possible, since they are easier to work with, as will be shown in the examples.

Also, every phase measurement yields an equation, but two gain measurements are necessary to form an equation, since gain is not specified.

4. Set up an iterative cycle which includes all of the relations chosen in Step 3. To satisfy the relations move the compensation poles or zeros nearest the point of a measurement, i.e., nearest to the fixed pole or zero used in defining the relation. No compensation pole or zero is moved twice during the cycle.

*It may be pointed out that a single pair of complex zeros may be realized through the use of position plus rate plus acceleration feedback. Therefore, it is not always necessary that zeros be accompanied by at least a like number of poles. Furthermore, since the complex zeros are in the feedback circuitry, the transient response of the system is not changed by their presence.

*Appendix II presents a brief discussion of the case in which the arcs do not intersect.

It is often convenient to choose new measurements as the compensation network begins to take form in order that the measurement be close to the pole or zero subject to being moved. This usually assures convergence of the iterative process. A convergence test might be used here, but due to the speed at which the work progresses, the convergence test will not usually save an appreciable amount of time. Even if convergence does not take place, a little experimentation should soon reveal a cycle involving measurements which will converge. In the case where $p + q > n - 1$, only a total of $(n - 1)$ compensation poles and zeros need to be adjusted during the iterative cycle.

5. Find any closed-loop poles resulting from the addition of open-loop poles to the compensation network. Conventional methods or iterative methods such as those demonstrated in the following examples may be used.

For the reader's convenience in studying the examples, the five steps are listed below:

1. Measure the phase and gain at the fixed, complex poles and zeros, both closed- and open-loop, using the poles and zeros as noted in 1, 2, 3, 4 and 5 above. It will help in directing the later work to list the phase and gain required of the compensation network to produce the poles and zeros at which the measurements were made.

2. Determine the number and approximate location of the poles and zeros which exactly satisfy the phase of both the open- and closed-loop systems and roughly equalize the gain among the poles of each system.

3. Given n fixed closed-loop poles, construct $(n - 1)$ independent equations from measurements at fixed open- or closed-loop poles or zeros. Choose as many phase equations as possible, since they are easier to work with, as will be shown in the examples.

4. Set up an iterative cycle which includes all of the relations chosen in Step 3. To satisfy the relations move the compensation poles or zeros nearest the point of a measurement, i.e., nearest to the fixed pole or zero used in defining the relation.

5. Find any closed-loop poles resulting from the addition of open-loop poles to the compensation network. Conventional methods or iterative methods such as those demonstrated in the following examples may be used.

Examples

To demonstrate the iterative method, let the system shown in Figure 1 be used with the added, fixed closed-loop pole at -10. (See Figure 2.) This makes four, fixed closed-loop poles. Therefore, three relations are necessary, since gain is not specified. Two of these may be phase relations at the two, complex poles, and one may be a gain relation at any of the fixed poles, say C. A total of at least three compensation poles and zeros will be required to effect a unique solution.

At least one compensation pole is required, since three open-loop poles are given.* Let this be placed on the real axis to the right of C and D, say at -24, since in this position the phase from C and D will be zero.

The phase requirement is measured at A and found to be 168° lead or 192° lag. At B it is found to be 252° lead or 108° lag. The arcs that satisfy these angles are drawn and a pair of intersections occur to give two complex zeros F.**

These zero may be accepted as part of the compensation network. The compensation network now has one pole and two zeros which supply the minimum number of points needed to satisfy equation (1).

To test whether these are sufficient to determine the required compensation network, a graphical iterative procedure is used. Start the first cycle by placing the complex zeros at the arc intersections. Next, the gain is measured at C and made to equal the gain at B by moving the open-loop pole E. By constructing two new arcs to account for the phase change at A and B due to the movement of E, the zeros are corrected next. The second cycle is carried out in the same way, and the work continues until no further movement of compensation pole and zeros is necessary. The final compensation network is shown in the figure (primes denote the final positions).

The second example demonstrates the speed attained by the combined use of trial-and-error and iterative methods in compensating an unstable system. In this example, only part of the closed-loop poles have to be forced in the s-plane to provide stability and a transient behavior that might be suitable in some cases. A compensation network is generated by forcing these poles. The other closed-loop pole, determined by the compensation network, fortuitously lies in a position that gives acceptable transient response. Since the number of poles and zeros in the compensation network is a function of the number of closed-loop poles that are forced, a simpler compensation network results.

Consider the open-loop system which contains the five poles shown in Figure 3. This is an unstable system. In an attempt to make the system stable, a closed-loop pole is placed at A. The phase is measured at A, and the phase lead required to create the pole is produced by adding the compensating zero at E, $(p + q \geq 1)$.

*The number of closed-loop poles must equal the number of open-loop poles or open-loop zeros.
**The intersections of the lag-arcs do not fix open-loop poles, since the arc from A was determined from the closed-loop phase requirements at A and thus, is the locus of closed-loop poles.

It is next desired to find the remaining closed-loop poles of the system, whose locations are affected by the addition of the compensation zero. The gain of the open-loop system required to produce the closed-loop pole at A is found by measuring the gain at A. This gain is a function of open-loop poles and zeros only. Preparatory to starting the first cycle in this problem, it is convenient to assume that the real closed-loop pole corresponding to the open-loop pole B is at B'. (A solution can be found if the closed-loop pole is assumed to be at B.) The first cycle then proceeds in the following way. The phase is measured at C, an open-loop pole, using all closed-loop poles and zeros, and the phase required to porduce C is determined in accordance with relation 1. The complex pair of poles which may be in the vicinity of C may be neglected in this measurement. The arc C' is drawn for the locus of complex poles satisfying that phase requirement. (It is evident, at this point, that the closed-loop poles are probably unstable, or at least one of them is, since the arc lies in the right-half plane. The iterative cycle described below for exactly locating the closed-loop poles is shown, therefore, only for instructive purposes.) The gain at C is made equal to the gain at A by placing the closed-loop pole at D'. (This may be done approximately on the first cycle by assuming the lower closed-loop pole is at the lower open-loop pole. After the upper pole is placed, the lower pole takes its conjugate position. The next cycle continues in a similar manner.) The gain at B is then made equal to the gain at A by moving the closed-loop pole B'.

The first cycle is now complete. The second cycle is started by measuring the phase at C, again neglecting the adjacent complex pair of closed-loop poles. Two complete cycles for this problem will most likely produce poles to the accuracy required for trial-and-error purposes. The final closed-loop poles other than A are D" and B".

Since the system is still unstable, another attempt at stabilization must be made. Figure 4 shows the next step that might be taken in the trial-and-error process. The phase at C will be altered in such a way as to force a pole into the left-half plane. If a pair of complex zeros is used to accomplish this, the residue of the resulting closed-loop pole may be made small by placing the zero close to the closed-loop pole. Now it is most likely that the zero will lie close to the closed-loop pole if the closed-loop pole is placed close to the open-loop pole. Therefore, the problem of stability and residue will be solved by forcing a closed-loop pole to exist adjacent to the open-loop pole by means of complex zeros. The stable pole at D will be forced simultaneously with the pole at A.

(Four closed-loop poles are to be forced. Therefore, $p + q \geq 3$.)

The iterative cycle may be carried out as follows, using only closed-loop pole relations in order not to include the closed-loop pole which must exist on the real axis. The phase lead requirement is measured at D; the zero at E is included in the measurement. Arc DD' is constructed so that a pair of complex zeros lying on this arc will satisfy the phase requirement. The gain at D is made equal to that at A by placing an upper-half plane zero on this arc. The lower zero is temporarily assumed to be at D'. The phase requirement is next measured at A and satisfied by moving the real zero E. The cycle is then repeated until the zeros, E' and F', are found. The closed-loop pole at B' is found by placing it so that the gain at B equals the gain at A. Note that the residue at B' will probably be small compared to the residue at A, since the zero, E', lies close to it.

The compensation network, just constructed, contains three zeros. If all the closed-loop poles had been fixed, a total of at least four poles and zeros would have been required.

Theory and Comparison with Cancellation Methods

The general theory underlying the method is presented in this section, with a comparison with the theory underlying cancellation methods.

Consider the feedback system shown in block diagram form below.

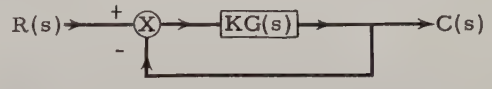

The expression for the closed-loop function is:

$$\frac{R(s)}{C(s)} = \frac{KG(s)}{1 + KG(s)} = Y(s) \qquad (2)$$

where K is a positive number.

A compensation network is to be selected, given the poles and zeros of Y(s) and some of the poles and zeros of G(s).* For example, G(s) may contain fixed poles and zeros, sometimes called the plant, and the poles and zeros of Y(s) may be defined by closed-loop specifications.

*It is assumed throughout this paper that all functions of s can be expressed as ratios of polynomials in s. Also G(s) is written in the following form:

$$G(s) = \frac{\prod_{i=1}^{m} (s - z_i)}{\prod_{i=1}^{n} (s - p_i)}$$

Let $G(s)$ be defined as,

$$G(s) = G_f(s)\, G_c(s)$$

where $G_f(s)$ is a rational function representing the plant poles and zeros, and $G_c(s)$ represents the compensation poles and zeros.

Substituting for $G(s)$ in equation (2),

$$Y(s) = \frac{KG_f(s)\, G_c(s)}{1 + KG_f(s)\, G_c(s)} \qquad (3)$$

Solving for $G_c(s)$,

$$G_c(s) = \frac{1}{G_f(s)} \cdot \frac{1}{K} \cdot \frac{Y(s)}{1 - Y(s)} \qquad (4)$$

It is obvious that if $G_c(s)$ is to be manufactured without modification of $Y(s)$, it must cancel out all poles and zeros of $G_f(s)$ which is the basis for cancellation compensation. However, if modification of $Y(s)$ is allowed, it may be possible to select a simpler network. Although the response of $Y(s)$ will be altered by such modifications, further modification of $Y(s)$ can be made to assure that it will meet closed-loop specifications.*

Let $Y(s)$ be defined as,

$$Y(s) = Y_f(s)\, Y_v(s) \qquad (5)$$

where $Y_f(s)$ represents the poles and zeros which are specified in the s-plane and $Y_v(s)$ contains the closed-loop poles and zeros resulting from added compensation open-loop poles and zeros.

Let

$$\left.\begin{aligned} G_f(s) &= \frac{N_{gf}}{D_{gf}} \\ Y_f(s) &= \frac{N_{yf}}{D_{yf}} \\ Y_v(s) &= \frac{N_{yv}}{D_{yv}} \end{aligned}\right\} \qquad (6)$$

Substituting equations (5) and (6) in equation (4),

$$G_c(s) = \frac{D_{gf}}{N_{gf}} \cdot \frac{1}{K} \cdot \frac{N_{yf} N_{yv}}{D_{yf} D_{yv} - N_{yf} N_{yv}} \qquad (7)$$

*In fulfilling closed-loop specifications, it should be remembered that any realizable part of the compensation network can be placed in the feedback part of the closed-loop system, thereby altering the closed-loop system performance. Therefore, all possible arrangements of the compensation network should be explored.

Thus equation (4) has been rewritten as equation (7) to show that by allowing $Y(s)$ to vary, a simpler compensation network may arise. For example, zeros of N_{gf} may become zeros of N_{yv} or $D_{yf} D_{yv} - N_{yf} N_{yv}$ may contain D_{gf} as a factor.

Conclusions

A graphical method has been presented for finding compensation networks given fixed open-loop and closed-loop poles and zeros. For any number of specified closed-loop poles and zeros, the minimum total number of compensation poles and zeros is given by equation (1).

The method assumes that at least some of the closed-loop poles and, possibly, zeros are known or specified. Phase and gain measurements at the fixed poles and zeros of the open- and closed-loop systems are made to determine the type of compensation network required. The phase and gain measurements also provide the information necessary for carrying out the iterative steps leading to the correct placement of the compensation poles and zeros. A minimum of phase and gain measurements is required. Thus the time required in carrying out this method is greatly reduced over other existing methods. A simple procedure for locating complex pairs of poles or zeros of the compensation network has been shown, so that it is almost as easy to use complex poles or zeros as real poles or zeros.

The method, in general, leads to simpler compensation networks than would result from the cancellation methods suggested by equation (4). Further simplification can result if the closed-loop system is not exactly specified, but allowed to move as do the compensation poles and zeros.

The use of this graphical method makes possible rapid gain and phase measurements by means of the Spirule or other tools. And, of course, the advantages of the s-plane are retained. Working with the graph also provides considerable insight on how to produce and manipulate a compensation network.

Appendix I

Technique for Constructing Complex Poles and Zeros

Figure 5 shows the geometrical relations that prove that the locus of complex conjugate poles or zeros, S_1 and S_2, producing a constant phase ϕ at a point P in the s-plane, is an arc of a circle passing through that point. The center of the circle lies on the real axis.

From the figure:

$$a = 90^\circ + \alpha + \beta$$

$$b = 90^\circ + \alpha$$

Hence, $a + b = \beta + 2\alpha + 180^\circ = \phi =$ angle contributed by complex pair at point P (1)

But $\beta + 2\alpha + \gamma = 180^\circ$ (2)

Subtracting equation (2) from equation (1)

$$360^\circ - \phi = \gamma = \text{a constant}$$

The vertex of γ, therefore, lies on an arc PP' of a circle whose center is on the real axis by a fundamental theorem of plane geometry.

The center, C, may readily be found as illustrated on the figure. Here the line $\overline{PC}$ is constructed at P to make the angle, θ. $\theta = \phi$ or $\phi - 180^\circ$, depending on whether ϕ is $<$ or $> 180^\circ$.

Appendix II

In the system shown in Figure 6, the phase lead requirements at A and B are 100° and 240°, respectively. The arcs resulting from these requirements fail to intersect, as shown. The points A' and B' are the locations of two zeros which satisfy the phase requirements. They are found by the following iterative procedure.

Since points A' and B' will always fall outside the interval (P, P'), a zero may be placed any point to the right of P' (the intersection of the arc A with the real axis). Let this point be A_1. The phase at B is then measured using this point as if it were a fixed zero. The point B_1 is located by finding the point on the real axis which satisfied the phase requirement at B. The phase is then measured similarly at A using the point B_1 as if it were a fixed zero, and placing the point A_2 on the real axis to satisfy the phase at A, thus completing the first cycle. The process is continued until only a negligible movement of the two points occurs. This method seems to require less time and work than any construction technique, tried to date, which exactly locates the desired points.

Figure 7 shows two arcs which fail to intersect in a somewhat different manner. The phase lead requirement at A is 75° and at B, 89°. To start, a zero may be placed at A_1; the phase is measured at B, and B_1 is placed to satisfy it. The next step gives A_2, but B_2 falls far to the left on the axis (completely off the graph). This suggests that there is no solution using two real zeros for this case. However, the zero to the left may be changed to a pole and placed on the graph at, say, B_3. Then convergence to the pole at B' and the zero at A', via B_4 and A_3, will take place. Thus, the choice of a usable combination of poles and zeros was guided by the iterative method in this example. More complicated examples have been worked in the same manner.

References

1. Truxal, J. G., Automatic Feedback Control System Synthesis, Chap. 5, McGraw-Hill Book Co., Inc., New York, 1955.

2. Aseltine, J. A., "Feedback System Synthesis by the Inverse Root-Locus Method," IRE Conv. Rec., Part II, March 1956, pp. 13-17.

3. Walters, L. G., "Optimum Lead-Controller Synthesis in Feedback-Control Systems," Trans. IRE, Vol. CT-1, No. 1, 1954, pp. 45-48.

4. Mortensen, R. E., "The Determination of Compensation Networks for Feedback Systems to Produce Specified Closed Loop Roots," STL Document (TR-59-0000-00781), 11 August, 1959.

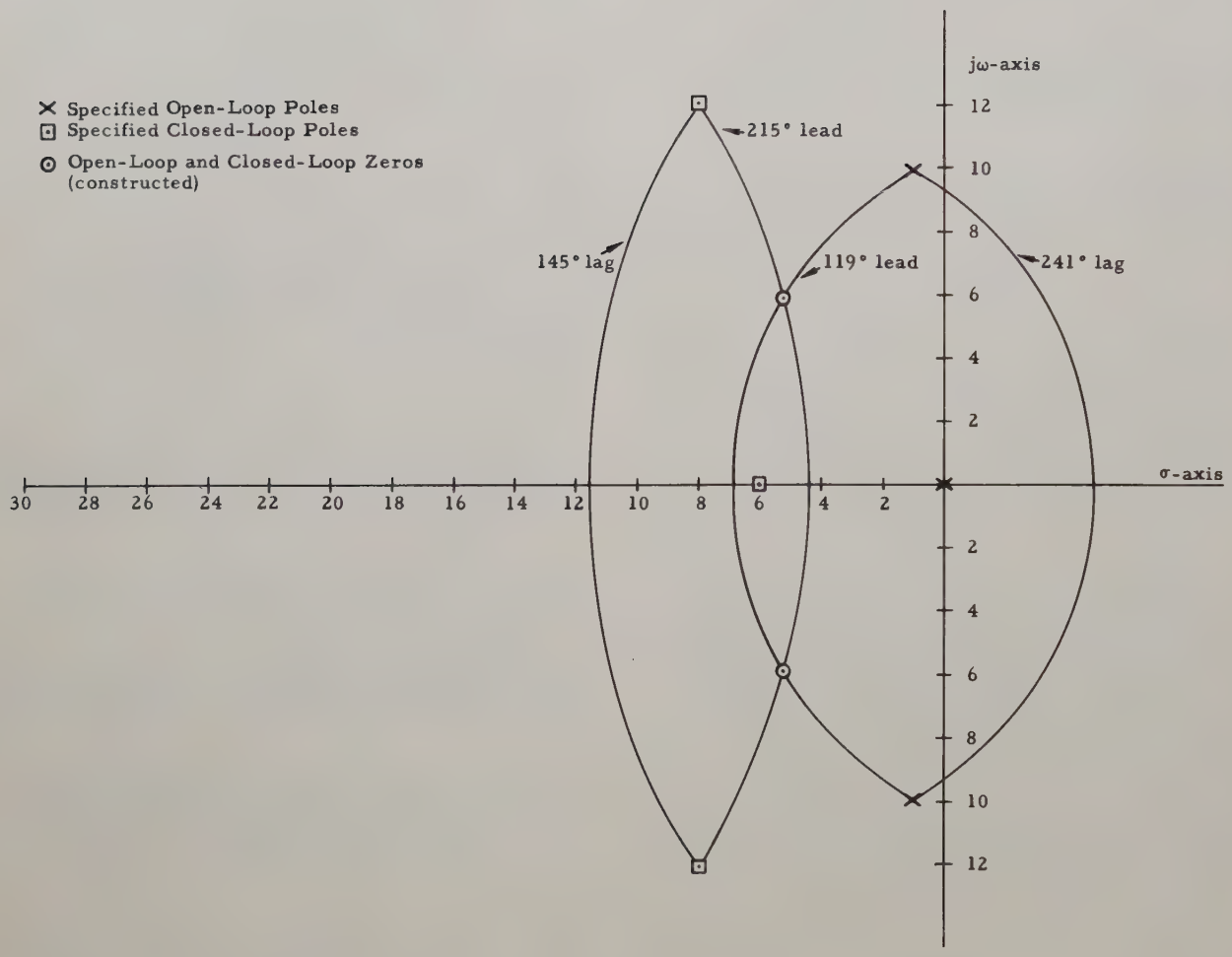
Specified Open-Loop Poles
Specified Closed-Loop Poles
Open-Loop and Closed-Loop Zeros (constructed)
jω-axis
σ-axis
215° lead
145° lag
119° lead
241° lag
30 28 26 24 22 20 18 16 14 12 10 8 6 4 2
12 10 8 6 4 2 2 4 6 8 10 12

Fig. 1.

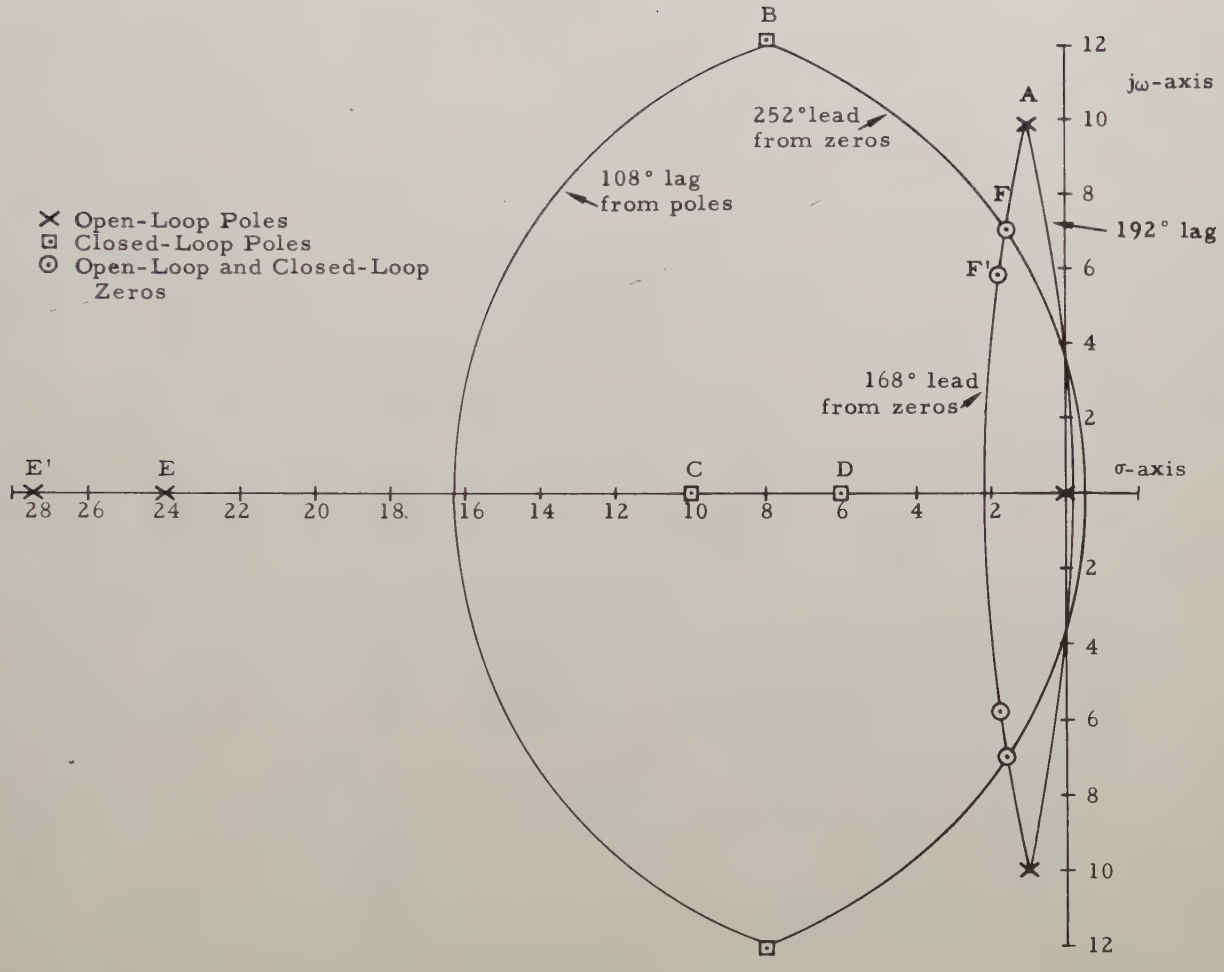
B
A
F
F'
E'
E
C
D
252° lead
from zeros
108° lag
from poles
168° lead
from zeros
192° lag
jω-axis
σ-axis
Open-Loop Poles
Closed-Loop Poles
Open-Loop and Closed-Loop
Zeros
28 26 24 22 20 18 16 14 12 10 8 6 4 2
12 10 8 6 4 2 2 4 6 8 10 12

Fig. 2.

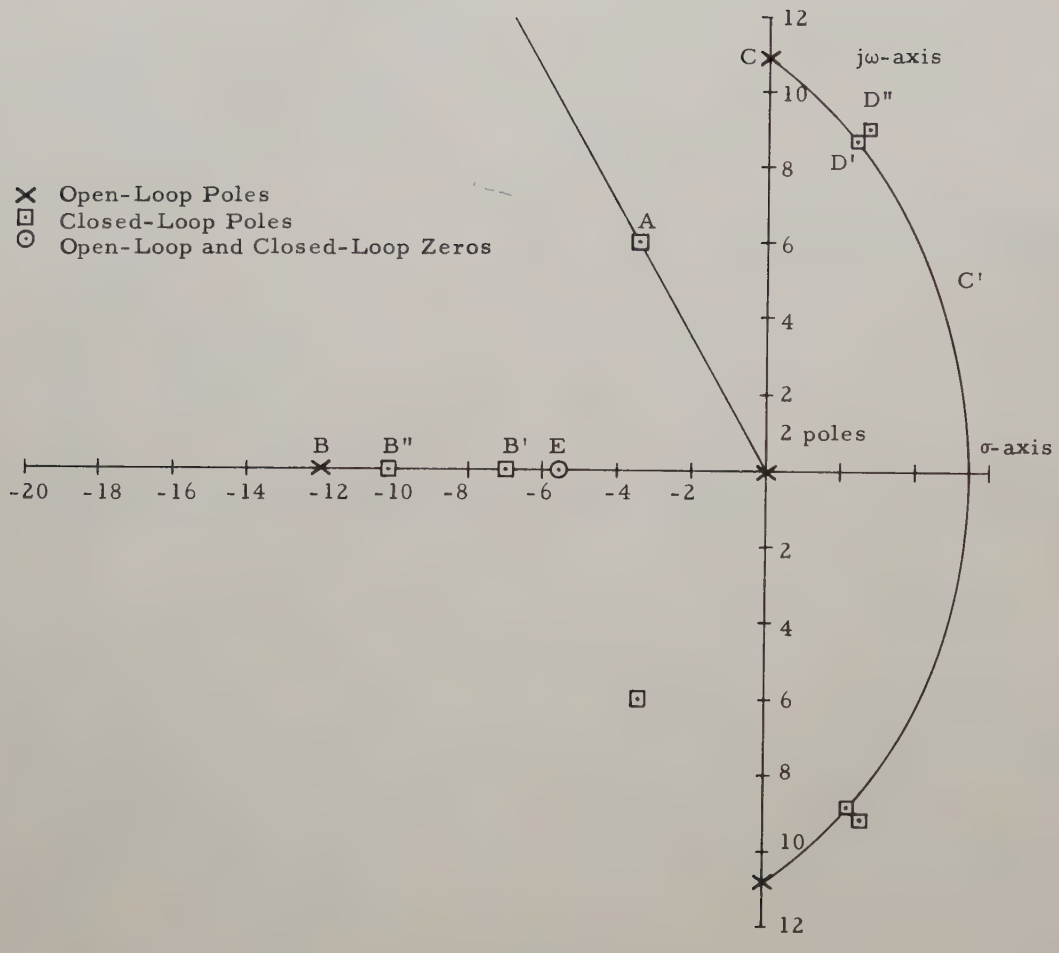
Open-Loop Poles
Closed-Loop Poles
Open-Loop and Closed-Loop Zeros
jω-axis
σ-axis
C
D"
D'
C'
A
B
B"
B'
E
2 poles
12
10
8
6
4
2
-20
-18
-16
-14
-12
-10
-8
-6
-4
-2

Fig. 3.

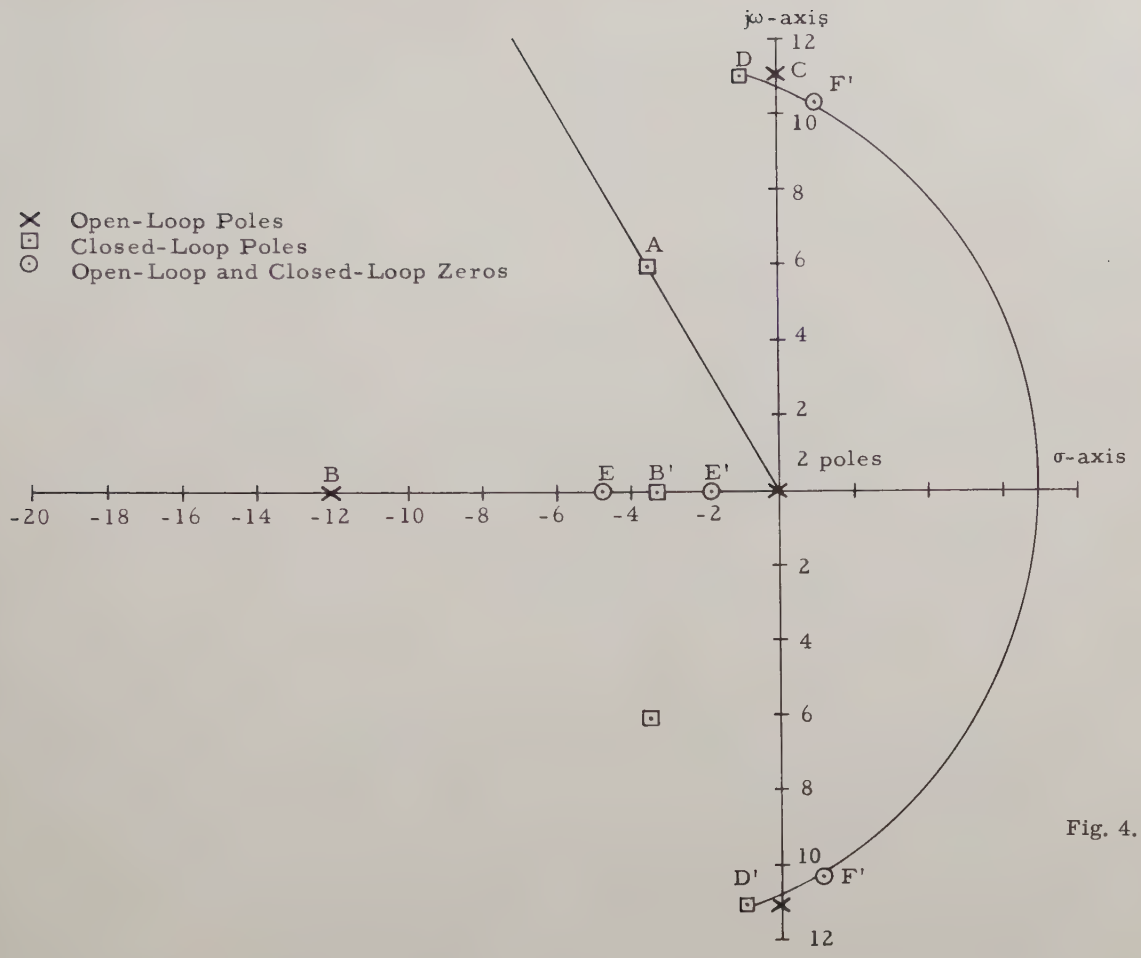
jω-axis
σ-axis
Open-Loop Poles
Closed-Loop Poles
Open-Loop and Closed-Loop Zeros
2 poles
A
B
C
D
E
B'
E'
F'
D'
12
10
8
6
4
2
-20
-18
-16
-14
-12
-10
-8
-6
-4
-2

Fig. 4.

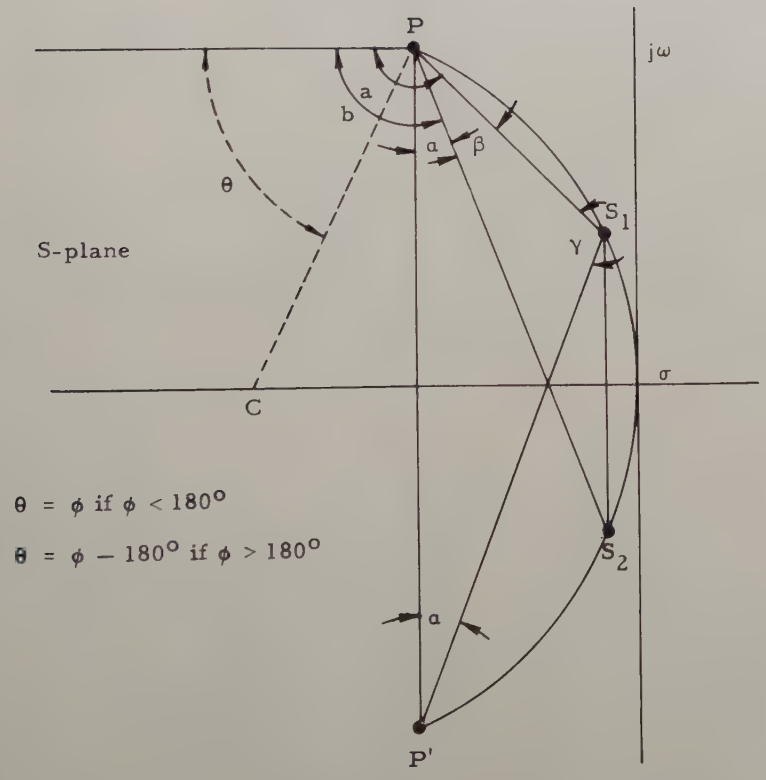
P
jω
a
b
α
β
θ
S-plane
S1
γ
σ
C
θ = φ if φ < 180°
θ = φ − 180° if φ > 180°
S2
α
P'

Fig. 5.

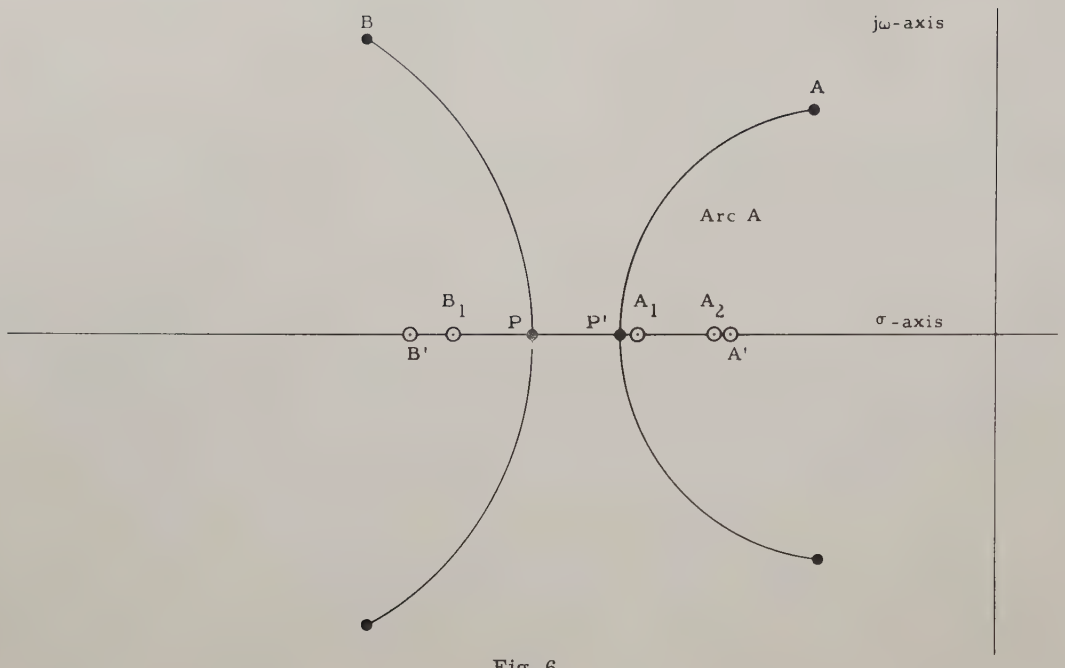
B
jω-axis
A
Arc A
B1
P
P'
A1
A2
σ-axis
B'
A'

Fig. 6.

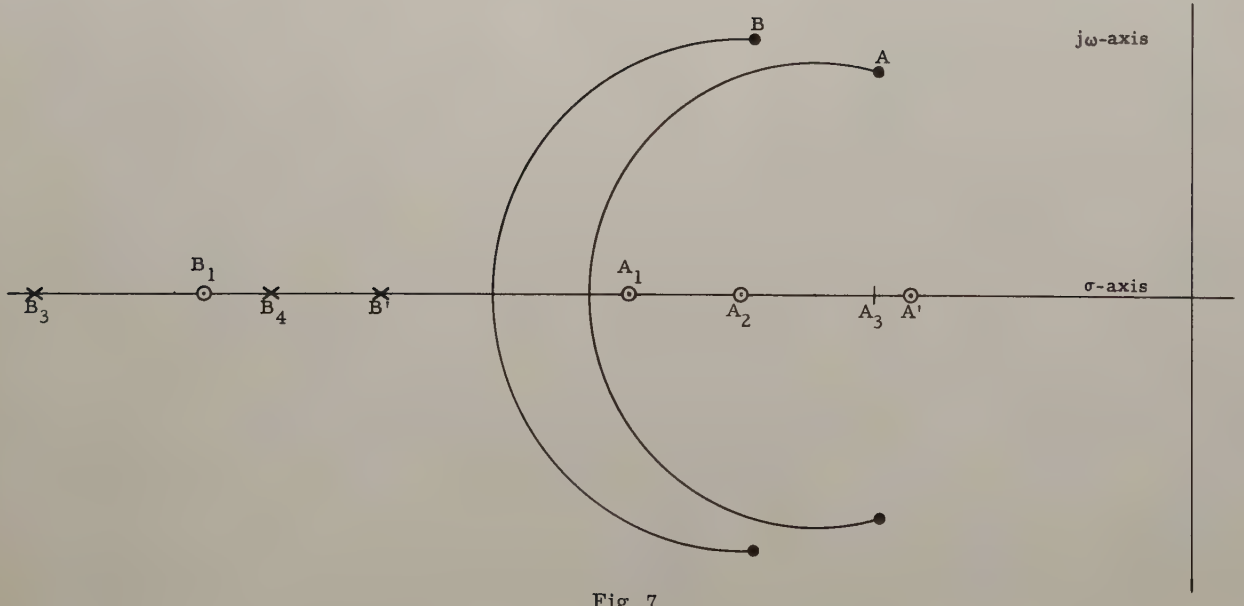
B
jω-axis
A
B1
A1
σ-axis
B3
B4
B'
A2
A3
A'

Fig. 7.

CALCULATING ZEROES OF FUNCTIONS ARISING IN VARIOUS CONTROL SYSTEM PROBLEMS

W. R. Evans
Aeronutronic, A Division of Ford Motor Company
Newport Beach, Calif.

Abstract

The paper considers three separate special cases of functions for which the zeroes are determined graphically. First, the spring constant of a structural member is replaced by a complex number to allow for hysteresis losses during vibration. The corresponding characteristic function has non-conjugate zeroes which are useful in calculating frequency response, but have no meaning for transient response. Secondly, vibration acting along the input axis of a pendulous accelerometer causing displacement of the proof mass; an in-phase cross vibration will cause a rectified torque. The real part of the compliance function is needed; knowing the zeroes is useful but not necessary in evaluating the integral over the frequency range by use of residues. Third, sampled-data systems have z transforms which often involve the sum of reciprocals of vectors. Finding real values of zeroes is simplified because only magnitudes need be considered; some graphical techniques can simplify the general vector problem. For each of the above problems alternate methods of calculation can be used; those presented are most apt to be of value to those engineers who are used to working with zeroes and poles.

This paper will be published by the AIEE.

RANDOM SAMPLING: ITS EFFECT ON SPECTRAL DENSITY

A. R. Bergen
University of California
Berkely, Calif.

Abstract

There are sampled-data systems of interest in which the sampling intervals are random variables. An example is a track-while-scan radar with a non-ideal blip scan ratio. In the statistical design of such systems it may be necessary to compute the spectral density of a random signal at the output of a random sampler. If the sampling intervals are independent, this spectral density may be determined from a complex convolution integral which, in many cases of practical interest, is easily evaluated in closed form by the method of residues. Consider a sampler which ideally operates periodically but actually misses samples with some probability. For this case the following result is obtained: the spectral density at the output of the non-ideal sampler is unchanged by replacing the non-ideal sampler by an ideal (periodic) sampler and adding to its output uncorrelated white noise of specified spectral density. When this result is used in the statistical design of a track-while-scan extrapolator it is found that the miss probability profoundly affects the system design. Neglect of this factor may, in fact, result in systems which are unstable in the mean square.

This paper is to be published in the Proceedings of the First IFAC Moscow Congress by Butterworth Scientific Publications in 1960.

SPECTRAL CHARACTERIZATION OF CONTROL SYSTEM NONLINEARITIES

R. B. McGhee

System Development Laboratories
Hughes Aircraft Company
Culver City, California

Summary

Control system feedback elements are subject to statistical variation from their desired characteristics due to manufacturing tolerances. For most feedback elements, this variation takes the form of a random nonlinear function of the input to the element. Analysis of the effects of such feedback errors is exceedingly difficult because the control system affected must be described by a random nonlinear differential equation. It is proposed that this difficulty be surmounted by computer simulation.

For purposes of simulation, a power spectrum is developed for the ensemble of feedback error functions. This power spectrum is then used to synthesize artificial nonlinearities in the simulation of the control system. By simulating groups of components with different statistical properties, production specifications can be generated based on parameters borrowed from noise theory such as power spectral density, noise bandwidth, rms error, etc.

This development is followed by two experimental examples which illustrate the application of the method and display the concept of bandwidth as applied to a feedback nonlinearity. It is shown that, in some situations, linearizing approximations permit analytic determination of the effects of random feedback error. In other problems, the utilization of power spectra permits the normalization of computer results.

Introduction

Control system components are manufactured to achieve a prescribed relationship between the input to a device and its output. The accuracy of this relationship depends upon production tolerances. The output of a production line thus consists of an ensemble of similar devices possessing statistical deviations from a desired characteristic. By the use of feedback control, the effects of such deviations are greatly reduced except in the very important case of irregularities associated with feedback elements. Such errors may add directly to the over-all system errors or even cause instability of the control loop. For most feedback elements, the variation from the desired input/output relationship takes the form of a random nonlinear function of the input to the element. An important example of such a nonlinearity is the deviation from linearity of a feedback potentiometer as a function of shaft angle. Another example of a nonlinear feedback error is the error introduced into the radar tracking system of a missile by the interaction of the missile's radome with the incident electromagnetic radiation. Both of these errors are random functions of an angle if an ensemble of devices is considered. If such a component is selected at random from a large production sample, the only statements that can be made, a priori, about its deviations from the desired characteristics are statistical statements.

When an element of this type is included in a control loop, a very serious complication of the mathematical description of the control system results. Unless statistical variations of the members of the ensemble of elements can be ignored (in which case no statistical characterization is required), the control system is described by a random nonlinear differential equation. This difficulty means that the control system performance cannot be determined by analysis except by a prohibitive amount of labor since an ensemble of nonlinear differential equations (one equation for each member of the ensemble of components considered) must be solved to determine the effects of component variability. If, in addition, the input to the control system is a random variable in time, one must certainly abandon analysis and resort to experiment to obtain system performance. This experimentation generally takes the form of simulation of the control system on an electronic computer. Unfortunately, such simulation is also quite difficult since it is not easy to say what constitutes a "typical" member of the group of components being considered. One solution to this problem is to undertake a physical simulation program utilizing a large number of component samples, closing the control loop with a computer if necessary. This may be quite effective for certain types of components. However, if the variables affected by the nonlinearity are not readily available in physical form, such simulation may be very difficult and costly. In the previously mentioned missile example, physical simulation requires construction of an electromechanical target simulator, a missile flight table, and considerable auxiliary equipment.

This paper outlines a computer simulation technique which permits a statistical evaluation of the effects of random nonlinearities on a control system without recourse to physical simulation. The technique rests on obtaining a "power" spectrum for the nonlinearity by measuring over a large sample of components. This "power" spectrum is then used to generate a family of functions having the same statistical properties as the

nonlinearities. By selecting members from this family, system performance can be evaluated on a computer for a collection of synthetic components. Finally, by simulating groups of components with different statistical properties, specifications can be generated based on parameters borrowed from noise theory such as power spectral density, noise bandwidth, rms error, etc. Specifications of this type may alleviate some manufacturing problems and at the same time permit a more realistic optimization of control system parameters. They may also aid considerably in the interpolation and extrapolation of simulation results for nonlinear systems.

The following paragraphs discuss the necessary definitions and describe the computer techniques required to realize the desired nonlinearity. Two examples illustrate the application of the method.

Measurement and Description of the Nonlinearity

Let $y(x)$ be a statistical nonlinear function of x. By "statistical", we mean that, a priori, only statistical properties of the function are known. The statistics are determined by measurements on a large number of similar devices. As a first step in analyzing $y(x)$, we transform the measured functions to a new set of functions with unity variance and zero mean,

$$z(x) = \frac{y(x) - \bar{y}(x)}{\sigma_y(x)} \tag{1}$$

where $\bar{y}(x)$ is the mean of $y(x)$ averaged over the available sample of nonlinearities and $\sigma_y^2(x)$ is the sample variance; i.e.,

$$\overline{y(x)} = \frac{1}{n} \sum_{j=1}^{n} y_j(x) \tag{2}$$

$$\sigma_y^2(x) = \frac{1}{n}\left[\sum_{j=1}^{n} y_j^2(x)\right] - \bar{y}^2(x) \tag{3}$$

The variable $y_j(x)$ is a specific function obtained by measurement of the j^{th} nonlinearity.

In practice, the family of functions, $y(x)$, will be defined only over a finite interval in x. Let the length of the interval be $2X$; i.e., $y(x)$ is defined over $a - X < x < a + X$. Outside this interval, let $z(x)$ be periodic:

$$z(x) = z(x + 2X) \tag{4}$$

Figure 1 illustrates a normalized periodic nonlinearity. The functions, $z(x)$, now exhibit a degree of regularity. A particular characteristic, $z_j(x)$, is similar to a noise voltage except that it is a function of a control system coordinate, x, rather than a function of time and it is, by definition, periodic. The sample statistics are stationary with regard to the mean and variance.

One might hope, therefore, to employ statistical parameters related to those commonly employed in the theory of stationary random noise to characterize the sample of nonlinearities. In the time domain, a noise voltage may be characterized by a correlation function. We therefore define a sample averaged correlation function for $z(x)$ as

$$R(x,\xi) = \overline{z(x)z(x+\xi)} \tag{5}$$

$$= \frac{1}{n} \sum_{j=1}^{n} z_j(x) z_j(x+\xi) \tag{6}$$

The argument averaged correlation function for the j^{th} member of the set of nonlinearities is defined as:

$$R_j(\xi) = \frac{1}{2X} \int_{-X}^{X} z_j(x) z_j(x+\xi)\,dx \tag{7}$$

$$= \overbrace{z_j(x) z_j(x+\xi)} \tag{8}$$

The argument and sample averaged correlation function is:

$$R(\xi) = \overbrace{R(x,\xi)} = \frac{1}{2Xn} \sum_{j=1}^{n} \int_{-X}^{X} z_j(x) z_j(x+\xi)\,dx \tag{9}$$

For $z(x)$, all of these autocorrelation functions are periodic in ξ with period $2X$ since, by definition,

$$z(x+\xi) = z(x+\xi+2X) \tag{10}$$

If the nonlinearity is stationary, then, as the number of samples approaches infinity,

$$R(\xi) \longrightarrow R(x,\xi) \tag{11}$$

so long as x and $x + \xi$ are confined to the basic interval of definition. Since $z_j(x)$ is a periodic random process, in general

$$R_j(\xi) \neq R(\xi) \tag{12}$$

so the family of nonlinearities is not ergodic.

Utilization of the correlation functions above corresponds to the time domain characterization of a noise voltage. It is also possible to specify and measure random functions in a transform or "frequency" domain. Again borrowing from noise theory, we can define a two sided power spectral density for $z(x)$ as:

$$G(f) = \lim_{\alpha \to \infty} \frac{1}{2\alpha} \overline{\left| \mathcal{F}_\alpha \left\{ z_j(x) \right\} \right|^2} \tag{13}$$

where $\mathcal{F}_\alpha$ is a Fourier transform of z over a finite interval, 2α:

$$\mathcal{F}_\alpha \left\{z_j(x)\right\} = \int_{-\alpha}^{\alpha} z_j(x) e^{-j2\pi fx} dx \qquad (14)$$

It should be noted that the dimensions of f are inverse x rather than inverse time. The Wiener-Khintchine relationhip states that $R(\xi)$ and $G(f)$ form a Fourier transform pair:[2]

$$G(f) = \int_{-\infty}^{\infty} e^{-j2\pi f\xi} R(\xi) d\xi \qquad (15)$$

$$R(\xi) = \int_{-\infty}^{\infty} e^{j2\pi f\xi} G(f) df \qquad (16)$$

A corollary result is

$$\overline{z^2(x)} = R(0) = \int_{-\infty}^{\infty} G(f) df = 1 \qquad (17)$$

To evaluate $G(f)$, we note that since $z(x)$ is periodic in an interval $2X$, a particular characteristic, $z_j(x)$, may be represented by a Fourier series:

$$z_j(x) = \frac{a_o}{2} + \sum_{k=1}^{\infty} \left\{a_{kj} \cos \omega_k x + b_{kj} \sin \omega_k x\right\} \qquad (18)$$

$$\omega_k = 2\pi f_k; \quad f_k = k\Delta f; \quad \Delta f = \frac{1}{2X}$$

where

$$a_{kj} = \frac{1}{X} \int_{-X}^{X} z_j(x) \cos \omega_k x \, dx$$

$$b_{kj} = \frac{1}{X} \int_{-X}^{X} z_j(x) \sin \omega_k x \, dx \qquad (19)$$

An analog or digital computer may be used to determine the a_{kj} and b_{kj} from measurements. Since the ensemble of nonlinearities is not ergodic, in general

$$a_{kj} \neq a_{k\ell} \qquad (20)$$

$$b_{kj} \neq b_{k\ell}$$

Rather, a_n and b_n are random variables whose distributions may be abstracted from the sample. The correlations between coefficients must be considered when constructing this distribution.

The two sided power spectral density (13) for such a function is:[1]

$$G(f) = \mathcal{F}\left\{R(\xi)\right\} = \frac{\overline{a_o^2}}{4} \delta(f) + \sum_{n=1}^{\infty} \frac{\overline{a_k^2} + \overline{b_k^2}}{4} \left[\delta(f - f_k) + \delta(f + f_k)\right] \qquad (21)$$

where

$$\overline{a_k^2} = \frac{1}{n} \sum_{j=1}^{n} a_{kj}^2$$

$$\overline{b_k^2} = \frac{1}{n} \sum_{j=1}^{n} b_{kj}^2 \qquad (22)$$

Thus the power spectral density for the sample of nonlinearities is obtainable either from harmonic analysis (21) or from the Fourier transform of the autocorrelation function (15).

Note that the power spectral density and correlation functions described above are themselves random variables since they are derived from sample statistics. That is, the functions obtained for $R(\xi)$ or $G(f)$ will vary depending upon which particular components are selected from the production line for testing. In order to minimize this effect, the number of production samples taken should be quite large. It will be assumed in the remainder of this paper that the sample is large enough to provide an adequate estimate of the ensemble (entire production) power spectrum.

In the following treatment, the sample power spectral density along with the sample mean, $\overline{y}(x)$, and the sample variance, $\sigma_y(x)$, is taken as the basic statistical description of the feedback error function, $y(x)$. Certainly, other statistical characterizations of the nonlinearity are possible. However, the power spectral density is one of the simplest measures which contains information regarding the frequency content of the nonlinearity. In the special case when the normalized functions, $z(x)$, are representable as samples drawn from a parent population whose ensemble statistics are stationary and Gaussian, the power spectral density is entirely adequate for a complete statistical description of the family of functions. The degree of departure of the nonlinearities from stationarity and a Gaussian amplitude distribution certainly has a bearing on the likelihood that the power spectral density is an adequate statistic. In some cases, it is probable that the validity of the spectral density as a description of the nonlinearities can be established only by simulation.

Simulation of the Nonlinearity By Harmonic Synthesis

Having obtained a statistical representation for the ensemble of feedback elements, it is now necessary to find a way of artificially creating such an element on a computer. The first simulation method which comes to mind is to represent the feedback functions by a random Fourier series (18). The coefficients, a_{kj} and b_{kj}, can be chosen from a table of random numbers having the same statistical properties as the data obtained by measurement of the sample (19). Alternatively, a noise generator with proper filtering may be used to generate the a_k and b_k for successive simulation runs. This representation of the nonlinearity will result in an ensemble having the proper power spectrum (21). However, the class of functions resulting from this expansion is somewhat more restrictive than all those satisfying (22) since phase information is preserved by considering both a_k and b_k whereas phase information is destroyed in forming the power spectrum (21). In keeping with the spirit of spectral characterization of the nonlinearities, we ought to neglect phase information and simply match the power of G(f) in a frequency interval, Δf. Thus we might well employ the synthetic set of nonlinearities:

$$z_j^*(x) = \frac{c_{oj}}{2} + \sum_{k=1}^{\infty} c_{kj} \cos(\omega_k x + \phi_{kj}) \qquad (23)$$

$$c_{kj} \geq 0$$

ϕ_{kj} = phase angle chosen from a uniform population distributed between 0 and 2π radians

If the ensemble of functions, $z^*(x)$, is to have the same spectral density as the set of functions, $z(x)$, then (due to the orthogonality of the sines and cosines of equation (18)) c_{kj} must be chosen from a distribution such that

$$E\left\{c_k^2\right\} \equiv \lim_{n \to \infty} \frac{1}{n} \sum_{j=1}^{n} c_{kj}^2 = \overline{a_k^2} + \overline{b_k^2} \qquad (24)$$

where $\overline{a_k^2}$ and $\overline{b_k^2}$ are the sample statistics of equation (22) and $E\{c_k^2\}$ denotes the expected value or population average of c_k^2. The form of the distribution of the c_k will not affect the power spectrum.

Equation (23) is still not amenable to simulation since it is an infinite series. Fortunately, any reasonable sort of nonlinearity will have a finite bandwidth; i.e., the power will be concentrated in relatively few harmonics of the fundamental frequency. When this is the case, the function $z_j^*(x)$ may be approximated by a finite number of Fourier components:

$$z_j^*(x) \cong z_j'(x) = \frac{c_{oj}'}{2} + \sum_{k=1}^{\infty} c_{kj}' \cos(\omega_k x + \phi_{kj}) \qquad (25)$$

where the c_{kj}' are obtained from operations on the c_{kj} and are all zero except for a finite number. One way of obtaining a statistical description for the c_{kj}' is to lump power from several frequencies (in $z^*(x)$) into a single frequency so that all the components of $z'(x)$ have more or less equal average power. On the other hand, it may be that the low frequency (or high frequency) terms of $z(x)$ are more important in the closed loop than other terms and should be reproduced more faithfully. The determination of just how to truncate the series is a matter of engineering judgement as in the practical truncation of any infinite series. Simulation of the complete control system can aid in this decision.

Once the desired mean square values of the coefficients have been determined, it is still necessary to mechanize a method of selecting values for the c_{kj}' and ϕ_k. While the ϕ_k is to be uniformly distributed, the only restriction on c_{kj}' is that the probability of negative values be zero (except for c_o). Both of these requirements are met by selecting a Rayleigh distribution for c_{kj}' and writing equation (25) in the alternate form

$$z_j'(x) = \frac{a_{oj}'}{2} + \sum_{k=1}^{\infty} a_{kj}' \cos \omega_k x + b_{kj}' \sin \omega_k x \qquad (26)$$

Now if a_{kj}' and b_{kj}' are drawn from a Gaussian population and are uncorrelated and furthermore

$$E\left\{a_{kj}'\right\} = E\left\{b_{kj}'\right\} = 0 \qquad (27)$$

$$E\left\{a_{kj}'^2\right\} = E\left\{b_{kj}'^2\right\} = \frac{1}{2} E\left\{c_{kj}'^2\right\}$$

then c_{kj}' will have the desired Rayleigh distribution and ϕ_{kj} will be uniformly distributed. Gaussian noise generators can be used to obtain the coefficients a_{nj}' and b_{nj}'. The zero frequency term, c_{oj}', may also be selected from a Gaussian zero mean source. Either time or frequency multiplexing techniques will permit substantially uncorrelated samples to be drawn from the same noise generator.

Once $z'(x)$ has been generated, a representation of the original function, $y(x)$ is obtained by multiplying $z'(x)$ by $\sigma_y^2(x)$ (equation 3) and adding $\bar{y}(x)$ (equation 2). These terms are easily generated on diode function generators or curve followers.

Simulation of the Nonlinearity With a Noise Generator

Just as the nonlinearity can be described either in the frequency domain or the argument domain, it can be synthesized in either domain. Consequently, an alternate technique for obtaining nonlinearities possessing the proper power spectrum is to utilize finite duration samples of the output of a noise generator of known spectral density. Rice[2] has shown that a sample of duration 2T drawn from a stationary Gaussian noise source has a representation

$$\hat{z}(t) = \frac{\alpha_o}{2} + \sum_{k=1}^{\infty} \alpha_k \cos \omega_k t + \beta_k \sin \omega_k t \qquad (28)$$

$$\omega_k = 2\pi f_k, \quad f_k = k\Delta f, \quad \Delta f = \frac{1}{2T}$$

where all the coefficients are uncorrelated random variables possessing a Gaussian distribution such that

$$E\left\{\alpha_k\right\} = E\left\{\beta_k\right\} = 0 \qquad (29)$$

$$E\left\{\alpha_k^2\right\} = E\left\{\beta_k^2\right\} = 2G_n(f_k)\Delta f = \frac{G_n(f_k)}{T}$$

$G_n(f)$ is the two sided spectral density of the noise generator. Now to obtain a noise source yielding samples with spectral density equal (on the average) to the spectral density of the nonlinearity (22), we choose

$$E\left\{\alpha_k^2 + \beta_k^2\right\} = \overline{a_k^2} + \overline{b_k^2} \qquad (30)$$

and

$$T = X \qquad (31)$$

so

$$\frac{2G_n(f_k)}{T} = \overline{a_k^2} + \overline{b_k^2} \qquad (32)$$

and

$$G_n(f_k) = T\,\frac{\overline{a_k^2} + \overline{b_k^2}}{2} \qquad (33)$$

It is possible to obtain the desired spectrum by shaping wide band noise with a passive filter. However, the parameter in the resultant noise process is time, rather than some control system coordinate, x, as desired. To remedy this deficiency, one may employ a curve follower or similar function generator. The noise voltage can be redrawn in conducting ink and then transferred to a curve follower. If the curve follower carriage is then commanded by the problem variable, x, the output of the device will be $\hat{z}(x)$, rather than $\hat{z}(t)$; i.e., the process of moving the curve from a plotting board to a curve follower performs a functional transformation:

$$\hat{z}(t) \longrightarrow \hat{z}(x) \qquad (34)$$

By drawing a series of such curves, one generates a sample which has the proper power spectrum in an average sense. Again, the actual feedback function, $y(x)$, is obtained by denormalization of $\hat{z}(x)$ using $\sigma_y(x)$ and $\bar{y}(x)$.

This technique has the advantage of requiring less computing equipment than the expansion in orthogonal functions. On the other hand, it is much easier to change the characteristic in the orthogonal function representation. The selection of one technique or the other depends upon the particular control system under study and the computing equipment available.

Application of the Spectral Description To a Tracking System

To illustrate the application of the power spectral density to the description of feedback elements, an elementary tracking system was simulated on an analog computer. Figure 2 is a block diagram of this system. The tracking accuracy of the basic servo was perturbed by the addition of a stationary, zero mean, Gaussian error, y, in the feedback signal (Figure 3). This error represents the deviation from linearity of the feedback element (potentiometer, synchro, etc.); i.e., the feedback signal, x_f, is given by

$$x_f(x) = x + y(x) \qquad (35)$$

Since the system is a hypothetical one, no analysis of measured feedback error functions was required. The performance of the perturbed system was measured by comparing it to a model system ($y = 0$) and calculating the error

$$\epsilon = x' - x \qquad (36)$$

The mean square value of ϵ (averaged over time)

$$\sigma_\epsilon^2 = \overline{\epsilon^2} \qquad (37)$$

was then measured as the performance index for each nonlinearity considered.

The feedback error functions, $y(x)$, were obtained from a noise source with spectral density

$$G_y(f) = \frac{G_o}{\left[1 + \tau_y^2(2\pi f)^2\right]^2} \qquad (38)$$

or

$$G_y(f) = \frac{4\tau_y\sigma_y^2}{\left[1 + \tau_y^2(2\pi f)^2\right]^2} \quad (39)$$

where

$$\sigma_y^2 = E\left\{y^2\right\} \quad (40)$$

Since the basic nonlinearities were assumed stationary and zero mean, no normalization or denormalization was required. From the power spectrum for y(x), one can deduce a noise bandwidth for the nonlinearity, B_y, in the usual way:

$$G_o B_y \equiv \sigma_y^2 = \int_{-\infty}^{\infty} G_y(f)df \quad (41)$$

so

$$B_y = \frac{\sigma_y^2}{G_o} = \int_{-\infty}^{\infty} \frac{df}{\left[1 + \tau_y^2(2\pi f)^2\right]^2} = \frac{1}{4\tau_y} \quad (42)$$

This is a two sided bandwidth; i.e., it includes both positive and negative frequencies as in equation (16). The units of B_y are inverse x. In this example, the servo output, x, is measured in degrees so the units of B_y are cycles per degree. The model servo system has a transfer function

$$\frac{x'}{w}(s) = \frac{1}{1 + s} \quad (43)$$

with the corresponding noise bandwidth:

$$B_s = \int_{-\infty}^{\infty} \frac{df}{1 + (2\pi f)^2} = \frac{1}{2} \text{ cps} \quad (44)$$

A dimensionless bandwidth ratio may be formed as

$$B = \frac{B_y \dot{w}}{B_s} = \frac{1}{2\tau_y} \quad (45)$$

The simulation experiment consisted of making a large number of computer runs with a different function, $(y_j(x))$ in the feedback path for each computer run. The relative bandwidth (B), rms nonlinearity (σ_ϵ) were recorded for each run. The results for functions having the same spectral properties were then averaged over the sample and plotted on Figure 4.

Figure 4 displays two distinct modes of servo operation. The first mode is labeled "linear filtering" and exists to the left of the line

$$B\sigma_\epsilon = .3 \quad (46)$$

In this region, it was observed during the simulation that the feedback nonlinearity had a minor effect on the output rate, $\dot{x}$, so

$$\dot{x} \cong \dot{w} = 1 \quad (47)$$

Now the time spectral content of the nonlinearity, y(x), depends upon $\dot{x}$; i.e., referring to Figure 3, if one sweeps across x at a uniform rate in time, then the spectral qualities of y(x) in terms of inverse x become spectral qualities in terms of inverse time or ordinary frequency. Thus, one would expect that in the "linear filtering" region the feedback nonlinearity can be replaced by a noise generator, thereby linearizing the analysis problem (Figure 5). The tracking error predicted by linear noise theory after this exchange is shown by the dotted lines on Figure 4. The agreement with measured error is indeed quite good. This analysis technique is a somewhat unexpected dividend accruing from the spectral characterization of y(x). Again referring to Figure 5, it should be noted that the exchange of y(x) for a noise generator is for purposes of analysis only. In the actual system simulated (Figure 2) the random process was the feedback nonlinearity.

Further inspection of the linear region of Figure 4 reveals the following phenomena:

1. When the dimensionless bandwidth ratio, B, (equation 45) is substantially less than 1, the servo output error is essentially the same as the feedback error. This results simply because the feedback nonlinearity varies sufficiently slowly that the servo output is able to track this error.

2. When B is greater than 1, the output error is considerably less than the feedback error. This results because the servo bandwidth is insufficient to follow rapid fluctuations in the feedback error.

Thus Figure 4 displays the rather novel concept of filtering a nonlinearity. Observation 2 above indicates that one might be able to trade accuracy for bandwidth in specifying a feedback element for this system. This is a prime motivation for utilizing a power spectrum to describe the element.

Equation (46) is an empirical result. The mechanism involved in the transition from the region of linear filtering to the region of nonlinear filtering is not understood at the present time. In the latter region, the servo displayed very different characteristics. During the simulation it was observed that the motion of the

output angle (as seen on the arm of the function generator producing y(x)) was very irregular. There was a tendency for the output angle to "hang up" on large positive slopes of the error function y(x) until an error peak was reached and then move rapidly over the characteristic until another large positive slope was encountered. This behavior can be explained qualitatively by phase plane analysis of the servo in the vicinity of an error peak. The net result of this irregular motion is an apparent narrow banding of the feedback nonlinearity; i.e., when the feedback error is stuck on a large positive error slope, the servo has sufficient time to null the error at the summing junction through the normal unity feedback loop so that the feedback error appears as an output error. No quantitative prediction of the observed results has been obtained for the nonlinear filtering region of Figure 4.

Figure 6 is a crossplot of Figure 4. The advantage of this presentation is that it permits a precise trade-off of feedback accuracy for error bandwidth (in the sense of equation 45). Consider for example, that the accuracy requirements of the servo (compared to the model system) were specified by

$$\sigma_\epsilon \leq .02 \text{ deg} \tag{48}$$

Then any combination of rms feedback error, σ_y, and nonlinearity relative bandwidth, B, lying below the line labeled $\sigma_\epsilon = .02$ would be acceptable. For example, if the relative bandwidth were 10, an rms feedback error as large as .07 deg would be acceptable. This is a quantitative expression of the intuitive feeling that large errors are not too important if the granularity is very fine.

Naturally, all of the quantitative results obtained apply only for the input selected, namely, a unit ramp. However, this constraint applies to the analysis of any nonlinear system whether the nonlinearities are random or not. Consideration of other inputs requires further simulation. If applicable, there is no reason why the input cannot also be a random process. In that event, the definition of dimensionless bandwidth would have to be altered. A suitable definition for purposes of normalization and linearization might be:

$$B \equiv \frac{B_y}{B_s} E\left\{\left|\dot{\theta}_i\right|\right\} \tag{49}$$

Application of the Spectral Description To a Missile Radome

Missiles possessing a tracking radar for gathering navigation information are provided with a protective covering or radome, which shields the radar reflector from the airstream. This radome interacts with the incident electromagnetic radiation in such a way as to shift the apparent location of the target from its actual location in space. The error between the true line of sight from the missile to the target and the line of sight to the apparent target location is termed the radome error. This error is a random function of the angles relating the antenna position to the missile body if an ensemble of radomes is considered. The radome error appears in the feedback path of the missile target tracking servo.

A homing missile navigating in a plane was simulated on an analog computer. Two types of hypothetical radomes were included in the simulation study. The first type was a truncated linear error as shown in Figure 7. The error is defined over $-\beta_{max} \leq \beta_o \leq \beta_{max}$. In the missile simulated, the deterioration of guidance accuracy due to the error introduced by the radome depended more upon the radome error slope,

$$k = \frac{\partial \eta}{\partial \beta} \tag{50}$$

than the error itself. Therefore, a spectral description of k rather than η was developed by making k periodic. The Fourier series for the resulting pulse train (Figure 8) is well known.

$$k(\beta) = \frac{a_o}{2} + \sum_{n=1}^{\infty} a_n \cos \frac{n\pi\beta}{2\beta_{max}} \tag{51}$$

$$a_o = \frac{mk_o}{\beta_{max}} \tag{52}$$

$$a_n = \frac{2k_o}{n} \sin \frac{n\pi m}{2\beta_{max}} = a_o \frac{\sin \alpha}{\alpha} \tag{53}$$

where

$$\alpha = \frac{n\pi m}{2\beta_{max}} \tag{54}$$

The power spectrum (21) for k thus consists of a train of delta functions with area $a_o^2/4$ in the central region and falling off at higher frequencies as shown in Figure 9. The height of each arrow in Figure 9 is proportional to the area of the delta function at that frequency. The separation between the delta functions is

$$\Delta f = \frac{1}{2\beta_{max}} \tag{55}$$

Introduction of the random phase angle, β_o, does not alter this power spectrum.

The noise bandwidth of the radome error derivative spectrum is found by determining the

frequency B/2 such that

$$\int_{-B/2}^{B/2} G_o \, df = \int_{-\infty}^{\infty} G(f)df = E\left\{k^2\right\} \quad (56)$$

i.e., the bandwidth B_k is that bandwidth which would be required to account for $E\{k^2\}$ if the area of the delta functions did not fall off at high frequencies. Now, from Figure 7 it is evident that

$$E\left\{k^2\right\} = \frac{k_o^2 m}{2\beta_{max}} = \frac{k_o a_o}{2} \quad (57)$$

Further, if

$$\frac{B}{2} = (\ell + \tfrac{1}{2})\Delta f \quad (58)$$

then

$$\int_{-B/2}^{B/2} G_o(f)df = (2\ell + 1)\frac{a_o^2}{4} \quad (59)$$

Combining (57) and (59)

$$(2\ell + 1)\frac{a_o^2}{4} = \frac{k_o a_o}{2} \quad (60)$$

$$2\ell + 1 = \frac{2k_o}{a_o} = \frac{2\beta_{max}}{m} \quad (61)$$

so

$$B = (2\ell + 1)\Delta f = \frac{2\beta_{max}}{m}\Delta f = \frac{1}{m} \quad (62)$$

Equations (62) and (57) will be taken as the spectral description of this type of radome along with the general low-pass shape of the power spectrum as shown in Figure 9.

The second type of radome simulated was a stationary, zero mean, Gaussian radome (Figure 10). Sample radomes were obtained by selecting finite samples from a noise generator with spectral density:

$$G_\eta(f) = \frac{G_o}{(1 + \tau_1^2\omega^2)(1 + \tau_2^2\omega^2)}$$

$$= \frac{2\sigma_\eta^2(\tau_1 + \tau_2)}{(1 + \tau_1^2\omega^2)(1 + \tau_2^2\omega^2)} \quad (63)$$

$$\tau_2 >> \tau_1$$

Then the spectrum for k is

$$G_k(f) = \frac{\omega^2 G_o}{(1 + \tau_1^2\omega^2)(1 + \tau_2^2\omega^2)}$$

$$= \frac{2\tau_1\tau_2(\tau_1 + \tau_2)\sigma_k^2\omega^2}{(1 + \tau_1^2\omega^2)(1 + \tau_2^2\omega^2)} \quad (64)$$

For $|\omega| > \frac{1}{\tau_2}$,

$$G_k(f) \cong \frac{2\tau_1\sigma_k^2}{1 + \tau_1^2\omega^2} \quad (65)$$

Thus, $G_k(f)$ has a low pass characteristic (except for a sharp dip at f = 0) as shown in Figure 11. The noise bandwidth is obtained from the integration of this spectral density

$$2\tau_1\sigma_k^2 B \cong \int_{-\infty}^{\infty} G_k(f)df = \sigma_k^2 \quad (66)$$

so

$$B = \frac{1}{2\tau_1} \text{ cps} \quad (67)$$

B is the bandwidth of the noise generator and is therefore a good estimate of the bandwidth of periodic samples drawn from the noise generator.

Repeated analog simulation runs were made with Gaussian noise (amplitude scintillation) added to the line of sight. The point of closest approach of the missile to the geometric center of the target (miss distance) was recorded for each run. After each series of five runs, the radome characteristic was changed (while holding the spectral content fixed). After twenty-five runs, the spectral content of the nonlinearity was changed. Figure 12 displays the normalized rms miss distances observed in the simulation experiment as a function of rms nonlinearity, k_{rms}, and bandwidth, B, for both types of radomes. The units of B are cycles per degree.

The remarkable characteristic of Figure 12 is that the two radomes, which differ so markedly in detail (see Figures 7 and 10), give substantially the same performance when their spectral qualities are the same.* This outcome of the experiment suggests that simulation results for one type of radome can be applied to other radomes having the same power spectral density. Such a normalization would provide a very substantial simplification of the simulation program required to evaluate the effects of various types of radomes. If one were to first make a series of computer runs with a Gaussian radome, for example, the behavior of the system with any other radome could be predicted simply be obtaining a power spectrum for the new radome. In some cases, it may be that the quality of this prediction would not be adequate for actual system evaluation, but nevertheless would provide an extrapolation and interpolation technique for greatly reducing the amount of simulation required.

If a crossplot of Figure 12 is made, one obtains a family of "trade-off" curves as in the previous example. Such a curve allows one to trade rms slope for bandwidth of the radome error derivative. Such a specification might alleviate manufacturing difficulties and at the same time permit a more realistic optimization of other system parameters.

Conclusions

This paper presents one method of characterizing an ensemble of nonlinearities. It is believed that the method provides a new point of view for the solution of a difficult class of nonlinear problems. In situations where the technique is applicable, it should furnish a useful set of specifications for quality control in the manufacture of control system feedback elements. The same set of specifications also provides a means for realistically simulating a feedback nonlinearity to aid in the design of the over-all control loop.

References

1. Lawson, James L., and Uhlenbeck, George E., Threshold Signals, McGraw-Hill, 1950.

2. Rice, S. O., "Mathematical Analysis of Random Noise," BSTJ, Vols. 23 and 24.

* This behavior is somewhat analogous to narrow band filtering of wide band noise in the time domain. In narrow band time filtering, the filter output tends toward Gaussian regardless of the input distribution and the mean square filter output is determined entirely by the input spectral density.

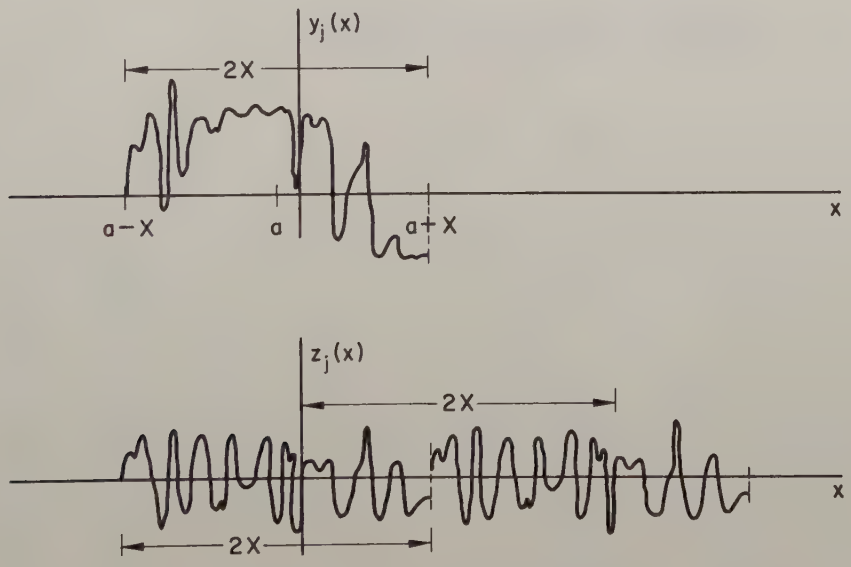

Fig. 1. Normalized Periodic Nonlinearity.

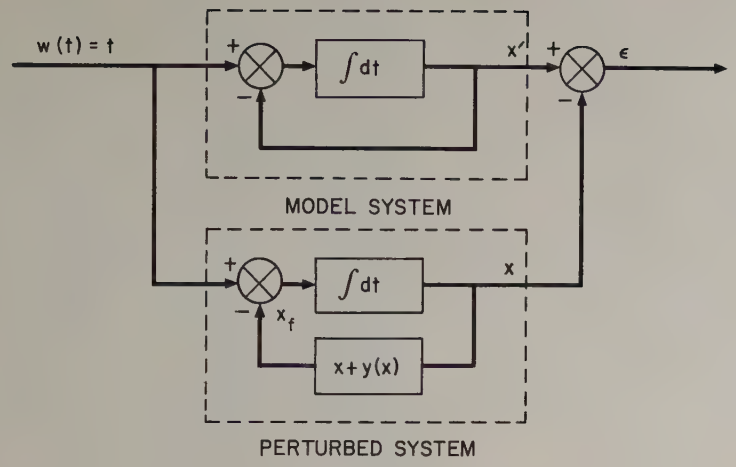

Fig. 2. Elementary Tracking System.

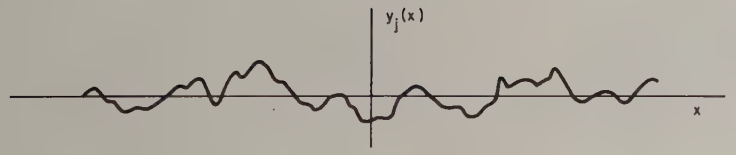

Fig. 3. Error in Feedback Element.

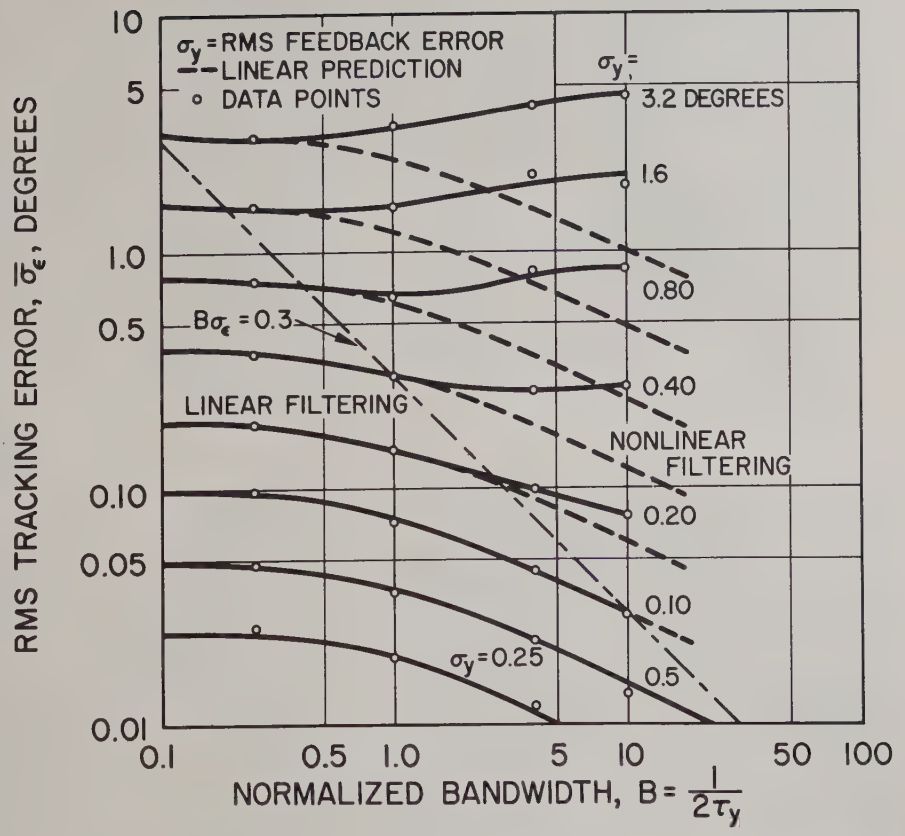

Fig. 4. RMS Tracking Error as a Function of RMS Feedback Error and Nonlinearity Bandwidth.

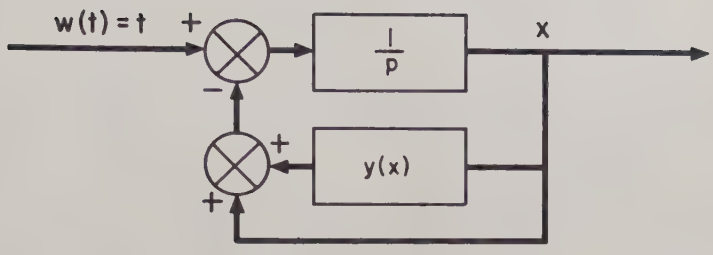

5a. ORIGINAL SYSTEM WITH FEEDBACK ERROR

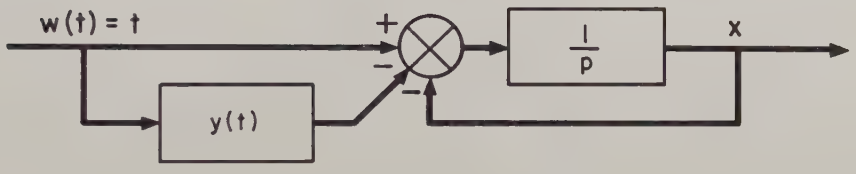

5b. INTERCHANGE OF x & t BASED ON $\dot{x} \cong \dot{w} = 1$

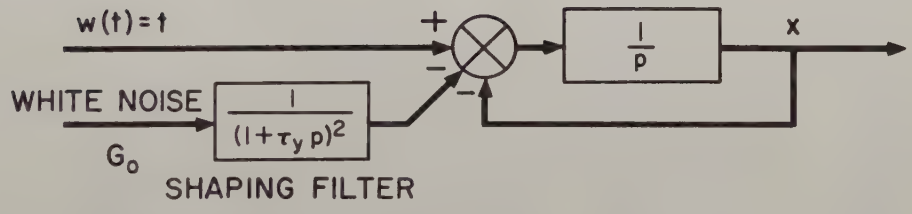

5c. REPLACEMENT OF y(t) BY A NOISE GENERATOR

Fig. 5. Calculation of Tracking Error in the Linear Region.

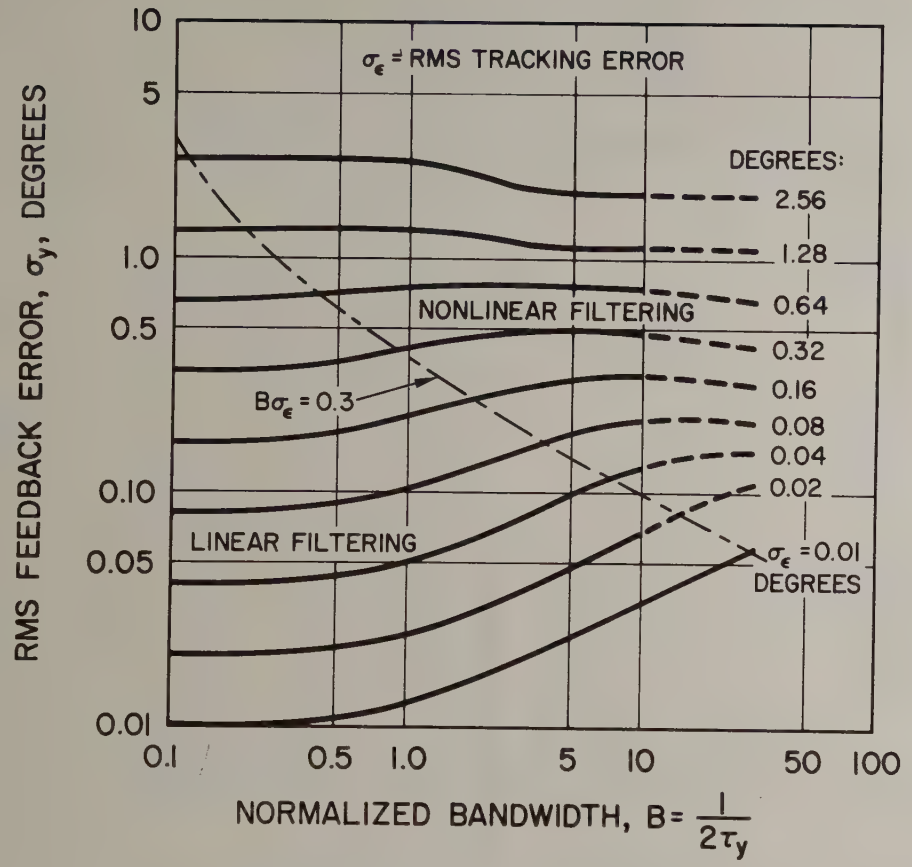

Fig. 6. Bandwidth-Error Trade-Off Curve.

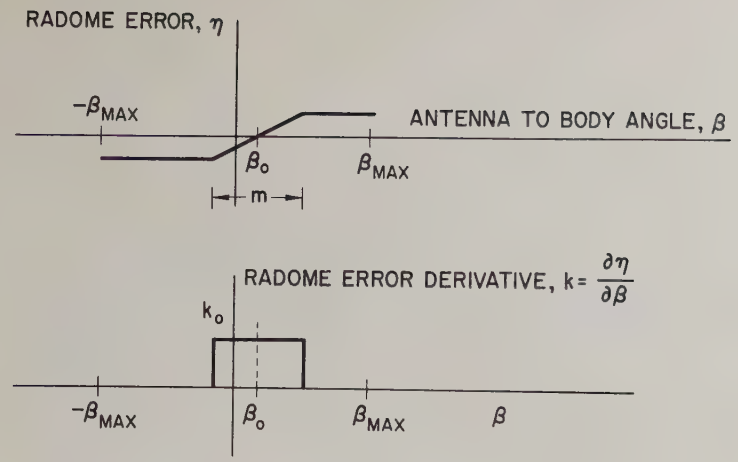

Fig. 7. Truncated Linear Radome Error.

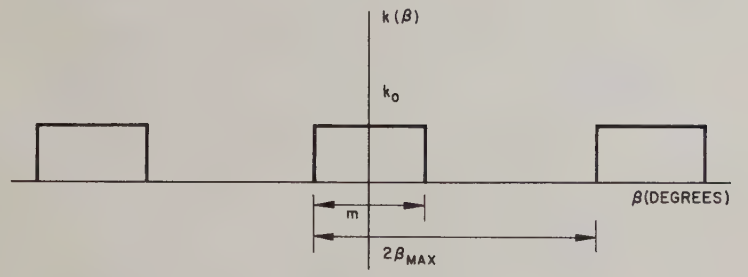

Fig. 8. Periodic Radome Error Derivative.

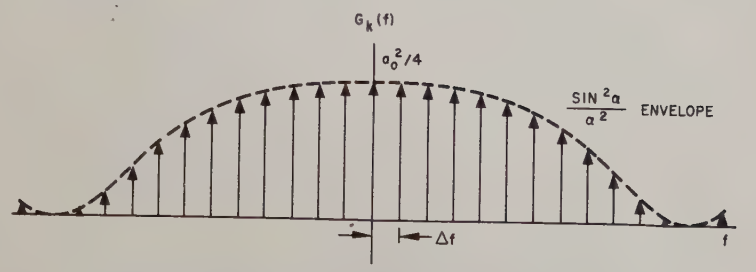

Fig. 9. Power Spectrum for Periodic Radome Error Derivative.

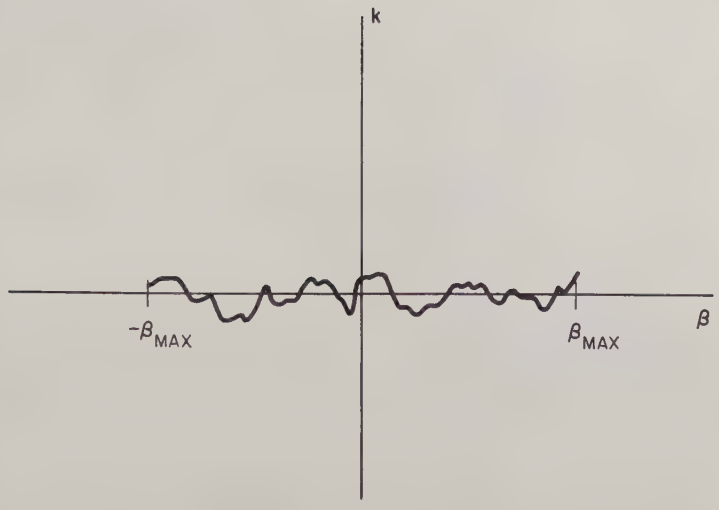

Fig. 10. Gaussian Radome Error Derivative.

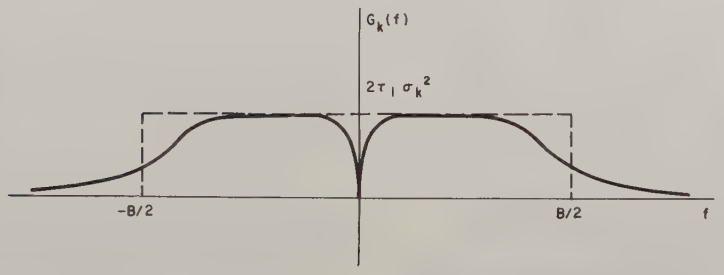

Fig. 11. Power Spectrum for Gaussian Radome Error Derivative.

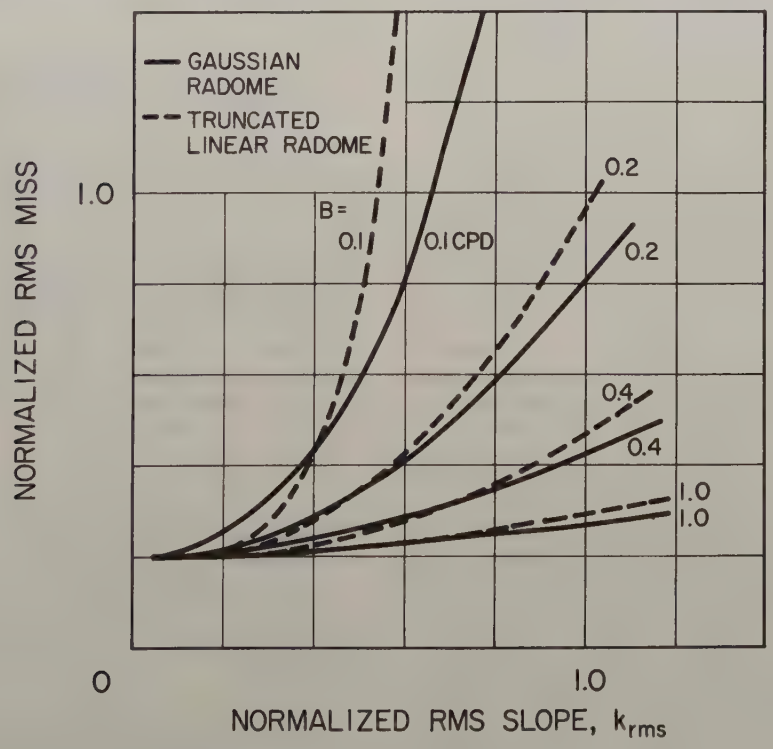

Fig. 12. Effect of Radome Bandwidth on RMS Miss Distance.

TECHNIQUES FOR THE OPTIMUM SYNTHESIS OF MULTIPOLE CONTROL SYSTEMS WITH RANDOM PROCESSES AS INPUTS

H. C. Hsieh
C. T. Leondes
University of California
Los Angeles, California

Summary

This report considers the general problem of obtaining the optimum multipole system when the inputs to the system are stationary random processes. The system under investigation is linear and time invariant. The input to each terminal shall consist of signal and noise.

The synthesis procedure is carried out under the basis that a fixed plant must be compensated in order to perform certain desired tasks. The design criterion employed is the minimum mean square error between actual outputs and ideal outputs of the system. A set of integral equations shall be obtained, which can be converted into algebraic equations through transformation. By solving these equations and using the method of undetermined coefficients, the transfer functions of the compensation can be uniquely determined.

1. Introduction to the Compensation of Fixed Plant

The synthesis procedure of a control system starts with the specifications for the system to be designed. These specifications would primarily include the types of signals and disturbances acting on the control system, the desired outputs from the system, the permissible error between the actual outputs and the desired outputs, and the configuration of the entire system. The designer seldom has complete freedom in choosing the system functions. There are always some fixed elements which must be included in the system in order to perform certain tasks. Under this situation, compensation must be introduced to the system in conjunction with the fixed elements so that the overall characteristics of the system would meet the specifications.

The systems under consideration are linear time-invariant multipole systems. A multipole system is defined as a system having n inputs and m outputs[1,4]. The input to each terminal shall consist of signal and noise which are both stationary random processes. There are fixed elements between all the input-output terminals. However, there is no constraint on the configuration of the compensators other than the practical one of physical realizability. This class of design problem is usually referred to as the semi-free configuration problem.

It is often necessary that systems contain feedback loops between inputs and outputs. Nevertheless the actual system with its feedback configuration can always be replaced by an equivalent system containing cascade combinations of compensators and fixed elements. With this simplified system, the synthesis procedure can frequently be expedited. The error of the output is defined as the difference between the actual output and the ideal output. The performance index used in the synthesis procedure is the minimum mean-square error[2,3].

Two different types of arrangement for the compensators are under investigation. In the first type, compensation is used in cascade with the individual fixed element of the plant. Mean-square error for each output terminal can be minimized independently. In the second arrangement, a controller which consists of a group of compensators is in cascade with the entire plant. Therefore, the controller itself is also multipole. It is necessary then to minimize the sum of the mean square errors for all the output terminals.

The derivation employed here is very conventional for this type of problem. A set of integral equations shall be obtained under the criterion of minimum mean square error. Transform method is then used to convert this set of integral equations into a set of algebraic equations. The transfer functions of the compensation can be determined by the technique of undetermined coefficients[5].

2. Basic System Equations with Cascade Compensators

In the following derivation for the system equations, we shall assume that it is possible to insert compensator in direct cascade with the individual fixed element of the plant. In practice, this may not be the case since the fixed plant usually represents an integrated system. However, the synthesis procedure for this simpler configuration is more apparent and instructive in illustrating the basic techniques to be employed. It shall also provide a better understanding for the design of a more complicated cascade controller to be considered in a later chapter.

The system considered is a linear time-invariant system. The inputs to the system shall consist of stationary stochastic signals $S_k(t)$ and noises $n_k(t)$. Thus, we have

$$i_k(t) = S_k(t) + n_k(t) \qquad (1)$$

The system configuration in matrix form is shown in Fig. 1.

It is evident that the input to each element of the plant can be expressed as

$$r_k(t)=\int_0^\infty q_{jk}(\tau_1)\, i_k(t-\tau_1)\, d\tau_1 \qquad (2)$$
$$k=1,2,\ldots n$$

where $q_{jk}(t)$ is weighting function of the compensator between k-input and j-output. The outputs of the system in terms of the inputs to the fixed elements are then

$$c_j(t)=\sum_{k=1}^{n}\int_0^\infty p_{jk}(\tau_2)\, r_k(t-\tau_2)\, d\tau_2 \qquad (3)$$
$$j=1,2,\ldots m$$

where $p_{jk}(t)$ is the weighting function of the fixed elements. Combining Eqs. (2) and (3), there results

$$c_j(t)=\sum_{k=1}^{n}\int_0^\infty q_{jk}(\tau_1)\, d\tau_1 \int_0^\infty p_{jk}(\tau_2)\, i_k(t-\tau_1-\tau_2)\, d\tau_2 \qquad (4)$$

which expresses the outputs in terms of inputs and the weighting functions of fixed elements and the cascade compensators.

Now, if we denote $D_{jk}(t)$ as the weighting function of an ideal system, then the desired output $z_j(t)$ can be seen to be

$$z_j(t)=\sum_{k=1}^{n}\int_{-\infty}^\infty D_{jk}(\tau_3)\, S_k(t-\tau_3)\, d\tau_3 \qquad (5)$$
$$j=1,2,\ldots m$$

Here the lower limit of the integration is extended to $-\infty$ to emphasize the fact that the ideal weighting functions can be physically unrealizable. Thus the errors between the actual and desired system outputs can be written as

$$\epsilon_j(t)=c_j(t)-z_j(t)$$
$$=\sum_{k=1}^{n}\int_0^\infty q_{jk}(\tau_1)\, d\tau_1 \int_0^\infty p_{jk}(\tau_2)\, i_k(t-\tau_1-\tau_2)\, d\tau_2$$
$$-\sum_{k=1}^{n}\int_{-\infty}^\infty D_{jk}(\tau_3)\, S_k(t-\tau_3)\, d\tau_3 \qquad (6)$$

A diagram of this general problem is shown in Figure 2 where, for simplicity, the matrix notation is adopted. The part of the diagram below the dotted line represents the actual system while the part above the dotted line represents the hypothetical ideal system together with comparator for generating the error signal.

After the error has been generated, we can proceed to find out the optimum weighting functions of the compensators so as to minimize its mean-square value.

The square of the error is

$$\epsilon_j^2(t)=c_j^2(t)-2\,c_j(t)\,z_j(t)+z_j^2(t) \qquad (7)$$

By taking the mathematical expectation of Eq. (7), we get the mean-square error in terms of the auto- and cross-correlation functions of the inputs and the system weighting functions. Thus, symbolically,

$$\overline{\epsilon_j^2}=\overline{c_j^2(t)}-2\,\overline{c_j(t)\,z_j(t)}+\overline{z_j^2(t)} \qquad (8)$$

Here the bar indicates the ensemble average.

The terms on the right side of Eq. (8) can be evaluated in the following manner:

$$c_j^2(t)=\overline{\left\{\sum_{k'=1}^{n}\int_0^\infty q_{jk'}(\tau_1')\, d\tau_1' \int_0^\infty p_{jk'}(\tau_2')\, i_{k'}(t-\tau_1'-\tau_2')\, d\tau_2'\right\}}$$
$$\times\overline{\left\{\sum_{k=1}^{n}\int_0^\infty q_{jk}(\tau_1)\, d\tau_1 \int_0^\infty p_{jk}(\tau_2)\, i_k(t-\tau_1-\tau_2)\, d\tau_2\right\}}$$
$$=\sum_{k'=1}^{n}\sum_{k=1}^{n}\int_0^\infty q_{jk'}(\tau_1')\, d\tau_1' \int_0^\infty p_{jk'}(\tau_2')\, d\tau_2' \int_0^\infty q_{jk}(\tau_1)\, d\tau_1$$
$$\times\int_0^\infty p_{jk}(\tau_2)\,\phi_{i_{k'}i_k}(\tau_1'+\tau_2'-\tau_1-\tau_2)\, d\tau_2 \qquad (9)$$

where the correlation function $\phi(\tau)$ is the ensemble average as defined by

$$\phi_{i_{k'}i_k}(\tau)=\overline{i_{k'}(t)\, i_k(t+\tau)}$$
$$=\overline{\left[S_{k'}(t)+n_{k'}(t)\right]\left[S_k(t+\tau)+n_k(t+\tau)\right]}$$

$$= \phi_{s_k,s_k}(\tau)+\phi_{s_k,n_k}(\tau)+\phi_{n_k,s_k}(\tau)+\phi_{n_k,n_k}(\tau) \quad (10)$$

If these stationary random processes possess the ergodic property, this ensemble average can then be replaced by time average performed on a single representative function of the ensemble.

Similarly,

$$\overline{z_j^2(t)} = \overline{\left\{\sum_{k'=1}^{n}\int_{-\infty}^{\infty} D_{jk'}(\tau_3')\, s_{k'}(t-\tau_3')\,d\tau_3'\right\}\left\{\sum_{k=1}^{n}\int_{-\infty}^{\infty} D_{jk}(\tau_3)\, s_k(t-\tau_3)\,d\tau_3\right\}}$$

$$= \sum_{k'=1}^{n}\sum_{k=1}^{n}\int_{-\infty}^{\infty} D_{jk'}(\tau_3')\,d\tau_3' \int_{-\infty}^{\infty} D_{jk}(\tau_3)\,\phi_{s_{k'},s_k}(\tau_3'-\tau_3)\,d\tau_3 \quad (11)$$

and

$$\overline{c_j(t)\,z_j(t)} =$$

$$\overline{\left\{\sum_{k'=1}^{n}\int_0^{\infty} g_{jk'}(\tau_1')\,d\tau_1'\int_0^{\infty} p_{jk'}(\tau_2')\,i_{k'}(t-\tau_1'-\tau_2')\,d\tau_2'\right\}\times\left\{\sum_{k=1}^{n}\int_{-\infty}^{\infty} D_{jk}(\tau_3)\,s_k(t-\tau_3)\,d\tau_3\right\}}$$

$$= \sum_{k'=1}^{n}\sum_{k=1}^{n}\int_0^{\infty} g_{jk'}(\tau_1')\,d\tau_1'\int_0^{\infty} p_{jk'}(\tau_2')\,d\tau_2' \int_{-\infty}^{\infty} D_{jk}(\tau_3)\,\phi_{i_{k'},s_k}(\tau_1'+\tau_2'-\tau_3)\,d\tau_3 \quad (12)$$

where $\phi_{i_{k'},s_k}(\tau) = \overline{i_{k'}(t)\,s_k(t+\tau)}$

$$= \overline{[s_{k'}(t)+n_{k'}(t)]\,[s_k(t+\tau)}$$

$$= \phi_{s_{k'},s_k}(\tau)+\phi_{n_{k'},s_k}(\tau) \quad (13)$$

Hence, by substituting Eqs. (9), (11) and (12) into Eq. (8), we obtain

$$\overline{\epsilon_j^2(t)} = \sum_{k'=1}^{n}\sum_{k=1}^{n}\int_0^{\infty} g_{jk'}(\tau_1')\,d\tau_1'\int_0^{\infty} p_{jk'}(\tau_2')\,d\tau_2' \int_0^{\infty} g_{jk}(\tau_1)\,d\tau_1$$

$$\times\int_0^{\infty} p_{jk}(\tau_2)\,\phi_{i_{k'},i_k}(\tau_1'+\tau_2'-\tau_1-\tau_2)\,d\tau_2$$

$$-2\sum_{k'=1}^{n}\sum_{k=1}^{n}\int_0^{\infty} g_{jk'}(\tau_1')\,d\tau_1'\int_0^{\infty} p_{jk'}(\tau_2')\,d\tau_2' \int_{-\infty}^{\infty} D_{jk}(\tau_3)\,\phi_{i_{k'},s_k}(\tau_1'+\tau_2'-\tau_3)\,d\tau_3$$

$$+\sum_{k'=1}^{n}\sum_{k=1}^{n}\int_{-\infty}^{\infty} D_{jk'}(\tau_3')\,d\tau_3'\int_{-\infty}^{\infty} D_{jk}(\tau_3)\,\phi_{s_{k'},s_k}(\tau_3'-\tau_3)\,d\tau_3 \quad (14)$$

In order to find out the condition for minimum mean-square error, let us introduce the arbitrarily unknown functions $v_{jk}(\tau)$ which are defined implicitly by the following equation:

$$\sum_{k=1}^{n}\int_0^{\infty} p_{jk'}(\tau_2')\,d\tau_2'\int_0^{\infty} v_{jk}(\tau_1)\,d\tau_1\int_0^{\infty} p_{jk}(\tau_2)\,\phi_{i_{k'},i_k}(\tau_1'+\tau_2'-\tau_1-\tau_2)\,d\tau_2$$

$$= \sum_{k=1}^{n}\int_0^{\infty} p_{jk'}(\tau_2')\,d\tau_2'\int_{-\infty}^{\infty} D_{jk}(\tau_3)\,\phi_{i_{k'},s_k}(\tau_1'+\tau_2'-\tau_3)\,d\tau_3 \quad \text{for } \tau_1' \geq 0 \quad (15)$$

Substituting Eq. (15) into Eq. (14) yields

$$\overline{\epsilon_j^2(t)} = \sum_{k'=1}^{n}\sum_{k=1}^{n}\int_0^{\infty} g_{jk'}(\tau_1')\,d\tau_1$$

$$\int_0^{\infty} p_{jk'}(\tau_2')\,d\tau_2'\int_0^{\infty} g_{jk}(\tau_1)\,d\tau_1$$

$$\times \int_0^\infty \rho_{jk}(\tau_2)\,\phi_{i_k,i_k}(\tau_1'+\tau_2'-\tau_1-\tau_2)\,d\tau_2$$

$$-2\sum_{k'=1}^{n}\sum_{k=1}^{n}\int_0^\infty q_{jk'}(\tau_1')\,d\tau_1'\int_0^\infty \rho_{jk'}(\tau_2')\,d\tau_2'$$
$$\int_0^\infty v_{jk}(\tau_1)\,d\tau_1$$

$$\times\int_0^\infty \rho_{jk}(\tau_2)\,\phi_{i_k,i_k}(\tau_1'+\tau_2'-\tau_1-\tau_2)\,d\tau_2$$

$$+\sum_{k'=1}^{n}\sum_{k=1}^{n}\int_{-\infty}^\infty D_{jk'}(\tau_3')\,d\tau_3'\int_{-\infty}^\infty D_{jk}(\tau_3)$$
$$\phi_{s_k,s_k}(\tau_3'-\tau_3)\,d\tau_3 \qquad (16)$$

By adding and substracting a summation term

$$\sum_{k'=1}^{n}\sum_{k=1}^{n}\int_0^\infty v_{jk'}(\tau_1')\,d\tau_1\int_0^\infty \rho_{jk}(\tau_2')\,d\tau_2'\int_0^\infty v_{jk}(\tau_1)\,d\tau_1$$
$$\times\int_0^\infty \rho_{jk}(\tau_2)\,\phi_{i_k,i_k}(\tau_1'+\tau_2'-\tau_1-\tau_2)\,d\tau_2$$

to Eq. (16), we shall have

$$\overline{\epsilon_j^2(t)} = \sum_{k'=1}^{n}\sum_{k=1}^{n}\int_{-\infty}^\infty D_{jk'}(\tau_3')\,d\tau_3'\int_{-\infty}^\infty D_{jk}(\tau_3)$$
$$\phi_{s_k,s_k}(\tau_3'-\tau_3)\,d\tau_3$$
$$-\sum_{k'=1}^{n}\sum_{k=1}^{n}\int_0^\infty v_{jk'}(\tau_1')\,d\tau_1'\int_0^\infty \rho_{jk'}(\tau_2')\,d\tau_2'$$
$$\int_0^\infty v_{jk}(\tau_1)\,d\tau_1$$
$$\times\int_0^\infty \rho_{jk}(\tau_2)\,\phi_{i_k,i_k}(\tau_1'+\tau_2'-\tau_1-\tau_2)\,d\tau_2$$
$$+\sum_{k'=1}^{n}\sum_{k=1}^{n}\int_0^\infty v_{jk'}(\tau_1')\,d\tau_1'\int_0^\infty \rho_{jk'}(\tau_2')\,d\tau_2'$$
$$\int_0^\infty v_{jk}(\tau_1)\,d\tau_1$$
$$\times\int_0^\infty \rho_{jk}(\tau_2)\,\phi_{i_k,i_k}(\tau_1'+\tau_2'-\tau_1-\tau_2)\,d\tau_2$$

$$-2\sum_{k'=1}^{n}\sum_{k=1}^{n}\int_0^\infty q_{jk'}(\tau_1')\,d\tau_1'\int_0^\infty \rho_{jk'}(\tau_2')\,d\tau_2'$$
$$\int_0^\infty v_{jk}(\tau_1)\,d\tau_1$$
$$\times\int_0^\infty \rho_{jk}(\tau_2)\,\phi_{i_k,i_k}(\tau_1'+\tau_2'-\tau_1-\tau_2)\,d\tau_2$$
$$+\sum_{k'=1}^{n}\sum_{k=1}^{n}\int_0^\infty q_{jk'}(\tau_1')\,d\tau_1'\int_0^\infty \rho_{jk'}(\tau_2')\,d\tau_2'$$
$$\int_0^\infty q_{jk}(\tau_1)\,d\tau_1$$
$$\times\int_0^\infty \rho_{jk}(\tau_2)\,\phi_{i_k,i_k}(\tau_1'+\tau_2'-\tau_1-\tau_2)\,d\tau_2$$
$$=\sum_{k'=1}^{n}\sum_{k=1}^{n}\int_{-\infty}^\infty D_{jk'}(\tau_3')\,d\tau_3'\int_{-\infty}^\infty D_{jk}(\tau_3)$$
$$\phi_{s_k,s_k}(\tau_3'-\tau_3)\,d\tau_3$$
$$-\sum_{k'=1}^{n}\sum_{k=1}^{n}\int_0^\infty v_{jk'}(\tau_1')\,d\tau_1\int_0^\infty \rho_{jk'}(\tau_2')\,d\tau_2'$$
$$\int_0^\infty v_{jk}(\tau_1)\,d\tau_1$$
$$\times\int_0^\infty \rho_{jk}(\tau_2)\,\phi_{i_k,i_k}(\tau_1'+\tau_2'-\tau_1-\tau_2)\,d\tau_2$$

$$+\left\{\sum_{k=1}^{n}\left[\overline{\int_0^\infty v_{jk}(\tau_1)\,d\tau_1\int_0^\infty \rho_{jk}(\tau_2)\,i_k(t-\tau_1-\tau_2)\,d\tau_2}\right.\right.$$
$$\left.\left.-\overline{\int_0^\infty q_{jk}(\tau_1)\,d\tau_1\int_0^\infty \rho_{jk}(\tau_2)\,i_k(t-\tau_1-\tau_2)\,d\tau_2}\right]\right\}^2 \qquad (17)$$

It is evident that the last term in Eq. (17) is always positive. In order to get a minimum error, we can, therefore, choose

$$\int_0^\infty v_{jk}(\tau_1)\,d\tau_1 \int_0^\infty \rho_{jk}(\tau_2)\, i_k(t-\tau_1-\tau_2)\,d\tau_2$$

$$= \int_0^\infty g_{jk}(\tau_1)\,d\tau_1 \int_0^\infty \rho_{jk}(\tau_2)\, i_k(t-\tau_1-\tau_2)\,d\tau_2$$

or

$$v_{jk}(\tau) = g_{jk}(\tau) \qquad \text{for all } k. \qquad (18)$$

Under this condition, Eq. (15) becomes

$$\sum_{k=1}^{n} \int_0^\infty \rho_{jk'}(\tau_2')\,d\tau_2' \int_0^\infty g_{jk}(\tau_1)\,d\tau_1 \int_0^\infty \rho_{jk}(\tau_2)\,\phi_{i_{k'} i_k}(\tau_1'+\tau_2'-\tau_1-\tau_2)\,d\tau_2$$

$$= \sum_{k=1}^{n} \int_0^\infty \rho_{jk'}(\tau_2')\,d\tau_2 \int_{-\infty}^\infty D_{jk}(\tau_3)\,\phi_{i_{k'} s_k}(\tau_1'+\tau_2'-\tau_3)\,d\tau_3$$

$$\text{for } \tau_1' \geqq 0 \qquad (19)$$

where $k' = 1, 2, \cdots n$

$j = 1, 2, \cdots m$

Here the term $p_{jk'}(\tau)$ is purposely retained on both sides of Eq. (19). Its usefulness will be evident from later treatment.

To show that Eq. (19) is not only the necessary condition for optimum system but also the sufficient one, let us replace the optimum weighting functions $q_{jk}(\tau)$ of the compensation by any arbitrary functions of the form $q_{jk}(\tau) + a_{jk}(\tau)$. Then the mean square error is

$$\overline{\epsilon_j^2(t)}' = \overline{\epsilon_j^2(t)} + 2\sum_{k'=1}^{n} \int_0^\infty a_{jk'}(\tau_1')\,d\tau_1' \left\{ \sum_{k=1}^{n} \int_0^\infty \rho_{jk'}(\tau_2')\,d\tau_2' \times \int_0^\infty g_{jk}(\tau_1)\,d\tau_1 \int_0^\infty \rho_{jk}(\tau_2)\,\phi_{i_{k'} i_k}(\tau_1'+\tau_2'-\tau_1-\tau_2)\,d\tau_2 \right.$$

$$\left. - \sum_{k=1}^{n} \int_0^\infty \rho_{jk'}(\tau_2')\,d\tau_2' \int_{-\infty}^\infty D_{jk}(\tau_3)\,\phi_{i_{k'} s_k}(\tau_1'+\tau_2'-\tau_3)\,d\tau_3 \right\}$$

$$+ \overline{\left\{ \sum_{k=1}^{n} \int_0^\infty a_{jk}(\tau_1)\,d\tau_1 \int_0^\infty \rho_{jk}(\tau_2)\, i_k(t-\tau_1-\tau_2)\,d\tau_2 \right\}^2} \qquad (20A)$$

where $\epsilon_j^2(t)$ is given by Eq. (14).

If now $q_{jk}(\tau)$'s satisfy the condition in Eq. (19), this mean square error becomes

$$\overline{\epsilon_j^2(t)}' = \overline{\epsilon_j^2(t)} + \overline{\left\{ \sum_{k=1}^{n} \int_0^\infty a_{jk}(\tau_1)\,d\tau_1 \int_0^\infty \rho_{jk}(\tau_2)\, i_k(t-\tau_1-\tau_2)\,d\tau_2 \right\}^2} \qquad (20B)$$

It is evident that the mean square error is not decreased by perturbing $q_{jk}(\tau)$. The condition shown in Eq. (19) is thus sufficient. This set of integral equations must be satisfied by the optimum weighting functions of the compensation.

The minimum mean square error can finally be expressed as

$$\overline{\epsilon_j^2(t)}_{min} = \sum_{k'=1}^{n} \sum_{k=1}^{n} \int_{-\infty}^\infty D_{jk'}(\tau_3')\,d\tau_3' \int_{-\infty}^\infty D_{jk}(\tau_3)\,\phi_{s_{k'} s_k}(\tau_3'-\tau_3)\,d\tau_3$$

$$- \sum_{k'=1}^{n} \sum_{k=1}^{n} \int_0^\infty g_{jk'}(\tau_1')\,d\tau_1' \int_0^\infty g_{jk}(\tau_1)\,d\tau_1 \int_0^\infty \rho_{jk'}(\tau_2')\,d\tau_2' \times \int_0^\infty \rho_{jk}(\tau_2)\,\phi_{i_{k'} i_k}(\tau_1'+\tau_2'-\tau_1-\tau_2)\,d\tau_2$$

$$j = 1, 2, \cdots m \qquad (21A)$$

or, in frequency domain,

$$\overline{\epsilon_j^2(t)_{min}} = \int_0^\infty G_{\epsilon\epsilon}(\omega)\,d\omega$$

$$= \sum_{k'=1}^{n}\sum_{k=1}^{n}\int_0^\infty (Yd)^*_{j_{k'}}(Yd)_{j_k} G_{s_{k'},s_k}\,d\omega$$

$$-\sum_{k'=1}^{n}\sum_{k=1}^{n}\int_0^\infty Q^*_{j_{k'}} Q_{j_k} P^*_{i_{k'}} P_{i_k} G_{i_{k'},i_k}\,d\omega \qquad (21B)$$

where $Yd(\omega)$, $Q(\omega)$ and $P(\omega)$ are the Fourier transforms of weighting functions D(t), q(t) and p(t) respectively; and the power spectral density $G(\omega)$ is the Fourier transform of correlation function $\phi(\tau)$ as expressed by

$$G(\omega) = \frac{1}{\pi}\int_{-\infty}^{\infty}\phi(\tau)\,e^{-j\omega\tau}\,d\tau$$

and

$$\phi(\tau) = \frac{1}{2}\int_{-\infty}^{\infty} G(\omega)\,e^{j\omega\tau}\,d\omega$$

3. Solutions for the Transfer Functions of Cascade Compensators

The n weighting functions of the compensators in associate with a particular output terminal j are related to all the known quantities by n integral equations of the type shown in Eq. (19). Explicit solutions for these weighting functions or their equivalent transfer functions can be obtained if the correlation functions of signals and noises are Fourier transformable. The technique in complex variables theory can then be fully employed.

Fortunately, the auto-correlation function of a general stationary random process and the cross-correlation function between two stationary random processes can be approximated in the least-square sense by

$$\phi_{xx}(\tau) = \sum_{k=1}^{n} A_k\,e^{-a_k|\tau|} \qquad (22)$$

and

$$\phi_{xy}(\tau) = \sum_{k=1}^{n} B_k\,e^{-b_k\tau} \quad \text{for } \tau > 0$$

$$= \sum_{k=1}^{n} C_k\,e^{c_k\tau} \quad \text{for } \tau < 0 \qquad (23)$$

Therefore, the Fourier transform of the correlation function, which is called the power spectral density, is always possible. These power spectral densities shall be fractional functions. In addition, the auto-power spectral density is a function in ω^2.

For convenience, let us rewrite Eq. (19).

$$\sum_{k=1}^{n}\int_0^\infty \rho_{j_{k'}}(\tau_2')\,d\tau_2 \int_0^\infty q_{j_k}(\tau_1)\,d\tau_1$$

$$\int_0^\infty \rho_{j_k}(\tau_2)\,\phi_{i_{k'},i_k}(\tau_1'+\tau_2'-\tau_1-\tau_2)\,d\tau_2$$

$$= \sum_{k=1}^{n}\int_0^\infty \rho_{j_{k'}}(\tau_2')\,d\tau_2 \int_{-\infty}^{\infty} D_{j_k}(\tau_3)$$

$$\phi_{i_{k'},s_k}(\tau_1'+\tau_2'-\tau_3)\,d\tau_3$$

$$\text{for } \tau_1' \geqq 0 \qquad (24)$$

Since this equation is true only for τ_1' equal to or greater than zero, certain modification must be made before taking the Fourier transform. Let us define a function $f_{jk'}(t)$ such that

$$f_{j_{k'}}(\tau_1') = 0 \quad \text{for } \tau_1' \geqq 0$$

and

$$f_{j_{k'}}(\tau_1') = \sum_{k=1}^{n}\int_0^\infty \rho_{j_{k'}}(\tau_2')\,d\tau_2'$$

$$\int_0^\infty q_{j_k}(\tau_1)\,d\tau_1 \int_0^\infty \rho_{j_k}(\tau_2)\,\phi_{i_{k'},i_k}(\tau_1'+\tau_2'-\tau_1-\tau_2)\,d\tau_2$$

$$-\sum_{k=1}^{n}\int_0^\infty \rho_{j_{k'}}(\tau_2')\,d\tau_2' \int_{-\infty}^{\infty} D_{j_k}(\tau_3)$$

$$\phi_{i_{k'},s_k}(\tau_1'+\tau_2'-\tau_3)\,d\tau_3$$

$$\text{for } \tau_1' < 0 \qquad (25)$$

Then

$$\sum_{k=1}^{n}\int_0^\infty \rho_{j_{k'}}(\tau_2')\,d\tau_2' \int_0^\infty q_{j_k}(\tau_1)\,d\tau_1$$

$$\int_0^\infty \rho_{jk}(\tau_2)\,\phi_{i_{k'},i_k}(\tau_1'+\tau_2'-\tau_1-\tau_2)\,d\tau_2$$

$$=\sum_{k=1}^{n}\int_0^\infty \rho_{jk'}(\tau_2')\,d\tau_2\int_{-\infty}^{\infty} D_{jk}(\tau_3)$$

$$\phi_{i_{k'},s_k}(\tau_1'+\tau_2'-\tau_3)\,d\tau_3+f_{j_{k'}}(\tau_1')$$

for all values of τ_1'. (26)

We can now take the Fourier transform on both sides of this equation. Eq. (26) thus becomes

$$\sum_{k=1}^{n}\rho^*_{jk'}\rho_{jk}\,G_{i_{k'}i_k}\,Q_{jk}$$

$$=\sum_{k=1}^{n}\rho^*_{jk'}(Yd)_{jk}\,G_{i_{k'},s_k}+\frac{1}{\pi}F^-_{jk'}$$

$k' = 1, 2, - - - n$ (27)

Here P and Q are the transfer functions of the fixed element and compensator respectively; and

$$G_{i_{k'},i_k}(\omega)=G_{s_{k'},s_k}(\omega)+G_{s_{k'},n_k}(\omega)$$

$$+G_{n_{k'},s_k}(\omega)+G_{n_{k'},n_k}(\omega) \quad (28)$$

$$G_{i_{k'},s_k}(\omega)=G_{s_{k'},s_k}(\omega)+G_{n_{k'},s_k}(\omega)$$

$$F^-_{jk}(\omega)=\int_{-\infty}^{0} f_{jk'}(t)\,e^{-j\omega t}\,dt \quad (29)$$

It is clear that $F^-_{jk}(\omega)$ contains poles in the lower half of the ω-plane only. In Eq. (27), the argument ω is omitted for simplicity.

We thus have feasibly transformed integral equations into ordinary linear algebraic equations. For every output terminal, there is a set of n equations of the type shown in Eq. (27). Therefore, the n transfer functions of the compensators associated with that particular output terminal can be obtained. A total of m x n equations would then determine all the transfer functions of the system compensators.

Let us introduce, for convenience, the symbols $M_{k'R}$ and $R_{jk'}$ which are defined as

$$M_{k'k}=\rho^*_{jk'}\,\rho_{jk}\,G_{i_{k'},i_k} \quad (30)$$

$$R_{jk'}=\sum_{k=1}^{n}\rho^*_{jk'}\,G_{i_{k'},s_k}\,(Yd)_{jk} \quad (31)$$

Then Eq. (27) can be written as

$$\sum_{k=1}^{n}M_{k'k}\,Q_{jk}=R_{jk'}+\frac{1}{\pi}F^-_{jk'}$$

$k' = 1, 2, - - - n$ (32)

or

$$M_{11}Q_{j1}+\cdots+M_{1k}Q_{jk}+\cdots+M_{1n}Q_{jn}=R_{j1}+\frac{1}{\pi}F^-_{j1}$$

$$M_{21}Q_{j1}+\cdots+M_{2k}Q_{jk}+\cdots+M_{2n}Q_{jn}=R_{j2}+\frac{1}{\pi}F^-_{j2}$$

$$\cdots\cdots\cdots\cdots\cdots\cdots$$

$$M_{k1}Q_{j1}+\cdots+M_{kk}Q_{jk}+\cdots+M_{kn}Q_{jn}=R_{jk}+\frac{1}{\pi}F^-_{jk}$$

$$\cdots\cdots\cdots\cdots\cdots\cdots \quad (32A)$$

$$M_{n1}Q_{j1}+\cdots+M_{nk}Q_{jk}+\cdots M_{nn}Q_{jn}=R_{jn}+\frac{1}{\pi}F^-_{jn}$$

In matrix form, Eq. (32A) appears as

$$\begin{bmatrix} M_{11} & M_{12}\cdots M_{1n}\\ M_{21} & M_{22}\cdots M_{2n}\\ \cdots & \cdots\\ M_{n1} & M_{n2}\cdots M_{nn}\end{bmatrix}\times\begin{Bmatrix} Q_{j1}\\ Q_{j2}\\ \vdots\\ Q_{jn}\end{Bmatrix}=\begin{Bmatrix} R_{j1}+\frac{1}{\pi}F^-_{j1}\\ R_{j2}+\frac{1}{\pi}F^-_{j2}\\ \cdots\\ R_{jn}+\frac{1}{\pi}F^-_{jn}\end{Bmatrix} \quad (33)$$

Therefore, we have

$$\begin{Bmatrix} Q_{j1}\\ Q_{j2}\\ \vdots\\ Q_{jn}\end{Bmatrix}=\frac{1}{M}\begin{bmatrix} A_{11} & A_{21}\cdots A_{n1}\\ A_{12} & A_{22}\cdots A_{n2}\\ \cdots & \cdots\\ A_{1n} & A_{2n}\cdots A_{nn}\end{bmatrix}\times\begin{Bmatrix} R_{j1}+\frac{1}{\pi}F^-_{j1}\\ R_{j2}+\frac{1}{\pi}F^-_{j2}\\ \cdots\\ R_{jn}+\frac{1}{\pi}F^-_{jn}\end{Bmatrix} \quad (34)$$

where

$$M = \begin{vmatrix} m_{11} & m_{12} \cdots m_{1n} \\ m_{21} & m_{22} \cdots m_{2n} \\ \cdots & \cdots \\ m_{n1} & m_{n2} \cdots m_{nn} \end{vmatrix} \qquad (35)$$

and $A_{k'k}$ = cofactor of the determinant M.

Let us now examine the nature of the determinant M. Since $G_{i_k i_k}$ is an even function in ω and

$$\rho^*_{jk}\ \rho_{jk} = |\rho_{jk}|^2$$

all the elements along the diagonal of the determinant will be fractional functions in ω^2 and will have zeros and poles placing symmetrically about both the real and imaginary axes. In addition, elements symmetrical with respect to the diagonal are complex conjugates to each other because

$$G_{i_{k'} i_k}(\omega) = G^*_{i_k i_{k'}}(\omega)$$

Thus this determinant is a Hermitian one.

$$M = \begin{vmatrix} m_{11} & m_{12} \cdots m_{1n} \\ m^*_{12} & m_{22} \cdots m_{2n} \\ \cdots & \cdots \\ m^*_{1n} & m^*_{2n} \cdots m_{nn} \end{vmatrix} \qquad (36)$$

The expansion of this determinant will then be a fractional function in ω^2.

If the function M satisfies the Wiener-Paley criterion

$$\int_{-\infty}^{\infty} \frac{|\log M(\omega)|}{1+\omega^2}\, d\omega < \infty \qquad (37)$$

then there exist two functions $M^+(\omega)$ and $M^-(\omega)$ such that

$$M(\omega) = M^+(\omega)\, M^-(\omega) \qquad (38)$$

and

$$M^+(\omega) = \left[M^-(\omega)\right]^* \qquad (39)$$

holds for real value of ω. Here $M^+(\omega)$ possesses poles and zeros in the upper half plane only and $M^-(\omega)$ has the complementary properties.

For the problem considered, the condition shown in Eq. (37) can be satisfied. Therefore, the factorization of M function into two functions is always possible. However, we shall limit ourselves to the case where M does not have zeros on the real axis.

From Eq. (34), the transfer functions of the compensators are obtained as

$$Q_{jk} = \frac{1}{m} \sum_{k'=1}^{n} A_{k'k} \left(R_{jk'} + \frac{1}{\pi} F^-_{jk'}\right)$$

$$k = 1, 2, \cdots n \qquad (40)$$

Under the condition that the function M can be factored into two functions M^+ and M^-, we shall have

$$Q_{jk} = \frac{1}{m^+ m^-} \sum_{k'=1}^{n} A_{k'k} \left(R_{jk'} + \frac{1}{\pi} F^-_{jk'}\right)$$

or

$$Q_{jk} M^+ = \frac{1}{m^-} \sum_{k'=1}^{n} A_{k'k} \left(R_{jk'} + \frac{1}{\pi} F^-_{jk'}\right) \qquad (41)$$

Since Q_{jk} must be a physically realizable transfer function, it can only have poles in the upper half of the ω-plane. Therefore, the left side of Eq. (41) possesses poles exclusively in the upper half plane. The right side of that equation can have poles over the entire ω-plane. Our next procedure now is to determine that component of the function which has all its poles in the upper half plane. Thus

$$Q_{jk} M^+ = \left[\frac{1}{m^-} \sum_{k'=1}^{n} A_{k'k} \left(R_{jk'} + \frac{1}{\pi} F^-_{jk'}\right)\right]^+ \qquad (42)$$

Let us now examine this equation in detail. The summation terms $\frac{1}{m^-} \sum_{k'=1}^{n} A_{k'k} R_{jk'}$ are completely known. Therefore, the upper-half-plane poles can be obtained and their residues can be evaluated. The second summation terms $\frac{1}{\pi m^-} \sum_{k'=1}^{n} A_{k'k} F^-_{jk'}$ are not completely specified at this moment because of the arbitrarily defined function $F^-_{jk'}$. However, we do know that $F^-_{jk'}/M^-$ can not have poles in the upper half plane. Thus the upper-half-plane poles can only come from the cofactor $A_{k'k}$. We can then decompose these summation terms as follows:

$$\frac{1}{\pi m^-} \sum_{k'=1}^{n} A_{k'k} F^-_{jk'} = \sum \frac{C_{il}}{(\omega - \gamma_i)^{\nu}} + L^- \qquad (43)$$

where L^- contains lower-half-plane poles only and γ_i's are upper-half-plane poles from $A_{k'k}$'s, which

can appear in multiplicity. Combining Eqs. (42) and (43), we finally get

$$Q_{jk} M^{+} = \left[\frac{1}{M^{-}} - \sum_{k'=1}^{n} A_{k'k} R_{jk'}\right]^{+} + \sum \frac{C_{il}}{(\omega - \gamma_i)^{\nu}}$$

or

$$Q_{jk} = \frac{1}{M^{+}} \left\{ \left[\frac{1}{M^{-}} - \sum_{k'=1}^{n} A_{k'k} R_{jk'}\right]^{+} + \sum \frac{C_{il}}{(\omega - \gamma_i)^{\nu}} \right\} \tag{44}$$

We have thus expressed the transfer functions of compensators in explicit form except the coefficients Cie's still need to be evaluated. This can be done by substituting Eq. (44) into any one of the simultaneous equations shown in Eq. (32A) and equating the residues of the same upper-half-plane poles. In other words,

$$\left[\sum_{k=1}^{n} P^{*}_{jk'} P_{jk} G_{i_{k'} i_k} Q_{jk}\right]^{+} = \left[\sum_{k=1}^{n} P^{*}_{jk'} G_{i_{k'} s_k} (Yd)_{jk}\right]^{+}$$

or

$$\left[\sum_{k=1}^{n} P_{jk} Q_{jk} G_{i_{k'} i_k}\right]^{+} = \left[\sum_{k=1}^{n} G_{i_{k'} s_k} (Yd)_{jk}\right]^{+} \tag{45}$$

We shall get a set of linear independent algebraic equations for Cie's. These coefficients can then be uniquely determined.

If the inputs to all terminals are not correlated with one another, then Eq. (27) reduces to

$$P^{*}_{jk} P_{jk} G_{i_k i_k} Q_{jk} = P^{*}_{jk} (Yd)_{jk} G_{i_k s_k} + F^{-}_{jk} \tag{46}$$

where

$$G_{i_k i_k}(\omega) = G_{s_k s_k}(\omega) + G_{s_k n_k}(\omega) + G_{n_k s_k}(\omega) + G_{n_k n_k}(\omega) \tag{47}$$

$$G_{i_k s_k}(\omega) = G_{s_k s_k}(\omega) + G_{n_k s_k}(\omega) \tag{48}$$

Thus $P^{*}_{jk} P_{jk} Q_{i_k i_k}$ is an even fractional function in ω and can be factored into two functions such that

$$P^{*}_{jk} P_{jk} G_{i_k i_k} = S^{+} S^{-} \tag{49}$$

Substituting Eq. (49) into Eq. (46), we have

$$S^{+} S^{-} Q_{jk} = P^{*}_{jk} (Yd)_{jk} G_{i_k s_k} + F^{-}_{jk}$$

and

$$Q_{jk} = \frac{1}{S^{+}} \left[\frac{1}{S^{-}} P^{*}_{jk} (Yd)_{jk} G_{i_k s_k}\right]^{+} \qquad k = 1, 2, - - - n \tag{50}$$

Therefore, for the uncorrelated case, the transfer functions of compensators can be determined independently. The minimum mean-square error is accordingly

$$\overline{\epsilon^{2}_{j}(t)}_{min} = \sum_{k=1}^{n} \int_{0}^{\infty} \left| (Yd)_{jk} \right|^{2} G_{s_k s_k} \, d\omega - \sum_{k=1}^{n} \int_{0}^{\infty} \left| Q_{jk} P_{jk} \right|^{2} G_{i_k i_k} \, d\omega \tag{51}$$

4. Effects of Fixed Elements on System Performance

Let us now investigate the effects on the system performance in the presence of fixed elements. To this end, Eq. (27) is rewritten for further consideration.

$$\sum_{k=1}^{n} P^{*}_{jk'} P_{jk} G_{i_{k'} i_k} Q_{jk} = \sum_{k=1}^{n} P^{*}_{jk'} (Yd)_{jk} G_{i_{k'} s_k} + F^{-}_{jk'}, \tag{52}$$

We recognize at once that the product $P_{jk} Q_{jk}$ is the over-all transfer function between the input terminal k and output terminal j. Intuitively, we may try to solve the over-all transfer function first and then to get the transfer function of the cascade compensator through the division of the over-all transfer function by the corresponding transfer function of the fixed element. Actually, this procedure is true only when the transfer functions of fixed elements are minimum phase. A minimum phase transfer function is one which does not have zeros lying in the right half of s-plane. Conversely, a non-minimum phase transfer function possesses zeros in the reight half-plane. It is

evident that when the fixed elements are non-minimum phase, the equivalent cascade compensator cannot be computed as the ratio of the over-all system function to the transfer function of the fixed element since such a ratio would contain poles in the right half-plane, therefore violating the requirement of stability.

Considering the case when the fixed elements are minimum phase, Eq. (27) can be reduced to

$$\sum_{k=1}^{n} G_{i_{k'}i_k} P_{jk} Q_{jk} = \sum_{k=1}^{n} G_{i_{k'}s_k} (Yd)_{jk} + H_{jk}^{-} \tag{53}$$

or

$$\sum_{k=1}^{n} G_{i_{k'}i_k} Y_{jk} = \sum_{k=1}^{n} G_{i_{k'}s_k} (Yd)_{jk} + H_{jk}^{-}, \tag{53A}$$

where

$$Y_{jk} = P_{jk} Q_{jk} \tag{54}$$

Thus the solution for this problem is the same as that of the free-configuration case[5]. The over-all system functions are independent of the transfer functions of the fixed elements and have been computed previously as

$$Y_{jk} = \frac{1}{G^{+}} \left\{ \left[\frac{1}{G^{-}} \sum_{k'=1}^{n} A_{k'k} N_{jk'} \right]^{+} \sum \frac{C_{il}}{(\omega - \gamma_i)^m} \right\} \tag{55}$$

where

$$G = \begin{vmatrix} G_{11}^{\phi} & G_{12}^{\phi} & \cdots & G_{1n}^{\phi} \\ \cdots & \cdots & \cdots & \cdots \\ G_{n1}^{\phi} & G_{n2}^{\phi} & \cdots & G_{nn}^{\phi} \end{vmatrix} = G^{+} G^{-}$$

$$N_{jk'} = \sum_{k=1}^{n} G_{i_{k'}s_k} (Yd)_{jk}$$

$A_{k'k}$ = cofactor of determinant G

γ_i = upper-half-plane poles from the cofactors

The transfer functions of the compensators are then

$$Q_{jk} = \frac{Y_{jk}}{P_{jk}} \tag{56}$$

Consequently, minimum-phase fixed elements impose no limitation on the system performance under the least mean-square error criterion.

When the fixed plant is non-minimum phase, Eq. (44) must be used to solve for the transfer functions of compensators. The over-all system functions are then given by the product of P_{jk} and Q_{jk} thus found. Therefore certain limitations on the system performance are definitely imposed by the fixed plant of non-minimum phase.

5. Synthesis of Optimum Cascade Controller

We are now going to consider the case where a controller is in cascade with the plant. The system diagram in matrix form is shown in Fig. 3.

It is obvious that the controller itself is also a multipole device. The outputs from this controller are the inputs to the plant. Thus $r_f(t)$ can be expressed as

$$r_f(t) = \sum_{k=1}^{n} \int_0^{\infty} g_{fk}(\tau_1) i_k(t-\tau_1) d\tau_1$$

$$f = 1, 2, - - - m \tag{57}$$

Similarly,

$$c_j(t) = \sum_{f=1}^{m} \int_0^{\infty} p_{jf}(\tau_2) r_f(t-\tau_2) d\tau_2$$

$$j = 1, 2, - - - n \tag{58}$$

By combining Eqs. (57) and (58) we obtain the final expression for the system outputs.

$$c_j(t) = \sum_{k=1}^{n} \sum_{f=1}^{m} \int_0^{\infty} g_{fk}(\tau_1) d\tau_1 \int_0^{\infty} p_{jf}(\tau_2) i_k(t-\tau_1-\tau_2) d\tau_2 \tag{59}$$

Since each element in the controller is closely related to all the system outputs, the total mean square error of the system must be minimized. This total error can easily be found as

$$\overline{\epsilon_T^2} = \sum_{j=1}^{n} \overline{\epsilon_j^2}$$

$$= \sum_{j=1}^{n} \left[\overline{c_j^2(t)} - 2\overline{c_j(t)\zeta_j(t)} + \overline{\zeta_j^2(t)} \right]$$

$$= \sum_{j=1}^{n} \sum_{f=1}^{m} \sum_{f=1}^{m} \sum_{k=1}^{n} \sum_{k=1}^{n} \int_0^\infty g_{f'k'}(\tau_1')\, d\tau_1' \int_0^\infty \rho_{jf'}(\tau_2')\, d\tau_2' \times \int_0^\infty g_{fk}(\tau_1)\, d\tau_1 \int_0^\infty \rho_{jf}(\tau_2)\, \phi_{i_{k'} i_k}(\tau_1' + \tau_2' - \tau_1 - \tau_2)\, d\tau_2$$

$$- 2 \sum_{j=1}^{n} \sum_{f'=1}^{m} \sum_{k'=1}^{n} \sum_{k=1}^{n} \int_0^\infty g_{f'k'}(\tau_1')\, d\tau_1' \int_0^\infty \rho_{jf'}(\tau_2')\, d\tau_2' \times \int_{-\infty}^\infty D_{jk}(\tau_3)\, \phi_{i_{k'} s_k}(\tau_1' + \tau_2' - \tau_3)\, d\tau_3$$

$$+ \sum_{j=1}^{n} \sum_{k'=1}^{n} \sum_{k=1}^{n} \int_{-\infty}^\infty D_{jk'}(\tau_3')\, d\tau_3' \int_{-\infty}^\infty D_{jk}(\tau_3)\, \phi_{s_{k'} s_k}(\tau_3' - \tau_3)\, d\tau_3 \tag{60}$$

where $\phi_{i_{k'} i_k}(\tau)$ and $\phi_{i_{k'} s_k}$ are given by Eqs. (10) and (13) respectively.

Let us now define a function v_{f_k} implicitly by the equation

$$\sum_{j=1}^{n} \sum_{f=1}^{m} \sum_{k=1}^{n} \int_0^\infty \rho_{jf'}(\tau_2')\, d\tau_2' \int_0^\infty v_{fk}(\tau_1)\, d\tau_1 \int_0^\infty \rho_{jf}(\tau_2)\, \phi_{i_{k'} i_k}(\tau_1' + \tau_2' - \tau_1 - \tau_2)\, d\tau_2$$

$$= \sum_{j=1}^{n} \sum_{k=1}^{n} \int_0^\infty \rho_{jf'}(\tau_2')\, d\tau_2 \int_{-\infty}^\infty D_{jk}(\tau_3)\, \phi_{i_{k'} s_k}(\tau_1' + \tau_2' - \tau_3)\, d\tau_3$$

$$\text{for } \tau_1' \gtrless 0 \tag{61}$$

Substituting Eq. (61) into Eq. (60), we shall find, by using the same method in chapter 2, that $\overline{\epsilon_T^2}$ assumes its minimum value when

$$v_{fk} = g_{fk} \tag{62}$$

Thus the integral equations which all the elements in the optimum controller must satisfy are

$$\sum_{j=1}^{n} \sum_{f=1}^{m} \sum_{k=1}^{n} \int_0^\infty \rho_{jf'}(\tau_2')\, d\tau_2 \int_0^\infty g_{fk}(\tau_1)\, d\tau_1 \int_0^\infty \rho_{jf}(\tau_2)\, \phi_{i_{k'} i_k}(\tau_1' + \tau_2' - \tau_1 - \tau_2)\, d\tau_2$$

$$= \sum_{j=1}^{n} \sum_{k=1}^{n} \int_0^\infty \rho_{jf'}(\tau_2')\, d\tau_2' \int_{-\infty}^\infty D_{jk}(\tau_3)\, \phi_{i_{k'} s_k}(\tau_1' + \tau_2' - \tau_3)\, d\tau_3$$

$$\text{for } \tau_1' \gtrless 0 \tag{63}$$

$f' = 1, 2, - - - m$

$k' = 1, 2, - - - n$

The minimum mean square error is then given by

$$\overline{\epsilon_T^2(t)}_{min} = \sum_{j=1}^{n} \sum_{k'=1}^{n} \sum_{k=1}^{n} \int_{-\infty}^\infty D_{jk'}(\tau_3')\, d\tau_3' \int_{-\infty}^\infty D_{jk}(\tau_3)\, \phi_{s_{k'} s_k}(\tau_3' - \tau_3)\, d\tau_3$$

$$- \sum_{j=1}^{n} \sum_{f'=1}^{m} \sum_{j=1}^{m} \sum_{k'=1}^{n} \sum_{k=1}^{n} \int_0^\infty g_{f'k'}(\tau_1')\, d\tau_1' \int_0^\infty \rho_{jf'}(\tau_2')\, d\tau_2'$$

$$\times \int_0^\infty q_{fk}(\tau_1)\,d\tau_1 \int_0^\infty \rho_{jf}(\tau_2)\,\phi_{i_{k'}i_k}(\tau_1'+\tau_2'-\tau_1-\tau_2)\,d\tau_2 \tag{64}$$

or, in frequency domain,

$$\overline{\epsilon_T^2(t)}_{min} = \sum_{j=1}^{n}\sum_{k'=1}^{n}\sum_{k=1}^{n}\int_0^\infty (Yd)^*_{jk'}\,(Yd)_{jk}\,G_{s_{k'}s_k}\,d\omega$$
$$-\sum_{j=1}^{n}\sum_{f'=1}^{m}\sum_{f=1}^{m}\sum_{k'=1}^{n}\sum_{k=1}^{n}\int_0^\infty Q^*_{f'k'}\rho^*_{jf'}\,Q_{fk}\rho_{jf}G_{i_{k'}i_k}\,d\omega \tag{65}$$

The technique used in solving Eq. (63) is exactly the same as that employed in the simple cascade compensators case. Let us define a function $X_{f'k'}(\tau_1')$ such that

$$\sum_{j=1}^{n}\sum_{f=1}^{m}\sum_{k=1}^{n}\int_0^\infty \rho_{jf'}(\tau_2')\,d\tau_2' \int_0^\infty q_{fk}(\tau_1)\,d\tau_1 \int_0^\infty \rho_{jf}(\tau_2)\,\phi_{i_{k'}i_k}(\tau_1'+\tau_2'-\tau_1-\tau_2)\,d\tau_2$$
$$-\sum_{j=1}^{n}\sum_{k=1}^{n}\int_0^\infty \rho_{jf'}(\tau_2')\,d\tau_2 \int_{-\infty}^\infty D_{ik}(\tau_3)\,\phi_{i_{k'}s_k}(\tau_1'+\tau_2'-\tau_3)\,d\tau_3 = X_{f'k'}(\tau_1') \tag{66}$$

and, from equation (63),

$$X_{f'k'}(\tau_1') = 0 \qquad \text{for } \tau_1' \geqq 0 \tag{67}$$

Taking Fourier transform of Eq. (66), we shall obtain

$$\sum_{j=1}^{n}\sum_{f=1}^{m}\sum_{k=1}^{n}\rho^*_{jf'}\rho_{jf}G_{i_{k'}i_k}Q_{fk} = \sum_{j=1}^{n}\sum_{k=1}^{n}\rho^*_{jf'}(Yd)_{jk}G_{i_k s_k} + \frac{1}{\pi}\bar{X}_{f'k'}$$

$$\text{for } f' = 1, 2, \cdots m \qquad k' = 1, 2, \cdots n \tag{68}$$

Thus these m x n equations shall determine the functions Q_{fk} uniquely. If we let

$$N_{fk}^{f'k'} = \left\{\sum_{j=1}^{n}\rho^*_{jf'}\rho_{jf}\right\}G_{i_{k'}i_k} \tag{69}$$

$$R^{f'k'} = \sum_{j=1}^{n}\sum_{k=1}^{n}\rho^*_{jf'}(Yd)_{jk}G_{i_{k'}s_k} \tag{70}$$

Eq. (68) in matrix form shall be

$$\left[N_{fk}^{f'k'}\right]\left\{Q_{fk}\right\} = \left\{R^{f'k'} + \frac{1}{\pi}\bar{X}_{f'k'}\right\} \tag{71}$$

Thus we have

$$\left\{Q_{fk}\right\} = \frac{1}{N}\left[A_{f'k'}^{fk}\right]\left\{R^{f'k'} + \frac{1}{\pi}\bar{X}_{f'k'}\right\} \tag{72}$$

Here $\left[N_{fk}^{f'k'}\right]$ and $\left[A_{f'k'}^{fk}\right]$ are mn x mn-square matrix. The index fk are used to number the columns and the index f'k' are used to number the rows. The sequence of variation for these index is to fix "f" or "f'" first and let "k" or "k'" assume the numbers from 1 to n. "f" or "f'" itself can go from 1 to m. N is the determinant of the matrix $\left[N_{fk}^{f'k'}\right]$ and $A_{fk}^{f'k'}$ are its cofactors.

It can easily be seen that this N determinant is also Hermitian. Therefore, factorization of this function $N(\omega)$ is possible.

$$N(\omega) = N^+(\omega)\,N^-(\omega) \tag{73}$$

Thus we have

$$Q_{jk} = \frac{1}{N^+N^-} \sum_{j'=1}^{m} \sum_{k'=1}^{n} A_{jk}^{j'k'} \left(R^{j'k'} + \frac{1}{\pi} \overline{X}_{j'k'}^{-} \right) \tag{74}$$

or

$$Q_{jk} = \frac{1}{N^+} \left\{ \left[\frac{1}{N^-} \sum_{j'=1}^{m} \sum_{k'=1}^{n} A_{jk}^{j'k'} R^{j'k'} \right]^{+} + \sum \frac{Cie}{(\omega - \gamma_i)^{\nu}} \right\} \tag{75}$$

where γ_i's are the upper-half-plane poles from the cofactors $A_{jk}^{j'k'}$'s. The coefficients Cie's can be determined by using the following equations;

$$\left[\sum_{j=1}^{n} \sum_{j'=1}^{m} \sum_{k=1}^{n} P_{jj'}^{*} P_{jj} G_{i_k i_k} Q_{jk} \right]^{+} = \left[\sum_{j=1}^{n} \sum_{k=1}^{n} P_{jj'}^{*} (Yd)_{jk} G_{i_{k'} s_k} \right]^{+} \tag{76}$$

We have shown then that the synthesis procedure for the cascade controller is similar to that for cascade compensators. The procedure would be amplified in working out a specific problem. (See the appendix.)

Appendix

Example For The Synthesis Of Optimum Cascade Compensators

The system under consideration shall have two input terminals and one output terminal. The transfer function of one of the fixed elements is non-minimum phase. The only cross-correlation between inputs at two terminals is the signals. White noises are taken as the disturbances. The various power spectral densities are given by

$$G_{s_1 s_1}(\omega) = \frac{1}{\omega^2+1} \qquad G_{s_2 s_2}(\omega) = \frac{2}{\omega^2+2}$$

$$G_{n_1 n_1}(\omega) = 0.2 \qquad G_{n_2 n_2}(\omega) = 0.5$$

$$G_{s_1 s_2}(\omega) = \frac{1}{\omega^2 + j\omega + 2}$$

The transfer functions of the two fixed elements are

$$P_{11}(s) = \frac{s-4}{s+4} \qquad P_{12}(s) = \frac{s+1}{s+3}$$

The desired output of the system is the sum of the second signal itself and the predicted value of the first signal through 1 second. Thus the desired system functions are

$$(Yd)_{11}(s) = e^{s} \qquad (Yd)_{12}(s) = 1$$

The system configuration is shown in Fig. A.

According to equation (27), we have the system equations as

$$P_{11}^{*} P_{11} G_{i_1 i_1} Q_{11} + P_{11}^{*} P_{12} G_{i_1 i_2} Q_{12} = P_{11}^{*} (Yd)_{11} G_{i_1 s_1} + P_{11}^{*} (Yd)_{12} G_{i_1 s_2} + \frac{1}{\pi} F_{11}^{-}$$

$$P_{12}^{*} P_{11} G_{i_2 i_1} Q_{11} + P_{12}^{*} P_{12} G_{i_2 i_2} Q_{12} = P_{12}^{*} (Yd)_{11} G_{i_2 s_1} + P_{12}^{*} (Yd)_{12} G_{i_2 s_2} + \frac{1}{\pi} F_{12}^{-} \tag{A-1}$$

From equation (28) and (29) we obtain

$$G_{i_1 s_1}(\omega) = G_{s_1 s_1}(\omega) = \frac{1}{\omega^2+1}$$

$$G_{i_1 s_2}(\omega) = G_{s_1 s_2}(\omega) = \frac{1}{\omega^2 + j\omega + 2} = \frac{1}{(\omega+j2)(\omega+j)}$$

$$G_{i_2 s_1}(\omega) = G_{s_2 s_1}(\omega) = G_{s_1 s_2}^{*}(\omega) = \frac{1}{\omega^2 - j\omega + 2} = \frac{1}{(\omega-j2)(\omega+j)}$$

$$G_{i_2 s_2}(\omega) = G_{s_2 s_2}(\omega) = \frac{2}{\omega^2+2}$$

$$G_{i_1 i_1}(\omega) = G_{s_1 s_1}(\omega) + G_{n_1 n_1}(\omega)$$

$$= \frac{1}{\omega^2+1} + 0.2 = \frac{0.2\omega^2+1.2}{\omega^2+1}$$

$$G_{i_1 i_2}(\omega) = G_{s_1 s_2}(\omega) = \frac{1}{\omega^2+j\omega+2} = \frac{1}{(\omega+j2)(\omega-j)}$$

$$G_{i_2 i_1}(\omega) = G_{s_2 s_1}(\omega) = \frac{1}{(\omega-j2)(\omega+j)}$$

$$G_{i_2 i_2}(\omega) = G_{s_2 s_2}(\omega) + G_{n_2 n_2}(\omega)$$

$$= \frac{2}{\omega^2+2} + 0.5 = \frac{0.5\omega^2+3}{\omega^2+2}$$

Now $P_{11}^*(\omega) P_{11}(\omega) = \frac{-j\omega-4}{-j\omega+4} \times \frac{j\omega-4}{j\omega+4} = 1$

$$P_{12}^*(\omega) P_{12}(\omega) = \frac{-j\omega+1}{-j\omega+3} \frac{j\omega+1}{j\omega+3} = \frac{\omega^2+1}{\omega^2+9}$$

Thus from equation (30),

$$M_{11} = P_{11}^* P_{11} G_{i_1 i_1} = \frac{0.2\omega^2+1.2}{\omega^2+1} \qquad \text{(A-2)}$$

$$M_{12} = P_{11}^* P_{12} G_{i_1 i_2} = \frac{-j\omega-4}{-j\omega+4} \times \frac{j\omega+1}{j\omega+3} \times \frac{1}{(\omega+j2)(\omega-j)} = \frac{\omega - j4}{(\omega+j4)(\omega-j3)(\omega+j2)}$$

(A-3)

$$M_{21} = P_{12}^* P_{11} G_{i_2 i_1} = M_{12}^* = \frac{\omega+j4}{(\omega-j4)(\omega+j3)(\omega-j2)}$$

(A-4)

$$M_{22} = P_{12}^* P_{12} G_{i_2 i_2} = \frac{(\omega^2+1)(0.5\omega^2+3)}{(\omega^2+9)(\omega^2+2)} \qquad \text{(A-5)}$$

$$M = \begin{vmatrix} M_{11} & M_{12} \\ M_{21} & M_{22} \end{vmatrix} = M_{11} M_{22} - M_{12} M_{21}$$

$$= \frac{0.2\omega^2+1.2}{\omega^2+1} \times \frac{(\omega^2+1)(0.5\omega^2+3)}{(\omega^2+9)(\omega^2+2)}$$

$$- \frac{\omega-j4}{(\omega+j4)(\omega-j3)(\omega+j2)} \times \frac{\omega+j4}{(\omega-j4)(\omega+j3)(\omega-j2)}$$

$$= \frac{\omega^6+16\omega^4+74\omega^2+124}{10(\omega^2+2)(\omega^2+4)(\omega^2+9)}$$

$$= \frac{(\omega-j3.11)(\omega+j3.11)(\omega-0.461-j1.836)}{10(\omega-j1.414)(\omega+j1.414)(\omega-j2)}$$

$$\frac{(\omega-0.461+j1.836)(\omega+0.461-j1.836)}{(\omega+j2)(\omega-j3)}$$

$$(\omega+0.461+j1.836)$$

(A-6)

Hence we can factor this M function into two terms:

$$M_+(\omega) = \frac{(\omega-j3.11)(\omega-0.461-j1.836)(\omega+0.461-j1.836)}{10(\omega-j1.414)(\omega-j2)(\omega-j3)}$$

(A-7)

$$M^{-}(\omega) = \frac{(\omega+j3.11)(\omega-0.461+j1.836)(\omega+0.461+j1.836)}{(\omega+j1.414)(\omega+j2)(\omega+j3)} \qquad (A\text{-}8)$$

(A) Determination of Q_{11}

$$A_{11} = M_{22} = \frac{(\omega^2+1)(0.5\omega^2+3)}{(\omega^2+9)(\omega^2+2)}$$

$$A_{21} = -M_{12} = -\frac{\omega-j4}{(\omega+j4)(\omega-j3)(\omega+j2)}$$

$$R_{11} = P_{11}^{*} G_{i_1 s_1}(Yd)_{11} + P_{11}^{*} G_{i_1 s_2}(Yd)_{12}$$

$$= \frac{(\omega-j4)\,e^{j\omega}}{(\omega+j4)(\omega^2+1)} + \frac{\omega-j4}{(\omega+j4)(\omega+j2)(\omega-j)}$$

$$R_{12}^{d} = P_{12}^{*} G_{i_2 s_1}(Yd)_{11} + P_{12}^{*} G_{i_2 s_2}(Yd)_{12}$$

$$= \frac{(\omega+j)\,e^{j\omega}}{(\omega+j3)(\omega-j2)(\omega+j)} + \frac{(\omega+j)\times 2}{(\omega+j3)(\omega^2+2)}$$

$$= \frac{e^{j\omega}}{(\omega+j3)(\omega-j2)} + \frac{2(\omega+j)}{(\omega+j3)(\omega^2+2)}$$

Thus we have

$$\frac{1}{M^{-}} \sum_{k'=1}^{2} A_{k'1} R_{1k'} = \frac{1}{M}\left[A_{11} R_{11} + A_{21} R_{12}\right]$$

$$= \frac{(\omega+j1.414)(\omega+j2)(\omega+j3)}{(\omega+j3.11)(\omega-0.461+j1.836)(\omega+0.461+j1.836)}$$

$$\times \left\{ \frac{(\omega^2+1)(0.5\omega^2+3)}{(\omega^2+9)(\omega^2+2)} \left[\frac{(\omega-j4)\,e^{j\omega}}{(\omega+j4)(\omega^2+1)} + \frac{\omega-j4}{(\omega+j4)(\omega+j2)(\omega-j)} \right] - \frac{\omega-j4}{(\omega+j4)(\omega-j3)(\omega+j2)} \right.$$

$$\left. \left[\frac{e^{j\omega}}{(\omega+j3)(\omega-j2)} + \frac{2(\omega+j)}{(\omega+j3)(\omega^2+2)} \right] \right\}$$

$$= \frac{(\omega-j4)(0.5\omega^4+4\omega^2+10)}{(\omega+j3.11)(\omega-0.461+j1.836)(\omega+0.461+j1.836)} \cdot \frac{e^{j\omega}}{(\omega-j1.414)(\omega-j2)(\omega-j3)(\omega+j4)}$$

$$+ \frac{0.5(\omega+j1.414)(\omega+j)(\omega-j4)}{(\omega+j3.11)(\omega-0.461+j1.836)(\omega+0.461+j1.836)(\omega-j3)(\omega+j4)}$$

$$= (Q_{11})_1 + (Q_{11})_2$$

The next step now is to find out that component of this function Q_{11}, which has all its poles in the upper half of the ω-plane.

$$(Q_{11})_1 = \left[\frac{A_1}{\omega-j1.414} + \frac{A_2}{\omega-j2} + \frac{A_3}{\omega-j3} + \frac{A_4}{\omega+j3.11} + \frac{A_5}{\omega-0.461+j1.836} + \frac{A_6}{\omega+0.461+j1.836} + \frac{A_7}{\omega+j4} \right] e^{j\omega}$$

It is evident that only the first three terms are useful in constituting the physically realizable transfer function. Hence we have

$$(q_{11})_1(t) = \frac{1}{2\pi} \int_{-\infty}^{\infty} \left[\frac{A_1 e^{j\omega}}{\omega-j1.414} + \frac{A_2 e^{j\omega}}{\omega-j2} + \frac{A_3 e^{j\omega}}{\omega-j3} \right] e^{j\omega t}\, d\omega$$

$$= A_1 j e^{-1.414(t+1)} + A_2 j e^{-2(t+1)} + A_3 j e^{-3(t+1)}$$

for $t + 1 > 0$

so that

$$(Q_{11})_1^+ = \int_0^\infty (q_{11})_1(t) e^{-j\omega t}\, dt$$

$$= \frac{A_1 e^{-1.414}}{\omega - j1.414} + \frac{A_2 e^{-2}}{\omega - j2} + \frac{A_3 e^{-3}}{\omega - j3}$$

$$= \frac{0.243\, A_1}{\omega - j1.414} + \frac{0.135\, A_2}{\omega - j2} + \frac{0.0498\, A_3}{\omega - j3} \qquad \text{(A-9)}$$

In a similar manner, we obtain

$$(Q_{11})_2^+ = \frac{B_1}{\omega - j3} \qquad \text{(A-10)}$$

All the coefficients are found to be

$$A_1 = j0.04217 \qquad B_1 = j0.008746$$

$$A_2 = -j0.01491$$

$$A_3 = j0.009058 \qquad \text{(A-11)}$$

The upper-half-plane poles from A_{11} and A_{21} are

$$\omega_1 = j1.414 \qquad \omega_2 = j3$$

Thus we have

$$(Q_{11})_3^+ = \frac{C_{11}}{\omega - j1.414} + \frac{C_{21}}{\omega - j3} \qquad \text{(A-12)}$$

Finally the transfer function Q_{11} is

$$Q_{11} = \left[(Q_{11})_1^+ + (Q_{11})_2^+ + (Q_{11})_3^+\right] / M^+$$

$$= \left[\frac{j0.04217 \times 0.243}{\omega - j1.414} + \frac{-j0.01491 \times 0.135}{\omega - j2} + \frac{j0.009058 \times 0.0498}{\omega - j3} + \frac{j0.008746}{\omega - j3} + \frac{C_{11}}{\omega - j1.414} + \frac{C_{21}}{\omega - j3}\right]$$

$$\times \frac{10(\omega - j1.414)(\omega - j2)(\omega - j3)}{(\omega - j3.11)(\omega - 0.461 - j1.836)(\omega + 0.461 - j1.836)}$$

$$= \frac{10}{(\omega - j3.11)(\omega - 0.461 - j1.836)(\omega + 0.461 - j1.836)}$$

$$\times \left[(C_{11} + C_{21} + j0.0174)\omega^2 - (5C_{11} + 3.414C_{21} + j0.07377)j\omega - 6C_{11} - 2.828C_{21} - j0.07896\right] \qquad \text{(A-13)}$$

(B) Determination of Q_{12}

$$A_{12} = -M_{21} = -\frac{\omega + j4}{(\omega - j4)(\omega + j3)(\omega - j2)}$$

$$A_{22} = M_{11} = \frac{0.2\omega^2 + 1.2}{\omega^2 + 1}$$

$$R_{11}^d = \frac{(\omega - j4)e^{j\omega}}{(\omega + j4)(\omega^2 + 1)} + \frac{\omega - j4}{(\omega + j4)(\omega + j2)(\omega - j)}$$

$$R_{12}^d = \frac{e^{j\omega}}{(\omega + j3)(\omega - j2)} + \frac{2(\omega + j)}{(\omega + j3)(\omega^2 + 2)}$$

Thus we obtain

$$\frac{1}{M^-} \sum_{k'=1}^{2} A_{k'2} R_{1k'}^d = \frac{1}{M^-}\left[A_{12} R_{11}^d + A_{22} R_{12}^d\right]$$

$$= \frac{(\omega + j1.414)(\omega + j2)(\omega + j3)}{(\omega + j3.11)(\omega - 0.461 + j1.836)(\omega + 0.461 + j1.836)}$$

$$\times \left\{\frac{-(\omega + j4)}{(\omega - j4)(\omega + j3)(\omega - j2)}\left[\frac{(\omega - j4)e^{j\omega}}{(\omega + j4)(\omega^2 + 1)} + \frac{\omega - j4}{(\omega + j4)(\omega + j2)(\omega - j)}\right] + \frac{0.2\omega^2 + 1.2}{\omega^2 + 1}\left[\frac{e^{j\omega}}{(\omega + j^3)(\omega - j2)} + \frac{2(\omega + j)}{(\omega + j3)(\omega^2 + 2)}\right]\right\}$$

$$\frac{0.2(\omega+j1.414)(\omega+j2)}{(\omega+j3.11)(\omega-0.461+j1.836)(\omega+0.461+j1.836)(\omega-j2)}e^{j\omega}$$

$$+\frac{0.4\omega^4+3\omega^2+7.6}{(\omega+3.11)(\omega-0.461+j1.836)(\omega+0.461+j1.836)(\omega-j)(\omega-j1.1414)(\omega-j2)}$$

$$= (Q_{12})_1 + (Q_{12})_2$$

Following the previous procedure, we get

$$(Q_{12})_1^+ = \frac{0.135\,A_1'}{\omega-j2} \qquad \text{(A-14)}$$

and

$$(Q_{12})_2^+ = \frac{B_1'}{\omega-j} + \frac{B_2'}{\omega-j1.414} + \frac{B_3'}{\omega-j2} \qquad \text{(A-15)}$$

These coefficients are found to be

$$A_1' = -j0.0358 \qquad B_1' = -j0.356$$
$$B_2' = j0.271$$
$$B_3' = -j0.04474 \qquad \text{(A-16)}$$

The upper half plane poles from A_{12} and A_{22} are $\omega_1' = j$, $\omega_2' = j2$, $\omega_3' = j4$. Thus we have

$$(Q_{12})_3^+ = \frac{C_{12}}{\omega-j} + \frac{C_{22}}{\omega-j2} + \frac{C_{32}}{\omega-j4} \qquad \text{(A-17)}$$

Finally we obtain

$$Q_{12} = \left[(Q_{12})_1^+ + (Q_{12})_2^+ + (Q_{12})_3^+\right]/M^+$$

$$= \left[\frac{-j0.0358\times0.135}{\omega-j2} - \frac{j0.356}{\omega-j} + \frac{j0.271}{\omega-j1.414} - \frac{j0.04474}{\omega-j2} + \frac{C_{12}}{\omega-j} + \frac{C_{22}}{\omega-j2} + \frac{C_{32}}{\omega-j4}\right]$$

$$\times \frac{10(\omega-j1.414)(\omega-j2)(\omega-j3)}{(\omega-j3.11)(\omega-0.461-j1.836)(\omega+0.461-j1.836)}$$

$$= \frac{10(\omega-j3)}{(\omega-j3.11)(\omega-0.461-j1.836)(\omega+0.461-j1.836)(\omega-j)(\omega-j4)}$$

$$\times\Big[(C_{12}+C_{22}+C_{32}-j0.1346)\omega^3 - j(7.414\,C_{12}+6.414\,C_{22}+4.414\,C_{32}-j1.06)\omega^2 - (16.48\,C_{12}+11.07\,C_{22}+6.242\,C_{32}-j2.623)\omega + j(11.31\,C_{12}+5.656\,C_{22}+2.828\,C_{32}-j2.139)\Big]$$

(A-18)

(C) Determination of the coefficients

In order to evaluate the coefficients C_{11}, C_{21}, C_{12}, C_{22}, and C_{32}, let us substitute Eqs. (A-13) and (A-18) into the first expression of Eq. (A-1) and find that component of the expression, which has all its poles in the upper half of the ω-plane. Thus, by Eqs. (45), we have

$$\left[\frac{\omega+j4}{\omega-j4}\times\frac{0.2\omega^2+1.2}{\omega^2+1}\times\frac{10\left[(C_{11}+C_{21}+j0.0174)\omega^2-(5C_{11}+3.414C_{21}+j0.07377)j\omega-6C_{11}-2.828C_{21}-j0.07896\right]}{(\omega-0.461-j1.836)(\omega+0.461-j1.836)(\omega-j3.11)}\right.$$

$$+\frac{\omega-j}{\omega-j3}\times\frac{1}{(\omega+j2)(\omega-j)}\times\frac{10(\omega-j3)\left[(C_{12}+C_{22}+C_{32}-j0.1346)\omega^3-(7.414C_{12}+6.414C_{22}+4.414C_{32}-j1.06)j\omega^2-(16.48C_{12}+11.07C_{22}+6.242C_{32}-j2.623)\omega+j(11.31C_{12}+5.656C_{22}+2.828C_{32}-j2.139)\right]}{(\omega-0.461-j1.836)(\omega+0.461-j1.836)(\omega-j4)(\omega-j)}\left.\right]^{+}$$

$$=\left[\frac{e^{j\omega}}{\omega^2+1}+\frac{1}{(\omega+j^2)(\omega-j)}\right]^{+} \qquad \text{(A-19)}$$

We then can equate the residues for the same upper-half-plane poles on both sides of the above equation. There are five poles in the upper half plane; namely,

$\omega_1 = j$ $\qquad$ $\omega_4 = 0.461 + j1.836$

$\omega_2 = j4$ $\qquad$ $\omega_5 = -0.461 + j1.836$

$\omega_3 = j3.11$

(A-20)

Through the evaluation of the residues of these poles, we shall get five independent equations in terms of C_{11}, C_{12}, C_{21}, C_{22}, and C_{32}. Thus these constants can be uniquely determined.

The five linear algebraic equations are found to be

$$8.668\,C_{11}+1.794\,C_{21}-0.7188\,C_{12}+0.3467\,C_{32} = j0.1633$$

(A-21)

$$4.996\,C_{11}+12.661\,C_{21}+0.002\,C_{12}+0.0004\,C_{22}-1.9778\,C_{32} = -j0.1507$$

(A-22)

$$0.448\,C_{11}+6.934\,C_{21}+0.952\,C_{12}+1.804\,C_{22}-2.258\,C_{32} = j0.0388$$

(A-23)

$$(2.5798+j1.771)\,C_{11}+(-1.2846+j0.8885)\,C_{21}+(0.4136-j0.5126)\,C_{12}+(1.1269+j0.6355)\,C_{22}+(0.00986+j0.28616)\,C_{32}=0.01667-j0.0443$$

(A-24a)

$$(2.5798-j1.771)\,C_{11}+(-1.2846-j0.8885)\,C_{21}+(0.4136+j0.5126)\,C_{12}+(1.1269-j0.6365)\,C_{22}+(0.00986-j0.28616)\,C_{32}=-0.01667-j0.0443$$

(A-25a)

Eqs. (A-24a) and (A-25a) can be combined to yield

$$2.5798\,C_{11}-1.2846\,C_{21}+0.4136\,C_{12}+1.1269\,C_{22}+0.00986\,C_{32} = -j0.0443$$

(A-24b)

$$1.771\,C_{11}+0.8885\,C_{21}-0.5126\,C_{12}+0.6365\,C_{22}+0.28616\,C_{32} = -j0.01667$$

(A-25b)

These coefficients are then determined as

$C_{11} = j0.02811$

$C_{21} = -j0.12512$

$C_{12} = -j0.51605$

$C_{22} = -j0.05116$

$C_{32} = -j0.65426$ (A-26)

The transfer functions for the compensators are then finally given as

$$Q_{11}(S) = 0.796\ \frac{S^2 + 2.692\,S + 1.334}{(S+3.11)(S+1.836-j0.461)(S+1.836+j0.461)} \qquad \text{(A-27)}$$

$$Q_{12}(S) = 13.5\ \frac{S^4 + 8.974S^3 + 29.56S^2 + 41.36\,S + 22.38}{(S+1)(S+3.11)(S+4)(S+1.836-j0.461)(S+1.836+j0.461)} \qquad \text{(A-28)}$$

References

1. Golomb, M., and E. Usdin: "A Theory Of Multi-Dimensional Servo Systems," J. of Franklin Inst., pp. 29-57, Jan. 1952.

2. Wiener, N.: "The Extrapolation, Interpolation, and Smoothing Of Stationary Time Series," John Wiley & Sons, Inc., New York, 1949.

3. Laning, J. H., Jr., and R. H. Battin: "Random Processes in Automatic Control," McGraw-Hill Book Company, Inc., New York, 1956.

4. Freeman, H.: "A Synthesis Method for Multipole Control Systems," Tech. Rept. T-15/B, Columbia University Electronics Research Laboratories, New York, April 1956.

5. Hsieh, H. C., and C. T. Leondes: "On The Optimum Synthesis of Multipole Control Systems in The Wiener Sense," IRE, National Convention Record, vol. 7, part 4, pp. 18-31, March 1959.

Acknowledgement

This research was supported by the United States Air Force under Contract No. AF49(638)438 monitored by the Air Force Office Of Scientific Research of the Air Research and Development Command.

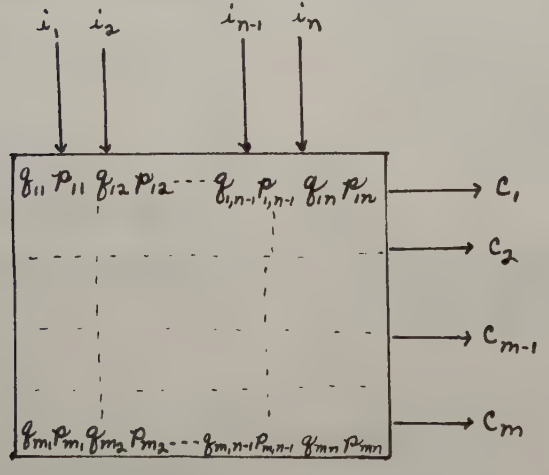

Fig. 1. n + m System with Cascade Compensators.

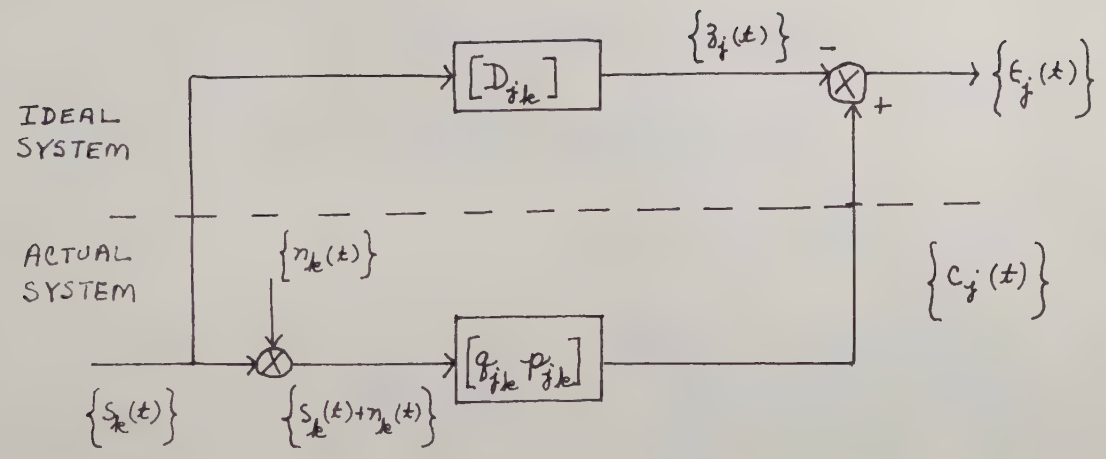

Fig. 2. Error Generation Diagram.

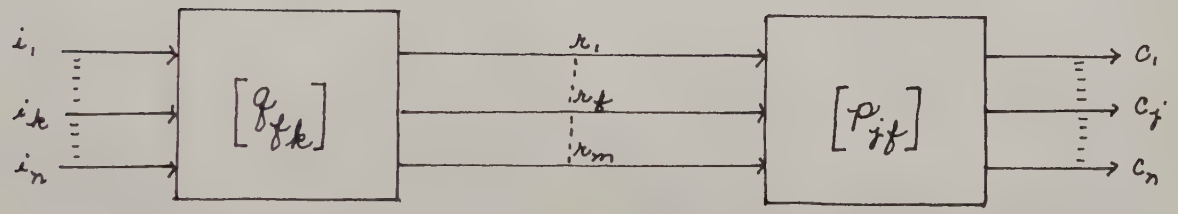

Fig. 3. System Diagram with Cascade Controller.

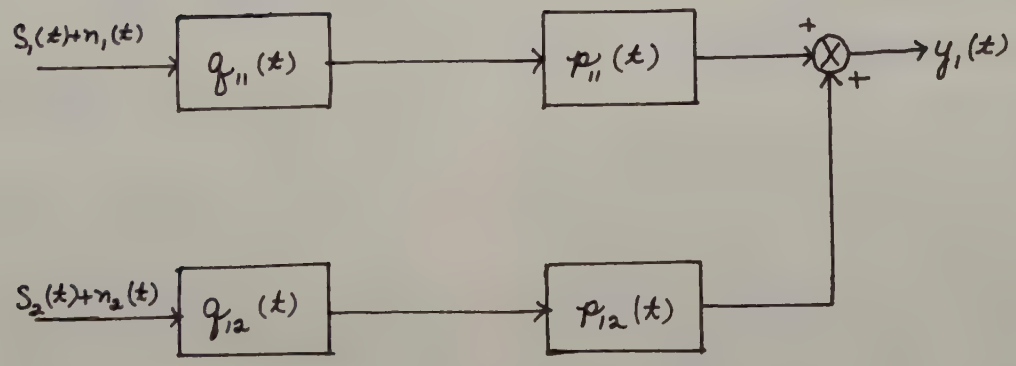

Fig. A. z + 1 poles system.

PREDICTOR-RELAY SERVOS WITH RANDOM INPUTS

Thomas R. Benedict

Cornell Aeronautical Laboratory, Inc.
Buffalo 21, New York

Summary

Part I contains an evaluation of a proposal by O. J. M. Smith on the control, by Wiener prediction and a non-linear combination of input and feedback signals, of a saturating element driving a primarily inertial load. This evaluation consists of simulation tests on a high-speed analog computer with actual continuous random Gaussian inputs. Results presented include: (1) Variation of the mean squared error with prediction time; (2) Optimum system parameter dependence upon input signal level; (3) For fixed saturating level, mean squared error comparisons between the predictor-relay servo, and the "McDonald" and "optimum relay" servo; (4) Effects of different input spectral width and location; and (5) Data on a variation of the basic predictor-relay servo, where minimal-error parameters become relatively independent of input signal level.

Part II is concerned with the error signal. The character of the error is discussed by examples from sinusoidal, transient, and random inputs. In an extension of a paper by K. Chuang and L. F. Kazda, the error probability density and distribution functions are found analytically, the results being valid for a class of compensated relay servos. The main result is that the large-amplitude error probability density is of a single-exponential form. Analog computer measurement of the error probability distribution function verifies the theory.

The Predictor-Relay Servo

Problem Statement

The intentional insertion into control systems of non-linear components has received considerable attention recently. Transducer weight, cost, and tolerances can be greatly reduced over an equivalent-error linear system.[1] See Fig. 1. A fixed saturation level F is assumed. The problem then is to specify the form and operation of the computer that will generate a control signal θ_c which will switch the non-linearity in such a way that some functional of the error signal θ_e is minimized. The optimum computer specifications will depend upon (1) the load characteristics, (2) the error functional to be minimized, and (3) the form of the input signal. An extensive literature treats the case of step and ramp input signals, for an nth order linear load and for the error criterion of minimum time for the error and its n-1 derivatives to be reduced to zero.[2] Solution is effected by phase-space analysis. These servo designs become definitely suboptimal when random signals (possessing non-zero acceleration) appear at the input.[3-5]

For the case of random input signals, the Booton quasi-linearization technique[6] may be applied to determine the optimal coefficients of an assumed proportional plus derivative control (linear control computer) of an inertial load.[7] This statistical technique would minimize the rms error under assumed topology of computer and known input spectrum. However, the nature of the saturating transducer and inertial load causes this assumed form to perform inferior to a computer with a chosen non-linearity in the switch computer and more sophisticated signal prediction and computation. Work at the University of California summarized by O. J. M. Smith[8] proposes a system which becomes the point of departure for this paper. It is an approximate, non-statistical phase plane method. A synthesis technique using a probabilistic model of the phase plane has not been announced.

Derivation of the Predictor-Relay Servo

Professor O. J. M. Smith[8] has outlined a method for predictor control of a saturating nonlinearity driving an inertial load, (see Fig. 1). In this analysis the following assumptions are made:

1) There is no load signal, θ_L. A variation here could be included in the same method without difficulty.

2) The saturating characteristic is pure, i.e.,

$$X(\theta_c) = F \frac{\theta_c}{|\theta_c|} \cdot \qquad (1)$$

It is known that slight deviations from this ideal characteristic do not adversely affect system performance.[1]

3) The input random variable has a high enough level and wide enough frequency band that the simpler McDonald servo is not suitable.

4) The input random variable has at the same time a low enough level and a narrow enough

frequency band that certain assumptions can be made regarding system response times. Throughout this paper, the input random variable will be considered to be a member of an ergodic stationary Gaussian random process.

The Smith method is one of approximate phase plane analysis and proceeds as follows, (see Fig. 2). One assumes the saturating element, at t = 0, is in the state $X = F_1$. Integrating X(t) then,

$$F_1 t_1 + F_2 t_2 = \dot{\theta}_o(\tau) - \dot{\theta}_o(0) \tag{2}$$

Integrating $\dot{\theta}_o(t)$,

$$\frac{1}{2}F_1 t_1^2 + F_2 t_1 t_2 + \frac{1}{2}F_2 t_2^2 = \theta_o(0) - \theta_o(\tau) + \tau\dot{\theta}_o(\tau) \tag{3}$$

Now define the new variables

$$\begin{aligned} \alpha &= -\left[\theta_o(0) - \theta_o(\tau) + \tau\dot{\theta}_o(\tau)\right] \\ \beta &= \dot{\theta}_o(\tau) - \dot{\theta}_o(0) \end{aligned} \tag{4}$$

The decision to switch comes at time $t = t_1$. For $t_1 = 0$ the switch time is the present instant; for $t_1 = 0$, eliminating t_2, one has a single equation expressing the variable state,

$$\alpha + \frac{\beta^2}{2F_2} \quad . \tag{5}$$

Letting β contain the sign and calling $F_2 = F$,

$$\alpha + \frac{\beta|\beta|}{F} = 0 \quad . \tag{6}$$

Eq. (6) then is the relation between α and β at switch time. One needs to derive a control signal, θ_c:

$$\theta_c = \alpha + \frac{\beta|\beta|}{F} \tag{7}$$

where the sign of θ_c will control the transducer action as in Fig. (1).

Actual signals α and β are selected from Eq. (4) by writing that

$$\dot{\theta}_e(\tau) = \theta_e(\tau) = 0 \tag{8}$$

This is to imply that after two trajectories (two forcing function reversals) from any starting conditions, error and its derivative are zero. This assumption is the now classical step taken in designing non-linear saturating systems to respond to step or ramp inputs, "extended" to the random input case. If Eq. (8) is to hold, the design equations for the predictor-compensated system become, with

$$\begin{aligned} \theta_e &= \theta_i - \theta_o \ , \\ \alpha &= \left[e^{j\omega\tau} - j\omega\tau e^{j\omega\tau}\right]\theta_i - \theta_o \\ \beta &= j\omega\tau^{j\omega\tau}\theta_i - j\omega\theta_o \end{aligned} \tag{9}$$

The system topology is shown in Fig. (3). Predictions of input and input derivative are needed.

The best prediction time τ is not developed in this method, when the input is random. Account is not taken of the fact that predictions will not be error-free. Most importantly, the method is, strictly speaking, only valid when the input is varying slowly enough that the system can "lock in" and approximate $\dot{\theta}_{e\tau} = \theta_{e\tau} = 0$ in actuality.

If the prediction time τ is made zero, the Smith design reduces the McDonald servo circuit of Fig. (4). When the input is varying slowly enough that future values are present values and derivatives are zero, no prediction is needed and the McDonald circuit, designed for transient inputs, serves well for random inputs.

This approximate design, then, should only be used for a certain class of random input signals. Furthermore it is not a true statistical design. However, as it appeared to be lacking a competitive design method, this Smith approach formed the starting point of the work described in this paper.

The work of the previous section calls out predictions of the input signal and its derivative for "optimum" control of the inertial load. The derivation of minimum-mean-square-error operators for future signal estimation, even in the presence of noise, is commonly available.[9] The transfer function for optimum linear prediction of a member of a stationary random process depends only upon the power spectral density, $\Phi_{ii}(\omega)$, of the input signal, and the power spectral density, $\Phi_{nn}(\omega)$, of any additive noise. It is assumed that signal-noise cross-correlation is zero.

The following notation is used, on the complex plane $\lambda = \omega + j\alpha$;

$$\Lambda(\omega) = \Phi_{ii}(\omega) + \Phi_{nn}(\omega)$$

$\Lambda^{+}(j\omega)$ = Factor of Λ having poles and zeros only in the upper half plane;

$\Lambda^{-}(j\omega)$ Factor of Λ having poles and zeros only in the lower half plane.

The well known result then, for the optimum linear predicting filter H_p for prediction time τ is

$$H_p(j\omega) = \frac{1}{2\pi\Lambda + (j\omega)} \int_0^\infty e^{-j\omega\tau} \int_{-\infty}^{\infty} \frac{\Phi_{ii}(\mu) e^{j\mu(t+\tau)}}{\Lambda - (j\mu)} d\mu dt \quad (10)$$

The estimating of future derivative is not discussed at all in the common works on control system statistics. However, the solution can be effected from straight forward application of Wiener's [10] techniques.

One arrives at the expedient result that the derivative prediction operator H_d is given by[11]

$$H_d(j\omega) = \frac{dH_p(j\omega)}{d\tau} = \frac{1}{2\pi\Lambda + (j\omega)} \int_0^\infty e^{j\omega t} \int_{-\infty}^{\infty} \frac{j\mu\Phi_{ii}(\mu) e^{j\mu(t+\tau)}}{\Lambda - (j\omega)} d\mu dt \quad (11)$$

These operators for two classes of input spectra are given in Fig. (5), for the zero noise case. The effect of flat noise on the operator is to add two simple poles to the transfer function (10) and (11), and vary the zeros slightly. The errors in prediction and derivative prediction may be derived. Analysis indicates that these optimum prediction filters perform better than truncated Taylor-servos operators even when spectrum estimates are crude. They also permit straightforward compensation for the effects of noise on the input.

Analog Simulation Technique

The electronic analog computer used in this study was built at the University of Wisconsin under the direction of Professor V. C. Rideout. It is a high speed computer, with a bandwidth from d-c to 10,000 cps. One second of real time then will correspond to one millisecond of computer time. This fast time capability makes it possible to measure statistical parameters in averaging times on the order of a few seconds. In the work to follow, computer integrators which perform the averaging are clamped every ten real-time seconds. Data was recorded both on a hot-wire recorder and by oscilloscope presentation. This rapid averaging rate is a necessity in investigations of this kind.

The "torque" saturating characteristic was obtained from a diode-operational amplifier unit. For output level of ten volts an input of .12 volts was sufficient to drive the unit into saturation. The small signal gain of approximately 80 thus realized, and the hysteresis width at signals below 1000 cps of .05 volts, is considered to represent an ideal limiter.

The signed squarer was obtained electronically by an input isolation stage followed by a piece of thyrite properly biased, as input to an operational amplifier stage. This characteristic may be approximated in practice more simply by a piecewise linear diode circuit. Philbrick-type electronic multipliers were used where multiplication, or the squaring of a function were required. A General Radio noise generator supplied the random input.

Simulation Results[12]

McDonald Servo

To begin with, the McDonald servo was simulated and subjected to the bandpass input spectrum of Fig. (5). The normalized mean-squared error was measured as a function of input level. The results are shown dasned in Fig. (6), for two widths Q = 2 and Q = 5 of input spectrum. There, the band center was 1 radian/sec. Error increased in a monotone fashion with input level. For fixed input level and band width, the error in general increased with center frequency. The behavior could be predicted from sine-wave input analysis of the McDonald servo, where maximum output acceleration limits the amplitude and frequency of acceptable input signals. However, this correlation between sine-wave and random signal behavior must be regarded cautiously. An experiment was made as follows: Generate a low pass spectrum (Fig. (5)) with identical band width as the band spectrum taken for Fig. (6); for Q = 2 this corresponds to T = 1.286. Measuring the error characteristics for this low pass case gives the data of Fig. (7). It is noted that within the range of acceptable error the behavior was identical. Analysis and corroborating tests lead to the conclusion that for relatively narrow band signals the McDonald servo operation is far more sensitive to band width than band location.

Predictor-Relay Servo

Next the predictor-relay servo of Fig. (3) was simulated. For prediction time $\tau = 0$, this servo reduces to the McDonald servo. Thus results for $\tau = 0$ in this section check comparable ones of the previous section. Mean squared error was measured for various prediction times τ and plotted, for Q = 2 band-pass input, on Fig. (8). It is apparent from Fig. (8) that for each input level there corresponds a unique prediction time τ for minimum mean squared error. In general, the optimal τ increased with input level. For small input power, this class of prediction-relay servos properly degenerates to the McDonald servo.

The optimal $-\tau$ prediction relay servo error characteristics are abstracted from Fig. (8) and plotted on Fig. (6) in solid lines.

The superiority of the predictor-relay servo is evident, as the range of possible input levels is markedly increased. A surprising result is

that the error level is decreased to a tolerable range at least up to $\overline{\theta_i}^2 = 12$ volts squared, where a prediction time τ of 0.9 computer seconds was used. Here the Wiener filters were operating at a per unit mean squared error of 0.16 and 0.47 for prediction and derivative prediction, respectively, for the Q = 2 case. Thus even rough estimates of future input values can be utilized to significantly reduce the mean squared error. Behavior in the low pass case was similar to that described above, with the exception that for large input the difference in error was not so striking.

Variation on the McDonald Servo

There is no sound reason to suppose that the control function

$$\theta_c = 2F\theta_e + \dot{\theta}_e|\dot{\theta}_e| \qquad (12)$$

designed for the step input case should be the optimum combination when the input is random. Letting instead

$$\theta_c = 2F\theta_e + \sigma\dot{\theta}_e|\dot{\theta}_e| \qquad (13)$$

tests were made to find what further decrease in mean squared error would result when σ is varied from unity. As in the predictor-relay tests in the previous section where minimal error obtained for a different prediction time τ for each value of input level, here the optimal σ varied with input level. For low levels, σ_{opt} was indistinguishable from unity. As input level $\overline{\theta_i}^2$ was increased, values of σ larger than unity were required for minimum error. For the input signal range tested, σ varied between 1.0 and 3.0. Results are plotted on Fig. (9), for the Q = 2, 5 band pass spectrum cases. The performance is indeed improved. However, the errors for optimal σ are still uniformly higher than those for the predictor-relay servo. Here compare the error curves of Fig. (9) with those of Fig. (6). Similar tests were made with narrower band spectra and with low pass spectra. This data is not presented here; however, the optimization of σ led to the same degree of improvement, and again σ_{opt} in each case was greater than unity. Thus emphasis on the error derivative improved the response.

Variations on the Predictor-Relay Servo

The results of the preceding section indicated that error derivative may well be weighted more strongly in the random signal case than for the input step change. Now it has been stated here that the predictor-relay servo is not necessarily an optimum system since several assumptions were made in its design. The tests reported on in this section were made to determine the extent to which the predictor-relay servo described above could be improved by computer optimization. Here as in the immediately preceding section, σ was made variable, that is, the weight given the signal β over that on α was computer optimized. Furthermore, the τ gain element in the α channel of Fig. (3) was varied independently of the lead time of the predictors. Increasing this τ gain provided additional weight on the predicted derivative of the input. Experimental optimization of lead time, τ, and σ then gave the computer-optimized results of Fig. (9). For each of the spectra tested this computer-optimized servo gave similar results.

Furthermore, for each spectrum is presented for the computer optimized case a single triplet of values of lead time, τ, and σ. Thus the servo parameters stood independent of input level, a beneficial feature for a practical system. Optimizing the triplet of values for each input level admitted slight additional improvement.

An attempt was made to further optimize the predictor-relay servo by an "adaptive" technique. The servo behavior was such that the optimal τ increased with input level. Thus a "linear" envelope detection circuit was set up on the computer to monitor the envelope magnitude. This signal was then multiplied in place of the τ amplifier in the α channel of Fig. (3). Thus in some proportional sense τ was made to increase with the short-time statistical level of the input wave. By adjusting the time constant of the detection filter and the magnitude of the multiplier output, this adaptive servo was optimized. Values of mean squared error only slightly smaller than those for the triplet-optimized predictor-relay servo described above could be attained. It was concluded that in applications the decrease in mean squared error would not warrant the additional circuitry.

Proportional-Plus-Derivative Control

A series of tests was conducted to determine the extent to which the simpler switch function

$$\theta_c = \theta_e + \lambda\dot{\theta}_e \qquad (14)$$

could be made to approach the quality of the McDonald servo with σ variable (Eq. (13)) and that of the predictor-relay servo. All data taken, although not presented here, indicated that for computer-optimized λ this simpler circuit could be made to perform roughly as well as the σ-variable McDonald servo, but in no case as well as the optimized predictor-relay servo.

Effect of Spectrum Change

The results given thus far for the predictor-relay servo are based on an input signal which actually possesses the spectra assumed in the predicting filter derivation. Of paramount practical importance is some indication of the degree to which the predictor-relay servo quality deteriorates with erroneous spectrum estimates. Tests

were conducted in this connection which indicated that while the predictor-relay servo was relatively sensitive to small spectrum changes, it continued to outperform the simpler configuration until actual spectra only remotely resembled the design spectra. For example, increasing the band width 15% for fixed power approximately doubled the McDonald servo error and only doubled the predictor-relay servo error.

The Error Signal

Discussion

It is well known that the response of a linear system to a Gaussian random input is also Gaussian. The response of a non-linear system to a Gaussian random input may or may not resemble a member of a Gaussian random process. Indeed, in most cases even the first probability density of the response will not be normal. When the error is not normally distributed it is often dangerous to rate the quality of a system by the size of its mean squared error (or variance, if the mean value is zero). Thus in a non-linear system the mean squared error may be very low because the error is zero 98% of the time, but exhibits wild excursions in the 2% of the time when the non-linear control system suddenly fails to stay "locked in". Short-time subharmonic oscillations may occur, or simply an input variable change too rapid for a torque-limited device to follow. Such short time bursts of error may be intolerable in an application, even though the "error power" or mean squared error is low.

The situations described above aptly characterize the predictor-relay control schemes studied in this paper. Instantaneous error plots show infrequent but large excursions. Thus the error probability density curves are more peaked at the origin, but have large-error tails which diminish more slowly than those for a normal (Gaussian) distribution. It is the purpose of this section to evaluate the actual probability distribution for the error in a class of non-linear control systems.

Analysis

Markoff Processes. Method of Fokker-Planck:[13] A continuous two-variable random process is called Markoff if all statistical information about the process is contained in the joint probability distribution W_2, where

$W_2(x_1, t_1 ; x_2, t_2)\, dx_1\, dx_2 =$

Joint probability of finding at time t_1 the variable represented by x_1 in the interval $(x_1, x_1 + dx_1)$, and at time t_2 the variable represented by x_2 in the interval $(x_2, x_2 + dx_2)$.

One writes a conditional probability p_2 such that

$p_2(x_1, x_2 ; t_1 \mid \xi_1, \xi_2 ; t_2)\, dx_1\, dx_2 =$

Probability of finding the variables in the intervals $(x_1, x_1 + dx_1)$ and $(x_2, x_2 + dx_1)$ at time t_1 given that the variables were in the intervals $(\xi_1, \xi_1 + d\xi_1)$ and $(\xi_2, \xi_2 + d\xi_2)$ at time t_2.

The first probability density

$w(x_1, x_2)\, dx_1\, dx_2 =$

Probability that at any time the variable represented by x_1 lies in the interval $(x_1, x_1 + dx_1)$ and x_2 lies in the interval $(x_2, x_2 + dx_2)$.

such that

$$\int_{-\infty}^{\infty}\int_{-\infty}^{\infty} w(x_1, x_2)\, dx_1\, dx_2 = 1$$

$$\int_{-\infty}^{\infty} w(x_1, x_2)\, dx_1 = p(x_2)$$

$$\int_{-\infty}^{\infty} w(x_1, x_2)\, dx_2 = p(x_1)$$

where the $p(x_i)$ represent probability densities for the individual processes.

Further,

$$\lim_{(t_1 - t_2) \to \infty} p_2(x_1, x_2 ; t_1 \mid \xi_1, \xi_2 ; t_2) = w(x_1, x_2)$$

the conditions at a given time being independent of values in the infinite past.

The basic equation for the theory of Markoff processes is the Smoluchowski or Chapmann-Kolmogoroff equation which states that

$$p_2(x_1, x_2 ; t_1 \mid \xi_1, \xi_2 ; t_2) = \int_{-\infty}^{\infty}\int_{-\infty}^{\infty} p_2(V_1, V_2 ; t \mid \xi_1, \xi_2 ; t_2)\, p_2(x_1, x_2 ; t_1 \mid V_1, V_2 ; t)\, dV_1\, dV_2 \qquad (15)$$

It has been shown that the above Smoluchowski equation reduces to a diffusion equation when, roughly, the variables are continuous in time. In this two-dimensional case, Eq. (15) reduces to the Fokker-Planck equation which follows. The angular brackets represent ensemble averages.

$$\frac{\partial p_2}{\partial t} = \frac{-\partial \beta_1 p_2}{\partial x_1} - \frac{\partial \beta_2 p_2}{\partial x_2}$$

$$+\frac{1}{2}\left[\frac{\partial^2 \beta_{11} p_2}{\partial x_1^2} + \frac{\partial^2 \beta_{12} p_2}{\partial x_1 \partial x_2} + \frac{\partial^2 \beta_{21} p_2}{\partial x_2 \partial x_1} + \frac{\partial^2 \beta_{22} p_2}{\partial x_2^2}\right] \qquad (16)$$

where

$$\beta_i = \lim_{\Delta t \to 0} \frac{\langle \Delta x_i \rangle}{\Delta t} \text{ and } \beta_{ij} = \lim_{\Delta t \to 0} \frac{\langle \Delta x_i \Delta x_j \rangle}{\Delta t}$$

Here interest lies in the steady solution, $t \to \infty$. Here $\frac{\partial p_2}{\partial t} = 0$ and the conditional probability distribution, p_2, reduces to the first probability distribution, w, defined above. Thus one has

$$0 = -\frac{\partial \beta_1 w}{\partial x_1} - \frac{\partial \beta_2 w}{\partial x_2}$$

$$+\frac{1}{2}\left[\frac{\partial^2 \beta_{11} w}{\partial x_1^2} + \frac{\partial^2 \beta_{12} w}{\partial x_1 \partial x_2} + \frac{\partial^2 \beta_{21} w}{\partial x_2 \partial x_1} + \frac{\partial^2 \beta_{22} w}{\partial x_2^2}\right] \qquad (17)$$

Eq. (17) may sometimes be solved for the probability density $w(x_1, x_2)$ for two selected variables in a non-linear or linear control system. x_1 and x_2 may be, for example, error and error derivative. This Fokker-Planck method represents the best statistical approach to phase plane analysis.[4]

Servo Analysis: Next the methods of the previous section are used to determine the error probability density function for the control system of Fig. (1). The "computer" is represented by $\theta_c = \theta_e + \lambda \dot{\theta}_e$. The load is initially allowed to possess damping and spring forces. λ, the proportion of derivative control, will be arbitrary. The presence of damping and "spring" forces in the load, is initially considered.

Label the non-linearity function $N(\theta_c)$. Thus the load dynamics satisfy the equation

$$N(\theta_e + \lambda \dot{\theta}_e) = \ddot{\theta} + a\dot{\theta}_o + b\theta_o ,$$

while the feedback equation is

$$\theta_e = \theta_i - \theta_o ;$$

combining equations,

$$\ddot{\theta}_e + a\dot{\theta}_e + b\theta_e + N(\theta_e + \lambda \dot{\theta}_e) = f(t) \qquad (18)$$

Eq. (18) is then the exact non-linear differential equation with error as dependent variable. The forcing function is

$$f(t) = \ddot{\theta}_i + a\dot{\theta}_i + b\theta_i ,$$

and effective input to the system. Now Eq. (18) is written in terms of two first-order differential equations, as in phase plane analysis. Let $x_1 = \theta_e$ and $x_2 = \dot{\theta}_e$ Eq. (18) becomes the system

$$\dot{x}_2 + a x_2 + b x_1 + N(x_1 + \lambda x_2) = f(t)$$
$$\dot{x}_1 = x_2 \qquad (19)$$

In order to determine the β_{ij} of Eq. (16) one integrates Eq. (19). As stated before, it is expected that the variables x_1 and x_2 change a small amount in small time increments. No such restriction is made on f(t). The following pair is thus obtained.

$$\Delta x_2 + a x_2 \Delta t + b x_1 \Delta t + N(x_1 + \lambda x_2)\Delta t = \int_t^{t+\Delta t} f(\tau)\, d\tau$$
$$\Delta x_1 = x_2 \Delta t \qquad (20)$$

With Eq. (20) now is evaluated the β_{ij} of Eq. (16)

$$\beta_1 = \lim_{\Delta t \to 0} \frac{\langle \Delta x_1 \rangle}{\Delta t} = \lim_{\Delta t \to 0} \frac{\langle x_2 \Delta t \rangle}{\Delta t} = x_2$$

$$\beta_2 = \lim_{\Delta t \to 0} \frac{\langle \Delta x_2 \rangle}{\Delta t} = \lim_{\Delta t \to 0} \frac{\left\langle -a x_2 \Delta t - b x_1 \Delta t - N(x_1 + \lambda x_2)\Delta t + \int_t^{t+\Delta t} f(\lambda)\, d\lambda \right\rangle}{\Delta t}$$
$$= -a x_2 - b x_1 - N(x_1 + \lambda x_2)$$

$$\beta_{11} = \lim_{\Delta t \to 0} \frac{\langle (\Delta x_1)^2 \rangle}{\Delta t} = \lim_{\Delta t \to 0} \frac{\langle (x_2 \Delta t)^2 \rangle}{\Delta t} = 0$$

$$\beta_{12} = \lim_{\Delta t \to 0} \frac{\langle \Delta x_1 \Delta x_2 \rangle}{\Delta t} = \lim_{\Delta t \to 0} \frac{\left\langle x_2 \Delta x_2 \Delta t + x_2 \Delta t \int_t^{t+\Delta t} f(\lambda)\, d\lambda \right\rangle}{\Delta t}$$
$$- \lim_{\Delta t \to 0} \frac{\langle (\Delta t)^2 [a x_2^2 + b x_1 x_2 + x_2 N(x_1 + \lambda x_2)] \rangle}{\Delta t} = 0$$

$$\beta_{21} = 0$$

$$\beta_{22} = \lim_{\Delta t \to 0} \frac{\langle (\Delta x_2)^2 \rangle}{\Delta t} = \lim_{\Delta t \to 0} \frac{\left\langle \left[\int_t^{t+\Delta t} f(\lambda) d\lambda - \Delta t \left\{ a x_2 + b x_1 + N(x_1 + \lambda x_2) \right\} \right]^2 \right\rangle}{\Delta t}$$

$$= \lim_{\Delta t \to 0} \frac{\left\langle \left[\int_t^{t+\Delta t} f(\lambda) d\lambda \right] \right\rangle}{\Delta t} = \lim_{\Delta t \to 0} \int_t^{t+\Delta t} \int_t^{t+\Delta t} \langle f(\lambda) f(t) \rangle d\lambda dt$$

If the autocorrelation function for the effective input f(t) is given by

$$\phi_{ff}(\tau) = 2D\delta(\tau)$$

that is, f(t) is effectively white Gaussian noise at strength 2D. Then

$$\beta_{22} = \lim_{\Delta t \to 0} \frac{\int_t^{t+\Delta t} \int_t^{t+\Delta t} 2D\delta(\tau - t) d\tau dt}{\Delta t} = 2D$$

The assumption that f(t) has an impulse autocorrelation function amounts to saying the f(t) has a flat frequency spectrum. While the latter is never strictly true, it often is approximately so. Thus, if θ_i possesses the spectrum

$$\Phi_{ii}(\omega) = \frac{1}{\omega^4}$$

and the system load is purely inertial, the effective input f(t) has a spectrum

$$\Phi_{ff}(\omega) = \left| (j\omega)^2 \right|^2 \Phi_{ii}(\omega) = 1 .$$

If the input is band limited and the load dynamics include damping and spring force,

$$\Phi_{ff}(\omega) = K \frac{\left| 1 + B_j \omega + J(j\omega)^2 \right|^2}{\left| 1 + 2\sigma j\omega\tau + (j\omega\tau)^2 \right|^2}$$

which may conceivably be flat well beyond any range of interest.

Combining the β_i and β_{ij} in Eq. (17) one obtains the Fokker-Planck equation:

$$0 = -\frac{\partial x_2 w}{\partial x_1} + \frac{\partial \left[a x_2 + b x_1 + N(x_1 + \lambda x_2) \right] w}{\partial x_2} + D \frac{\partial^2 w}{\partial x_2^2} \qquad (21)$$

This equation for $w(x_1, x_2)$ will be solved for the case of the saturating transducer

$$N(x_1 + \lambda x_2) = F \frac{x_1 + \lambda x_2}{|x_1 + \lambda x_2|}$$

First consider the half of the x_1, x_2 phase plane where $(x_1 + \lambda x_2) > 0$ Try

$$w(x_1, x_2) = e^{-\frac{a}{2D} x_2^2} G(x_1) .$$

This product of functions inserted in Eq. (21) leads to

$$0 = x_2 e^{-\frac{a}{2D} x_2^2} \left[G(x_1) \left\{ \frac{aF}{D} + \frac{ab}{D} x_1 \right\} + \frac{dG_1(x_1)}{dx_1} \right]$$

whence

$$G(x_1) = K \exp - \left\{ \frac{aF}{D} x_1 + \frac{ab}{2D} x_1^2 \right\}$$

In a precisely similar fashion, for $(x_1 + \lambda x_2) < 0$,

$$G(x_1) = K \exp - \left\{ -\frac{aF}{D} x_1 + \frac{ab}{2D} x_1^2 \right\}$$

so that anywhere on the phase plane

$$w(x_1, x_2) = K \exp - \frac{a}{2D} x_2^2 \exp \left\{ -\frac{aF}{D} \frac{x_1 + \lambda x_2}{|x_1 + \lambda x_2|} \cdot x_1 - \frac{ab}{2D} x_1^2 \right\} \qquad (22)$$

For $\lambda = 0$ the probability density for the error derivative, x_2, is found from

$$p(x_2) = \int_{-\infty}^{\infty} w(x_1, x_2) dx_1$$

to be normal. The probability density for the

error, x_1, is found from

$$p(x_2)=\int_{-\infty}^{\infty} w(x_1, x_2)\,dx_2$$

for $b=\lambda=0$ and suitable normalization to be

$$p(x_1)=p(\theta_e)=\frac{1}{\sqrt{2}\,\sigma_e}\,e^{-\sqrt{2}\,\frac{|\theta_e|}{\sigma_e}} \qquad (23)$$

a result which will be of considerable interest. Integrating again, one obtains the probability distribution function

$$P(\theta_e)=\frac{1}{2}\,e^{\sqrt{2}\,\frac{\theta_e}{\sigma_e}}\ ,\ \theta_e\le 0$$

$$P(\theta_e)=\frac{1}{2}+\frac{1}{2}\left[1-e^{-\sqrt{2}\,\frac{\theta_e}{\sigma_e}}\right]\ ,\ \theta_e\ge 0 \qquad (24)$$

Eq. (22) is studied further for the case b = 0, and arbitrary $\lambda>0$. Thus

$$p(\theta)=K\int_{-\infty}^{\infty} exp-\frac{a}{2D}x^2\,exp-\frac{aF}{D}\frac{\theta_e+\lambda x}{|\theta_e+\lambda x|}\,\theta_e\,dx$$

$$=\sqrt{\frac{2\pi D}{a}}\,K\cosh\frac{aF}{D}\theta_e-2K\sinh\frac{aF}{D}\theta_e\int_0^{\frac{\theta_e}{\lambda}}e^{-\frac{a}{2D}x^2}dx, \qquad (25)$$

again an even non-negative function. Eq. (25) represents the error probability density for arbitrary λ. Letting $\lambda\to 0$ and considering the sign of θ_e reduces this equation to Eq. (23).

Integrating Eq. (25) once more gives the error probability distribution function

$$P(\theta_e)=\sqrt{\frac{2\pi D}{a}}\,\frac{DK}{aF}\sinh\frac{aF}{D}\theta_e$$

$$-\frac{2KD}{aF}\cosh\frac{aF}{D}\theta_e\int_0^{\frac{\theta_e}{\lambda}}e^{-\frac{a}{2D}x^2}dx$$

$$+\frac{2KD}{aF\lambda}\int_{-\infty}^{\theta_e}\cosh\frac{aF}{D}\mu\,e^{-\frac{a}{2D}\frac{\mu^2}{\lambda^2}}d\mu$$

where for proper normalization,

$$K=\frac{\frac{a}{b}\sqrt{\frac{a}{b}}F}{\sqrt{2\pi}}\,e^{-\frac{aF^2\lambda^2}{2D}}$$

The important result is that the integral terms of Eq. (26) have significant effect only in the neighborhood of the origin of θ_e. The distribution (26) approaches asymptotically the $\lambda=0$ case (Eq. (24)) for large θ_e.

A development exactly similar to the one above may be made for a servo with a non-linearity in the switch control computer. For example, consider a modified McDonald servo, where $\theta_c=\theta_e+\lambda\dot{\theta}_e\,|\dot{\theta}_e|$ instead of the control $\theta_c=\theta_e+\lambda\dot{\theta}_e$ given above. Again the $\dot{\theta}_e$ vs. θ_e phase plane is separated into two parts, corresponding to $\theta_c>0$ and for $\theta_c<0$. The Fokker-Planck equation is integrated once in the same way. Then the error probability density is found by integration just as in Eq. (25) except that the upper limit on the final indefinite integral would be $\sqrt{\theta_e/\lambda}$. The probability distribution function in this case then approaches that of a simple exponential even more rapidly than for the linear switch control computer case.

Simulation Results

Error probability distribution functions were measured for each of the control computers of the previous sections. The distribution function of Eq. (23) served as a large error asymptote and a small error bound (negative error u.b. positive error l.b.) for all measured distribution functions. For each servo studied, the normalized error probability distribution functions' departure from the Gaussian decreased with band width, and decreased with input level. In general the inclusion of additional control circuitry represented a more normal error curve. Representative curves are given on Fig. (10), plotted on normal probability paper.

Conclusion

Analog tests indicated that inclusion of prediction circuitry indeed reduced rms error in a saturating servo system with a random input. Straightforward application of the Smith method did yield a helpful guide to design. However, tests indicated that in applications, simulation would be necessary to establish servo-computer parameters which would be less sensitive to input statistics.

A method is illustrated which yields the error probability distribution function for a class of compensated relay servos. A generalization of the analytic results would indicate that a large class of compensated relay servos with Gaussian random input yield a simple exponential large error probability density.

Acknowledgement

The author gratefully acknowledges the guidance of Professor Vincent C. Rideout of the University of Wisconsin during the course of this study. Financial support was received from the Wisconsin Alumni Research Foundation and the National Science Foundation.

Bibliography

1. Kendall, P. E. and Bogner, I., "Research in Non-Linear Mechanics as Applied to Servomechanisms", WADC Tech. Rep. No. 53-521 Wright-Patterson AFB, Ohio; December, 1953.

2. Bushaw, D. W., "Differential Equations with a Discontinuous Forcing Term", Experimental Towing Tank Report No. 469, Stevens Inst. of Technology; January, 1953.

3. Caldwell, R. R. and Rideout, V. C., "A Differential Analyzer Study of Certain Nonlinearly Damped Servomechanisms", AIEE Trans., Paper No. 53-107, pp. 165-169; January, 1953.

4. Hopkin, A. M. and Wang, P. K. C., "A Relay-Type Feedback Control System Designed for Random Inputs", AIEE Trans., Paper No. 59-218; February, 1959.

5. Kalman, R. E., "Analysis and Design Principles of Second and Higher Order Saturating Servomechanisms", AIEE Trans., Paper No. 55-551, pp. 294-308; 1955.

6. Booton, R. C., Mathews, M. V. and Seifert, W. W., "Non-Linear Servomechanisms with Random Inputs", DACL Report No. 70; August, 1953.

7. Leland, H. R., "Response of Certain Non-Linear Systems to Random Inputs", Proc. NEC, Vol. 14, pp. 698-708; October 1958.

8. Smith, O. J. M., "Feedback Control Systems", McGraw-Hill Book Company, Inc., New York; 1958.

9. Laning, J. H. and Battin, R. H., "Random Processes in Automatic Control", McGraw-Hill Book Company, Inc., New York; 1956.

10. Wiener, N., "Extrapolation, Interpolation, and Smoothing of Stationary Time Series", John Wiley and Sons, Inc., New York; 1950.

11. Zakai, M., "On a Property of Wiener Filters", IRE PGIT Trans., Vol. 1T-5, No. 1, pp.15-17; March, 1959

12. Benedict, T. R., "A Study of Predictor-Relay Servos with Random Inputs", Ph.D. Thesis, University of Wisconsin, Madison, Wisconsin; 1959.

13. Wang, M. C. and Uhlenbeck, G. E.,"On the Theory of the Brownian Motion II", in "Noise and Stochastic Processes", ed. by Nelson Wax, Dover Publications, Inc., New York, pp. 113-132; 1954.

14. Chuang, K. and Kazda, L. F., "A Study of Non-Linear Systems with Random Inputs", AIEE Trans., Paper No. 59-147; February, 1959.

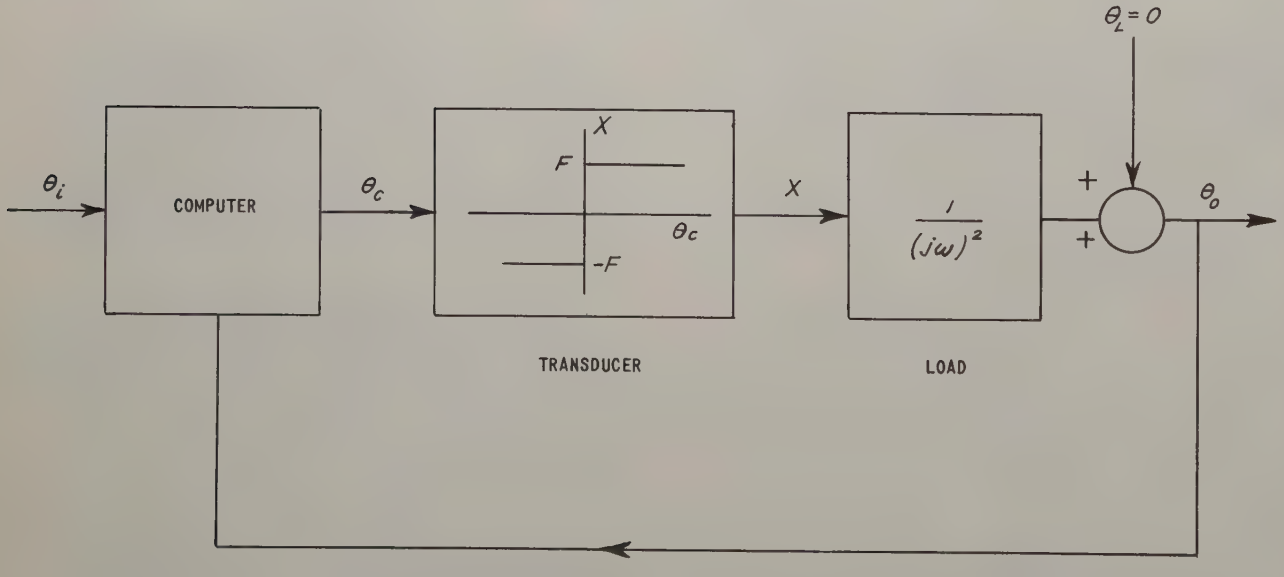

Fig. 1. Relay Control of an Inertial Element.

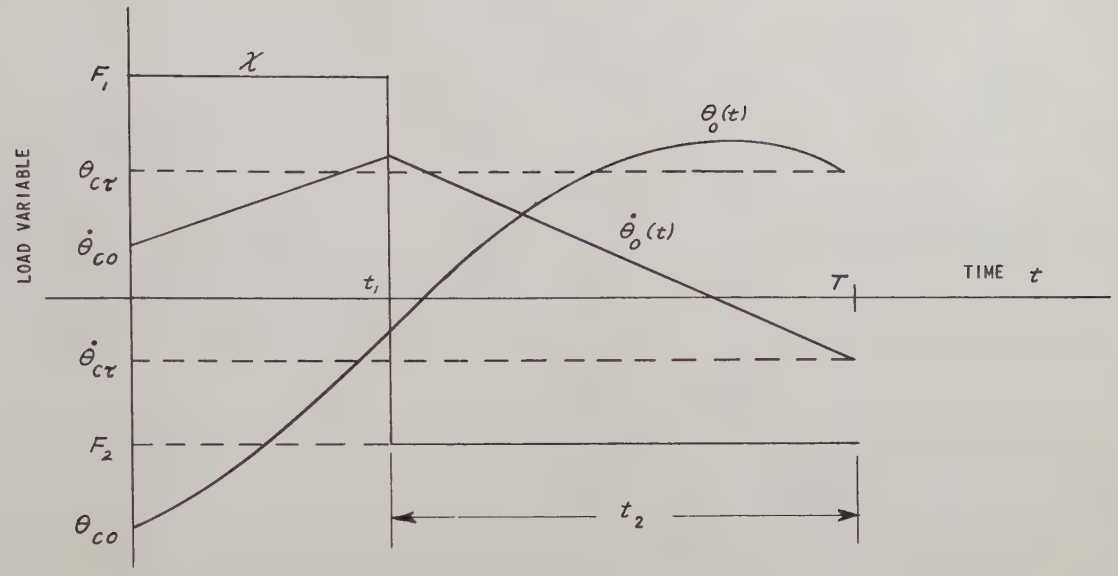

Fig. 2. Dynamic Variables in an Inertial Load.

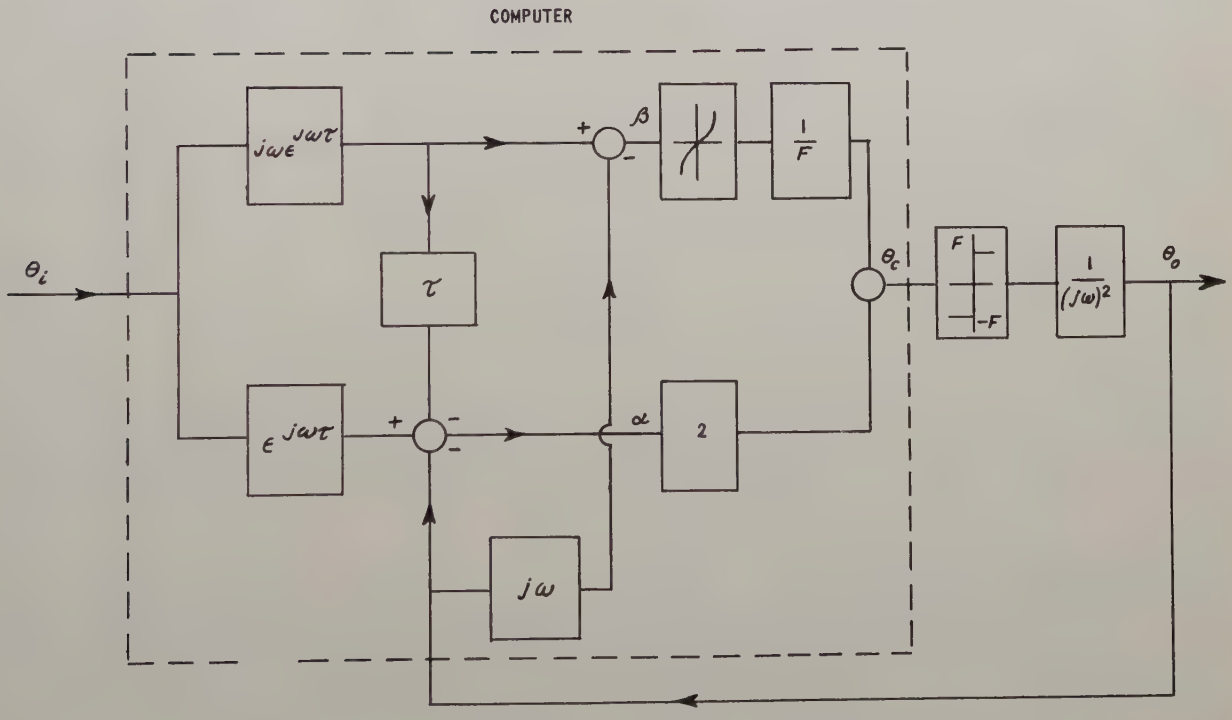

Fig. 3. System Topology of a Predictor-Relay Servo.

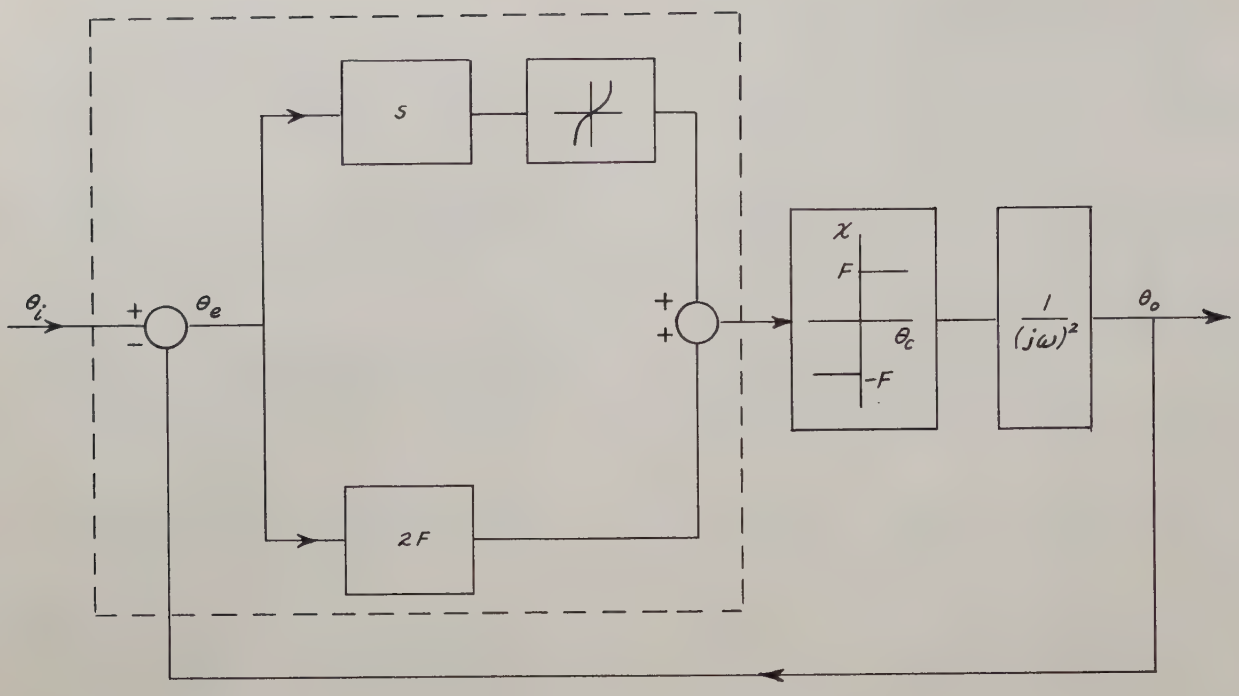

Fig. 4. The McDonald Servo.

SIGNAL SPECTRUM	OPTIMUM PREDICTOR $H_p(j\omega)$ OPTIMUM DERIVATIVE-PREDICTOR $H_d(j\omega)$
$\frac{A}{(\omega^2+\omega_0^2)^2}$	$H_p(j\omega) = \epsilon^{-\omega_0\tau}\left[(1+\omega_0\tau)+j\omega\tau\right]$ $H_d(j\omega) = \omega_0\,\epsilon^{-\omega_0\tau}\left[-\omega_0\tau + j\frac{\omega}{\omega_0}(1-\omega_0\tau)\right]$
$\frac{A}{\left\lvert 1+j\frac{\omega}{Q\omega_0}+\left(j\frac{\omega}{\omega_0}\right)^2\right\rvert^2}$	$H_p(j\omega) = \frac{\epsilon^{-\xi\tau}}{\sqrt{1-\xi^2}}\sin\sqrt{1-\xi^2}\,\tau\left[\left(\sqrt{1-\xi^2}\cot\sqrt{1-\xi^2}\,\tau+\xi\right)+j\omega\right]$ $H_d(j\omega) = \frac{\epsilon^{-\xi\tau}}{\sqrt{1-\xi^2}}\sin\sqrt{1-\xi^2}\,\tau\left[-1+j\omega\left(\sqrt{1-\xi^2}\cot\sqrt{1-\xi^2}\,\tau-\xi\right)\right]$ $Q=\frac{1}{2\xi} \qquad \omega_0 = 1.0$

Fig. 5. Prediction Operators.

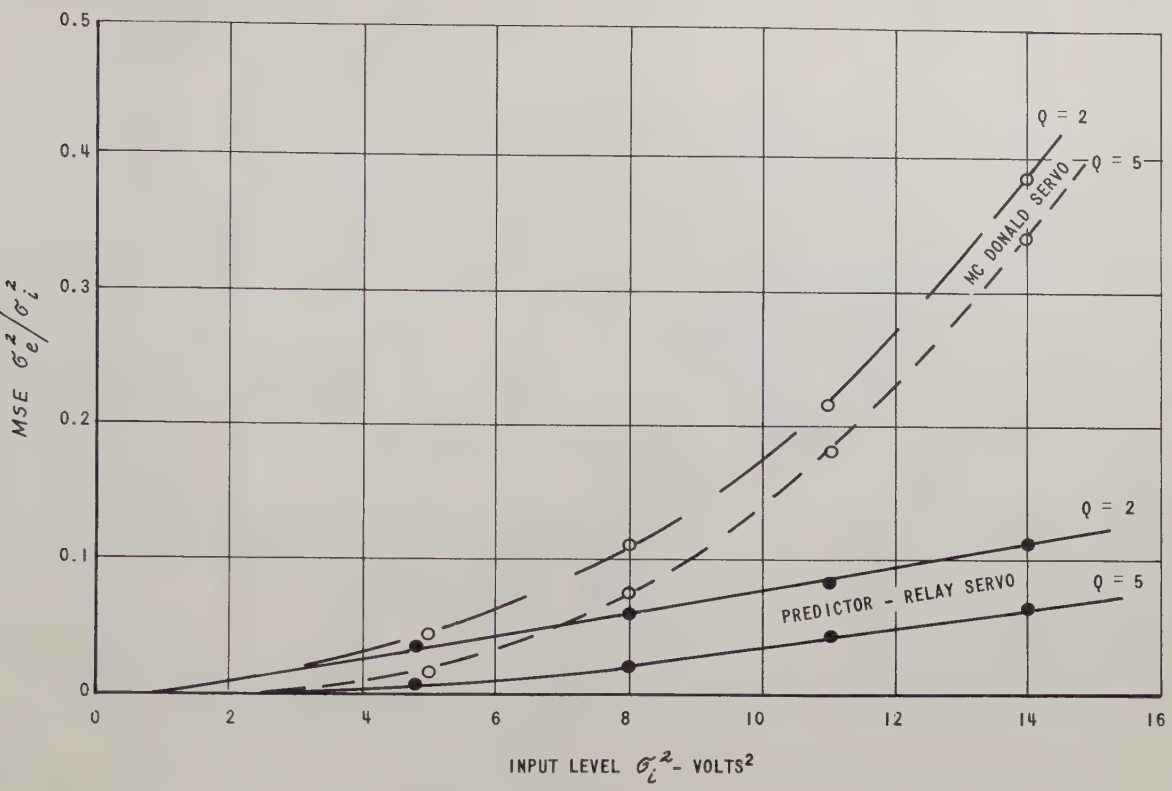

Fig. 6. Comparison of Optimal - τ Predictor-Relay Servo with McDonald Servo for Bandpass Spectra.

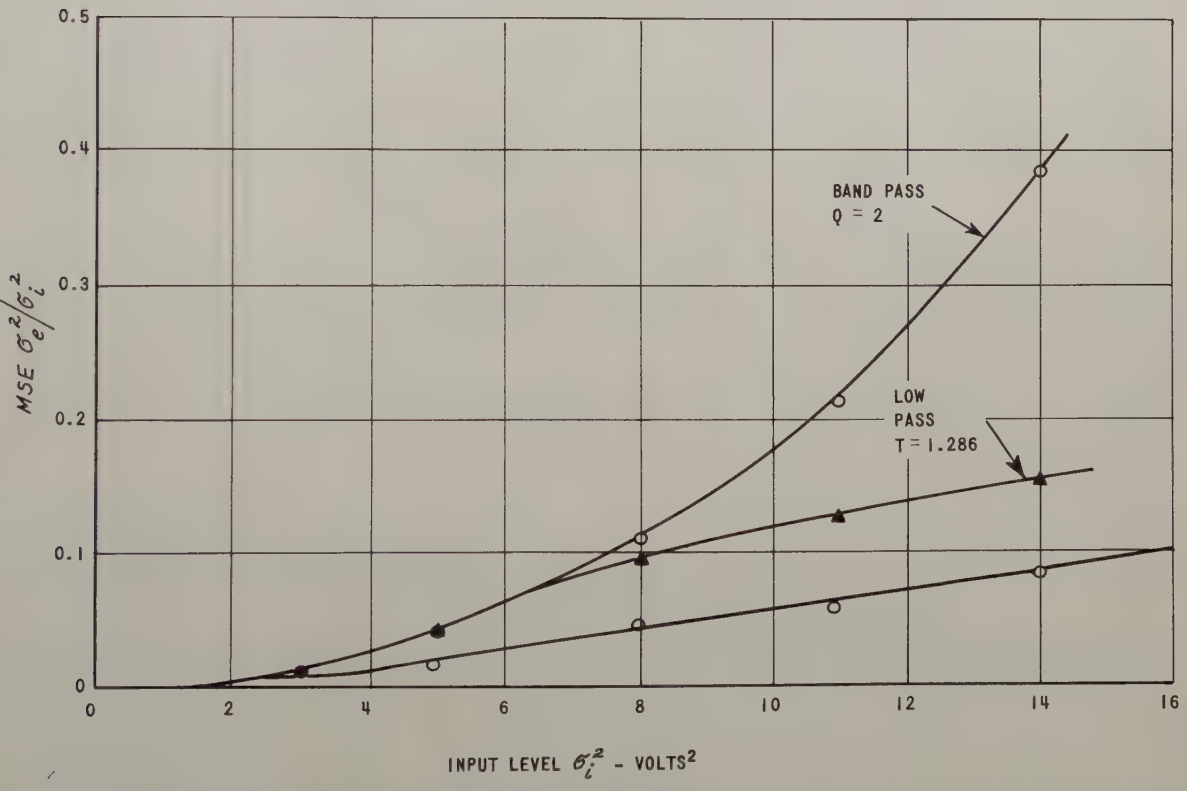

Fig. 7. Comparison of McDonald Servo Error for Equal Bandwidth Low Pass and Band Pass Input Spectra.

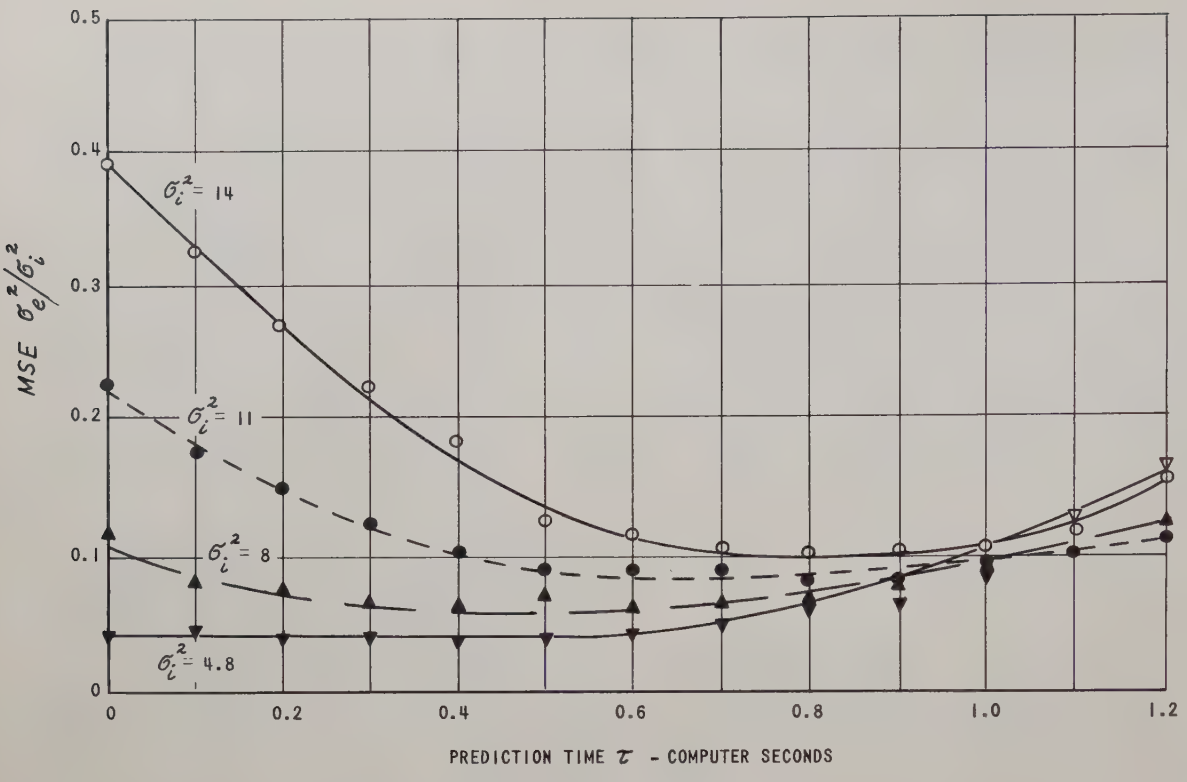

Fig. 8. Predictor-Relay Servo Errors. Q = 2

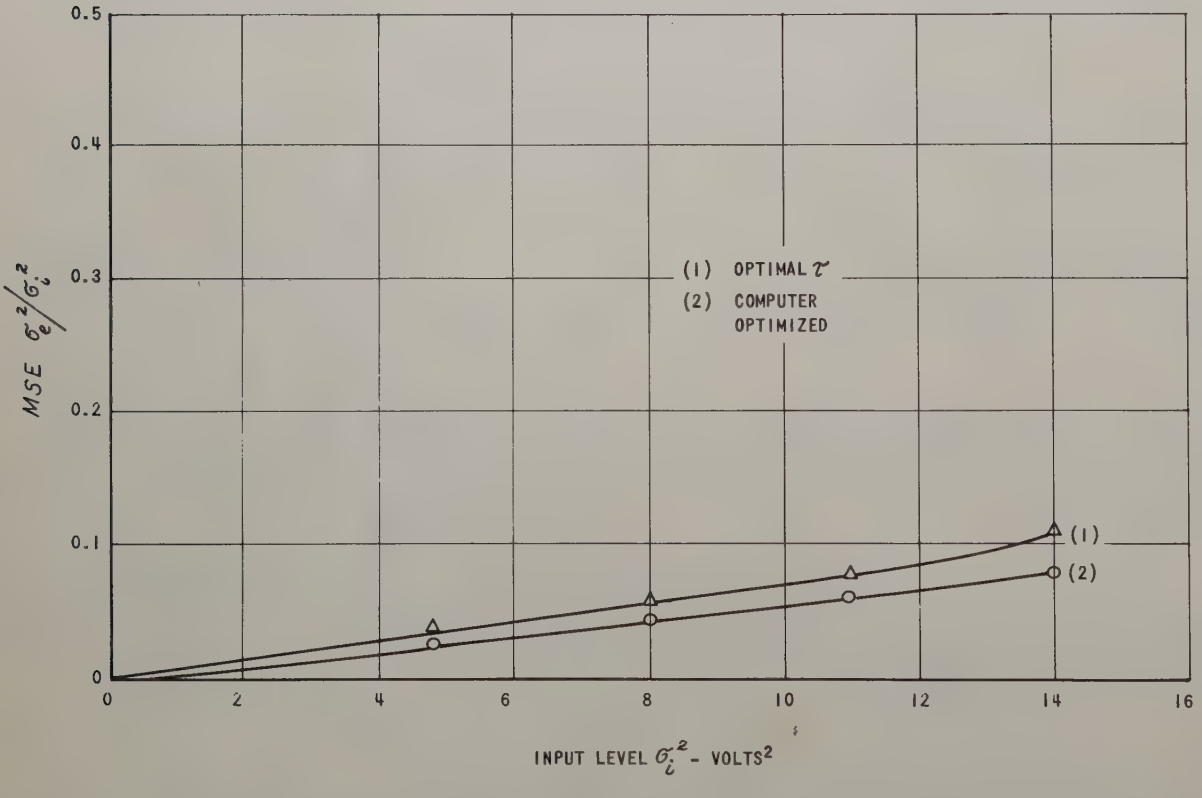

Fig. 9. Computer-Optimized Predictor-Relay Servo Error. Band Pass Input. Q = 2

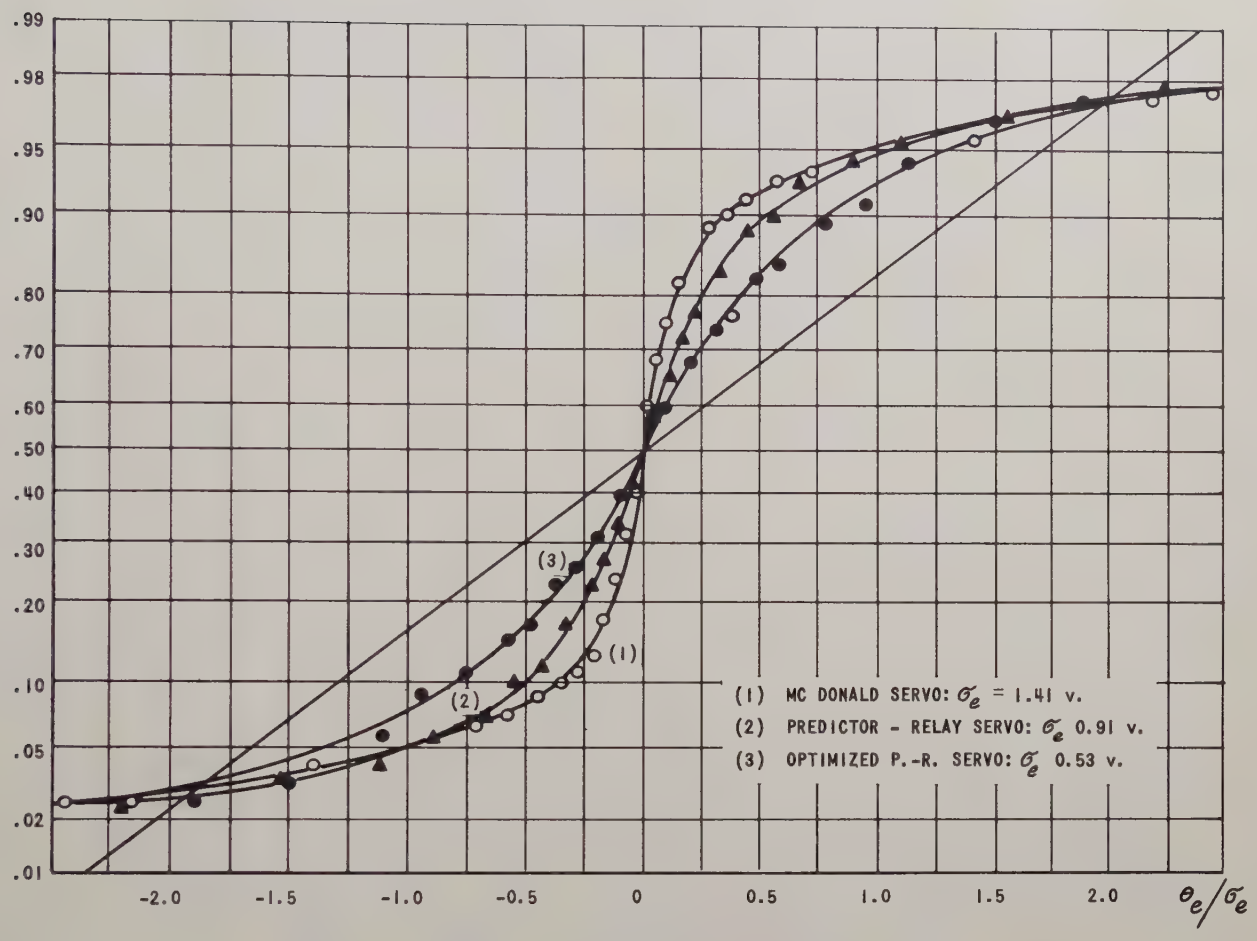

Fig. 10. Comparison of Three Systems $Q = 5 \quad \sigma_i^2 = 11.0\ v^2$.

INSTITUTIONAL LISTINGS

The IRE Professional Group on Automatic Control is grateful for the assistance given by the firms listed below, and invites application for Institutional Listings from other firms interested in the field of Automatic Control.

PHILCO CORP., GOVERNMENT & INDUSTRIAL DIV., 4700 Wissahickon Ave., Philadelphia 44, Pa.
Transac S-2000 All Transistor, Large-Scale Data-Processing Systems; Transac Computers

RAMO-WOOLDRIDGE, DIV. OF THOMPSON RAMO WOOLDRIDGE INC., P.O. Box 90534, Airport Station, Los Angeles 45, Calif.
Electronic Research and Development

The charge for an Institutional Listing is $75.00 per issue or $125.00 for two consecutive issues. Applications for Institutional Listings and checks made out to the Institute of Radio Engineers, Inc.) should be sent to Mr. L. G. Cumming, Technical Secretary, Institute of Radio Engineers, Inc., 1 East 79th Street, New York 21, N. Y.